Vinitakhatri Ji

Vinita_thesis_Revised__2_

Thesis

Document Details

Submission ID
trn:oid:::27535:125422881

Submission Date
Dec 31, 2025, 1:01 PM GMT+5:30

Download Date
Dec 31, 2025, 1:48 PM GMT+5:30

File Name
Vinita_thesis_Revised__2_.pdf

File Size
15.4 MB

285 Pages

119,822 Words

571,736 Characters

9% Overall Similarity

The combined total of all matches, including overlapping sources, for each database.

Filtered from the Report

- Bibliography
- Quoted Text
- Cited Text
- Small Matches (less than 10 words)

Exclusions

- 6 Excluded Sources

Match Groups

713 Not Cited or Quoted 9%
Matches with neither in-text citation nor quotation marks

0 Missing Quotations 0%
Matches that are still very similar to source material

0 Missing Citation 0%
Matches that have quotation marks, but no in-text citation

0 Cited and Quoted 0%
Matches with in-text citation present, but no quotation marks

Top Sources

4% Internet sources
6% Publications
2% Submitted works (Student Papers)

Match Groups

- **713** Not Cited or Quoted 9%
  Matches with neither in-text citation nor quotation marks
- **0** Missing Quotations 0%
  Matches that are still very similar to source material
- **0** Missing Citation 0%
  Matches that have quotation marks, but no in-text citation
- **0** Cited and Quoted 0%
  Matches with in-text citation present, but no quotation marks

Top Sources

4% Internet sources
6% Publications
2% Submitted works (Student Papers)

Top Sources

The sources with the highest number of matches within the submission. Overlapping sources will not be displayed.

1	Internet	dspace.dtu.ac.in:8080 2%
2	Internet	diposit.ub.edu <1%
3	Publication	Javier de Cruz Pérez, Joan Solà Peracaula. " Running vacuum in Brans & Dicke the... <1%
4	Publication	Yogesh Bhardwaj, C. P. Singh. "Matter creation cosmology with generalized Chapl... <1%
5	Publication	Simran Kaur, C.P. Singh. "Constraints on holographic dark energy model with ma... <1%
6	Publication	Tanmay Nandi, Amitava Choudhuri. "Bulk viscous matter with decaying vacuum ... <1%
7	Internet	export.arxiv.org <1%
8	Student papers	Delhi Technological University on 2017-02-09 <1%
9	Publication	Simran Kaur, C. P. Singh. "Evolution of holographic dark energy model with adiab... <1%
10	Publication	Simran Kaur, C P Singh. "Viscous cosmology in holographic dark energy with Gra... <1%

11	Publication	Tanmay Nandi, Amitava Choudhuri. "Bulk viscous matter interacting with decayi... <1%
12	Publication	Yogesh Bhardwaj, C P Singh. "Constraining the variable generalized Chaplygin ga... <1%
13	Internet	hdl.handle.net <1%
14	Publication	C. P. Singh, Joan Solà Peracaula. "Friedmann cosmology with decaying vacuum de... <1%
15	Publication	Ajay Kumar, C. P. Singh. "The generalized second law of thermodynamics in visco... <1%
16	Publication	Cao, Shulei. "Cosmological Constraints from Standardized Non-CMB Observation"... <1%
17	Student papers	University of Sheffield on 2023-09-16 <1%
18	Publication	C. P. Singh, Ajay Kumar. "Holographic dark energy, matter creation, and cosmic a... <1%
19	Student papers	NIT Imphal on 2022-06-29 <1%
20	Publication	Manungu Kiveni, Jo. "A Search for WIMP Dark Matter using an Optimized Chi-squ... <1%
21	Publication	C. P. Singh, Ajay Kumar. "Quintessence behavior via matter creation cosmology", ... <1%
22	Internet	www.arxiv-vanity.com <1%
23	Student papers	Indian School of Mines on 2025-07-20 <1%
24	Student papers	University of Sheffield on 2018-07-23 <1%

25 Student papers
Birla Institute of Technology and Science Pilani on 2020-04-08 <1%

26 Student papers
Chandigarh University on 2025-06-26 <1%

27 Publication
C. P. Singh, Simran Kaur. "Probing bulk viscous matter-dominated model in Brans... <1%

28 Student papers
Manipur University, Imphal on 2025-03-24 <1%

29 Student papers
iimcal on 2025-03-04 <1%

30 Student papers
NIT Imphal on 2021-04-27 <1%

31 Publication
Eleonora Di Valentino, Jackson Levi Said, Adam Riess, Agnieszka Pollo et al. "The C... <1%

32 Publication
Ramadan, Omar Fawzy Muhammed. "Scalar Fields in Cosmology and Their Applic... <1%

33 Internet
doi.org <1%

34 Student papers
Delhi Technological University on 2017-02-12 <1%

35 Student papers
Delhi Technological University on 2024-05-03 <1%

36 Student papers
University of Ioannina on 2022-02-04 <1%

37 Publication
Sabla, Vivian I.. "New Physics in the Age of Precision Cosmology", Dartmouth Coll... <1%

38 Publication
"The Hubble Constant Tension", Springer Science and Business Media LLC, 2024 <1%

39 Publication
Ryan, Joseph. "Observational Constraints on the Cosmological Expansion Rate an... <1%

40 Publication
Peter Coles. "The Routledge Companion to the New Cosmology", Routledge, 2019 <1%

41 Publication
Utpal Sarkar. "Particle and Astroparticle Physics", CRC Press, 2019 <1%

42 Publication
Izadi, Yousef. "Modified Gravity Theories: Cosmological Tests and Black Hole Ther... <1%

43 Publication
Arthur Diniz Meirelles. "Optimization of the CMB-galaxy cross-correlation signal f... <1%

44 Publication
John Senior, Éva Gyarmathy. "The Ethics, Psychology, and Theology of AI - Explori... <1%

45 Publication
Antonini, Stefano. "Holographic Cosmological Models and the AdS/CFT Correspon... <1%

46 Publication
Bagherian, Hengameh. "Building Beyond the Standard Model: Tools from Cosmol... <1%

47 Publication
Norriss S. Hetherington. "Encyclopedia of Cosmology (Routledge Revivals) - Histor... <1%

48 Publication
Mukhopadhyay, Utpal. "Accelerating Universe and i›-Dark Energy.", Jadavpur Uni... <1%

49 Publication
Sailer, Noah. "Towards Accurate Cosmology From CMB Secondaries and Large-Sc... <1%

50 Publication
Daniel J. Denis. "Multivariate Statistics and Machine Learning - An Introduction to... <1%

51 Student papers
Chandigarh University on 2025-06-26 <1%

52 Publication
Yennapureddy, Manoj Kumar . "New Theoretical Ideas in Cosmology Driven by Hi... <1%

53 Publication

Greene, Kylar L.. "Challenging ΛCDM: Unraveling Cosmic Distances, Dark Sector P... <1%

54 Publication

Mutlu Yuksel, Yigit Aydede. "Causal Inference and Machine Learning - In Economi... <1%

55 Publication

Pablo William Rodrigues de Lima. "Nonstandard cosmologies with gravitationally... <1%

56 Publication

Sobotka, Alexander C.. "Altering the Pre-Recombination Expansion History with H... <1%

57 Student papers

NIT Imphal on 2022-07-20 <1%

58 Publication

Richard E. Plant. "Spatial Data Analysis in Ecology and Agriculture Using R", CRC P... <1%

59 Publication

Chen, Shu-Fan. "Tracing the Origins: Cosmological Information in the Large-Scale ... <1%

60 Publication

Kamalinejad, Farshad. "Constraining Cosmology With Higher-Order Summary Sta... <1%

61 Publication

Satyanshu K. Upadhyay, Umesh Singh, Dipak K. Dey, Appaia Loganathan. "Curren... <1%

62 Publication

Surrao, Kristen Marie. "Optimizing Parameter Inference and Foreground Remova... <1%

63 Publication

V.L. Ginzburg. "About Science, Myself and Others", CRC Press, 2019 <1%

A STUDY ON EVOLUTION AND DYNAMICS OF DARK ENERGY MODELS IN COSMOLOGY

A Thesis Submitted

in Partial Fulfillment of the Requirements

for the Degree of

DOCTOR OF PHILOSOPHY

In

Mathematics

by

Vinita Khatri

(2K20/PHDAM/501)

Under the Supervision of

Prof. Chandra Prakash Singh

(Delhi Technological University)

DEPARTMENT OF APPLIED MATHEMATICS

DELHI TECHNOLOGICAL UNIVERSITY

(Formerly Delhi College of Engineering)

BAWANA ROAD, NEW DELHI-110042, INDIA.

DECEMBER, 2025

CANDIDATE'S DECLARATION

I, Vinita Khatri (2K20/PHDAM/501), a PhD student in the Department of Applied Mathematics, hereby declare that the thesis entitled **"A Study on Evolution and Dynamics of Dark energy models in Cosmology"** which is submitted by me to the Department of Applied Mathematics, Delhi Technological University, Delhi in partial fulfillment of the requirement for the award of the degree of "Doctor of Philosophy in Mathematics", is original and not copied from any source without proper citation. This work has not previously formed the basis for the award of any Degree, Diploma Associateship, Fellowship or other similar title or recognition.

Place: DTU, Delhi **(Vinita Khatri)**

Date: 2K20/PHDAM/501

CERTIFICATE

This is to certify that the thesis entitled, **"A Study on Evolution and Dynamics of Dark energy models in Cosmology"** submitted by **Ms. Vinita Khatri** (2K20/PHDAM/501), for the award of **Doctor of Philosophy in Mathematics** of Delhi Technological University, New Delhi, India embodies original work done by her under my supervision.

(Prof. Chandra Prakash Singh)
Supervisor and Associate Head
Department of Applied Mathematics
Delhi Technological University
New Delhi, India.

(Prof. R. Srivastava)
Professor and Head
Department of Applied Mathematics
Delhi Technological University
New Delhi, India.

Date:

ACKNOWLEDGEMENTS

I feel deeply grateful to all those who have supported and encouraged me throughout my Ph.D. journey. Their invaluable guidance and motivation, right from the beginning, have played a significant role in helping me reach this important milestone. It is with heartfelt appreciation that I take this opportunity to thank each one of them.

First and foremost, I would like to express my profound gratitude and respect to my supervisor, Prof. Chandra Prakash Singh, Department of Applied Mathematics, Delhi Technological University (DTU), Delhi. His continuous support, thoughtful guidance, and insightful suggestions have been instrumental at every stage of my research. Even during the difficult times of the COVID-19 pandemic, he remained a source of motivation and stability. He gave me the freedom to explore my ideas while offering constructive feedback and encouragement. He is a great thinker for looking new perceptions and ways to understand the reality around us. Working under his supervision has been a great learning experience, and I am truly thankful for his time, dedication, and mentorship.

I am also sincerely thankful to Prof. R. Srivastava, Head, Department of Applied Mathematics, DTU, for providing the necessary resources and valuable suggestions during the progress of my work. I extend my warm thanks to all the faculty members and research scholars in the department for their support, motivation, and friendly interactions that made this journey smoother.

I express my thanks to Departmental Research Committee (DRC) and Student Research Committee (SRC) members who have given the constructive suggestions to improve the quality of the research.

I would like to thank to the cosmology community whose works on General Relativity and Cosmology, has help me a lot to complete my thesis work.

My sincere appreciation goes to the academic and administrative branches of DTU for providing a conducive environment and all necessary facilities to carry out my research. I also thank the office staff of the Department of Applied Mathematics for their consistent help and cooperation.

I gratefully acknowledge Delhi Technological University (DTU) for awarding me the fellowship, which made it possible for me to pursue and complete my Ph.D. work.

On a personal note, I wish to express my heartfelt gratitude to my parents and my husband for their unconditional love, constant encouragement, and emotional support

throughout my academic journey. Their faith in me has been my greatest strength. I also thank my brother and sisters for their affection, support, and understanding, which have always encouraged me to keep moving forward.

Further I want to thank my friends and colleagues from DTU, Dr. Simran Kaur, Dr. Milan Srivastava, Mr.Yogesh Bhardwaj and Mr. Lokesh Chander, who have made this journey memorable by constantly bringing motivation, enthusiasm, fun and friendship to me.

Last but not least, I thank to the almighty God for granting me the strength, wisdom, and perseverance to overcome every challenge along the way for successful completion of this thesis. Thank you.

Date: **(VINITA KHATRI)**

Place: DTU, Delhi, India. **2K20/PHDAM/501**

Preface

Cosmology is a branch of science which deals with the study of the origin of Universe, its evolution, and its eventual fate.

Cosmology has been classified into two categories in contemporary science: Physical cosmology and Observational Cosmology. The study of the Universe's formation, evolution, and the physics behind it, is known as physical cosmology. Observational cosmology investigates the direct evidence of the Universe's formation and structure using telescopes and other tools. Cosmological models are studied using the combination of theories and observations. These models incorporate ideas as well as data gathered from observations. Cosmology integrates developments from a wide range of scientific fields, such as relativity, quantum mechanics, particle physics, nuclear physics, astrophysics, and plasma physics.

Nicolaus Copernicus' discovery that the Earth rotates around the Sun in the early $1500s$ marked the beginning of modern cosmology. Isaac Newton's discovery in the late $1600s$ that objects in space functioned in accordance with the same rules of physics as objects on Earth was an additional breakthrough. Early in the $20th$ century, Albert Einstein's theory of relativity provided a model of spacetime, establishing the way to modern physical cosmology.

Contemporary cosmologists assert that the Universe is made up of far more than the ordinary matter we encounter daily. Most scientists believe that a significant portion of the Universe is composed of *Dark energy* and *Dark matter*. According to this theory, about two-thirds of the Universe is composed of dark energy. The dark energy is believed to be the force that defies gravity and permits the Universe to expand - a phenomenon known as cosmic acceleration. According to this concept, dark matter makes up an additional 26% of the cosmos. Scientists are unable to directly detect this hypothetical kind of matter since it does not emit or absorb light and only interacts with regular matter through gravity.

The most plausible and effective candidate of dark energy is the cosmological

constant introduced by Albert Einstein. Several alternative models have been proposed to explain the Universe's observed accelerated expansion which includes scalar field theories, Chaplygin gas, holographic dark energy and Ricci dark energy, and several other dark energy models. The decaying vacuum energy density and bulk viscosity have recently been investigated as additional potential explanations for the universe's current accelerated expansion.

The objective of this thesis is to investigate how decaying vacuum and bulk viscosity contribute to the explanation of dark energy phenomena in the context of a spatially homogenous and isotropic flat Friedmann-Lemaître-Robertson-Walker metric in general relativity and its modified theories. Using observational data, we fit the model to the proposed model and extract the relevant information on the decaying vacuum energy density and bulk viscosity. The first chapter serves as an introduction. The research that was published as research articles in reputable, peer-reviewed publications served as the basis for chapters 2–6. The conclusion and future directions of the thesis work are covered in the final chapter. Each chapter starts with an overview of the work accomplished in that chapter.

Date : **(VINITA KHATRI)**

Place : DTU, New Delhi, India.

1

Dedicated

to

My Family

Contents

List of Tables

List of Figures

Chapter 1

Introduction

In this chapter we present an elementary discussion on some basic concepts and an overview of General Relativity and Cosmology. We present the Einstein's discovery of General Relativity, the idea of expanding Universe, cosmological principle, metric of spacetime, Friedmann-Lemaître-Robertson-Walker line element, Einstein's field equations, Friedmann equations. It also delves into introduction of cosmological constant in the Einstein's field equations and its importance in cosmology. We particularly emphasize the time varying cosmological constant models in depth throughout this thesis. A discussion on the thermodynamics of dissipative phenomena, such as bulk viscosity is presented. The fundamental components of the Λ-Cold-Dark-Matter (or ΛCDM) also known as the standard model of cosmology along with some important alternatives to the ΛCDM are briefly discussed. This section also analyzes recent observational data, including Type Ia supernovae, the Hubble constant, baryon acoustic oscillations, cosmic microwave background radiation , and f(z)$\sigma_8(z)$. Additionally, a concise overview of significant cosmological and geometric parameters is provided. The chapter concludes by outlining the research's motivation and structural roadmap.

§1. Introduction

General Theory of Relativity, introduced by Albert Einstein in 1915 and published in 1916 [1], represents a pivotal advancement in understanding of gravity, offering a revolutionary conceptual framework. It proposes that gravity is the curvature of four-dimensional spacetime, guiding the formation and evolution of the Universe on the largest scales. Cosmology, which investigates the origins, evolution, and large-scale dynamics of the Universe, operates within this framework. Thus, it is one of the key applications of general relativity, focusing on the interplay between cosmic structures and their long-term behavior. Over recent decades, the insights provided by cosmology have deepened, through both theoretical models and observational data. One of the significant advances in cosmology has been the identification of enigmatic entities such as dark matter and dark energy. Over the past two decades, the standard cosmological model, known as the Lambda-Cold-dark-matter model, has gained prominence. This model offers a comprehensive explanation of the Universe's expansion and evolution, though certain anomalies within the model suggest the need for further refinements beyond its current formulation.

The subsequent sections explore key topics that illustrate both historical advancements and ongoing developments in the field of cosmology.

1.1 Cosmology

Cosmology is a branch of science which deals with the study of the origin of Universe, its evolution, and its ultimate fate. Under cosmology, scientists study about the origin and evolution of the Universe, large scale structures and their dynamics. The geocentric model proposed by Ptolemy, which placed the Earth at the center of the Universe, dominated for more than a thousand years. During the Renaissance, Nicolaus Copernicus revolutionized this perspective with the heliocentric model, where Earth and other planets orbit around the Sun, laying the foundation for modern cosmology. Johannes Kepler's laws of planetary motion and Galileo Galilei's telescopic observations provided strong evidence for the heliocentric view, but Isaac Newton's law of universal gravitation in the $17th$ century unified these advances with a robust mathematical framework for comprehending gravitational interactions. Newtonian mechanics assumed absolute space and time, but this notion was fundamentally chal-

lenged in the early $20th$ century by Albert Einstein. The disk structure of the Milky Way was discovered by the $18th$ and $19th$ centuries, but the Herschels' initial observations put the Solar System at its center. Shapley rectified this in the $20th$ century, demonstrating that the Solar System is displaced from the center of the Galaxy. Baade later demonstrated that the Milky Way is a typical galaxy among billions in a dynamic Universe. These discoveries, combined with evidence of cosmic expansion and relic radiation, established that the Big Bang theory describes how the Universe has been evolving since its birth in a hot, dense state billions of years ago, a process described by the Big Bang theory. Thus, the modern cosmology is based on the Big Bang theory, where the Universe is considered as emerged out of the Big Bang, which occurred about 13.8 billion years ago. Cosmology assumes the homogeneous and isotropic Universe, which is justified on the large scales of larger than 100 Mpc.

1.2 General Theory of Relativity

The major breakthrough in modern cosmology came in 1915 when Albert Einstein introduced the *General Theory of Relativity (GTR)*, which provided a new understanding of gravity. Rather than being a force as described by Newton, Einstein's theory showed that gravity is the manifestation of the curvature of spacetime caused by mass and energy [1]. This revolutionary idea allowed scientists to describe the dynamics of celestial bodies and the structure of the Universe in a completely new light.

Einstein's general theory of relativity is a classical field theory of gravitation. It includes and surpasses Newton's theory, which only applies to particles travelling slowly (in relation to the speed of light) in a weak, stationary gravitational field. General Relativity may naturally account for the potential for a repulsive gravitational force to arise from a constant "vacuum energy density". Such an agent is a fundamental component of contemporary cosmological models of the Big Bang (the inflationary cosmology) and the accelerating Universe (containing a dark energy). GTR depends on two fundamental principles: the principle of general covariance and the principle of equivalence.

The **Principle of general covariance** states that the laws of physics must be expressed in a form that remains valid in any coordinate system. This requires that all physical laws be formulated using covariant equations, ensuring that they hold true regardless of the observer's frame of reference. These equations often take the form

of tensors, which inherently have the same structure in all coordinate systems.

The **Principle of Equivalence** is another cornerstone of GTR, proposing that the effects of gravitational force on a mass are locally indistinguishable from the pseudo-force felt in an accelerated reference frame. In simple terms, an observer in free fall within a gravitational field will not be able to discern the presence of gravitation. This principle is well-tested in experimental settings, such as within our solar system. This principle underscores the relationship between inertial mass and gravitational mass, showing that they are equivalent. The principle of equivalence has profound implications for general relativity and has been validated to a high degree of precision through experimental observations.

1.3 Cosmological Principle

The Cosmological Principle, abbreviated as CP, is the foundation of modern cosmology, which allows cosmologists to use simple, symmetric equations to describe the Universe's evolution. It states that the Universe is uniformly isotropic and homogeneous, when viewed on a sufficiently large scale at any given cosmic time. This assumption holds for scales exceeding 100 megaparsecs (Mpc). In essence, the principle suggests that the Universe appears identical from any location in space. Let's briefly explain these concepts.

- **Isotropy** indicates that the Universe appears the same when observed in any direction, meaning there are no special directions in space. An isotropic Universe also lacks a center, as it looks the same from any vantage point. The alignment of the Earth's poles provides an example of orientation, yet the Universe remains uniform in all directions regardless of position.

- **Homogeneity** refers to the notion that the Universe looks the same everywhere. This means there is no preferred or special place in the Universe. On large scales, homogeneity implies that the average distribution of matter is uniform throughout the Universe, making its structure relatively smooth over vast distances.

While the concepts of isotropy and homogeneity might seem similar, they refer to different aspects of the Universe's structure. Consequently, according to the cosmological principle, the physical laws are universal. The same laws and models that

apply to Earth can be extended to distant stars, galaxies, and all regions of the Universe. In other words, CP is a foundational assumption which allows scientists to apply physics universally and model the theories and its expansion history. It is important to note that fundamental physical constants (such as the gravitational constant, electron mass, and speed of light) are assumed to remain consistent throughout space and time. When extending the cosmological principle to infinity, we arrive at the **perfect cosmological principle**, which states that the Universe has always been both homogeneous and isotropic across all time. There are plenty of observations that support the Cosmological Principle. Specifically: the isotropy of cosmological signals, including the cosmic microwave background radiation (CMBR), the large-scale distribution of matter (large-scale structures), and the recession of distant galaxies (Hubble's Law).

1.4 Expansion of the Universe

Cosmological interpretation for red-shifts of spectral lines from galaxies is that the Universe is expanding. The velocity of recession of a galaxy is proportional to its distance from any observer. The red-shift provides the velocity of galaxy. It is measured by the quantity

$$z = \frac{\lambda_0 - \lambda_e}{\lambda_e}, \tag{1.1}$$

where λ_0 and λ_e are the observed and emitted wavelengths respectively. According to Doppler effect, the wavelength of a light emitted by a cosmic object receding away from an observer with a velocity v is found to increase as compared to its wavelength measured in a laboratory. The relation between the red-shift z of a cosmic object and its receding velocity v is

$$z+1 = \frac{\sqrt{1+v/c}}{\sqrt{1-v/c}}. \tag{1.2}$$

For non-relativistic case $(v << c)$, we have $z = v/c$. Since all cosmic objects show red-shift and if the Doppler effect is valid, it shows that all the objects are moving away from us, i.e., the Universe is expanding.

It was first used to measure a galaxy's velocity by Vesto Slipher around 1912 and it was systematically applied by Edwin Hubble in 1926 during an observation on galaxies.

Hubble realized that there was a relation between the distance of a galaxy and its

red-shift. He found that the velocity of recession v of a galaxy was proportional to its distance r from an observer. Mathematically, it can be expressed as

$$v = H_0\, r \tag{1.3}$$

where the proportionality constant H_0 is known as Hubble's constant. It measures the rate at which the Universe is expanding. It also helps to determine the age of the Universe, size and history. However, its precise value is presently a major point of debate as the different measurements yield very conflicting results which creates so-called Hubble tension. We will discuss about Hubble tension in later section of this chapter.

1.5 Metric of space-time

In the three-dimensional Euclidean space, the distance ds between the two neighbouring points (x,y,z) and $x+dx, y+dy, z+dz$ is given by

$$ds^2 = dx^2 + dy^2 + dz^2, \tag{1.4}$$

where ds is called the line element.

The idea of distance was extended by Riemann to a space of N-dimensions. Thus, the distance ds between two adjacent points whose coordinates in any system are x^μ $(\mu = 1,2,...N)$ and $x^\mu + dx^\mu$, is given by

$$ds^2 = g_{\mu\nu} dx^\mu\, dx^\nu, \quad (\mu,\ \nu = 1,2,3,...N) \tag{1.5}$$

where $g_{\mu\nu}$ are functions of x^μ, known as metric tensor or fundamental tensor. This quadratic differential formulation is known as Riemannian metric.

Einstein's general theory of relativity provides an excellent description of gravitational physics. It is a geometric theory of gravity - gravitational phenomena are attributed as reflecting the underlying curved spacetime. An important idea is the metric of space-time, which describes the physical distance between points. The metric of space-time interprets the geometry of the Universe, and the ideas of luminosity and distances in cosmology.

General Relativity is formulated in a four-dimensional Riemannian space. An inter-

val ds, invariant with respect to coordinate transformations, is related to the coordinates dx^μ of the spacetime manifold through the metric whose line element is given by

$$ds^2 = g_{\mu\nu}dx^\mu dx^\nu, \qquad (\mu,\nu = 0,1,2,3) \tag{1.6}$$

where $(x^0,\, x^1,\, x^2,\, x^3) = (ct,\, x,\, y,\, z)$ and $g_{\mu\nu}$ transforms according to

$$\tilde{g}_{ij} = \frac{\partial x^\lambda}{\partial \tilde{x}^i}\frac{\partial x^\sigma}{\partial \tilde{x}^j} g_{\lambda\sigma} \tag{1.7}$$

In the line element (1.6), dx^μ and dx^ν are contravariant tensor, $g_{\mu\nu}$ is a covariant tensor of rank-2 and is a symmetric tensor, i.e., $g_{\mu\nu} = g_{\nu\mu}$. The line element (1.6) represents the curved geometry and $g_{\mu\nu}$ is a function of the coordinates.

The contravariant metric tensor corresponding to $g_{\mu\nu}$ is denoted by $g^{\mu\nu}$ and is defined by

$$g_{\mu\nu}g^{\nu\lambda} = \delta^\lambda_\mu \tag{1.8}$$

where δ^λ_μ is the Kronecker delta with $\delta^\lambda_\mu = 1$ when $\lambda = \mu$ and zero otherwise.

The metric that is used to describe the Universe on large scales is known as the Friedmann-Lemaître-Robertson-Walker (FLRW) line element. It is based on the assumption of Cosmological Principle. The FLRW metric was developed by Alexander Friedmann [2, 3], Georges Lemaître [4], Howard P. Robertson [5, 6] and Arthur Geoffrey Walker [7].

In spherical coordinates (r, θ, ϕ), the FLRW metric for contracting or expanding Universe that is homogeneous and isotropic on large scales is given by

$$ds^2 = -c^2dt^2 + a^2(t)\left[\frac{dr^2}{1-kr^2} + r^2(d\theta^2 + sin^2\theta d\phi^2)\right], \tag{1.9}$$

where k is a constant representing the curvature of the space. The constant k is taken to be $\{-1,\, 0,\, +1\}$ for negative, zero or positive curvature respectively, and $a(t)$ is the scale factor of the Universe. It measures the universe's expansion rate. It is a function of time alone and it tells us how physical separations are growing with time.

1.6 Einstein's Field Equations

In the General Theory of Relativity (GTR), the metric is the fundamental field characterising the geometric and gravitational properties of spacetime, and so the action

must be a functional of $g_{\mu\nu}$. The Einstein-Hilbert action gives the Einstein field equations through the stationary action principle. In metric signature $(-, +, +, +)$, the gravitational part of the action is given by

$$S = \frac{1}{2\kappa}\int R\sqrt{-g}\, d^4x, \tag{1.10}$$

where R is the Ricci scalar, $g = \det(g_{\mu\nu})$ and $\kappa = 8\pi G c^{-4}$ is the Einstein gravitational constant (G is the Newtonian gravitational constant and c is the speed of light in vacuum). The minus sign under the square-root arises due to the Lorentz spacetime.

The full action with any matter field $\mathscr{L}_m$, appearing in the theory is given by

$$S = \int \left[\frac{1}{2\kappa}R + \mathscr{L}_m\right]\sqrt{-g}\, d^4x, \tag{1.11}$$

where $\mathscr{L}_m$ represents the Langragian density for the matter fields.

Varying the action with respect to the metric tensor $g_{\mu\nu}$ and applying the principal of least action, we arrive at the Einstein's field equations

$$G_{\mu\nu} = \frac{8\pi G}{c^4}T_{\mu\nu}, \tag{1.12}$$

The **left hand side** of (1.12) represents the geometry of spacetime where $G_{\mu\nu}$ is the Einstein tensor, which measure the curvature of spacetime and is given by

$$G_{\mu\nu} = R_{\mu\nu} - \frac{1}{2}g_{\mu\nu}R, \tag{1.13}$$

where

$$R = g^{\mu\nu}R_{\mu\nu}, \tag{1.14}$$

and

$$R_{\mu\nu} = R^{\lambda}_{\mu\lambda\nu} = \frac{\partial}{\partial x^{\lambda}}\Gamma^{\lambda}_{\mu\nu} - \frac{\partial}{\partial x^{\nu}}\Gamma^{\lambda}_{\mu\lambda} + \Gamma^{\lambda}_{\mu\nu}\Gamma^{\delta}_{\lambda\delta} - \Gamma^{\lambda}_{\mu\delta}\Gamma^{\delta}_{\nu\lambda}, \tag{1.15}$$

where $\Gamma^{\lambda}_{\mu\nu}$ is the Christoffel symbol given by:

$$\Gamma^{\lambda}_{\mu\nu} = \frac{1}{2}g^{\lambda\rho}\left(\frac{\partial g_{\rho\mu}}{\partial x^{\nu}} + \frac{\partial g_{\rho\nu}}{\partial x^{\mu}} - \frac{\partial g_{\mu\nu}}{\partial x^{\rho}}\right). \tag{1.16}$$

The **right hand side** $\left(\frac{8\pi G}{c^4}T_{\mu\nu}\right)$ in (1.12) represents the distribution of mass, energy and momentum within the spacetime where $T_{\mu\nu}$ is the stress-energy tensor (or

energy-momentum tensor). [1]

1.7 Energy-momentum tensor

The energy-momentum tensor describes the presence and motion of gravitating matter. Let us discuss the energy-momentum tensor for a particular case of a "*perfect fluid*", which is a mathematical idealisation but one which is a good approximate description of the gravitating matter in many cosmological models.

The simplest type of relativistic fluid is known as '**dust**' which means that a collection of particles that are at all rest with respect to Lorentz frame. However, the particles within a fluid element will have random motions, and these will give rise to pressure in the fluid. There is also an exchange of energy with its neighbours via **heat conduction**, and there may be **viscous forces** present between neighbouring fluid elements which are directed parallel to the interface between neighbouring fluid element, and that result in a **shearing** of the fluid. A relativistic fluid element is said to be a **perfect fluid** if the fluid element has no heat conduction or viscous forces. It follows that dust is the special case of a pressure-free perfect fluid. The perfect fluid form of energy-momentum tensor is extremely important and common. Cosmologists find that it is nearly perfect description of the Universe on large scales.

For a perfect fluid, the energy-momentum tensor $T_{\mu\nu}$ is solely determined by the energy density ρ and pressure p, which is given by

$$T_{\mu\nu} = (\rho + p)u_\mu u_\nu - (u^\alpha u_\alpha)pg_{\mu\nu}, \tag{1.17}$$

where u represents the velocity of an observer in the fluid's rest frame, and $u^\alpha u_\alpha = u^2 = u.u$ equals to $+1$ for the signature $(+, -, -, -)$ and -1 for signature $(-, +, +, +)$. However, in the present thesis, we adopt the signature $(-, +, +, +)$ for which the above energy-momentum tensor for perfect fluid modifies to

$$T_{\mu\nu} = (\rho + p)u_\mu u_\nu + pg_{\mu\nu}, \tag{1.18}$$

The conservation of the energy-momentum tensor requires that $T^{\mu\nu}_{;\nu} = 0$, which gives

$$\dot{\rho} + 3\frac{\dot{a}}{a}(\rho + p) = 0, \tag{1.19}$$

[1] In the present thesis, we assume the speed of light in vacuum $c = 1$ in relativistic unit.

where an overdot represents the derivative with respect to the cosmic time t.

When Einstein formulated the field equations (1.12) of general relativity, he believed that the Universe was static as the expansion of the Universe had not been discovered. However, he found that his theory of general relativity did not permit it. In order to make a static Universe, he therefore modified his equation by adding the so-called "*cosmological constant*" to his equation (1.12) as follows:

$$G_{\mu\nu} + \Lambda g_{\mu\nu} = 8\pi G\, T_{\mu\nu}, \tag{1.20}$$

where Λ is the *cosmological constant* and it has the dimension of $[Length]^{-2}$. Sometimes, we measure it in the unit $[time]^{-2}$. The above form of the Einstein field equations is the standard established by Charles W. Misner, Kip S. Thorne and, John Archibald Wheeler [8, 9]. It is frequently abbreviated **MTW**. MTW uses the $(-, +, +, +)$ sign convention.

Apart from the static solution mentioned above, there are, of course, many dynamic solutions with the cosmological constant. These models were first studied by Lemaître so they are known as Lemaître models. In recent years, other motivations have been found for introducing a cosmological constant term and such a term arises in many different contexts. Introducing cosmological term as a fictitious 'fluid' with energy-momentum tensor $T^{(\Lambda)}_{\mu\nu}$ given by

$$T^{(\Lambda)}_{\mu\nu} = (\rho_\Lambda + p_\Lambda)\, u_\mu u_\nu + p_\Lambda g_{\mu\nu} = \frac{\Lambda g_{\mu\nu}}{8\pi G}, \tag{1.21}$$

This tensor describes a vacuum state with an energy density ρ_Λ and pressure p_Λ that are fixed constants and given by

$$\rho_\Lambda = \frac{\Lambda}{8\pi G}, \quad p_\Lambda = -\frac{\Lambda}{8\pi G}. \tag{1.22}$$

Thus, the existence of cosmological constant is equivalent to the existence of vacuum energy and a pressure of negative sign. Now, Eq. (1.20) can be written as follows:

$$G_{\mu\nu} = 8\pi G \left(T_{\mu\nu} + T^{(\Lambda)}_{\mu\nu}\right). \tag{1.23}$$

Properties of the Einstein tensor:

- $G_{\mu\nu}$ vanishes when spacetime is flat.

- $G_{\mu\nu}$ is constructed from the Riemann tensor and the metric.

- $G_{\mu\nu}$ is different from other tensors that can be constructed from the Riemann tensor and the metric by the demands:
  (1) $G_{\mu\nu}$ is linear in Riemann.
  (2) $G_{\mu\nu}$ (like $T_{\mu\nu}$) is symmetric.
  (3) $G_{\mu\nu}$ (like $T_{\mu\nu}$) obeys Bianchi identity, $G^{\mu\nu}_{;\nu} = 0$.

1.8 Friedmann Universe

The Einstein field equations (1.20) for the FLRW line element (1.9) and energy-momentum tensor (1.18) yield the following two equations:

$$\frac{\dot{a}^2}{a^2} = \frac{8\pi G}{3}\rho - \frac{k}{a^2} + \frac{\Lambda}{3}, \tag{1.24}$$

$$\frac{\ddot{a}}{a} = -\frac{4\pi G}{3}(\rho + 3p) + \frac{\Lambda}{3}, \tag{1.25}$$

Equation (1.24) is the well known **Friedmann equation** [2], which provides the fundamental description of the expansion of the Universe. The second Eq. (1.25) is known as **acceleration equation**. Different choices of matter content lead to different cosmological solutions. A positive Λ gives a positive contribution of $\ddot{a}$, and so acts effectively as a repulsive force. If the cosmological constant is sufficiently large, it can overcome the gravitational attraction represented by the first term and lead to an accelerating Universe.

Introducing the cosmological constant term as a fluid with energy density ρ_Λ and pressure p_Λ as given in Eq. (1.22), Equations (1.24) and (1.25) can be modified as (In relativistic unit, assuming the speed of light in vacuum $c = 1$)

$$H^2 = \frac{8\pi G}{3}(\rho + \rho_\Lambda) - \frac{k}{a^2} \tag{1.26}$$

$$\dot{H} + H^2 = -\frac{4\pi G}{3}\left[(\rho + \rho_\Lambda) + 3(p + p_\Lambda)\right], \tag{1.27}$$

where $H = \frac{\dot{a}}{a}$ is Hubble parameter. We use Hubble parameter as function of cosmic time. However, it is Hubble constant, H_0 for its present value, which is the proportionality constant of Hubble's law. Normally, Hubble parameter decreases with time for instance, as the expansion is slowed by gravitational attraction of the matter in the

Universe.

The conservation equation (1.19) with the inclusion of vacuum energy is rewritten as

$$\dot{\rho} + 3H(\rho + p) = -\dot{\rho_\Lambda}. \tag{1.28}$$

In cosmology, matter and energy are usually characterized by an **equation of state**, which links pressure and energy density as

$$p = w\rho, \quad -1 \leq w \leq 1 \tag{1.29}$$

where w is the equation of state (EoS) parameter. This EoS parameter is extremely important in cosmology to describe the different phases of the Universe. For instance, $w = 0$ describes the matter-dominated phase, $w = 1/3$ leads the radiation-dominated phase whereas $w = -1$ describes the cosmological constant (vacuum energy dominated phase). Applying to a fluid with a given equation of state, the Friedmann equations yield the time evolution and geometry of the Universe as a function of the fluid density.

1.9 Lambda-Cold-Dark-Matter model

The Lambda-Cold-Dark-Matter, abbreviated as ΛCDM model is a parametrization of the Big-Bang cosmological model. In this model, the Universe contains three major components:

- **Dark energy:** Represented by the cosmological constant Λ, it accounts for approximately 68% of the total energy density of the Universe and is responsible for the observed accelerated expansion.
- **Cold dark matter (CDM):** It constitutes about 27% of the Universe's energy content. CDM interacts gravitationally but not electromagnetically, explaining why it does not emit, absorb, or reflect light.
- **Baryonic matter:** The ordinary matter that makes up stars, planets, and galaxies, comprising roughly 0.04% of the Universe's energy density.

The ΛCDM model is also known as standard concordance model. This is the simplest model that provides a reasonably good account of the following properties of cosmos:

- Existence and structure of the cosmic microwave background.
- The large scale structure in the distribution of galaxies.
- The accelerating expansion of the Universe.

The ΛCDM model is based on three postulates: Cosmological Principle, lines of spacetime (geodesics) intersect at only one point, and general relativity assumes the correct theory on the cosmological scales. The Greek letter Λ represents the cosmological constant which is currently associated with vacuum energy or dark energy in empty space. This vacuum energy plays an important role in explaining the accelerating expansion of the space against the attractive effects of gravity. A cosmological constant has negative pressure, $p_\Lambda = -\rho_\Lambda$. It explains the Universe's early evolution with great precision, especially when compared with the observed CMB, the distribution of galaxies, and the large-scale structure of the Universe. Additionally, the model accurately predicts the growth of cosmic structures over billions of years. However, despite its success, the ΛCDM model has its own set of limitations, particularly concerning the late-time behavior of the Universe and the nature of its key components.

In the Friedmann Universe, the density parameter Ω is expressed as the ratio of actual (or observed) density ρ to the critical density ρ_c. This parameter determines the overall geometry of the Universe. When $\Omega = 1$, the Universe is flat (Euclidean).

An expression for the critical density is found by assuming $\Lambda = 0$ and setting the normalized spatial curvature k equal to zero. Substitution of these values in the Friedmann's first equation (1.26) gives

$$\rho_c = \frac{3H^2}{8\pi G}. \tag{1.30}$$

The density parameter is thus defined as

$$\Omega = \frac{\rho}{\rho_c} = \frac{8\pi G\rho}{3H^2}. \tag{1.31}$$

It is to be noted that ρ used in the above equation is the total energy density of the Universe. Our Universe contains several different types of matter, this notation can be used not only for total density but also for each individual component of the density. It is the sum of a number of different components including both normal dark matter as well as dark energy suggested by the observations. We can write as

$$\Omega = \Omega_b + \Omega_{dm} + \Omega_{rad} + \Omega_\Lambda. \tag{1.32}$$

where Ω_b is the density parameter of baryonic matter, Ω_{dm} for dark matter, Ω_{rad} for radiation and Ω_Λ for dark energy. The total density parameter is roughly 1.02. The observations reveals that we live in a dark energy dominated Universe with $\Omega_\Lambda = 0.73$, $\Omega_{dm} = 0.23$ and $\Omega_b = 0.04$. Thus, we live in a flat (Ω is very closed to 1) Universe.

Since the densities of various species scale as different powers of a, e.g., $\rho_{dm} \propto a^{-3}$ for dark matter, $\rho_{rad} \propto a^{-4}$ for radiation and ρ_Λ stays constant. Therefore, the Friedmann equation (1.26) for $\Omega_k = 0$ can be conveniently rewritten in terms of various density parameters as

$$H(a) = H_0\sqrt{(\Omega_{dm}+\Omega_b)a^{-3} + \Omega_{rad}a^{-4} + \Omega_\Lambda}, \tag{1.33}$$

23 where H_0 is the present value of Hubble parameter. As we know that the scale factor is related to the redshift of the light by the relation $(1+z) = a^{-1}$ (assuming the parametrizing the scale factor at present day, $a(t_0) = 1$). Thus, the above equation for the evolution of Hubble parameter can be rewritten as

$$H(z) = H_0\sqrt{(\Omega_{dm}+\Omega_b)(1+z)^3 + \Omega_{rad}(1+z)^4 + \Omega_\Lambda}. \tag{1.34}$$

Observations show that the radiation density is very small today, $\Omega_{rad} \sim 10^{-4}$. Neglecting this term, we have

$$H(z) = H_0\sqrt{(\Omega_{dm}+\Omega_b)(1+z)^3 + \Omega_\Lambda}. \tag{1.35}$$

The analytic solution of scale factor of the above equation for neglecting Ω_b is obtained as

$$a(t) = (\Omega_m/\Omega_\Lambda)^{1/3}\sinh^{2/3}(t/t_\Lambda), \tag{1.36}$$

where $t_\Lambda \equiv 2/(3H_0\sqrt{\Omega_\Lambda})$.

1.10 Challenges

Despite of the widespread success of ΛCDM model, cosmologists find that the model has some following issues.

- **Fine-tuning problem:** The observed value of the cosmological constant Λ is extremely small compared to theoretical predictions from quantum field theory, leading to a severe mismatch of scales.

25

- **Cosmic coincidence problem:** It is unclear why the energy densities of dark energy and matter are of the same order of magnitude in the present epoch, even though they evolve differently over time.

As the precise mechanism behind cosmic acceleration remains unknown, alternative explanations for dark energy have been explored due to the limitations of the cosmological constant. In general relativity, the dynamics of vacuum energy and the cosmological constant, represented by Λ, are equivalent. A significant fine-tuning issue for Λ is revealed when cosmological data has been compared with estimates of vacuum energy from quantum field theory (QFT) calculations. Refer to Ref.[10] for further details. The density ρ_Λ is specifically estimated to be around 10^{-47}GeV^4 [11] based on existing findings. The Planck scale, at about 10^{76} GeV^4, is the natural scale for vacuum energy density, indicating a 123-order-of-magnitude difference. The difference is more than 55 orders of magnitude even if we take into account a fictitious vacuum state post-electroweak phase transition at roughly 10^8 GeV^4. Refer to [12] for a more comprehensive examination of these concerns.

The so-called *cosmic coincidence* problem [13] is another noteworthy challenge with Λ. This problem occurs because, the density of the cosmological constant stays constant throughout time, whereas the density of matter decreases as the Universe expands. Currently, their densities seem to be nearly equal, which is quite coincidental. The ramifications make this even more perplexing: if Λ had dominated earlier, galaxies might not have formed; if it had dominated later, the Universe would still be decelerating, which could have resulted in younger structures like some stellar clusters [14].

Another way to interpret this cosmic coincidence is as a fine-tuning of the Universe's initial conditions. The ratio of ρ_Λ to the matter density ρ_m can be used as an example. It scales roughly as a^3, where a is the scale factor. $\rho_\Lambda/\rho_m \approx 10^{-96}$ is the result of extrapolating this relationship to the Planck scale at $a \approx 10^{-32}$. A method that precisely adjusts this ratio with 96 significant digits would be required at such high energies. Any divergence would contradict current observations and suggest radically different cosmic models.

We are currently at an impasse. While Λ is the most successful dark energy option, it is also prevalent with these fine-tuning problems. This circumstance leads to a quest for alternatives, which can include changes to GR itself or new theories of gravity. There are so many conflicting hypotheses in the field that it is difficult to choose a

leading candidate. Refer to [15] for a clear overview of the topic.

1.11 Cosmic Tensions and Small-Scale Problems

The research in cosmology is currently facing several significance gaps in understanding the evolution and dynamics of the Universe, especially dark matter and dark energy. The standard ΛCDM model faces challenges and discrepancies with the observations. In what follows, we describe a more detailed the research gaps in cosmology.

1. *Nature of dark matter and dark energy:* Dark matter and dark energy are two major components in the Universe. Dark matter and dark energy are estimated to be about 27% and 68% of the Universe which are invisible. Dark matter interacts gravitationally and affects the movement of the galaxies which makes it undetectable by telescope. Its existence can be realized only due to gravitational effects. On the other hand, dark energy is thought to be a force that permeates all of space. Observations like Type Ia supernova reveals that dark energy is responsible for driving an accelerated expansion of the Universe. However, the fundamental properties of these quantities are still unknown. Cosmological constant (CC) and cosmic coincidence are major problems with ΛCDM model which highlight a fundamental gap between theoretical expectations and observational data.

2. *Hubble tension:* The Hubble constant represents the rate at which the Universe is expanding. The Hubble constant derived from two observations, namely, Cosmic Distance Ladder and Cosmic Microwave Background (CMB) are not consistent. The Cosmic Distance Ladder measures high value of Hubble constant than the CMB method. This discrepancy is known as Hubble tension. This shows that the standard ΛCDM is not the complete model which gives a sign of new physics beyond the standard ΛCDM model.

3. σ_8 *tension:* The σ_8 is a cosmological parameter that quantifies the clustering of matter in the Universe. It helps to determine how much matter (both visible and dark) is clustered in different cosmic regions. The σ_8 tension gives the mismatch in the value of σ_8 as obtained by CMB measurements (higher value) and cosmic shear / lensing surveys (lower value). The higher value of σ_8 signifies the more

clumpy Universe where as lower value of σ_8 indicates a more uniform distribution of matter. This discrepancy challenges the ΛCDM model, the standard model of cosmology.

1.12 Alternatives to the ΛCDM

In this section, we discuss some of the alternative models to the concordance cosmological model that have been proposed over the time. These models have one thing in common: they all deviate, though in different ways, from the theoretical framework that ΛCDM is based on. Cosmologists are encouraged to investigate potential alternative theories since, as is generally known, the ΛCDM model, despite its effectiveness in many areas, does not provide a completely satisfactory explanation for the Universe's accelerating expansion. Finding models that offer a more physically based mechanism for this expansion is not the only objective but resolving the known tensions within the concordance model is also a goal.

It should be noted that although ΛCDM has been successful in explaining cosmological observations, promising alternatives should not deviate much from its theoretical predictions. For instance, certain models may provide a better description of large-scale structure data while reproducing Cosmic Microwave Background (CMB) observations as precisely as ΛCDM by accounting for small changes in the cosmological constant. Furthermore, competing models will be subject to stricter constraints as new, extremely accurate measurements become available, which will assist us in identifying models that do not fit observational data effectively. It is crucial to have an open mind and consider all reasonable options in the possibilities.

1.12.1 Running vacuum models

The fundamental idea of the running vacuum models is that the vacuum energy density in cosmology is a time-dependent quantity rather than a constant value. It is difficult to conceptualize a vacuum energy density that has not changed since the beginning of time in an expanding Universe. A more conventional approach would be to think of a smoothly fluctuating vacuum energy density that changes in response to cosmological parameters like the scale factor $a(t)$ or the Hubble rate $H(t)$. This idea is supported by theoretical physics, specifically Quantum Field Theory (QFT) in curved space-time, in addition to being evident from a cosmological perspective [16, 17].

Considering the renormalized zero-point energy (ZPE) contribution from quantum fluctuations of a non-minimally coupled scalar field in the FLRW metric, which is essential in understanding the variation of ρ_Λ when shifting from one scale to another. If we know the observed value at a certain scale, we can evaluate ρ_Λ at a different scale. Let us examine the vacuum energy density at the current energy scale, represented by $M = H_0$, where H_0 is the current Hubble parameter, using the grand unified theory (GUT) scale $M_X \approx 10^{16}\,\text{GeV}$. Since we are concerned with the present Universe, we can ignore terms of order $\mathscr{O}(H^4)$, such as $\dot{H}^2$, $H\ddot{H}$, and $\dot{H}H^2$, thus the expression is

$$\rho_\Lambda(M = H_0) \equiv \rho_0^\Lambda = \rho_\Lambda(M_0 = M_X) + \frac{3}{16\pi^2}\left(\xi - \frac{1}{6}\right) H_0^2 \left[M_X^2 + m^2 \ln\left(\frac{H_0}{M_X}\right)^2\right]. \tag{1.37}$$

Here, ρ_0^Λ denotes the observational measurement of the vacuum energy at present. This expression can be simplified by introducing a running parameter ν_{eff}:

$$\rho_0^\Lambda = \rho_\Lambda(M_0 = M_X) + \frac{3\,\nu_{eff}}{8\pi} H_0^2 M_{Pl}^2, \tag{1.38}$$

where

$$\nu_{eff} = \frac{1}{2\pi}\left(\frac{1}{6} - \xi\right)\frac{M_X^2}{M_{Pl}^2}\left(1 + \frac{m^2}{M_X^2}\ln\left(\frac{H_0}{M_X}\right)^2\right). \tag{1.39}$$

This dimensionless parameter ν_{eff} is non-zero as long as $\xi \neq \frac{1}{6}$. Given that $M_X^2/M_{Pl}^2 \ll 1$, we can expect this value to be relatively small. Applying (1.37) again, now relating the vacuum energy density ρ_Λ at $M = H$ to the previously obtained value (1.38) at $M_0 = M_X$, we get

$$\rho_\Lambda(H) = \rho_0^\Lambda - \frac{3\,\nu_{eff}}{8\pi} H_0^2 M_{Pl}^2 + \frac{3\,\nu_{eff}(H)}{8\pi} H^2 M_{Pl}^2, \tag{1.40}$$

with

$$\nu_{eff}(H) = \frac{1}{2\pi}\left(\frac{1}{6} - \xi\right)\frac{M_X^2}{M_{Pl}^2}\left(1 + \frac{m^2}{M_X^2}\ln\left(\frac{H}{M_X}\right)^2\right). \tag{1.41}$$

As our focus is on the post-inflationary Universe, we assume that the Hubble parameter $H(a)$ at any scale factor a does not differ significantly from the current Hubble parameter H_0. This permits the approximation $\nu_{eff}(H) \simeq \nu_{eff}$. Consequently, the running vacuum energy density becomes

$$\rho_\Lambda(H) \simeq \rho_\Lambda^0 + \frac{3\,\nu_{eff}}{8\pi}\left(H^2 - H_0^2\right) M_{Pl}^2 = \rho_\Lambda^0 + \frac{3\,\nu_{eff}}{8\pi G_N}\left(H^2 - H_0^2\right), \tag{1.42}$$

where in the last equality we used $M_{Pl}^2 \equiv 1/G_N$ (non-reduced Planck mass).

For positive ν_{eff}, this expression can be interpreted as vacuum energy decaying into matter, with a larger value in the past. Conversely, for $\nu_{eff} < 0$, the effect is reversed, which is particularly relevant for interacting models. For further details on this, see Refs. [18, 19, 20, 21, 22, 23]. Although Eq.(1.42) only accounts for the zero-point energy (ZPE) from scalar fields, it provides an ansatz to study phenomenological models of running vacuum energy.

In fact, Eq.(1.42) can be derived as a special case of a broader expression for the vacuum energy density that relates to the renormalization group equation, providing a framework based on quantum field theory (QFT):

$$\frac{d\rho_\Lambda}{d\ln\alpha^2} = \frac{1}{4\pi^2}\sum_i \left[a_i M_i^2\alpha^2 + b_i\alpha^4 + c_i\frac{\alpha^6}{M_i^2} + \cdots\right], \tag{1.43}$$

which encodes quantum corrections from bosonic and fermionic fields through dimensionless coefficients a_i, b_i, c_i, with M_i the particle masses. The scale α is typically identified with $\alpha \sim aH^2 + b\dot{H}$, and only even powers of H or $\dot{H}$ enter $\rho_\Lambda(H)$ by covariance. Integrating (1.43), one obtains for the current Universe

$$\rho_\Lambda(H) = \frac{3}{8\pi G_N}\left(c_0 + \nu H^2 + \mu\dot{H}\right) + \mathcal{O}(H^4), \tag{1.44}$$

where μ and ν are dimensionless parameters, and c_0 is a constant of mass dimension 2 in natural units. We keep $c_0 \neq 0$ to ensure a smooth ΛCDM limit when the dimensionless parameters vanish. These coefficients can be computed in QFT from ratios of particle masses to the Planck mass, and may be interpreted as β-functions for the running of the vacuum energy density [17]. Theoretically one expects $\mu, \nu \sim 10^{-6}$–10^{-3} [17], but their values must be determined phenomenologically by confronting the models with cosmological data.

Accordingly, RVMs are tested and compared to various observational data, including the Pantheon, BAO measurements, Cosmic chronometers and significant $f(z)\sigma_8(z)$ observations. The results depend on the data set used; however, they consistently show that RVMs are preferred over the ΛCDM model.

1.12.2 Brans-Dicke theory

Brans-Dicke (BD) theory, which is also known as scalar-tensor theory is an alternative theory of gravitation to Einstein's GTR which was formulated by Robert H. Dicke and Carl H. Brans [24, 25] on the basis of Jordan's work. This scalar-tensor theory is consistent with Mach's principle (that inertia comes from the Universe's matter) and Dirac's large number hypothesis (LNH). In this theory, in addition to the tensor field that describes the geometry of spacetime, a scalar field is also included. The effective gravitational constant G is replaced by a time-varying scalar field ϕ, and a new coupling parameter ω_{BD} was introduced.

The action of GR (1.11) for BD theory in Jordan frame is generalized as follows [26, 27] [2]

$$S = \frac{1}{16\pi}\int d^4x\sqrt{-g}\left(\phi R - \frac{\omega_{BD}}{\phi}\partial_a\phi\partial^a\phi\right) + \int d^4x\sqrt{-g}\mathscr{L}_m, \tag{1.45}$$

where $g = |g_{\mu\nu}|$, $\sqrt{-g}d^4x$ is the four-dimensional volume form, and $\mathscr{L}_m$ is the matter Lagrangian density.

Varying the action (1.45) with respect to the metric $g_{\mu\nu}$, the field equations of the BD theory are

$$R_{\mu\nu} - \frac{1}{2}g_{\mu\nu}R - \frac{\omega_{BD}}{\phi^2}\left(\phi_{,\mu}\phi_{,\nu} - \frac{1}{2}g_{\mu\nu}\phi_{,\alpha}\phi^{,\alpha}\right) - \frac{1}{\phi}\left(\phi_{,\mu;\nu} - g_{\mu\nu}\Box\phi\right) = \frac{8\pi}{\phi}T_{\mu\nu}(\text{matter}), \tag{1.46}$$

On the other hand, a preference that ϕ be part of "matter" gives the same result but in different form

$$R_{\mu\nu} - \frac{1}{2}g_{\mu\nu}R = \frac{8\pi}{\phi}T_{\mu\nu}(\text{matter}) + \frac{\omega_{BD}}{\phi^2}\left(\phi_{,\mu}\phi_{,\nu} - \frac{1}{2}g_{\mu\nu}\phi_{,\alpha}\phi^{,\alpha}\right) + \frac{1}{\phi}\left(\phi_{,\mu;\nu} - g_{\mu\nu}\Box\phi\right), \tag{1.47}$$

Varying with respect to ϕ, we get the following scalar field equation (wave equation)

$$\Box\phi = \frac{8\pi}{2\omega_{BD}+3}T(\text{matter}), \tag{1.48}$$

where ϕ is the scalar field, ω_{BD} is the dimensionless Dicke coupling constant and $\Box$ is the Laplace operator or covariant wave operator, $\Box\phi = \phi^{;a}_{;a}$, and $T = T^{\mu}_{\mu}$ is the trace of energy-momentum tensor.

[2] We use natural units, with $= c = 1$ and $G_N = 1/M_{Pl}^2$, where $M_{Pl} \approx 1.22 \times 10^{19}$GeV is the Planck mass. The sign convention follows $(-,+,+,+)$.

The BD field equations (1.47) in a flat FLRW metric (1.9) for perfect fluid energy-momentum tensor (1.18) yield

$$3H^2 = \frac{8\pi}{\phi}\rho - 3H\frac{\dot{\phi}}{\phi} + \frac{\omega_{BD}}{2}\left(\frac{\dot{\phi}}{\phi}\right)^2 \tag{1.49}$$

$$-2\dot{H} - 3H^2 = \frac{8\pi}{\phi}p + \frac{\ddot{\phi}}{\phi} + 2H\frac{\dot{\phi}}{\phi} + \frac{\omega_{BD}}{2}\left(\frac{\dot{\phi}}{\phi}\right)^2, \tag{1.50}$$

while Eq. (1.48) results to

$$\frac{\ddot{\phi}}{\phi} + 3H\frac{\dot{\phi}}{\phi} = \frac{8\pi}{\phi}\frac{(\rho - 3p)}{(3+2\omega_{BD})}. \tag{1.51}$$

The first two equations reduce to the conventional Friedmann and pressure equations of GR given a constant $\phi = 1/G$, whereas the third equation requires $\omega_{BD} \to \infty$ for consistency. Since matter and the BD field do not interact, we can construct a local covariant conservation law that is analogous to GR by combining these equations. This can be verified through explicit calculations. Although the procedure is more complicated than in GR, the final result is identical:

$$\dot{\rho} + 3H(\rho + p) = \sum_N \dot{\rho}_N + 3H(\rho_N + p_N) = 0, \tag{1.52}$$

where all of the components-baryons, dark matter, radiation, neutrinos, and vacuum are added together. We implement an approach that during significant stages of cosmic evolution, each component conserves independently.

1.13 Viscous Cosmology

In standard cosmological models, the cosmic fluid is often assumed to be *perfect*, implying that it is devoid of any dissipative processes such as viscosity or heat conduction. However, this idealized case does not fully capture the physical reality of the universe. In more realistic models, it is necessary to consider the effects of dissipation, particularly when dealing with large-scale cosmological evolution, early Universe dynamics, or structure formation.

Viscous cosmology deals with the effect of bulk viscosity-a type of internal friction in fluids in GR which explain the cosmic expansion, particularly the current cosmic acceleration of the universe. The cosmic fluid has resistance to expansion (viscosity)

which generates a negative pressure, responsible for acceleration, mimicking dark energy and provides the alternate of ΛCDM. In the context of cosmology, viscosity is related to thermodynamic processes and can manifest in two forms: *bulk viscosity* and *shear viscosity*. Bulk viscosity is particularly relevant in cosmological models due to its isotropic nature, meaning it affects the Universe's expansion rate without introducing directional dependence.

In a cosmological setting, bulk viscosity arises when the cosmic fluid expands or contracts too rapidly for the system to maintain thermodynamic equilibrium. As a result, the pressure of the fluid is modified by an additional dissipative term, which acts to restore equilibrium. The bulk viscosity serves as an effective mechanism for reducing the deceleration of the universe, and under certain conditions, it can lead to an accelerated expansion similar to the effects of dark energy.

1.13.1 Thermodynamic of Bulk Viscosity

In physical systems, bulk viscosity can be interpreted as a deviation from local thermodynamic equilibrium. In a cosmological fluid, bulk viscosity appears when the fluid cannot adjust quickly enough to changes in the expansion rate. This dissipative process introduces a resistance to the expansion, which is described by an effective pressure term that accounts for the deviation from equilibrium.

The general form of the pressure in a cosmological fluid with bulk viscosity is modified as:

$$P = p + \Pi, \tag{1.53}$$

where p is the thermodynamic pressure and Π is the dissipative pressure. For bulk viscosity, the dissipative pressure is typically given by:

$$\Pi = -3\zeta H, \tag{1.54}$$

where H is the Hubble parameter, and ζ is the bulk viscosity coefficient, which governs the strength of the viscous effects. The negative sign indicates that viscosity acts to resist the expansion of the Universe. The energy-momentum tensor of a relativistic fluid with bulk viscosity as the only dissipative phenomena is given by

$$T_{\mu\nu} = (\rho + p + \Pi)u_\mu u_\nu + (p + \Pi)g_{\mu\nu}, \tag{1.55}$$

where ρ is the energy density, p is the equilibrium pressure, Π is the bulk viscous pressure and u_μ is the four-velocity of the fluid.

The particle flow vector N^α is given by

$$N^\alpha = nu^\alpha, \tag{1.56}$$

where n is the particle number density. For the scond order deviations from equilibrium, the entropy flow vector S^α is given by [28]

$$S^\alpha = sN^\alpha - \frac{\tau\Pi^2}{2\zeta T}u^\alpha, \tag{1.57}$$

where s is entropy per particle, τ is the relaxation time, T is the temperature and ζ is the bulk viscous coefficient. The balance equation is given by

$$N^\alpha_{;\alpha} = 0, \quad \text{and} \quad T^{\mu\nu}_{;\nu} = 0 \tag{1.58}$$

which give

$$\dot{n} + \Theta n = 0 \quad \text{and} \quad \dot{\rho} = -\Theta(\rho + p + \Pi), \tag{1.59}$$

respectively, where $\Theta \equiv u^\alpha_{;\alpha}$ is the fluid expansion and $\dot{n} \equiv n_{,\alpha}u^\alpha$, etc. Using the above equations with Gibbs relation $Tds = d\frac{\rho}{n} + pd\frac{1}{n}$, we get

$$nT\dot{s} = -\Theta\Pi. \tag{1.60}$$

From (1.57) and (1.59), we get the entropy production density as

$$S^\alpha_{;\alpha} = -\frac{\Pi}{T}\left[\Theta + \frac{\tau}{\zeta}\dot{\Pi} + \frac{1}{2}\Pi T\left(\frac{\tau}{\zeta T}u^\alpha\right)_{;\alpha}\right]. \tag{1.61}$$

Now, $S^\alpha_{;\alpha} \geq 0$ implies the evolution equation

$$\Pi + \tau\dot{\Pi} = -\zeta\Theta - \frac{1}{2}\Pi\tau\left[\Theta + \frac{\dot{\tau}}{\tau} - \frac{\dot{\zeta}}{\zeta} - \frac{\dot{T}}{T}\right]. \tag{1.62}$$

One can observe that Eq. (1.62) reduces to the Eckart theory, $\Pi = -\zeta\theta$ in the relaxation limit $\tau \to 0$. If the bracket term on the right hand side of (1.62) can be neglected compared to the viscous term $-\zeta\Theta$, i.e., if the condition $\Theta + \frac{\dot{\tau}}{\tau} - \frac{\dot{\zeta}}{\zeta} - \frac{\dot{T}}{T} = 0$, we get the

truncated theories

$$\Pi + \tau\dot{\Pi} = -\zeta\Theta. \tag{1.63}$$

The study of bulk viscosity in cosmology dates back to the work of Eckart [29] and Landau and Lifshitz [30], who first laid the foundations for relativistic viscous hydrodynamics. These early models treated viscosity as a first-order deviation from equilibrium, leading to a causal formulation of dissipative processes. However, such models were later shown to suffer from non–causal behavior and instability under certain conditions. A more refined treatment was developed by Israel and Stewart [28], who introduced a second–order relativistic theory of viscosity, known as the full causal theory. This framework allowed for a more accurate description of non-equilibrium states in cosmology, particularly during the early universe.

One of the primary motivations for considering bulk viscosity in cosmological models is that it can potentially remove singularities, such as the initial singularity in the Big Bang model. Several authors have explored the idea that bulk viscosity could drive the inflationary phase of the early universe, allowing for a smooth transition to the radiation-dominated era. Furthermore, viscous models have been shown to produce late-time acceleration, mimicking the effects of dark energy. The concept of *viscous dark energy* has been developed to characterize models in which the bulk viscosity of the cosmic fluid plays the role traditionally assigned to dark energy in driving the accelerated expansion.

Recent research has shown that viscous effects can play a crucial role in the late-time acceleration of the universe. By introducing a large enough bulk viscosity coefficient, the deceleration of the Universe can be halted, and an accelerated expansion phase can be triggered without the need for an exotic dark energy component. This opens up the possibility of explaining cosmic acceleration within the framework of standard thermodynamics and fluid dynamics, rather than invoking unknown forms of energy.

One key result of viscous cosmology is the realization that singularities, such as the initial Big Bang singularity, can be avoided. The introduction of viscosity smooths the evolution of the universe, leading to non-singular models that are free from the divergences that typically arise in perfect fluid models. This has motivated many authors to explore the implications of viscous cosmology in both the early and late stages of cosmic evolution.

Moreover, viscous dark energy models have gained significant attention as they of-

fer a potential solution to the dark energy problem. By treating the bulk viscosity as a dynamic property of the cosmic fluid, these models can account for the observed acceleration while remaining consistent with observational data. However, the exact nature of bulk viscosity in cosmology is still not well understood, and further research is required to constrain its value and behavior through observations.

1.14 Cosmological Parameters

The cosmological parameters are the fundamental quantities that characterize the dynamics, structure, and development of the Universe. The following is a list of the key cosmological parameters:

1.14.1 Hubble Parameter

Hubble parameter is defined as the rate of expansion of the universe and is given by

$$H = \frac{\dot{a}(t)}{a(t)} \tag{1.64}$$

where a represents the cosmic scale factor and an over-dot describes the derivative with respect to cosmic time t. It determines the scale of the universe and the rate at which distant galaxies are receding due to cosmic expansion. The current value of the Hubble parameter is referred to as the Hubble constant and is represented by the proportionality constant in Hubble's law, H_0. The modest differences in values obtained from different approaches (local versus early universe measurements) are referred to as the "Hubble tension". The Planck Collaboration [31] anticipates $H_0 = 67.4 \pm 0.5\ kms^{-1}Mpc^{-1}$, while Riess et al. (also known as R21)[32] reported $73.04 \pm 1.04\ kms^{-1}Mpc^{-1}$ at a 5σ confidence level. These are the significant ramifications to confirming the Hubble tension. The Hubble constant has become even more important to understand the composition and expansion history of the Universe.

1.14.2 Deceleration Parameter

The deceleration parameter is a way quantifying the rate at which the Universe is expanding. It is defined as follows:

$$q = -\frac{a\ddot{a}}{\dot{a}^2} = -1 - \frac{\dot{H}}{H^2}\,, \tag{1.65}$$

Since the above equation contains $\ddot{a}$, thus it describes how the expansion of Universe is accelerating. It serves as an indicator for the Universe's acceleration or deceleration phase. A positive value of q indicates the Universe's decelerated phase, while a negative value indicates its accelerated phase. As a result, it is a crucial parameter for verifying the Universe's phase transition, which is symbolized by the shift in the deceleration parameter's sign. Two phase transitions have occurred in our Universe: early time inflation to decelerated expansion and decelerated expansion to late time accelerated expansion. Analysis of type Ia supernovae observations in [33, 34] have revealed that $q_0 < 0$, signifying the deceleration parameter is negative and the universe is expanding at an accelerated rate.

1.14.3 Effective equation of state parameter

In modern cosmology, the effective equation of state parameter, denoted w_{eff}, characterizes the overall pressure-to-energy density ratio of the total cosmic fluid driving the expansion of the Universe. It is a useful diagnostic quantity that encapsulates the combined dynamical effect of all components-such as matter, radiation, and dark energy-on the background evolution. By definition,

$$w_{eff} \equiv \frac{p_{tot}}{\rho_{tot}}, \tag{1.66}$$

where p_{tot} and ρ_{tot} are the total pressure and energy density, respectively.

Using the Friedmann equations for a spatially flat FLRW metric, w_{eff} can be expressed directly in terms of the Hubble parameter. Combining the acceleration equation (1.25) with the first Friedmann equation (1.24), one finds

$$w_{eff} = -1 - \frac{2}{3}\frac{\dot{H}}{H^2}. \tag{1.67}$$

Equivalently, in terms of the dimensionless Hubble parameter $h(z) \equiv H(z)/H_0$, we may write

$$w_{eff}(z) = -1 + \frac{1}{3}(1+z)\frac{d\ln h^2(z)}{dz}. \tag{1.68}$$

1.15 Cosmographic Parameters

We may observe behaviour of the Universe through many cosmological models by studying cosmological parameters such as the Hubble parameter H, the decelera-

tion parameter q, and the effective equation of state parameter ω_{eff}. However, some of these parameters exhibit the same behavior across various dark energy models. Therefore, in order to properly comprehend dark energy models, cosmographic parameters are needed. The evolution of Universe in presence of cosmological data has been studied using the cosmographic technique that utilizes a Taylor expansion of the scale factor. We know that the Hubble parameter (H) and deceleration parameter (q) are related to the first and second order derivative of the scale factor, respectively. The jerk (j) parameter and snap (s) parameter are related to third and fourth order derivative of the scale factor These quantities are defined as [35]

$$j \equiv \frac{1}{aH^3}\frac{d^3a}{dt^3}, \quad s \equiv \frac{1}{aH^4}\frac{d^4a}{dt^4} \tag{1.69}$$

These parameters can also be expressed in terms of redshift and are computed as

$$j(z) = q(z) + 2q^2(z) + (1+z)\frac{dq}{dz}(z), \tag{1.70}$$

$$s(z) = -(1+z)\frac{dj}{dz}(z) - 2j(z) - 3j(z)q(z). \tag{1.71}$$

These parameters are dimensionless, and a Taylor expansion of the scale factor about t_0 provides

$$a(t) = a_0\{1 + H_0(t-t_0) - \frac{1}{2}q_0H_0^2(t-t_0)^2 + \frac{1}{3!}j_0H_0^3(t-t_0)^3 + \frac{1}{4!}s_0H_0^4(t-t_0)^4 + O[(t-t_0)^5]\} \tag{1.72}$$

In the concordance ΛCDM model, the jerk parameter is constant and equal to 1. As anticipated by the observations, for any DE model other than ΛCDM, the jerk parameter is consistently positive and the snap parameter exhibits transitional behavior similar to the deceleration parameter. Thus these parameters demonstrates how any DE model is different from the ΛCDM model.

1.16 Observational analysis

In cosmology, observational analysis plays a crucial role in validating theoretical models and improving our understanding of the composition and evolution of the Universe. Cosmological models, especially the concordance ΛCDM model, is significantly influenced as a result of observational achievements such as the discovery of dark matter and dark energy. This process depends on the precise observations

of cosmological phenomena such as, baryon acoustic oscillations (BAO), the Hubble data(cosmic chronometers), type Ia supernovae and structure formation data $f(z)\sigma_8(z)$. Cosmologists can use these data to refine model parameters for increased accuracy by comparing observed data with theoretical predictions. Complex statistical techniques such as the Monte Carlo Markov Chain (MCMC) approach is frequently used in this process. Applications such as the Python-based “emcee" package, created by Foreman-Mackey and associates [36] is employed to explore the parameter space of the model by alternating between several sets of values according to likelihood and convergence on regions that best fit the observations. This method involves ‘jumping’ randomly from one set of parameter values to another in order to explore the parameter space. The rule determining whether a jump is accepted or declined is based on how likely the new point is in comparison to the old. As a result, the algorithm typically leans toward the areas with the highest likelihood, which fits best to the data. With the help of these mechanisms, cosmologists can rapidly integrate a variety of datasets, allowing them to examine new or improved cosmological models and investigate late-time cosmic acceleration enabling a deeper and more precise understanding of the universe’s complex dynamics and the forces influencing its evolution. We adhere to the following some of these datasets in this thesis that are significant when considering late time acceleration.

1.16.1 Supernova Type Ia Datasets:

Type Ia supernovae (SNeIa) are among the most powerful cosmological probes, widely employed as standardizable candles to measure extragalactic distances and trace the expansion history of the Universe. In this thesis, we focus on the statistical treatment of SNeIa data within a Bayesian framework, emphasizing methodological and theoretical aspects rather than detailed modeling of systematic uncertainties.

We consider three progressively expanded compilations of SNeIa observations. The first comprises 40 binned data points in the redshift interval $0.014 \leq z \leq 1.612$, drawn from the Pan-STARRS1 (PS1) Medium Deep Survey [37]. The second, known as the *Pantheon* sample, incorporates this PS1 subset along with data from the Sloan Digital Sky Survey (SDSS), the Supernova Legacy Survey (SNLS), low-redshift surveys, and the Hubble Space Telescope (HST), resulting in a total of 1048 SNeIa spanning $0.01 < z < 2.3$ [37]. The third and most comprehensive compilation is the *Pan-*

theon+ dataset, which extends Pantheon by including additional low-redshift SNeIa–particularly those in galaxies with Cepheid distance measurements–yielding 1701 light curves from 1550 distinct supernovae over the redshift range $0.00122 \leq z \leq 2.2613$ [38, 39].

The fundamental observable in SNeIa cosmology is the apparent magnitude m, defined as

$$m = -\frac{5}{2}\log_{10}\left(\frac{F}{F_0}\right), \tag{1.73}$$

where F is the measured flux and F_0 is a reference flux calibrated such that $m = 0$ for a standard source.

47 The absolute magnitude M represents the apparent magnitude an object would have at a fiducial luminosity distance of 10 parsecs. The distance modulus μ, which links m and M, is given by

$$\mu = m - M = 5\log_{10}\left(\frac{d_L}{10\text{ pc}}\right), \tag{1.74}$$

where d_L is the luminosity distance. In cosmological units (megaparsecs), this is commonly expressed as

$$\mu(z;\theta) = 5\log_{10}\left(\frac{D_L(z;\theta)}{1\text{ Mpc}}\right) + 25, \tag{1.75}$$

with the model-dependent luminosity distance

$$D_L(z;\theta) = \frac{c(1+z)}{H_0}\int_0^z \frac{dz'}{E(z';\theta)}, \tag{1.76}$$

1 where $E(z;\theta) = H(z;\theta)/H_0$, c is the speed of light, and θ denotes the set of cosmological parameters.

In the Pantheon analysis, the goodness–of–fit is quantified via a χ^2 statistic:

$$\chi^2_{\text{Pan}} = \Delta\mu^{\text{T}}\mathbf{C}^{-1}\Delta\mu, \tag{1.77}$$

where $\Delta\mu = \mu^{\text{obs}} - \mu^{\text{model}}$, and $\mathbf{C} = \mathbf{D}_{\text{stat}} + \mathbf{C}_{\text{sys}}$ is the full covariance matrix accounting for both statistical and systematic uncertainties [40].

The Pantheon+ analysis introduces a critical refinement: it incorporates Cepheid-calibrated distance moduli for SNeIa hosted in galaxies with direct distance measurements. This breaks the degeneracy between the Hubble constant H_0 and the absolute magnitude M, which is otherwise treated as a nuisance parameter. Specifically, the

residual vector $\mathbf{D}$ in the χ^2 expression is redefined as

$$D_i = \begin{cases} m_i - M - \mu_i^{\text{Ceph}} & \text{if } i \in \text{Cepheid hosts}, \\ m_i - M - \mu(z_i;\theta) & \text{otherwise}, \end{cases} \tag{1.78}$$

where μ_i^{Ceph} denotes the Cepheid-inferred distance modulus for host i. Consequently, the Pantheon+ likelihood is constructed as

$$\chi^2_{\text{SNeIa}} = \mathbf{D}^{\text{T}} \mathbf{C}^{-1}_{\text{Pantheon+}} \mathbf{D}, \tag{1.79}$$

with $\mathbf{C}_{\text{Pantheon+}}$ encoding the updated covariance structure that includes correlations from photometric calibration, peculiar velocities, and other systematics [39]. This approach allows M to be constrained independently through the Cepheid anchor, thereby enabling tighter and more robust inferences on cosmological parameters, particularly H_0, within a joint analysis framework.

1.16.2 Hubble dataset(cosmic chronometers)

A key observational approach in modern cosmology involves using passively evolving early-type galaxies as cosmic chronometers to directly measure the Hubble parameter $H(z)$ across cosmic time. This method relies on the differential aging of stellar populations in such galaxies, enabling model-independent estimates of the expansion rate at various redshifts. Current compilations of these measurements span the redshift interval $0.07 < z < 1.965$, drawing from multiple independent surveys to improve the statistical robustness of cosmological inferences.

The foundational set of cosmic chronometer (CC) data consists of 32 measurements, as compiled in Table III of [41]. The agreement between theoretical predictions and these observations is assessed using the chi-squared statistic:

$$\chi^2_{\text{CC}} = \sum_{i=1}^{32} \frac{[H_{th}(z_i,\theta) - H_{obs}(z_i)]^2}{\sigma_H^2(z_i)}, \tag{1.80}$$

where $H_{th}(z_i,\theta)$ denotes the Hubble parameter predicted by a given cosmological model with parameter vector θ, $H_{obs}(z_i)$ is the measured value at redshift z_i, and $\sigma_H(z_i)$ represents the associated observational uncertainty.

To enhance constraining power, we employ an extended sample of 36 $H(z)$ mea-

surements -referred to as Observational Hubble Data (OHD) -which integrates complementary probes:

- 31 data points obtained via the cosmic chronometer technique [42];
- 2 measurements inferred from the baryon acoustic oscillation (BAO) feature in the Lyman-α forest, either from its autocorrelation or cross-correlation with quasars [43, 44];
- 3 correlated measurements derived from the radial BAO signal in the distribution of galaxies at $z = 0.38$, 0.51, and 0.61 [45].

For the first 33 uncorrelated entries (31 CC + 2 Lyman-α), the contribution to the total chi-squared is:

$$\chi^2_{CC+Ly\alpha} = \sum_{i=1}^{33} \frac{[H_{obs}(z_i) - H_{th}(z_i)]^2}{\sigma_i^2}, \tag{1.81}$$

with σ_i denoting the reported uncertainty of the i-th measurement.

The final three data points from galaxy clustering are statistically correlated, necessitating the use of their full covariance matrix. Following [45], the covariance matrix is given by:

$$\mathbf{C} = \begin{bmatrix} 3.65 & 1.78 & 0.93 \\ 1.78 & 3.65 & 2.20 \\ 0.93 & 2.20 & 4.45 \end{bmatrix},$$

and the residual vector between observed and theoretical values is:

$$\mathbf{A} = \begin{bmatrix} H_{obs}(0.38) - H_{th}(0.38) \\ H_{obs}(0.51) - H_{th}(0.51) \\ H_{obs}(0.61) - H_{th}(0.61) \end{bmatrix}.$$

The corresponding chi-squared term is computed as:

$$\chi^2_{gal} = \mathbf{A}^T \mathbf{C}^{-1} \mathbf{A}. \tag{1.82}$$

The total chi-squared for the complete 36-point OHD sample is thus:

$$\chi^2_{H(z),36} = \chi^2_{CC+Ly\alpha} + \chi^2_{gal}. \tag{1.83}$$

This multi-probe compilation provides a stringent and largely model–independent test

of cosmological scenarios through direct measurements of the Universe's expansion history.

1.16.3 Baryon Acoustic Oscillations

Baryon acoustic oscillations (BAOs) provide a powerful standard ruler for probing the expansion history of the Universe. In this analysis, we employ three complementary BAO data configurations to test cosmological models: (i) a joint BAO+CMB dataset calibrated to the CMB sound horizon, (ii) a dimensionless BAO estimator $d_z(z) = r_s(z_d)/D_V(z)$, and (iii) the latest anisotropic BAO measurements from the Dark Energy Spectroscopic Instrument Data Release 2 (DESI DR2). Each approach offers distinct advantages and redshift coverage, enabling robust cross-validation of model predictions.

- **BAO+CMB:** We adopt the widely used BAO+CMB compilation that combines low and intermediate-redshift isotropic BAO measurements with the CMB-inferred angular diameter distance to last scattering. This dataset includes six effective redshifts from the $6dF$ Galaxy Survey ($z = 0.106$), SDSS Main Galaxy Sample ($z = 0.35$), BOSS CMASS ($z = 0.57$), and WiggleZ ($z = 0.44, 0.60, 0.73$) [46, 47, 48, 49]. The CMB anchor uses $d_A(z_*)$ with $z_* \approx 1090$ [50]. The chi-squared is constructed from the ratios $d_A(z_*)/D_V(z_i)$ as

$$\chi^2_{\rm BAO/CMB} = \mathbf{A}^{\rm T}\mathbf{C}^{-1}\mathbf{A}, \tag{1.84}$$

where C^{-1} represents the inverse of the covariance matrix [51] given by

$$C^{-1} = \begin{bmatrix} 0.52552 & -0.03548 & -0.07733 & -0.00167 & -0.00532 & -0.00590 \\ -0.03548 & 24.97066 & -1.25461 & -0.02704 & -0.08633 & -0.09579 \\ -0.07733 & -1.25461 & 82.92948 & -0.05895 & -0.18819 & -0.20881 \\ -0.00167 & -0.02704 & -0.05895 & 2.91150 & -2.98873 & 1.43206 \\ -0.00532 & -0.08633 & -0.18819 & -2.98873 & 15.96834 & -7.70636 \\ -0.00590 & -0.09579 & -0.20881 & 1.43206 & -7.70636 & 15.28135 \end{bmatrix} \tag{1.85}$$

and the residual vector $\mathbf{A}$ is given by

$$A = \begin{bmatrix} \frac{d_A(z_*,\theta)}{D_v(0.106,\theta)} - 30.84 \\ \frac{d_A(z_*,\theta)}{D_v(0.35,\theta)} - 10.33 \\ \frac{d_A(z_*,\theta)}{D_v(0.57,\theta)} - 6.72 \\ \frac{d_A(z_*,\theta)}{D_v(0.44,\theta)} - 8.41 \\ \frac{d_A(z_*,\theta)}{D_v(0.6,\theta)} - 6.66 \\ \frac{d_A(z_*,\theta)}{D_v(0.73,\theta)} - 5.43 \end{bmatrix} \tag{1.86}$$

This approach assumes a fixed sound horizon calibrated by CMB data and tests consistency of late-time expansion.

- **BAO$_{d_z}$:** An alternative isotropic BAO statistic uses the dimensionless quantity

$$d_z(z,\theta) = \frac{r_s(z_d)}{D_V(z,\theta)}, \tag{1.87}$$

13 where $r_s(z_d)$ is the comoving sound horizon at the baryon drag epoch z_d, computed as

$$r_s(z_d) = \int_{z_d}^{\infty} \frac{c_s(z)}{H(z,\theta)}\, dz, \tag{1.88}$$

with sound speed $c_s(z) = c/\sqrt{3(1+\bar{R}(z))}$ and $\bar{R}(z) \propto (1+z)^{-1}$. The dilation scale $D_V(z)$ is defined as

$$D_V(z) = \left[(1+z)^2 d_A^2(z) \frac{cz}{H(z)}\right]^{1/3}. \tag{1.89}$$

This formulation, used in [52] and subsequent works [53, 54], avoids explicit dependence on CMB calibration and instead treats $r_s(z_d)$ as a derived quantity from the cosmological model. The corresponding χ^2 is computed from differences between observed and predicted d_z values, assuming uncorrelated errors.

- **BAO DESI DR2:** We further incorporate the most recent BAO results from the Dark Energy Spectroscopic Instrument Data Release 2 [55], which provide high-precision, anisotropic constraints across seven tracer populations: BGS, LRG1, LRG2, LRG3+ELG1, ELG2, QSO, and Lyα. These yield 13 independent BAO measurements at effective redshifts $z_{\rm eff} = 0.295, 0.51, 0.706, 0.934, 1.321, 1.484,$ and 2.33, with multiple tracers at some redshifts.

  The DESI DR2 analysis reports constraints on the transverse and radial BAO scales normalized by the sound horizon at drag, $r_s(z_d)$ (with $z_d \simeq 1060$) is given

in (1.88).

The relevant distance measures are the transverse comoving distance

$$D_M(z) = \int_0^z \frac{c}{H(z',\theta)}\, dz', \tag{1.90}$$

the Hubble distance $D_H(z) = c/H(z,\theta)$, and the angle-averaged distance

$$D_V(z) = \left[z D_M^2(z) D_H(z)\right]^{1/3}. \tag{1.91}$$

For each tracer, the data vector $\mathbf{Y}$ consists of one or more of the ratios $D_M(z)/r_s(z_d)$, $D_H(z)/r_s(z_d)$, and $D_V(z)/r_s(z_d)$, depending on the survey geometry and redshift. The chi-squared contribution is then

$$\chi^2_{\rm DESI} = \Delta\mathbf{Y}^{\rm T}\, \mathbf{C}^{-1}_{\rm BAO}\, \Delta\mathbf{Y}, \tag{1.92}$$

where $\Delta\mathbf{Y}$ is the difference between observed and model-predicted values, and $\mathbf{C}^{-1}_{\rm BAO}$ is the published inverse covariance matrix for the full DESI DR2 BAO dataset [56, 57].

1.16.4 $f(z)\sigma_8(z)$ data (Growth data)

To complement the geometric probes discussed earlier, we also employ measurements of the growth rate of cosmic structure. Specifically, we use the so-called "Gold-17" compilation, which comprises 18 independent estimates of the combined growth observable $f(z)\sigma_8(z)$ derived from redshift-space distortions (RSD) in large-scale structure (LSS) surveys. These data points are compiled in Table III of Nesseris et al.[58] and represent some of the most robust low-redshift constraints on the evolution of matter perturbations.

The linear growth rate of matter density fluctuations, $f(z)$, quantifies how perturbations evolve with cosmic expansion and is defined as

$$f(z) = \frac{d\ln\delta_m}{d\ln a} = -(1+z)\frac{1}{\delta_m(z)}\frac{d\delta_m}{dz}, \tag{1.93}$$

where $\delta_m(z)$ is the linear matter density contrast, $a = 1/(1+z)$ is the scale factor, and primes denote derivatives with respect to redshift z.

The amplitude of matter fluctuations is characterized by $\sigma_8(z)$, which denotes the root-mean-square mass fluctuation within spheres of radius $8h^{-1}$ Mpc, extrapolated

to redshift z using linear theory:

$$\sigma_8(z) = \sigma_8 \frac{\delta_m(z)}{\delta_m(0)}, \tag{1.94}$$

where $\sigma_8 \equiv \sigma_8(z=0)$ is the present-day value.

The product $f(z)\sigma_8(z)$ provides a convenient, nearly model-independent probe of structure growth, as it minimizes degeneracies between growth and bias in RSD analysis. Substituting Eqs. (1.93) and (1.94), it can be expressed as

$$f\sigma_8(z) = -(1+z)\frac{\sigma_8}{\delta_m(0)}\frac{d\delta_m}{dz}. \tag{1.95}$$

To compare theoretical predictions with observations, we adopt a Gaussian likelihood. The corresponding chi-squared statistic for the $f\sigma_8$ dataset is given by

$$\chi^2_{f\sigma_8} = \sum_{i=1}^{18} \frac{\left[f\sigma_8(z_i;\theta) - (f\sigma_8)_i^{\rm obs}\right]^2}{\sigma_i^2}, \tag{1.96}$$

where $(f\sigma_8)_i^{\rm obs}$ and σ_i are the measured value and 1σ uncertainty of the i-th data point, respectively, and θ denotes the set of cosmological parameters that determine the growth history $\delta_m(z;\theta)$. This form assumes uncorrelated errors across the 18 measurements, consistent with the treatment in Quelle & Maroto (2020) [59].

1.16.5 H_0 Prior

The Hubble constant, denoted H_0, characterizes the present-day expansion rate of the Universe. A notable discrepancy–often termed the “Hubble tension” has emerged between determinations of H_0 based on early-Universe observations and those derived from local distance-ladder methods. Analyses of the cosmic microwave background (CMB) by the *Planck* satellite, assuming the standard ΛCDM cosmology, yield a value of $H_0 = 67.4 \pm 0.5\ \mathrm{km\,s^{-1}\,Mpc^{-1}}$ [31]. On the other hand, the SH0ES collaboration has pursued a late–Universe approach using Cepheid-variable–calibrated Type Ia supernovae. Their 2019 analysis (R19) reported $H_0 = 73.04 \pm 1.04\ \mathrm{km\,s^{-1}\,Mpc^{-1}}$ [60], and this was subsequently updated in 2021 (R21) to $H_0 = 73.2 \pm 1.3\ \mathrm{km\,s^{-1}\,Mpc^{-1}}$ [32]. The difference between the *Planck* and SH0ES results stands at approximately 5σ, challenging the standard cosmological model or pointing to unaccounted systematics.

1.17 Model Selection Criterion

In this thesis, we assess the statistical significance of the data fitting and the observational compatibility of the models by applying the well-known Akaike Information Criterion (AIC), the Bayesian Information Criterion (BIC), and the Deviance Information Criterion (DIC).

1.17.1 Akaike information criteria and Bayesian information criteria

When comparing competing models that aim to describe the same physical phenomenon, two widely used statistical tools are the Akaike Information Criterion (AIC) and the Bayesian Information Criterion (BIC). Both criteria balance the goodness of fit of a model with its complexity, penalizing models that require a larger number of free parameters. While AIC originates from information theory and is rooted in a frequentist framework, BIC arises from an asymptotic approximation to the Bayesian marginal likelihood (or evidence).

In cosmology, AIC and BIC have been utilized to discriminate cosmological models based on the penalization associated with the number of parameters that the model needs to explain the data. By using statistical analysis, we can identify which models are “more favorable" by considering the dataset and number of parameters. The AIC is defined as [61]

$$\mathrm{AIC} = \chi^2_{\mathrm{min}} + \frac{2dN}{N-d-1}, \tag{1.97}$$

where N denotes the total number of data points, d is the number of free parameters in the model, and χ^2_{min} is the minimum chi-squared value obtained from the best-fit parameters. To compare a candidate model k against the standard ΛCDM model (denoted as model l), we compute the difference

$$\Delta\mathrm{AIC}_{k,l} = \mathrm{AIC}_k - \mathrm{AIC}_l. \tag{1.98}$$

A negative value of $\Delta\mathrm{AIC}_{k,l}$ indicates that model k is preferred over ΛCDM. Following conventional interpretation thresholds given by Liddle[62], we classify the strength of evidence as follows:

- $\Delta\mathrm{AIC}_{k,l} < 2$: strong evidence in favor of model k,
- $2 \leq \Delta\mathrm{AIC}_{k,l} \leq 4$: moderate (or average) evidence,

- $4 < \Delta\mathrm{AIC}_{k,l} \leq 7$: weak (or little) evidence,
- $\Delta\mathrm{AIC}_{k,l} > 8$: essentially no evidence supporting model k over ΛCDM.

In contrast, the BIC is given by [63]

$$\mathrm{BIC} = \chi^2_{\mathrm{min}} + d \ln N. \tag{1.99}$$

The difference $\Delta\mathrm{BIC}_{k,l} = \mathrm{BIC}_k - \mathrm{BIC}_l$ is interpreted as evidence *against* model k relative to the reference ΛCDM model. The standard interpretation is:

- $0 \leq \Delta\mathrm{BIC}_{k,l} < 2$: not enough evidence against model k,
- $2 \leq \Delta\mathrm{BIC}_{k,l} < 6$: positive evidence against model k,
- $6 \leq \Delta\mathrm{BIC}_{k,l} < 10$: strong evidence against model k,
- $\Delta\mathrm{BIC}_{k,l} \geq 10$: very strong evidence against model k.

Both criteria rely on the assumption that the models being compared are fitted to the same dataset. Moreover, while AIC tends to favor more complex models (as its penalty grows linearly with d), BIC imposes a stronger penalty for additional parameters- especially for large N and thus generally prefers simpler models.

1.17.2 Deviance information criteria

In addition to AIC and BIC, the Deviance Information Criterion (DIC) [62] provides a Bayesian framework for model comparison that naturally incorporates the trade-off between goodness of fit and model complexity. It is particularly well–suited for analysis based on posterior samples, such as those obtained from Markov Chain Monte Carlo (MCMC) methods. The DIC is built upon the concept of the effective number of parameters, denoted p_D, which quantifies the Bayesian complexity of a model. It is defined as

$$p_D = \overline{D(\theta)} - D(\overline{\theta}), \tag{1.100}$$

where $D(\theta) = -2 \ln \mathscr{L}(\theta)$ is the deviance, $\mathscr{L}(\theta)$ is the likelihood for parameter vector θ, and the bar indicates the posterior mean. Thus, p_D measures the difference between the average deviance and the deviance evaluated at the posterior mean.
Under the common assumption of a Gaussian likelihood, the deviance coincides with

the chi–squared statistic up to an additive constant, allowing us to equivalently write

$$p_D = \overline{\chi^2(\theta)} - \chi^2(\overline{\theta}), \tag{1.101}$$

where $\chi^2(\theta) = -2\ln\mathscr{L}(\theta)$. The DIC is then defined as

$$\mathrm{DIC} \equiv D(\overline{\theta}) + 2p_D = \overline{D(\theta)} + p_D. \tag{1.102}$$

This expression penalizes model complexity through p_D, while $D(\overline{\theta})$ reflects the fit quality at the posterior mean. In the regime where parameters are tightly constrained and the posterior is approximately Gaussian, p_D approaches the actual number of free parameters d, and DIC behaves similarly to AIC rather than BIC, due to its relatively milder penalty on complexity.

To compare a candidate cosmological model k with the standard ΛCDM model l, we define the DIC difference as

$$\Delta\mathrm{DIC}_{k,l} = \mathrm{DIC}_k - \mathrm{DIC}_l. \tag{1.103}$$

Since a lower DIC value indicates a more favorable balance between fit and complexity, a *negative* $\Delta\mathrm{DIC}_{k,l}$ implies that model k is preferred over model l, whereas a *positive* value indicates that ΛCDM provides a better description of the data under the DIC criterion.

1.17.3 Ongoing Research and research gaps:

Researchers are actively working on refining measurements, developing new techniques, and exploring different theoretical models to try and resolve the cosmological constant, cosmic coincidence, Hubble tension and σ_8 tension. They are also working on understanding of galaxy formation, properties of black holes and neutron stars. In existing research, researchers are working on modified theories to explore the nature of the Universe.

The biggest research gap include understanding dark matter, dark energy and cosmic acceleration where we are still uncovering. Different measurements show a conflicting results of H_0 and σ_8 raising the Hubble tension and σ_8 tension, and bridging gaps between small-scale astrophysics and large-scale cosmology.

1.18 Motivation

Analysis carried out by various researchers demonstrate that the Universe recently went transition from a decelerating to an accelerating expansion [11, 33, 34, 64, 65, 66, 67]. These observations are consistent with the concordance ΛCDM model. This accelerated phase of the universe is mainly explained by two well-known theories. The first involves changes to conventional General Relativity, while the second involves the addition of a component called dark energy, which has an equation of state $w < -1/3$ and a strong negative pressure.

In this regard, it is important to note that the existence of negative pressure is a significant component for accelerated expansion. When physical systems deviate from their thermodynamic equilibrium states, this sort of stress arises spontaneously in many different circumstances. Such states are generally associated with phase transitions, and the presence of negative pressure appears to be inevitable for certain systems.

Several publications have highlighted that bulk viscous fluid can generate an accelerating expansion of the Universe. Some authors [68, 69] investigated the impact of bulk viscosity in the framework of inflation and discovered that the bulk viscous fluid can lead to an accelerated expansion of the Universe. Many authors [70, 71, 72, 73, 74, 75] have discussed the late time expansion of the Universe by including the viscous term in the cosmic fluid.

Our aim is to achieve a more complete and accurate understanding about the origin, evolution and fate of the Universe. Tensions in key cosmological parameters H_0, S_8, and σ_8 suggest the necessity of a more comprehensive framework to address these fundamental gaps while aligning with precise observational data. Several explanations have been proposed to resolve the tensions. *This includes: New physics beyond ΛCDM model, systematic errors in measurement and modification in GTR*. These research gaps to understand the evolution of the Universe motivate me to investigative the alternative theories beyond ΛCDM model. Modified gravity seeks to address key gaps in standard cosmology, particularly inflation, dark matter, and dark energy. Broadly, modifications to General Relativity fall into two categories: introducing new fields or altering the geometric structure of spacetime. This study focuses on both categories, which have been instrumental in explaining cosmic acceleration without the need of an explicit dark energy component. In particular, some modified gravity models offer

viable solutions to the H_0 tension, especially through late-time modifications. Some research suggest that the cosmological constant is not a constant but varies with time which gives a new sight to understand the evolution of the Universe, especially dark matter and dark energy. This thesis is dedicated to address the above issues by studying the decaying vacuum model with bulk viscosity in General Relativity and its alternative theories.

1.19 Organization of thesis work

The thesis entitled *"A Study on Evolution and Dynamics of Dark Energy models in Cosmology"* comprises of six chapters. A summary of the thesis and future scope of the work are also provided. The list of publications and the bibliography are given at the end of the thesis.

Chapter 1 titled *"Introduction"* presents a brief study on Einstein's general theory of relativity, spacetime and cosmological models. It gives a brief overview of the model for explaining the Universe's accelerated expansion that have been proposed in the literature. The thermodynamics of dissipative processes of bulk viscosity has been discussed. A brief survey of running vacuum models has been carried out. We have briefly discussed the cosmological parameters, since they are vital in the study of cosmological models. Finally, the chapter discusses key cosmological observations that provide insights into the nature of the Universe and validate theoretical models. Some of the latest observational data such as Type Ia supernovae (SNe), Hubble data (CC), Baryon acoustic oscillations (BAO) and Growth data ($f(z)\sigma_8(z)$) are discussed. Hence, chapter 1 establishes a context of the thesis work, explains its purpose and offers tools to accomplish the objectives.

Chapter 2 titled *"Viscous fluid dynamics with decaying vacuum energy density"* introduces the analytical and observational consequences of cosmology inspired by dissipative phenomena with varying vacuum energy density (VED) for a spatially flat, homogeneous and isotropic FLRW geometry. We have assumed the interaction of two components: viscous dark matter and vacuum energy density. We have solved the field equations by assuming the most general form of bulk viscous coefficient, viz., $\zeta = \zeta_0 + \zeta_1 H + \zeta_2(\ddot{a}/aH)$. We have also explored three particular cases of bulk

viscosity, namely (1) $\zeta = \zeta_0$; (2) $\zeta = \zeta_1 H$; (3) $\zeta = \zeta_0 + \zeta_1 H$ to observe the effect of viscosity with varying VED. We have used the varying VED of the functional form $\rho_\Lambda = c_0 + 3\nu H^2$ in all of viscous models presented above. It has been observed that all these viscous $\Lambda(t)$ models expand exponentially with cosmic time t. The models show the transition from decelerated phase to accelerated phase in late time. The matter energy density, $\rho_m(t)$ approaches to a finite value in late time evolution of the Universe. The value of χ^2_{red} is less than unity with every data sets which show that the model is in a very good fit with these observational data sets. The jerk parameter remains positive and less than unity in past, and eventually tends to unity in late-time. Thus, the jerk parameter deviates in early time but it attains the same value as ΛCDM in late-time. To discriminate the viscous $\Lambda(t)$ with the ΛCDM, we have examined them using the selection criterion. *The content of this chapter has been published as a research paper "Viscous fluid dynamics with decaying vacuum energy density",* Physical Review D*, American Physical Society,* **109***, 023508 (2024).*

Chapter 3 titled *"Interacting bulk viscous model with decaying vacuum density"* explores a cosmological model composed of a viscous dark matter interacting with decaying vacuum energy in a spatially flat Universe. In the first part, we have found the analytical solution of different cosmological parameters by assuming the physically viable forms of bulk viscosity and decaying vacuum density with the interaction term. The second part is dedicated to constrain free parameters of the interacting viscous model with decaying vacuum energy by employing latest observational data of $Pantheon+$, Cosmic Chronometer and $f(z)\sigma_8(z)$. We have found that the interacting model just deviate very slightly from well-known concordance ΛCDM model and can alleviate effectively the current H_0 tension between local measurement by R21 and global measurement by Planck 2018, and the excess in the mass fluctuation amplitude σ_8 essentially vanish in this context. We have reported the Hubble constants as $H_0 = 72.100^{+1.700}_{-1.700}$, and $72.200^{+1.000}_{-2.000}$ $kms^{-1}Mpc^{-1}$, deceleration parameters as $q_0 = -0.532^{+0.022}_{-0.024}$, and $-0.531^{+0.022}_{-0.022}$, and equation of state parameters as $w_0 = -0.689^{+0.016}_{-0.016}$, and $-0.688^{+0.016}_{-0.016}$ for ΛCDM and interacting models, respectively. It has been found that the interacting model is in good agreement with ΛCDM. Further, we have discussed the amplitude of matter power spectrum σ_8 and its associated parameter S_8 using $f(z)\sigma_8(z)$ data. Finally, the information selection criterion and Bayesian inference have been discussed to distinguish the interacting model with ΛCDM model. *The content of this chapter has been published in the form of*

a research paper, "Exploring interacting bulk viscous model with decaying vacuum density" Astronomy and Computing, *Elsevier(Science Direct),* **53**, *100992 (2025).*

In **Chapter 4** titled *"Interacting viscous running vacuum model in FLRW Universe"*, we have discussed the dynamics of interacting viscous model with time-varying cosmological constant, $\Lambda(t)$, which is a natural generalization of the standard ΛCDM model in FLRW) spacetime. The $\Lambda(t)$ is motivated by different cosmological approaches. Recent investigations involving the renormalization of quantum field theory (QFT) in curved spacetime yield a time-varying Λ, so-called running vacuum model (RVM) in which it acquires a dynamical component through quantum effects. We discuss both the background and perturbation equations for viscous RVM using a more generalized parametrization form of vacuum density. We employ the cosmic data, namely distant Type Ia Supernovae (Pantheon+), Baryonic Acoustic Oscillations DESI, Cosmic Chronometers and growth data. We anchor ΛCDM and viscous RVM on two Hubble constant priors of Planck2018 and SH0ES R22 that reflect the Hubble tension. Using these data samples we assess the viability and compare viscous RVM with the standard ΛCDM model. The Gelman-Rubin statistic (or R-hat statistic) is used to assess the convergence of Markov Chain Monte Carlo (MCMC) simulations. We also discuss the stability of viscous RVM using information criterion such as AIC, BIC and DIC. The constraints on parameters show that the viscous RVM is consistent with the standard ΛCDM model and alleviates the Hubble tension up to 0.569σ. *The content of this chapter has been published as a research paper, "Interacting model of bulk viscous and decaying vacuum energy "* Physical Letters B, *Elsevier(Science Direct),* **871**, *139994 (2025).*

In **Chapter 5** titled *"Time-varying vacuum energy models in Brans-Dicke theory"*, we have constrained the time-varying VED models in Brans-Dicke (BD) theory within the framework of a flat FLRW space-time by using the latest observational data. In the first step, the analytical solution of field equations have been found by considering the two functional forms of cosmological constant, viz. power-series form: $\Lambda = n_1 H + n_2 H^2$ and power-law form: $\Lambda \propto a^{-n}$, where n_1, n_2 and n are all constants, and H and a are the Hubble parameter and scale factor, respectively. Then, to test the viability of the models, the latest data sample such as Hubble $H(z)$ data, Type Ia supernovae and baryon acoustic oscillations have been used to constrain the model parameters. We have applied the Markov Chain Monte Carlo

(MCMC) method to find the best-fit values of the space parameters of both the models. The cosmological implications of the models have been discussed by using the best-fit values of parameters. It has found that both the models are in good agreement with the datasets and are consistent with the analytical solutions. We have used jerk parameter and selection criteria (AIC and BIC) to find the consistency of the proposed models with the observation as compared to ΛCDM model. Both the models explain the late-time acceleration of the Universe. *The content of this chapter has been published in the form of a research paper "Constraining the time-varying vacuum energy models in Brans-Dicke theory",* Astrophysics and Space Science*, Springer,* **368***, 16 (2023).*

In **Chapter 6** titled "*Brans-Dicke cosmology with cosmological term* $\Lambda(H) = c_0 + 3\nu H^2$", we have studied the dynamics of a flat FLRW cosmological model by considering varying VED in BD cosmology. For this purpose, we have considered the well-motivated VED of the form $\Lambda(H) = c_0 + 3\nu H^2$, where c_0 and ν are dimensionless constants. We first adopt a theoretical method to find the exact solutions for various cosmological parameters of two models, namely Λ_{RG1} and Λ_{RG2}. In Λ_{RG1} model, the scale factor evolves as a power-law expansion which gives the deceleration parameter a constant value. Hence, this type of model does not show the transition phase. The second model Λ_{RG2} describes the transition phase from deceleration to acceleration. In the second part, we have performed two joint likelihood analysis in order to find the constrain on the main free parameters of the Λ_{RG2} model using the latest observational data sets including SNe Pantheon, $H(z)$ data, BAO/CMB data and local H_0 by SH0ES. Performing the two different combination of datasets, we have found that the model shows prior decelerated epoch followed by late time accelerated epoch. We have also compared the decaying VED with traditional Λ cosmology, which help us to define the evolution of the VED model. The results show that varying VED model in BD theory is consistent with data and the cosmic evolutions are in good agreement with the concordance ΛCDM and BD with constant Λ models. The AIC and BIC selection criteria have also been discussed. *The content of this chapter has been published as a research paper "Brans-Dicke cosmology with cosmological term* $\Lambda(H) = c_0 + 3\nu H^2$*",* Physics of the Dark Universe*, Elsevier(Science Direct),* **42***, 101300 (2023).*

Chapter 7 titled *"Conclusion, Future Scope and Social Impact"* presents the conclusion of this thesis work and the research strategy for the future. The impacts of bulk viscosity and decaying vacuum energy density in a few cosmological models have been examined in the current thesis. To illustrate the early and late-time development of the Universe, we have addressed different forms of cosmological constant Λ and bulk viscous coefficient ζ. We have further examined the linear perturbation growth of some models to study the current σ_8 and H_0 tensions. In the context of other cosmological models or hypotheses, these forms might be crucial for the study of the universe. We think there is a lot of potential for studying many cosmic events with these forms. In the future, we intend to add more modified theories and other forms of time–varying cosmological constant $\Lambda(t)$.

Finally, the thesis concludes with a bibliography and a list of the author's publications.

****

Chapter 2

Viscous fluid dynamics with decaying vacuum energy density

In this chapter [1], we explore an alternative cosmological model which contains a viscous fluid with decaying vacuum energy that diminishes over time. The model describes a transition from deceleration towards accelerated expansion of the Universe. It potentially solve the Hubble tension when fit into the observational data. It shows a good agreement with standard ΛCDM model.

Highlights:

☞ A spatially isotropic and homogeneous flat FLRW spacetime is considered for studying the evolution and dynamics of the Universe.

☞ Assumes decaying vacuum energy (VED) instead of a constant cosmological constant which decays over cosmic time.

☞ Presents a modified the Einstein's equations to include bulk viscosity and decaying vacuum energy.

☞ Such cosmological models create a richer system than a simple non-interacting scenario.

☞ The solutions for Hubble parameter, scale factor, deceleration parameter, equation of state parameter and energy density as a function of redshift are obtained.

☞ This model explains a transition from deceleration to accelerating Universe where the deceleration parameter q approaches to -1 in late time of its evolution.

[1] This chapter is based on a published research paper, " Viscous fluid dynamics with decaying vacuum energy density, *Physical Review D* **109**, 023508 (2024)".

☞ Uses the MCMC methods with observational data like Pantheon, cosmic chronometer, BAO, to constrain model's parameters.

☞ Analyzes the matter fluctuations (structure formation) to know how the viscous decaying models affect the galaxy and structure growth.

☞ Plots the trajectories of various cosmological parameters to analyze the dynamics and late time evolution of the Universe.

☞ Discuss the model selection criterion (AIC and BIC) to compare the proposed model with the standard ΛCDM model.

☞ Presents the findings in Conclusion section.

2.1 Introduction

Different observations such as luminosity distances of type Ia supernova, measurements of anisotropy of cosmic microwave background (CMB) and gravitational lensing have confirmed that our Universe is spatially flat and expanding with an accelerated rate. It has been observed that the Universe contains a mysterious dominant component, called dark energy (DE) with large negative pressure, which leads to this cosmic acceleration [33, 34, 45, 76, 77, 78, 79]. In literature, several models have been proposed to explain the current accelerated expansion of the Universe. The two most accepted DE models are that of a cosmological constant and a slowly varying rolling scalar field (quintessence models)[80, 81, 82, 83].

The cosmological constant Λ(CC for short), initially introduced by Einstein to get the static universe, is a natural candidate for explaining DE phenomena with equation of state parameter equal to -1. The natural interpretation of CC arises as an effect of quantum vacuum energy. Thus, the cold dark matter based cosmology together with a CC, called the ΛCDM cosmology, is preferred as the standard model for describing the current dynamics of the Universe. It is mostly consistent with the current cosmological observations. However, despite of its success, the ΛCDM model has several strong problems due to its inability to renormalize the energy density of quantum vacuum, obtaining a discrepancy of ~ 120 orders of magnitude between its predicted and observed value, so-called CC or fine-tuning problem [10, 84, 85]. It also has the coincidence problem, i.e., why the Universe transition, from decelerated to an accelerated

phase, is produced at late times [13].

Many models have been proposed to tackle these issues. One of the possible proposal is to incorporate energy transfer among the cosmic components. In this respect, the models with time–varying vacuum energy density (VED), also known as 'decaying vacuum cosmology'(DVC) seems to be promising. The idea of a time-varying VED models ($\rho_\Lambda = \Lambda(t)/8\pi G$) is physically more viable than the constant Λ [86, 87, 88, 89]. Although no fundamental theory exists to describe a time-varying vacuum, a phenomenological technique has been suggested to parametrize $\Lambda(t)$. Such attempts suggest that decaying VED model provides the possibility of explaining the acceleration of the Universe as well as it solves both cosmological constant and coincidence problems [16, 90, 91, 92, 93, 94, 95, 96, 97, 98, 99, 100, 101, 102, 103, 104, 105, 106, 107, 108, 109, 110].

On the other hand, in recent years, the observations suggest that the Universe is permeated by dissipative fluids. Based on the thermodynamics point of view, phenomenological exotic fluids are supposed to play the role for an alternative DE models. It has been known since long time ago that a dissipative fluid can produce acceleration during the expansion of the universe [111, 112]. The bulk and shear viscosity are most relevant parts of dissipative fluid. The dynamics of homogeneous cosmological models has been studied in the presence of viscous fluid and has application in studying the evolution of the Universe.

Eckart [29] extended a classical irreversible thermodynamics from Newtonian to relativistic fluids. He proposed the simplest non-causal theory of relativistic dissipative phenomena of first order which was later modified by Landau and Lifshitz [30]. The Eckart theory has some important limitations. It has been found that all the equilibrium states are unstable [113] and the signals can propagate through the fluids faster than the speed of light [114]. Therefore, to resolve theses issues, Israel and Stewart [28] proposed a full causal theory of second order. When the relaxation time goes to zero, the causal theory reduces to the Eckart's first order theory. Thus, taking the advantage of this limit of vanishing relaxation time at late time, it has been used widely to describe the recent accelerated expansion of the Universe. An exhaustive reviews on non-causal and causal theories of viscous fluids can be found in Refs.[115, 116, 117, 118, 119, 120, 121, 122, 123, 124, 125, 126]. In recent years, the direct observations indicate for viscosity dominated late epoch of accelerating expansion of the Universe. In this respect, many authors have explored the viability of a bulk viscous Universe to explain the present accelerated expansion of the Universe

cf.[72, 74, 75, 127, 128, 129, 130, 131, 132, 133, 134, 135, 136, 137, 138, 139, 140, 141, 142, 143, 144, 145].

In Eckart theory, the effective pressure of the cosmic fluid is modeled as $\Pi = -3\zeta H$, where ζ is bulk viscous coefficient and H the Hubble parameter. Bulk viscous coefficient can be assumed as a constant or function of Hubble parameter. It allows to explore the presence of interacting terms in the viscous fluid. Since the imperfect fluid should satisfy the equilibrium condition of thermodynamics, the pressure of the fluid must be greater than the one produced by the viscous term. To resolve this condition, it is useful to add an extra fluid such as cosmological constant. Many authors [146, 147, 148, 149] have studied viscous cosmological models with constant or with time-dependent cosmological constant. Hu and Hu [146] have investigated a bulk viscous model with cosmological constant by assuming bulk viscous proportional to the Hubble parameter. Herrera-Zamorano et al. [147] have studied a cosmological model filled with two fluids under Eckart formalism, a perfect fluid as DE mimicking the dynamics of the CC, while a non-perfect fluid as dark matter with viscosity term.

In this chapter, we focus on discussing the dynamics of viscous Universe which consider the first order deviation from equilibrium, i.e., Eckart formalism with decaying VED. Using different versions of bulk viscous coefficient ζ, we find analytically the main cosmological functions such as the scale factor, Hubble parameter, matter density, deceleration and equation of state parameters. We have discussed the effect of viscous model with varying VED in perturbation level. We implement the perturbation equation to obtain the growth of matter fluctuations in order to study the contribution of this model in structure formation. We perform a Bayesian MCMC analysis to constrain the parameter spaces of the model using three different combinations involving observational data from type Ia supernovae (Pantheon), Hubble data (cosmic chronometers), Baryon acoustic oscillations and $f(z)\sigma_8(z)$ measurements. We compare our model and concordance ΛCDM to understand the effects of viscosity with decaying vacuum by plotting the evolutions of the deceleration parameter, equation of state parameter and Hubble parameter. We also study the selection information criterion such as AIC and BIC to analyze the stability of the model.

The work of this chapter is organized as follows. In Section 2.2, we present the basic cosmological equations of FLRW geometry with bulk viscosity and decaying VED. In Section 2.3, we find the solution of the field equations by assuming the most general form of bulk viscous coefficient. Section 2.4 is devoted to study the evolutions of some particular forms of bulk viscous coefficient with varying VED. We discuss the growth

rate equations that govern the perturbation in Section 2.5. Section 2.6 presents the observational data and method to be used to constrain the proposed model. The results and discussion on the evolution of the various parameters are presented in Section 2.7. In Section 2.8, we present the selection information criterion to distinguish the presented model with concordance ΛCDM. Finally, we conclude our finding in Section 2.9.

2.2 Viscous model with varying-Λ

We assume a homogeneous, isotropic and spatially flat FLRW metric in spherical coordinates

$$ds^2 = -c^2dt^2 + a^2(t)\left[dr^2 + r^2(d\theta^2 + sin^2\theta d\phi^2)\right]. \tag{2.1}$$

The large scale dynamics of (2.1) is described by the Einstein field equations, which include the cosmological constant Λ and is given by

$$G_{\mu\nu} = R_{\mu\nu} - \frac{1}{2}g_{\mu\nu}R = 8\pi G(T_{\mu\nu} + g_{\mu\nu}\rho_\Lambda). \tag{2.2}$$

We introduce a bulk viscous fluid through the energy-momentum tensor which is given by [150]

$$T_{\mu\nu} = (\rho_m + P)u_\mu u_\nu + g_{\mu\nu}P, \tag{2.3}$$

where u^μ is the fluid four-velocity, ρ_m is the density of matter and P is the pressure which is composed of the equilibrium pressure p_m of the matter fluid plus the viscous pressure Π, i.e., $P = p_m + \Pi$. The viscous effect can be defined by the viscous pressure $\Pi = -3\zeta H$, where ζ is the bulk viscous coefficient and H is the Hubble parameter. The bulk viscous coefficient ζ is assumed to be positive on thermodynamical grounds. Therefore, it makes the effective pressure as a negative value which leads to modification in energy-momentum tensor of perfect fluid.

If we denote the total energy-momentum tensor $T_{\mu\nu} + g_{\mu\nu}\rho_\Lambda$ as modified $\tilde{T}_{\mu\nu}$ on right hand side of field equations (2.2), then the modified $\tilde{T}_{\mu\nu}$ can be assumed the same form as $T_{\mu\nu}$, that is, $\tilde{T}_{\mu\nu} = (\rho + p)u_\mu u_\nu + g_{\mu\nu}p$, where $\rho = \rho_m + \rho_\Lambda$ and $p = p_m - 3\zeta H + p_\Lambda$ are the total energy density and pressure, respectively. Further, we assume that the bulk viscous fluid is the non-relativistic matter with $p_m = 0$. Thus, the contribution to the total pressure is only due to the sum of negative viscous pressure, $-3\zeta H$ and vacuum energy pressure, $p_\Lambda = -\rho_\Lambda$.

Using the modified energy-momentum tensor as discussed above, the Einstein field equations (2.2) describing the evolution of FLRW Universe dominated by bulk viscous matter and vacuum energy yield

$$3H^2 = \rho = \rho_m + \rho_\Lambda, \tag{2.4}$$

$$2\dot{H} + 3H^2 = -p = 3\zeta H + \rho_\Lambda. \tag{2.5}$$

where $H = \dot{a}/a$ is the Hubble parameter and an over dot represents the derivative with respect to cosmic time t. In this chapter, we propose the evolution of the Universe based on decaying vacuum models, i.e., vacuum energy density as a function of the cosmic time. From (2.2), the Bianchi identity $\nabla^\mu G_{\mu\nu} = 0$ gives

$$\nabla^\mu \tilde{T}_{\mu\nu} = 0, \tag{2.6}$$

or, equivalently,

$$\dot{\rho}_m + 3H(\rho_m + p_m - 3\zeta H + \rho_\Lambda + p_\Lambda) = -\dot{\rho}_\Lambda, \tag{2.7}$$

which imply that the there is a coupling between a dynamical Λ term and viscous CDM. Therefore, there is some energy exchange between the viscous CDM fluid and vacuum. Using the equation of state of the vacuum energy $p_\Lambda = -\rho_\Lambda$ and $p_m = 0$, Eq. (2.7) leads to

$$\dot{\rho}_m + 3H(\rho_m - 3\zeta H) = -\dot{\rho}_\Lambda. \tag{2.8}$$

Now, combining (2.4) and (2.8), we get

$$\dot{H} + \frac{3}{2}H^2 = \frac{1}{2}\rho_\Lambda + \frac{3}{2}\zeta H. \tag{2.9}$$

The evolution equation (2.9) has three independent unknown quantities, namely, H, ζ and ρ_Λ. We get the solution only if ζ and ρ_Λ are specified. In what follows, we discuss the dynamics of the Universe depending on the specific forms of ρ_Λ and ζ.

2.3 Solution of field equations

In this chapter, we parameterize the functional form of ρ_Λ as a function of Hubble parameter. The motivation for a function $\rho_\Lambda = \rho_\Lambda(H)$ can be assumed from different points of view. Although the correct functional form of ρ_Λ is not known, a quantum

field theory (QFT) approach within the context of the renormalization group (RG) was proposed in Refs.[151, 152] and further studied by many authors [16, 17, 95, 100, 153, 154]. In Ref. [97], the following ratio has been defined between the two fluid components:

$$\gamma = \frac{\rho_\Lambda - \rho_{\Lambda_0}}{\rho_m + \rho_\Lambda}, \tag{2.10}$$

where ρ_{Λ_0} is a constant vacuum density. If $\rho_\Lambda = \rho_{\Lambda_0}$, then $\gamma = 0$, and we get ΛCDM model. On the other hand, if $\rho_{\Lambda_0} \neq 0$, then we get

$$\rho_\Lambda = \rho_{\Lambda 0} + \gamma(\rho_m + \rho_\Lambda) = \rho_{\Lambda 0} + 3\gamma H^2. \tag{2.11}$$

The above proposal was first considered by Shapiro and Solà [155] in context of RG. Many authors have studied the evolution of the Universe by assuming this form [96, 101, 107]. Hereafter, we shall focus on the simplest form of ρ_Λ which evolves with the Hubble rate. Specifically, in this chapter we consider

$$\rho_\Lambda = c_0 + 3\nu H^2, \tag{2.12}$$

where $c_0 = 3H_0^2(\Omega_{\Lambda 0} - \nu)$ is fixed by the boundary condition $\rho_\Lambda(H_0) = \rho_{\Lambda 0}$. The suffix '0' denotes the present value of the parameter. The dimensionless coefficient ν is the vacuum parameter and is expected to be very small value $|\nu| \ll 1$. A non-zero value of it makes possible the cosmic evolution of the vacuum.

The choice of ζ generates different viscous models and in literature there are different approaches to assume the evolution of bulk viscosity. In this chapter, we consider the most general form of the bulk viscous term ζ , which is assumed to be the sum of three terms: the first term is a constant, ζ_0, the second term is proportional to the Hubble parameter $H = \dot{a}/a$ which is related to the expansion and the third term is proportional to the acceleration, $\ddot{a}/\dot{a}$. Thus, we assume the parametrization of bulk viscous coefficient in the form[73, 141, 142, 143, 156, 157]

$$\zeta = \zeta_0 + \zeta_1 \frac{\dot{a}}{a} + \zeta_2 \frac{\ddot{a}}{\dot{a}}, \tag{2.13}$$

where ζ_0, ζ_1 and ζ_2 are constants to be determined by the observations. The term $\ddot{a}/\dot{a}$ in Eq. (2.13) can be written as $\ddot{a}/aH$. The basic idea about the assumption of ζ in Eq.(2.13) is that the dynamic state of the fluid influences its viscosity in which the transport viscosity is related to the velocity and acceleration.

Using Eqs.(2.12) and (2.13), the differential equation for the Hubble parameter (2.9) finally reduces to

$$\left(1-\frac{3}{2}\zeta_2\right)\dot{H}+\frac{3}{2}(1-\zeta_1-\zeta_2-\nu)H^2-\frac{3}{2}\zeta_0 H-\frac{1}{2}c_0=0, \tag{2.14}$$

which on integration, it gives

$$H=\frac{\zeta_0}{2(1-\zeta_1-\zeta_2-\nu)}+\sigma\left(\frac{1+e^{-3(1-\zeta_1-\zeta_2-\nu)\sigma t}}{1-e^{-3(1-\zeta_1-\zeta_2-\nu)\sigma t}}\right), \tag{2.15}$$

where $\sigma=\sqrt{\left(\frac{\zeta_0}{2(1-\zeta_1-\zeta_2-\nu)}\right)^2+\frac{H_0^2(\Omega_{\Lambda 0}-\nu)}{(1-\zeta_1-\zeta_2-\nu)}}$.

The above equation simplifies to give

$$H=\frac{\zeta_0}{2(1-\zeta_1-\zeta_2-\nu)}+\sigma\coth\left(\frac{3}{2}\frac{(1-\zeta_1-\zeta_2-\nu)\sigma}{(1-\frac{3}{2}\zeta_2)}t\right). \tag{2.16}$$

Using the Hubble parameter $H=\dot{a}/a$, the scale factor of the model $a(t)$ with the condition $a(t_0)=1$ is given by

$$a=e^{\frac{\zeta_0}{2(1-\zeta_1-\zeta_2-\nu)}t}\left[\sinh\left(\frac{3}{2}\frac{(1-\zeta_1-\zeta_2-\nu)\sigma}{(1-\frac{3}{2}\zeta_2)}t\right)\right]^{\frac{2(1-\frac{3}{2}\zeta_2)}{3(1-\zeta_1-\zeta_2-\nu)}}, \tag{2.17}$$

which shows that the scale factor increases exponentially as t increases. From (2.17), one can observe that, in general, it is not possible to express cosmic time t in terms of the scale factor a. It is possible only if the viscous coefficient terms are zero. In the absence of bulk viscosity, we obtain the result of decaying vacuum model as discussed in Ref.[100]. Further, for constant Λ, the solution reduced to the ΛCDM model with no viscosity.

It is worthwhile to compute the evolution of matter energy density as a function of scale factor (or redshift) or function of cosmic time. Using (2.12) and (2.13), the continuity equation (2.8) takes the form

$$\dot{\rho_m}+3(1-\nu)H\rho_m=9(1-\nu)\left(\zeta_0+\zeta_1\frac{\dot{a}}{a}+\zeta_2\frac{\ddot{a}}{\dot{a}}\right)H^2. \tag{2.18}$$

The solution of above equation involves a big expression. Therefore, we avoid to write the expression for matter density. However, we present the numerical solution of this equation for different combinations of viscous and ν terms in Fig. 2.1. It is observed

that the matter energy density decreases as t increases and it approaches to the finite value as $t \to \infty$. However, in the absence of viscous terms, $\rho_m \to 0$ as $t \to \infty$.

Using (1.65), the deceleration parameter is calculated as

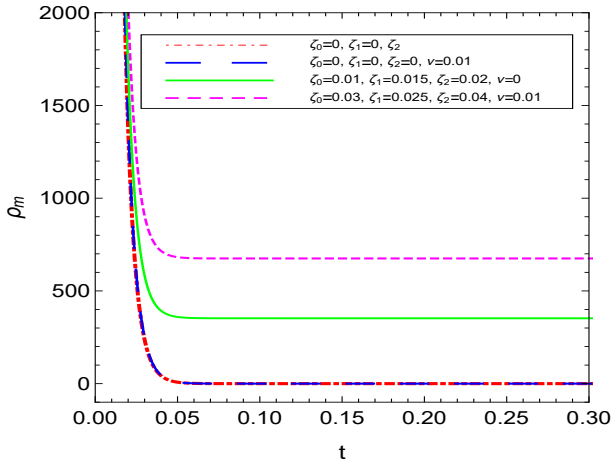

Figure 2.1: The matter energy density as a function of cosmic time t for decaying vacuum with $\zeta = \zeta_0 + \zeta_1 \frac{\dot{a}}{a} + \zeta_2 \frac{\ddot{a}}{\dot{a}}$

.

$$q = -1 + \frac{3}{2} \frac{\frac{(1-\zeta_1-\zeta_2-\nu)}{(1-\frac{3}{2}\zeta_2)} \sigma^2 \csc^2 h(\frac{3}{2} \frac{(1-\zeta_1-\zeta_2-\nu)}{(1-\frac{3}{2}\zeta_2)} \sigma t)}{\left(\frac{\zeta_0}{2(1-\zeta_1-\zeta_2-\nu)} + \sigma \coth(\frac{3}{2} \frac{(1-\zeta_1-\zeta_2-\nu)}{(1-\frac{3}{2}\zeta_2)} \sigma t) \right)^2}. \tag{2.19}$$

From (2.19), we observe that the model transits from decelerated phase to accelerated phase. As t increases, the deceleration parameter decreases and as $t \to \infty$, it approaches to $q = -1$. The rate of deceleration parameter attaining to -1 depends on the viscous terms.

For sake of completeness, we discuss another important cosmological parameter, known as effective equation of state (EoS) parameter. Using (2.16), Eq.(1.67) gives

$$w_{eff} = -1 + \frac{\frac{(1-\zeta_1-\zeta_2-\nu)}{(1-\frac{3}{2}\zeta_2)} \sigma^2 \csc^2 h(\frac{3}{2} \frac{(1-\zeta_1-\zeta_2-\nu)}{(1-\frac{3}{2}\zeta_2)} \sigma t)}{\left(\frac{\zeta_0}{2(1-\zeta_1-\zeta_2-\nu)} + \sigma \coth(\frac{3}{2} \frac{(1-\zeta_1-\zeta_2-\nu)}{(1-\frac{3}{2}\zeta_2)} \sigma t) \right)^2}. \tag{2.20}$$

It can be observed that the effective EoS parameter decreases to negative values and finally saturated to $w_{eff} = -1$ corresponding to a de Sitter epoch in future time of evolution.

2.4 Some particular solutions

In order to calculate specific expressions for cosmological parameters of viscous model with decaying vacuum energy, let us analyze three particular popular proposals depending on the choice of ζ defined in Eq.(2.13)

***Case I*: $\zeta = \zeta_0$ = const**

This is the simplest parametrization of Eckart's bulk viscosity model. Many authors [75, 117, 128, 129, 130, 144, 145, 158, 159, 160] have studied the viscous cosmological models with constant bulk viscous coefficient. In this case, the evolution equation (2.14) reduces to

$$\dot{H} + \frac{3}{2}(1-\nu)H^2 - \frac{3}{2}\zeta_0 H = \frac{1}{2}c_0. \tag{2.21}$$

Solving (2.21) or directly taking $\zeta_1 = \zeta_2 = 0$ in (2.16), for $\nu < 1$, we get

$$H = \frac{\zeta_0}{2(1-\nu)} + \sigma_1 \coth\left(\frac{3}{2}(1-\nu)\sigma_1 t\right), \tag{2.22}$$

where

$\sigma_1 = \sqrt{(\frac{\zeta_0}{2(1-\nu)})^2 + \frac{H_0^2(\Omega_{\Lambda 0}-\nu)}{(1-\nu)}}$. It can be observed that the solution reduces to the standard Λ for $\zeta_0 = 0$ and $\nu = 0$, whereas for $\zeta_0 = 0$ and $\nu \neq 0$ it gives the solution for $\Lambda(t)$ model from quantum field theory[100]. The scale factor is given by

$$a(t) = e^{\frac{\zeta_0}{2(1-\nu)}t}\left(\sinh(\frac{3}{2}(1-\nu)\sigma_1 t)\right)^{\frac{2}{3(1-\nu)}}, \tag{2.23}$$

which shows that the scale factor increases exponentially as t increases. From (2.23), one can observe that, in general, it is not possible to express cosmic time t in terms of the scale factor a. It is possible only if $\zeta_0 = 0$. In the absence of bulk viscosity, we obtain the result of decaying vacuum model as discussed in Ref.[100]. Further, for constant Λ, the solution reduced to the ΛCDM model with no viscosity.

The deceleration parameter and effective EoS parameter are respectively given by

$$q = -1 + \frac{3}{2}\frac{(1-\nu)\sigma_1^2 \csc^2 h(\frac{3}{2}(1-\nu)\sigma_1 t)}{\left(\frac{\zeta_0}{2(1-\nu)} + \sigma_1 \coth(\frac{3}{2}(1-\nu)\sigma_1 t)\right)^2}, \tag{2.24}$$

and

$$w_{eff} = -1 + \frac{(1-\nu)\sigma_1^2 \csc^2 h(\frac{3}{2}(1-\nu)\sigma_1 t)}{\left(\frac{\zeta_0}{2(1-\nu)} + \sigma_1 \coth(\frac{3}{2}(1-\nu)\sigma_1 t)\right)^2}. \tag{2.25}$$

The time evolutions of q and w_{eff} are similar to the evolutions of these parameters as discussed for general form of viscous term in Sect. 2.3.

The continuity equation (2.18) in this case has the form

$$\dot{\rho_m} + 3(1-\nu)H\rho_m = 9(1-\nu)\zeta_0 H^2 \tag{2.26}$$

Solving (2.26), one may find the time evolution of the matter density. We will only present a numerical solution of this equation. In Fig. 2.2 we plot the time evolution of matter energy density $\rho_m(t)$ for different combinations of ζ_0 and ν. This figure shows that the matter density diverges at beginning of the cosmic evolution and decreases as t increases, and finally approaches to a finite value as $t \to \infty$ for $\zeta \neq 0$ and $\nu \neq 0$. In the absence of viscosity or decaying vacuum energy, the matter energy density tends to zero as $t \to \infty$.

Case II: $\zeta = \zeta_0 + \zeta_1 H$

We assume that the bulk viscous coefficient is a linear combination of two terms: ζ_0 and $\zeta_1 H$, i.e., $\zeta = \zeta_0 + \zeta_1 H$. In literature, many authors [72, 142, 143] have assumed such a form of ζ to study the dynamics of Universe. In this case, Eq.(2.14) reduces to

$$\dot{H} + \frac{3}{2}(1-\zeta_1-\nu)H^2 - \frac{3}{2}\zeta_0 H = \frac{1}{2}c_0. \tag{2.27}$$

Solving Eq. (2.27) or directly putting $\zeta_2 = 0$ in Eq.(2.16), the solution for Hubble parameter for $(\zeta_1 + \nu) < 1$ is given by

$$H = \frac{\zeta_0}{2(1-\zeta_1-\nu)} + \sigma_2 \coth\left(\frac{3}{2}(1-\zeta_1-\nu)\sigma_2 t\right), \tag{2.28}$$

where $\sigma_2 = \sqrt{\left(\frac{\zeta_0}{2(1-\zeta_1-\nu)}\right)^2 + \frac{H_0^2(\Omega_{\Lambda 0}-\nu)}{(1-\zeta_1-\nu)}}$. The corresponding expression for the scale factor in normalized unit has the form

$$a = e^{\frac{\zeta_0}{2(1-\zeta_1-\nu)}t}\left[\sinh\left(\frac{3}{2}(1-\zeta_1-\nu)\sigma_2 t\right)\right]^{\frac{2}{3(1-\zeta_1-\nu)}}. \tag{2.29}$$

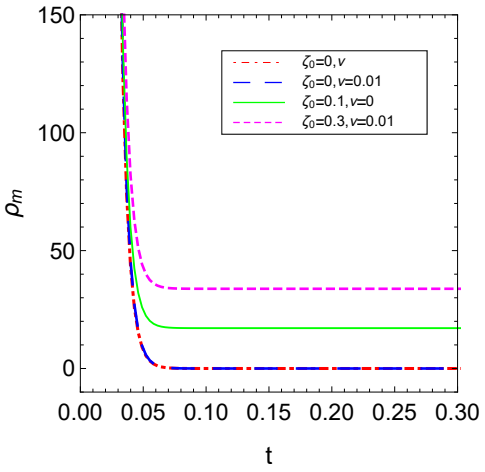

Figure 2.2: The time evolution of matter energy density for decaying vacuum model with viscosity $\zeta = \zeta_0$.

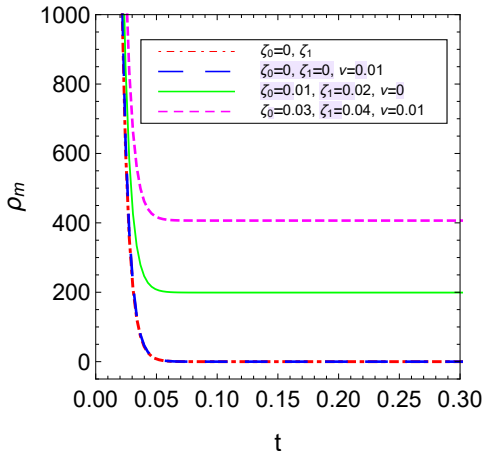

Figure 2.3: The time evolution of matter energy density for decaying vacuum model with viscosity $\zeta = \zeta_0 + \zeta_1 H$

The respective deceleration parameter and effective EoS parameter are calculated as

$$q = -1 + \frac{3(1-\zeta_1-\nu)\sigma_2^2 \csc^2 h(\frac{3}{2}(1-\zeta_1-\nu)\sigma_2 t)}{2\left(\frac{\zeta_0}{2(1-\zeta_1-\nu)} + \sigma_2 \coth(\frac{3}{2}(1-\zeta_1-\nu)\sigma_2 t)\right)^2}, \tag{2.30}$$

and

$$w_{eff} = -1 + \frac{(1-\zeta_1-\nu)\sigma_2^2 \csc^2 h(\frac{3}{2}(1-\zeta_1-\nu)\sigma_2 t)}{\left(\frac{\zeta_0}{2(1-\zeta_1-\nu)} + \sigma_2 \coth(\frac{3}{2}(1-\zeta_1-\nu)\sigma_2 t)\right)^2}. \tag{2.31}$$

The time evolutions of q and w_{eff} are similar to the evolutions of these parameters as discussed for general form of viscous term in Sect.2.3.

The continuity equation (2.18) in this case has the form

$$\dot{\rho_m} + 3(1-\nu)H\rho_m = 9(1-\nu)(\zeta_0 H^2 + \zeta_1 H^3). \tag{2.32}$$

We only present a numerical solution of Eq.(2.32). In Fig. 2.3 we plot the time dependent matter energy density $\rho_m(t)$ for different combinations of ζ_0, ζ_1 and ν. It is observed from figure that the matter density diverges at beginning of the cosmic evolution and decreases as time passes, and finally approaches to a finite value as $t \to \infty$ for $\zeta \neq 0$, $\zeta_1 \neq 0$ and $\nu \neq 0$. In the absence of viscous terms or decaying vacuum energy, the matter energy density tends to zero as $t \to \infty$.

Case III: $\zeta = \zeta_1 H$

Finally, let us consider the case where bulk viscous coefficient is proportional to the Hubble parameter, i.e., $\zeta = \zeta_1 H$. Such a form of ζ has been studied by many authors [115, 116, 117, 131, 142, 146]. In this case, the evolution equation (2.14) for Hubble parameter reduces to

$$\dot{H} + \frac{3}{2}(1-\zeta_1-\nu)H^2 - \frac{1}{2}c_0 = 0. \tag{2.33}$$

The above equation with change of a variable from t to $x = \ln a$ can be written as

$$\frac{dh^2}{dx} + 3(1-\zeta_1-\nu)h^2 = 3(\Omega_{\Lambda 0}-\nu), \tag{2.34}$$

where $h = H/H_0$ is the dimensionless Hubble parameter and $\Omega_{\Lambda 0} = \rho_{\Lambda 0}/3H_0^2$. Assuming $(\zeta_1+\nu) < 1$ and using the normalized scale factor -redshift relation, $a = (1+z)^{-1}$, we can express the normalized Hubble function $E(z) \equiv H(z)/H_0$ as

$$E(z) = \frac{1}{(1-\zeta_1-\nu)^{1/2}} \times \left[(1-\zeta_1-\Omega_{\Lambda 0})(1+z)^{3(1-\zeta_1-\nu)} + \Omega_{\Lambda 0} - \nu\right]^{1/2}. \tag{2.35}$$

From the above equation, it is clear that for $\nu = 0$ and $\zeta_1 = 0$, we recover exactly the ΛCDM expansion model whereas only $\zeta_1 = 0$ gives the solution obtained in Ref.[107]. It is observed that at very late time we get an cosmological constant dominated era, $H \approx H_0\sqrt{\frac{\Omega_{\Lambda 0}-\nu}{(1-\zeta_1-\nu)}}$, which implies a de Sitter phase of the scale factor. Using $H = \dot{a}/a$, the solution for the scale factor in terms of cosmic time t is given by

$$a = \left(\frac{(1-\zeta_1-\Omega_{\Lambda 0})}{\Omega_{\Lambda 0}-\nu}\right)^{\frac{1}{3(1-\zeta_1-\nu)}} \times \left[\sinh\left(\frac{3}{2}\sqrt{(1-\zeta_1-\nu)(\Omega_{\Lambda 0}-\nu)}\, H_0\, t\right)\right]^{\frac{2}{3(1-\zeta_1-\nu)}} \tag{2.36}$$

It can be observed that the scale factor evolves as power-law expansion, i.e., $a \propto t^{2/3(1-\zeta_1-\nu)}$ for small values of t whereas it expands exponentially, i.e., $a \propto \exp\sqrt{\frac{(\Omega_{\Lambda 0}-\nu)}{3(1-\zeta_1-\nu)}}H_0 t$ for large values of time t. In other words, the model expands with decelerated rate in early time of its evolution and expands with accelerated rate in late time of its evolution.

From Eq. (2.36), we can find the cosmic time in terms of the scale factor, which is given by

$$t(a) = \frac{2}{3H_0\sqrt{(1-\zeta_1-\nu)(\Omega_{\Lambda 0}-\nu)}} \sinh^{-1}\left[\left(\frac{a}{a_I}\right)^{\frac{3(1-\zeta_1-\nu)}{2}}\right] \tag{2.37}$$

where $a_I = \left(\frac{(1-\zeta_1-\Omega_{\Lambda 0})}{(\Omega_{\Lambda 0}-\nu)}\right)^{1/3(1-\zeta_1-\nu)}$.

Using (2.35), the value of q in terms of redshift is calculated as

$$q(z) = -1 + \frac{3}{2}\frac{(1-\zeta_1-\Omega_{\Lambda 0})(1+z)^{3(1-\zeta_1-\nu)}}{\left[\frac{(\Omega_{\Lambda 0}-\nu)}{(1-\zeta_1-\nu)} + \left(1-\frac{(\Omega_{\Lambda 0}-\nu)}{(1-\zeta_1-\nu)}\right)(1+z)^{3(1-\zeta_1-\nu)}\right]} \tag{2.38}$$

The above equation shows that the dynamics of q depends on the redshift which describes the transition of the Universe from decelerated to accelerated phase. We observe that as $z \to -1$, $q(z)$ approaches to -1. However, the model decelerates or accelerates if $\Omega_{\Lambda 0} = \nu$, which gives $q = -1 + 1.5(1-\zeta_1-\nu)$. Thus, a cosmological constant is required for a transition phase. Also, for $z = 0$, we find the present value of q which is given by

$$q_0 = -1 + 1.5(1-\zeta_1-\Omega_{\Lambda 0}). \tag{2.39}$$

The transition redshift, z_{tr} of the Universe can be calculated as

$$z_{tr} = -1 + \left(\frac{2(\Omega_{\Lambda 0}-\nu)}{(3(1-\zeta_1-\nu)-2)(1-\zeta_1-\Omega_{\Lambda 0})}\right)^{\frac{1}{3(1-\zeta_1-\nu)}}. \tag{2.40}$$

In this case, the effective EoS parameter is defined by $w_{eff} = -1 - \frac{1}{3}\frac{d\ln h^2}{dx}$, where $x = \ln a$ and $h = H/H_0$. Using Eq. (2.35), we get

$$w_{eff}(z) = -1 + \frac{(1-\zeta_1-\Omega_{\Lambda 0})(1+z)^{3(1-\zeta_1-\nu)}}{\left[\frac{(\Omega_{\Lambda 0}-\nu)}{(1-\zeta_1-\nu)} + \left(1-\frac{(\Omega_{\Lambda 0}-\nu)}{(1-\zeta_1-\nu)}\right)(1+z)^{3(1-\zeta_1-\nu)}\right]} \tag{2.41}$$

The present value of w_{eff} at $z = 0$ is given by

$$w_{eff}(z=0) = -1 + (1-\zeta_1-\Omega_{\Lambda 0}). \tag{2.42}$$

We can observe that the model will accelerate provided $3w_{eff}(z=0)+1 = -2+3(1-\zeta_1-\Omega_{\Lambda 0}) < 0$.

Let us discuss the behavior of the matter energy density in this model as a function of scale factor (or redshift). Transforming the time derivative into derivative with respect to the scale factor, the conservation equation (2.18) reduces to a differential equation for matter density,

$$\frac{d\rho_m}{da} + \frac{3(1-\nu)}{a}\rho_m = \frac{9(1-\nu)\zeta_1}{a}H^2, \tag{2.43}$$

Using (2.35) into (2.43) and integrating, we find

$$\rho_m = \left(\rho_{m0} - \frac{3\zeta_1 H_0^2(\Omega_{\Lambda 0} - \nu)}{(1-\zeta_1-\nu)}\right) a^{-3(1-\zeta_1-\nu)} + \frac{3\zeta_1 H_0^2(\Omega_{\Lambda 0} - \nu)}{(1-\zeta_1-\nu)}, \tag{2.44}$$

where $\rho_{m0} = \rho_m(a=1)$ is the present matter density. Substituting Eq. (2.36) in the above equation, one may obtain the explicit time evolution of the matter density if desired. It can be observed from Eq. (2.44) that the matter density does no longer evolve as $\rho_m = \rho_{m0}\, a^{-3}$. There is a correction in the exponent of the scale factor and some additional constant terms. This is due to the fact that matter is exchanging energy from vacuum and viscous term. We also note that as $t \to \infty$, $\rho_m = 3\zeta_1 H_0^2(\Omega_{\Lambda 0} - \nu)/(1-\zeta_1-\nu)$, i.e, matter density does not approach zero in infinitely far future due to viscosity. In the absence of viscous term, the matter density tends to zero as $t \to \infty$. The detail discussion on the evolutions of matter energy density and other cosmological parameters of this particular model is presented in Section 2.7.

In the following Section, we constrain the parameters of this model by using the latest observational data sets and analyze the evolutions of all above discussed various cosmological parameters using the best-fit values. We compare the proposed model with the existing model through the stability criteria.

2.5 Growth of perturbations

In cosmic structure formation it is assumed that the present abundant structure of the Universe is developed through gravitational amplification of small density perturbations generated in its early evolution. In this section, we briefly discuss the linear perturbation within the framework of viscous fluid with varying $\Lambda(t)$. We refer the reader to Refs. [161, 162] for the detailed perturbation equations since here we have discussed some basic equations only. The differential equation for the matter density contrast $\delta_m \equiv \delta\rho_m/\rho_m$ for our model considered here can be approximated as follows [163]:

$$\delta_m'' + \left(\frac{3}{a} + \frac{H'(a)}{H(a)}\right)\delta_m' - \frac{4\pi G\rho_m}{H^2(a)}\frac{\delta_m}{a^2} = 0 \tag{2.45}$$

where prime represents derivative with respect to the scale factor a. The above second-order differential equation turns out to be accurate since the main effects come from the different expression of the Hubble function. We consider the Hubble function as obtained in *case III of Sect. 2.4*. Equation (2.45) describes the smoothness

of the matter perturbation in extended viscous $\Lambda(t)$ model.

The linear growth rate of the density contrast, f, which is related to the peculiar velocity in the linear theory [164] is defined as

$$f(a) = \frac{d\ln D_m(a)}{d\ln a}, \tag{2.46}$$

where $D_m(a) = \delta_m(a)/\delta_m(a=1)$ is the linear growth function. The weighted linear growth rate, denoted by $f\sigma_8$, is the product of the growth rate $f(z)$, defined in (2.46), and $\sigma_8(z)$. Here, σ_8 is the root-mean-square fluctuation in spheres with radius $8h^{-1}$ Mpc scales [165, 166], and it is given by [167]

$$\sigma_8(z) = \frac{\delta_m(z)}{\delta_m(z=0)}\sigma_8(z=0). \tag{2.47}$$

Using (2.46) and (2.47), the weighted linear growth rate is given by

$$f\sigma_8(z) = -(1+z)\frac{\sigma_8(z=0)}{\delta_m(z=0)}\frac{d\delta_m}{dz}. \tag{2.48}$$

In what follows, we perform the observational analysis of case III of Section 2.4 to estimate the parameters of the model and analyse the evolution and dynamics of the model in detail.

2.6 Data and methodology

In this section, we present the data and methodology used in this work. We constrain the parameters of the $GR-\Lambda$CDM and $\zeta = \zeta_1 H$ with varying Λ models using a large, robust and latest set of observational data which involve observations from: (i) distant type Ia supernovae (SNe Ia); (ii) a compilation of cosmic chronometer measurements of Hubble parameter $H(z)$ at different redshifts; (iii) baryonic acoustic oscillations (BAO); and (iv) $f(z)\sigma_8(z)$ data. A brief description of each of datasets are as follows:

- **SNe Ia sample (Pantheon data):** We use the recent SNe Ia data points, the so-called Pantheon sample which includes 1048 data points of luminosity distance in the redshift range $0.01 < z < 2.26$ [37].
- **BAO measurements:** We have used 6 points of BAO data-sets from several surveys, which includes the Six Degree Field Galaxy Survey (6dFGS),the Sloan

Digital Sky Survey (SDSS), and the LOWZ samples of the Baryon Oscillation Spectroscopic Survey(BOSS))[52, 168, 169].

- **Hubble measurements $H(z)$ (CC):** We use 32 CC data points of the Hubble parameter measured by differential age technique [41] between the redshift range $0.07 \leq z \leq 1.965$ and are determined by cosmic chronometric technique (CC).
- $\mathbf{f(z)\sigma_8(z)}$ **data :** We use 18 data points of "Gold -17" compilation of robust and independent measurements of weighted linear growth $f(z)\sigma_8(z)$ obtained by various galaxy surveys as complied in Table III as mentioned in [58].

Using the observational data as discussed above, we use the Markov Chain Monte Carlo (MCMC) method by employing EMCEE python package [36] to explore the parameter spaces of viscous model with decaying vacuum density as discussed in case III of Sect. 2.4 by utilizing different combinations of data sets. The combinations are as follows:

- **BASE**: The combination of two datasets $SNe\ Ia + BAO$ is termed as "BASE", whose the joint χ^2 function is defined as $\chi^2_{tot} = \chi^2_{SNe\ Ia} + \chi^2_{BAO}$.
- $+\mathbf{CC}$: We combine CC data to the BASE, where $\chi^2_{tot} = \chi^2_{SNe\ Ia} + \chi^2_{BAO} + \chi^2_{H(z)}$.
- $+\mathbf{f\sigma_8(z)}$: The BASE data is complemented with CC and $f\sigma_8$, where $\chi^2_{tot} = \chi^2_{SNe\ Ia} + \chi^2_{BAO} + \chi^2_{H(z)} + \chi^2_{f\sigma_8}$.

We consider the ΛCDM model as a reference model and its parameters are also constrained with the above sets of data.

2.7 Results and Discussion

In this section, we present the main results obtained through the observational data on the viscous $\Lambda(t)$ model of the form $\zeta = \zeta_1 H$ with $\Lambda = c_0 + 3\nu H^2$ (Refers to case III of Sect.2.4). We also present the cosmological observation for ΛCDM model using the three combination of datasets. The viscous $\Lambda(t)$ model has 4 free parameter spaces $\{H_0, \Omega_\Lambda, \zeta_1, \nu\}$, where as ΛCDM has 2 free parameters $\{H_0, \Omega_\Lambda\}$. We calculate the best-fit values by minimizing the combination of χ^2 function for above defined data sets. We also provide the fitting values of the ΛCDM for comparison with the viscous

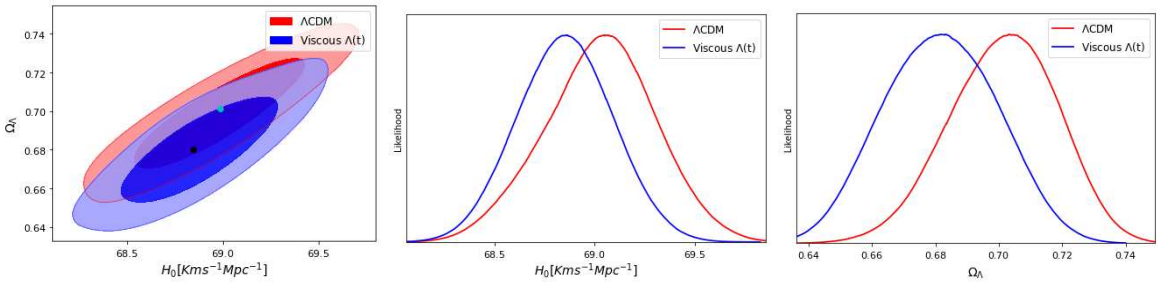

Figure 2.4: Two-dimensional confidence contours of the $H_0 - \Omega_\Lambda$ and one dimensional posterior distributions of H_0, Ω_Λ for the ΛCDM and viscous $\Lambda(t)$ models using "*BASE*" data. The green and black dot on the contour represents the best fit value of ΛCDM and viscous $\Lambda(t)$ models respectively.

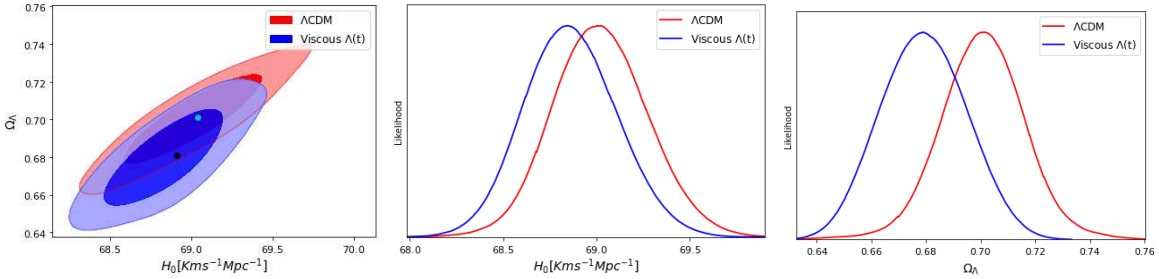

Figure 2.5: Two-dimensional confidence contours of the $H_0 - \Omega_\Lambda$ and one dimensional posterior distributions of H_0, Ω_Λ for the ΛCDM and viscous $\Lambda(t)$ models using "$+CC$" data. The green and black dot on the contour represents the best fit value of ΛCDM and viscous $\Lambda(t)$ models respectively.

$\Lambda(t)$ model. The constraints of the statistical study are presented in Tables 2.1 and 2.2. Figures 2.4–2.6 show the $1\sigma(68.3\%)$ and $2\sigma(95.4\%)$ confidence level (CL) contours with marginalized likelihood distributions for the cosmological parameters of ΛCDM and viscous $\Lambda(t)$ models considering combination of different datasets, respectively. It is observed from Tables 2.1 and 2.2 that the constraints on the parameter spaces of ΛCDM and viscous with $\Lambda(t)$ are nearly the same.

Using best-fit values of parameters obtained from $BASE$, $+CC$ and $+f\sigma_8$ data into Eq.(2.38), the evolutions of the deceleration parameter with respect to the redshift are shown in Figs.2.7–2.9 for viscous $\Lambda(t)$ model along with the ΛCDM model. It is observed that with each data set $q(z)$ varies from positive to negative and show the similar trajectory that is comparable to the ΛCDM model. Thus, both the models depict a transition from the early decelerated phase to the late-time accelerated phase. Further, $q(z)$ approaches to -1 in late-time of evolution. Thus, the models successfully generate late-time cosmic acceleration along with a decelerated expansion in the past. Figures 2.7–2.9 show that the transition from decelerated to accelerated phase

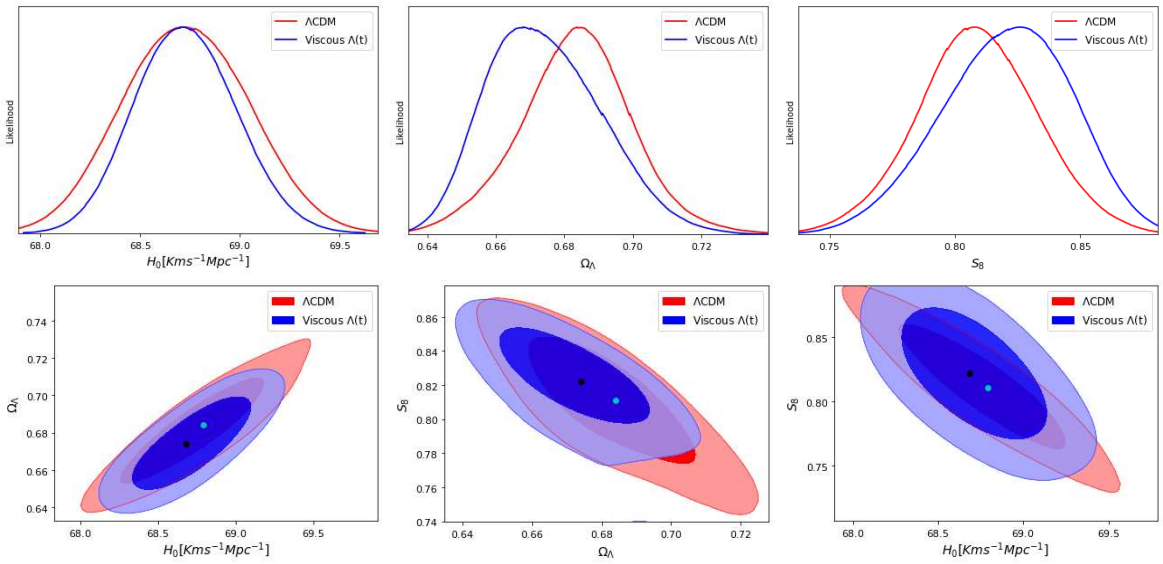

Figure 2.6: Two-dimensional confidence contours of $H_0 - \Omega_\Lambda$, $\Omega_\Lambda - S_8$ and $H_0 - S_8$ and one-dimensional posterior distributions of H_0, Ω_Λ and S_8 for the ΛCDM and viscous $\Lambda(t)$ models using "$+ f\sigma_8$" data. The green and black dot on the contour represents the best fit value of ΛCDM and viscous $\Lambda(t)$ models respectively.

Table 2.1: Constraints on parameters of ΛCDM for different set of observation data. Here "BASE" denotes "SNe Ia+BAO".

ΛCDM			
Parameter	BASE	+CC	$+f\sigma_8$
H_0	$68.987^{+0.263}_{-0.276}$	$69.001^{+0.238}_{-0.223}$	$68.793^{+0.193}_{-0.221}$
Ω_Λ	$0.701^{+0.013}_{-0.020}$	$0.699^{+0.016}_{-0.015}$	$0.684^{+0.015}_{-0.014}$
σ_8	–	–	$0.794^{+0.014}_{-0.015}$
S_8	–	–	$0.811^{+0.022}_{-0.022}$
z_{tr}	$0.670^{+0.038}_{-0.038}$	$0.674^{+0.035}_{-0.035}$	$0.625^{+0.041}_{-0.041}$
q_0	$-0.549^{+0.020}_{-0.023}$	$-0.551^{+0.020}_{-0.020}$	$-0.523^{+0.025}_{-0.025}$
w_0	$-0.699^{+0.013}_{-0.015}$	$-0.701^{+0.013}_{-0.013}$	$-0.682^{+0.017}_{-0.017}$
$t_0(Gyr)$	$13.73^{+0.017}_{-0.017}$	$13.69^{+0.015}_{-0.015}$	$13.54^{+0.013}_{-0.013}$

Table 2.2: Constraints on parameters of viscous Λ(t) model using different set of observation data.

Viscous Λ(t)			
Parameter	BASE	+CC	$+f\sigma_8$
H_0	$68.843^{+0.274}_{-0.238}$	$68.913^{+0.262}_{-0.261}$	$68.684^{+0.259}_{-0.241}$
Ω_Λ	$0.680^{+0.018}_{-0.020}$	$0.684^{+0.013}_{-0.020}$	$0.674^{+0.012}_{-0.016}$
ζ_1	$0.006^{+0.007}_{-0.004}$	$0.006^{+0.008}_{-0.004}$	$0.003^{+0.005}_{-0.002}$
ν	$0.004^{+0.003}_{-0.003}$	$0.003^{+0.004}_{-0.002}$	$0.003^{+0.004}_{-0.002}$
σ_8	–	–	$0.790^{+0.008}_{-0.010}$
S_8	–	–	$0.822^{+0.019}_{-0.019}$
z_{tr}	$0.664^{+0.031}_{-0.042}$	$0.665^{+0.031}_{-0.037}$	$0.626^{+0.028}_{-0.038}$
q_0	$-0.533^{+0.025}_{-0.020}$	$-0.535^{+0.023}_{-0.020}$	$-0.516^{+0.022}_{-0.017}$
w_0	$-0.689^{+0.017}_{-0.013}$	$-0.690^{+0.015}_{-0.013}$	$-0.677^{+0.014}_{-0.011}$
$t_0(Gyr)$	$13.52^{+0.019}_{-0.019}$	$13.48^{+0.017}_{-0.017}$	$13.47^{+0.013}_{-0.015}$

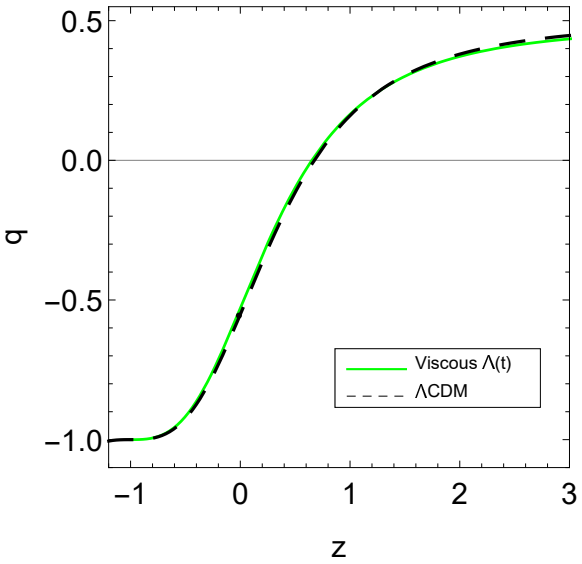

Figure 2.7: The redshift evolution of the deceleration parameter for viscous $\Lambda(t)$ using "*BASE*" dataset. The evolution of deceleration parameter in the standard ΛCDM model is also shown as the dashed curve. A dot denotes the current value of q (hence q_0).

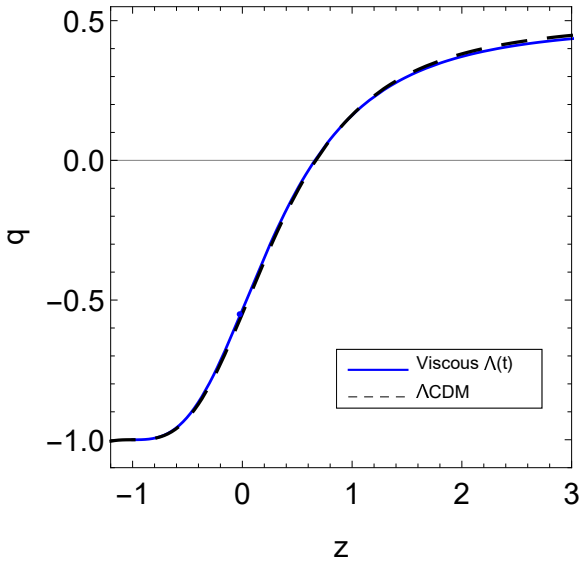

Figure 2.8: The redshift evolution of the deceleration parameter for viscous $\Lambda(t)$ using "$+CC$" dataset. The evolution of deceleration parameter in the standard ΛCDM model is also shown as the dashed curve. A dot denotes the current value of q (hence q_0).

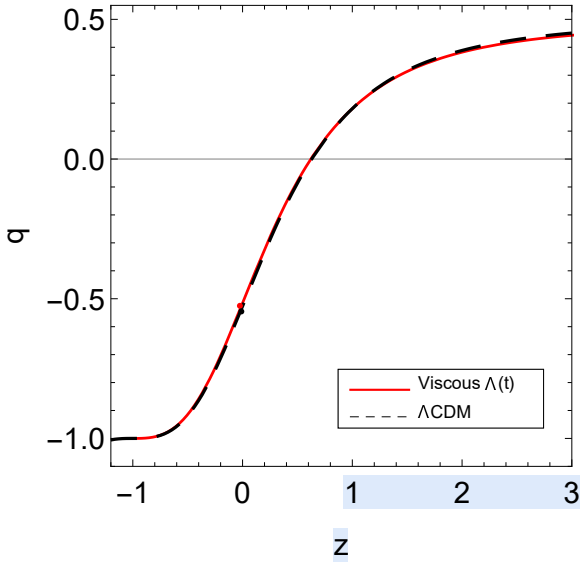

Figure 2.9: The redshift evolution of the deceleration parameter for viscous $\Lambda(t)$ using "$+f\sigma_8$" dataset. The evolution of deceleration parameter in the standard ΛCDM model is also shown as the dashed curve. A dot denotes the current value of q (hence q_0).

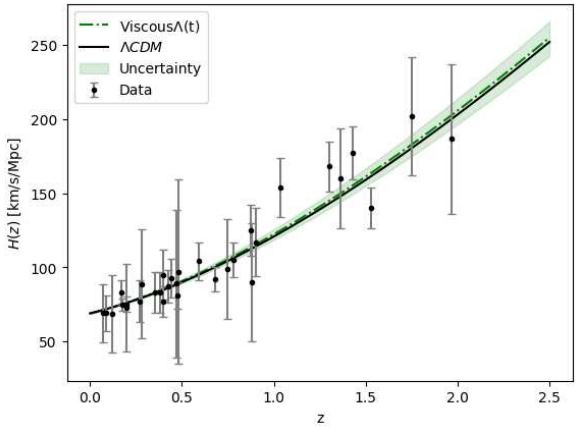

Figure 2.10: Best fits using "*BASE*" data set over $H(z)$ data for viscous $\Lambda(t)$ (green dot-dashed line) and ΛCDM (black solid line) are shown. The grey points with uncertainty bars correspond to the 32 *CC* sample.

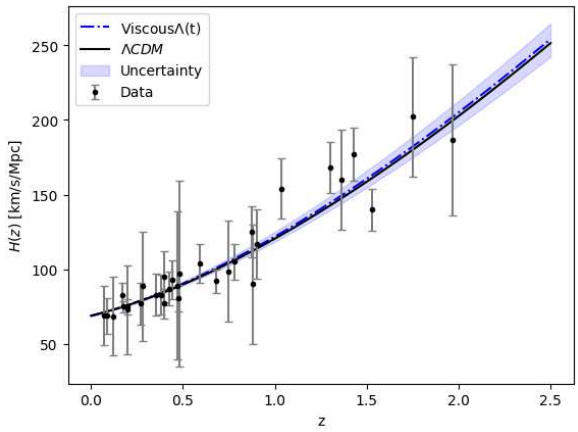

Figure 2.11: Best fits using "$+CC$" data set over $H(z)$ data for viscous $\Lambda(t)$ (blue dot-dashed line) and ΛCDM (black solid line) are shown. The grey points with uncertainty bars correspond to the 32 *CC* sample.

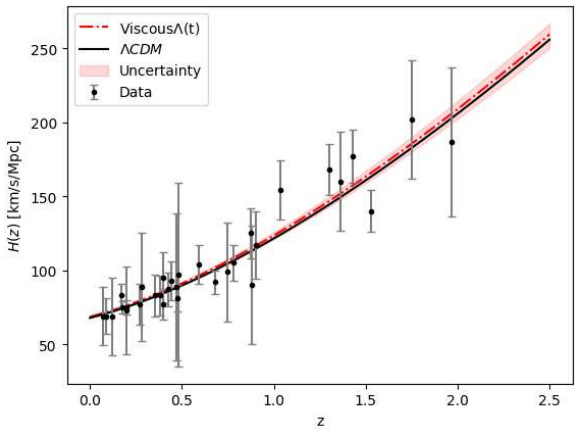

Figure 2.12: Best fits using "$+f\sigma_8$" data set over $H(z)$ data for viscous $\Lambda(t)$ (red dot-dashed line) and ΛCDM (black solid line) are shown. The grey points with uncertainty bars correspond to the 32 *CC* sample.

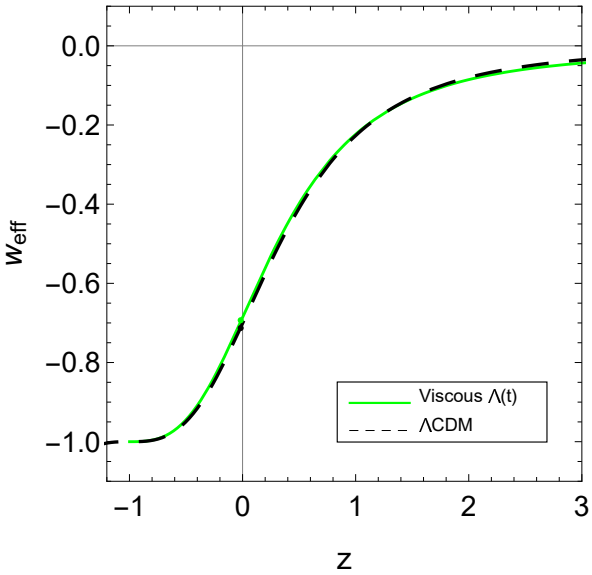

Figure 2.13: Effective EoS parameter as a function of redshift z for viscous $\Lambda(t)$ using "*BASE*" dataset. The evolution of EoS parameter in the standard ΛCDM model is also represented as the dashed curve. A dot denotes the present value of the EoS parameter.

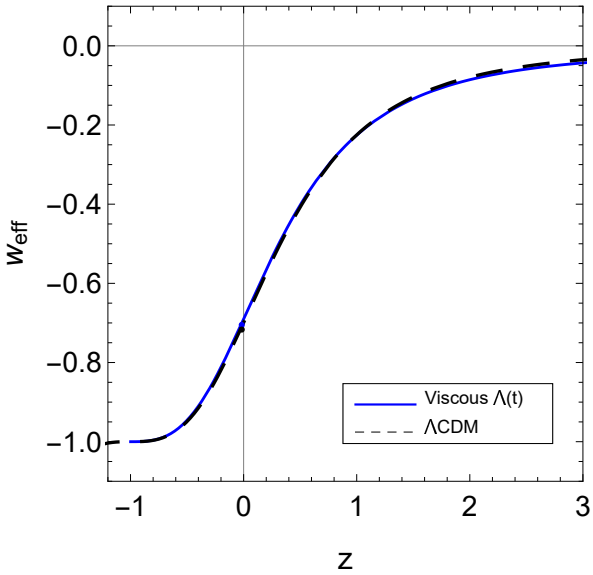

Figure 2.14: Effective EoS parameter as a function of redshift z for viscous $\Lambda(t)$ using "$+CC$" dataset. The evolution of EoS parameter in the standard ΛCDM model is also represented as the dashed curve. A dot denotes the present value of the EoS parameter.

take place at redshift $z_{tr} = 0.664^{+0.031}_{-0.042}$ with *BASE* data, $z_{tr} = 0.665^{+0.031}_{-0.037}$ with $+CC$ data and $z_{tr} = 0.626^{+0.028}_{-0.037}$ with $+f\sigma_8$ data. The datasets *BASE*, $+CC$ and $+f\sigma_8$ yield the present deceleration parameter q_0 as $-0.533^{+0.025}_{-0.020}$, $-0.535^{+0.023}_{-0.020}$ and $-0.516^{+0.022}_{-0.017}$ respectively (cf. Table 2.2). The present values of z_{tr} and q_0 are very close and thus are in good agreement to ΛCDM as presented in Table 2.1.

The evolutions of the Hubble parameter $H(z)$ of viscous $\Lambda(t)$ model with respect to the redshift are shown in Figs. 2.10–2.12. Throughout the expansion, viscous $\Lambda(t)$ is coinciding with the ΛCDM model and the model paths cover majority of the dataset with the error bar of Hubble parameter, indicating that the viscous $\Lambda(t)$ agrees well with the ΛCDM model for all the three combination of datasets. In the considered cosmological scenario, the present age of the Universe are found to be $t_0 \approx 13.52\ Gyr$, $t_0 \approx 13.48\ Gyr$ and $t_0 \approx 13.47\ Gyr$ respectively as presented in Table 2.2. The ages thus obtained are very much compatible with that obtained from the ΛCDM model with the same datasets (cf.Table 2.1).

Using the best-fit values of parameters in Eq.(2.41) , the evolutions of the effective EoS parameter w_{eff} are shown in Figs. 2.13–2.15. We conclude that for large redshifts, w_{eff} has small negative value $w_{eff} > -1/3$ and in future the model asymptotically approaches to $w_{eff} = -1$. The trajectory of w_{eff} for *BASE* and $+CC$ datasets coincides with the evolution of ΛCDM model. However, it slightly varies with the best-

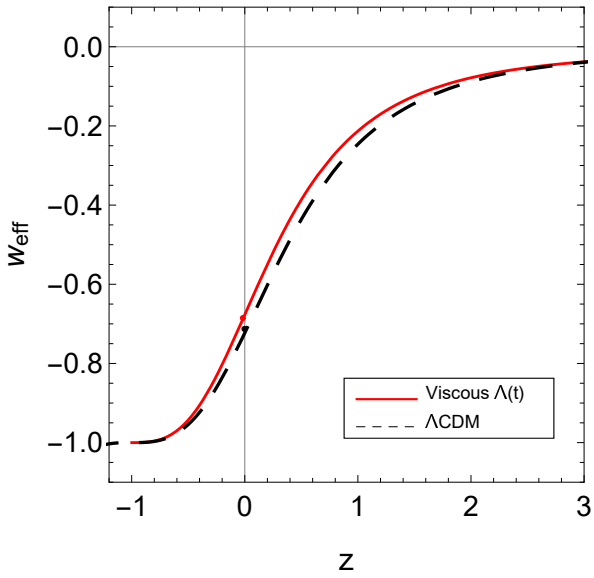

Figure 2.15: Effective EoS parameter as a function of redshift z for viscous $\Lambda(t)$ using "$+f\sigma_8$" dataset. The evolution of EoS parameter in the standard ΛCDM model is also represented as the dashed curve. A dot denotes the present value of the EoS parameter.

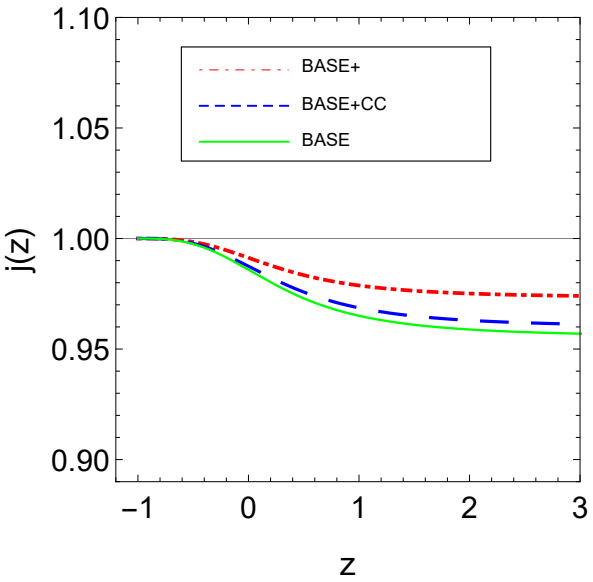

Figure 2.16: Jerk parameter $j(z)$ with redshift z using best-fit values of parameters for viscous $\Lambda(t)$ model. The horizontal line represents the ΛCDM model.

Table 2.3: Values of Chi-squared, reduced Chi-squared, AIC and BIC of ΛCDM and viscous $\Lambda(t)$ models. The ΛCDM model is considered as reference model to calculate the ΔAIC and ΔBIC.

Values	BASE		+CC		$+f\sigma_8$	
	ΛCDM	viscous Λ(t)	ΛCDM	viscous Λ(t)	ΛCDM	viscous Λ(t)
χ^2	518.017	515.074	525.457	522.390	842.630	831.112
d	2	4	2	4	2	4
N	1054	1054	1086	1086	1104	1104
χ^2_{red}	0.492	0.498	0.484	0.481	0.764	0.755
AIC	522.028	523.055	529.468	530.427	846.641	839.112
BIC	531.938	542.915	539.438	550.351	856.643	859.139
ΔAIC	–	1.026	–	0.959	–	−7.492
ΔBIC	–	10.977	–	10.913	–	2.496

fit values obtained through $+f\sigma_8(z)$ data points. It can be observed that the viscous Λ(t) model behaves like a quintessence in early time and cosmological constant in late-time. The present values of w_{eff} are found to be $-0.689^{+0.017}_{-0.013}$, $-0.690^{+0.015}_{-0.013}$ and $-0.677^{+0.014}_{-0.011}$ with $BASE$, $+CC$ and $+f\sigma_8$ datasets respectively, which are very close to the current value of ΛCDM model as presented in Table 2.1.

From Tables 2.1 and 2.2, let us discuss the present value H_0 of Hubble parameter in case of viscous Λ(t) and ΛCDM models. The viscous $\Lambda(t)$ model gives $H_0 = 68.843^{+0.274}_{-0.238}$ km/s/Mpc with $BASE$ data, the $+CC$ data gives $H_0 = 68.913^{+0.262}_{-0.261}$ km/s/Mpc and, finally, the $+f\sigma_8$ renders the present value: $H_0 = 68.684^{+0.259}_{-0.241}$ km/s/Mpc. Recently, the local measurement $H_0 = 73.04 \pm 1.04$ km/s/Mpc from Riess et al.[32] exhibits a strong tension with the Planck 2018 release $H_0 = 67.4 \pm 0.5$ km/s/Mpc [31] at the 4.89σ confidence level. The residual tensions of our fitting results with respect to the latest local measurement $H_0 = 73.04 \pm 1.04$ km/s/Mpc [32] are 3.92σ, 3.85σ and 4.07σ respectively.

Let us focus on σ_8 and S_8 which play very relevant role in structure formation. The best-fit values of these parameters for ΛCDM and viscous $\Lambda(t)$ models using $BASE + CC + f\sigma_8$ data are reported in Tables 2.1 and 2.2, respectively. We can read off $\sigma_8 = 0.794^{+0.014}_{-0.015}$ for ΛCDM model (cf.Table 2.1), whereas the viscous $\Lambda(t)$ model prediction is $\sigma_8 = 0.790^{+0.008}_{-0.010}$ (cf. Table 2.1. This is a very good result, which can be rephrased in terms of the fitting value of the related LSS observable $S_8 = \sigma_8\sqrt{(1-\Omega_\Lambda)/0.3}$ quoted in the Tables 2.1 and 2.2: $S_8 = 0.811 \pm 0.022$ for ΛCDM and $S_8 = 0.822 \pm 0.019$ for viscous Λ(t) model. The values of σ_8 and S_8 for viscous $\Lambda(t)$ model is compatible for 1σ confidence level with ΛCDM. Our result predicts that the tensions in σ_8 and S_8 are reduced to 0.23σ and -0.38σ, respectively. The behavior of $f(z)\sigma_8(z)$ as a function of redshift is plotted in Fig. 2.17. We can see that the evolution of $f\sigma_8$ for both viscous $\Lambda(t)$ and ΛCDM models are consistent with the observational data points.

Table 2.3 presents the χ^2 and reduced χ^2 of ΛCDM and viscous $\Lambda(t)$ models, respectively for the used datasets. To compute reduced χ^2, denoted as χ^2_{red}, we use $\chi^2_{red} = \chi^2_{min}/(N-d)$, where N is the total number of data points and d is the total number of fitted parameters, which differs for the various models. It should be noted that when a model is fitted to data, a value of $\chi^2_{red} < 1$ is regarded as the best fit, whereas a value of $\chi^2_{red} > 1$ is regarded as a poor fit. In our observations, we have used $N = 1054$ data points for BASE (SNIa and BAO), $N = 1086$ data points for BASE+CC and $N = 1104$ data points for BASE+CC+$f\sigma_8$. The number of free parameters of viscous $\Lambda(t)$ is $d = 4$

where as for ΛCDM it is $d = 2$. Using these information, the χ^2_{red} for both the models are given in Table 2.3. It can be observed that the value of χ^2_{red} is less than unity with every data sets for both the models which show that the both models are in a very good fit with these observational data sets and the observed data are consistent with the considered models.

Using the three combination of data sets, we are also interested in investigating the cosmographical aspects of the models, such as jerk parameter, which is defined in 1.15. As we know that the jerk parameter provide us the simplest approach to search for departures from the ΛCDM model. It is noted that for ΛCDM model, $j = 1$(const.) always. Thus, any deviation from $j = 1$ would favor a non-ΛCDM model. In contrast to deceleration parameter which has negative values indicating accelerating Universe, the positive values of the jerk parameter show an accelerating rate of expansion. In Fig.2.16, the evolutions of jerk parameter are shown for ΛCDM and viscous $\Lambda(t)$ models using the best-fit values of parameters obtained from three combination of datasets. It is obvious from the figure that this parameter remains positive and less than unity in past, and eventually tends to unity in late-time. Thus, the jerk parameter deviates in early time but it attains the same value as ΛCDM in late-time.

Using the best-fit values of parameters from Table 2.2 in Eq.(2.44), we plot the matter energy density as a function of redshift for different combinations of datasets in Fig.2.18. It is observed that the matter density was too large at the beginning of the cosmic evolution. As $z \to -1$, the matter energy density tends to a finite value for all combinations of datasets.

2.8 Selection criterion

To evaluate which model provides a better fit, we rely on the Akaike Information Criterion (AIC) and the Bayesian Information Criterion (BIC). These criteria have been explained in Section 1.17.1 and are useful for comparing models based on their statistical performance. According to equations (1.97) and (1.99), models with lower AIC and BIC values are considered more consistent with the observational data. For this comparison, it is necessary to choose a reference model. Here, the ΛCDM model is taken as the reference model.

The values of ΔAIC and ΔBIC with respect to ΛCDM as the referring model are shown in Table 2.3. According to our results, $\Delta AIC(\Delta BIC) = 1.026(10.977)$ with re-

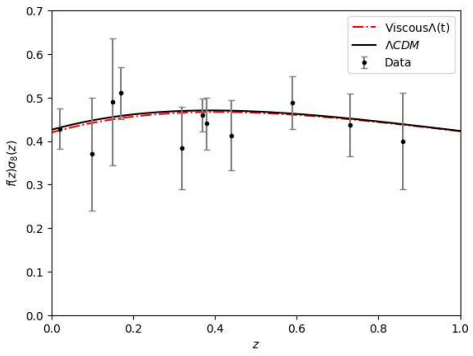

Figure 2.17: Theoretical curves for the $f(z)\sigma_8(z)$ corresponding to ΛCDM and viscous $\Lambda(t)$ model along with some of the data points employed in our analysis. To generate this plot we have used the best-fit values of the cosmological parameters listed in Tables 2.1 and 2.2 for "$+f\sigma_8$" data.

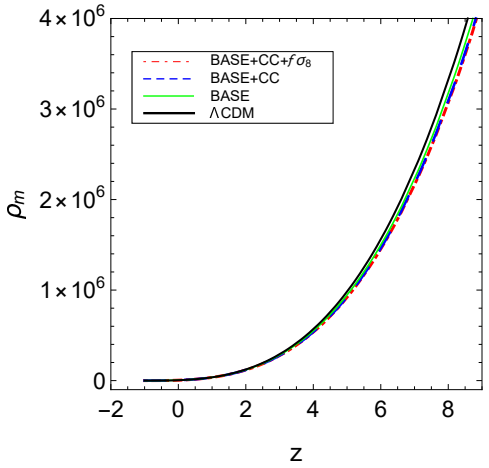

Figure 2.18: The matter energy density as a function of redshift for decaying vacuum with viscous term $\zeta = \zeta_1 H$ using the best fit values obtained from different combinations of datasets.

spect to the $BASE$ dataset, $\Delta AIC(\Delta BIC) = 0.959(10.913)$ with $+CC$ dataset, and for $+f\sigma_8$ dataset, we have $\Delta AIC(\Delta BIC) = -7.492(2.416)$. Thus, under AIC there is "strong evidence in favor" of the viscous $\Lambda(t)$ model where as under BIC, there is "strong evidence against" the viscous $\Lambda(t)$ model with $BASE$ and $+CC$ dataset and "positive evidence against" the model with $+f\sigma_8$ dataset.

2.9 Conclusion

In this chapter, we have studied the analytical and observational consequences of cosmology inspired by dissipative phenomena in fluids according to Eckart theory with varying VED scenarios for spatially flat homogeneous and isotropic FLRW geometry. We have assumed the interaction of two components: viscous dark matter and vacuum energy density satisfying the conservation equation (2.8). We have solved the field equations by assuming the most general form of bulk viscous coefficient, viz., $\zeta = \zeta_0 + \zeta_1 H + \zeta_2(\ddot{a}/aH)$. We have also explored three particular cases of bulk viscosity, namely (1) $\zeta = \zeta_0$; (2) $\zeta = \zeta_1 H$; (3) $\zeta = \zeta_0 + \zeta_1 H$ to observe the effect of viscosity with varying VED. These viscous models have different theoretical motivations, but not all of them are able to constraint observationally. We have constrained only the viscous model $\zeta = \zeta_1 H$ with varying VED. The motivation of the present chapter is to

study the dynamics and evolutions of a wide class of viscous models with time varying vacuum energy density in the light of the most recent observational data. Current observations do not rule out the possibility of varying DE. It has been observed that the dynamical Λ could be useful to solve the coincidence problem. Although the functional form of $\Lambda(t)$ is still unknown, a quantum field theory (QFT) approach has been proposed within the context of the renormalization group (RG). Thus, we have used the varying VED of the functional form $\rho_\Lambda = c_0 + 3\nu H^2$ in all of viscous models presented in this chapter. The motivation for this functional form stems from the general covariance of the effective action in QFT in curved geometry. It has been shown that the $\Lambda(t)$ provides either a particle production processes or increasing the mass of the viscous dark matter particles. In what follows, we summarize the main results of the four different viscous $\Lambda(t)$ models.

In case of the viscous $\Lambda(t)$ models with $\zeta = \zeta_0$, $\zeta = \zeta_0 + \zeta_1 H$ and $\zeta = \zeta_0 + \zeta_1 H + \zeta_2(\ddot{a}/aH)$, we have found the analytical solutions of the various cosmological parameters, like $H(t)$, $a(t)$, $\rho_m(t)$, $q(t)$ and $w_{eff}(t)$. It has been observed that all these three viscous $\Lambda(t)$ models expand exponentially with cosmic time t. The models show the transition from decelerated phase to accelerated phase in late time. The matter energy density, $\rho_m(t)$ approaches to a finite value in late time evolution of the Universe. This happens due to the presence of bulk viscosity. The deceleration parameter $q(t)$ tends to -1 as $t \to \infty$. It is important to note that it is $H(z)$ that is actually the observable quantity in cosmology which can be examined with current observations. However, assuming suitable choice of model parameters, we have discussed numerically the evolutions and dynamics of these models.

In case of viscous $\Lambda(t)$ model with $\zeta = \zeta_1 H$, we have obtained the various cosmological parameters. We have performed a joint likelihood analysis in order to put the constrain on the main parameters by using the three different combinations of observational data: BASE, $+CC$ and $+f\sigma_8$. To discriminate our model with the concordance ΛCDM model, we have also performed the statistical analysis for ΛCDM by using the same observational datasets. Our finding shows that this viscous $\Lambda(t)$ model can accommodate a late time accelerated expansion. It has been observed that we can improve significantly the performance of the model by using $BASE + CC + f\sigma_8$.

From observational consistency points of view, we have examined the evolution of the viscous $\Lambda(t)$ model on Hubble parameter, deceleration parameter and equation of state parameter by using the best-fit values of parameters. It has been observed that the model depicts transition from an early decelerated phase to late-time accel-

erated phase and the transition takes place at $z_{tr} = 0.664^{+0.031}_{-0.042}$ with $BASE$ data, $z_{tr} = 0.665^{+0.031}_{-0.037}$ with $+CC$ data and $z_{tr} = 0.626^{+0.028}_{-0.037}$ with $+f\sigma_8$ data. The present viscous $\Lambda(t)$ model has $q_0 = -0.533^{+0.025}_{-0.020}$, $q_0 = -0.535^{+0.023}_{-0.020}$ and $q_0 = -0.516^{+0.022}_{-0.017}$ respectively. Thus, both z_{tr} and q_0 values are in good agreement with that of ΛCDM model. The ages of the Universe obtained for this model with each dataset are very much compatible with the ΛCDM model. The proposed model has small negative value of EoS parameter for large redshifts and asymptotically approaches to cosmological constant for small redshifts. Thus, the viscous $\Lambda(t)$ model behaves like quintessence in early time and cosmological constant in late-time. The residual tensions of our fitting results with respect to the latest local measurement $H_0 = 73.04 \pm 1.04$ km/s/Mpc [32] are 3.92σ, 3.85σ and 4.07σ, respectively. In Ref. [170], the authors found $H_0 = 69.13 \pm 2.34$ km/s/Mpc assuming the ΛCDM. Such result almost coincides with H_0 that we obtained in Tables 2.1 and 2.2 for ΛCDM and viscous $\Lambda(t)$ models. We have explored the σ_8 and S_8 parameters using the combined datasets of $BASE + CC + f\sigma_8$. The constraints on σ_8 and S_8 from this combined analysis are $\sigma_8 = 0.790^{+0.008}_{-0.010}$ and $S_8 = 0.822^{+0.019}_{-0.019}$, respectively which are very close to the values of ΛCDM. The tension of our fitting results in σ_8 and S_8 for viscous $\Lambda(t)$ model with respect to respective σ_8 and S_8 of ΛCDM are 0.23σ and -0.38σ, respectively. The evolution of $f\sigma_8$ as displayed in Fig. 2.17 shows that the behaviour of $f\sigma_8$ is consistent with the observational data points. It has been noticed that the best-fit results are consistent in the vicinity of Planck data [31].

It has been observed that the value of χ^2_{red} is less than unity with every data sets which show that the model is in a very good fit with these observational data sets and the observed data are consistent with the considered model. The jerk parameter remains positive and less than unity in past, and eventually tends to unity in late-time. Thus, the jerk parameter deviates in early time but it attains the same value as ΛCDM in late-time.

To discriminate the viscous $\Lambda(t)$ with the ΛCDM, we have examined the selection criterion, namely, AIC and BIC. According to the selection criteria ΔAIC, we have found that the viscous $\Lambda(t)$ model is “positively favored" over the ΛCDM model for $BASE$, $+CC$ and $+f\sigma_8$ datasets. Similarly, with respect to ΔBIC our model has a “very strong evidence against" the model for $BASE$ and $+CC$ datasets whereas when we add $+f\sigma_8$ dataset, there is “no significant evidence against" the model. As a concluding remark we must point out that the viscous models with decaying VED may be preferred as potential models to examine the dark energy models beyond the concordance cos-

mological constant. The viscous effects with decaying VED can drive an accelerated expansion of the Universe.

****

Chapter 3

Interacting bulk viscous model with decaying vacuum density

In this chapter [1], we study an interacting decaying vacuum energy with bulk viscosity which creates a more complex cosmological model. It is assumed that they can exchange energy with each other with the aim to explain the accelerated expansion of the Universe in a better way. It has been shown that how coupled decaying vacuum and dissipative effects influence the structure formation, Hubble constant and late time expansion of the Universe.

Highlights:

☞ Discusses the cosmological model of bulk viscosity and decaying vacuum energy within the framework of FLRW spacetime.

☞ Instead of a constant cosmological constant, decaying vacuum energy $\rho_\Lambda = c_0 + 3\nu H^2$ is assumed, which decreases with time.

☞ A viscous fluid linked to dark matter, described in Eckart formalism is assumed with the bulk viscous coefficient proportional to Hubble parameter.

☞ Combines the viscous with decaying vacuum to form a single framework to explore their combined effects.

☞ An energy exchange between dark matter containing viscous term and decaying vacuum through the interaction term $Q = 3\alpha\rho_m H$.

☞ The solutions for Hubble parameter, deceleration parameter and effective EoS

[1] This chapter is based on a published research paper " Exploring interacting bulk viscous model with decaying vacuum density, *Astronomy and Computing* **53**, 100992 (2025)".

parameter in terms of redshift are obtained.

☞ Uses the MCMC method for Pantheon+, cosmic chronometer and $f(z)\sigma_8(z)$ data to find the best fit values of model's parameter.

☞ Analyzes the matter fluctuations (structure formation) to know how the interacting viscous decaying models affect the galaxy and structure growth.

☞ Plots the trajectories of various cosmological parameters to analyze the dynamics and late time evolution of the Universe.

☞ Uses model selection criterion (AIC, BIC and DIC) and Bayesian inference to compare the proposed model with the standard ΛCDM model.

☞ Some particular solutions with $\zeta = \zeta_0$ and $\zeta = \zeta_0 + \zeta_1 H$ are obtained.

☞ Main results are discussed in the last section.

3.1 Introduction

In modern cosmology, understanding the two dark components of the Universe – DE and DM, remains one of the most challenging problems. The discovery of the accelerated expansion of the Universe [33, 34] has motivated research on the composition of these dark sectors. DM, which interacts only gravitationally, explains galaxy rotation curves [171], with proposed candidates such as scalar fields and supersymmetry particles [172, 173, 174]. DE, with negative pressure, is considered responsible for the cosmic acceleration, and various models have been proposed such as the cosmological constant (CC), phantom energy, quintessence, Chaplygin gas, and modified gravity [83, 175, 176]. The ΛCDM model, which incorporates CC as DE, remains the standard model but faces theoretical issues like the fine-tuning and coincidence problems [10, 85].

In recent years, dynamical DE models have been proposed to address these problems. A prominent class is time-varying VED models, especially the running vacuum models (RVMs) proposed in Ref. [17, 155] on the basis of renormalization group (RG) formalism of QFT in curved spacetime. In the context of RVMs, it is considered that the VED evolves slowly with the cosmic expansion. It has been illustrated that both the background and linear perturbation levels of the cosmic evolutions can be described by the RVMs. The vacuum energy is typically determined in curved space-times using renormalization group procedures, which depend on the Hubble

parameter H and its time derivative and is given by the form $\rho_\Lambda(H,\dot{H}) = M_{Pl}^2\Lambda(H,\dot{H})$ [16]. Many works have studied the time-varying VED models. In recent years, the RVMs have been carefully confronted against many cosmological data, which have received a significant success [23, 87, 88, 90, 93, 94, 99, 100, 101, 102, 103, 104, 105, 107, 110, 161, 177, 178, 179, 180, 181, 182, 183, 184], and these models have shown success in fitting various cosmological datasets.

Another interesting approach is viscous fluid cosmology, which considers irreversible processes as a possible cause of cosmic acceleration. Bulk viscosity, consistent with the cosmological principle, is most relevant. Two main formulations exist: the non-causal first-order Eckart theory [29] and the causal second–order Israel–Stewart theory [28]. Despite its known limitations [113, 114], the Eckart theory is widely used due to its simplicity. Many studies have examined bulk viscous models with constant or evolving ζ [72, 75, 115, 117, 118, 120, 127, 128, 129, 130, 131, 133, 134, 135, 136, 141, 142, 143, 144, 145, 146, 156, 185, 186, 187, 188, 189, 190, 191]. These studies show that bulk viscosity can drive late-time acceleration.

Decaying vacuum energy density and viscous fluid models are two appealing theoretical models that have been separately studied by many authors to solve some of problems facing by standard ΛCDM model. Despite the success of decaying VED and viscous fluid models, it should be noted that they have, separately, limitations in describing the entire cosmological evolution. Recently, the authors in Refs. [147, 192, 193, 194] have combined the viscous with decaying vacuum to form a single framework to explore their combined effects. Additionally, the standard assumption that DM and DE do not interact lacks physical justification. Interacting dark energy (IDE) models consider energy exchange between DM and DE while conserving total energy, and have been explored as possible solutions to cosmological tensions such as the H_0 and σ_8 discrepancies [22, 119, 195, 196, 197, 198, 199, 200, 201, 202, 203, 204, 205, 206, 207]. These studies suggest that interactions can affect both background dynamics and structure formation. In chapter 2, we have successfully performed a combined cosmological model of viscous and decaying VED into a single cosmological setting and have investigated their cosmological implications using observational data.

In light of the aforementioned discussions, it has been observed that the interacting scenario that include dynamical dark energy have attracted the interest in literature as they are efficient to resolve the H_0 and σ_8 tensions. In this chapter we investigate a cosmological model for a spatially flat FLRW Universe including two components:

a non-perfect and interacting viscous dark matter, and VED that interact with viscous dark matter in Eckart's approach. We analyze the dynamics of interacting model by constraining the free parameters by performing a MCMC method using the latest observational data. Further, we investigate how our interacting viscous model with decaying VED affects the perturbation level. To investigate the role of this model in structure formation, we employ the perturbation equation to determine the growth of matter fluctuations. Finally, we study the evolutions of various cosmological parameters and compare the perfect fluid case that corresponds to the ΛCDM model through the model selection criteria and Bayesian evidence analysis.

This chapter is organised as follows. In Section 3.2, we present the general features of the proposed cosmological model for a spatially flat FLRW Universe where dissipative effects are present with interacting decaying VED. Section 3.3 deals with the analysis on Structure formation and perturbation equations. We present in Section 3.4 the cosmological probes that are used to constrain the model. Section 3.5 gives the results and discussions on various cosmological parameters with the trajectories and compares the proposed model with the concordance ΛCDM using information criterion and the Bayesian inference. The main results of the work are summarized and discussed in Section 3.6. Two more solutions are also presented in Appendix.

3.2 Interacting dark energy model

We start with a homogeneous, isotropic and spatially flat FLRW metric in spherical coordinates as given in (2.1). The Einstein field equations are given by

$$R_{\mu\nu} - \frac{1}{2} g_{\mu\nu} R = 8\pi G \tilde{T}_{\mu\nu}, \tag{3.1}$$

where $\tilde{T}_{\mu\nu} = T_{\mu\nu} + g_{\mu\nu}\rho_\Lambda$ is the total energy-momentum tensor, which accounts for contribution of viscous dark matter and vacuum energy.

In this chapter, we propose to study the cosmological dynamics of the Universe which include the interaction between the dark matter component including dissipation through a bulk viscous coefficient and a VED described by running coupling depending on the Hubble parameter (hereafter we refer interacting viscous $\Lambda(t)$ model).

The energy-momentum tensor, $T_{\mu\nu}$ for viscous matter is given by [29]

$$T_{\mu\nu} = (\rho_m + P) u_\mu u_\nu + g_{\mu\nu} P \tag{3.2}$$

where ρ_m is the energy density of DM, u_μ is the associated four-velocity and $P = p_m + \Pi$ is the sum of pressure of fluid contributed from the equilibrium pressure, p_m and the non-equilibrium pressure, Π due to bulk viscosity.

The viscous fluid in homogeneous and isotropic cosmological models is determined by its bulk viscosity. The Eckart's formalism serves as the basis for this theory [29]. It is basically obtained from the second order theory of non-equilibrium thermodynamics in the limit of vanishing relaxation time which was proposed by Israel and Stewart [28]. Inspired by the viscosity behavior in fluid mechanics, being proportional to the speed, we assume $\Pi = -3\zeta H$, where H is the Hubble parameter and ζ is the bulk viscous coefficient, which is assumed to be positive on thermodynamic grounds. Furthermore, we consider the non-relativistic matter with $p_m = 0$ to be the bulk viscous fluid. Therefore, the sum of the vacuum energy pressure, $p_\Lambda = -\rho_\Lambda$ and viscous pressure $\Pi = -3\zeta H$ are the components contributing to the total pressure. These two extra ingredients have been introduced to get a more realistic fluid description of DM and DE and also a suitable comparison with ΛCDM model.

In the presence of a non-gravitational interaction between viscous dark matter and decaying vacuum energy, which is characterized by a coupling function $Q(t)$, also known as the interacting rate, the Friedmann equation and conservation equations can be written as

$$3H^2 = \rho_m + \rho_\Lambda, \tag{3.3}$$

$$\dot{\rho}_m + 3H\rho_m = 9\zeta H^2 + Q(t), \tag{3.4}$$

$$\dot{\rho}_\Lambda + 3H(\rho_\Lambda + p_\Lambda) = -Q(t), \tag{3.5}$$

where dot denotes derivative with respect to the cosmic time t. In Eqs.(3.4) and (3.5), $Q(t)$ denotes the interaction function providing the rate of energy transfer between viscous dark matter and decaying VED. It is to be noted that $Q(t) < 0$ gives energy transfer from viscous DM to decaying vacuum energy where as $Q(t) > 0$ gives energy transfer from decaying vacuum energy to viscous DM. Once the interaction function $Q(t)$ is specified, the background dynamics of the model can be found using (3.3)-(3.5). We can define $Q(t)$ by two ways: either by deriving the interaction function from some fundamental physics at the Lagrangian level or by assuming at phenomenological level and testing using observational data. Due to the absence of a fundamental physical theory, we will consider the second approach by assuming the interaction

function as [208, 209]

$$Q = 3\alpha\rho_m H, \tag{3.6}$$

where the term α denotes the dimensionless coupling parameter and included in the fitting vector of free parameters which is to be constrained by the observational dataset.

For decaying VED, we assume a phenomenological application of renormalization group analysis, which can be written as [23, 183]

$$\rho_\Lambda = c_0 + 3\nu H^2, \tag{3.7}$$

where $c_0 = 3H_0^2(\Omega_\Lambda - \nu)$ is the additive constant and fixed by the boundary condition $\rho_\Lambda(H_0) = \rho_{\Lambda 0}$. In this scenario, ν is the dimensionless vacuum parameter and is naturally anticipated to have extremely small magnitude i.e. $|\nu| \ll 1$. Thus, the positive magnitude of ν enables the vacuum's cosmic evolution. In this instance, we will fit ν to the cosmological data set by taking it as a free parameter.

Substituting (3.6) into (3.4), we get

$$\dot{\rho}_m = 9\zeta H^2 - 3(1-\alpha)\rho_m H \tag{3.8}$$

From (3.3)-(3.8), we get the following Hubble evolution equation,

$$\dot{H} + \frac{3}{2}(1-\alpha)H^2 = \frac{3}{2}\frac{\zeta}{(1-\nu)}H + \frac{1}{2}\left(\frac{1-\alpha}{1-\nu}\right)c_0. \tag{3.9}$$

The above evolution equation (3.9) has H and ζ as unknown quantities. We can get the solution of H only if the functional form of ζ is specified. We consider the bulk viscous coefficient ζ as proportional to the expansion rate of the Universe, i.e., to the Hubble parameter H, which can be expressed as [115, 116, 117, 131, 146]

$$\zeta = \zeta_1 H \tag{3.10}$$

where ζ_1 is a dimensionless constant to be estimated from the observations. Substituting this relation into (3.9), we get

$$\dot{H} + \frac{3}{2}\left(\frac{(1-\nu)(1-\alpha) - \zeta_1}{1-\nu}\right)H^2 - \frac{1}{2}\left(\frac{1-\alpha}{1-\nu}\right)c_0 = 0. \tag{3.11}$$

The preceding equation with a variable change from t to $x = \log a$ together with $c_0 = 3H_0^2(\Omega_\Lambda - \nu)$ can be written as

$$\frac{dh^2}{dx} + 3\left(\frac{(1-\nu)(1-\alpha)-\zeta_1}{1-\nu}\right)h^2 = 3\left(\frac{(\Omega_\Lambda-\nu)(1-\alpha)}{1-\nu}\right), \tag{3.12}$$

where $h = H/H_0$ represents the Hubble parameter which is dimensionless and $\Omega_\Lambda = \rho_\Lambda/3H_0^2$. Assuming $(1-\nu)(1-\alpha)-\zeta_1 > 0$ and employing the redshift relation to the normalised scale factor, $a = (1+z)^{-1}$, Eq.(3.12) gives

$$E^2(z) = \tilde{\Omega}_{m,0}(1+z)^{3\left(\frac{(1-\nu)(1-\alpha)-\zeta_1}{(1-\nu)}\right)} + \tilde{\Omega}_{\Lambda,0}, \tag{3.13}$$

where

$$\tilde{\Omega}_{\Lambda,0} = \frac{(\Omega_\Lambda-\nu)(1-\alpha)}{(1-\nu)(1-\alpha)-\zeta_1}, \tag{3.14}$$

and

$$\tilde{\Omega}_{m,0} = 1 - \frac{(\Omega_\Lambda-\nu)(1-\alpha)}{(1-\nu)(1-\alpha)-\zeta_1} = 1 - \tilde{\Omega}_{\Lambda,0}. \tag{3.15}$$

In Eq.(3.13), $E(z) = H/H_0$ is dimensionless Hubble parameter and $\Omega_{i,0}$ (i = DM,DE) represents the current value of density parameter of viscous DM and decaying vacuum energy. For $E(0) = 1$, we have $\tilde{\Omega}_{m,0} + \tilde{\Omega}_{\Lambda,0} = 1$. The scale factor of expansion can be calculated by using $H = \dot{a}/a$ and integrating the equation (3.13), the solution for the scale factor $a(t)$ is given by

$$a(t) = \left(\frac{\tilde{\Omega}_{m,0}}{\tilde{\Omega}_{\Lambda,0}}\right)^{\frac{(1-\nu)}{3[(1-\alpha)(1-\nu)-\zeta_1]}} \left(\sinh^{2/3}\left(\frac{t}{\tilde{t}}\right)\right)^{\frac{(1-\nu)}{(1-\alpha)(1-\nu)-\zeta_1}}, \tag{3.16}$$

where $\tilde{t} \equiv 2/(3H_0\sqrt{\frac{[(1-\nu)(1-\alpha)-\zeta_1](1-\alpha)(\Omega_\Lambda-\nu)}{(1-\nu)^2}})$. It can be observed from (3.16) that the scale factor reduces to $a(t) = (\Omega_{m,0}/\Omega_{\Lambda,0})^{1/3}\ \sinh^{2/3}(t/\tilde{t})$ for $\alpha = 0$, $\zeta_1 = 0$ and $\nu = 0$, which is the analytical solution of the scale factor for ΛCDM model. It can be observed from above equation that the scale factor varies as $a \propto t^{\frac{2(1-\nu)}{3[(1-\nu)(1-\alpha)-\zeta_1]}}$ during early times which the power-law expansion of the Universe. For late-time evolution the scale factor varies as $a \propto \exp\sqrt{\frac{(\Omega_\Lambda-\nu)}{3(1-\zeta_1-\nu)}}H_0 t$, which implies the de Sitter Universe.

To investigate the decelerated and accelerated phases of the expansion of the Universe as well as its transition during the evolution, we explore a crucial cosmological parameter, called 'deceleration parameter'. It is defined in Section 1.14.2. Using

(3.13) into (1.65), the deceleration parameter q in terms of redshift z is given by

$$q(z) = -1 + \frac{3}{2(1-v)} \left(\frac{((1-\alpha)(1-\Omega_\Lambda) - \zeta_1)(1+z)^{3\left(\frac{(1-v)(1-\alpha)-\zeta_1}{(1-v)}\right)}}{\frac{(\Omega_\Lambda - v)(1-\alpha)}{(1-v)(1-\alpha)-\zeta_1} + \left(1 - \frac{(\Omega_\Lambda - v)(1-\alpha)}{(1-v)(1-\alpha)-\zeta_1}\right)(1+z)^{3\left(\frac{(1-v)(1-\alpha)-\zeta_1}{(1-v)}\right)}} \right) \tag{3.17}$$

The aforementioned equation demonstrates how the redshift affects the dynamics of q . We note that the value of $q(z)$ approaches -1 in the future (negative redshift). Furthermore, we determine the present value of q for $z = 0$, denoted as (q_0), which is given by

$$q_0 = -1 + \frac{3}{2(1-v)} \left[(1-\alpha)(1-\Omega_\Lambda) - \zeta_1 \right]. \tag{3.18}$$

For $q_0 > 0$, the Universe exhibits expanding behaviour and goes through a deceleration phase. For $-1 < q_0 < 0$, represents the current state of the Universe which is the expanding and accelerating Universe.

For the sake of completion, we further calculate effective EoS parameter w_{eff} as a function of redshift z,

$$w_{eff}(z) = -1 + \frac{1}{(1-v)} \left(\frac{((1-\alpha)(1-\Omega_\Lambda) - \zeta_1)(1+z)^{3\left(\frac{(1-v)(1-\alpha)-\zeta_1}{(1-v)}\right)}}{\frac{(\Omega_\Lambda - v)(1-\alpha)}{(1-v)(1-\alpha)-\zeta_1} + \left(1 - \frac{(\Omega_\Lambda - v)(1-\alpha)}{(1-v)(1-\alpha)-\zeta_1}\right)(1+z)^{3\left(\frac{(1-v)(1-\alpha)-\zeta_1}{(1-v)}\right)}} \right) \tag{3.19}$$

At $z = 0$, the present value of w_{eff} is determined by

$$w_{eff}(z=0) = -1 + \frac{1}{(1-v)} \left[(1-\alpha)(1-\Omega_\Lambda) - \zeta_1 \right]. \tag{3.20}$$

3.3 Growth of perturbations

The presence of cosmological fluctuations influences the background cosmology in which the perturbations evolve. Hence for the complete analysis of our interacting viscous $\Lambda(t)$ model we must take into account the effects on the large scale structure (LSS) formation data, which we incorporate into our observational analysis, in order to fully confront the model. As a result, we must take the matter density perturbations into consideration. Details on this portion of the analysis has been provided in many references [161, 162]. Here, we simply cite the resulting differential equation, which is entirely consistent with the analysis of [194] and references therein. For the interacting viscous $\Lambda(t)$ model, we use the standard perturbations equation for the linear matter

density contrast $\delta_m \equiv \delta\rho_m/\rho_m$ as given below:

$$\delta_m'' + \left(\frac{3}{a} + \frac{H'(a)}{H(a)}\right)\delta_m' - \frac{4\pi G\rho_m}{H^2(a)}\frac{\delta_m}{a^2} = 0. \tag{3.21}$$

Here $()' \equiv d/da$ represents the derivative with respect to the scale factor. The aforementioned approximation to structure formation is sufficient for considering the primary consequences originate from the distinct expression of the Hubble function as compared to the ΛCDM. Thus, the preceding second-order differential equation (3.21) seems to be accurate. We examine the Hubble function (3.13) as it was determined in Sect. 3.2. The smoothness of the matter perturbation in the interacting viscous $\Lambda(t)$ model is described by the equation (3.21).

The weighted linear growth, $f(z)\sigma_8(z)$, is typically used to compare the theoretical calculations with the structure formation data in the linear regime. Here, $\sigma_8(z)$ represents the r.m.s. mass fluctuations on $R_8 = 8h^{-1}$ Mpc at redshift z and $f(z) = d\ln\delta_m(a)/d\ln(a)$ is the growth factor. The details of the calculation are provided in Sect. 1.16.4.

3.4 Data and methodology

In this section, we use a variety of observational data and methodology in order to constrain the model parameters of ΛCDM and interacting viscous Λ(t) models which comprise observations from: (i) Pantheon+ dataset; (ii) Hubble dataset(Cosmic Chronometers); and (iii) $f(z)\sigma_8(z)$ dataset. The following provide an overview of each data set.

- **SNe Ia sample (Pantheon+ data):** We consider an updated Pantheon+ sample [38] which is the successor of the Pantheon sample. This compilation comprises of 1701 light curves gathered by 1550 type Ia supernovae (SNe), providing detailed information for cosmological analysis. In addition to the most recent SNe sightings, the Pantheon+ collection expands upon earlier SNe compilations and offers a broad range of redshifts ranging from $z = 0.00122$ to 2.2613..

- **Hubble measurements $H(z)$ (Cosmic chronometers):** In our analysis, we employ a compilation of 32 data points of the Hubble parameter derived through the differential age technique [41] in the redshift range $0.07 \leq z \leq 1.965$ with errors.

Table 3.1: Flat prior used on various parameters during statistical analysis.

Parameters	Priors
H_0	$[50, 100]$
Ω_Λ	$(0, 1]$
ζ_1	$(0, 1]$
ν	$(0, 1]$
α	$(0, 1]$
σ_8	$[0.6, 1.2]$

Table 3.2: The values of parameters for ΛCDM and interacting viscous $\Lambda(t)$ models for combination of Pantheon+, Hubble(CC) and $f(z)\sigma_8(z)$ observational datasets.

Parameter	ΛCDM	Interacting viscous $\Lambda(t)$
H_0	$72.100^{+1.7}_{-1.7}$	$72.200^{+1.000}_{-2.000}$
Ω_Λ	$0.688^{+0.029}_{-0.028}$	$0.679^{+0.033}_{-0.034}$
M	$-19.293^{+0.048}_{-0.048}$	$-19.291^{+0.051}_{-0.054}$
ζ_1	$-$	$0.010^{+0.011}_{-0.010}$
ν	$-$	$0.005^{+0.005}_{-0.005}$
α	$-$	$-0.004^{+0.005}_{-0.005}$
σ_8	$0.748^{+0.055}_{-0.055}$	$0.738^{+0.062}_{-0.058}$
S_8	$0.762^{+0.053}_{-0.055}$	$0.762^{+0.055}_{-0.052}$
q_0	$-0.532^{+0.022}_{-0.024}$	$-0.531^{+0.022}_{-0.022}$
z_{tr}	$0.643^{+0.041}_{-0.041}$	$0.648^{+0.042}_{-0.042}$
w_0	$-0.689^{+0.016}_{-0.016}$	$-0.688^{+0.016}_{-0.016}$
$t_0(Gyr)$	$13.74^{+0.019}_{-0.021}$	$13.75^{+0.023}_{-0.021}$

- $\mathbf{f(z)\sigma_8(z)}$ **data :** Finally, in this work we use the recent “Gold -17" compilation consisting of 18 independent measurements of $f(z)\sigma_8(z)$. These data points are based on Redshift Space Distortion (RSD) measurements from various observations of the Large Scale Structure (LSS) and complied in Table III of Ref. [58].

Based on the EMCEE [36] python module, we employ the Markov Chain Monte Carlo(MCMC) statistical technique to examine the parameter space of our cosmological models and minimise the χ^2 function for both ΛCDM and interacting viscous $\Lambda(t)$ models. We consider the joint analysis by assuming the sum of all χ^2 functions:

$$\chi^2_{tot} = \chi^2_{Pan+} + \chi^2_{CC} + \chi^2_{f\sigma_8(z)}. \tag{3.22}$$

To perform this analysis, we choose uniform priors for the parameters of models which is listed in Table 3.1.

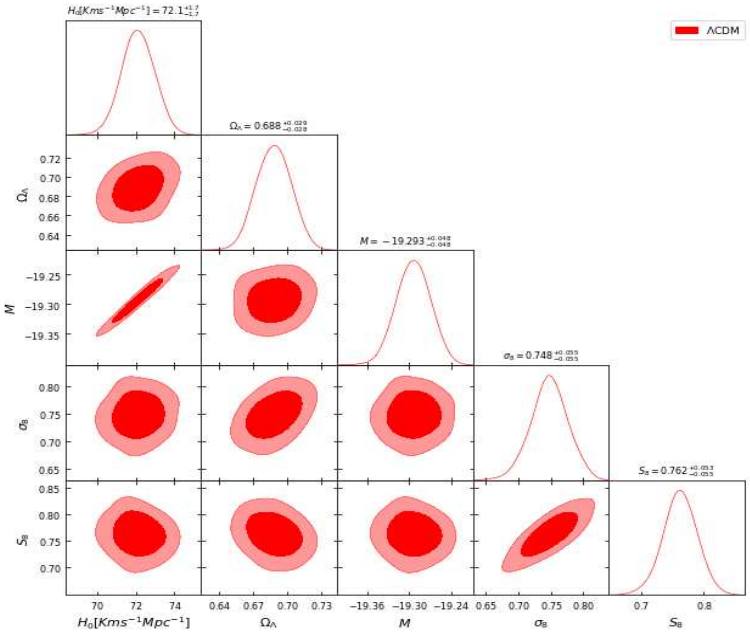

Figure 3.1: The one-dimensional marginalized distributions and two-dimensional contour plots of ΛCDM model at 68.3% and 95.4% confidence levels using combined data of *Pantheon+*, *CC* & $f(z)\sigma_8(z)$.

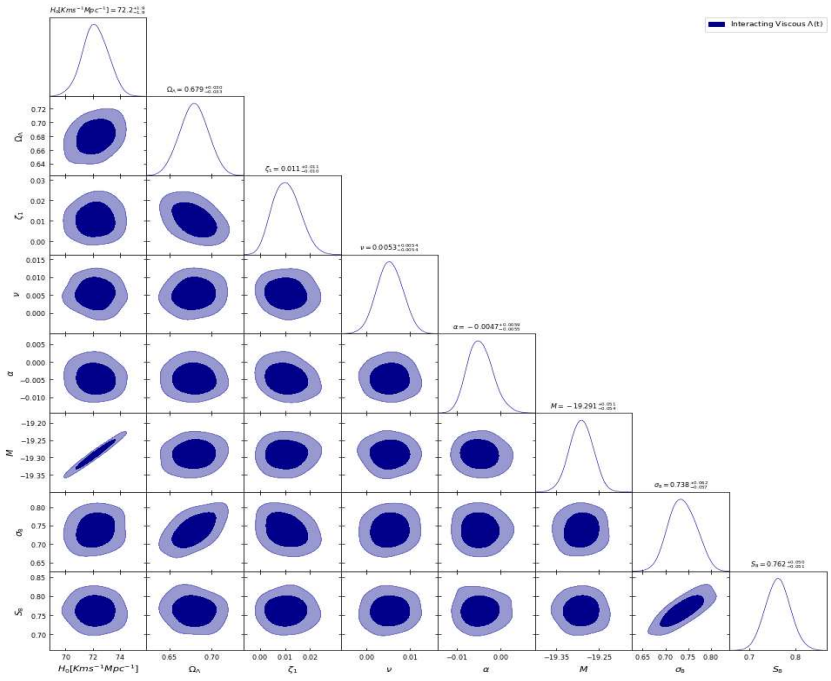

Figure 3.2: The one-dimensional marginalized distributions and two-dimensional contour plots of interacting viscous $\Lambda(t)$ model at 68.3% and 95.4% confidence levels using combined data of *Pantheon+*, *CC* & $f(z)\sigma_8(z)$.

3.5 Result and discussion

In this section, we present the results of our observational analysis on ΛCDM and interacting viscous $\Lambda(t)$ models, including both the constraints and cosmological parameters from the current data. In the first subsection, we will present the parameters constraints achieved by observational analysis using the data discussed in Sect.3.4. In second subsection, we will implement the Bayesian inference, and in last subsection, we will examine the model comparison through information criterion.

3.5.1 Parameter constraints

The best-fit values of parameters of ΛCDM and interacting viscous $\Lambda(t)$ models using a combined $CC + f(z)\sigma_8(z) + Pan+$ data are summarized in Table 3.2. Figures 3.1 and 3.2 show the 68.3% and 95.4% confidence regions and marginalized likelihood distributions for ΛCDM and interacting viscous $\Lambda(t)$ models, respectively. The GetDist code [210] is utilised to retrieve their mean values and the aforementioned Figs. 3.1–3.2. In what follows we discuss the constraints on different cosmological as well as model parameters.

It is noted that the H_0 determined by Riess et al. (2022) is $73.04 \pm 1.04\ kms^{-1}Mpc^{-1}$, so-called R21 where as Planck Collaboration [79] predicts $H_0 = 67.4 \pm 0.5\ kms^{-1}Mpc^{-1}$ at 5σ confidence level. This discrepancy is recognized as “Hubble tension". For ΛCDM model we obtain $H_0 = 72.100^{+1.7}_{-1.7}\ kms^{-1}Mpc^{-1}$. This is in tension with both Planck [79] and R21 [32] results at 2.65σ and 0.47σ respectively. For interacting viscous $\Lambda(t)$ model, we obtain $H_0 = 72.200^{+1.000}_{-2.000}\ kms^{-1}Mpc^{-1}$ which is tension with both Planck and R21 results at 3.03σ and 0.46σ respectively. In other words, the H_0 measurement of interacting viscous $\Lambda(t)$ model is consistent with R21. The evolutions of $H(z)$ with redshift z are shown in Fig.3.3 which predict that the trajectories cover majority of dataset with error bars of $H(z)$. This means that the interacting viscous $\Lambda(t)$ model agrees with the combination of dataset as well as ΛCDM model.

In the interacting viscous $\Lambda(t)$ model, we obtain the viscosity coefficient, ζ_1 as $0.011^{+0.011}_{-0.010}$ and ν as $0.005^{+0.005}_{-0.005}$. The coupling parameter of the interaction term, α is calculated as $-0.004^{+0.005}_{-0.005}$. The negative value of α indicates that there is a possibility of the dark matter to decay into the dark energy.

Using the best-fit values, the evolutions of deceleration parameter with redshift for

ΛCDM and interacting viscous $\Lambda(t)$ models with errors are plotted in Fig.3.4. The trajectories show that the models have transition from decelerating phase to accelerating phase at transition redshift z_{tr}=$0.643^{+0.041}_{-0.041}$ and z_{tr} =$0.648^{+0.042}_{-0.042}$, respectively. The present value of deceleration parameter are found to be q_0= $-0.532^{+0.022}_{-0.024}$ and q_0 = $-0.531^{+0.022}_{-0.022}$. These values of q_0 are within the range of the observational results, i.e., $q_0 = -0.64 \pm 0.12$ [79]. In late time of evolution, $q(z)$ approaches to -1 in both models which is the future de Sitter phase.

In Fig.3.5, we plot the effective EoS parameter as a function of redshift for best-fit values of ΛCDM and interacting viscous $\Lambda(t)$ models. It is observed that $w_{\text{eff}} \to -1$ in the late-time in both the models, which implies that the models correspond to de Sitter phase in late-time. Using the best-fit, we get the present EoS parameters $w_{\text{eff}}(z=0) = -0.689 \pm 0.016$ and $w_{\text{eff}}(z=0) = -0.688 \pm 0.016$, respectively.

Next, we explore another tension between the theoretical prediction of the growth rate of matter perturbations with the observational growth rate data points for ΛCDM and interacting viscous $\Lambda(t)$ models. For both models the constraints on σ_8 and S_8 are given in Table 3.2. The amplitude of the matter power spectrum (σ_8) and its associated parameter $S_8 = \sigma_8\sqrt{(1-\Omega_\Lambda)/0.3}$ may be determined using the $f(z)\sigma_8(z)$ dataset and it is further possible to calculate the σ_8/S_8 tension. The combined dataset gives $\sigma_8 = 0.748^{+0.055}_{-0.055}$ and $S_8 = 0.762^{+0.053}_{-0.055}$ in the ΛCDM model and $\sigma_8 = 0.738^{+0.062}_{-0.057}$ and $S_8 = 0.762^{+0.055}_{-0.052}$ in interacting viscous $\Lambda(t)$ model. Our results are perfectly consistent with the combined use of the SDSS and KiDS/Viking data which gives $\sigma_8 = 0.760^{+0.025}_{-0.020}$ and $S_8 = 0.766^{+0.020}_{-0.014}$ [211]. It is to be noted that Planck collaboration gives $\sigma_8 = 0.806 \pm 0.005$ and $S_8 = 0.811 \pm 0.011$. Thus, the interacting viscous $\Lambda(t)$ model is in 1.14σ tension in σ_8 and 0.91σ tension in S_8 with the corresponding values of Planck [79]. These tensions are not as large compared to H_0 tension as discussed above. This confirms that the measurement of σ_8 and S_8 using $CC + Pan+$ with $f(z)\sigma_8(z)$ data is fully consistent with ΛCDM. The trajectories of $f(z)\sigma_8(z)$ for ΛCDM and interacting viscous $\Lambda(t)$ models are plotted in Fig.3.6. It can be observed that both the models are consistent with the observational data points.

Let us discuss the interacting viscous $\Lambda(t)$ model by defining a dimensionless parameter, known as jerk parameter, j. This parameter is purely kinematical and is associated with the third order derivative of the scale factor $a(t)$. It is defined in 1.15 It can provide us the deviation of any model from the ΛCDM model. It is noted that jerk parameter always has constant value $j = 1$ for ΛCDM model. We report $j_0 = 0.992$ in interacting viscous $\Lambda(t)$ model which is quite comparable to the ΛCDM model. We plot

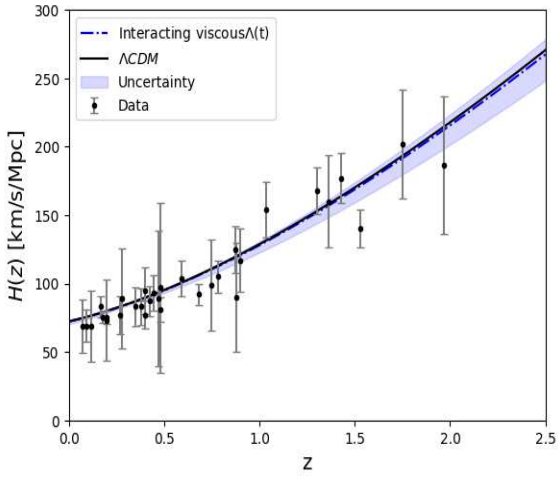

Figure 3.3: The evolution of Hubble function $H(z)$ with redshift z. The solid black line corresponds to the ΛCDM model and the dashed blue line corresponds to the interacting viscous $\Lambda(t)$ model. The $H_{obs}(z)$ data are also plotted with their error bars.

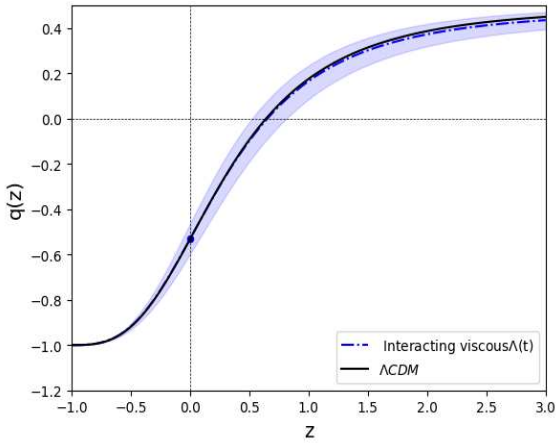

Figure 3.4: The evolution of $q(z)$ with redshift z for interacting viscous $\Lambda(t)$ model and ΛCDM model using the best fit values. The present value q_0 is represented by a dot.

the evolution of jerk parameter with respect to the redshift as shown in Fig.3.7. We observe that the trajectory of $j(z)$ deviates from ΛCDM in early phase where as it approaches to $j = 1$ as $z \to -1$. Thus, jerk parameter points us the effects of interacting viscous $\Lambda(t)$ model over the ΛCDM model.

3.5.2 Model selection

In this section, we will discuss mainly reduced Chi-square and model selection criterion to observe the compatibility of the proposed model.

Let us first calculate the reduced Chi-square, χ^2_{red}, which is defined as $\chi^2_{red} = \chi^2_{min}/dof$. Here, dof denotes the degree of freedom which is equal to the number of observational data points (N) minus the number of parameters (K). It is

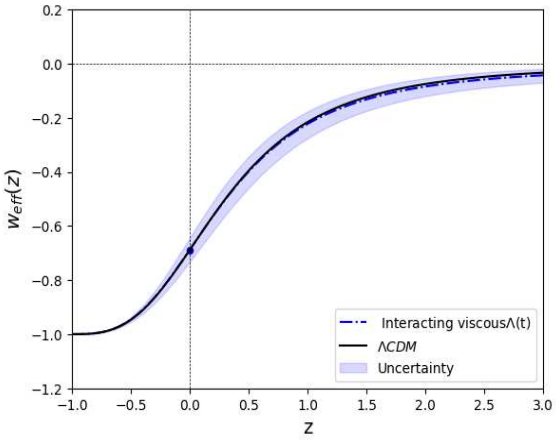

Figure 3.5: The evolution of w_{eff} with redshift z for interacting viscous $\Lambda(t)$ model and ΛCDM model using the best fit values. The present value of $w_{eff}(z=0)$ is represented by a dot.

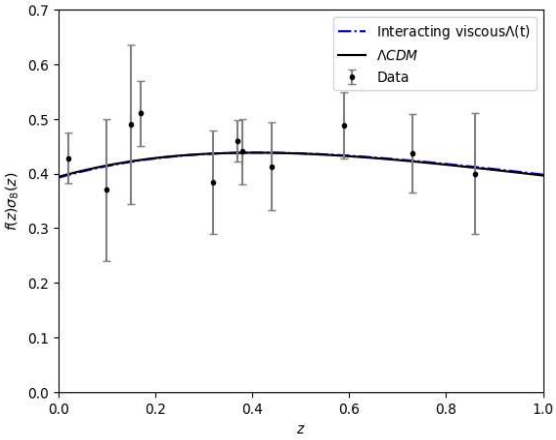

Figure 3.6: The evolution of $f(z)\sigma_8(z)$ with redshift z for interacting viscous$\Lambda(t)$ model and ΛCDM model using the best fit values.

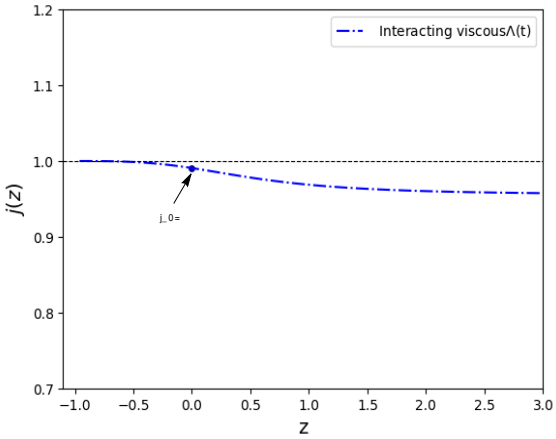

Figure 3.7: The evolution of $j(z)$ with redshift z for interacting viscous $\Lambda(t)$ model the best fit values. The present value of $j_0(z=0)$ is represented by a dot and the horizontal line $j=1$ represents ΛCDM model.

to be noted that we have used $N = 1751$ and $K = 3$ in ΛCDM and $K = 6$ in interacting viscous $\Lambda(t)$ model with same number of data points. Table 3.4 presents the χ^2 and χ^2_{red} of ΛCDM and interacting viscous $\Lambda(t)$ models, respectively. It is noted that a value $\chi^2_{red} < 1$ gives the best-fit with the data. We observed that both the models have the reduced χ^2 less than unity (for ΛCDM, $\chi^2_{red} = 0.447$ and for interacting viscous $\Lambda(t)$ model, it is $\chi^2_{red} = 0.448$). This shows that both the models are in very good fit with the observational data.

We discuss the another method which provides the statistical comparison of the proposed model with ΛCDM model. In this regard, there are two model selection criterion, namely, Akaike information criteria (AIC) and Bayesian information criteria (BIC) [61, 63]. These selection criterion allow to compare models with different degree of freedom. They are defined in section 1.17.1. In these approaches, the model with low values of AIC(BIC) is preferred by data. Considering the AIC (BIC) of ΛCDM model as reference model, denoted as $AIC_\Lambda(BIC_\Lambda)$, we compute $\Delta AIC = AIC_{model} - AIC_{\Lambda CDM}(\Delta BIC = BIC_{model} - BIC_{\Lambda CDM})$.

Table 3.4 displays the values of AIC (BIC) and corresponding ΔAIC (ΔBIC) for interacting viscous $\Lambda(t)$ model. According to our results, we have $\Delta AIC = 6.670$ and $\Delta BIC = 23.039$. This shows that there is “less support in favor" of the interacting viscous $\Lambda(t)$ model as far as AIC is concerned where as BIC gives “strong evidence against" the interacting viscous $\Lambda(t)$ model. This indicates that the evidence against our model is overwhelmingly strong and it is not the best-fit for the data according to BIC. This discrepancy arises because AIC tends to be more inclusive in model selection. Generally, AIC is more lenient with additional parameters, while BIC penalizes them. Thus, AIC limits the number of parameters, making it worthwhile.

3.5.3 Bayesian Inference

The Bayesian evidence serves as the foundation for assessing a model’s performance in light of the data. In Bayesian data analysis, the correlation between the data, the model or hypotheses, and the prior knowledge is characterized by the joint probability distributions. Given the observed data, the conditional probability distribution of the unknowns can be used to uniquely infer the posterior distribution using Bayes theorem. The key statistic of Bayesian model selection is the Bayesian evidence $\mathscr{E}$ [212, 213], which is employed in a model comparison problem by integrating the product of likelihood and posterior over the entire parametric space of the model.

Table 3.3: "Jeffreys' scale" for evaluating the strength of evidence between two comparing models, M_i versus M_j. The right column provides the convention for denoting the different levels of evidence above these thresholds.

$\ln \mathscr{B}_{ij}$	Strength of Evidence
< 1.0	Inconclusive
1.0	Weak evidence
2.5	Moderate evidence
5.0	Strong evidence

It is defined as [62, 214, 215, 216]

$$\mathscr{E}(D|M) = \int_M \mathscr{L}(D|\Theta, M)\mathscr{P}(D|\Theta, M)d\Theta. \tag{3.23}$$

On the right-hand side, Θ is a set of free parameters for the given data D, M stands for the model, the vertical bar reads as 'given', and $\mathscr{L}$ and $\mathscr{P}$ stand for likelihood and prior probability distribution function of those parameters before the data, respectively.

In cosmology, this concept has been utilized extensively [217, 218]. When comparing two models, M_i versus M_j, one is interested in the ratio of the models' evidences known as $Bayes\ factor$, which is given by:

$$\mathscr{B}_{ij} \equiv \frac{\mathscr{E}_i}{\mathscr{E}_j} \tag{3.24}$$

Here, B_{ij} indicates the support for model i over model j.

Bayes factors are typically interpreted using the Jeffreys' scale [212] which measures the strength of the evidence, given in Table 3.3. We accomplish this by estimating the values of the logarithm of Bayes factor $(\ln \mathscr{B})$ and the Bayesian evidence $(\ln \mathscr{E})$. Using the dataset and the priors mentioned in Table 3.1, the values of $\mathscr{E}$ and $\mathscr{B}$ are determined. We assume the ΛCDM as the reference model.

The results for the Bayesian evidence $(\ln \mathscr{E})$ and Bayes factor $(\ln \mathscr{B})$ for both ΛCDM and interacting viscous Λ(t) models examined in this work are summarized in Table 3.4. We find that the $\ln \mathscr{B}$ for interacting viscous Λ(t) model with respect to the ΛCDM model is obtained as 2.577 and thus the Bayesian evidence analysis shows that our model is "moderately supported" by the considered priors and dataset on Jeffreys' scale.

Table 3.4: Summary of $\ln\mathscr{E}$, $\ln\mathscr{B}$, χ^2, χ^2_{red}, *AIC* and *BIC* for the ΛCDM and interacting viscous $\Lambda(t)$ models for the following:

Values	ΛCDM	Interacting viscous$\Lambda(t)$
$\ln\mathscr{E}$	-793.120 ± 0.473	-795.697 ± 0.532
$\ln\mathscr{B}$	–	2.577
χ^2	781.708	782.344
K	3	6
N	1751	1751
χ^2_{red}	0.447	0.448
AIC	787.722	794.392
ΔAIC	–	6.670
BIC	804.112	827.152
ΔBIC	–	23.039

3.6 Conclusion

Inspired by dissipative phenomena and decaying vacuum energy, we have discussed some cosmological consequences of an alternative mechanism of accelerating Universe based on a class of interacting viscous model with decaying vacuum energy, referred as interacting viscous $\Lambda(t)$ model. The coupling between viscous fluid and vacuum energy density has been made through a coupling parameter, Q. Within the framework of Eckart thermodynamic theory the non-equilibrium pressure, Π is proportional to the Hubble parameter H with proportionality constant ζ, i.e., $\Pi=-3\zeta(t)H$. Thus, the effective pressure is assumed as sum of barotropic pressure, bulk viscous pressure and pressure due to vacuum energy, i.e., $\bar{p}=p_m+\Pi+p_\Lambda$. In the first part of work, we have obtained some main results for the scale factor, the Hubble parameter, the deceleration parameter, jerk parameter and EoS parameter by assuming the interaction term $Q=3\alpha\rho_m H$. Although the nature of bulk viscosity and time-varying vacuum energy density are unknown, we have assumed $\zeta=\zeta_1 H$ for bulk viscous coefficient and $\rho_\Lambda=c_0+3\nu H^2$ for vacuum energy density. One can expect that the viscosity is affected by the expansion rate of the Universe and varying VED from the general covariance of the effective action in QFT. We have investigated the growth perturbation of interacting viscous $\Lambda(t)$ model. In the second part of this work, we have performed the Bayesian analysis using the latest background probes such as SNe Pantheon+, cosmic chronometer and $f(z)\sigma_8(z)$. We have compared the interacting viscous $\Lambda(t)$ model with ΛCDM using the Bayesian inference and model selection criterion such as AIC and BIC. The results show that the standard ΛCDM

model is reproduced in the absence of parameters ζ, α and v. In what follows, we summarize the main points of our analysis.

The constraints on model free parameters have been reported in Table 3.2. The best-fit value of H_0 according to a combination of Pantheon+, CC and $f(z)\sigma_8(z)$ is $H_0 = 72.200^{+1.000}_{-2.000}\ kms^{-1}Mpc^{-1}$, which is tension with both Planck and R21 results at 3.03σ and 0.46σ ,respectively. In other words, the tension in H_0 measurement is almost resolved in interacting viscous $\Lambda(t)$ model with respect to R21. The best fit values of present q and w_{eff} are $q_0 = -0.532^{+0.022}_{-0.024}$ and $w_{\text{eff}}(z=0) = -0.688 \pm 0.016$, respectively. From Fig.3.4, it has been observed that the interacting viscous $\Lambda(t)$ model exhibits transition from an early decelerated phase to late-time accelerated phase and the transition takes place at $z_{tr} = 0.648^{+0.042}_{-0.042}$ which is close proximity $z_{tr} = 0.643^{+0.041}_{-0.041}$ to that of ΛCDM model. It has been found that the value of $\chi^2_{red} < 1$ which shows that the interacting viscous $\Lambda(t)$ model is in very good fit with the used data points. The jerk parameter remains positive and less than one in past, and tends to unity in late-time.

We have explored the σ_8 and S_8 parameters for ΛCDM and interacting viscous $\Lambda(t)$ models using the combined data set of Pantheon+, CC and $f(z)\sigma_8(z)$. The constraints on σ_8 and S_8 in interacting viscous $\Lambda(t)$ model are $\sigma_8 = 0.738^{+0.062}_{-0.057}$ and $S_8 = 0.762^{+0.055}_{-0.057}$ which are very close to ΛCDM model as reported in Table 3.2. The tensions of our fitting results in σ_8 and S_8 with respect to Plank results [79] are 1.14σ and 0.91σ, respectively. The evolution of $f(z)\sigma_8(z)$ has been plotted in Fig. 3.6 which shows that it is consistent with the observational data points.

It is noted that cosmological models are testable from the abundance of observational data as discussed above. However, an important distinction must be made between parameter fitting and model selection. As we know that the parameter fitting simply tells us how well a model fit the data. Model selection such as Bayesian inference and AIC and BIC are necessary to discriminate the proposed model with the existing model. The Bayesian inference analysis demonstrated the interacting viscous Λ(t) model is moderately supported by the considered dataset and priors. Further, there has been increasing interest in applying information criterion such as AIC and BIC for model selection. We have examined the models using AIC and BIC for a fairer comparison. We have observed that the interacting viscous $\Lambda(t)$ model has “less support" according to the selection criteria ΔAIC. On contrary, with respect to ΔBIC, interacting viscous $\Lambda(t)$ model has “strong evidence against" the model with the considered datasets.

As a concluding remark we must point out that despite its intrinsic nature of bulk viscosity and decaying vacuum energy and its interaction are not well understood yet, the work presented in this chapter suggests a possible description for resolving the H_0 and σ_8 tensions in cosmology. In principle, to give a robust approach for investigating the dark energy model beyond ΛCDM, background dynamics should be considered. Taking into account such interaction between the dark components may provide an opportunity to explain the present accelerating Universe. Indeed considering the interaction between the viscous fluid and decaying vacuum energy potentially enables us to resolve tensions in cosmological parameters.

Appendix

13 The main aim in this appendix is to present some more analytical solutions of the cosmological parameters of the interacting viscous model with decaying vacuum energy density based on the different choices of ζ.

Solution with $\zeta = \zeta_0$

It is the most simple parametric form of the bulk viscous coefficient. Many authors [75, 128, 129, 160] have studied the viscous cosmological models with constant bulk viscous coefficient. Using $\zeta = \zeta_0$ in Eq.(3.9), the Hubble evolution equation deduces the form

$$\dot{H} + \frac{3}{2}(1-\alpha)H^2 - \frac{3}{2}\frac{\zeta_0 H}{(1-\nu)}H = \frac{1}{2}\left(\frac{1-\alpha}{1-\nu}\right)c_0. \tag{3.25}$$

Solving (3.25) with the condition $H(t_0) = H_0$, we get

$$H = \frac{\zeta_0}{2(1-\nu)(1-\alpha)} + k\coth\left(\frac{3}{2}(1-\alpha)kt\right). \tag{3.26}$$

where $k = \frac{\zeta_0{}^2 + 4(\Omega_\Lambda - \nu)(1-\nu)(1-\alpha)^2 H_0{}^2}{4(1-\nu)^2(1-\alpha)^2}$.

Integrating again with the condition $a(t_0) = 1$, we obtain the scale factor

$$a(t) = e^{\frac{\zeta_0}{2(1-\nu)(1-\alpha)}t}\left[\sinh\left(\frac{3}{2}(1-\alpha)kt\right)\right]^{\frac{2}{3(1-\alpha)}}, \tag{3.27}$$

Using (3.26), the deceleration parameter q and Effective EoS parameter w_{eff} are respectively given by

$$q = -1 + \frac{3}{2}\frac{(1-\alpha)k^2\csc^2 h(\frac{3}{2}(1-\alpha)kt)}{\left(\frac{\zeta_0}{2(1-\nu)(1-\alpha)} + k\coth(\frac{3}{2}(1-\alpha)kt)\right)^2}. \tag{3.28}$$

$$w_{eff} = -1 + \frac{(1-\alpha)k^2\csc^2 h(\frac{3}{2}(1-\alpha)kt)}{\left(\frac{\zeta_0}{2(1-\nu)(1-\alpha)} + k\coth(\frac{3}{2}(1-\alpha)kt)\right)^2}. \tag{3.29}$$

Solution with $\zeta = \zeta_0 + \zeta_1 H$

This form of bulk viscous coefficient has been discussed by several authors and the references therein [72]. For $\zeta = \zeta_0 + \zeta_1 H$, where ζ_0 and ζ_1 are constants, the Eq. (3.9) simplifies into

$$\dot{H} + \frac{3}{2}(1-\alpha)H^2 - \frac{3}{2}\frac{\zeta_1 H^2}{(1-\nu)} - \frac{3}{2}\frac{\zeta_0 H}{(1-\nu)} = \frac{1}{2}\left(\frac{1-\alpha}{1-\nu}\right)c_0, \tag{3.30}$$

which can be integrated to calculate the Hubble function and the scale factor

$$H = \frac{\zeta_0}{2((1-\alpha)(1-\nu)-\zeta_1)} + k_1\ \coth\left(\frac{3}{2}\frac{((1-\alpha)(1-\nu)-\zeta_1)}{(1-\nu)}k_1 t\right), \tag{3.31}$$

$$a = e^{\frac{\zeta_0 t}{2((1-\alpha)(1-\nu)-\zeta_1)}} \times \left[\sinh\left(\frac{3}{2}\frac{((1-\alpha)(1-\nu)-\zeta_1)}{1-\nu}k_1 t\right)\right]^{\frac{2(1-\nu)}{3((1-\alpha)(1-\nu)-\zeta_1)}}, \tag{3.32}$$

where $k_1 = \frac{{\zeta_0}^2 + 4((1-\alpha)(1-\nu)-\zeta_1)((\Omega_\Lambda-\nu)(1-\alpha))H_0^2}{4((1-\nu)(1-\alpha)-\zeta_1)^2}$.

With this, we can calculate the deceleration parameter q and effective equation of state parameter w_{eff}, which are respectively given by

$$q = -1 + \frac{3(1-\zeta_1-\nu)\sigma_1^2\csc^2 h(\frac{3}{2}(1-\zeta_1-\nu)\sigma_1 t)}{2\left(\frac{\zeta_0}{2(1-\zeta_1-\nu)} + \sigma_1\coth(\frac{3}{2}(1-\zeta_1-\nu)\sigma_1 t)\right)^2} \tag{3.33}$$

and

$$w_{eff} = -1 + \frac{(1-\zeta_1-\nu)\sigma_1^2\csc^2 h(\frac{3}{2}(1-\zeta_1-\nu)\sigma_1 t)}{\left(\frac{\zeta_0}{2(1-\zeta_1-\nu)} + \sigma_1\coth(\frac{3}{2}(1-\zeta_1-\nu)\sigma_1 t)\right)^2} \tag{3.34}$$

****

Chapter 4

Interacting viscous running vacuum model in FLRW Universe

In this chapter [1] , we combine the two alternative ideas to a standard ΛCDM: bulk viscosity from dissipative mechanism and running vacuum energy from quantum field theory within the framework of FLRW metric.

Highlights of the chapter:

☞ Presents a running vacuum model with bulk viscosity in FLRW spacetime.

☞ Running vacuum model (RVM): A vacuum energy density (a cosmological constant), which changes with cosmic time and assume the form $\rho_\Lambda = 3\left[c_0 + \frac{2}{3}\mu\dot{H}(z) + \nu H^2(z)\right]$.

☞ Bulk viscosity: Creating a non-ideal fluid added to the pressure of dark matter, which is parametrized as $\zeta = \zeta_1 H$.

☞ Modified equations: Friedmann equations governing the cosmic expansion are modified by including bulk viscosity and RVM term.

☞ The combined model allows for a more complex, non-static description of the dark energy and matter.

☞ Test model with the latest observational data like, Pantheon+, BAO DESI, CC and growth data to find the best-fit values of parameters.

[1] This chapter is based on a published research paper " Interacting model of bulk viscous and decaying vacuum energy, *Physics Letters B* **871**, 139994 (2025)".

☞ Uses Gelman-Rubin statistic (or R-hat statistic) to assess the convergence of MCMC simulations.

☞ Discuss the stability of viscous RVM using information critetion like AIC, BIC and DIC.

☞ The viscous RVM is consistent with the standard ΛCDM model and alleviates the Hubble tension up to 0.569σ.

☞ The model shows a smooth transition from a matter-dominated era to an accelerating vacuum-dominated era.

☞ Concludes the results in conclusion section.

4.1 Introduction

Many cosmological observations indicate that General theory of Relativity (GTR) may not be the only ultimate theory which explains this accelerating phenomena. Therefore, it compels to modify either in matter part or gravitational part of Einstein field equations. The simplest modification is the introduction of cosmological constant(CC), Λ, into the Einstein field equations. A flat Friedmann-Lemaître-Robertson-Walker (FLRW) model with CC-term, known as ΛCDM (Λ plus Cold Dark matter) model of cosmology [219, 220], is considered as the most effective model to explain the accelerating expansion of the Universe. However, this model suffers several theoretical and observational difficulties. Some remarkable examples are the cosmological constant problem and the coincidence problem(see, e.g., [10, 16, 175, 221] for a review).

Nowadays, Hubble tension is one of the most intriguing problem with ΛCDM, which refers mismatching between the value of the Hubble constant H_0 inferred from early-Universe probes such as Planck CMB data [79] and direct local distance ladder measurements such as Type Ia supernovae and Cepheid variable stars [196, 222, 223]. In particular, the Planck collaboration gives $H_0 = 67.4 \pm 0.50\ kms^{-1}Mpc^{-1}$, while the $SH0ES$ collaboration finds $H_0 = 73.04 \pm 1.04\ kms^{-1}Mpc^{-1}$, a tension of 4.89σ. Another tension pertains to S_8 parameter, defined as $S_8 \equiv \sigma_8\sqrt{\Omega_m/0.3}$, where Ω_m is the fractional matter density and σ_8 is the variance of matter density field at $8Mpc$ scales. This tension refers mismatch in measurements of matter density fluctuations today as

inferred from the CMB and galaxy surveys [224]. Due to these theoretical and observational shortcomings, it is necessary to look beyond the ΛCDM model.

In literature, many cosmological models have been proposed to provide a conceptual framework for physical interpretation to DE. The most compelling representative for the DE is the CC, Λ which is traditionally connected to VED through $\rho_\Lambda = \Lambda/8\pi G$, where G is the Newton's gravitational constant. Recent developments in QFT suggest that the issues related to vacuum energy and its connection to the Λ-term can be largely resolved. Moreover, a time-evolving Λ (or dynamical DE) could help in alleviating the problems faced by ΛCDM model [87, 88, 89, 182, 225, 226, 227, 228, 229, 230, 231, 232, 233, 234, 235, 236, 237, 238, 239, 240]. Motivated by perturbation of QFT in curved spacetime, running vacuum models (RVMs) [180, 244] and viscous DM models [72, 74, 75, 111, 112, 127, 128, 129, 130, 131, 132, 133, 134, 135, 136, 137, 138, 139, 140, 141, 144, 145, 241, 242] have been explored to alleviate these tensions. The works show that viscous DM and RVMs are capable in alleviating some limitations of ΛCDM, and attempts have been made to combine both frameworks [146, 147, 148, 149, 191, 194, 243]. Solá and Gómez-Valent[180], and Moreno-Pulido and Solá [244] proposed a dynamical VED called in the literature 'running vacuum model'(RVM) in which the effective VED appears as an expansion in powers of the Hubble function and its time derivatives, i.e., $\rho_{vac} = \rho_{vac}(H, \dot{H}, \ddot{H}..)$. In RVMs, the dynamical dependency of the VED yields from proper renormalization of quantum effects in QFT in curve spacetime. Thus, the potential dynamics of VED is well motivated from different fundamental perspectives, and therefore, it creates the interest to study the dynamical VED in cosmology. One can find more literature review on RVMs in Refs. [108, 245, 246, 247, 248] and therein.

The other dark component is the cold dark matter(CDM) which is commonly described by pressureless fluid and is responsible for structure formation of the Universe. The first attempt towards developing a general theory of dissipation in relativistic imperfect fluids was carried out by Eckart [29] and in a somewhat different formulation by Landau and Lifshitz[30]. These theories were further developed by Israel and Stewart[28]. The possibility of explaining late-time accelerated expansion of the Universe, as an influence of the effective negative pressure due to bulk viscosity in the cosmic fluids, was first studied in [111, 112] and since then several authors [72, 74, 75, 127, 128, 129, 130, 131, 132, 133, 134, 135, 136, 137, 138, 139, 140, 141, 144, 145, 241, 242] have included bulk viscosity in cosmological models.

The works discussed above show that viscous DM models and a running VED mod-

els are capable in alleviating some of the tensions associated with the ΛCDM model. But these theories have separately some physical limitations to describe the entire evolution of the Universe. However, we can anticipate a more comprehensive physical scenario by combining these two theories to overcome the limitations of each individual approach. Such attempts have been carried out in Refs.[146, 147, 148, 149, 194, 243].

In the light of aforementioned outlines, the main motivation of the present work is to address whether incorporating viscous DM with dynamical vacuum energy into a flat FLRW framework could provide a completely consistent cosmological evolution. In Ref.[194], the authors have explored the late-time evolution of the Universe through viscous DM and decaying vacuum with particular parametrization of decaying vacuum and bulk viscous coefficient $\zeta = \zeta_1 H$. This chapter aims to examine the cosmological evolution by considering a more general parametrization for a running VED along with a simple parametrization of bulk viscous coefficient within Eckart's framework of relativistic non-perfect fluids. As a first step we shall determine the analytical solutions for Hubble function, deceleration parameter and effective equation of state parameter using certain phenomenological assumptions on bulk viscous coefficient and vacuum energy. It is learnt that viscous DM and RVM type of cosmological models can help to improve the best-fit to cosmological observations. Using latest observational data set, such as SNeIa (Pantheon+), BAO (DESI), Cosmic Chronometer (CC) and $f(z)\sigma_8(z)$, we find the best-fit values of parameters to check whether further improvement of the tensions can be attained as compared to ΛCDM model. The Gelman-Rubin statistic (or R-hat statistic) is used to assess the convergence of MCMC simulations. To analyze the stability of our model, we additionally study information criterion such as AIC, BIC and DIC to discuss the stability of the model.

This chapter is structured as follows: In Sec. 4.2 we introduce the mathematical formalism of bulk viscosity with RVM, evolution equations and motivation for assumptions on bulk viscous DM and running VED. In Sec.4.3 we find the analytical solutions for the Hubble parameter, scale factor, equation of state parameter and deceleration parameter. In Sec. 4.4 we analyze the stability of our cosmological model using the scalar perturbation approach. In Sec.4.5, we provide a brief overview of the various observational data used in this work as well as the method employed to constraint the free parameters of the models. We use two datasets: Baseline (SNeIa, CC and BAO(DESI)) and Baseline +$f(z)\sigma_8(z)$ through out the chapter. We also use the priors of Hubble constant of Planck2018 and SH0ES R22 with these datasets. The results

are discussed in Sec. 4.6. In Sec. 4.7 we discuss the convergence diagnostic of Gelman-Rubin for our proposed model. The selection information criteria are presented in Sec. 4.8. Finally, the main findings are summarized in Sec. 4.9.

4.2 Viscous RVM

Let us consider a cosmological framework described by the spatially homogeneous and isotropic flat FLRW metric (2.1). As we know that the simplest explanation for the current observations is the unclumped form of energy density corresponds to positive Λ whose presence modifies the Einstein field equations to

$$G_{\mu\nu} = 8\pi G T_{\mu\nu} + \Lambda g_{\mu\nu}, \tag{4.1}$$

where the symbols have their usual meaning. We consider the presence of two cosmic fluids: running VED and viscous DM. The first fluid represents a vacuum energy density described from the renormalization of QFT in curve spacetime which depends on the Hubble parameter and its time derivatives, $\rho_\Lambda = \rho_\Lambda(H,\dot{H})$. The energy-momentum tensor for the vacuum energy can be assumed to have the same form as $T_{\mu\nu}$, that is,

$$T^{\Lambda}_{\mu\nu} = (\rho_\Lambda + p_\Lambda)u_\mu u_\nu + g_{\mu\nu}p_\Lambda \tag{4.2}$$

where ρ_Λ and p_Λ are the energy density and pressure, respectively for vacuum energy. For vacuum energy density we have $p_\Lambda = -\rho_\Lambda$.

As a second fluid, we assume the imperfect fluid characterized by bulk viscous coefficient as a part of pressureless cold dark matter. The energy-momentum tensor, $T_{\mu\nu}$, for such a viscous fluid modifies to [150]

$$T_{\mu\nu} = (\rho_m + P)u_\mu u_\nu + g_{\mu\nu}P, \tag{4.3}$$

where ρ_m denotes the matter density of the fluid, μ^μ is the associated fluid's four-velocity and $P = p_m - 3\zeta H$.

In this chapter, we combine these two components in a single cosmological scenario and explore their cosmological implications.Considering $p_m = 0$, the Einstein's field equations (4.1) yield

$$3H^2 = \rho = \rho_m + \rho_\Lambda, \tag{4.4}$$

$$2\dot{H}+3H^2=-p=3\zeta H+\rho_\Lambda, \tag{4.5}$$

As usual, the dot sign denotes derivative with respect to the cosmic time. In this work, we present a theory of the Universe's evolution based on time varying VED. From (4.1), the Bianchi identity imply that the coupling between vacuum energy and viscous CDM fluid must be of the type

$$u_\mu T^{\mu\nu}_{;\nu}=-u^\mu\left(\Lambda g^{\mu\nu}\right)_{;\nu}, \tag{4.6}$$

or, equivalently,

$$\dot{\rho}_m+3H(\rho_m-3\zeta H)=-\dot{\rho}_\Lambda, \tag{4.7}$$

This suggest that viscous CDM and varying Λ term are coupled. As a result, there is certain energy exchange amongst vacuum and the viscous CDM fluid. From equations (4.4) and (4.7) together, the evolution equation for Hubble parameter is given by

$$\dot{H}+\frac{3}{2}H^2=\frac{1}{2}\rho_\Lambda+\frac{3}{2}\zeta H. \tag{4.8}$$

4.3 Solution of Field Equations

There are three independent unknown quantities, namely, H, ρ_Λ and ζ in the evolution equation (4.8). One can obtain the solution only when both ρ_Λ and ζ are defined. As previously mentioned, we shall consider the framework of FLRW spacetime in our study. Within the RVM, the generic low-energy form of the VED has been phenomenologically investigated on several prior times and with an impressive level of success. Moreover, it has consistently shown to be very competitive with the ΛCDM and even capable of outperforming the latter's fitting performance. In this chapter, we examine to what extent a viscous dark matter plus running vacuum framework is consistent with current cosmological data to describe the late-time expansion of the Universe. Motivated by the explicit QFT calculations on a FLRW background, the VED in the RVM takes following form [244, 246]

$$\rho_\Lambda=3\left[c_0+\frac{2}{3}\mu\dot{H}(z)+\nu H^2(z)\right], \tag{4.9}$$

where μ and ν are dimensionless parameters and expect that the values of these parameters should be less than one. The value of the additive constant c_0 is fixed by

the boundary condition $\rho_\Lambda(H_0) = \rho_{\Lambda 0}$ and the two evolving components, H^2 and $\dot{H}$ are independent and dimensionally homogeneous. Notice that in above equation (4.9), the parameter μ has an explicit factor $2/3$ for convenience. Additionally, for $\mu, \nu \to 0$, the model smoothly reduce to the concordance ΛCDM.

In literature various methods have been proposed for assuming the evolution of bulk viscosity and different viscous models are produced depending on the choice of ζ. In this chapter, we examine the bulk viscous term ζ is proportional to the Hubble parameter, i.e, to the expansion rate of the Universe which can be expressed as [115, 117, 131, 142, 146, 249]:

$$\zeta = \zeta_1 H. \tag{4.10}$$

Using (4.9) and (4.10), the evolution equation (4.8) has in the following form.

$$(1-\mu)\dot{H} + \frac{3}{2}(1-\nu-\zeta_1)H^2 = \frac{3}{2}c_0. \tag{4.11}$$

We can find the additive constant $c_0 = H_0^2[\Omega_\Lambda - \nu + \mu(1-\Omega_\Lambda - \zeta_1)]$, where $\Omega_{i,0} = \rho_{i,0}/\rho_{cr,0}$ with $\rho_{cr,0} = 3H_0^2/8\pi G$ is the current critical density at $a = 1$. Now, equation (4.11) immediately gives the Hubble function as

$$H^2(z) = H_0^2\left(\tilde{\Omega}_{\Lambda,0} + \tilde{\Omega}_{m,0}(1+z)^{3\left(\frac{1-\nu-\zeta_1}{1-\mu}\right)}\right), \tag{4.12}$$

where

$$\tilde{\Omega}_{\Lambda,0} = \frac{(\Omega_\Lambda - \nu) + \mu(1-\Omega_\Lambda - \zeta_1)}{(1-\nu-\zeta_1)}, \tag{4.13}$$

and

$$\tilde{\Omega}_{m,0} = 1 - \frac{(\Omega_\Lambda - \nu) + \mu(1-\Omega_\Lambda - \zeta_1)}{(1-\nu-\zeta_1)} = 1 - \tilde{\Omega}_{vac,0}. \tag{4.14}$$

Solving Eq. (4.12), we can find the evolution of various cosmological parameters of our model. Given the multiplicity of particles in Grand Unified Theory (GUT), the theoretical value of ν must be below 1. In the calculations carried out in [244], the coefficients μ, ν are expected to be of order $\approx M_X^2/m_{Pl}^2 << 1$, being M_X of order of a typical GUT scale. An estimate of ν in QFT indicates that it is of order 10^{-3} at most [17]. Here, we consider the fact that μ must be small and positive (i.e $0 < \mu << 1$) since the term $(1/1+z)^{3\left(\frac{1-\nu-\zeta_1}{1-\mu}\right)} \to 0$ for virtually any $(1/1+z) < 1$. Further ν can have any sign with $|\nu| << 1$.

By utilizing $H = \dot{a}/a$ and integrating the equation (4.12), one may determine the scale

factor which is given by

$$a(t) = \left(\frac{\tilde{\Omega}_{m,0}}{\tilde{\Omega}_{\Lambda,0}}\right)^{\frac{(1-\mu)}{3(1-\nu-\zeta_1)}} \left(\sinh^{2/3}\left(\frac{t}{\tilde{t}}\right)\right)^{\frac{(1-\mu)}{(1-\nu-\zeta_1)}}, \tag{4.15}$$

where $\tilde{t} \equiv 2/(3H_0\sqrt{\frac{(1-\nu-\zeta_1)[(\Omega_\Lambda-\nu)+\mu(1-\Omega_\Lambda-\zeta_1)]}{(1-\mu)^2}})$. It is evident from the above equation (4.15) that for $\nu = 0$, $\mu = 0$ and $\zeta_1 = 0$, the scale factor reduces to the ΛCDM model, i.e. $a(t) = (\Omega_{m0}/\Omega_{\Lambda 0})^{1/3}\ \sinh^{2/3}(t/\tilde{t})$. The above equation shows that the scale factor varies as $a \propto t^{\frac{2(1-\mu)}{3(1-\nu-\zeta_1)}}$ during early Universe expansion, which is power-law expansion. Further, the scale factor varies as $a \propto \exp\sqrt{\frac{(\Omega_\Lambda-\nu)+\mu(1-\Omega_\Lambda-\zeta_1)}{3(1-\zeta_1-\nu)}}H_0 t$ for late-time evolution, which implies the de Sitter universe. It follows that the model expands with deceleration in the early stages followed by acceleration in the later stages.

In order to investigate the decelerated and accelerated phases of the expansion of the Universe and the evolution during this time, we examine a crucial cosmological parameter, known as the 'deceleration parameter' q, which is defined in Section 1.65. Using (4.12) into (1.65), the value of deceleration parameter q in terms of redshift is calculated as

$$q(z) = -1 + \frac{3}{2(1-\mu)}\left[\frac{(1-\nu-\zeta_1) - [(\Omega_\Lambda-\nu)+\mu(1-\Omega_\Lambda-\zeta_1)](1+z)^{3\left(\frac{1-\nu-\zeta_1}{1-\mu}\right)}}{\left[\frac{(\Omega_\Lambda-\nu)+\mu(1-\Omega_\Lambda-\zeta_1)}{(1-\nu-\zeta_1)} + \left(1 - \frac{(\Omega_\Lambda-\nu)+\mu(1-\Omega_\Lambda-\zeta_1)}{(1-\nu-\zeta_1)}\right)(1+z)^{3\left(\frac{1-\nu-\zeta_1}{1-\mu}\right)}\right]}\right]. \tag{4.16}$$

Moreover, we compute q_0, the current value of q at $z = 0$, which is obtained as

$$q_0 = -1 + \frac{3}{2(1-\mu)}\left[(1-\zeta_1-\Omega_\Lambda) + \mu(1-\Omega_\Lambda-\zeta_1)\right]. \tag{4.17}$$

In order to help us better understand the accelerated phase, we consider another parameter, called as the equation of state (EoS) parameter w_{eff}, that is described in section 1.67. Using (4.12), we obtain

$$w_{eff}(z) = -1 + \frac{1}{(1-\mu)}\left[\frac{(1-\nu-\zeta_1) - [(\Omega_\Lambda-\nu)+\mu(1-\Omega_\Lambda-\zeta_1)](1+z)^{3\left(\frac{1-\nu-\zeta_1}{1-\mu}\right)}}{\left[\frac{(\Omega_\Lambda-\nu)+\mu(1-\Omega_\Lambda-\zeta_1)}{(1-\nu-\zeta_1)} + \left(1 - \frac{(\Omega_\Lambda-\nu)+\mu(1-\Omega_\Lambda-\zeta_1)}{(1-\nu-\zeta_1)}\right)(1+z)^{3\left(\frac{1-\nu-\zeta_1}{1-\mu}\right)}\right]}\right]. \tag{4.18}$$

Further, we compute the present value of $w_{eff}(z=0)$ which is determined as

$$w_{eff}(z=0) = -1 + \frac{1}{(1-\mu)}\left[(1-\zeta_1-\Omega_\Lambda) + \mu(1-\Omega_\Lambda-\zeta_1)\right]. \tag{4.19}$$

4.4 Growth of perturbations

The LSS observable $f(z)\sigma_8(z)$, which is primarily determined by Redshift Space Distortion measurements, plays a crucial role in understanding the formation of structures in the universe. In this section, we want to discuss a few points that will enable us to quickly review why improving the description of structure can also benefit our model in contrast to GR. In terms of the linear density contrast between the matter perturbations, $\delta_m = \delta\rho_m/\rho_m$, the precise differential equation is expressed as

$$\delta_m'' + \left(\frac{3}{a} + \frac{H'(a)}{H(a)}\right)\delta_m' - \frac{3}{2}\Omega_m(a)\frac{\delta_m}{a^2} = 0, \tag{4.20}$$

where the primes denote the derivative with respect to the scale factor. The $\Omega_m(a)$ can be derived from $\Omega_m(a) = 1 - \Omega_\Lambda(a)$ where

$$\Omega_\Lambda(a) = \nu + \frac{1}{H^2(a)}\left[H_0^2\left\{\left(\Omega_\Lambda(a=1) - \nu\right) + \mu\left(1 - \Omega_\Lambda(a=1) - \zeta_1\right)\right\} + \frac{2}{3}\mu a H(a) H'(a)\right]. \tag{4.21}$$

The above equation utilizes the Hubble function that corresponds to the model under consideration. Due to the different Hubble function expression in each model, the above approximation for the structure formation equation is accurate.

In Ref.[194], equation (4.20) turns to be a very good approximation for the analysis of the matter perturbations and thus for present analysis, equation (4.20) is adequate. Details on this aspect of the analysis have been provided in numerous references [161, 162]. Furthermore, in these references the impact is evaluated in considerable detail and the model's ability to reduce S_8 tension is predicated using the same fundamental process. Here, we shall utilize the Hubble function determined in Section-4.3, equation (4.12) to perform our analysis of the matter perturbation in Viscous RVM. The linear LSS regime's investigation is conveniently implemented using the weighted linear growth $f(z)\sigma_8(z)$, where $f(z)$ is the growth factor and is described by $f(z) = d\ln\delta_m/d\ln a$. Here, $\sigma_8(z)$ is the RMS mass fluctuation in spheres with radius $8h^{-1}$ Mpc scales. The calculation specifics are given in the Section 1.16.4.

4.5 Dataset and Methodology

This section briefly describes the observational datasets and the statistical analysis methodology. We use following diverse array of observational datasets, which include latest Pantheon+ obtained from observations of Type Ia Supernovae (SNeIa), cosmic chronometer (CC), Baryonic Acoustic Oscillations (BAO) and $f(z)\sigma_8(z)$ to perform the statistical inference. We also consider two independent Hubble constant measurements that lead to the Hubble ten-

sions [79, 223].

- **SNeIa dataset:Pantheon+:** The Pantheon+ analysis extends the Pantheon dataset by including Cepheid distance measurements to galaxies in the extended dataset of SNeIa. We use Pantheon+ SNeIa compilation [37, 38, 39] which includes the apparent magnitudes and redshifts corresponding to 1701 light curves in the redshift range $0.001 \leq z \leq 2.2613$ that were collected from 1550 SNeIa.
- **H(z) dataset: CC:** Depending on the basis of the relative age of passively evolving galaxies, we employ the most recent estimates of 32 CC data points, precise estimates, and model-independent data in the redshift region $0.07 < z < 1.965$. We have taken into account the impact of the established correlations between the different data points as described in[250].The computation of full covariance matrix for cosmic chronometers has been described in Ref. [250].
- **BAO dataset:** We use the most recent 13 BAO measurements from DESI DR2 including the BGS, LRG1, LRG2, LRG3+ELG1, ELG2, QSO and Lyα samples at effective redshifts z_{eff} = 0.295, 0.51, 0.706, 0.934, 1.321, 1.484 and 2.33, respectively. We use the Dark Energy Spectroscopic Instrument (DESI) BAO measurements from the Data Release 2 [251].
- $\mathbf{f(z)\sigma_8(z)}$ **data :** In this chapter, we utilize the recent compilation of “Gold-17" data which consists of 18 independent measurements of $f(z)\sigma_8(z)$. These data points are compiled in Table III of Ref.[58] and are essentially determined from RSD measurements from many observations of the Large Scale Structure (LSS).
- **Hubble constant measurements:** In the background of the Hubble tension, we use the Hubble constant estimated by the Planck ($H_0^{P18} = 67.4 \pm 0.5\ kms^{-1}Mpc^{-1}$ [79]) collaborations and the SH0ES ($H_0^{R22} = 73.04 \pm 1.04\ kms^{-1}Mpc^{-1}$ [223]). We take these values as priors in the parameter space of ΛCDM and viscous RVM models.

The details regarding the minimized χ^2 values for the datasets presented above are provided in Section 1.16. Statistical analysis is performed using MontePython code *emcee* [36] of Python library. In this code, MCMC method [252] is used to perform the statistical analysis on the input data to constrain the parameters of the viscous RVM. As a comparison, we perform a similar MCMC for the ΛCDM model, also based on the same likelihood. The following combinations are employed for our study:

- **Baseline**: It consists of combination of 3 datasets, namely $SNe\ Ia + CC + BAO$ and the joint χ^2 function is $\chi^2_{Baseline} = \chi^2_{SNe\ Ia} + \chi^2_{CC} + \chi^2_{BAO}$.

- **Baseline +f(z)σ_8(z)**: In this combination, Baseline dataset is complemented $f\sigma_8$, where $\chi^2_{Baseline+f\sigma_8} = \chi^2_{SNe\,Ia} + \chi^2_{CC} + \chi^2_{BAO} + \chi^2_{f\sigma_8}$.

In the next section, we use MCMC sampling technique and the *emcee* library together with the above two splices of full data to see how the results are affected by minimising their respective χ^2 values, that correspond to the likelihood by $\mathscr{L} \propto exp\left(-\frac{\chi^2}{2}\right)$. We built two competing models with each datasets by taking into account the Planck and SH0ES measurements of the Hubble constant as independent priors, while the rest of the cosmological parameters take the initial flat priors. We refer to the models as $P18$ (with the prior H_0^{18}) and $R22$ (with the prior H_0^{22}) for simplicity.

4.6 Results

Let us explore the evolution of the primary cosmological parameters for the best-fit values of the parameters derived from Baseline and Baseline+$f(z)\sigma_8(z)$ datasets with $P18$ and $R22$ priors, rspectively. Tables 4.1 and 4.2 show the constraints on full and subsets of the data, respectively for ΛCDM and viscous RVM models. These results are obtained with a reasonable Gelman-Rubin convergence criterion of $R-1 = 10^{-2}$, which has been discuss in Section 4.7. Figures 4.1 and 4.2 depict the $1-\sigma$ and $2-\sigma$ contour plots of ΛCDM and viscous RVM from Baseline and Baseline+$f(z)\sigma_8(z)$ datasets with $P18$ and $R22$, respectively.

As we know that the one of the key cosmological parameter in cosmology is current value of the Hubble parameter. Recent observations have revealed differences in the Hubble constant H_0 between Planck CMB data [79] and SH0ES-calibrated SNe[223]. This discrepancy is described as “Hubble tension" which is one of the most lingering tensions in cosmology. Note that the Planck Collaboration [79] predicts $H_0^{P18} = 67.4 \pm 0.5 \quad kms^{-1}Mpc^{-1}$, while Riess et al.[223] estimates a higher value of $H_0^{R22} = 73.04 \pm 1.04 \quad kms^{-1}Mpc^{-1}$. This leads to a tension at the level of 4.89σ. Tables 4.1 and 4.2 demonstrate that the present value of H_0 for the viscous RVM are $H_0^{P18} = 67.403 \pm 0.49 \quad kms^{-1}Mpc^{-1}$ and $H_0^{R22} = 72.212 \pm 1.0 \quad kms^{-1}Mpc^{-1}$ from Baseline, respectively, which has 4.318σ level of tension. In contrast, H_0 obtained for ΛCDM model are $H_0^{P18} = 67.410 \pm 0.49 \quad kms^{-1}Mpc^{-1}$ and $H_0^{R22} = 72.776 \pm 0.99 \quad kms^{-1}Mpc^{-1}$, respectively with Baseline, respectively. This leads to a tension at the level of 4.857σ.

Similarly, we have reported the present H_0 for the proposed viscous RVM as $H_0^{P18} = 67.416 \pm 0.48 \quad kms^{-1}Mpc^{-1}$ and $H_0^{R22} = 72.212 \pm 1.0 \quad kms^{-1}Mpc^{-1}$, respectively obtained from Baseline+$f(z)\sigma_8(z)$, which leads to a tension of 4.323σ level. The ΛCDM model have $H_0^{P18} = 67.391 \pm 0.51$ $kms^{-1}Mpc^{-1}$ and $H_0^{R22} = 72.678 \pm 1.00 \quad kms^{-1}Mpc^{-1}$ which has a tension of 4.709σ level. The analysis of present values of Hubble constant show that the viscous RVM minimizes the Hubble tension up to 0.569σ and 0.564σ, respectively with the datasets used for this observation.

Table 4.1: Cosmological constraints on ΛCDM model by Baseline and Baseline+$f(z)\sigma_8(z)$ with Hubble constants priors by the Planck (P18) and the SH0ES (R22) values, respectively, obtained via MCMC analysis.

Model	Dataset	H_0	Ω_Λ	r_d	M	σ_8	S_8
ΛCDM	Baseline+P18	67.410 ± 0.49	0.690 ± 0.008	148.810 ± 1.5	-19.438 ± 0.016	–	–
	Baseline+R22	72.776 ± 0.99	0.691 ± 0.009	137.998 ± 2.1	-19.272 ± 0.030	–	–
ΛCDM	Baseline+f(z)σ_8(z)+ P18	67.391 ± 0.51	0.692 ± 0.007	149.060 ± 1.4	-19.437 ± 0.017	0.753 ± 0.026	0.751 ± 0.022
	Baseline+f(z)σ_8(z)+R22	72.678 ± 1.00	0.693 ± 0.008	138.290 ± 2.1	-19.275 ± 0.030	0.752 ± 0.028	0.762 ± 0.024

The Hubble constant values also remain consistent with the Planck measurement regardless of the prior used.

Figure 4.3 show the evolutions of $H(z)$ with redshift z for ΛCDM and viscous RVM using the baseline+P18 and Baseline+R22, respectively. Figure 4.4 is same as in Figure 4.3 but considering the results obtained with the Baseline+$f(z)\sigma_8(z)$ dataset. It is observed that the trajectories cover the majority of the dataset with $H(z)$ error bars. This indicates that both the datasets used for analysis agree with the viscous RVM. Further, in the current scenario the present age of the Universe is $13.7Gyr$ which is compatible with ΛCDM model with same combination of datasets.

Table 4.2: Cosmological constraints on viscous RVM by Baseline and Baseline+$f(z)\sigma_8(z)$ with Hubble constants priors by the Planck (P18) and the SH0ES (R22) values, respectively, obtained via MCMC analysis.

Model	Dataset	H_0	Ω_Λ	ζ_1	ν	μ	r_d	M	σ_8	S_8
viscous RVM	Baseline+P18	67.403 ± 0.49	0.667 ± 0.012	0.013 ± 0.004	0.005 ± 0.003	0.004 ± 0.003	148.49 ± 1.5	-19.435 ± 0.017	–	–
	Baseline+R22	72.212 ± 1.0	0.669 ± 0.013	0.012 ± 0.005	0.006 ± 0.003	0.003 ± 0.002	137.81 ± 2.2	-19.271 ± 0.031	–	–
viscous RVM	Baseline+f(z)σ_8(z)+P18	67.416 ± 0.48	0.670 ± 0.011	0.012 ± 0.005	0.006 ± 0.003	0.004 ± 0.003	148.62 ± 1.4	-19.435 ± 0.016	0.745 ± 0.028	0.782 ± 0.021
	Baseline+f(z)σ_8(z)+R22	72.212 ± 1.0	0.669 ± 0.013	0.012 ± 0.004	0.006 ± 0.002	0.004 ± 0.002	137.81 ± 2.1	-19.271 ± 0.030	0.749 ± 0.027	0.784 ± 0.024

Focusing on the deceleration parameter q, which plays a crucial role in describing deceleration, acceleration or transition of the Universe, we find present values of $q(z)$ for viscous RVM $q_0 = -0.520 \pm 0.014$ and $q_0 = -0.523 \pm 0.013$ with transition redshift $z_{tr} = 0.646 \pm 0.009$ and $z_{tr} = 0.650 \pm 0.007$, respectively for the Baseline with P18 and R22, whereas Baseline+$f(z)\sigma_8(z)$ dataset with P18 and R22 give $q_0 = -0.523 \pm 0.015$ and $q_0 = -0.524 \pm 0.016$ with $z_{tr} = 0.650 \pm 0.009$ nd $z_{tr} = 0.653 \pm 0.009$, respectively (see, Table 4.3). These value of q_0 are quite comparable to those obtained by the ΛCDM model. The evolution of $q(z)$ with redshift z for viscous RVM

Table 4.3: Present values of cosmological parameters for ΛCDM and viscous RVM with Hubble constant priors by the Planck (P18) and the SH0ES (R22) values.

Model	Dataset	q_0	$w_{eff}(z=0)$	z_{tr}	t_0(Gyr)	j_0
ΛCDM	Baseline+P18	-0.535 ± 0.012	-0.690 ± 0.009	0.645 ± 0.007	13.775 ± 0.256	1
	Baseline+ R22	-0.537 ± 0.014	-0.691 ± 0.008	0.648 ± 0.005	13.790 ± 0.268	1
ΛCDM	Baseline+f(z)σ_8(z)+ P18	-0.538 ± 0.012	-0.692 ± 0.008	0.649 ± 0.007	13.787 ± 0.245	1
	Baseline+f(z)σ_8(z)+ R22	-0.539 ± 0.013	-0.693 ± 0.007	0.652 ± 0.008	13.811 ± 0.288	1
Viscous RVM	Baseline+P18	-0.520 ± 0.014	-0.680 ± 0.006	0.646 ± 0.009	13.805 ± 0.284	0.978 ± 0.004
	Baseline+ R22	-0.523 ± 0.013	-0.681 ± 0.009	0.650 ± 0.007	13.834 ± 0.274	0.978 ± 0.006
Viscous RVM	Baseline+f(z)σ_8(z)+ P18	-0.523 ± 0.015	-0.682 ± 0.008	0.650 ± 0.009	13.825 ± 0.240	0.979 ± 0.007
	Baseline+f(z)σ_8(z)+R22	-0.524 ± 0.016	-0.683 ± 0.007	0.653 ± 0.009	13.839 ± 0.249	0.980 ± 0.005

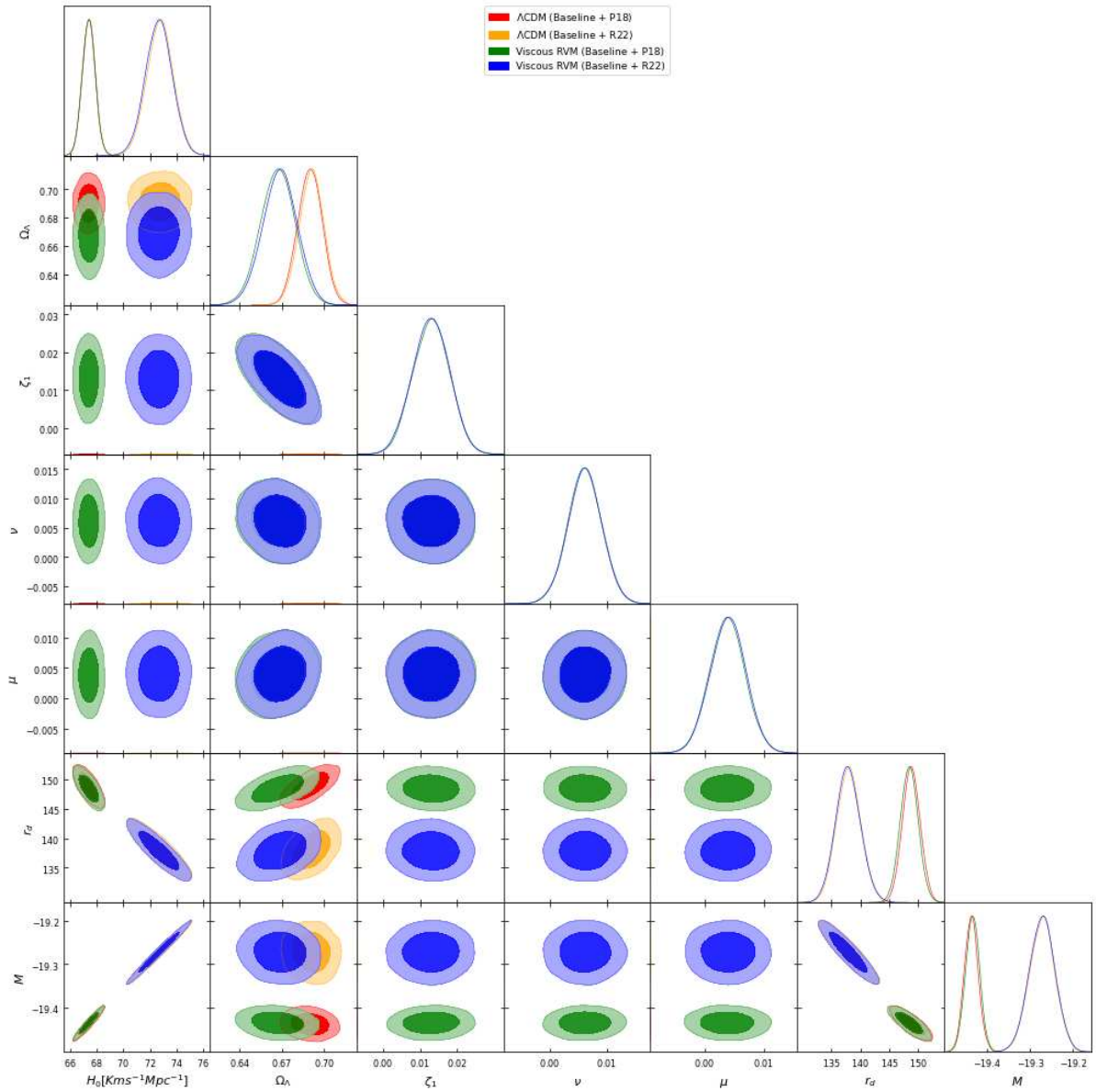

Figure 4.1: Likelihood contours on the ΛCDM and viscous RVM cosmological parameters with the Baseline dataset + the Hubble constant priors from the Planck (P18) and the SH0ES (R22) values at $1-\sigma$ and $2-\sigma$ confidence levels.

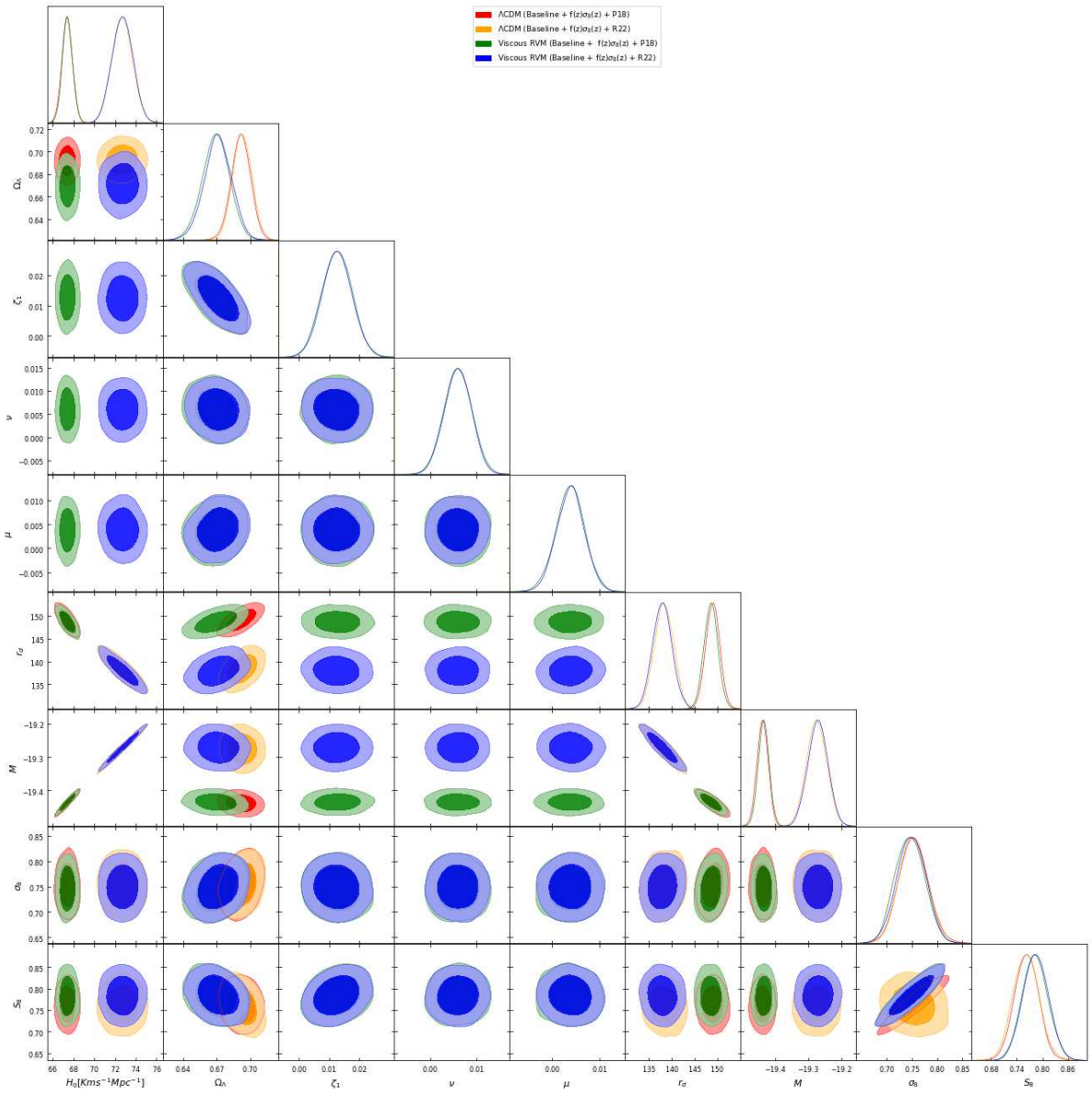

Figure 4.2: The same as in Fig.4.1 but for the Baseline+$f(z)\sigma_8(z)$ dataset + the Hubble constant priors from the Planck (P18) and the SH0ES (R22) values at $1-\sigma$ and $2-\sigma$ confidence levels.

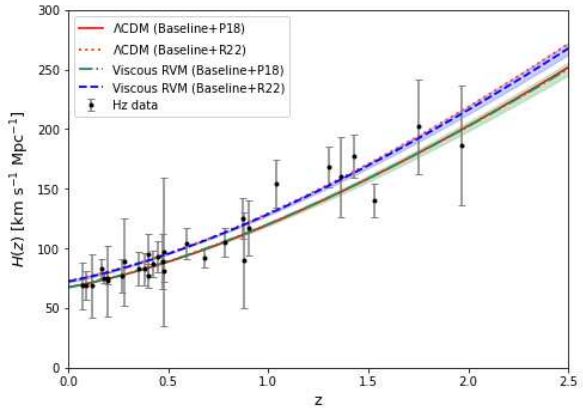

Figure 4.3: The evolution of $H(z)$ with z for ΛCDM model and viscous RVM, using Baseline dataset. The 32 observational data points of $H(z_i)$ are displayed with their associated error bars.

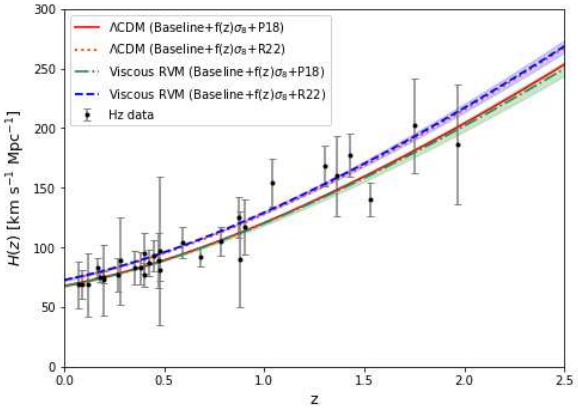

Figure 4.4: The same as in figure 4.3 but considering the results obtained with the Baseline+$f(z)\sigma_8(z)$ dataset.

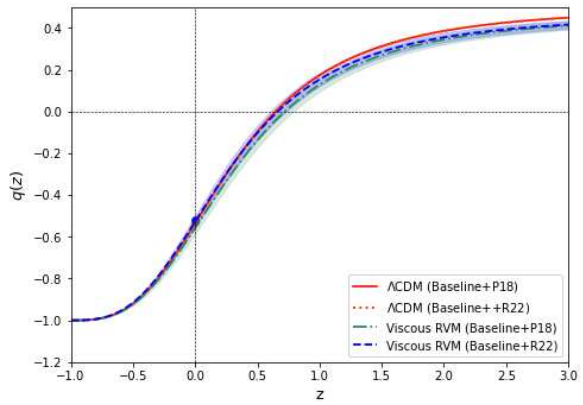

Figure 4.5: Deceleration parameter with redshift z for the ΛCDM model and viscous RVM, using the results obtained from the Baseline dataset.

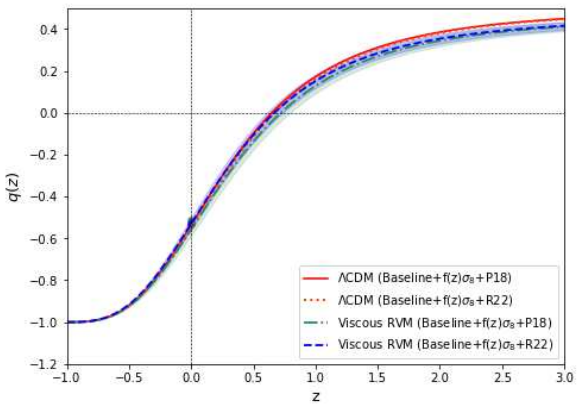

Figure 4.6: The same as in figure 4.5 but considering the results obtained with the Baseline+$f(z)\sigma_8(z)$ dataset.

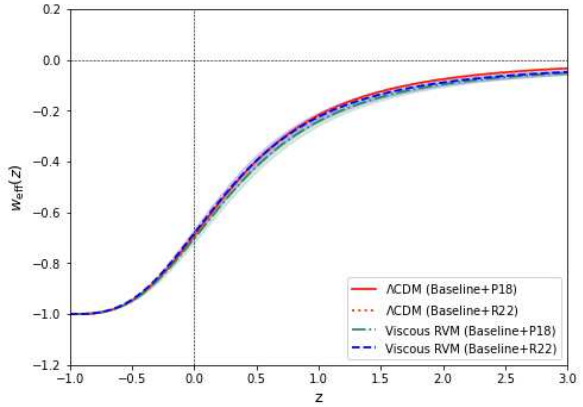

Figure 4.7: Effective equation of state parameter with redshift z for the ΛCDM model and viscous RVM, using the results obtained from the Baseline dataset.

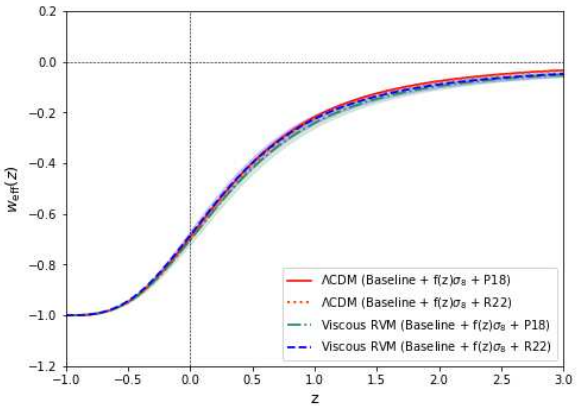

Figure 4.8: The same as in figure 4.7 but considering the results obtained with the Baseline+$f(z)\sigma_8(z)$ dataset.

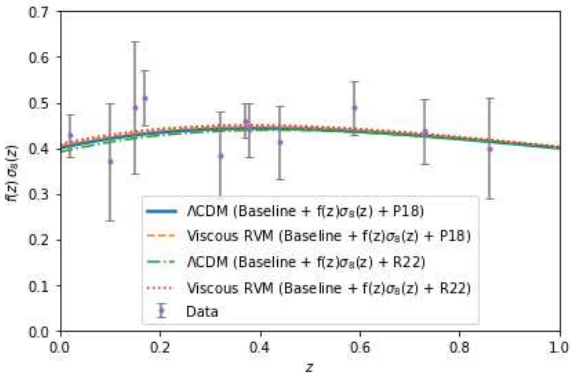

Figure 4.9: $f(z)\sigma_8(z)$ with redshift z for the ΛCDM model and viscous RVM, using the results obtained from the Baseline+$f(z)\sigma_8(z)$ dataset.

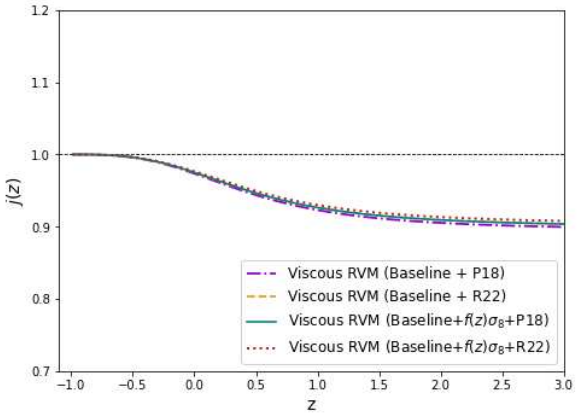

Figure 4.10: Jerk parameter for Viscous RVM using the results obtained with the Baseline and Baseline+$f(z)\sigma_8(z)$ dataset.

models with errors are plotted in Figs. 4.5 and 4.6, respectively for these two combinations of datasets. As $q(z)$ evolves, it clearly shows that Universe has decelerated in the past ($q > 0$) and accelerated recently ($q < 0$). In both models, $q(z)$ approaches -1 in the late-time, corresponding to the future de Sitter phase. The plots also demonstrate that the evolution of $q(z)$ for viscous running vacuum model is consistently compatible with the ΛCDM model across these datasets. We find that the best-fit values of q_0 and z_{tr} align well with the predictions of ΛCDM model and other previous findings by many researchers using different approaches [189, 194, 253, 254, 255].

Further, based on the estimated model parameters, the evolutions of the effective equation of state parameter, $w_{eff}(z = 0)$ are shown in Figs. 4.7 and 4.8 for all dataset combinations. In both models, it is found that the Universe transits from quintessence to de Sitter phase. The present effective EoS parameters for viscous RVM with respect to Baseline and Baseline+$f(z)\sigma_8(z)$ along with P18 and R22 are align with the theoretical predictions for the present value of ΛCDM model.

As we know that the second tension in cosmology is referred as the growth tension. This arises as the result of the discrepancy between the Planck value of the cosmological parameters Ω_m and σ_8 from weak gravitational lensing survey, cluster counts,and the redshift space distortion data. Given the degenerate impacts of these two parameters in lensing surveys, typically weighted amplitude of matter fluctuations $S_8 = \sigma_8\sqrt{(1-\Omega_\Lambda)/0.3}$ is employed as a parameter to compare the consistency with other observations. The weak gravitational lensing surveys provide constraints via cosmic shear, e.g. $S_8 = 0.759^{+0.024}_{-0.021}$ from the Kilo-Degree Survey (KiDS-1000)[256] which is in 3σ tension with the prediction of the Planck Legacy analysis of the cosmic microwave background. The values of σ_8 and S_8 for viscous RVM are $\sigma_8 = 0.745 \pm 0.028$ and $S_8 = 0.782 \pm 0.021$ using Baseline+$f(z)\sigma_8(z)$ with P18, and $\sigma_8 = 0.749 \pm 0.027$ and $S_8 = 0.784 \pm 0.024$ for Baseline+$f(z)\sigma_8(z)$ with R22. We find reasonable

results for the matter sector including the perturbation. These values of $S_8(\sigma_8)$ are aligned with the KiDS-1000 [256]. However, viscous RVM shows a difference of 1.36σ with P22 and 1.27σ with R22 when compare with $S_8(\sigma_8) = 0.814^{+0.011}_{-0.012}(0.802^{+0.022}_{-0.018})$ of KiDS-Legacy [257]. We present the redshift evolution of the growth rate parameter $f\sigma_8(z)$ for ΛCDM and viscous RVM, compared against recent observational measurement of $f\sigma_8(z)$ (see Tables 4.1 and 4.2). These comparisons are shown in Fig. 4.9. We constraint viscous RVM by Baseline+$f(z)\sigma_8(z)$ with P18 and R22 which closely follow the ΛCDM curve.

The results of MCMC analysis for χ^2 and reduced Chi-squared $\chi^2_{red} = \chi^2_{min}/(N-d)$, where N and d are respectively the total number of data points used and number of free parameters, for ΛCDM and viscous RVM are reported in Table 4.5. It is noted that we have $N = 1747$ for Baseline and $N = 1765$ for Baseline+$f\sigma_8$ including P18 or R22. In viscous RVM, $d = 5$ and in ΛCDM, we have $d = 2$. Table 4.5 reveals that the χ^2_{red} is less than unity for both the models with both combinations of datasets. Note that a value of $\chi^2_{red} < 1$ is considered the best-fit with data while $\chi^2_{red} > 1$ is considered a bad fit. This indicates that both the models fit these observational data sets quite effectively and that the observed data are compatible with the concerned models.

As a supplementary information, we include an additional purely kinematical parameter, which is called the jerk parameter $j(z)$ and is described in 1.70. It provide us with the departure of our model from the ΛCDM model. It is observed that for the ΛCDM model, jerk parameter always has a constant value of $j = 1$. The evolution of $j(z)$ for the viscous RVM and ΛCDM model are plotted in Fig. 4.10 using the best-fit parameter values derived from two different combinations of dataset. The positive value of $j(z)$ indicates an accelerating expansion of the Universe. The present values of jerk parameter for viscous RVM are $j_0 = 0.978 \pm 0.004$ for Baseline +P18 and $j_0 = 0.978 \pm 0.006$ for Baseline+R22 dataset, and $j_0 = 0.979 \pm 0.007$ for Baseline+$f\sigma_8(z)$ +P18 and $j_0 = 0.980 \pm 0.005$ for Baseline+$f\sigma_8(z)$ +R22 dataset, which slight deviation from the ΛCDM model. However, in late time, jerk parameter tends to 1 for all datasets.

4.7 Convergence diagnostics

Convergence diagnostics is a tool which is used to assess the stability state of the MCMC simulation. This diagnostics ensure the validity and reliability of the result obtained from MCMC analysis. The Gelman-Rubin (GR) diagnostic is one of the most commonly used techniques to evaluate the convergence of MCMC simulations. This diagnostic works by running multiple Markov chains, denoted as $\{X_{i0}, X_{i1}, \ldots, X_{in-1}\}$ for $i = 1, \ldots, m$, with each chain initialized from an over-dispersed starting distribution compared to the target distribution π. Gelman and Rubin[258] presented approaches to construct such initial distributions, although

in practice, these starting points are often selected arbitrarily. When running these m parallel chains, two variance estimators are computed for a variable $X \sim \pi$. The first is the within-chain variance:

$$W = \sum_{i=1}^{m} \sum_{j=0}^{n-1} (X_{ij} - \bar{X}_i)^2 / (m(n-1)) \tag{4.22}$$

where $\bar{X}_i$ is the mean of the ith chain.

The second is the pooled (between-chain) variance estimate:

$$\hat{V} = \frac{n-1}{n} W + \frac{B}{n} \tag{4.23}$$

where

$$B = n \left(\sum_{i=1}^{m} \frac{(\bar{X}_i - \bar{X}_{..})^2}{m-1} \right) \tag{4.24}$$

with $\bar{X}_{..}$ representing the overall mean across all chains.

Gelman and Rubin [258] suggested comparing the ratio of the pooled to the within-chain variance, known as the potential scale reduction factor (PSRF):

$$\hat{R} = \frac{\hat{V}}{W} \tag{4.25}$$

A value of $\hat{R}$ close to 1 indicates convergence. As more samples are drawn and the chains mix, $\hat{R}$ approaches 1.

In this chapter, to assess the convergence of our Markov Chain Monte Carlo sampling, we execute four independent chains using the emcee package. Each chain was initialized from a different starting position to ensure diverse exploration of the parameter space. We ran each chain for a total of 5000 iterations. To eliminate the influence of initial transients, we treat the first 2000 samples from each chain as burn-in and excluded them from all subsequent analyses. After discarding these burn-in samples, we evaluate convergence by calculating the Gelman-Rubin statistic $\hat{R}$ for each model parameter. The $\hat{R}$ values of parameters of ΛCDM and viscous RVM model are given in Table 4.4 which shows that both the models converge to 1 for both datasets, indicating that the chains had converged satisfactorily. In addition, we visualize the sampling behavior by plotting trace plots for each parameter of ΛCDM and viscous RVM models using baseline and baseline+ $f(z)\sigma(z)$ datasets, respectively as shown in figures 4.11–4.18, which further confirm that the chains are well-mixed and stable after burn-in.

Table 4.4: The $\hat{R}$ values of parameters for ΛCDM and viscous RVM models with Hubble constant priors by the Planck (P18) and the SH0ES (R22) values.

Model	Dataset	H_0	Ω_Λ	ζ_1	ν	μ	r_d	M	σ_8
ΛCDM	Baseline+P18	1.0003	1.0002	–	–	–	1.0005	1.0004	–
	Baseline+R22	1.0003	1.0000	–	–	–	1.0002	1.0003	–
ΛCDM	Baseline+f(z)σ_8(z)+ P18	1.0000	1.0000	–	–	–	1.0000	1.0000	1.0008
	Baseline+f(z)σ_8(z)+ R22	1.0000	1.0000	–	–	–	1.0001	1.0000	1.0000
Viscous RVM	Baseline+P18	1.0000	1.0000	1.0004	1.0001	1.0006	1.0000	1.0000	–
	Baseline+ R22	1.0008	1.0001	1.0002	1.0007	1.0001	1.0006	1.0006	–
Viscous RVM	Baseline+f(z)σ_8(z)+P18	1.0003	1.0000	1.0006	1.0000	1.0004	1.0002	1.0003	1.0000
	Baseline+f(z)σ_8(z)+ R22	1.0008	1.0000	1.0002	1.0009	1.0000	1.0009	1.0007	1.0000

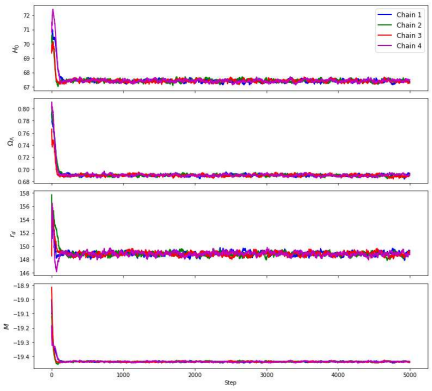

Figure 4.11: Trace plot ΛCDM model using Baseline dataset with P18.

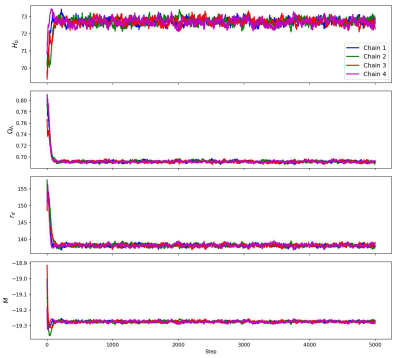

Figure 4.12: Trace plot ΛCDM model using Baseline dataset with R22.

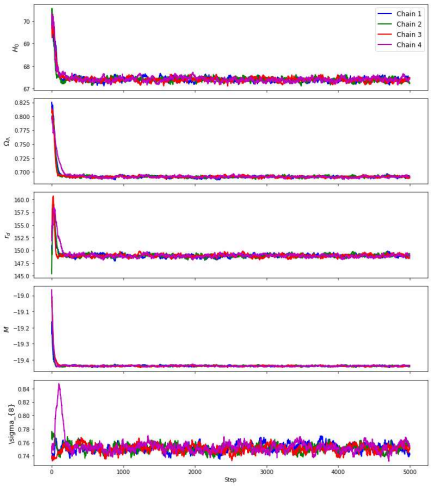

Figure 4.13: Trace plot ΛCDM model using Baseline + f(z)$\sigma_8(z)$ dataset with P18.

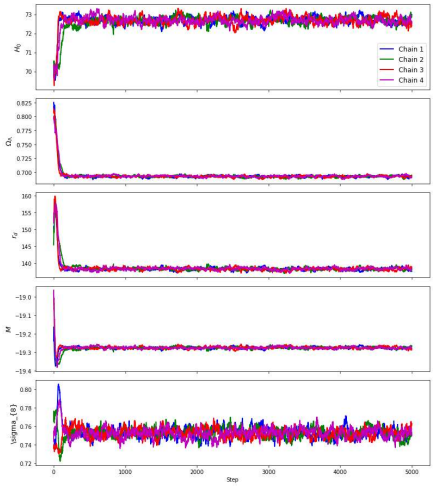

Figure 4.14: Trace plot ΛCDM model using Baseline + f(z)$\sigma_8(z)$ dataset with R22.

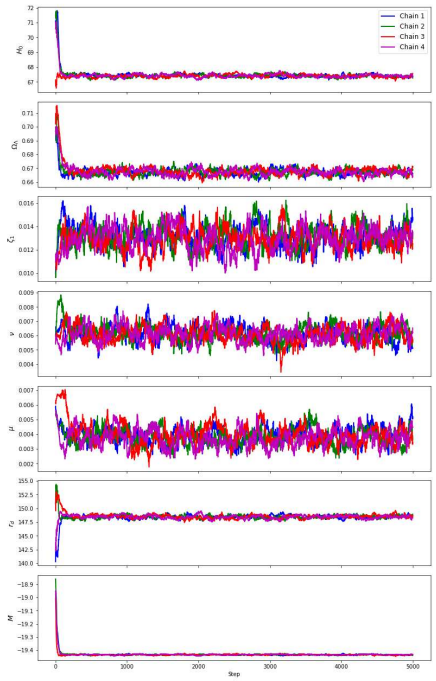

Figure 4.15: Trace plot Viscous RVM using Baseline dataset with P18.

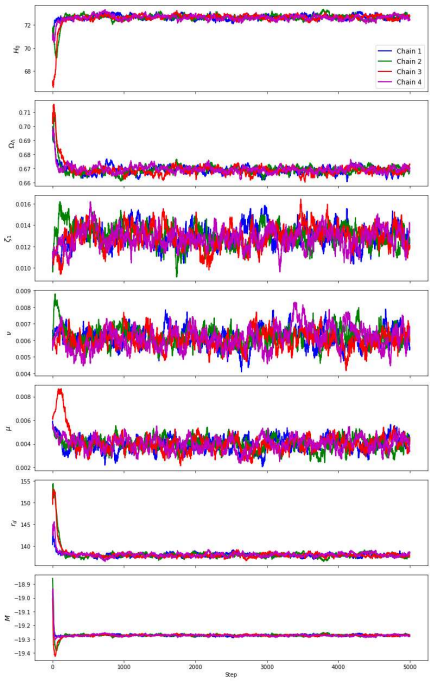

Figure 4.16: Trace plot Viscous RVM using Baseline dataset with R22.

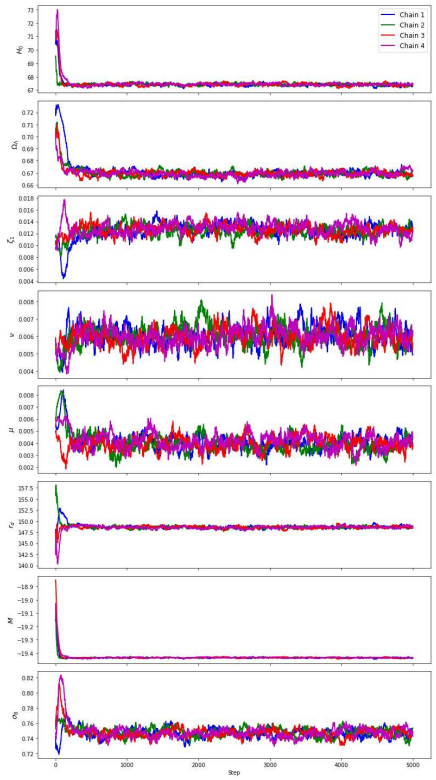

Figure 4.17: Trace plot Viscous RVM using Baseline + f(z)$\sigma_8(z)$ dataset with P18.

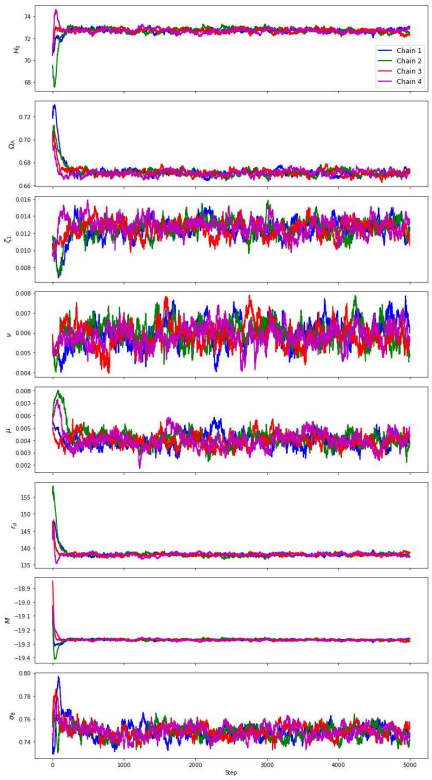

Figure 4.18: Trace plot Viscous RVM using Baseline + f(z)$\sigma_8(z)$ dataset with R22.

Table 4.5: The reduced chi-squared $\chi^2_{red} = \chi^2/N - d$, AIC, BIC, DIC values for viscous RVM model with the Hubble constant Priors by the Planck (P18) and the SH0ES (R22) values.

Model	Dataset	χ^2_{min}	d	N	χ^2_{red}	AIC	BIC	DIC	ΔAIC	ΔBIC	ΔDIC
ΛCDM	Baseline+P18	1581.053	2	1747	0.906	1585.053	1595.984	1585.969	–	–	–
	Baseline+R22	1582.420	2	1747	0.907	1586.420	1597.351	1586.222	–	–	–
ΛCDM	Baseline+f(z)σ_8(z)+P18	1593.451	2	1765	0.903	1597.451	1608.403	1597.411	–	–	–
	Baseline+f(z)σ_8(z)+ R22	1594.890	2	1765	0.905	1598.890	1609.841	1599.567	–	–	–
Viscous RVM	Baseline+P18	1573.334	5	1747	0.903	1583.334	1610.662	1585.404	−1.719	14.678	−0.565
	Baseline+R22	1573.531	5	1747	0.903	1583.531	1610.859	1586.044	−2.889	13.508	−0.178
Viscous RVM	Baseline+f(z)σ_8(z)+ P18	1587.194	5	1765	0.902	1597.194	1624.573	1598.255	−0.257	16.170	0.844
	Baseline+f(z)σ_8(z)+R22	1589.721	5	1765	0.903	1599.721	1627.100	1600.326	0.831	17.259	0.759

4.8 Model Selection Statistics

Finally, we assess the statistical relevance of the data fitting and the observational compatibility of the models by applying the well-known Akaike Information Criterion (AIC), the Bayesian Information Criterion (BIC), and the Deviance Information Criterion (DIC). These criteria evaluate fitted models against a reference model. The details on minimized χ^2 of above datasets are given in section 4.6.

Table 4.5 displays the values of ΔAIC, ΔBIC and ΔDIC assuming the ΛCDM as the referring model. We find the values of $(\Delta AIC, \Delta BIC, \Delta DIC) = (-1.719, 14.678, -0.565)$ for Baseline+P18 and $(\Delta AIC, \Delta BIC, \Delta DIC) = (-2.889, 13.508, -0.178)$ for Baseline+R22, and $(\Delta AIC, \Delta BIC, \Delta DIC) = (-0.257, 16.170, 0.844)$ for Baseline+$f(z)\sigma_8(z) + P18$ and $(\Delta AIC, \Delta BIC, \Delta DIC) = (0.831, 17.259, 0.759)$ for Baseline+$f(z)\sigma_8(z) + R22$. The values of $\Delta AIC(\Delta DIC)$ show that the datasets have strong support in favor of viscous RVM model. In contrast, the evaluation based on ΔBIC, we find that both the datasets exhibit a strong support for the ΛCDM model.

This discrepancy arises because AIC (DIC) tends to be more inclusive in model selection. The BIC imposes a stronger penalty on models with more number free parameters than AIC(DIC) and that the penalization function is proportional to the number of points in the dataset.

4.9 Conclusion

In this chapter, we have examined a bulk viscous cosmological model in the framework of time-varying vacuum energy density, where the bulk viscosity coefficient is proportional to the Hubble parameter H. Additionally, we have assumed a generic form of the VED which is proportional to $\dot{H}$ and H. This type of model has been the subject of discussions in the literature [16, 95, 180, 259, 260] and the references therein. These models have withstand numerous benchmark tests against all kinds of contemporary data with success and proved their robustness and viability as strong competitors to the standard ΛCDM model.

This is true not only in terms of their ability to fit the recent cosmological data, but also important in terms of elevating the significance of the ΛCDM and its extensions in the context of theoretical physics. The primary distinctive characteristic of the RVM is predicting the existence of dynamical dark energy (DDE) related with the vacuum. In other words, the running vacuum manifests itself as a type of DDE, but it is actually (quantum) vacuum, and not merely an additional phenomenon taken out of the dark energy's blackbox to imitate or replace the core idea of vacuum energy in QFT. Since the VED in QFT must be renormalized, the rigid cosmological term Λ does not exist in the RVM paradigm. The renormalization scale is dynamic; hence, the calculated quantum corrections result in a time-evolving VED with the expansion [260]. In the context of QFT in curved spacetime, precise calculations have recently reinforced the general structure of the RVM. As mentioned in the references [244, 245, 246], the smooth VED dynamics in the RVM was long anticipated based on semi-qualitative renormalization group arguments and it was only confirmed recently in an entire QFT context. In RVM framework, a true cosmological constant does not exist and it is reasonable to assert that a rigid parameter of this kind, is not predicted in renormalizable QFT [260].

Regarding the analysis presented in this chapter, we have focused on the implementation of viscous RVM, in order to facilitate a better comparison with earlier studies, especially the most recent one in Ref. [194]. In our approach, we have described a novel and comprehensive parametrization of bulk viscous coefficient and VED. The viscous RVM has one additional parameter μ. The dynamical component of the VED is proportional to the scalar of curvature, $\dot{H}$ and H^2, with its coefficient μ and ν respectively. Although such a coefficient can be analytically explained in QFT, in practical application it has to be fitted to the overall cosmological data because it depends on the masses of all the quantized matter fields. We have employed the chosen parameterizations in order to derive analytical solutions for different cosmological parameters, including $H(z)$, $a(t)$, $q(z)$, $w(z)$ and $j(z)$.

We have validated our findings using observational data from a wide range of sources, which comprises of, SNeIa pantheon+, CC, BAO and $f(z)\sigma_8(z)$ datasets. The priors of the present Hubble constant from Planck and SH0ES have been implied with these two datasets. Applying the MCMC methodology, the constraints of the model parameters of ΛCDM and viscous RVM have been estimated which are presented in Tables 4.1 and 4.2. When a global fit is made to the cosmological dataset using two different combinations, including the Baseline and Baseline+ $f(z)\sigma_8(z)$, and the rigid option $\nu, \mu, \zeta = 0$ (i.e., Λ=constant corresponding to the ΛCDM model) is compared with the viscous RVM ($\nu, \mu, \zeta \neq 0$), we observed that a mild dynamics of the cosmic vacuum ($\nu, \mu \sim 10^{-3}$) and viscosity ($\zeta \sim 0.01$) is strongly preferred. We have evaluated convergence by calculating the Gelman-Rubin statistic $\hat{R}$ for each model parameter. The $\hat{R}$ values of parameters of ΛCDM and viscous RVM model

are given in Table 4.4 which shows that both the models converge to 1 for both datasets, indicating that the chains had converged satisfactorily. The analysis of present values of Hubble constant show that the viscous RVM minimizes the Hubble tension up to 0.569σ and 0.564σ, respectively with the datasets used for this observation. The Hubble constant values also remain consistent with the Planck measurement regardless of the prior used. In other words, the MCMC analysis naturally favors the Planck value of H_0. This holds when both the Baseline and Baseline $+f(z)\sigma_8(z)$ have been considered. We have also found the reasonable results for the matter sector including the perturbation. These values of $S_8(\sigma_8)$ are aligned with the KiDS-1000 [256]. However, viscous RVM shows a difference of 1.36σ with P22 and 1.27σ with R22 when compare with $S_8(\sigma_8) = 0.814^{+0.011}_{-0.012}(0.802^{+0.022}_{-0.018})$ of KiDS-Legacy [257]. The analysis of other cosmological parameters such as deceleration parameter, EoS parameters and jerk parameter and their corresponding present values reveal that the viscous RVM describes the Universe transits from a decelerated phase to accelerated phase. The comparison with ΛCDM model demonstrates the efficacy of our parametrization of viscous RVM in determining the late-time cosmic acceleration.

We have reported the model selection criteria such as AIC, BIC and DIC of proposed viscous RVM with reference to the ΛCDM model. According to ΔAIC(ΔDIC), viscous RVM has “strong evidence in favour", and as far as ΔBIC is concerned, we have obtained the values > 10 and hence strong support of ΛCDM model.

To conclude, it is intriguing that the interacting viscous DM and vacuum energy density, i.e., viscous RVM provides the present values of Hubble constant which alleviates the Hubble tension. The viscous RVM which have been considered seems to be consistent with ΛCDM model in terms of evolution and present values of cosmological parameters such as the Hubble parameter, deceleration parameter, EoS parameter and jerk parameter. Our model is able to explain the accelerated expansion of the Universe with the consistency of observational datasets. Our findings imply that the dark energy is most likely dynamical and assumes the running vacuum form with viscosity. The potential for late-time new physics in the dark sector, which may be concealed behind these ongoing cosmological tensions, cannot yet be ruled out.

****

Chapter 5

Time-varying vacuum energy models in Brans-Dicke theory

In this chapter [1], we discuss decaying vacuum energy model, which suggests that vacuum energy is not constant but decreases as Universe expands, in a modified theory of gravity, known as Brans-Dicke (BD) theory. The solution of the field equations lead to late-time acceleration and model's parameters are consistent with the observations.

Highlights:

☞ Presents a cosmological model with decaying vacuum and bulk viscosity in the framework of FLRW spacetime in Brans-Dicke theory.

☞ Instead of constant Λ, a time-varying vacuum energy density ρ_Λ as a truncated power series of Hubble parameter up to second order, $\Lambda(t) = n_1 H + n_2 H^2$ and power-law $\Lambda(t) = 3\gamma a^{-n}$ are assumed to find the solutions of the proposed models.

☞ The BD theory introduces a scalar field ϕ in place of $1/G$ which permeates spacetime which distinguishes from the standard ΛCDM model.

☞ The scalar field ϕ is assumed to be related to the scale factor a by a power-law relation, $\phi = \phi_0 a(t)^\varepsilon$, where ϕ_0 and ε are constants.

☞ Analytical solutions of two proposed models are obtained for Hubble parameter in terms of redshift.

[1] This chapter is based on a published research paper "Constraining the time-varying vacuum energy models in Brans-Dicke theory, *Astrophysics and Space Science* **368**, 16 (2023)".

☞ Observational analysis are performed using SNe Ia, Hubble data and BAO by MCMC simulation method.

☞ The different cosmological parameters show that there is a smooth transition from decelerated phase to the late-time accelerated phase approaching to de Sitter model.

☞ The information criterion AIC and BIC suggest that both the models have strong evidence in favor over the ΛCDM model.

☞ Presents a summary of findings in last section.

5.1 Introduction

In the current view of modern cosmology, the nature and origin behind the current accelerating expansion of the Universe constitute a major problem. The analysis and interpretation of many observational data like Type Ia supernova [34, 261, 262], galaxy clustering [263], Cosmic microwave background radiation [264] and other cosmological observations [11, 67, 265, 266, 267] provide a cosmic expansion of the Universe that involves a recent accelerated expansion. This phenomena has been discussed either by adding an energy component in energy-momentum tensor usually called Dark energy (DE) which has negative pressure, or modifying the General theory of relativity. The Cosmological constant (CC), which was initially introduced by Albert Einstein to make the static Universe, is a natural and simplest candidate of DE. This DE model, so-called standard Lambda-cold dark matter (ΛCDM) model, fits accurately the current observational data and describes well the observed Universe, but faces two serious problems, namely, the fine-tuning and the cosmological coincidence problems [10, 176].

In the recent years, these longstanding problems have galvanized a variety of alternative theories beyond the ΛCDM model, including a dynamical Λ instead of just assuming the Λ as a constant. The $\Lambda(t)$ model is based on vacuum quantum fluctuations in the curved space-time, and the resulting effective vacuum energy density depends on the space-time curvature which decays from high initial values to smaller ones as the Universe expands [268]. In Quantum field theory, the renormalization group [269] describes a dynamical vacuum energy, in which the Λ-term varies as $\Lambda \sim H^2$, and a number of flat FLRW models have been studied by assuming the vacuum energy density as a truncated power-series in terms of Hubble parameter H [97, 99, 100, 101, 102, 103, 105, 107, 270, 271, 272].

On the other hand, the scalar–tensor theories have been reconsidered extensively in literature, in particular, the Brans–Dicke theory. Brans and Dicke [24] introduced this scalar–tensor

theory to incorporate the Mach's principle in general relativity. In this theory, a scalar field ϕ is included in the Einstein–Hilbert action that makes the Newtonian gravitational constant G as a function of coordinates. We replace the gravitational constant G by an inverse of time-varying scalar field ϕ, which couples to gravity with a coupling parameter ω. However, in the limit $\omega \to \infty$, BD theory reduces to the corresponding general relativity.

In recent years, this theory has received significant attention as it successfully describes the early inflationary era and late-time evolution of the Universe. Many authors [130, 144, 145, 184, 273, 274, 275, 276, 277, 278, 279, 280, 281, 282, 283, 284, 285, 286, 287, 288, 289, 290, 291, 292, 293] have extensively studied FLRW model in the framework of BD theory. Since the vacuum energy models have the dynamical behavior, it is more suitable to consider the models in a dynamical framework such as BD theory.

In this chapter, we extend the successful approach recently presented on BD cosmology with decaying vacuum energy by Singh and Sol$\grave{a}$ (2021) [184] with the some suitable form of $\Lambda(t)$. Here, we assume two different functional form of time-varying Λ: a power series up to the second order of H and a power-law form. We focus our attention on exact solutions and discuss the observational aspects of $\Lambda(t)$ models in the framework of BD theory. Additionally, we perform a Bayesian MCMC method to constrain the space parameters using the observational data of SNe Ia, Hubble data and BAO. Using the best-fit values of parameters we discuss the evolution of the Universe through Hubble parameter, deceleration and equation of state parameters, and check the consistency of the analytical solution so far obtained for the both models. The model selection criteria and jerk parameters are also discussed and compared the models with the standard ΛCDM model.

The chapter is organized as follows: In Sect. 5.2, we propose the model and basic field equations in BD theory with cosmological constant. The analytical solutions of the field equations are presented in Sects. 5.3 and 5.4 with two different functional forms of $\Lambda(t)$. In Sect. 5.5, we discuss the latest observational data and method to constrain the main parameters of our vacuum models. In Sect. 5.6, we analyze the models by using the best-fit values of model parameters. Section 5.7 discusses the statistical criteria of AIC and BIC in respect of the models along with ΛCDM. In Sect. 5.8, we draw our conclusions.

5.2 BD field equations with varying–$\Lambda(t)$

The action of Einstein-Hilbert in Jordan frame for BD theory defined in Eq. (1.45) is modified by inclusion of cosmological constant Λ to [293, 294]

$$S = \int d^4x\sqrt{-g}\left[\frac{1}{16\pi}\left(\phi R - \frac{\omega_{BD}}{\phi}\partial_a\phi\partial^a\phi\right) - \rho_\Lambda\right] + \int d^4x\sqrt{-g}\mathscr{L}_m, \tag{5.1}$$

where $g = |g_{\mu\nu}|$, $\sqrt{-g}d^4x$ is the four-dimensional volume form, and $\mathscr{L}_m$ is the matter Lagrangian density. Assume that the cosmological constant Λ implies as vacuum energy density with EoS $p_\Lambda = -\rho_\Lambda$.

Varying the action (5.1) with respect to the metric $g_{\mu\nu}$, the field equations of the BD theory are

$$R_{\mu\nu} - \frac{1}{2}g_{\mu\nu}R = \frac{8\pi}{\phi}\left(T_{\mu\nu}(\text{matter}) - g_{\mu\nu}\rho_\Lambda\right) + \frac{\omega_{BD}}{\phi^2}\left(\phi_{,\mu}\phi_{,\nu} - \frac{1}{2}g_{\mu\nu}\phi_{,\alpha}\phi^{,\alpha}\right) + \frac{1}{\phi}\left(\phi_{,\mu;\nu} - g_{\mu\nu}\Box\phi\right), \tag{5.2}$$

Varying with respect to ϕ, we get the following scalar field equation (wave equation)

$$\Box\phi = \frac{8\pi}{2\omega_{BD}+3}\left(T(\text{matter}) + \frac{\Lambda}{8\pi}\phi\right), \tag{5.3}$$

where ϕ is the scalar field, ω_{BD} is the dimensionless Dicke coupling constant and $\Box$ is the Laplace operator or covariant wave operator, $\Box\phi = \phi^{;a}_{;a}$, and $T = T^{\mu}_{\mu}$ is the trace of energy-momentum tensor.

The field equations of BD theory defined in Eq.(5.2) can be rewritten as

$$R_{\mu\nu} - \frac{1}{2}g_{\mu\nu}R = \frac{8\pi}{\phi}\tilde{T}_{\mu\nu} + \frac{8\pi}{\phi}T^{BD}_{\mu\nu}, \tag{5.4}$$

where $\tilde{T}_{\mu\nu} \equiv T_{\mu\nu} - g_{\mu\nu}\rho_\Lambda$ is the total energy-momentum tensor, that is, the sum of the matter and vacuum contributions. Here $\rho_\Lambda = \Lambda/8\pi G = \Lambda\phi/8\pi$ is the vacuum energy density and $T_{\mu\nu} = (\rho_m + p_m)\,u_\mu u_\nu + p_m\, g_{\mu\nu}$ is the ordinary energy-momentum tensor of perfect fluid, where ρ_m is the energy density of matter, p_m is the corresponding pressure and u_μ is the four-velocity vector. Thus, we consider $\tilde{T}_{\mu\nu}$ as a perfect fluid form of energy-momentum tensor which is given by

$$\tilde{T}_{\mu\nu} = (\rho + p)\,u_\mu u_\nu + p\, g_{\mu\nu}, \tag{5.5}$$

where $\rho = \rho_m + \rho_\Lambda$ and $p = p_m + p_\Lambda$.

In Eq. (5.4), $T^{BD}_{\mu\nu}$ is considered as

$$T^{BD}_{\mu\nu} = \frac{1}{8\pi}\left[\frac{\omega_{BD}}{\phi}\left(\nabla_\mu\phi\nabla_\nu\phi - \frac{1}{2}g_{\mu\nu}\nabla_\alpha\phi\nabla^\alpha\phi\right) + \nabla_\mu\nabla_\nu\phi - g_{\mu\nu}\nabla_\alpha\nabla^\alpha\phi\right], \tag{5.6}$$

which is assumed to be perfect fluid like form of BD energy-momentum tensor

$$T^{BD}_{\mu\nu} = (\rho_{BD} + p_{BD})u_\mu u_\nu + p_{BD}g_{\mu\nu}, \tag{5.7}$$

where

$$\rho_{BD} = \frac{1}{8\pi}\left[\frac{\omega_{BD}}{2}\left(\frac{\dot{\phi}^2}{\phi}\right) - 3H\dot{\phi}\right], \tag{5.8}$$

$$p_{BD} = \frac{1}{8\pi}\left[\frac{\omega_{BD}}{2}\left(\frac{\dot{\phi}^2}{\phi}\right) + 2H\dot{\phi} + \ddot{\phi}\right], \tag{5.9}$$

For energy-momentum tensors (5.5) and (5.6), the BD field equations for FLRW metric (2.1) yield

$$3H^2 + 3H\frac{\dot{\phi}}{\phi} - \frac{\omega_{BD}}{2}\frac{\dot{\phi}^2}{\phi^2} = \frac{8\pi}{\phi}\rho, \tag{5.10}$$

$$2\dot{H} + 3H^2 + \frac{\ddot{\phi}}{\phi} + 2H\frac{\dot{\phi}}{\phi} + \frac{\omega_{BD}}{2}\frac{\dot{\phi}^2}{\phi^2} + = -\frac{8\pi}{\phi}p, \tag{5.11}$$

$$\ddot{\phi} + 3H\dot{\phi} = \frac{8\pi}{(2\omega_{BD}+3)}(\rho - 3p). \tag{5.12}$$

The consistency of the BD field equations (5.4) yield

$$\nabla_\nu\left(R^{\mu\nu} - \frac{1}{2}g^{\mu\nu}R\right) = 0 = \nabla_\nu\left(\frac{8\pi}{\phi}\tilde{T}^{\mu\nu} + \frac{8\pi}{\phi}T^{\mu\nu}_{BD}\right). \tag{5.13}$$

Assuming that the matter with vacuum and scalar field conserve separately, i.e., $\tilde{T}^{\mu\nu}$ obeys the usual conservation law, $\nabla_\nu\tilde{T}^{\mu\nu} = 0$, which leads to

$$\dot{\rho_m} + 3H(\rho_m + p_m) = -\dot{\rho_\Lambda}. \tag{5.14}$$

One should note here that the EoS of the vacuum energy density follows the same usual form, i.e., $p_\Lambda(t) = -\rho_\Lambda(t) = -\phi\Lambda(t)/8\pi$ despite it evolves with time. From (5.13), we obtain

$$8\pi\tilde{T}^{\mu\nu}\,\nabla_\nu\left(\frac{1}{\phi}\right) + \nabla_\nu\left(\frac{8\pi}{\phi}T^{\mu\nu}_{BD}\right) = 0, \tag{5.15}$$

which simplifies to

$$\dot{\rho}_{BD} + 3H(\rho_{BD} + p_{BD}) = (\rho_m + \rho_\Lambda + \rho_{BD})\frac{\dot{\phi}}{\phi}. \tag{5.16}$$

In this chapter, we assume that the scalar field ϕ is related to scale-factor a by a power-law relation [273, 295, 296]:

$$\phi = \phi_0\, a(t)^\varepsilon, \tag{5.17}$$

where ϕ_0 and ε are constants. Using (5.17) into (5.10), we get

$$H^2 = \frac{2}{(6 + 6\varepsilon - \omega_{BD}\varepsilon^2)}\frac{8\pi}{\phi}(\rho_m + \rho_\Lambda), \tag{5.18}$$

where $\Lambda = 8\pi\rho_\Lambda/\phi$. One can find that the standard cosmology is recovered in the limit of $\varepsilon \to 0$.

Finally, using (5.14) and (5.18), we find

$$\dot{H} + \frac{(3+\varepsilon)}{2}H^2 = \frac{3\Lambda}{(6 + 6\varepsilon - \omega_{BD}\varepsilon^2)}. \tag{5.19}$$

In the following sections, we find the exact solutions with two forms of $\Lambda(t)$: power-series and power-law forms.

5.3 A power series $\Lambda(t)$ model

In this chapter, we first assume the time-varying Λ as a truncated power series of the Hubble parameter up to the second order [hereafter, PS-model], that is, [99, 100, 297]

$$\Lambda(t) = n_1 H + n_2 H^2, \tag{5.20}$$

where n_1 is a constant with dimension of H, while n_2 is a dimensionless constant. The first term, i.e., $\Lambda \propto H$ was discussed in Refs.[102, 103, 105, 270] where as the second term, i.e., $\Lambda \propto H^2$ was proposed in [87, 298]. Thus, Eq.(5.20) is a combination of linear and quadratic form of $\Lambda(t)$. Using (5.20) into (5.19), we get

$$\dot{H} + \left(\frac{3+\varepsilon}{2} - \frac{3n_2}{(6+6\varepsilon-\omega_{BD}\varepsilon^2)}\right) H^2 = \frac{3n_1 H}{(6+6\varepsilon-\omega_{BD}\varepsilon^2)}. \tag{5.21}$$

Now, considering the current value of Λ as $\Lambda_0 = 3H_0^2\Omega_\Lambda$, where Ω_Λ is the density parameter for vacuum, Eq. (5.20) gives $n_1 = H_0(\beta - 3\Omega_m)$, where $\Omega_\Lambda = 1 - \Omega_m$. Here, Ω_m is the matter density parameter. Using this value of n_1, Eq.(5.21) can be rewritten as

$$\frac{dh}{dx} + \left(\frac{(3+\varepsilon)(6+6\varepsilon-\omega_{BD}\varepsilon^2) - 6(3-\beta)}{2(6+6\varepsilon-\omega_{BD}\varepsilon^2)}\right) h = \frac{3(\beta-3\Omega_m)}{(6+6\varepsilon-\omega_{BD}\varepsilon^2)} \tag{5.22}$$

where $x = ln\, a$ and $h = H/H_0$ is the dimensionless Hubble parameter and $\beta = 3 - n_2$ (or $|n_2| << 1$). It is obvious from (5.22) that $\beta > 3\Omega_m$, where $0 < \beta < 3$.

On solving (5.22), the dimensionless Hubble parameter as a function of the scalar factor can be written as

$$h(a) = \frac{6(\beta-3\Omega_m)}{(3+\varepsilon)(6+6\varepsilon-\omega_{BD}\varepsilon^2) - 6(3-\beta)} + \left(1 - \frac{6(\beta-3\Omega_m)}{(3+\varepsilon)(6+6\varepsilon-\omega_{BD}\varepsilon^2) - 6(3-\beta)}\right) a^{-k} \tag{5.23}$$

where $k = \frac{(3+\varepsilon)(6+6\varepsilon-\omega_{BD}\varepsilon^2)-6(3-\beta)}{2(6+6\varepsilon-\omega_{BD}\varepsilon^2)}$. It is to be noted that for $\varepsilon \to 0$, we recover the result obtained in Ref. [297] and further for $\beta \to 3$ i.e. $n_2 \to 0$ and $\varepsilon \to 0$, we recover the dynamical Λ solution derived in Ref. [103].

Considering $a = (1+z)^{-1}$, we can define the normalized Hubble expansion $E(z)$ as

$$E(z) = \frac{H}{H_0} = \tilde{\Omega}_{\Lambda 1} + \tilde{\Omega}_{m1}(1+z)^k, \tag{5.24}$$

where

$$\tilde{\Omega}_{\Lambda 1} = 1 - \tilde{\Omega}_{m1} = \frac{6(\beta - 3\Omega_m)}{(3+\varepsilon)(6+6\varepsilon - \omega_{BD}\varepsilon^2) - 6(3-\beta)}. \tag{5.25}$$

One can observe that for $\varepsilon \to 0$ and $\beta \to 3$, Eq.(5.25) reduces to $\tilde{\Omega}_{\Lambda 1} = \Omega_\Lambda$. Assuming the scale factor to unity at present, i.e., $a_0 = 1$, the scale factor evolves with time as

$$a(t) = \left(\frac{e^{(k\tilde{\Omega}_{\Lambda 1} H_0\, t)} - 1 + \tilde{\Omega}_{\Lambda 1}}{\tilde{\Omega_{\Lambda 1}}} \right)^{1/k} \tag{5.26}$$

It is obvious from (5.26) that the scale factor varies as $a \sim t^{1/k}$, i.e., power-law expansion during the early times. Therefore, the model expands with decelerated rate. It is followed by a transition to an accelerating epoch where the scale factor varies $a \sim \exp(\tilde{\Omega}_{\Lambda 1} H_0\, t)$ in late time.

The observational data suggest that the accelerated expansion of the Universe is a recent phenomenon. It means that the Universe might be decelerated phase in the early epoch when there was no DE or when its effect was subdominant. Therefore, the Universe must have a transition from decelerating to accelerating phase. In this context, the deceleration parameter plays an important role to describe the evolution history of the Universe. For this model, the deceleration parameter in terms of redshift is calculated as

$$q(z) = -1 + \frac{k\, \tilde{\Omega}_{m1}\, (1+z)^k}{\tilde{\Omega}_{\Lambda 1} + \tilde{\Omega}_{m1}\, (1+z)^k}. \tag{5.27}$$

The present-day value q_0 can be found by putting $z = 0$ in (5.27), which is given by

$$q_0 = k\, \tilde{\Omega}_{m1} - 1. \tag{5.28}$$

We now discuss the deceleration-acceleration transition redshift, z_{tr} which is defined as a redshift where $q(z) = 0$ and it is given by

$$z_{tr} = -1 + \left[\frac{2(6+6\varepsilon - \omega_{BD}\varepsilon^2)\, \tilde{\Omega}_{\Lambda 1}}{((1+\varepsilon)(6+6\varepsilon - \omega_{BD}\varepsilon^2) - 6(3-\beta))\, \tilde{\Omega}_{m1}} \right]^{1/k}, \tag{5.29}$$

At this stage, we also discuss another important parameter, known as equation of state (EoS) parameter which describes the dynamics of the Universe. In this model, we discuss the effective EoS parameter, which is defined as $w_{eff} = -1 - \frac{2a}{3}\frac{dh}{da}$. Using (5.23) in this expression, we get

$$w_{eff}(z) = -1 + \frac{2k\tilde{\Omega}_{m1}}{3h}(1+z)^k. \tag{5.30}$$

The present value of EoS parameter is given by

$$w_{eff}(z=0) = -1 + \frac{2k}{3}\tilde{\Omega}_{m1}. \tag{5.31}$$

The condition for acceleration of the present universe is given by

$$3w_{eff}(z=0)+1=2\left(-1+k\tilde{\Omega}_{m1}\right). \tag{5.32}$$

It should ne noted here that for an accelerated expansion of the Universe the effective EoS parameter must be $w_{eff}<(-1/3)$. This condition is satisfied if $\tilde{\Omega}_{m1}<1/k$, which is also compatible with the analysis of deceleration parameter as given in Eq.(5.28). From Eq. (5.30), it is found that $w_{eff}(z)\to -1$ as $z\to -1$, i.e., as $a\to\infty$. Thus, the model exhibits to de Sitter Universe and coincides with the ΛCDM model in later stages of its evolution.

In what follows, we check the consistency of the model. Using (5.8), (5.9) and (5.18) into (5.16), we get

$$2(\omega_{BD}\varepsilon-3)\dot{H}+(\omega_{BD}\varepsilon^2+6\omega_{BD}\varepsilon-12)H^2=0. \tag{5.33}$$

We substitute the solution of Hubble function H from (5.24) into (5.33), we get

$$2k(\omega_{BD}\varepsilon-3)\tilde{\Omega}_{m1}(1+z)^k+(12-\omega_{BD}\varepsilon^2-6\omega_{BD}\varepsilon)(\tilde{\Omega}_{\Lambda 1}+\tilde{\Omega}_{m1}(1+z)^k)=0. \tag{5.34}$$

It can be observed that, in general, the above equation is not satisfied. However, we can get a relation between the constants at present epoch, i.e., for $z=0$, which is given by

$$2k(\omega_{BD}\varepsilon-3)\tilde{\Omega}_{m1}+(12-\omega_{BD}\varepsilon^2-6\omega_{BD}\varepsilon)=0. \tag{5.35}$$

Once we get the best-fit values of model parameters by observations, we can check the consistency of the Eq. (5.35) for the present epoch.

5.4 A power-law $\Lambda(t)$ model

Bertolami (1986) [177], Ozer and Taha (1987)[179], and Chen and Wu (1990) [240] have studied the model with vacuum energy density in general relativity which evolves as $\Lambda\propto a^{-2}$. In the following, we assume that the vacuum energy density evolves as the general power of the scale factor (hereafter PL-model):

$$\Lambda(a)=3\gamma a^{-n}, \tag{5.36}$$

where γ is a constant. Using (5.36) in (5.19) and simplifying, we get

$$\frac{dH^2}{da}+\frac{(3+\varepsilon)}{a}H^2=\frac{18\gamma}{(6+6\varepsilon-\omega_{BD}\varepsilon^2)}a^{-n-1}. \tag{5.37}$$

Using the present value of vacuum energy density, $\Lambda_0 = 3H_0^2\Omega_\Lambda$ into (5.36), we get $\gamma = \Omega_\Lambda H_0^2$. Using this value of γ, the solution of (5.37) with $H(a=1) = H_0$ in terms of redshift is given by

$$E(z) = \frac{H}{H_0} = \left[\tilde{\Omega}_{m2}(1+z)^{(3+\varepsilon)} + \tilde{\Omega}_{\Lambda 2}(1+z)^n\right]^{1/2}. \tag{5.38}$$

where

$$\tilde{\Omega}_{\Lambda 2} = \frac{18\Omega_\Lambda}{(6+6\varepsilon-\omega_{BD}\varepsilon^2)(3+\varepsilon-n)}, \tag{5.39}$$

and

$$\tilde{\Omega}_{m2} = 1 - \frac{18\Omega_\Lambda}{(6+6\varepsilon-\omega_{BD}\varepsilon^2)(3+\varepsilon-n)}. \tag{5.40}$$

The deceleration parameter is obtained as

$$q = -1 + \frac{1}{2}\frac{(3+\varepsilon)\tilde{\Omega}_{m2}(1+z)^{(3+\varepsilon)} + n\tilde{\Omega}_{\Lambda 2}(1+z)^n}{\tilde{\Omega}_{m2}(1+z)^{(3+\varepsilon)} + \tilde{\Omega}_{\Lambda 2}(1+z)^n}. \tag{5.41}$$

It is clear from (5.41) that $q(z)$ tends to -1 in the future (negative redshifts). The present value q_0 is obtained as

$$q_0 = -1 + \frac{(3+\varepsilon)\tilde{\Omega}_{m2} + n\tilde{\Omega}_{\Lambda 2}}{2}. \tag{5.42}$$

The transition redshift is given by

$$z_{tr} = \left(\frac{(2-n)\tilde{\Omega}_{\Lambda 2}}{(1+\varepsilon)\tilde{\Omega}_{m2}}\right)^{1/(3+\varepsilon-n)} - 1, \tag{5.43}$$

where as the effective EoS parameter is calculated as

$$w_{eff} = -1 + \frac{1}{3}\frac{(3+\varepsilon)\tilde{\Omega}_{m2}(1+z)^{(3+\varepsilon)} + n\tilde{\Omega}_{\Lambda 2}(1+z)^n}{\tilde{\Omega}_{m2}(1+z)^{(3+\varepsilon)} + \tilde{\Omega}_{\Lambda 2}(1+z)^n}. \tag{5.44}$$

The w_{eff} at $z=0$ is obtained as

$$w_{eff}(z=0) = -1 + \frac{1}{3}\left((3+\varepsilon)\tilde{\Omega}_{m2} + n\tilde{\Omega}_{\Lambda 2}\right). \tag{5.45}$$

From above equation, we observe that the condition for acceleration of the present Universe $3w_{eff}(z=0)+1<0$ is satisfied if $(3+\varepsilon)\tilde{\Omega}_{m2} + n\tilde{\Omega}_{\Lambda 2} < 2$, which is also compatible with the analysis of deceleration parameter. From Eq. (5.45), it is found that $w \to -1$ as $z \to -1$, i.e., as $a \to \infty$. Thus, the model attains to de Sitter Universe and coincides with the ΛCDM model in late time evolution.

Let us check also the consistency of the model. Substituting the solution of Hubble function

$H(z)$ obtained in Eq. (5.38) in Eq. (5.33), we get

$$(\omega_{BD}\varepsilon-3)[(3+\varepsilon)\tilde{\Omega}_{m2}a^{-(3+\varepsilon)}+n\tilde{\Omega}_{\Lambda 2}a^{-n}]-(\omega_{BD}\varepsilon^2+6\omega_{BD}\varepsilon-12)[\tilde{\Omega}_{m2}a^{-(3+\varepsilon)}+\tilde{\Omega}_{\Lambda 2}a^{-n}]=0. \tag{5.46}$$

We can get the relation between the constants at present epoch which is as follows.

$$(\omega_{BD}\varepsilon-3)[(3+\varepsilon)\tilde{\Omega}_{m2}+n\tilde{\Omega}_{\Lambda 2}]-(\omega_{BD}\varepsilon^2+6\omega_{BD}\varepsilon-12)=0. \tag{5.47}$$

We will check the above consistency equation for the model once the best-fit values of model parameters by observations are obtained.

5.5 Data Sample and methodology

In this section we discuss the observational constraints on the free parameters of PS and PL models by using the latest observational data of $H(z)$, Type Ia supernovae and baryon acoustic oscillations.

- **Hubble data:** We employ 30 $H(z)$ measurements obtained via the differential age method [299] for passively evolving galaxies in the redshift range $0.07 \leq z \leq 1.965$ [23]. These data points are uncorrelated with the BAO points.

- **Type Ia Supernovae:** For SNe constraints, we adopt the Pantheon sample of 1048 SNe covering $0.01 < z < 2.3$ [37]. Accounting for varying G [283, 300], we modify μ (1.74) given in section 1.16.1. Simple analytical models of light curve predict that the SNe peak luminosity is proportional to the mass of nickel synthesized which in turn, to a good approximation, is a fixed fraction of the Chandrasekhar mass $(M_{Ni} \propto M_{Ch})$, which satisfies $M \propto G^{-3/2}$ [283, 301, 302]. Based on the fact that luminosity $L \propto M_{Ch}$, a modification is required to the absolute magnitude of a SNe in the case of varying G. Thus, for the luminosity distance we have $L \propto G^{-3/2}$, i.e., for a slow decrease of G with time, the distant supernovae should be dimmer than predicted for a standard scenario. Using the definition of absolute magnitude

$$M = -2.5 \log \frac{L}{L_{\odot}}, \tag{5.48}$$

the modulus distance relation (1.74) must be corrected as [283, 300]

$$\mu^{th}(z,\mathbf{p}) = 5\ \log_{10}[d_L(z,\mathbf{p})/10\ pc] + \frac{15}{4}\log\frac{G}{G_0} + \mathscr{M}, \tag{5.49}$$

Since, in BD theory, $G \propto \psi^{-1}$, where $\psi = \psi_0 a^{\varepsilon}$, we rewrite (5.49) as

$$\mu^{th}(z,\mathbf{p}) = 5\ \log_{10}[d_L(z,\mathbf{p})/10\ pc] + \frac{15}{4}\varepsilon \log(1+z) + \mathscr{M}. \tag{5.50}$$

where **p** is the set of parameters.

- **Baryon acoustic oscillations (BAO_{dz}):** We adopt six d_z measurements from [52]. The values of z_i, $d_{z,obs}$, $\sigma_{z,i}$ can be found in Table 3 of Blake et al(2011) [52].

The data description of SNe, $H(z)$ and BAO_{dz} data are given in Section 1.16. Using the above cosmological observations, we adopt the Markov Chain Monte Carlo (MCMC) method to find the best-fit value of model parameters of viscous model. The χ^2 for each data, namely, χ^2_{SNe}, $\chi^2_{H(z)}$ and χ^2_{BAO} are given in equations (1.77), (1.80) and (1.84) respectively.

5.6 Results and discussion

In our analysis, we use the publicly available MCMC sampling algorithm in emcee python library [36] to generate the chain. In MCMC method, the best-fit of the parameters are maximized by using the probability function $\mathscr{L} \propto \exp(-\chi^2/2)$.

In order to find the best fit, we minimize the overall χ^2 function using two different combinations of datasets, namely, $DS1 : \chi^2_{min} = \chi^2_{SNe} + \chi^2_{H(z)}$ and $DS2 : \chi^2_{min} = \chi^2_{SNe} + \chi^2_{H(z)} + \chi^2_{BAO_{dz}}$. The main cosmological parameters are ε, ω_{BD} and H_0 which are common for both models. In addition to this PS model has two extra parameters Ω_m and β, and PL model has two extra parameters n and Ω_Λ. We constrain the space parameters in three models: ΛCDM, PS and PL. The contours of our statistical analyses are shown in Figs.5.1–5.3 and best-fit values of parameters are summarized in Table 5.1 that arise from the joint analysis described above. Using fitting values of parameters of ΛCDM, PS and PL models, a comparative study of PS and PL models with concordance ΛCDM are as follows:

In PS model, we find $\Omega_m = 0.344^{+0.023}_{-0.024}$ and $\Omega_m = 0.341^{+0.026}_{-0.024}$ from $DS1$ and $DS2$, respectively which are subsequently higher than the respective values $\Omega_m = 0.313^{0.018}_{-0.016}$ and $\Omega_m = 0.314^{+0.015}_{-0.018}$ of ΛCDM model. However, these results are close to $\Omega_m = 0.32^{+0.01}_{-0.02}$ obtained in Ref. (Basilakos et al.2009) in general relativity.

The respective transition from deceleration to acceleration takes place at the redshift $z_{tr} = 0.735^{+0.051}_{-0.180}$ and $z_{tr} = 0.735^{+0.064}_{-0.180}$, which show that the transitions occur earlier than ΛCDM model as mentioned in Table 5.2, and also $z_{tr} = 0.660$ as obtained in Ref. [31].

The present values of q and w_{eff} are listed in Table 5.2 which show that the q_0 and $w_{eff}(z=0)$ of PS model are lower than the ΛCDM obtained from $DS1$ dataset. However, these values,

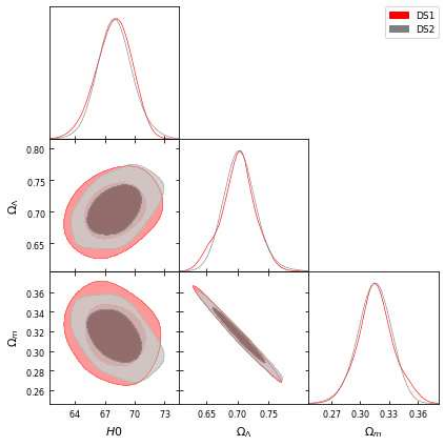

Figure 5.1: Two-dimensional confidence contours and one -dimensional posterior distributions on free parameters in ΛCDM model obtained from the datasets $DS1 : SNe + H(z)$ (red contours) and $DS2 : SNe + H(z) + BAO_{dz}$ (grey contours)

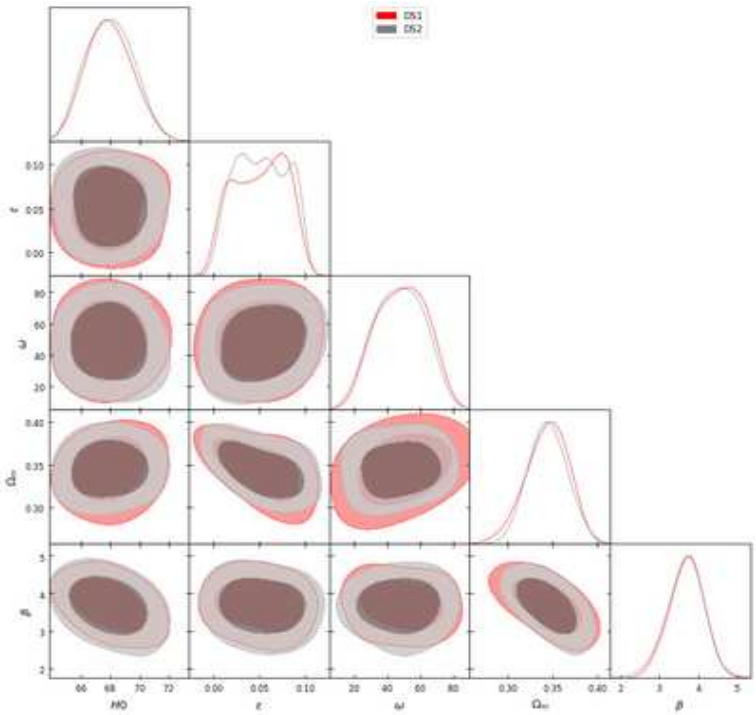

Figure 5.2: Two-dimensional confidence contours and one -dimensional posterior distributions on free parameters in the PS model obtained from the datasets $DS1 : SNe + H(z)$ (red contours) and $DS2 : SNe + H(z) + BAO_{dz}$ (grey contours)

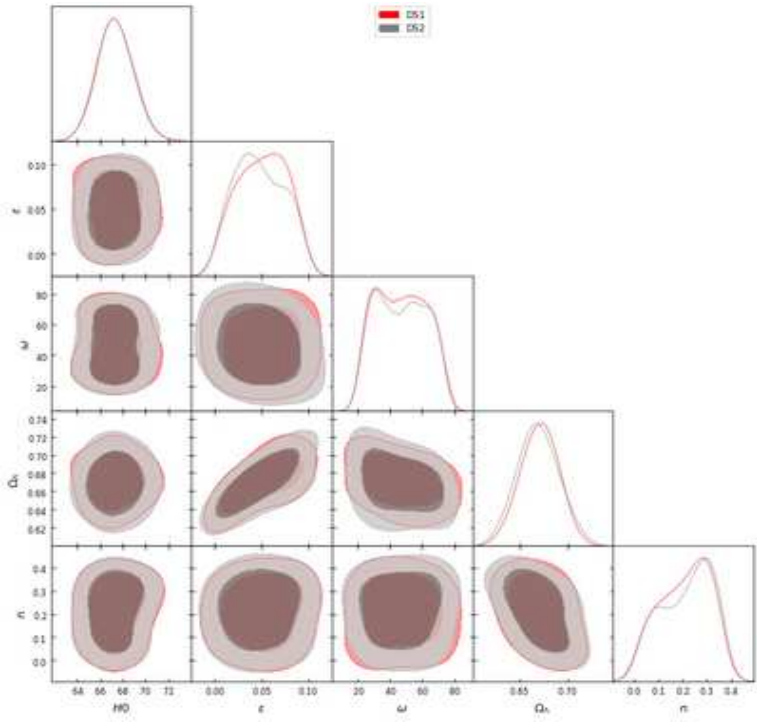

Figure 5.3: Two-dimensional confidence contours and one -dimensional posterior distributions on free parameters in the PL model obtained from datasets $DS1 : SNe + H(z)$ (red contours) and $DS2 : SNe + H(z) + BAO_{dz}$ (grey contours)

Table 5.1: The fit values of parameters of ΛCDM, PS and PL models, respectively obtained from $DS1 : SNe + H(z)$ and $DS2 : SNe + H(z) + BAO_{dz}$ datasets. The H_0 parameter is expressed in $Kms^{-1}Mpc^{-1}$

$Models \rightarrow$	ΛCDM		PS		PL	
$Parameters \downarrow$	$DS1$	$DS2$	$DS1$	$DS2$	DS1	DS2
H_0	$68.179^{+2.008}_{-1.670}$	$68.126^{+1.311}_{-1.788}$	$67.801^{+1.688}_{-1.634}$	$67.706^{+1.617}_{-1.575}$	$67.266^{+1.440}_{-1.683}$	$67.182^{+1.615}_{-1.612}$
ε	–	–	$0.036^{+0.032}_{-0.037}$	$0.036^{+0.031}_{-0.037}$	$0.038^{+0.034}_{-0.030}$	$0.038^{+0.035}_{-0.029}$
ω_{BD}	–	–	$48.234^{+18.385}_{-19.161}$	$48.384^{+18.593}_{-19.664}$	$46.489^{+20.241}_{-18.530}$	$46.151^{+19.415}_{-19.238}$
β	–	–	$3.710^{+0.414}_{-0.447}$	$3.709^{+0.419}_{-0.417}$	–	–
n	–	–	–	–	$0.219^{+0.101}_{-0.136}$	$0.222^{+0.116}_{-0.136}$
Ω_m	$0.313^{+0.018}_{-0.016}$	$0.314^{+0.015}_{-0.018}$	$0.344^{+0.023}_{-0.024}$	$0.341^{+0.026}_{-0.024}$	–	–
Ω_Λ	$0.708^{+0.023}_{-0.027}$	$0.706^{+0.027}_{-0.022}$	–	–	$0.672^{+0.021}_{-0.021}$	$0.669^{+0.021}_{-0.021}$
χ^2_{min}	569.617	10684.353	553.587	10659.909	544.063	10633.291
AIC	575.639	10690.355	563.642	10669.964	554.685	10643.346
ΔAIC	–	–	11.997	20.391	20.954	47.029
BIC	578.714	10693.458	568.750	10675.084	559.226	10684.474
ΔBIC	–	–	9.964	18.374	19.488	8.984

Table 5.2: The transition value z_{tr} and the present values of q, w_{eff} of ΛCDM, PS and PL models, respectively.

$Model \rightarrow$	ΛCDM		PS		PL	
$Values \downarrow$	$DS1$	$DS2$	DS1	DS2	DS1	DS2
z_{tr}	$0.651^{+0.048}_{-0.048}$	$0.647^{+0.055}_{-0.055}$	$0.735^{+0.051}_{-0.180}$	$0.735^{+0.064}_{-0.180}$	$0.667^{+0.045}_{-0.052}$	$0.607^{+0.045}_{-0.052}$
q_0	$-0.541^{+0.032}_{-0.032}$	$-0.535^{+0.031}_{-0.031}$	$-0.770^{+0.23}_{-0.23}$	$-0.780^{+0.23}_{-0.23}$	$-0.459^{+0.018}_{-0.018}$	$-0.459^{+0.018}_{-0.018}$
$w_{eff}(z=0)$	$-0.694^{+0.021}_{-0.021}$	$-0.690^{+0.021}_{-0.021}$	$-0.850^{+0.15}_{-0.15}$	$-0.850^{+0.16}_{-0.16}$	$-0.639^{+0.012}_{-0.012}$	$-0.639^{+0.012}_{-0.012}$

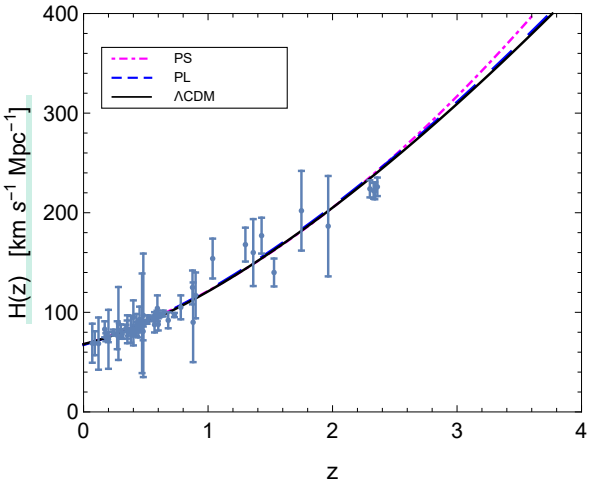

Figure 5.4: Best fits over $H(z)$ obtained from $DS1$ dataset . The grey bars show the data points of $H(z)$

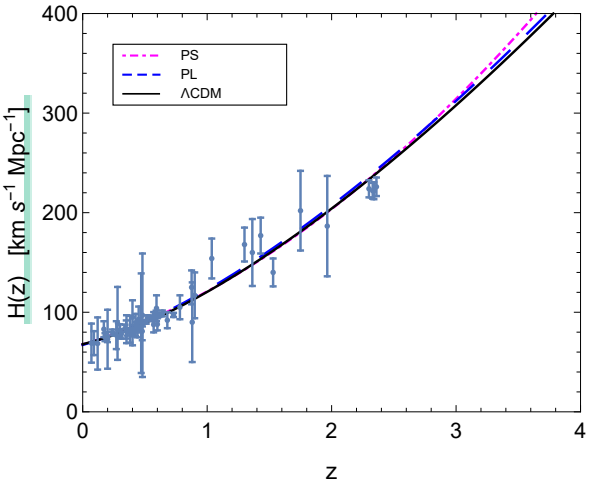

Figure 5.5: Best fits over $H(z)$ obtained from $DS2$ dataset . The grey bars show the data points of $H(z)$

which are obtained with dataset $DS2$, are little-bit higher than ΛCDM model. From Figs. 5.6 and 5.8, we observe that as $z \rightarrow -1$, both q and EoS parameter w_{eff} tend to -1. The present values of Hubble parameter are $H_0 = 67.801^{+1.688}_{-1.634}$ $Kms^{-1}Mpc^{-1}$ and $H_0 = 67.706^{+1.617}_{-1.575}$ $Kms^{-1}Mpc^{-1}$, which are good agreement with Planck result (Aghanim et al.2018), where $H_0 = 67.7 \pm 0.46$ $Kms^{-1}Mpc^{-1}$. However, these values are slightly lower than the values of ΛCDM obtained from the same datasets.

In this model, we have two extra free parameters, namely ε and β with respect to the Λ CDM model. In dataset $DS1$ we find $\varepsilon = 0.036^{+0.032}_{-0.037}$ and $\beta = 3.710^{+0.414}_{-0.447}$ whereas for $DS2$ dataset, we have $\varepsilon = 0.036^{+0.031}_{-0.037}$ and $\beta = 3.709^{+0.419}_{-0.417}$.

The χ^2 is an important quantity which is used to data fitting process. In this analysis, we find $\chi^2 = 553.587$ and $\chi^2 = 10659.909$, respectively with respect to $DS1$ and $DS2$ datasets. The reduced chi-square is defined as $\chi^2_{red} = \chi^2_{min}/\nu$, where $\nu = (N - n)$ is the degree of freedom (dof). Here, N is total number of combined data, which are 1078 and 1084 and n is the number of estimated free parameters of model, which is 5 for each dataset $DS1$ and $DS2$, respectively.

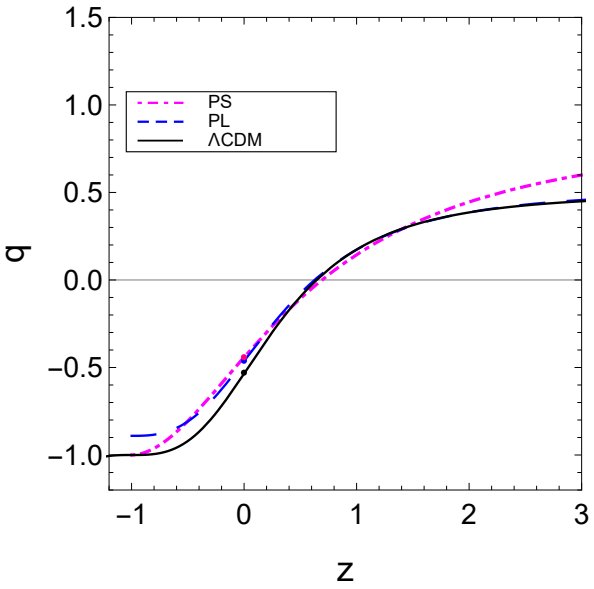

Figure 5.6: Plot of evolution of deceleration parameter with redshift using fitting values of parameters obtained from $DS1$ dataset. The dot denotes the present value of deceleration parameter

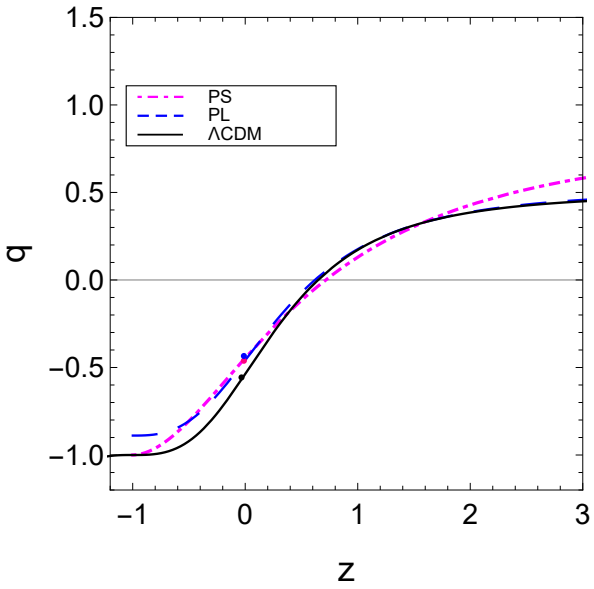

Figure 5.7: Plot of evolution of deceleration parameter with redshift using fitting values of parameters obtained from $DS1$ dataset. The dot denotes the present value of deceleration parameter.

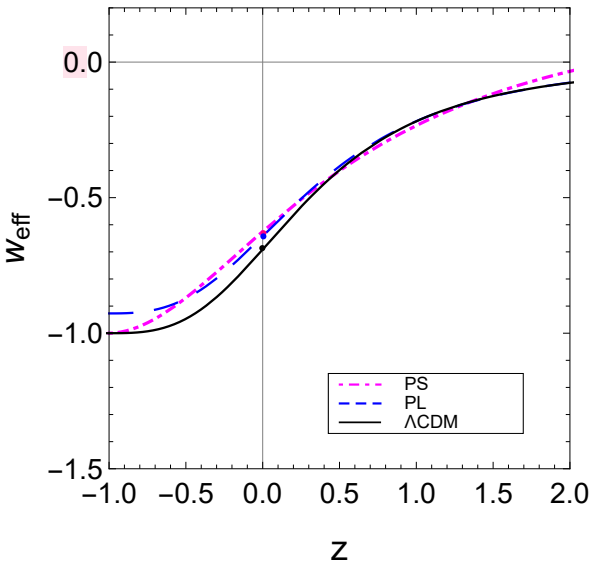

Figure 5.8: Plot of evolution of EoS parameter with redshift using fitting values of parameters obtained by $DS1$ dataset. The dot denotes the present value of EoS parameter.

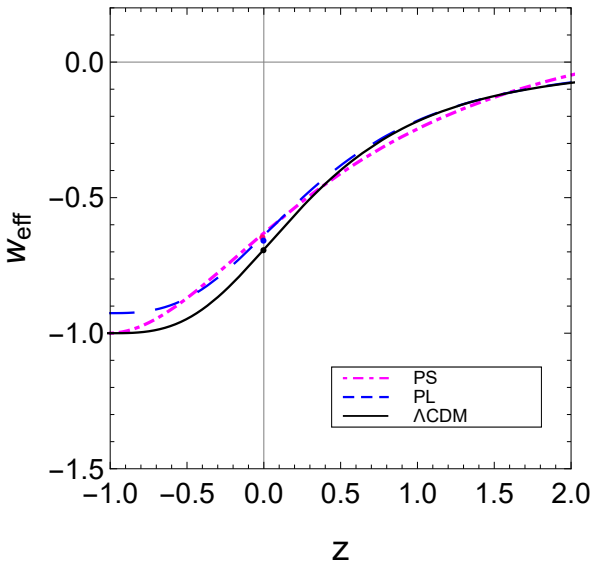

Figure 5.9: Plot of evolution of EoS parameter with redshift using fitting values of parameters obtained by $DS2$ dataset. The dot denotes the present value of EoS parameter.

If $\chi^2_{red} \leq 1$, then the fit is good and the observed data is consistent with the proposed model. For PS model, it is $\chi^2_{red} = 0.515$ and $\chi^2_{red} = 9.879$, respectively. Thus, the data $DS1$ is compatible with the considered model.

An another way to analyze the departure from the concordance ΛCDM model is through the *jerk parameter* (j), which is defined in section1.15. This parameter gives the information about the dynamics of DE corresponding to $j(z) = 1$ (constant) for ΛCDM model. Any deviation from $j = 1$ would favor a non-ΛCDM model. The plot of jerk parameter $j(z)$ is shown in Fig. 5.10 using the best-fit values of parameters obtained from DS1 and DS2 datasets in (**??**). It is found that $j(z) \to 1$ as $z \to -1$ which incorporates the flat ΛCDM model well in late times. The current value $j(z)$ at $z = 0$ is $j_0 = 0.6214$ and $j_0 = 0.6247$ with DS1 and DS2 datasets, respectively which differ from $j_0 = 1$ at present-day.

In PL **model**, we find $\Omega_\Lambda = 0.672 \pm 0.021$ from $DS1$ and $\Omega_\Lambda = 0.669 \pm 0.021$ from $DS2$, which

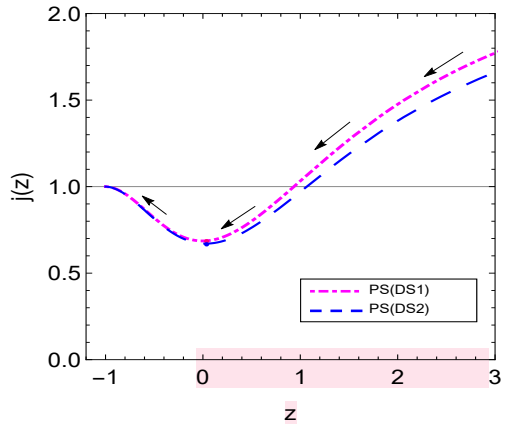

Figure 5.10: Plot of evolution of jerk parameter $j(z)$ with redshift z using fitting values of parameters of model PS. The horizontal line represents the ΛCDM model.

are comparatively lower than the value $\Omega_\Lambda = 0.708^{+0.023}_{-0.027}$ and $\Omega_\Lambda = 0.706^{+0.027}_{-0.022}$, respectively. The redshift transition values are $z_{tr} = 0.667^{+0.045}_{-0.052}$ and $z_{tr} = 0.607^{+0.045}_{-0.052}$, which are consistent with the values of ΛCDM model.

The present values of Hubble constant for this model are $H_0 = 67.266^{+1.440}_{-1.683}$ and $H_0 = 67.182^{+1.615}_{-1.612}$ obtained from DS1 and DS2 datasets which are slightly lower than the values of ΛCDM model. The evolution of $H(z)$ for this model with ΛCDM are shown in Fig. 5.4 and 5.5. The present values of q are higher than ΛCDM model whereas the $w_{eff}(z = 0)$ are very closed to standard model (Refer to Table 5.2). From Fig. 5.6–5.9, we observe that as $z \to \infty$, $q \to -0.779$ and -0.802, where as $w_{eff} \to -0.850$ and -0.864 for datastes $DS1$ and $DS2$, respectively. This model shows the quintessence-like behavior $(-1 < w \leq 0)$ in late-time evolution. This model has two extra parameters, namely ε and n with respect to the ΛCDM model. The best-fit values of these parameters are $\varepsilon = 0.038^{+0.034}_{-0.030}$ and $n = 0.219^{+0.101}_{-0.136}$ from $DS1$ dataset, and $\varepsilon = 0.038^{+0.035}_{-0.029}$ and $n = 0.222^{+0.116}_{-0.136}$ from $DS2$. The values of n are much larger than the value $n = -0.06 \pm 0.04$ obtained in Ref.[100].

The respective chi-square values from DS1 and DS2 datasets are $\chi^2 = 544.063$ and $\chi^2 = 10633.291$ for which $\chi^2_{red} = 0.507$ and $\chi^2_{red} = 9.854$. Thus, the χ^2_{red} is less than unity for $DS1$ dataset which show that the the model provides a very good fit to this dataset.

The plot of jerk parameter $j(z)$ as a function of redshift z is shown in Fig. 5.11 using the best-fit values of parameters obtained from DS1 and DS2 datasets. It is observed that the model PL deviates from the ΛCDM model at current epoch ($j_0 = 0.6004$ and $j_0 = 0.6574$, respectively) as well as $z \to -1$. These deviations from ΛCDM model need attention which would be found to know the real cause behind the cosmic acceleration.

It is to be noted that the best-fit values of parameters obtained from DS1 and DS2 datasets for both the models satisfy the consistency equations (5.35) and (5.47), respectively. Thus, the models PS and PL are also analytically consistent.

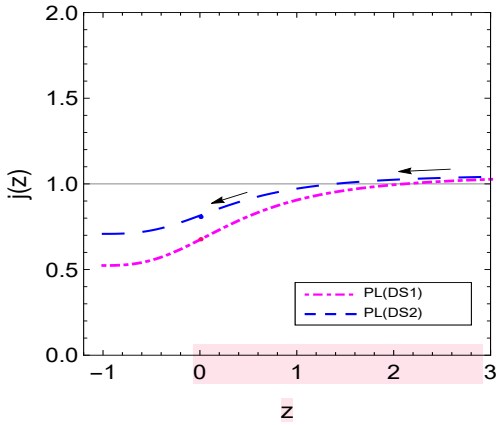

Figure 5.11: Plot of evolution of jerk parameter $j(z)$ with redshift z using fitting values of parameters of model PL. The horizontal line represents the ΛCDM model.

5.7 Selection Criteria

In order to compare the proposed models with ΛCDM, we implement the selection information criteria in terms of the strength of the evidence according to Akaike information criteria (AIC) [61] and Bayesian information criteria (BIC) [63]. These information criteria penalize the presence of extra degree of freedom (d.o.f.). For detail discussion about these criteria, we refer to Section 1.17.1. The AIC and BIC and their difference values ΔAIC and ΔBIC for models PS and PL with reference to the corresponding values of AIC and BIC of ΛCDM model are given in Table 5.1.

According to AIC and BIC in $DS1$ dataset, we find $\Delta AIC(\Delta BIC) = 11.997(9.964)$ for PS model whereas it is $\Delta AIC(\Delta BIC) = 20.954(19.488)$ for PL model. Similarly, in $DS2$ dataset, we find $\Delta AIC(\Delta BIC) = 20.391(18.374)$ for PS model and $\Delta AIC(\Delta BIC) = 47.029(8.984)$ for PL model. These values suggest that according to AIC, there is a *very strong evidence in favor* whereas as per BIC there is a *strong evidence in favor* of these two models.

5.8 Conclusion

In this chapter, we have discussed the dynamics of a flat FLRW model in BD theory with varying vacuum energy density. We have assumed two different functional forms of vacuum energy density, namely power series expansion in H up to the second order excluding constant term and power-law form in terms of scale factor, in order to parametrize the vacuum energy density. In the first step, we have solved the BD field equations analytically using these two forms of vacuum energy density. These two models have different theoretical solutions. We have discussed the cosmological consequences of cosmic acceleration based on these two forms of interacting Λ scenarios. Secondly, We have performed two different combinations of joint likelihood analysis $DS1 = SNe + H(z)$ and $DS2 = SNe + H(z) + BAO_{dz}$ for each model including ΛCDM model in order to put the constraints on the main free parameters by χ^2 minimizing technique. It is noted that there are extra parameters, namely ε and β in PS model, and ε and n in PL model with respect to the ΛCDM model. The fit values of these free parameters are provided in Table 5.1.

Figures 5.1–5.3 show the two-dimensional confidence contours and one-dimensional posterior distributions on the free parameters in ΛCDM, PS and PL models obtained from datasets. The best-fit values of the models parameters, transition redshift z_{tr}, q_0 and $w_{eff}(z=0)$ are displayed in the Tables 5.1 and 5.2, respectively. Using the fitting values we have discussed the dynamical behavior of various cosmological parameters, like $H(z)$, $q(z)$, $w_{eff}(z)$ and $j(z)$ by plotting the trajectories of evolution with redshift as shown in Figs. 5.4–5.11. In view of the observational datasets, we find datasets $DS1$ and $DS2$ are very much compatible for the considered models. The present values H_0, q_0 and $w_{eff}(z=0)$ are very close to the ΛCDM model. However, the current value of jerk parameter j_0 deviates from concordance model. We have found that the PS model behaves as a de Sitter model in late-time evolution of the Universe where as the PL model behaves as a quintessence DE with an EoS lying in $(-1 < w \leq 0)$. The χ^2_{red} implies the same goodness of the models considered here. Also, using the best-fit values of models parameters, we have found that the consistency equations (5.35) and (5.47) for the both models are satisfied. In what follows, we have summarized our main results in more detail.

Assuming ΛCDM as a reference model, we have discussed the performance of these two proposed models. We have found that both the models PS and PL show a smooth transition from deceleration $(q > 0)$ epoch to acceleration $(q < 0)$ epoch in recent past. The trajectories of $q(z)$ clearly show that the models generate decelerated expansion in past and late time cosmic acceleration in present. Figures 5.6 and 5.7 also show the transition from decelerated to accelerated expansion happen in the range $0.667 \leq z_{tr} \leq 0.735$ which are comparatively same

as ΛCDM model. The parameters $q(z)$, w_{eff} and $j(z)$ tend to ΛCDM model in late-time evolution in PS model. In PL model, these parameters do not tend to respective values of ΛCDM in late-time evolution. It has been observed that both the models are well consistent with $H(z)$ data at low redshifts. Therefore, we conclude that both the models are well fitted with the present $H(z)$ data.

As for as the AIC and BIC statistical criteria is concerned, we have discussed these two parameters for the models against the ΛCDM to observe the performance of each model beyond the standard concordance ΛCDM model and have analyzed any deviation against or in favor of these models. According to ΔAIC and ΔBIC we have found large positive values which show that PS and PL models have $strong\ evidence\ in\ favor$ over the ΛCDM model with reference to datasets $DS1$ and $DS2$.

We therefore conclude that, within the framework of Brans-Dicke theory paired with an appropriate form of time varying cosmological constant can successfully account for the observed accelerated expansion of the universe.

****

Chapter 6

Brans-Dicke cosmology with cosmological term $\Lambda(H) = c_0 + 3\nu H^2$

In this chapter [1], we study the dynamics of a flat FLRW cosmological model by considering dynamical VED in BD cosmology. Two different forms of VED are discussed to explain the evolution of the Universe.

Highlights:

☞ A spatially homogenous and isotropic flat FLRW Universe is considered in Brans-Dicke theory for the dynamics of the model.

☞ Assumes the cosmological constant a dynamical parameter, that is, it varies with Universe's expansion.

☞ Analyzes the physical behaviours of various cosmological parameters using phenomenological decaying–laws as $\Lambda(t) = 3\nu H^2$, so-called Λ_{RG1} model and $\Lambda = c_0 + 3\nu H^2$, so-called Λ_{RG2} model.

1 ☞ In Λ_{RG1} model, the scale factor evolves as a power-law expansion which gives a constant value of deceleration parameter. Hence it does not show the transition.

☞ Performs the MCMC simulations with two different combintion of observational datasets, 2 including SNe Ia (Panthoen sample), BAOs and CMB, Hubble data and local Hubble constant $H_0 = 73.5 \pm 1.4 \ kmS^{-1}Mpc^{-1}$ as measured by SH0ES for Λ_{RG2} model

☞The deceleration parameter and EoS parameter trajectories show that there is a smooth

[1]This chapter is based on a published research paper "Brans-Dicke cosmology with cosmological term $\Lambda(H) = c_0 + 3\nu H^2$, *Physics of the Dark Universe* **42**, 101300 (2023)".

transition from deceleration to late-time acceleration and approach to -1 in late time.

☞ Discuss the selection criterion, AIC and BIC to analyze the model's stability.

☞ Summary in conclusion section.

6.1 Introduction

Bertolami [177], and Ozer and Taha [179] proposed a cosmological model of time-varying cosmological constant, $\Lambda(t)$ and claimed that it could be a possible candidate of DE. Later on, many authors [87, 182, 303, 304, 305] have studied the cosmological model with time-varying cosmological constant. The renormalization of quantum field theory (QFT) provides a time-varying VED in which the Λ component evolves as $\Lambda \sim H^2$, where H is the Hubble parameter [269]. Wang and Meng [110] have given a more interesting and realistic decay law. Although, there exists no fundamental theory to model the time-varying VED, a phenomenological approach has been proposed to parametrize $\Lambda(t)$. In literature, many authors [16, 90, 91, 92, 93, 94, 95, 96, 100, 101, 102, 103, 104, 105, 107, 271, 306] have carried out analysis on decaying VED in which VED has been phenomenologically assumed in various possible ways, as a function of scale factor or Hubble parameter. Such attempts suggest that decaying VED model describe not only the acceleration of the Universe but also solve both cosmological constant and coincidence problems.

Although Einstein's GTR is a very successful theory, the research on its alternative theories are getting a lot of attention during the last two decades. There are many reasons behind the alternative theories. The motivation comes from the attempt to quantize gravity, which requires higher order modifications on the EinsteinHilbert (EH) action. Some motivation comes from the dark components (DE and DM) which might be the effects caused by the modifications on large scales of GR. It may also possible due to the unification of gravity with other forces, which requires the modifications on EH action

Brans and Dicke [24] proposed a scalar tensor theory of gravitational field based on Mach's principal and Dirac's large number hypothesis (LNH), known as Brans-Dicke (BD) theory of gravitation. BD theory is a modified theory of Einstein's general theory of relativity. It involves the non-linear kinetic terms for the BD scalar field. In this theory, the Newtonian gravitational constant G is replaced by a time-varying scalar field, and a new coupling parameter ω_{BD} is introduced. It is generally assumed that General Relativity is recovered in the limit $\omega_{BD} \to \infty$.

The action and field equations for BD theory are well-known. They involve the ordinary (tensor) gravitational field of GR, $g_{\mu}\nu$, but also the scalar BD field ϕ and the (dimensionless)

BD parameter, ω_{BD}. We include the cosmological constant associated to vacuum energy density, ρ_Λ as a fundamental ingredient of the theory. In fact, we wish to consider the same matter and vacuum components as in the concordance ΛCDM except that we replace GR paradigm by the BD one. Vacuum dynamics, and in general dynamical DE can be phenomenologically favorable, even if not firmly established yet. The idea that the DE could be not just the cosmological constant of Einstein equations but a dynamical variable, or just some appropriate function of the cosmic time, i.e., there must be some decay-law of vacuum energy density, sometimes on purely phenomenological grounds. In particular, models with time-dependent VED seem to be promising. Many of these models, however, are of pure phenomenological nature since these models are parametrized in a totally ad hoc manner and having no obvious connection with any fundamental theory, therefore, these need testing. This kind of theory was renewed, owing to its association with superstrings theories [133, 274, 275, 276, 277, 278, 279, 293, 294, 295, 296, 307, 308, 309, 310, 311]. In recent years, many authors [144, 145, 161, 181, 184, 281, 282, 283, 312] have studied BD theory with cosmological constant in explaining the DE phenomena.

In this work, we combine BD gravity with the idea of dynamical DE. More especially, we show that if one tries to encapsulate the slow evolution of the BD field in terms of the current GR paradigm, the effective theory that emerges is a variant of the ΛCDM framework in which $\rho_\Lambda$acquires a time-evolving component and plays the role of an approximate dynamical VED. Although the correct form of this varying VED is not known, a quantum field theory (QFT) approach within the context of renormalization group (RG) have been proposed phenomenologically. Therefore, we assume the phenomenological form of the dependence of the cosmological constant on the square of the Hubble parameter with a constant term. In the absence of this square term of Hubble parameter, it reduces to the concordance ΛCDM model. Thus, due to this additional term, the model deviate from the ΛCDM. Our analysis includes both analytical and observational. We perform the joint statistical analysis using the latest observational data including Hubble data, Type Ia Supernova Pantheon data, baryon acoustic oscillation data and cosmic microwave background data, and local Hubble constant, H_0 by SH0ES. The evolution of various cosmological parameters such as Hubble parameter, deceleration parameter and equation of state parameter have been discussed.

We have organized the chapter as follows. Section 6.2 presents the model and field equations of a flat FLRW cosmological model in BD theory with varying cosmological constant. In Section 6.3, we present the exact solution for two different models depending on the choice of VED. In Section 6.4, we describe the datasets used in this chapter and the method to constraint the free parameters of the model. The results are discussed in detail for the various cosmological parameters such as deceleration parameter, Hubble parameter and equation of state parameter in Section 6.5. Section 6.6 discusses the model selection criteria of AIC and

BIC of the models assuming ΛCDM as a reference model. In Section 6.7, we conclude the main findings of our work.

6.2 The field equations in BD theory

Let us recall that Eq. (5.4) of cosmological constant contribution to the curvature of space-time is represented by $\Lambda g_{\mu\nu}$ term on the right hand side of BD field equations

$$R_{\mu\nu} - \frac{1}{2} g_{\mu\nu} R = \frac{8\pi}{\phi} \tilde{T}_{\mu\nu} + \frac{8\pi}{\phi} T^{BD}_{\mu\nu}, \tag{6.1}$$

and

$$\nabla_\alpha \nabla^\alpha \phi = \frac{8\pi}{(2\omega_{BD}+3)} (T^{m\lambda}_{\lambda} - 4\rho_\Lambda), \tag{6.2}$$

where the modified $\tilde{T}_{\mu\nu}$ is given by $\tilde{T}_{\mu\nu} = T_{\mu\nu} + g_{\mu\nu}\rho_\Lambda$. Here $\rho_\Lambda = \Lambda\phi/8\pi$ is the VED in BD theory associated with the presence of Λ (with pressure $p_\Lambda = -\rho_\Lambda$) and $T_{\mu\nu}$ is the energy-momentum tensor for dark matter. Modelling the expanding Universe as a perfect fluid wih velocity four-vector field u_μ, we have

$$\tilde{T}_{\mu\nu} = (\rho + p)\, u_\mu u_\nu + p\, g_{\mu\nu}, \tag{6.3}$$

with $\rho = \rho_m + \rho_\Lambda$ and $p = p_m + p_\Lambda$, where ρ_m and ρ_Λ are the matter energy density and VED, respectively, while p_m and p_Λ are the corresponding thermodynamical pressure and vacuum pressure, respectively. In this work, we consider the pressure of dust matter containing the dark matter, $p_m = 0$.

The energy-momentum tensor for BD scalar, $T^{BD}_{\mu\nu}$ in (6.1) is defined by

$$T^{BD}_{\mu\nu} = \frac{1}{8\pi}\left[\frac{\omega_{BD}}{\phi}\left(\nabla_\mu\phi\nabla_\nu\phi - \frac{1}{2}g_{\mu\nu}\nabla_\alpha\phi\nabla^\alpha\phi\right) + \left(\nabla_\mu\nabla_\nu\phi - g_{\mu\nu}\nabla_\alpha\nabla^\alpha\phi\right)\right], \tag{6.4}$$

By assuming the above generalized energy-momentum tensor and a spatially flat FLRW metric (2.1), The indepenent BD field equaiotns reduce to as follows:

$$3H^2 + 3H\frac{\dot{\phi}}{\phi} - \frac{\omega_{BD}}{2}\frac{\dot{\phi}^2}{\phi^2} = \frac{8\pi}{\phi}\rho, \tag{6.5}$$

$$2\dot{H} + 3H^2 + \frac{\ddot{\phi}}{\phi} + 2H\frac{\dot{\phi}}{\phi} + \frac{\omega_{BD}}{2}\frac{\dot{\phi}^2}{\phi^2} = -\frac{8\pi}{\phi}p, \tag{6.6}$$

$$\ddot{\phi} + 3H\dot{\phi} = \frac{8\pi}{(2\omega_{BD}+3)}(\rho - 3p). \tag{6.7}$$

where an overdot means derivative with respect to cosmic time t and $H = \dot{a}/a$ is the Hubble parameter. The Bianchi identity of $\nabla_\nu G^{\mu\nu} = 0$ in Eq.(6.1) leads to the following consistency relation.

$$\nabla_\nu \left(R^{\mu\nu} - \frac{1}{2} g^{\mu\nu} R \right) = 0 = \nabla_\nu \left(\frac{8\pi}{\phi} \tilde{T}^{\mu\nu} + \frac{8\pi}{\phi} T^{\mu\nu}_{BD} \right). \tag{6.8}$$

Let us assume that $\tilde{T}_{\mu\nu}$ obeys the usual energy conservation equation $\tilde{T}^{\mu\nu}_{;\nu} = 0$, which gives

$$\dot{\rho_m} + 3(\rho_m + p_m)\frac{\dot{a}}{a} = -\dot{\rho_\Lambda}. \tag{6.9}$$

We assume that $T^{BD}_{\mu\nu}$ regards as a perfect fluid, i.e., $T^{BD}_{\mu\nu} = (\rho_{BD} + p_{BD}) u_\mu u_\nu + p_{BD} g_{\mu\nu}$, where

$$\rho_{BD} = \frac{1}{8\pi} \left[\frac{\omega_{BD}}{2} \left(\frac{\dot{\phi}^2}{\phi} \right) - 3H\dot{\phi} \right], \tag{6.10}$$

$$p_{BD} = \frac{1}{8\pi} \left[\frac{\omega_{BD}}{2} \left(\frac{\dot{\phi}^2}{\phi} \right) + 2H\dot{\phi} + \ddot{\phi} \right]. \tag{6.11}$$

Now, using (6.9) the Bianchi identity equation (6.8) gives

$$8\pi \tilde{T}^{\mu\nu} \nabla_\nu \left(\frac{1}{\phi} \right) + \nabla_\nu \left(\frac{8\pi}{\phi} T^{\mu\nu}_{BD} \right) = 0, \tag{6.12}$$

which simplifies to

$$\dot{\rho}_{BD} + 3H(\rho_{BD} + p_{BD}) = (\rho_m + \rho_\Lambda + \rho_{BD}) \frac{\dot{\phi}}{\phi}. \tag{6.13}$$

Let us assume that the BD scalar ϕ varies as a power-law of the scale factor [295, 296, 308], which is given by

$$\phi = \phi_0 \, a(t)^\varepsilon, \tag{6.14}$$

where ϕ_0 and ε are constants. The value of ε is assumed to be small in order to make the consistency with G. Therefore, large ω_{BD} results the product $\varepsilon\omega_{BD}$ as an order unity [295]. It is noted that the Cassini experiment set a very high lower bound on ω_{BD}.

It is interesting to note that in Ref.[161] such power-law form of BD scalar has been assumed to study the dynamics of BD cosmology with a cosmological term. It has been observed that the power-law form of BD scalar can conveniently improve the fitting of the cosmological data [312]. Therefore, we expect that this assumption would also be helpful in a different form of time-varying VED model in BD theory.

Thus, using the power-law form of BD scalar, Eq. (6.5) reduces to

$$H^2 = \frac{2}{(6 + 6\varepsilon - \omega_{BD}\varepsilon^2)} \frac{8\pi}{\phi} (\rho_m + \rho_\Lambda). \tag{6.15}$$

Equation (6.15) shows that the standard cosmology of general relativity can be recovered in the limit of $\varepsilon \to 0$. Considering the dust matter $p_m = 0$, Eqs. (6.9) and (6.15) give a single

evolution equation for Hubble parameter as

$$\dot{H}+\frac{(3+\varepsilon)}{2}H^2=\frac{3}{(6+6\varepsilon-\omega_{BD}\varepsilon^2)}\frac{8\pi}{\phi}\rho_\Lambda=\frac{3\Lambda}{(6+6\varepsilon-\omega_{BD}\varepsilon^2)}, \tag{6.16}$$

where $\rho_\Lambda=\Lambda/8\pi G=\Lambda\phi/8\pi$. The above equation is solvable once we know the functional form of Λ. In the next Section, we find the solution of Eq.(6.16) using time-dependent cosmological constant.

6.3 Solution with time-varying Λ

In this chapter, we assume $\Lambda(t)$ as a combination of constant term and a quadratic term in H [107, 161], that is,

$$\Lambda(H)=c_0+3\nu H^2, \tag{6.17}$$

where c_0 and ν are constants. The motivation for assuming variable Λ of the form (6.17) originates from quantum field theory (QFT)[313], for a detail review, see, Refs.[97, 99, 247]. This functional form of $\Lambda(t)$ has been used to study the evolution of the cosmic star formation rate and constrained the model parameter $\nu\leq 0.1$ [99, 101].

It is to be noted that in Ref. [184], the authors have studied the Friedmann cosmology with decaying vacuum energy in BD theory with $\Lambda=c_0$ and $\Lambda=\sigma H$. It has been found that cosmological model with constant Λ gives the consistent results where as the model with $\Lambda=\sigma H$ does not show consistency with the observational data used. Therefore, we extend our work by assuming the functional form of $\Lambda(H)$ as defined in (6.17) with the possibility that it would describe the current accelerating Universe and fit well with the latest observational data. The following two subsections study two different cosmological models depending on the choice of Λ component defined in Eq. (6.17), namely $\Lambda=3\nu H^2$ and $\Lambda=c_0+3\nu H^2$ and perform the qualitative and observational analysis(see, the model $\Lambda=c_0$ in Ref.[184]).

6.3.1 Model with $\Lambda\propto H^2$

We assume that the cosmological term is proportional to the quadratic Hubble parameter (hereafter, Λ_{RG1} model). This form of $\Lambda(t)$ can be obtained from Eq.(6.17) by setting $c_0=0$, which gives [87, 239, 314, 315, 316]

$$\Lambda(H)=3\nu H^2, \tag{6.18}$$

where v is a constant and is expected to be $|v| \ll 1$. Using (6.18) into (6.16), we get

$$H' + \left(\frac{3+\varepsilon}{2} - \frac{9v}{(6+6\varepsilon-\omega_{BD}\varepsilon^2)}\right)\frac{H}{a} = 0, \tag{6.19}$$

where a prime represents dH/da. On solving (6.19), we get

$$H(z) = H_0\,(1+z)^{\left(\frac{3+\varepsilon}{2} - \frac{9v}{6+6\varepsilon-\omega_{BD}\varepsilon^2}\right)}, \tag{6.20}$$

where H_0 denotes the current Hubble parameter at $t = 0$ and $z = (a_0/a) - 1$ is the redshift (thereafter, we take $a_0 = 1$). Using $H = \dot{a}/a$, the scale factor is given by

$$a = \left[\left(\frac{3+\varepsilon}{2} - \frac{9v}{(6+6\varepsilon-\omega_{BD}\varepsilon^2)}\right)H_0 t\right]^{\frac{1}{\left(\frac{3+\varepsilon}{2} - \frac{9v}{6+6\varepsilon-\omega_{BD}\varepsilon^2}\right)}}, \tag{6.21}$$

We find the power-law solution of the scale factor which shows that the model decelerates, marginally inflates or accelerates depending on $\left(\frac{3+\varepsilon}{2} - \frac{9v}{(6+6\varepsilon-\omega_{BD}\varepsilon^2)}\right) > 1$, $\left(\frac{3+\varepsilon}{2} - \frac{9v}{(6+6\varepsilon-\omega_{BD}\varepsilon^2)}\right) = 1$ or $\left(\frac{3+\varepsilon}{2} - \frac{9v}{(6+6\varepsilon-\omega_{BD}\varepsilon^2)}\right) < 1$, respectively.

Using (6.21) in to (1.65), we get the deceleration parameter as $q = \left(\frac{3+\varepsilon}{2} - \frac{9v}{(6+6\varepsilon-\omega_{BD}\varepsilon^2)}\right) - 1$, which is a constant. This shows that the model either decelerates ($q > 0$), marginally inflates ($q = 0$) or accelerates ($q < 0$) depending on the bracket term is greater, equal or less than one. Thus, the model does not describe transition from decelerating phase to accelerating phase. We can say that, this model does not fit the present observational data as desired. In general, a time varying q describes the phase transition.

Let us test the consistency of the solution obtained for this model. Using (6.5), (6.10) and (6.11), Eq. (6.13) gives

$$2\varepsilon(\omega_{BD}\varepsilon - 3)\dot{H} = \varepsilon(12 - \omega_{BD}\varepsilon^2 - 6\omega_{BD}\varepsilon)H^2. \tag{6.22}$$

Using the solution (6.20) into (6.22), one can get

$$2(\omega_{BD}\varepsilon - 3)\left(\frac{3+\varepsilon}{2} - \frac{9v}{(6+6\omega_{BD} - \omega_{BD}\varepsilon^2)}\right) - \left(\omega_{BD}\varepsilon^2 + 6\omega_{BD}\varepsilon - 12\right) = 0, \tag{6.23}$$

which gives a relation between the constants.

6.3.2 Model with $\Lambda = c_0 + 3vH^2$

In the previous subsection, we observe that the form $\Lambda = 3vH^2$ gives power-law solution and constant value of deceleration parameter, which shows that the Λ_{RG1} model can not describe the current transition phase of the Universe. Therefore, to observe the phase transition we

now consider the form of Λ with the addition of a constant c_0, i.e., $\Lambda = c_0 + 3\nu H^2$ as defined in Eq.(6.17). This type of model (hereafter Λ_{RG2} model) was first proposed in Ref.[155] using renormalization group (RG) in quantum field theory, which have been further extensively studied in the literature, cf. Refs.[97, 99, 101, 317].

Using (6.17), Eq.(6.16) reduces to

$$\frac{dH^2}{dx} + \left(\frac{3+\varepsilon}{2} - \frac{9\nu}{(6+6\varepsilon-\omega_{BD}\varepsilon^2)}\right)H^2 = \frac{6c_0}{(6+6\varepsilon-\omega_{BD}\varepsilon^2)}, \tag{6.24}$$

where $x = lna$. By defining $\Lambda_0 = 3H_0^2\Omega_\Lambda$, Eq. (6.17) gives $c_0 = 3H_0^2(\Omega_\Lambda - \nu)$, where "0" represents the present cosmic time. Therefore, Eq. (6.24) can be rewritten as

$$\frac{dH^2}{dx} + \left(\frac{3+\varepsilon}{2} - \frac{9\nu}{(6+6\varepsilon-\omega_{BD}\varepsilon^2)}\right)H^2 = \frac{18H_0^2(\Omega_\Lambda - \nu)}{(6+6\varepsilon-\omega_{BD}\varepsilon^2)}, \tag{6.25}$$

The solution of (6.25) in terms of redshift is given by

$$H^2(z) = H_0^2\left[\frac{18(\Omega_\Lambda-\nu)}{(3+\varepsilon)(6+6\varepsilon-\omega_{BD}\varepsilon^2)-18\nu} + \left(1 - \frac{18(\Omega_\Lambda-\nu)}{(3+\varepsilon)(6+6\varepsilon-\omega_{BD}\varepsilon^2)-18\nu}\right)(1+z)^k\right], \tag{6.26}$$

where $k = \left(\frac{(3+\varepsilon)(6+6\varepsilon-\omega_{BD}\varepsilon^2)-18\nu}{(6+6\varepsilon-\omega_{BD}\varepsilon^2)}\right)$.

Using the dimensionless Hubble parameter $E(z) = H/H_0$, Eq.(6.26) can be represented as

$$E^2(z) = \tilde{\Omega}_\Lambda + \tilde{\Omega}_m(1+z)^k, \tag{6.27}$$

where

$$\tilde{\Omega}_\Lambda = 1 - \tilde{\Omega}_m = \frac{18(\Omega_\Lambda-\nu)}{(6+6\varepsilon-\omega_{BD}\varepsilon^2)(3+\varepsilon)-18\nu} \tag{6.28}$$

From above equations it is to be noted that the solution (22) of the Ref.[184] in case of standard BD model with constant cosmological constant can be recovered by taking $\nu = 0$ and further $\varepsilon = 0$ gives the standard ΛCDM regime, the standard scaling law of non-relativistic matter and a strictly constant VED [99]. Again, in the absence of BD theory $\varepsilon = 0$, i.e. $\phi = \phi_0 = 1/G$ and $\nu \neq 0$, the model Λ_{RG2} reduces to the the ΛCDM regime, the standard scaling law of non-relativistic matter and varying VED [97, 99].

We observe from (6.27) that in the limit $a \to 0$, the Hubble parameter, $H \approx H_0\tilde{\Omega}_m a^{-k/2}$, which implies that the model decelerates. However, in the limit $a \to \infty$, we have $H \approx H_0\sqrt{\tilde{\Omega}_\Lambda}$, which corresponds to a pure de Sitter phase. Thus, the model transits from a decelerated phase to a late time accelerated phase.

Integrating and simplifying (6.26), the scale factor has the solution

$$a(t) = \left(\frac{\tilde{\Omega}_m}{\tilde{\Omega}_\Lambda}\right)^{1/k} \sinh^{2/k}\left(\frac{k\sqrt{\tilde{\Omega}_\Lambda}}{2}H_0\, t\right). \tag{6.29}$$

It is observed that at early times the scale factor varies as $a \propto t^{2/k}$, i.e, power-law expansion and during late-time, it varies as $a \propto \exp\left(\sqrt{\tilde{\Omega}_\Lambda}\, H_0 t\right)$, which shows the de Sitter phase of the Universe.

The Hubble parameter in terms of cosmic time t is given by

$$H(t) = H_0 \sqrt{\tilde{\Omega}_\Lambda}\, \coth\left(\frac{k\sqrt{\tilde{\Omega}_\Lambda}}{2} H_0 t\right), \tag{6.30}$$

whereas the cosmic time t in terms of the scale factor a is expressed by

$$t(a) = \frac{2}{k\sqrt{\tilde{\Omega}_\Lambda}\, H_0} sinh^{-1}\left(\sqrt{\frac{\tilde{\Omega}_\Lambda}{\tilde{\Omega}_m}}\, a^{k/2}\right). \tag{6.31}$$

Thus, the current age t_0 of the Universe is given by

$$t_0 = \frac{2(6+6\varepsilon-\omega_{BD}\varepsilon^2)}{(3+\varepsilon)(6+6\varepsilon-\omega_{BD}\varepsilon^2)\sqrt{\tilde{\Omega}_\Lambda} H_0} sinh^{-1}\left(\sqrt{\frac{\tilde{\Omega}_\Lambda}{\tilde{\Omega}_m}}\right). \tag{6.32}$$

It is straight forward to calculate the deceleration parameter q which is obtained as

$$q(z) = -1 + \frac{k\tilde{\Omega}_m(1+z)^k}{2\left[\tilde{\Omega}_{\Lambda 1} + \tilde{\Omega}_m(1+z)^k\right]}. \tag{6.33}$$

Now, the present value of q corresponds to $z = 0$ is calculated as

$$q_0 = -1 + \frac{1}{2}\frac{(3+\varepsilon)(6+6\varepsilon-\omega_{BD}\varepsilon^2) - 18\Omega_\Lambda}{(6+6\varepsilon-\omega_{BD}\varepsilon^2)}. \tag{6.34}$$

We observe that the present transition from decelerated to accelerated phase, $q(\text{at } z=0) = 0$ occurs at $18(\Omega_\Lambda = (1+\varepsilon)(6+6\varepsilon-\omega_{BD}\varepsilon^2)$. The transition redshift, z_{tr} at $q(z) = 0$ is given by

$$z_{tr} = \left[\frac{2(6+6\varepsilon-\omega_{BD}\varepsilon^2)\tilde{\Omega}_\Lambda}{[(1+\varepsilon)(6+6\varepsilon-\omega_{BD}\varepsilon^2) - 18\nu]\tilde{\Omega}_m}\right]^{1/k} - 1 \tag{6.35}$$

For sake of completeness, we discuss another parameter known as equation of state (EoS) parameter w, which also describes the different phases of the evolution of the Universe. It is observed that $3w+1<0$ describes the accelerated expansion of the Universe. The EoS parameter (hereafter, effective EoS parameter, w_{eff}) is defined by

$$w_{eff} = -1 - \frac{2}{3}\frac{aH'}{H}. \tag{6.36}$$

For this model, we have

$$w_{eff} = -1 + \frac{1}{3}\frac{k\tilde{\Omega}_m(1+z)^k}{[\tilde{\Omega}_\Lambda + \tilde{\Omega}_m\,(1+z)^k]}. \tag{6.37}$$

The above equation gives w_{eff} at $z=0$ as

$$w_{eff}(z=0) = -1 + \frac{1}{3}\frac{(3+\varepsilon)(6+6\varepsilon-\omega_{BD}\varepsilon^2)-18\Omega_\Lambda}{(6+6\varepsilon-\omega_{BD}\varepsilon^2)}. \tag{6.38}$$

The condition $3w_{eff}(z=0)+1<0$ is satisfied if $18\Omega_\Lambda > (1+\varepsilon)(6+6\varepsilon-\omega_{BD}\varepsilon^2)$. From Eq. (6.37), it is observed that $w_{eff}\to -1$ as $z\to -1$. Thus, the model corresponds to the ΛCDM model.

Substituting the solution (6.26) into the consistency equation (6.22), we obtain

$$k(\omega_{BD}\varepsilon-3)\tilde{\Omega}_m a^{-k} + (12-\omega_{BD}\varepsilon^2-6\omega_{BD}\varepsilon)[\tilde{\Omega}_\Lambda + \tilde{\Omega}_m a^{-k}] = 0. \tag{6.39}$$

One can observe that the above equation are not always consistent. Therefore, we assume that this equation satisfies at present, i.e. $a=a_0=1$. Thus, Equation (6.39) at present reduces to

$$k(\omega_{BD}\varepsilon-3)\tilde{\Omega}_m - (\omega_{BD}\varepsilon^2+6\omega_{BD}\varepsilon-12) = 0, \tag{6.40}$$

where $\tilde{\Omega}_\Lambda + \tilde{\Omega}_m = 1$.

6.4 Data and statistical method

In this section we will discuss the observational data and the statistical method to constraint the parameters of model.

6.4.1 Data

In our analysis, we use the most recent and relevant observational data as follows:

- **SNe (Pantheon sample):** We use 40 binned data points in the redshift range $0.014 \leq z \leq 1.62$ from the Pantheon sample [37].
- **BAOs and CMB:** We use BAO measurements from SDSS(R), 6dF, BOSS CMASS and WiggleZ surveys, combined with CMB data [46, 48, 49, 318].
- **Hubble data:** We use 36 measurements of $H(z)$ including 31 from CC technique, 2 from Lyman-α, and 3 from radial BAO signals [42, 43, 44, 45].
- **Local Hubble constant:** We use $H_0 = 73.5 \pm 1.4\ Km\ s^{-1}\ Mpc^{-1}$ as measured by SH0ES [319].

The details of the minimized χ^2 values for each dataset are provided in Section 1.16.

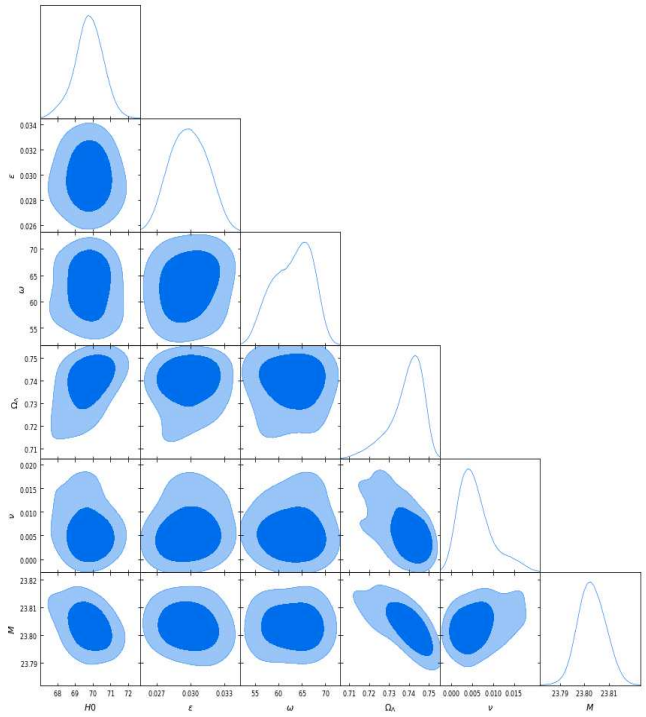

Figure 6.1: The $2-$ dimensional contours and $1-$ dimensional posterior distribution of the free parameters of Λ_{RG2} model using the combined dataset $DS1 = SNe + H(z) + BAO/CMB + H_0$.

6.4.2 Statistical method

We study two combinations of data set, labeled as $DS1 : SNe + BAO/CMB + H(z) + H_0$ and $DS2 : SNe + BAO/CMB + H(z)$ to minimize the total χ^2 -function of the model. The corresponding chi-squared are defined as

$$\chi^2_{DS1} = \chi^2_{Pan} + \chi^2_{BAO/CMB} + \chi^2_{H(z)36} + H_0, \tag{6.41}$$

and

$$\chi^2_{DS2} = \chi^2_{Pan} + \chi^2_{BAO/CMB} + \chi^2_{H(z)36}. \tag{6.42}$$

We perform a Bayesian Markov Chain Monte Carlo (MCMC) analysis based on *EMCEE* module [36]. In our study, we assume prior values for model parameters, viz., $60 \leq H_0 \leq 80$, $0 < \varepsilon < 1$, $0 < \omega_{BD} \leq 500$, $0 < \nu < 1$ and $0.6 \leq \Omega_\Lambda \leq 0.8$.

Table 6.1: Constraints of the parameters, and AIC and BIC for ΛCDM model obtained from joint analysis of data sets DS1 and DS2 [184].

Sample	Ω_Λ	H_0	χ^2_{min}	AIC	BIC
$DS1$	$0.680^{+0.015}_{-0.010}$	$71.545^{+1.175}_{-0.820}$	34.78	40.78	48.04
$DS2$	$0.690^{+0.032}_{-0.028}$	$68.545^{+2.102}_{-1.742}$	34.69	40.69	47.91

Table 6.2: Constraints on the parameters, and AIC and BIC for Λ_{RG2} model obtained from joint analysis of data sets DS1 and DS2.

$Parameters \downarrow$	$DS1$	$DS2$
ε	$0.029^{+0.002}_{-0.002}$	$0.029^{+0.002}_{-0.002}$
ν	$0.005^{+0.004}_{-0.003}$	$0.007^{+0.007}_{-0.005}$
ω	$68.870^{+3.968}_{-5.192}$	$62.673^{+4.736}_{-5.527}$
Ω_Λ	$0.741^{+0.006}_{-0.010}$	$0.730^{+0.011}_{-0.017}$
H_0	$69.780^{+0.801}_{-0.717}$	$67.951^{+1.076}_{-1.145}$
χ^2_{min}	41.03	38.82
AIC	51.03	48.82
BIC	63.13	60.85
ΔAIC	10.25	8.13
ΔBIC	15.09	12.94

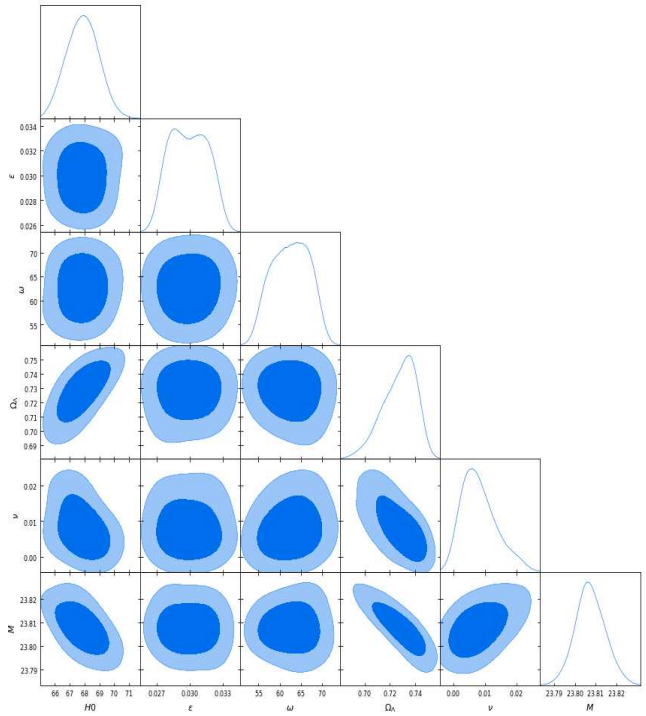

Figure 6.2: The $2-$ dimensional contours and $1-$ dimensional posterior distribution of the free parameters of Λ_{RG2} model using the combined dataset $DS2 = SNe + H(z) + BAO/CMB$.

6.5 Results and discussion

In this section, we present the main results obtained by observational data sets: DS1 and DS2, and describe the physical properties of the vacuum model accordingly. We summarize the best-fit of free parameters of Λ_{RG2} model in Tables 6.2. To make a comparison with the Λ_{RG2} model, we also present the fitting values of ΛCDM (cf. Table 6.1). The contour maps of parameters Ω_Λ, ε, ω_{BD} and ν of Λ_{RG2} model with $1\sigma(68.3\%)$ and $2\sigma(95.4\%)$ confidence level are shown in Figs.6.1 and 6.2, respectively.

Figures 6.3 and 6.4 present the evolution of the deceleration parameter for the best fit values of parameters obtained from DS1 and DS2 data sets for Λ_{RG2} model. It is observed that $q(z)$ with each data set varies with redshift z from positive to negative and show the same trajectory as ΛCDM model. Thus, the model shows transition from early deceleration to the late time acceleration. It can be observed that $q(z) \to -1$ in late-time of evolution. Figures 6.3 and 6.4 also show that the transition from decelerated to accelerated phase occurs at the redshift $z_{tr} = 0.707^{+0.094}_{-0.707}$ with DS1 data and $z_{tr} = 0.678^{+0.013}_{-0.011}$ with DS2 data (cf. Table 6.4). The joint datasets DS1 and DS2 yield the present deceleration parameter q_0 as $-0.572^{+0.067}_{-0.015}$ and $-0.555^{+0.016}_{-0.023}$, respectively. These results show that the parameters z_{tr} and q_0 are in good agreement with that of ΛCDM model (cf. Table 6.3).

Using the parameter constraints in analytical solution of Hubble parameter (6.26), the evolutions of the Hubble parameter $H(z)$ with the error bar of Hubble data set are shown

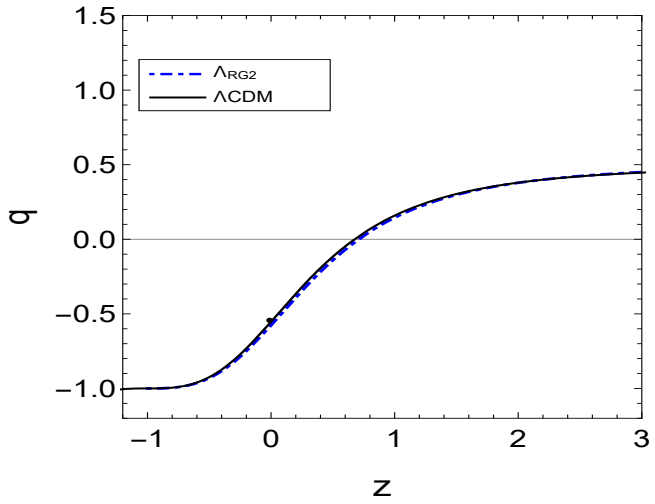

Figure 6.3: Figure shows the evolution of the deceleration parameter for Λ_{RG2} and ΛCDM using data combination DS1. A dot on a curve represents the current value q_0.

Table 6.3: Values of z_{tr}, q_0 ,$w_{eff}(z=0)$ and t_0 for ΛCDM model [184]

Sample	z_{tr}	q_0	$w_{eff}(z=0)$	t_0
$DS1$	$0.701^{+0.024}_{-0.020}$	$-0.594^{+0.014}_{-0.018}$	$-0.729^{+0.009}_{-0.012}$	$13.48^{+0.450}_{-0.230}$ Gyr
$DS2$	$0.672^{+0.028}_{-0.025}$	$-0.554^{+0.024}_{-0.030}$	$-0.703^{+0.016}_{-0.020}$	$13.69^{+0.09}_{-0.09}$ Gyr

in Figs.6.5 and 6.6. For sake of comparison the ΛCDM model is also plotted. The cosmic evolution of Λ_{RG2} is coinciding each other through out the expansion history with ΛCDM model. The trajectories of the model for both data sets DS1 and DS2 cover most of the data set of error bar of Hubble parameter, which shows that the Λ_{RG2} model is in good agreement with ΛCDM model.

In this cosmological scenario, the current age of the Universe with each dataset are found to be $t_0 = 14.07^{+0.018}_{-0.022}\ Gyr$ and $t_0 = 13.95^{0.020}_{-0.020}\ Gyr$, respectively. The age of the Universe obtained are very much compatible with that obtained from the ΛCDM (cf. Table 6.3), and $t_0 \approx 14.37\ Gyr$ and $t_0 \approx 13.7$ obtained through the combined data set of WMAP, BAO and SNe [266]. Using data set DS1, the present value of Hubble parameter is extracted as $H_0 = 69.780^{+0.801}_{-0.717}\ Kms^{-1}Mpc^{-1}$, which is slightly lower than $H_0 = 71.545^{+1.175}_{-0.820}\ Kms^{-1}Mpc^{-1}$ based on the observation from ΛCDM model applied to DS1 dataset. With DS2 dataset, it is $H_0 = 67.951^{+1.076}_{-1.145}\ Kms^{-1}Mpc^{-1}$ which is consistent with the observational value of ΛCDM model $H_0 = 68.545^{+2.102}_{-1.742}\ Kms^{-1}Mpc^{-1}$. These values show a variation from $H_0 = 71.9^{+2.6}_{-2.7}\ Kms^{-1}Mpc^{-1}$ of WMAP sky survey [266].

The evolution of effective EoS parameters w_{eff} are shown in Figs.6.7 and 6.8 for Λ_{RG2} and ΛCDM models obtained through the combined data sets DS1 and DS2. We may conclude

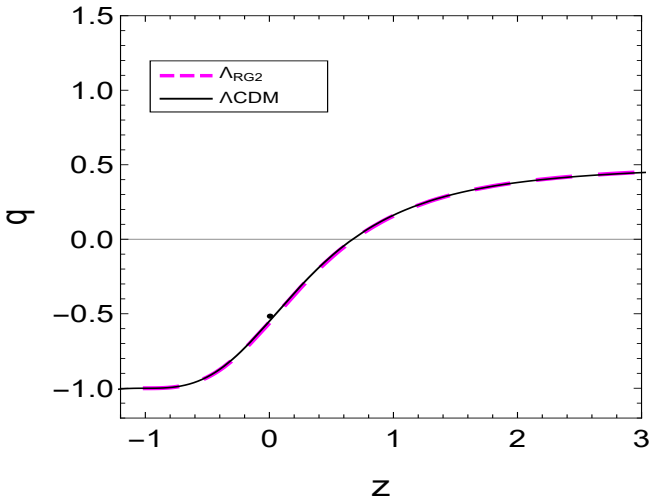

Figure 6.4: Figure shows the evolution of the deceleration parameter for Λ_{RG2} and ΛCDM using data combination DS2. A dot on a curve represents the current value q_0.

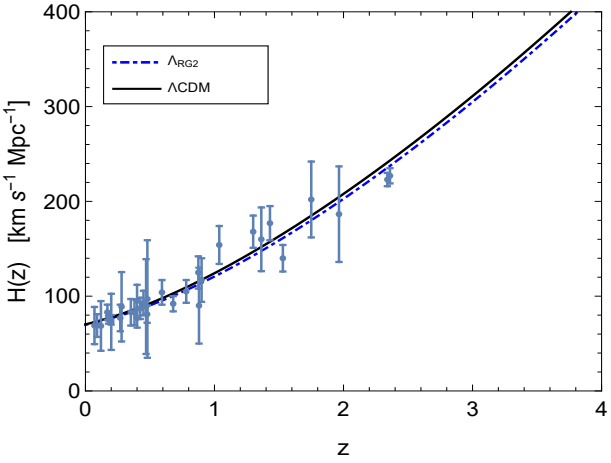

Figure 6.5: Best fits using DS1 data set over $H(z)$ data for Λ_{RG2} (blue dash-dot line) and ΛCDM (black solid line) are shown. The grey points with uncertainty bars correspond to the 36 $H(z)$ sample.

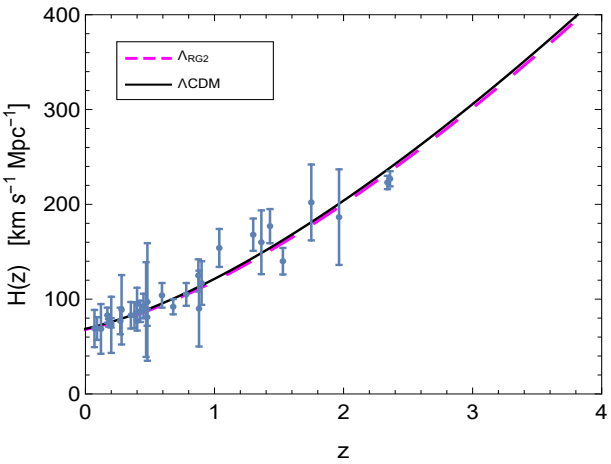

Figure 6.6: Best fits using DS2 data set over $H(z)$ data for Λ_{RG2} (magenta dashed line) and ΛCDM (black solid line) are shown. The grey points with uncertainty bars correspond to the 36 $H(z)$ sample.

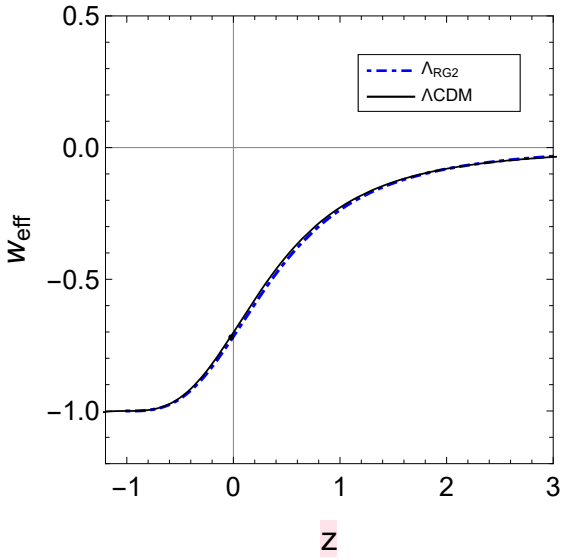

Figure 6.7: Figure shows the evolution of effective EoS parameter as a function of redshift z for Λ_{RG2} and ΛCDM using data combination DS1. A dot on a curve represents the current value $w_{eff}(z=0)$.

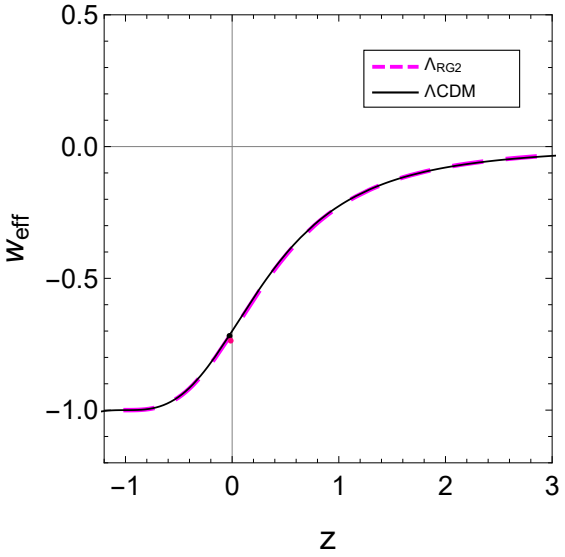

Figure 6.8: Figure shows the evolution of effective EoS parameter as a function of redshift z for Λ_{RG2} and ΛCDM using data combination DS2. A dot on a curve represents the current value $w_{eff}(z=0)$.

Table 6.4: Values of z_{tr}, q_0, $w_{eff}(z=0)$ and t_0 for Λ_{RG2} model.

Sample	z_{tr}	q_0	$w_{eff}(z=0)$	t_0
*DS*1	$0.707^{+0.094}_{-0.077}$	$-0.571^{+0.067}_{-0.015}$	$-0.714^{+0.004}_{-0.009}$	$14.07^{+0.018}_{-0.022}$ Gyr
*DS*2	$0.678^{+0.013}_{-0.011}$	$-0.555^{+0.016}_{-0.023}$	$-0.703^{+0.011}_{-0.015}$	$13.95^{+0.020}_{-0.020}$ Gyr

that for large redshifts, w_{eff} has small negative value $w_{eff} > -1/3$ and in future the model asymptotically approaches to $w_{eff} = -1$. The each trajectory of w_{eff} coincides with the evolution of ΛCDM model. The Λ_{RG2} model behaves like a quintessence. The present value of w_{eff} is found to be $-0.714^{+0.004}_{-0.009}$ and $-0.703^{+0.011}_{-0.015}$ with DS1 and DS2 datasets, respectively, which are very close to the current value of w_{eff} of ΛCDM model (cf.Table 6.3).

The combined data sets DS1 and DS2 give the minimal chi-squared viz. χ^2 as 41.038 and 38.820, respectively. Let us calculate the reduced χ^2_{red}, which can be obtained as $\chi^2_{red} = \chi^2_{min}/(N-d)$, where N is the total number of data and d is the number of fitted parameters, which vary for the different models. In our observation, we have used $N = 83$ data points for DS1: 40 data points of SNe Pantheon, 36 Hubble data, 6 data set of BAO/CMB and 1 of local Hubble constant H_0, $N = 82$ data points for DS2 consists of 40 data points of SNe Pantheon, 36 Hubble data, 6 data set of BAO/CMB, and $d = 5$ for Λ_{RG2} model. Using these information, we get $\chi^2_{red} = 0.526$ and 0.504, respectively with DS1 and DS2 data sets which provide a very good fit with these observation data sets. A model with $\chi^2_{red} < 1$ or closer to 1 is considered as a best-fit where as $\chi^2_{red} > 1$ is considered a bad fit.

6.6 Selection Criterion

We now study model selection information criteria like, Akaike Information Criterion (AIC)[61] and Bayesian Information Criterion (BIC)[63] for Λ_{RG2} and ΛCDM models.

Based on our $\Delta AIC(\Delta BIC)$ results given in Table 6.2 for Λ_{RG2} model with reference to ΛCDM, we find $\Delta AIC(\Delta BIC) = 10.25(15.09)$ for $DS1$ dataset whereas in $DS2$ dataset, it is $\Delta AIC(\Delta BIC) = 8.13(12.94)$. These values suggest that Λ_{RG2} model is not supported from a model selection point of view. These results show that BIC penalizes the free parameters more strongly than AIC.

6.7 Conclusion

In this chapter, we have discussed the dynamics of a flat FLRW model with decaying VED in BD theory. Many authors, as mentioned in introductory part, have studied the FLRW model with varying Λ in GR assuming the phenomenological form of $\Lambda(t)$. We have considered the cosmological model in dynamical BD theory of gravity to explore the role played by the scalar field and varying $\Lambda(t)$ in describing the late-time evolution of the Universe. It is here worthy to mention that the authors [184] studied the FLRW spacetime with varying vacuum density in BD theory by assuming the forms $\Lambda = c_0$ and $\Lambda = \sigma H$ and found that $\Lambda = \sigma H$ model does not satisfy the consistency condition whereas the model with constant Λ in BD theory satisfies

remarkably well the consistency equation.

We have studied a flat FLRW model in BD theory by assuming two different functional forms of VED, viz. $\Lambda_{RG1} : \Lambda = 3\nu H^2$ and $\Lambda_{RG2} : \Lambda = c_0 + 3\nu H^2$. We have found that Λ_{RG1}-model does not able to fit with the observational data. This model gives power-law expansion of the Universe which does not show the phase transition. The Universe decelerates or accelerates depending on the values of model parameters. A similar discussion has been carried out by many authors [87, 99]. On the other hand, the Λ_{RG2} model is well compared with standard ΛCDM model. Firstly, we have obtained the analytical solution of the basic cosmological functions of flat FLRW model in BD theory for these two models. The second part of the work consists of performing a Bayesian MCMC analysis using two different joint combinations of observational data of SNe Pantheon, $H(z)$ data, BAO/CMB and local Hubble constant to obtain the best fit parameters for Λ_{RG2} model. We have constrained the parameter ν using these observational data and found to be $0.005^{+0.004}_{-0.003}$ with DS1 data and $0.007^{+0.007}_{-0.005}$ with DS2 data.

The observational data sets DS1 and DS2 yield the density parameter Ω_Λ as $0.741^{+0.006}_{-0.010}$ and $0.730^{+0.011}_{-0.017}$, respectively. If we look the consistency of the Λ_{RG2} model, Eq. (6.40) must be satisfied by using best fit values of the free parameters of the model obtained numerically as listed in Table 6.2 or it gives the same value of one of the free parameters of the model. Hence, using the best fit values of parameters of DS1 and DS2 listed in Table 6.2 into the consistency relation (6.40), we found the free parameter Ω_Λ as 0.723 and 0.730, respectively. These results of Ω_Λ are perfectly consistent with the values of Ω_Λ as mentioned above obtained from the observations using DS1 and DS2 datasets (cf. Table 6.2). In what follows, we summarize the main results of our analysis.

Based on the best-fit values of model parameters obtained from two different combined datasets, the evolution of the cosmological quantities have been plotted as a function of redshift. In case of Λ_{RG2} model, we have observed that the scale factor expands with decelerated rate in early times and accelerated at late-time of the evolution. We have estimated the deceleration-acceleration transition redshift that takes place at $z_{tr} = 0.707^{+0.094}_{-0.707}$ and $z_{tr} = 0.678^{+0.678}_{-0.011}$, which are consistent with the ΛCDM model. The deceleration parameter exhibits a transition from decelerated phase to an accelerated phase. The effective EoS parameter is small negative values at high redshift but tend to -1 as $z \to -1$, showing the ΛCDM behavior.

Using the best fit values, the current age of the Universe are found to be $t_0 \sim 14.07$ Gyr and $t_0 \sim 13.95$ Gyr from DS1 and DS2 datasets, respectively. In Figs. 6.5 and 6.6 , we have plotted the best fitting curve over Hubble data points and have presented a comparison with ΛCDM model. It has been found that Λ_{RG2} model is well fitted along with ΛCDM. According to the Chi-square and hence reduced chi-square values, this model is also good agreement to data. However, the model is not in favor with respect to the selection information criteria of AIC and

BIC.

In the final remark, we have discussed the possibility, in contrast to ΛCDM case, that Λ is not a constant but a function of the cosmic time, i.e., $\rho_\Lambda = \rho_\Lambda(t)$. This varying VED is perfectly allowed within the FLRW metric in a dynamical frame of BD theory. It has been observed that the choice of functional form of Λ is very important in describing the dynamics of the Universe, especially the late time acceleration. In the absence of BD theory, we recover exactly the varying vacuum models as discussed in Ref. [97, 99]. At very late time we get an effective cosmological constant dominated era that implies a pure de Sitter phase of the scale factor. In summary, the Λ_{RG2} model successfully reproduces the expected epochs and shows a good agreement with the ΛCDM model.

****

Chapter 7

Conclusion, Future Scope and Social Impact

7.1 Conclusion

Einstein's general theory of relativity is the fundamental basis for modern cosmology, which describes the interactions of matter, energy, space and time. Cosmological models are theoretical frameworks which are used in cosmology to explain the Universe's expansion. As we know that the most accepted cosmological model is the ΛCDM model which is based on the Einstein's GTR. It provides a reasonably good account of the properties of existence and structure of the cosmic microwave background, the large scale structure in the distribution of galaxies and the accelerating expansion of the Universe. The faster expansion has been attributed to the DE with negative pressure. The Λ term which was introduced by Einstein to make the Universe as a static, is currently associated with the vacuum energy or dark energy in empty space which is used to explain the accelerating expansion of space. The ΛCDM model, which contains (cold dark Matter (CDM) to explain the clustering, flat spatial geometry, fits accurately the current observational data. It has the equation of state $p_\Lambda = -\rho_\Lambda$, with $w = -1$. However, the ΛCDM suffers from, among others, two fundamental problems: fine-tuning problem and the coincidence problem.

Over the past decade, it has been observed that one of the main attempts to solve the issues of ΛCDM model is based on the idea that vacuum energy density is not a constant but a time-dependent quantity, i.e., $\Lambda = \Lambda(t)$. There are a number of interesting works on Λ–variable models as we have already discussed in the Introductory chapters. The decaying vacuum provides the repulsive force which drives the accelerated expansion of the Universe. It can affect the growth of cosmic structures, putting constraints on the decay rate. In most of

the work, the decaying vacuum models have been proposed on phenomenological grounds. In recent years, many authors have presented the a more fundamental approach for the decaying vacuum models which are based on the quantum field theory (QFT).

On the other hand, the viscous cosmology is an interesting alternative to understand the accelerated expansion of the Universe. The bulk viscosity in a cosmic fluid creates the necessary negative pressure, responsible for accelerated expansion of the Universe. It can potentially describe both DM and DE using single viscous fluid component which simplifies our understanding about the Universe. The origin of the bulk viscosity in physical system is due to its deviation from local thermodynamic equilibrium. The energy-momentum tensor of bulk viscous component it that of an imperfect fluid with a first-order deviation from the thermodynamic equilibrium. The effective pressure was proposed by Eckart [29] for relativistic dissipative processes in thermodynamics system out of local equilibrium. In spite of the problems of the Eckart theory, it has been widely used by many authors due to simplified form. Bulk viscous model has been used to explain the observed acceleration of the Universe by assuming that the approximation of vanishing relaxation time is valid for this purpose. In this thesis, we also assume a vanishing relaxation time, so that, in this limit the Eckart theory is a good approximation to the Israel–Stewart theory. In this context, it is convenient to mention that Hiscock et al. showed that flat FLRW cosmological models with bulk viscous Boltmann gas expand more rapidly using Eckart theory.

In this thesis, we have combined the decaying vacuum with the bulk viscosity in a spatially homogeneous and isotropic FLRW metric in General Relativity and its alternative theories, like Brans-Dicke theory. These type of cosmological models provide a richer, more dynamic picture of the Universe's expansion and offer plausible solutions to the current cosmological puzzles. In order to evaluate the theoretical predictions using the vast amount of cosmological data that we presently have access to, the related studies have been conducted by carefully examining the predictions at the background and perturbation levels. Finding evidence of new physics that helps to ease some of the tensions that affect the ΛCDM is the ultimate objective. As previously said, because the concordance hypothesis is generally consistent with a substantial amount of cosmological data, it has remained strong and uncontested for a very long time. This characteristic makes it impractical to search for models that behave considerably differently from the ΛCDM; instead, one should examine models that show minor deviations from the standard model in significant domains. We have thoroughly examined the Running Vacuum Models (RVMs). They are characterized by having time-evolving vacuum energy density, whose functional form is inspired by quantum field theory (QFT) in curved space-time. We have studied different forms of decaying vacuum energy density in this thesis.

Finally, the Brans and Dicke (BD) gravity model was thoroughly examined at the conclusion of the thesis. This model's primary characteristic is that a dynamical scalar field $G(t) = 1/\phi(t)$,

linked to the curvature, takes the place of the Newtonian constant coupling G. As a result, the metric field mediates the gravitational interaction for both the aforementioned scalar field and the General Relativity (GR) case. A dimensionless parameter in the theory is called the BD-parameter and is represented by ω_{BD}. We take into account the presence of the constant ρ_Λ in the action, unlike in the model's initial formulation. In this sense, the model has two additional d.o.f. compared to the standard model, namely the ω_{BD} parameter indicated above and the initial value of the BD scalar field. As a result, we must impose the limits $\omega_{BD} \to \infty$ and $\phi \to G_N$ in order to recover the ΛCDM. As we've seen, having these two degrees of freedom is essential for solving the H_0-tension and σ_8-tension.

Let us summarize the main conclusions obtained in this thesis:

- In chapter 2 we have studied the analytical and observational consequences of cosmology inspired by dissipative phenomena in fluids according to Eckart theory with varying VED scenarios for spatially flat homogeneous and isotropic FLRW geometry. We have assumed the interaction of two components: viscous dark matter and vacuum energy density. We have solved the field equations by assuming the most general form of bulk viscous coefficient, viz., $\zeta = \zeta_0 + \zeta_1 H + \zeta_2(\ddot{a}/aH)$. We have also explored three particular cases of bulk viscosity, namely (1) $\zeta = \zeta_0$; (2) $\zeta = \zeta_1 H$; (3) $\zeta = \zeta_0 + \zeta_1 H$ to observe the effect of viscosity with varying VED. We have used the varying VED of the functional form $\rho_\Lambda = c_0 + 3\nu H^2$ in all of viscous models presented above. It has been observed that all these viscous $\Lambda(t)$ models expand exponentially with cosmic time t. The models show the transition from decelerated phase to accelerated phase in late time. The matter energy density, $\rho_m(t)$ approaches to a finite value in late time evolution of the Universe. The value of χ^2_{red} is less than unity with every data sets which show that the model is in a very good fit with these observational data sets. The jerk parameter remains positive and less than unity in past, and eventually tends to unity in late-time. Thus, the jerk parameter deviates in early time but it attains the same value as ΛCDM in late-time. To discriminate the viscous $\Lambda(t)$ with the ΛCDM, we have examined them using the selection criterion.

- In chapter 3, we have extended the work of chapter 2 and discussed some cosmological consequences of an alternative mechanism of accelerating Universe based on a class of interacting viscous model with decaying vacuum energy, referred as interacting viscous $\Lambda(t)$ model. The coupling between viscous fluid and vacuum energy density has been made through a coupling parameter, Q. The interaction term is taken to be $Q = 3\alpha\rho_m H$. We have assumed $\zeta = \zeta_1 H$ for bulk viscous coefficient and $\rho_\Lambda = c_0 + 3\nu H^2$ for vacuum energy density. We have investigated the growth perturbation of interacting viscous

$\Lambda(t)$ model and performed the Bayesian analysis using the latest background probes such as SNe Pantheon+, cosmic chronometer and $f(z)\sigma_8(z)$. We have discovered that indeed the interaction between the viscous fluid and decaying vacuum energy potentially resolved tensions in cosmological parameters.

- Additionally, Chapter 4 explores another bulk viscous cosmological model in the framework of time varying vacuum energy density, where the bulk viscosity coefficient is proportional to the hubble parameter H. Additionally, we have assumed a specific form of the vacuum energy density which is proportional to the scalar of curvature, $\dot{H}$ and H^2. We have discovered that the VED with viscosity is keeping pace with the expansion of the universe. When a global fit is made to the cosmological dataset using two different combinations, including the Baseline(SNIa + BAO + H(z)) and Baseline+ $f(z)\sigma_8(z)$, and the rigid option $\nu, \mu, \zeta = 0$ (i.e., Λ=constant corresponding to the ΛCDM model) is compared with the Viscous RVM ($\nu, \mu, \zeta \neq 0$), we discovered that a mild dynamics of the cosmic vacuum and viscosity is strongly preferred. Further the model alleviates the Hubble tension up to 0.569σ.

- In chapter 5, we have discussed the dynamics of a flat FLRW model in BD theory with varying vacuum energy density by using combination of two datasets $DS1 = SNe + H(z)$ and $DS2 = SNe + H(z) + BAO_{dz}$. We have found the analytical solution of field equations by considering the two functional forms of cosmological constant, viz. power-series(PS) form: $\Lambda = n_1 H + n_2 H^2$ and power-law(PL) form: $\Lambda \propto a^{-n}$, where n_1, n_2 and n are all constants, and H and a are the Hubble parameter and scale factor, respectively. Assuming ΛCDM as a reference model, we have discussed the performance of these two proposed models. We have found that both the models PS and PL show a smooth transition from deceleration $(q > 0)$ epoch to acceleration $(q < 0)$ epoch in recent past. The parameters $q(z)$, w_{eff} and $j(z)$ tend to ΛCDM model in late-time evolution in PS model. In PL model, these parameters do not tend to respective values of ΛCDM in late-time evolution. It has been observed that both the models are well consistent with $H(z)$ data at low redshifts. In order to examine different cosmological parameters, we have used the MCMC method to constrain the model parameters and then, we have compared them using the information criterion techniques.

- In chapter 6, we have enchanced our work and studied a flat FLRW model in BD theory by assuming two different functional forms of VED, viz. $\Lambda_{RG1} : \Lambda = 3\nu H^2$ and $\Lambda_{RG2} : \Lambda = c_0 + 3\nu H^2$. We have found that Λ_{RG1}-model was unable to fit with the observational data as this model gave power-law expansion of the Universe which did not show the phase transition. On the other hand, the Λ_{RG2} model was well compared with standard ΛCDM model. Firstly, we have obtained the analytical solution of the basic

cosmological functions for these two models and then performed a Bayesian MCMC analysis using two different joint combinations of observational data of SNe Pantheon, $H(z)$ data, BAO/CMB and local Hubble constant to obtain the best fit parameters for Λ_{RG2} model. The deceleration parameter exhibited a transition from decelerated phase to an accelerated phase and the effective EoS parameter has small negative values at high redshift but tend to -1 as $z \to -1$, showing the ΛCDM behavior. It has been observed that the choice of functional form of Λ is very important in describing the dynamics of the Universe, especially the late time acceleration. In the absence of BD theory, we recover exactly the varying vacuum models. At very late time we got an effective cosmological constant dominated era that implies a pure de Sitter phase of the scale factor. In summary, the Λ_{RG2} model successfully reproduced the expected epochs and shows a good agreement with the ΛCDM model.

7.2 Future Scope

One can plan the following by continuing the present thesis work as a future scope:

- As we know that the current decaying VED and viscous cosmology are often phenomenological. In future we one focus on developing models grounded in fundamental physics, like Quantum field theory (QFT) in curved spacetime to provide a solid foundation of decaying vacuum and viscosity.
- This might help to unify inflationary and late-time acceleration at one platform.
- In the thesis work, we have observed that the combined cosmological models have the potential to resolve the current discrepancies in the ΛCDM model.
- We have also observed that combined models have shown in alleviating H_0 and σ_8 tensions. Further investigations and refinement could give better results.
- Since the dissipative processes are the thermodynamical dynamics in which generalized second law of thermodynamics, will play an important role for study.
- One can focus on phase–space analysis to examine the stability and evolution of the Universe.
- Future study will delve in deeper knowledge of structure formation at perturbation level.
- Using latest advanced observational data, one can find more tighter constraints and explore their potential to solve H_0 and σ_8 tensions.

7.3 Social Impact

Although this thesis is rooted in theoretical cosmology, its social impact lies in how it strengthens the foundations on which modern astrophysics is built and how it improves the way we interpret evidence about the Universe. By developing and testing alternative models for cosmic acceleration–especially those using bulk viscosity and decaying (or running) vacuum energy–the work directly engages with well–known limitations of the standard ΛCDM framework, including the coincidence and fine-tuning problems.

A key societal benefit of this research is methodological reliability. The thesis emphasizes confronting theory with observation using multiple datasets–Type Ia supernovae, Hubble expansion data, BAO, and large scale structure, rather than relying on a single measurement. This multi–probe approach contributes to a culture of verification in science, where results are judged by consistency across evidence. In practical terms, with improved models researchers can analyse future data more accurately and reduce errors that come from systematic mismodelling. This work also addresses a broader challenge in cosmology: reducing persistent tensions in key measurements. The proposed interaction between running vacuum energy and bulk viscosity is presented as a promising route in improving the current tensions, particularly the H_0 and σ_8 tensions. If such alternatives continue to perform well, they can guide how the community prioritizes follow up observations and what kinds of measurements are most decisive.

Finally, the thesis has an educational and capacity building impact. By working within established frameworks (GTR, FLRW geometry) while also extending to modified gravity through Brans–Dicke theory, it demonstrates how new ideas can be tested without abandoning scientific discipline. The use of MCMC parameter estimation and model comparison methods further supports training in modern data driven research skills that transfer well to other fields requiring rigorous statistical inference. Beyond observational tests, this research engages with fundamental questions about the Universe's origin and ultimate fate, and it has cultural value by supporting public scientific literacy.

****

Bibliography

[1] A. Einstein; The foundation of the general theory of relativity, Ann. Phys. **49**, 769 (1916); Sitz. Preuss. Akad. Wiss. Phys. 1, 142 (4) (1917); Ann. Phys. **69**, 436 (1922).

[2] A. Friedmann; *Über die Krümmung des Raumes*, Z. Phys. **10**, 377–386 (1922).

[3] A. Friedmann; *Über die Möglichkeit einer Welt mit konstanter negativer Krümmung des Raumes*, Z. Phys. **21**, 326–332 (1924).

[4] G. Lemaître; *The Expanding Universe*, Mon. Not. R. Astron. Soc. **91**, 490–501 (1931).

[5] H. P. Robertson; *Kinematics and World-Structure*, Astrophys. J. **82**, 284–301 (1935).

[6] H. P. Robertson; *Kinematics and World-Structure III*, Astrophys. J. **83**, 257–271 (1936).

[7] A. G. Walker; *On Milne's theory of world-structure*, Proc. Lond. Math. Soc. **s2-42**, 90–127 (1937).

[8] Charles W. Misner, Kip S. Thorne, John Archibald Wheeler; *Gravitation* San Francisco: W. H. Freeman. ISBN 978-0-7167-0344-0 (1973).

[9] Charles W. Misner, Kip S. Thorne, John Archibald Wheeler, David I. Kaiser; *Gravitation* Princeton University Press. ISBN 9780691177793 (2017).

[10] S. Weinberg; *The cosmological constant problem*, Rev. Mod. Phys. **61**, 1–23 (1989).

[11] P. A. R. Ade et al.; *Planck 2015 results*, Astron. Astrophys. **594**, A13 (2016).

[12] J. Martin; *Everything you always wanted to know about the cosmological constant problem (but were afraid to ask)*, C. R. Phys. **13**, 566–665 (2012).

[13] I. Zlatev, L. Wang, and P. J. Steinhardt; *Quintessence, cosmic coincidence, and the cosmological constant*, Phys. Rev. Lett. **82**, 896–899 (1999).

[14] H. Velten, R. F. vom Marttens, and W. Zimdahl; *Aspects of the cosmological "coincidence problem"*, Eur. Phys. J. C **74**, 3160 (2014).

[15] L. Amendola and S. Tsujikawa; *Dark Energy: Theory and Observations*, Cambridge University Press (2010).

[16] J. Solà; *Cosmological constant and vacuum energy: old and new ideas*, J. Phys. Conf. Ser. **453**, 012015 (2013).

[17] J. Solà; *Dark energy: A quantum fossil from the inflationary Universe?*, J. Phys. A **41(16)**, 164066 (2008).

[18] A. Gómez-Valent, V. Pettorino, and L. Amendola; *Update on coupled dark energy and the H_0 tension*, Phys. Rev. D **101**, 123513 (2020).

[19] L. P. Chimento, A. S. Jakubi, D. Pavón, and W. Zimdahl; *Interacting quintessence solution to the coincidence problem*, Phys. Rev. D **67**, 083513 (2003).

[20] G. Olivares, F. Atrio-Barandela, and D. Pavón; *Observational constraints on interacting quintessence models*, Phys. Rev. D **71**, 063523 (2005).

[21] V. Salvatelli et al.; *Indications of a late-time interaction in the dark sector*, Phys. Rev. Lett. **113**, 181301 (2014).

[22] W. Yang et al.; *Tale of stable interacting dark energy, observational signatures, and the H_0 tension*, J. Cosmol. Astropart. Phys. **09**, 019 (2018).

[23] J. Solà, A. Gómez-Valent, and J. de Cruz Pérez; *The H_0 tension in light of vacuum dynamics in the Universe*, Phys. Lett. B **774**, 317–324 (2017).

[24] C. Brans and R. H. Dicke; *Mach's principle and a relativistic theory of gravitation*, Phys. Rev.(series I) **124**, 925–935 (1961).

[25] C. H. Brans; *Mach's principle and a relativistic theory of gravitation. II*, Phys. Rev.(series I), **125(6)**, 2194–2201 (1962).

[26] J. M. Cervero and P. G. Estevez; *General solutions for a cosmological Robertson-Walker metric in the Brans-Dicke theory*, Gen. Relativ. Gravit., **15(4)**, 351–356 (1983).

[27] K. Uehara and C. W. Kim; *Brans-Dicke cosmology with cosmological constant*, Phys.Rev. D, **26(10)**, 2575–2579 (1982).

[28] W. Israel and J. M. Stewart; *Thermodynamics of nonstationary and transient effects in a relativistic gas*, Phys. Lett. A **58**, 213–215 (1976).

[29] C. Eckart; *The thermodynamics of irreversible processes. III. Relativistic theory of the simple fluid*, Phys. Rev. **58**, 919 (1940).

[30] L. D. Landau and E. M. Lifshitz; *Fluid Mechanics*, Pergamon Press, Oxford (1959).

[31] N. Aghanim et al. (Planck Collaboration); *Planck 2018 results. VI. Cosmological parameters*, Astron. Astrophys. **641**, A6 (2020).

[32] A. G. Riess et al.; *A comprehensive measurement of the local value of the Hubble constant with* $1\,\mathrm{km\,s^{-1}\,Mpc^{-1}}$ *uncertainty from the hubble space telescope and the SH0ES Team*, Astrophys. J. Lett. **934**, L7 (2022).

[33] A. G. Riess et al.; *Observational Evidence from Supernovae for an Accelerating Universe and a Cosmological Constant*, Astron. J. **116**, 1009–1038 (1998).

[34] S. Perlmutter et al.; *Measurements of* Ω *and* Λ *from 42 High-Redshift Supernovae*, Astrophys. J. **517**, 565–586 (1999).

[35] M. Visser; *Jerk, snap and cosmological equation of state*, Class. Qunatum Grav., **21(11)**, 2603 (2004).

[36] D. Foreman-Mackey, D. W. Hogg, D. Lang, and J. Goodman; *emcee: The MCMC Hammer*, Publ. Astron. Soc. Pac. **125**, 306–312 (2013).

[37] D. M. Scolnic et al.; *The Complete Light-curve Sample of Spectroscopically Confirmed SNe Ia from Pan-STARRS1 and Cosmological Constraints from the Combined Pantheon Sample*, Astrophys. J. **859**, 101 (2018).

[38] D. Scolnic et al.; *The Pantheon+ Analysis: The Full Data Set and Light-curve Release*, Astrophys. J. **938**, 113 (2022).

[39] D. Brout et al.; *The Pantheon+ Analysis: Cosmological Constraints*, Astrophys. J. **938**, 110 (2022).

[40] A. Conley et al.; *Supernova Constraints and Systematic Uncertainties from the First Three Years of the Supernova Legacy Survey*, Astrophys. J. Suppl. Ser. **192**, 1 (2011).

[41] M. Moresco et al.; *Unveiling the Universe with emerging cosmological probes*, Living Rev. Relativ. **25**, 6 (2022).

[42] M. Moresco et al.; *Improved constraints on the expansion rate of the Universe up to* $z \sim 1.1$ *from the spectroscopic evolution of cosmic chronometers*, J. Cosmol. Astropart. Phys. **2012**(08), 006 (2012).

[43] T. Delubac et al.; *Baryon acoustic oscillations in the Ly*α *forest of BOSS DR11 quasars*, Astron. Astrophys. **574**, A59 (2015).

[44] A. Font-Ribera et al.; *Quasar–Lyman α forest cross-correlation from BOSS DR11: Baryon acoustic oscillations*, J. Cosmol. Astropart. Phys. **2014**(05), 027 (2014).

[45] S. Alam et al. (BOSS Collaboration); *The clustering of galaxies in the completed SDSS-III Baryon Oscillation Spectroscopic Survey: cosmological analysis of the DR12 galaxy sample*, Mon. Not. R. Astron. Soc. **470**, 2617–2652 (2017).

[46] F. Beutler et al.; *The 6dF Galaxy Survey: Baryon Acoustic Oscillations and the Local Hubble Constant*, Mon. Not. R. Astron. Soc. **416**, 3017–3032 (2011).

[47] A. J. Ross et al.; *The clustering of the SDSS DR7 main Galaxy Sample – I. A 4 per cent distance measure at redshift 0.15*, Mon. Not. R. Astron. Soc. **449**, 835–847 (2015).

[48] L. Anderson et al.; *The clustering of galaxies in the SDSS–III Baryon Oscillation Spectroscopic Survey: baryon acoustic oscillations in the Data Releases 10 and 11 Galaxy samples*, Mon. Not. R. Astron. Soc. **441**, 24–62 (2014).

[49] C. Blake et al., *The WiggleZ Dark Energy Survey: joint measurements of the expansion and growth history at z<1*, Mon. Not. R. Astron. Soc. **425**, 405–414 (2012).

[50] P.A.R. Ade et al.(Planck Collaboration); *Planck 2015 results. XIII. Cosmological parameters*, Astron. Astrophys. **594**, A13 (2016).

[51] M.V. Santos, R.R.R. Reis and I. Waga; *Constraining the cosmic deceleration–acceleration transition with type Ia supernova, BAO/CMB and H(z) data*, J. Cosmol. Astropart. Phys. **2016**(02), 066 (2016).

[52] C. Blake et al.; *The WiggleZ Dark Energy Survey: mapping the distance–redshift relation with baryon acoustic oscillations*, Mon. Not. R. Astron. Soc. **418**, 1707–1724 (2011).

[53] A. G. Valent, E. Karimkhani and J. Sola; *Background history and cosmic perturbations for a general system of self–conserved dynamical dark energy and matter*, J. Cosmol. Astropart. Phys. **2015**(12), 048 (2015).

[54] A. G. Valent, J. Sola and S.Basilakos; *Dynamical vacuum energy in the expanding Universe confronted with observations: a dedicated study*, J. Cosmol. Astropart. Phys. **2015**(01), 004 (2015).

[55] A. G. Adame et al.; *DESI 2024 VI: Cosmological constraints from the measurements of baryon acoustic oscillations*, J. Cosmol. Astropart. Phys. **2025**(02), 021 (2025).

[56] CobayaSampler Collaboration, *DESI BAO Data Repository*, https://github.com/CobayaSampler/DESI_BAO_data.

[57] CobayaSampler Collaboration, *DESI BAO Covariance Matrix File*, https://github.com/CobayaSampler/DESI_BAO_data.

[58] S. Nesseris, G. Pantazis, and L. Perivolaropoulos; *Tension and constraints on modified gravity parametrizations of $G_{eff?}(z)$ from growth rate and Planck data*, Phys. Rev. D **96**, 023542 (2017).

[59] A. Quelle and A. L. Maroto; *On the tension between growth rate and CMB data*, Eur. Phys. J. C **80**, 369 (2020).

[60] A. G. Riess et al.; *Large Magellanic Cloud Cepheid Standards Provide a 1% Foundation for the Determination of the Hubble Constant and Stronger Evidence for Physics Beyond ΛCDM*, Astrophys. J. **876**, 85 (2019).

[61] H. Akaike; *A new look at the statistical model identification*, IEEE Trans. Autom. Control **19**, 716–723 (1974).

[62] A. R. Liddle; *Information criteria for astrophysical model selection*, Mon. Not. R. Astron. Soc. **377**, L74–L78 (2007).

[63] G. Schwarz; *Estimating the dimension of a model*, Ann. Stat. **6**, 461–464 (1978).

[64] G. Hinshaw et al.; *Nine-Year Wilkinson Microwave Anisotropy Probe (WMAP) observations: Cosmological parameter results*, Astrophys. J. Suppl. **208**, 19 (2013).

[65] C.L. Bennett et al.; *Nine-Year Wilkinson Microwave Anisotropy Probe (WMAP) Observations: Final maps and results*, Astrophys. J. Suppl. **208**, 20 (2013).

[66] L. Anderson et al.; *The clustering of galaxies in the SDSS-III Baryon Oscillation spectroscopic survey: Baryon Acoustic Oscillations in the data release 9 spectroscopic galaxy sample*, Mon. Not. Roy. Astron. Soc. **427**, 3435–3467 (2012).

[67] P.A.R. Ade et al.; *Planck 2013 results. I. Overview of products and scientific results (Planck Collaboration)*, Astron. Astrophys. **571**, A1 (2014).

[68] T. Padmanabhan and S. M. Chitre; *Viscous universes*, Phys. Lett. A **120**, 433–436 (1987).

[69] B. Cheng; *Bulk viscosity in the early Universe*, Phys. Lett. A **160(4)**, 329–338 (1991).

[70] J.C. Fabris, S.V.B. Goncalves, R.S. Ribeiro; *Bulk viscosity driving the acceleration of the Universe*, Gen.Rel.Grav. **38**, 495–406 (2006).

[71] B. Li and J. D. Barrow; *Does bulk viscosity create a viable unified dark matter model?*, Phys. Rev. D **79**, 103521 (2009).

[72] A. Avelino and U. Nucamendi; *Exploring a matter–dominated model with bulk viscosity to drive the accelerated expansion of the Universe*, J. Cosmol. Astropart. Phys. **2010**(08), 009 (2010).

[73] A. Avelino et al.; *Bulk viscous matter-dominated Universes: asymptotic properties*, J. Cosmol. Astropart. Phys. **2013**(08), 012 (2013).

[74] A. Sasidharan, T.K. Mathew and M. S. Divya; *Bulk viscous matter and recent acceleration of the universe*, Eur. Phys. J. C **75**, 348 (2015).

[75] A. Avelino and U. Nucamendi; *Can a matter-dominated model with constant bulk viscosity drive the accelerated expansion of the Universe?*, J. Cosmol. Astropart. Phys. **04**, 006 (2009).

[76] C. L. Bennett et al.; *First-Year Wilkinson Microwave Anisotropy Probe (WMAP) Observations: Preliminary Maps and Basic Results*, Astrophys. J. Suppl. Ser. **148**, 1–27 (2003).

[77] M. Tegmark et al.; *Cosmological parameters from SDSS and WMAP*, Phys. Rev. D **69**, 103501 (2004).

[78] M. H. Amante et al.; *Testing dark energy models with a new sample of strong-lensing systems*, Mon. Not. R. Astron. Soc. **498**, 6013–6033 (2020).

[79] N. Aghanim et al. (Planck Collaboration); *Planck 2018 results. VI. Cosmological parameters*, Astron. Astrophys. **641**, A6 (2020).

[80] L. Wang, R. R. Caldwell, J. P. Ostriker, and P. J. Steinhardt; *Cosmic concordance and quintessence*, Astrophys. J. **530**, 17 (2000).

[81] R. R. Caldwell, R. Dave, and P. J. Steinhardt; *Quintessential cosmology novel models of cosmological structure formation*, Astrophys. Space Sci. **261**, 303–310 (1998).

[82] P. J. Steinhardt; *A quintessential introduction to dark energy*, Phil. Trans. R. Soc. A **361**(1812), 2497–2513 (2003).

[83] P. J. E. Peebles and B. Ratra; *The cosmological constant and dark energy*, Rev. Mod. Phys. **75**, 559–606 (2003).

[84] S. M. Carroll; *The cosmological constant*, Living Rev. Relativ. **4**, 1 (2001).

[85] T. Padmanabhan; *Cosmological constant—the weight of the vacuum*, Phys. Rep. **380**, 235–320 (2003).

[86] K. Freese, F. C. Adams, J. A. Frieman, and E. Mottola; *Cosmology with decaying vacuum energy*, Nucl. Phys. B **287**, 797–814 (1987).

[87] J. C. Carvalho, J. A. S. Lima, and I. Waga; *Cosmological consequences of a time-dependent Λ term*, Phys. Rev. D **46**, 2404 (1992).

[88] J. A. S. Lima and J. M. F. Maia; *Deflationary cosmology with decaying vacuum energy density*, Phys. Rev. D **49**, 5597 (1994).

[89] J. A. S. Lima; *Thermodynamics of decaying vacuum cosmologies*, Phys. Rev. D **54**, 2571 (1996).

[90] E. Elizalde, S. Nojiri, S. D. Odintsov, and P. Wang; *Dark energy: Vacuum fluctuations, the effective phantom phase, and holography*, Phys. Rev. D **71**(10), 103504 (2005).

[91] J. S. Alcaniz and J. A. S. Lima; *Interpreting cosmological vacuum decay*, Phys. Rev. D **72**, 063516 (2005).

[92] J. Solà and H. Stenfancic; *Dynamical dark energy or variable cosmological parameters?*, Mod. Phys. Lett. A **21**, 479–494 (2006).

[93] F. E. M. Costa and J. S. Alcaniz; *Cosmological consequences of a possible Λ–dark matter interaction*, Phys. Rev. D **81**, 043506 (2010).

[94] C. Pigozzo, M. A. Dantas, S. Carneiro, and J. S. Alcaniz; *Observational tests for $\Lambda(t)$CDM cosmology*, J. Cosmol. Astropart. Phys. **2011**(08), 022 (2011).

[95] J. Solà; *Cosmologies with a time dependent vacuum*, J. Phys. Conf. Ser. **283**, 012033 (2011).

[96] J. Grande, J. Solà, S. Basilakosweinberg, and M. Plionis; *Hubble expansion and structure formation in the "running FLRW model" of the cosmic evolution*, J. Cosmol. Astropart. Phys. **2011**(08), 007 (2011).

[97] E.L.D. Perico, J.A.S. Lima, S. Basilakos and J. Solà; *Complete cosmic history with a dynamical $\Lambda = \Lambda(H)$ term*, Phys. Rev. D **88**, 063531 (2013).

[98] M. Szydłowski and A. Stachowski; *Cosmology with decaying cosmological constant–exact solutions and model testing*, J. Cosmol. Astropart. Phys. **2015(10)**, 066 (2015).

[99] S. Basilakos; *Cosmological implications and structure formation from a time varying vacuum*, Mon. Not. R. Astron. Soc. **395**, 2347–2355 (2009).

[100] S. Basilakos, M. Plionis, and J. Solà; *Hubble expansion & structure formation in time-varying vacuum models*, Phys. Rev. D **80**, 083511 (2009).

[101] D. Bessada and O. D. Miranda; *Probing a cosmological model with a* $\Lambda = \Lambda_0 + 3\beta H^2$ *decaying vacuum*, Phys. Rev. D **88**, 083530 (2013).

[102] H. A. Borges and S. Carneiro; *Friedmann cosmology with decaying vacuum density*, Gen. Relativ. Gravit. **37**, 1385–1394 (2005).

[103] S. Carneiro, C. Pigozzo, H. A. Borges, and J. S. Alcaniz; *Supernova constraints on decaying vacuum cosmology*, Phys. Rev. D **74**, 023532 (2006).

[104] H. A. Borges, S. Carneiro, J. C. Fabris, and C. Pigozzo; *Evolution of density perturbations in decaying vacuum cosmology*, Phys. Rev. D **77**, 043513 (2008)

[105] S. Carneiro, M. A. Dantas, C. Pigozzo, and J. S. Alcaniz; *Observational constraints on late-time* $\Lambda(t)$ *cosmology*, Phys. Rev. D **77**, 083504 (2008).

[106] A. Gómez-Valent, E. Karimkhani, and J. Solà; *Background history and cosmic perturbations for a general system of self-conserved dynamical dark energy and matter*, J. Cosmol. Astropart. Phys. **2015**(12), 048 (2015), arXiv:1509.03298 [astro-ph.CO].

[107] A. P. Jayadevan, M. Mukesh, and T. K. Mathew; *Probing the dynamical system and thermal behaviors of the model* $\Lambda_0 + 3\beta H^2$, Astrophys. Space Sci. **364**, 67 (2019).

[108] J. Solà and A. Gómez-Valent; *The* $\bar{\Lambda}$*CDM cosmology: From inflation to dark energy through running vacuum*, Int. J. Mod. Phys. D **24**, 1541003 (2015).

[109] E. A. Novikov; *Quantum modification of general relativity*, Electron. J. Theor. Phys. **13(35)**, 79–90 (2016).

[110] P. Wang and X. Meng; *Can vacuum decay in our Universe?*, Class. Quantum Grav. **22**, 283–294 (2005).

[111] W. Zimdahl, D. J. Schwarz, A. B. Balakin, and D. Pavón; *Cosmic antifriction and accelerated expansion*, Phys. Rev. D **64**, 063501 (2001).

[112] A. B. Balakin, D. Pavón, D. J. Schwarz, and W. Zimdahl; *Curvature force and dark energy*, New J. Phys. **5**, 85 (2003).

[113] W. A. Hiscock and L. Lindblom; *Generic instabilities in first–order dissipative relativistic fluid theories*, Phys. Rev. D **31**, 725 (1985).

[114] I. Müller; *Zum Paradoxon der Wärmeleitungstheorie*, Z. Phys. **198**, 329 (1967).

[115] C. P. Singh, S. Kumar, and A. Pradhan; *Early viscous universe with variable gravitational and cosmological 'constants'*, Class. Quantum Grav. **24**, 455 (2007).

[116] I. Brevik and S. D. Odintsov; *Cardy–Verlinde entropy formula in viscous cosmology*, Phys. Rev. D **65**, 067302 (2002).

[117] Ø. Grøn; *Viscous inflationary universe models*, Astrophys. Space Sci. **173**, 191 (1990).

[118] K. Bamba and S. D. Odintsov; *Inflation in a viscous fluid model*, Eur. Phys. J. C **76**, 18 (2016).

[119] J. X. Wang and X. H. Meng; *Effects of new viscosity model on cosmological evolution*, Mod. Phys. Lett. A **29(03)**, 1450009 (2014).

[120] R. Maartens; *Dissipative cosmology*, Class. Quantum Grav. **12**, 1455 (1995).

[121] A. A. Coley, R. J. van den Hoogen, and R. Maartens; *Qualitative viscous cosmology*, Phys. Rev. D **54**, 1393 (1996).

[122] W. Zimdahl; *Bulk viscous cosmology*, Phys. Rev. D **53**, 5483 (1996).

[123] I. Brevik and A. Hallanger; *Randall–Sundrum model in the presence of a brane bulk viscosity*, Phys. Rev. D **69**, 024009 (2004).

[124] C. P. Singh; *Bulk Viscous cosmology in the early universe*, Pramana J. Phys. **71(1)**, 33–48 (2008).

[125] I. Brevik, O. Gorbunova, and D. Saez-Gomez; *Casimir effects near the big rip singularity in viscous cosmology*, Gen. Relativ. Grav. **42**, 1513 (2010).

[126] H. Velten, J. Wang, and X. H. Meng; *Phantom dark energy as an effect of bulk viscosity*, Phys. Rev. D **88**, 123504 (2013).

[127] J. R. Wilson, G. J. Mathews, and G. M. Fuller; *Bulk viscosity, decaying dark matter, and the cosmic acceleration*, Phys. Rev. D **75**, 043521 (2007).

[128] M.-G. Hu and X.-H. Meng; *Bulk viscous cosmology: statefinder and entropy*, Phys. Lett. B **635**, 186 (2006).

[129] I. Brevik and O. Gorbunova; *Dark energy and viscous cosmology*, Gen. Relativ. Gravit. **37**, 2039 (2005).

[130] C. P. Singh and A. Kumar; *Ricci dark energy model with bulk viscosity*, Eur. Phys. J. Plus **133**, 312 (2018).

[131] C. P. Singh and P. Kumar; *Friedmann model with viscous cosmology in modified $f(R,T)$ gravity theory*, Eur. Phys. J. C **74**, 3070 (2014).

[132] G. M. Kremer and F. P. Devecchi; *Viscous cosmological models and accelerated universes*, Phys. Rev. D **67**, 047301 (2003).

[133] J. C. Fabris, S. V. B. Gonçalves, and R. S. Ribeiro; *Bulk viscosity driving the acceleration of the Universe*, Gen. Relativ. Grav. **38**, 495 (2006).

[134] G. J. Mathews, N. Q. Lan, and C. Kolda; *Late decaying dark matter, bulk viscosity and the cosmic acceleration*, Phys. Rev. D **78**, 043525 (2008).

[135] A. Avelino and U. Nucamendi; *Constraining a matter-dominated cosmological model with bulk viscosity proportional to the Hubble parameter*, AIP Conf. Proc. **1083**, 1 (2008).

[136] B. D. Normann and I. Brevik; *Characteristic properties of two different viscous cosmology models for the future Universe*, Mod. Phys. Lett. A **32**, 1750026 (2017).

[137] A. Avelino, U. Nucamendi and F. S. Guzmán; *Constraining a bulk viscous matter-dominated cosmological model using SNe Ia, CMB and LSS*, AIP Conf. Proc. **1026**, 300 (2008).

[138] D. Wang, Y.J. Yan and X.H. Meng; *Constraining viscous dark energy models with the latest cosmological data*, Eur. Phys. J. C **77(10)**, 660 (2017).

[139] C. P. Singh and A. Kumar; *Viscous Ricci dark energy and generalized second law of thermodynamics in modified $f(R,T)$ gravity*, Mod. Phys. Lett. A **33**, 1850225 (2018).

[140] C. P. Singh and M. Srivastava; *Viscous cosmology in new holographic dark energy model and the cosmic acceleration*, Eur. Phys. J. C **78**, 190 (2018).

[141] J. Ren and X.-H. Meng; *Cosmological model with viscosity media (dark fluid) described by an effective equation of state*, Phys. Lett. B **633**, 1 (2006).

[142] X.-H. Meng, J. Ren, and M.-G. Hu; *Friedmann cosmology with a generalized equation of state and bulk viscosity*, Commun. Theor. Phys. **47**, 379 (2007).

[143] X.-H. Meng and X. Dou; *Friedmann cosmology with bulk viscosity: a concrete model for dark energy*, Commun. Theor. Phys. **52**, 377 (2009).

[144] C. P. Singh and Simran Kaur, *Probing bulk viscous matter-dominated model in Brans–Dicke theory*, Astrophys. Space Sci. **365**, 2 (2020).

[145] C. P. Singh and A. Kumar; *Observational constraints on viscous Ricci dark energy model*, Astrophys. Space Sci. **364**, 94 (2019).

[146] J. Hu and H. Hu; *Viscous universe with cosmological constant*, Eur. Phys. J. Plus **135**, 718 (2020).

[147] L. Herrera-Zamorano et al.; *Constraints and cosmography of ΛCDM in presence of viscosity*, Eur. Phys. J. C **80**, 637 (2020).

[148] C. P. Singh; *Viscosity effects on the early universe with time-varying constants*, Nuovo Cimento B **122**, 89 (2007).

[149] C. P. Singh and S. Kumar; *Viscous fluid cosmology with a cosmological constant*, Astrophys. Space Sci. **323**, 407 (2009).

[150] S. Weinberg; *Gravitation and Cosmology: Principles and Applications of the General Theory of Relativity*, John Wiley & Sons (1972).

[151] S. L. Adler; *Einstein gravity as a symmetry-breaking effect in quantum field theory*, Rev. Mod. Phys. **54**, 729 (1982).

[152] L. Parker and D. J. Toms; *Renormalization group and nonlocal terms in the curved-spacetime effective action: weak-field results*, Phys. Rev. D **32**, 1409 (1985).

[153] I. L. Shapiro and J. Solà; *On the possible running of the cosmological "constant"*, Phys. Lett. B **682**, 105 (2009).

[154] F. Andrade-Oliveira, F. E. M. Costa and J. A. S. Lima; *Decaying vacuum cosmology and its scalar field description*, Class. Quantum Grav. **31**, 045004 (2014).

[155] I.L. Shapiro and J. Solà; *The scaling evolution of the cosmological constant*, J. High Energy Phys. **2002(02)**, 006 (2002).

[156] I. Brevik, Ø. Grøn, J. de Haro, S. D. Odintsov, and E. N. Saridakis; *Viscous cosmology for early- and late-time universe*, Int. J. Mod. Phys. D **26**, 1730024 (2017).

[157] A. Sasidharan and T. K. Mathew; *Phase space analysis of bulk viscous matter dominated universe*, J. High Energy Phys. **06**, 138 (2016).

[158] C. P. Singh and Ajay Kumar; *Holographic Ricci dark energy with constant bulk viscosity in $f(R,T)$ gravity*, Grav. Cosmol. **25**, 58 (2019).

[159] T. Padmanabhan and S. M. Chitre; *Viscous universes*, Phys. Lett. A **120**, 433 (1987).

[160] A. Montiel and N. Bretón; *Probing bulk viscous matter-dominated models with gamma-ray bursts*, J. Cosmol. Astropart. Phys. **08**, 023 (2011).

[161] J. Solà Peracaula, J. de Cruz Pérez and A. Gómez-Valent; *Possible signals of vacuum dynamics in the Universe*, Mon. Not. R. Astron. Soc. **478**, 4357 (2018).

[162] A. Gómez-Valent and J. Solà Peracaula; *Density perturbations for running vacuum: a successful approach to structure formation and to the σ_8-tension*, Mon. Not. R. Astron. Soc. **478**, 126 (2018).

[163] J. de Cruz Pérez and J. Solà Peracaula; *Running vacuum in Brans & Dicke theory: a possible cure for the σ_8 and H_0 tensions*, Phys. Dark Universe **43**, 101406 (2024).

[164] P. J. E. Peebles; *Principles of Physical Cosmology*, Princeton University Press (1993).

[165] Y.-S. Song and W. J. Percival; *Reconstructing the history of structure formation using redshift distortions*, J. Cosmol. Astropart. Phys. **10**, 004 (2009).

[166] D. Huterer et al.; *Growth of cosmic structure: probing dark energy beyond expansion*, Astropart. Phys. **63**, 23 (2015).

[167] S. Nesseris and L. Perivolaropoulos; *Testing ΛCDM with the growth function $\delta(a)$: current constraints*, Phys. Rev. D **77**, 023504 (2008).

[168] W. J. Percival et al.; *Baryon acoustic oscillations in the Sloan Digital Sky Survey Data Release 7 galaxy sample*, Mon. Not. R. Astron. Soc. **401**, 2148 (2010).

[169] R. Giostri et al.; *From cosmic deceleration to acceleration: new constraints from SN Ia and BAO/CMB*, J. Cosmol. Astropart. Phys. **03**, 027 (2012).

[170] Y. Wang, L. Xu, and G.-B. Zhao; *A measurement of the Hubble constant using galaxy redshift surveys*, Astrophys. J. **849**, 84 (2017).

[171] M. Persic, P. Salucci, and F. Stel; *The universal rotation curve of spiral galaxies–I. The dark matter connection*, Mon. Not. R. Astron. Soc. **281**, 27–47 (1996).

[172] J. Magana and T. Matos; *The scalar field dark matter model and its implications*, J. Phys. Conf. Ser. **378**, 012012 (2012).

[173] A. Hernandez-Almada and M. A. Garcia-Aspeitia; *Observational constraints on the interacting dark energy scenario*, Int. J. Mod. Phys. D **27**, 1850031 (2018).

[174] S. P. Martin; *A supersymmetry primer*, Adv. Ser. Dir. High Energy Phys. **18**, 1–98 (1998).

[175] V. Sahni and A. Starobinsky; *The case for a positive cosmological Λ -term*, Int. J. Mod. Phys. D **9**, 373 (2000).

[176] E. J. Copeland, M. Sami, and S. Tsujikawa; *Dynamics of dark energy*, Int. J. Mod. Phys. D **15**, 1753–1935 (2006).

[177] O. Bertolami; *Time-dependent cosmological term*, Nuovo Cimento B **93**, 36–42 (1986).

[178] J. M. Overduin and F. I. Cooperstock; *Evolution of the scale factor with a variable cosmological term*, Phys. Rev. D **58**, 043506 (1998).

[179] M. Ozer and O. Taha; *A model of the universe free of cosmological problems*, Nucl. Phys. B **287**, 776–786 (1987).

[180] J. Solà and A. Gómez-Valent; *The $\bar{\Lambda}$CDM cosmology: from inflation to dark energy through running Λ*, Int. J. Mod. Phys. D **24**, 1541003 (2015).

[181] J. Solà, A. Gómez-Valent, J. de Cruz Pérez, and C. Moreno-Pulido; *Brans–Dicke gravity with a cosmological constant smoothes out ΛCDM tensions*, Astrophys. J. Lett. **886**, L6 (2019), arXiv:1909.02554.

[182] P. J. E. Peebles and B. Ratra; *Cosmology with a time–variable cosmological "constant"*, Astrophys. J. **325**, L17–L20 (1988).

[183] V. Khatri and C. P. Singh; *Brans–Dicke cosmology with cosmological term $\Lambda(H) = c_0 + 3\nu H^2$*, Phys. Dark Univ. **42**, 101300 (2023).

[184] C. P. Singh and J. Solà; *Friedmann cosmology with decaying vacuum density in Brans–Dicke theory*, Eur. Phys. J. C **81**, 960 (2021).

[185] G. L. Murphy; *Big-bang model without singularities*, Phys. Rev. D **8**, 4231 (1973).

[186] T. Padmanabhan and S. M. Chitre; *Viscous universes*, Phys. Lett. A **120**, 433–436 (1987).

[187] A. Sasidharan and T. K. Mathew; *Bulk viscous matter and recent acceleration of the universe*, Eur. Phys. J. C **75**, 348 (2015).

[188] D. Wang, Y.-J. Yan, and X.-H. Meng; *Constraining viscous dark energy models with the latest cosmological data*, Eur. Phys. J. C **77**, 660 (2017).

[189] A. Hernández-Almada; *Cosmological test on viscous bulk models using Hubble parameter measurements and type Ia supernovae data*, Eur. Phys. J. C **79**, 751 (2019).

[190] M. Xin-He and D. Xu; *Friedmann Cosmology with Bulk Viscosity: A Concrete Model for Dark Energy*, Commun. Theor. Phys. **52(2)**, 377 (2009).

[191] N. Mostafapoor and Ø. Grøn; *Viscous ΛCDM universe models*, Astrophys. Space Sci. **333**, 357–368 (2011).

[192] A. Ashoorioon and Z. Davari; *Dark Matter Cosmology with Varying Viscosity: A Possible Resolution to the S_8 Tension*, Astrophys. J. **959(2)**, 120 (2023).

[193] N. Cruz et al.; *Exploring models of running vacuum energy with viscous dark matter from a dynamical system perspective*, Phys. Dark Univ. **42**, 101351 (2023).

[194] C. P. Singh and V. Khatri; *Viscous fluid dynamics with decaying vacuum energy density*, Phys. Rev. D **109**, 023508 (2024).

[195] R. C. Nunes, S. Pan, and E. N. Saridakis; *New constraints on interacting dark energy*, Phys. Rev. D **94**, 023508 (2016).

[196] E. Di Valentino, A. Melchiorri, and O. Mena; *Can interacting dark energy solve the H_0 tension?*, Phys. Rev. D **96**, 043503 (2017).

[197] E. Di Valentino, A. Melchiorri, O. Mena, and S. Vagnozzi; *Interacting dark energy in the early 2020s: A promising solution to the H_0 and cosmic shear tensions*, Phys. Dark Univ. **30**, 100666 (2020).

[198] L. Wang et al.; *Constraints on interacting dark energy models from time–delay cosmography with seven lensed quasars*, Mon. Not. Roy. Astron. Soc. **514**, 1433-1440 (2022).

[199] S. Gariazzo, E. Di Valentino, O. Mena, and R. C. Nunes; *Late–time interacting cosmologies and the Hubble constant tension*, Phys. Rev. D **106**, 023530 (2022).

[200] J.-H. Chen, S. Zhou, and Y.-J. Wang; *Evolution of Interacting Viscous Dark Energy Model in Einstein Cosmology*, Chin. Phys. Lett. **28**, 029801 (2011).

[201] G. M. Kremer and O. A. S. Sobreiro; *Bulk Viscous Cosmological Model with Interacting Dark Fluids*, Braz. J. Phys. **42**, 77–83 (2012).

[202] A. Avelino; *Interacting viscous matter with a dark energy fluid*, AIP Conf. Proc. **1473**, 98–107 (2012).

[203] T. Harko and F. S. N. Lobo; *Irreversible thermodynamic description of interacting dark energy-dark matter cosmological models*, Phys. Rev. D **87**, 044018 (2013).

[204] A. Hernández-Almada et al.; *Stability analysis and constraints on interacting viscous cosmology*, Phys. Rev. D **101**, 063516 (2020).

[205] A. Marcel van der Westhuizen and A. Abebe; *Interacting dark energy: clarifying the cosmological implications and viability conditions*, J. Cosmol. Astropart. Phys. **2024(01)**, 048 (2024).

[206] X.-M. Chen, Y. Gong, and E. N. Saridakis; *Phase–space analysis of interacting phantom cosmology*, J. Cosmol. Astropart. Phys. **04**, 001 (2009).

[207] X.-M. Chen, Y. Gong, and E. N. Saridakis; *The transient acceleration from time–dependent interacting dark energy models*, Internat. J. Theoret. Phys. **53**, 469–481 (2014).

[208] I. Brevik, V. V. Obukhov, and A. V. Timoshkin; *Dark Energy Coupled with Dark Matter in Viscous Fluid Cosmology*, Astrophys. Space Sci. **355**, 399–403 (2015).

[209] S. Nojiri and S. D. Odintsov; *Unified cosmic history in modified gravity: from F(R) theory to Lorentz non–invariant models*, Phys. Rep. **505**, 59–144 (2011).

[210] A. Lewis; *GetDist: a Python package for analysing Monte Carlo samples*, J. Cosmol. Astropart. Phys. **2025(08)**, 025 (2025).

[211] C. Heymans et al.; *KiDS-1000 Cosmology: Multi-probe weak gravitational lensing and spectroscopic galaxy clustering constraints*, Astron. Astrophys. **646**, A140 (2021).

[212] H. Jeffreys; *Theory of Probability* (Oxford University Press, Oxford, 1961).

[213] D. J. C. MacKay; *Information Theory, Inference, and Learning Algorithms* (Cambridge University Press, Cambridge, 2003).

[214] A. R. Liddle, P. Mukherjee, D. Parkinson, and Y. Wang; *Present and future evidence for evolving dark energy*, Phys. Rev. D **74**, 123506 (2006).

[215] P. Mukherjee, D. Parkinson, and A. R. Liddle; *A Nested Sampling Algorithm for Cosmological Model Selection*, Astrophys. J. **638**, L51 (2006).

[216] R. Trotta; *Applications of Bayesian model selection to cosmological parameters*, Mon. Not. Roy. Astron. Soc. **378**, 72 (2007).

[217] B. Santos, N. Chandrachani Devi, and J. S. Alcaniz; *Bayesian comparison of nonstandard cosmologies using type Ia supernovae and BAO data*, Phys. Rev. D **95**, 123514 (2017).

[218] W. J. C. da Silva and R. Silva; *Growth of matter perturbations in the extended viscous dark energy models*, Eur. Phys. J. C **81**, 403 (2021).

[219] P. J. E. Peebles; *Tests of cosmological models constrained by inflation*, Astrophys. J. **284**, 439 (1984).

[220] P. J. E. Peebles; *Principles of Physical Cosmology*, Princeton University Press (1993).

[221] L. Perivolaropoulos and F. Skara; *Challenges for ΛCDM: An update*, New Astron. Rev. **95**, 101659 (2022).

[222] W. L. Freedman; *Cosmology at a crossroads*, Nat. Astron. **1**, 121 (2017).

[223] A. G. Riess and L. Breuval; *The Local Value of H_0*, arXiv:2308.10954 (2023).

[224] R. Dalal et al.; *Hyper Suprime–Cam Year 3 results: Cosmology from cosmic shear power spectra*, Phys. Rev. D **108**, 123519 (2023).

[225] A. M. Abdel-Rahman; *The cosmological constant (Λ) as a possible primordial link to Einstein's theory of gravity, the properties of hadronic matter and the problem of creation*, Nuovo Cim. B **102**, 225–228 (1988).

[226] A. M. Abdel-Rahman; *Singularity-free decaying-vacuum cosmologies*, Phys. Rev. D **45**, 3497 (1992).

[227] J. D. Barrow; *The deflationary universe: an instability of the de Sitter universe*, Phys. Lett. B **180**, 335 (1986).

[228] J. D. Barrow and P. Parsons; *Behavior of cosmological models with varying G*, Phys. Rev. D **55**, 1906 (1997).

[229] A. Beesham; *Bianchi type I cosmological models with variable G and Λ*, Gen. Relativ. Gravit. **26**, 159 (1994).

[230] M. S. Berman; *Cosmological models with a variable cosmological term*, Phys. Rev. D **43**, 1075 (1991).

[231] T. Damour, G. W. Gibbons, and J. H. Taylor; *Limits on the variability of G using binary-pulsar data*, Phys. Rev. Lett. **61**, 1151 (1988).

[232] T. B. Enginol; *An inflationary cosmology with varying G*, Phys. Lett. A **139**, 127 (1989).

[233] D. Kalligas, P. Wesson, and C. W. F. Everitt; *Flat FRW models with variable G and Λ*, Gen. Relativ. Gravit. **24**, 351 (1992).

[234] D. Kalligas, P. S. Wesson, and C. W. F. Everitt; *Bianchi type I cosmological models with variable G and Λ: a comment*, Gen. Relativ. Gravit. **27**, 645 (1995).

[235] Y. K. Lau; *The large number hypothesis and Einstein's theory of gravitation*, Aust. J. Phys. **38**, 547 (1985).

[236] Y. K. Lau and S. J. Prokhovnik; *The large numbers hypothesis and a relativistic theory of gravitation*, Aust. J. Phys. **39**, 339 (1986).

[237] T. Singh, A. Beesham, and W. S. Mbokazi; *Bulk viscous cosmological models with variable G and Λ*, Gen. Relativ. Gravit. **30**, 573 (1998).

[238] R. F. Sistero; *Cosmology with G and Λ coupling scalars*, Gen. Relativ. Gravit. **23**, 1265 (1991).

[239] I. Waga; *Decaying vacuum flat cosmological models–Expressions for some observable quantities and their properties*, Astrophys. J. **414**, 436 (1993).

[240] W. Chen and Y.S. Wu; *Implications of a cosmological constant varying as R^{-2}*, Phys. Rev. D **41**, 695 (1990).

[241] X.H. Meng, J. Ren, and M.G. Hu; *Friedmann cosmology with a generalized equation of state and bulk viscosity*, Commun. Theor. Phys. **47**, 379 (2007).

[242] X.H. Meng and X. Dou; *Friedmann cosmology with bulk viscosity: a concrete model for dark energy*, Commun. Theor. Phys. **52**, 377 (2009).

[243] N. Cruz et al.; *Exploring models of running vacuum energy with viscous dark matter from a dynamical system perspective*, Phys. Dark Univ. **42**, 101351 (2023).

[244] C. Moreno-Pulido and J. Solà Peracaula; *Running vacuum in quantum field theory in curved spacetime: renormalizing $\rho_{\rm vac}$ without $\sim m^4$ terms*, Eur. Phys. J. C **80**, 692 (2020).

[245] C. Moreno-Pulido and J. Solà Peracaula; *Renormalizing the vacuum energy in cosmological spacetime: implications for the cosmological constant problem*, Eur. Phys. J. C **82**, 551 (2022).

[246] C. Moreno-Pulido and J. Solà Peracaula; *Equation of state of the running vacuum*, Eur. Phys. J. C **82**, 1137 (2022).

[247] J. Solà; *Brans–Dicke gravity: from Higgs physics to (dynamical) dark energy*, Int. J.Mod. Phys. D **27**, 1847029 (2018), arXiv:1805.09810.

[248] J. Solà, A. Gómez-Valent, and J. de Cruz Pérez; *First Evidence of Running Cosmic Vacuum: Challenging the Concordance Model*, Astrophys. J. **836**, 43 (2017).

[249] I. Brevik; *Cardy–Verlinde entropy formula in the presence of a general cosmological state equation*, Phys. Rev. D **65**, 127302 (2002).

[250] M. Moresco et al.; *Setting the Stage for Cosmic Chronometers. II. Impact of Stellar Population Synthesis Models Systematics and Full Covariance Matrix*, Astrophys. J. **898**, 82 (2020).

[251] M. A. Karim et al.(DESI Collaboration); *DESI DR2 Results II: Measurements of Baryon Acoustic Oscillations and Cosmological Constraints*, Phys. Rev. D **112**, 083515 (2025).

[252] W.K. Hastings; *Monte Carlo sampling methods using Markov chains and their applications*, Biometrika **57**, 97–109 (1970).

[253] M.Koussour; *A model-independent method with phantom divide line crossing in Weyl-type $f(Q,T)$ gravity*, Chin. J. Phys. **83**, 454–466 (2023).

[254] M. Koussour, N. Myrzakulov, S. Myrzakulova, and M. Sofuoglu; *A comprehensive parametrization approach for the Hubble parameter in scalar field dark energy models*, Results Phys. **55**, 107166 (2023), arXiv:2311.02727.

[255] D. Wang, et al.; *Observational constraints on a logarithmic scalar field dark energy model and black hole mass evolution in the Universe*, Eur. Phys. J. C **83**, 670 (2023).

[256] M. Asgari et al.; *KiDS-1000 Cosmology: Cosmic shear constraints and comparison between two-point statistics*, Astron. Astrophys. **645**, A104 (2021), arXiv:2007.15633.

[257] B. Stolzner et al.; *KiDS-Legacy: Consistency of cosmic shear measurements and joint cosmological constraints with external probes*, Astron. Astrophys. **702**, A169 (2025), arXiv:2503.19442.

[258] A. Gelman and D. B. Rubin; *Inference from iterative simulation using multiple sequences*, Statist. Sci. **7**(4), 457–472 (1992).

[259] J. Solà; *Vacuum energy and cosmological evolution*, AIP Conf. Proc. **1606**, 19–37 (2014).

[260] J. S. Peracaula; *The cosmological constant problem and running vacuum in the expanding universe*, Phil. Trans. Roy. Soc. Lond. A **380**, 20210182 (2022).

[261] A. G. Riess et al.; *Type Ia supernova discoveries at $z > 1$ from the Hubble Space Telescope: evidence for past deceleration and constraints on dark energy evolution*, Astrophys. J. **607**, 665–687 (2004).

[262] P. Astier et al.; *The Supernova Legacy Survey: Measurement of Ω_M, Ω_Λ, and w from the first year data set*, Astron. Astrophys. **447**, 31–48 (2006).

[263] H. Feldman et al.; *An estimate of Ω_m without conventional priors*, Astrophys. J. **596**, L131–L134 (2003).

[264] D. N. Spergel et al. (WMAP Collaboration); *Three-Year Wilkinson Microwave Anisotropy Probe (WMAP) Observations: Implications for cosmology*, Astrophys. J. Suppl. Ser. **170**, 377–408 (2007).

[265] A. G. Sánchez et al.; *The clustering of galaxies in the SDSS–III Baryon Oscillation Spectroscopic Survey: cosmological implications of the large–scale two–point correlation function*, Mon. Not. R. Astron. Soc. **425**, 415–437 (2012).

[266] E. Komatsu et al. (WMAP Collaboration); *Five-Year Wilkinson Microwave Anisotropy Probe (WMAP) Observations: Cosmological Interpretation*, Astrophys. J. Suppl. Ser. **180**, 330–376 (2009).

[267] E. Komatsu et al. (WMAP Collaboration); *Seven-Year Wilkinson Microwave Anisotropy Probe (WMAP) Observations: Cosmological Interpretation*, Astrophys. J. Suppl. Ser. **192**, 18 (2011).

[268] S. Carneiro; *On the vacuum entropy and the cosmological constant*, Int. J. Mod. Phys. D **12**, 1669–1676 (2003).

[269] I. L. Shapiro and J. Solà; *Scaling behavior of the cosmological constant and the possible existence of new forces and new light degrees of freedom*, Phys. Lett. B **475**, 236–246 (2000).

[270] R. Schützhold; *Small cosmological constant from the QCD trace anomaly*, Phys. Rev. Lett. **89**, 081302 (2002).

[271] M. Szydłowski and A. Stachowski; *Cosmology with decaying cosmological constant–exact solutions and model testing*, J. Cosmol. Astropart. Phys. **2015**(10), 066 (2015).

[272] J. A. S. Lima, S. Basilakos, and J. Solà; *Expansion history with decaying vacuum: a complete cosmological scenario*, Mon. Not. R. Astron. Soc. **431**, 923–931 (2013).

[273] L. O. Pimentel; *Exact cosmological solutions in the scalar–tensor theory with cosmological constant*, Astrophys. Space Sci. **112**, 175–183 (1985).

[274] A. E. Montenegro Jr. and S. Carneiro; *Exact solutions of Brans–Dicke cosmology with decaying vacuum density*, Class. Quantum Gravity **24**, 313 (2007).

[275] C. P. Singh; *FRW models with particle creation in Brans–Dicke theory*, Astrophys. Space Sci. **338**, 411–419 (2012).

[276] P. Kumar and C. P. Singh; *New agegraphic dark energy model in Brans–Dicke theory with logarithmic form of scalar field*, Astrophys. Space Sci. **362**, 52 (2017).

[277] C. P. Singh and P. Kumar; *Holographic Dark Energy in Brans–Dicke Theory with Logarithmic Form of Scalar Field*, Int. J. Theor. Phys. **56**, 3297–3310 (2017).

[278] S. Ghaffari et al.; *Tsallis holographic dark energy in the Brans–Dicke cosmology*, Eur. Phys. J. C **78**, 706 (2018).

[279] P. Mukherjee and S. Chakrabarti; *Exact solutions and accelerating universe in modified Brans–Dicke theories*, Eur. Phys. J. C **79**, 681 (2019).

[280] J. de Cruz Pérez and J. Solà; *Brans–Dicke cosmology mimicking running vacuum*, Mod. Phys. Lett. A **33**, 1850228 (2018), arXiv:1809.03329.

[281] J. Solà, A. Gómez-Valent, J. de Cruz Pérez, and C. Moreno-Pulido; *Brans–Dicke cosmology with a Λ-term: a possible solution to ΛCDM tensions*, Class. Quantum Gravity **37**, 245003 (2020).

[282] S. Kaur and C. P. Singh; *Constraints on holographic dark energy model with matter creation in Brans–Dicke theory and thermodynamic analysis*, Phys. Dark Universe **33**, 100869 (2021).

[283] E. Karimkhani and A. Khodam-Mohammadi; *Hubble–rate–dependent dark energy in Brans–Dicke cosmology*, Astrophys. Space Sci. **364**, 177 (2019).

[284] M. Arik and M. C. Çalik; *Can Brans–Dicke scalar field account for dark energy and dark matter?*, Mod. Phys. Lett. A **21**, 1241–1248 (2006).

[285] M. Arik, M. C. Çalik, and M. B. Sheftel; *Friedmann equation for Brans–Dicke cosmology*, Int. J. Mod. Phys. D **17**, 225–235 (2008).

[286] N. Banerjee and D. Pavón; *A quintessence scalar field in Brans–Dicke theory*, Class. Quantum Grav. **18**, 593–601 (2001).

[287] V. B. Johri and D. Kalyani; *Cosmological models with constant deceleration parameter in Brans–Dicke theory*, Gen. Relativ. Gravit. **26**, 1217–1232 (1994).

[288] A. A. Sen, S. Sen, and S. Sethi; *Dissipative Fluid in Brans Dicke theory and late time acceleration*, Phys. Rev. D **63**, 107501 (2001).

[289] S. Sen and A. A. Sen; *Late-time acceleration in Brans–Dicke theory*, Phys. Rev. D **63**, 124006 (2001).

[290] M. Sharif and S. A. A. Shah; *A study of pilgrim dark energy model in Brans–Dicke theory*, Mod. Phys. Lett. A **34**(12), 1950083 (2019).

[291] Shri Ram and C. P. Singh; *Early universe in Brans–Dicke cosmology.*, Nuovo Cimento B **114(3)**, 245–251 (1999).

[292] L. Xu, Z. Liu, J. Lu, and W. Li; *Cosmic constraints on holographic dark energy in Brans–Dicke theory via Markov–Chain Monte–Carlo method*, Mod. Phys. Lett. A **25**, 1441–1454 (2010).

[293] K. Uehara and C. W. Kim; *Brans–Dicke cosmology with the cosmological constant*, Phys. Rev. D **26**, 2575 (1982).

[294] H. Kim; *Brans–Dicke theory as a unified model for dark matter and dark energy*, Mon. Not. R. Astron. Soc. **364**, 813–822 (2005).

[295] N. Banerjee and D. Pavón; *Holographic dark energy in Brans–Dicke theory*, Phys. Lett. B **647**, 477–481 (2007).

[296] A. Sheykhi; *Interacting agegraphic dark energy models in Brans–Dicke theory*, Phys. Rev. D **81**, 023525 (2010).

[297] F. A. Oliveira, F. E. M. Costa, and J. A. S. Lima; *Decaying vacuum cosmology and its scalar field description*, Class. Quantum Grav. **31**, 045004 (2014).

[298] J. Grande, J. Solà, and H. Štefančić; *ΛXCDM: A cosmon model solution to the cosmological coincidence problem?*, J. Cosmol. Astropart. Phys. **2006**(08), 011 (2006).

[299] D. Stern et al.; *Cosmic chronometers: constraining the equation of state of dark energy. I: $H(z)$ measurements*, J. Cosmol. Astropart. Phys. **2010**(02), 008 (2010).

[300] J.X. Li et al.; *Cosmological constraint on Brans–Dicke model*, Res. Astron. Astrophys. **15**, 2151–2162 (2015).

[301] J. Gómez-Gomar, J. Isern, and P. Jean; *Prospects for Type Ia supernova explosion mechanism identification with gamma-rays*, Mon. Not. R. Astron. Soc. **295**, 1–10 (1998).

[302] A. M. Khokhlov, E. Müller, and P. Höflich; *Light curves of Type Ia supernova models with different explosion mechanisms*, Astron. Astrophys. **270**, 223–248 (1993).

[303] O. Bertolami; *Time–dependent cosmological term*, Nuovo Cimento B **93**, 36–42 (1986).

[304] J. S. Alcaniz and J. M. F. Maia; *Current and future supernova constraints on decaying Λ cosmologies*, Phys. Rev. D **67**, 043502 (2003).

[305] J. D. Barrow and T. Clifton; *Cosmologies with energy exchange*, Phys. Rev. D **73**, 103520 (2006).

[306] A. Gómez–Valent and J. Solà; *Vacuum models with a linear and a quadratic term in H: structure formation and number counts analysis*, Mon. Not. R. Astron. Soc. **448**, 2810–2821 (2015).

[307] N. Banerjee and D. Pavón; *Cosmic acceleration without quintessence*, Phys. Rev. D **63**, 043504 (2001).

[308] L. O. Pimentel; *Exact cosmological solutions in the scalar–tensor theory with cosmological constant*, Astrophys. Space Sci. **112**, 175–183 (1985).

[309] L. Amendola, C. Quercellini, D. Tocchini–Valentini, and A. Pasqui; *Constraints on the interaction and self–interaction of dark energy from cosmic microwave background*, Astrophys. J. **583**, L53–L56 (2003).

[310] T. Clifton and J. D. Barrow; *Decaying gravity*, Phys. Rev. D **73**, 104022 (2006).

[311] G. Olivares, F. Atrio-Barandela, and D. Pavon; *Dynamics of interacting quintessence models: observational constraints*, Phys. Rev. D **77**, 063513 (2008).

[312] J. de Cruz Pérez and J. Solà; *Brans–Dicke cosmology mimicking running vacuum*, Mod. Phys. Lett. A **33**, 1850228 (2018), arXiv:1809.03329.

[313] I.L. Shapiro; *Effective Action of Vacuum: Semiclassical Approach*, Class. Quant. Gravity **25** 103005 (2008).

[314] J. M. Salim and I. Waga; *Thermodynamic constraints on a time–dependent Λ model*, Class. Quantum Gravity **10**, 1767–1774 (1993).

[315] R. C. Arcuri and I. Waga; *Growth of density inhomogeneities in Newtonian cosmological models with variable Λ*, Phys. Rev. D **50**, 2928–2931 (1994).

[316] A. I. Arbab; *Cosmological models with variable cosmological and gravitational constants and bulk viscous models*, Gen. Relativ. Gravit. **29**, 61–74 (1997).

[317] S. Basilakos, D. Polarski, and J. Solà; *Generalizing the running vacuum energy model and comparing with the entropic-force models*, Phys. Rev. D **86**, 043010 (2012).

[318] N. Padmanabhan et al.; *A 2% distance to* $z = 0.35$ *by reconstructing baryon acoustic oscillations — I. Methods and application to the Sloan Digital Sky Survey*, Mon. Not. R. Astron. Soc. **427**, 2132–2145 (2012).

[319] M. J. Reid, D. W. Pesce, and A. G. Riess; *An improved distance to NGC 4258 and its implications for the Hubble constant*, Astrophys. J. Lett. **886**, L27 (2019).

****

List of Publications

1. C.P. Singh, **Vinita Khatri**; *Viscous fluid dynamics with decaying vacuum energy density*, Physical Review D, American Physical Society, **109**, 023508 (2024). https://doi.org/10.1103/PhysRevD.109.023508 (**SCIE, Impact Factor: 5.3**).

2. **Vinita Khatri**, C.P. Singh, Milan Srivastava; *Exploring interacting bulk viscous model with decaying vacuum density*, Astronomy and Computing, Elsevier(Science Direct), **53**, 100992 (2025). https://doi.org/10.1016/j.ascom.2025.100992 (**SCIE, Impact Factor: 1.8**).

3. **Vinita Khatri**, C.P. Singh; *Interacting model of bulk viscous and decaying vacuum energy*, Physics Letters B, Elsevier(Science Direct), **871**, 139994 (2025). https://doi.org/10.1016/j.physletb.2025.139994 (**SCIE, Impact Factor: 4.5**).

4. **Vinita Khatri**, C.P. Singh; *Constraining the time-varying vacuum energy models in Brans-Dicke theory*, Astrophysics and Space Science, Springer, **368**, 16 (2023). https://doi.org/10.1007/s10509-023-04173-7 (**SCIE, Impact Factor: 1.5**).

5. **Vinita Khatri**, C.P. Singh; *Brans-Dicke cosmology with cosmological term* $\Lambda(H) = c_0 + 3\nu H^2$, Physics of the Dark Universe, Elsevier(Science Direct), **42**, 101300 (2023). https://doi.org/10.1016/j.dark.2023.101300 (**SCIE, Impact Factor: 6.4**).

Papers Presented in International Conferences

- Presented on **"Bulk viscous cosmology with decaying vacuum model"** in Cosmology@CCSP_1: An Inaugural Conference on Current Status of Cosmology, organized by The Thanu Padmananbhan Centre for Cosmology and Science Popularization (CCSP), SGT University, Gurugram, Delhi-NCR during October 17-19, 2022.

- Presented on **"Observational constrains on time-varying vacuum energy models in Brans-Dicke theory"** in the International Conference of The Mathematical Society-BHU on Recent Trends in Mathematical and Computational Sciences (RTMCS), organized by the DST-Centre for Interdisciplinary Mathematical Sciences, Institute of Science, Banaras Hindu University, Varanasi during February 3-5, 2023.

- Presented on **"Decaying vacuum energy models in Brans-Dicke theory"** in 2nd International Conference on Recent Advances in Mathematical Sciences and Interdisciplinary Areas (RAMSIA-2023), organized by Department of Mathematics, Institute of Applied Sciences and Humanities, GLA University, Mathura during June 22-24, 2023.

Viscous fluid dynamics with decaying vacuum energy density

C. P. Singh* and Vinita Khatri†

Department of Applied Mathematics, Delhi Technological University, Delhi-110042, India

(Received 26 September 2023; accepted 14 December 2023; published 5 January 2024)

In this work, we investigate the dynamics of bulk viscous models with decaying vacuum energy density (VED) in a spatially homogeneous and isotropic flat Friedmann-Lemaître-Robertson-Walker spacetime. We particularly are interested to study the viscous models which consider first-order deviation from equilibrium, i.e., the Eckart theory. In the first part, using the most general form of bulk viscous coefficient, we find the analytical solutions of main cosmological parameters, like Hubble parameter, scale factor, matter density, deceleration parameter, and equation of state parameter, and discuss the evolutions of the models accordingly. We also discuss the cosmological consequences of the evolutions and dynamics of three particular viscous models with decaying VED depending on the choices of bulk viscous coefficient. We examine the linear perturbation growth of the model to see if it survives this further level of scrutiny. The second part of the work is devoted to constrain one of the viscous models, viz., $\zeta \propto H$, where ζ is the bulk viscous coefficient and H is the Hubble parameter, using three different combinations of data from type Ia supernovae (Pantheon), $H(z)$ (cosmic chronometers), baryon acoustic oscillation, and $f(z)\sigma_8(z)$ measurements with the Markov chain Monte Carlo method. We show that the considered model is compatible with the cosmological probes and the ΛCDM recovered in late time of the evolution of the Universe. Finally, we obtain selection information criteria (Akaike information criteria and Bayesian information criteria) to study the stability of the models.

DOI: 10.1103/PhysRevD.109.023508

I. INTRODUCTION

Different observations such as luminosity distances of type Ia supernova, measurements of anisotropy of cosmic microwave background (CMB), and gravitational lensing have confirmed that our Universe is spatially flat and expanding with an accelerated rate. It has been observed that the Universe contains a mysterious dominant component, called dark energy (DE) with large negative pressure, which leads to this cosmic acceleration [1–7]. In the literature, several models have been proposed to explain the current accelerated expansion of the Universe. The two most accepted DE models are that of a cosmological constant and a slowly varying rolling scalar field (quintessence models) [8–11].

The cosmological constant Λ (CC for short), initially introduced by Einstein to get the static Universe, is a natural candidate for explaining DE phenomena with the equation of state parameter equal to −1. The natural interpretation of CC arises as an effect of quantum vacuum energy. Thus, the cold-dark-matter-based cosmology together with a CC, called ΛCDM cosmology, is preferred as the standard model for describing the current dynamics of the Universe. It is mostly consistent with the current cosmological observations. However, despite its success, the ΛCDM model has several strong problems due to its inability to renormalize the energy density of quantum vacuum, obtaining a discrepancy of ∼120 orders of magnitude between its predicted and observed value, the so-called CC or fine-tuning problem [12–14]. It also has the coincidence problem, i.e., why the Universe transition, from decelerated to an accelerated phase, is produced at late times [15].

Many models have been proposed to tackle these issues. One possible proposal is to incorporate energy transfer among the cosmic components. In this respect, the models with time-varying vacuum energy density (VED), also known as "decaying vacuum cosmology," seems to be promising. The idea of a time-varying VED model [$\rho_\Lambda = \Lambda(t)/8\pi G$] is physically more viable than the constant Λ [16–19]. Although no fundamental theory exists to describe a time-varying vacuum, a phenomenological technique has been suggested to parametrize $\Lambda(t)$. In the literature, many authors [20–41] have carried out analyses on decaying vacuum energy in which the time-varying vacuum has been phenomenologically modeled as a function of time in various possible ways, as a function of the Hubble parameter. Such attempts suggest that the decaying VED model provides the possibility of explaining the acceleration of the Universe as well as it solves both cosmological constant and coincidence problems.

*cpsingh@dce.ac.in
†vinitakhatri_2k20phdam501@dtu.ac.in

Shapiro and Solà [42], and Solà [43] proposed a possible connection between cosmology and quantum field theory on the basis of renormalization group (RG) which gives the idea of running vacuum models (RVMs), characterized by VED ρ_Λ; see Refs. [32,35,39] for a review. The RVM has been introduced to solve the coincidence problem where the term Λ is assumed to be varying with the Hubble parameter H. Carneiro *et al.* [27] proposed that the vacuum term is proportional to the Hubble parameter: $\Lambda(a) \propto H(a)$. However, this model fails to fit the current CMB data. It is interesting to note that RG in quantum field theory (QFT) provides a time-varying vacuum, in which $\Lambda(t)$ evolves as $\Lambda \propto H^2$ [44]. Basilakos [28] proposed a parametrization of the functional form of $\Lambda(t)$ by applying a power series expansion in H up to the second order. Recently, a large class of cosmologies has been discussed where VED evolves like a truncated power series in the Hubble parameter H; see Refs. [45,46], and references therein.

On the other hand, in recent years, the observations suggest that the Universe is permeated by dissipative fluids. Based on the thermodynamics point of view, phenomenological exotic fluids are supposed to play the role for an alternative DE models. It has been known since a long time ago that a dissipative fluid can produce acceleration during the expansion of the Universe [47,48]. The bulk and shear viscosity are the most relevant parts of dissipative fluid. The bulk viscosity characterizes a change in volume of the fluid which is relevant only for the compressed fluids. The shear viscosity characterizes a change in shape of a fixed volume of the fluid which represents the ability of particles to transport momentum. In general, shear viscosity is usually used in connection with the spacetime anisotropy, whereas bulk viscosity plays the role in isotropic cosmological models. The dynamics of homogeneous cosmological models has been studied in the presence of viscous fluid and has application in studying the evolution of the Universe.

Eckart [49] extended a classical irreversible thermodynamics from Newtonian to relativistic fluids. He proposed the simplest noncausal theory of relativistic dissipative phenomena of first order which was later modified by Landau and Lifshitz [50]. The Eckart theory has some important limitations. It has been found that all the equilibrium states are unstable [51] and the signals can propagate through the fluids faster than the speed of light [52]. Therefore, to resolve theses issues, Israel and Stewart [53] proposed a full causal theory of second order. When the relaxation time goes to zero, the causal theory reduces to Eckart's first-order theory. Thus, taking advantage of this limit of vanishing relaxation time at late time, it has been used widely to describe the recent accelerated expansion of the Universe. An exhaustive reviews on noncausal and causal theories of viscous fluids can be found in Refs. [54–67]. In recent years, direct observations indicate for a viscosity-dominated late epoch of accelerating expansion of the Universe. In this respect, many authors have explored the viability of a bulk viscous Universe to explain the present accelerated expansion of the Universe; cf. [68–89].

In Eckart theory, the effective pressure of the cosmic fluid is modeled as $\Pi = -3\zeta H$, where ζ is the bulk viscous coefficient and H the Hubble parameter. The bulk viscous coefficient can be assumed as a constant or function of the Hubble parameter. It allows one to explore the presence of interacting terms in the viscous fluid. Since the imperfect fluid should satisfy the equilibrium condition of thermodynamics, the pressure of the fluid must be greater than the one produced by the viscous term. To resolve this condition, it is useful to add an extra fluid such as cosmological constant. Many authors [90–94] have studied viscous cosmological models with constant or with time-dependent cosmological constant. Hu and Hu [93] have investigated a bulk viscous model with cosmological constant by assuming bulk viscous proportional to the Hubble parameter. Herrera-Zamorano, Hernández-Almada, and García-Aspeitia [94] have studied a cosmological model filled with two fluids under Eckart formalism, a perfect fluid as DE mimicking the dynamics of the CC, while a nonperfect fluid as dark matter with viscosity term.

In this paper, we focus on discussing the dynamics of a viscous Universe which consider the first-order deviation from equilibrium, i.e., Eckart formalism with decaying VED. Using different versions of bulk viscous coefficient ζ, we find analytically the main cosmological functions such as the scale factor, Hubble parameter, matter density, deceleration, and equation of state parameters. We discuss the effect of a viscous model with varying VED in perturbation level. We implement the perturbation equation to obtain the growth of matter fluctuations in order to study the contribution of this model in structure formation. We perform a Bayesian Markov chain Monte Carlo (MCMC) analysis to constrain the parameter spaces of the model using three different combinations involving observational data from type Ia supernovae (Pantheon), Hubble data (cosmic chronometers), baryon acoustic oscillations, and $f(z)\sigma_8(z)$ measurements. We compare our model and concordance ΛCDM to understand the effects of viscosity with decaying vacuum by plotting the evolutions of the deceleration parameter, equation of state parameter, and Hubble parameter. We also study the selection information criterion such as Akaike information criteria (AIC) and Bayesian information criteria (BIC) to analyze the stability of the model.

The work of the paper is organized as follows. In Sec. II, we present the basic cosmological equations of Friedmann-Lemaître-Robertson-Walker (FLRW) geometry with bulk viscosity and decaying VED. In Sec. III, we find the solution of the field equations by assuming the most general form of bulk viscous coefficient. Section IV is

devoted to study the evolutions of some particular forms of bulk viscous coefficient with varying VED. We discuss the growth rate equations that govern the perturbation in Sec. V. Section VI presents the observational data and method to be used to constrain the proposed model. The results and discussion on the evolution of the various parameters are presented in Sec. VII. In Sec. VIII, we present the selection information criterion to distinguish the presented model with concordance ΛCDM. Finally, we conclude our findings in Sec. IX.

II. VISCOUS MODEL WITH VARYING Λ

Let us start with the FLRW metric in the flat space geometry as the case favored by observational data:

$$ds^2 = -dt^2 + a^2(t)[dr^2 + r^2(d\theta^2 + \sin^2\theta d\phi^2)], \quad (1)$$

where (r, θ, ϕ) are the comoving coordinates and $a(t)$ is the scale factor of the Universe. The large-scale dynamics of (1) is described by the Einstein field equations, which include the cosmological constant Λ, and is given by

$$G_{\mu\nu} = R_{\mu\nu} - \frac{1}{2}g_{\mu\nu}R = 8\pi G(T_{\mu\nu} + g_{\mu\nu}\rho_\Lambda), \quad (2)$$

where $G_{\mu\nu}$ is the Einstein tensor, $\rho_\Lambda = \Lambda/8\pi G$ is the vacuum energy density (the energy density associated to the CC vacuum term), and $T_{\mu\nu}$ is the energy-momentum tensor of matter. It is to be noted that for simplicity we use geometrical units $8\pi G = c = 1$. We introduce a bulk viscous fluid through the energy-momentum tensor which is given by [95]

$$T_{\mu\nu} = (\rho_m + P)u_\mu u_\nu + g_{\mu\nu}P, \quad (3)$$

where u^μ is the fluid four-velocity, ρ_m is the density of matter, and P is the pressure which is composed of the barotropic pressure p_m of the matter fluid plus the viscous pressure Π, i.e., $P = p_m + \Pi$. The origin of bulk viscosity is assumed as a deviation of any system from the local thermodynamic equilibrium. According to the second law of thermodynamics, the reestablishment to thermal equilibrium is a dissipative processes which generates entropy. Because of generation of entropy, there is an expansion in the system through a bulk viscous term.

In homogeneous and isotropic cosmological models, the viscous fluid is characterized by a bulk viscosity. It is mostly based on Eckart's formalism [49], which can be obtained from the second-order theory of nonequilibrium thermodynamics proposed by Israel and Stewart [53] in the limit of vanishing relaxation time. The viscous effect can be defined by the viscous pressure $\Pi = -3\zeta H$, where ζ is the bulk viscous coefficient and H is the Hubble parameter. The bulk viscous coefficient ζ is assumed to be positive on thermodynamical grounds. Therefore, it makes the effective pressure as a negative value which leads to modification in the energy-momentum tensor of perfect fluid.

If we denote the total energy-momentum tensor $T_{\mu\nu} + g_{\mu\nu}\rho_\Lambda$ as modified $\tilde{T}_{\mu\nu}$ on the right-hand side of field equations (2), then the modified $\tilde{T}_{\mu\nu}$ can be assumed the same form as $T_{\mu\nu}$; that is, $\tilde{T}_{\mu\nu} = (\rho + p)u_\mu u_\nu + g_{\mu\nu}p$, where $\rho = \rho_m + \rho_\Lambda$ and $p = p_m - 3\zeta H + p_\Lambda$ are the total energy density and pressure, respectively. Furthermore, we assume that the bulk viscous fluid is the nonrelativistic matter with $p_m = 0$. Thus, the contribution to the total pressure is due to only the sum of negative viscous pressure $-3\zeta H$ and vacuum energy pressure $p_\Lambda = -\rho_\Lambda$.

Using the modified energy-momentum tensor as discussed above, the Einstein field equations (2) describing the evolution of the FLRW Universe dominated by bulk viscous matter and vacuum energy yield

$$3H^2 = \rho = \rho_m + \rho_\Lambda, \quad (4)$$

$$2\dot{H} + 3H^2 = -p = 3\zeta H + \rho_\Lambda, \quad (5)$$

where $H = \dot{a}/a$ is the Hubble parameter and an overdot represents the derivative with respect to cosmic time t. In this paper, we propose the evolution of the Universe based on decaying vacuum models, i.e., vacuum energy density as a function of the cosmic time. From (2), the Bianchi identity $\nabla^\mu G_{\mu\nu} = 0$ gives

$$\nabla^\mu \tilde{T}_{\mu\nu} = 0 \quad (6)$$

or, equivalently,

$$\dot{\rho}_m + 3H(\rho_m + p_m - 3\zeta H + \rho_\Lambda + p_\Lambda) = -\dot{\rho}_\Lambda, \quad (7)$$

which imply that there is a coupling between a dynamical Λ term and viscous CDM. Therefore, there is some energy exchange between the viscous CDM fluid and vacuum. Using the equation of state of the vacuum energy $p_\Lambda = -\rho_\Lambda$ and $p_m = 0$, Eq. (7) leads to

$$\dot{\rho}_m + 3H(\rho_m - 3\zeta H) = -\dot{\rho}_\Lambda. \quad (8)$$

Now, combining (4) and (8), we get

$$\dot{H} + \frac{3}{2}H^2 = \frac{1}{2}\rho_\Lambda + \frac{3}{2}\zeta H. \quad (9)$$

The evolution equation (9) has three independent unknown quantities, namely, H, ζ, and ρ_Λ. We get the solution only if ζ and ρ_Λ are specified. In what follows, we discuss the dynamics of the Universe depending on the specific forms of ρ_Λ and ζ.

III. SOLUTION OF FIELD EQUATIONS

In this paper, we parametrize the functional form of ρ_Λ as a function of the Hubble parameter. The motivation for a function $\rho_\Lambda = \rho_\Lambda(H)$ can be assumed from different points of view. Although the correct functional form of ρ_Λ is not known, a QFT approach within the context of the RG was proposed in Refs. [96,97] and further studied by many authors [29,32,35,43,98,99]. In Ref. [36], the following ratio has been defined between the two fluid components:

$$\gamma = \frac{\rho_\Lambda - \rho_{\Lambda_0}}{\rho_m + \rho_\Lambda}, \tag{10}$$

where ρ_{Λ_0} is a constant vacuum density. If $\rho_\Lambda = \rho_{\Lambda_0}$, then $\gamma = 0$, and we get the ΛCDM model. On the other hand, if $\rho_{\Lambda_0} \neq 0$, then we get

$$\rho_\Lambda = \rho_{\Lambda 0} + \gamma(\rho_m + \rho_\Lambda) = \rho_{\Lambda 0} + 3\gamma H^2. \tag{11}$$

The above proposal was first considered by Shapiro and Solà [42] in the context of RG. Many authors have studied the evolution of the Universe by assuming this form [33,34,41]. Hereafter, we shall focus on the simplest form of ρ_Λ which evolves with the Hubble rate. Specifically, in this paper, we consider

$$\rho_\Lambda = c_0 + 3\nu H^2, \tag{12}$$

where $c_0 = 3H_0^2(\Omega_{\Lambda 0} - \nu)$ is fixed by the boundary condition $\rho_\Lambda(H_0) = \rho_{\Lambda 0}$. The suffix "0" denotes the present value of the parameter. The dimensionless coefficient ν is the vacuum parameter and is expected to be very small value $|\nu| \ll 1$. A nonzero value of it makes possible the cosmic evolution of the vacuum.

The choice of ζ generates different viscous models, and in the literature there are different approaches to assume the evolution of bulk viscosity. In this paper, we consider the most general form of the bulk viscous term ζ, which is assumed to be the sum of three terms: The first term is a constant, ζ_0, the second term is proportional to the Hubble parameter $H = \dot{a}/a$, which is related to the expansion, and the third term is proportional to the acceleration, $\ddot{a}/\dot{a}$. Thus, we assume the parametrization of bulk viscous coefficient in the form [67,72,73,79,82,100,101]

$$\zeta = \zeta_0 + \zeta_1 \frac{\dot{a}}{a} + \zeta_2 \frac{\ddot{a}}{\dot{a}}, \tag{13}$$

where ζ_0, ζ_1, and ζ_2 are constants to be determined by the observations. The term $\ddot{a}/\dot{a}$ in Eq. (13) can be written as $\ddot{a}/aH$. The basic idea about the assumption of ζ in Eq. (13) is that the dynamic state of the fluid influences its viscosity in which the transport viscosity is related to the velocity and acceleration.

Using Eqs. (12) and (13), the differential equation for the Hubble parameter (9) finally reduces to

$$\left(1 - \frac{3}{2}\zeta_2\right)\dot{H} + \frac{3}{2}(1 - \zeta_1 - \zeta_2 - \nu)H^2 - \frac{3}{2}\zeta_0 H - \frac{1}{2}c_0 = 0, \tag{14}$$

which on integration gives

$$H = \frac{\zeta_0}{2(1 - \zeta_1 - \zeta_2 - \nu)} + \sigma\left(\frac{1 + e^{-3(1-\zeta_1-\zeta_2-\nu)\sigma t}}{1 - e^{-3(1-\zeta_1-\zeta_2-\nu)\sigma t}}\right), \tag{15}$$

where $\sigma = \sqrt{\left(\frac{\zeta_0}{2(1-\zeta_1-\zeta_2-\nu)}\right)^2 + \frac{H_0^2(\Omega_{\Lambda 0}-\nu)}{(1-\zeta_1-\zeta_2-\nu)}}$.

The above equation simplifies to give

$$H = \frac{\zeta_0}{2(1 - \zeta_1 - \zeta_2 - \nu)} + \sigma \coth\left(\frac{3}{2}\frac{(1 - \zeta_1 - \zeta_2 - \nu)\sigma}{(1 - \frac{3}{2}\zeta_2)}t\right). \tag{16}$$

Using the Hubble parameter $H = \dot{a}/a$, the scale factor of the model $a(t)$ with the condition $a(t_0) = 1$ is given by

$$a = e^{\frac{\zeta_0}{2(1-\zeta_1-\zeta_2-\nu)}t}\left[\sinh\left(\frac{3}{2}\frac{(1 - \zeta_1 - \zeta_2 - \nu)\sigma}{(1 - \frac{3}{2}\zeta_2)}t\right)\right]^{\frac{2(1-\frac{3}{2}\zeta_2)}{3(1-\zeta_1-\zeta_2-\nu)}}, \tag{17}$$

which shows that the scale factor increases exponentially as t increases. From (17), one can observe that, in general, it is not possible to express cosmic time t in terms of the scale factor a. It is possible only if the viscous coefficient terms are zero. In the absence of bulk viscosity, we obtain the result of decaying vacuum model as discussed in Ref. [29]. Furthermore, for constant Λ, the solution reduced to the ΛCDM model with no viscosity.

It is worthwhile to compute the evolution of matter energy density as a function of scale factor (or redshift) or function of cosmic time. Using (12) and (13), the continuity equation (8) takes the form

$$\dot{\rho_m} + 3(1-\nu)H\rho_m = 9(1-\nu)\left(\zeta_0 + \zeta_1\frac{\dot{a}}{a} + \zeta_2\frac{\ddot{a}}{\dot{a}}\right)H^2. \tag{18}$$

The solution of the above equation involves a big expression. Therefore, we avoid writing the expression for matter density. However, we present the numerical solution of this equation for different combinations of viscous and ν terms in Fig. 1. It is observed that the matter energy density decreases as t increases, and it approaches to the finite value as $t \to \infty$. However, in the absence of viscous terms, $\rho_m \to 0$ as $t \to \infty$.

To discuss the decelerated and accelerated phases and its transition during the evolution of the Universe, we study a

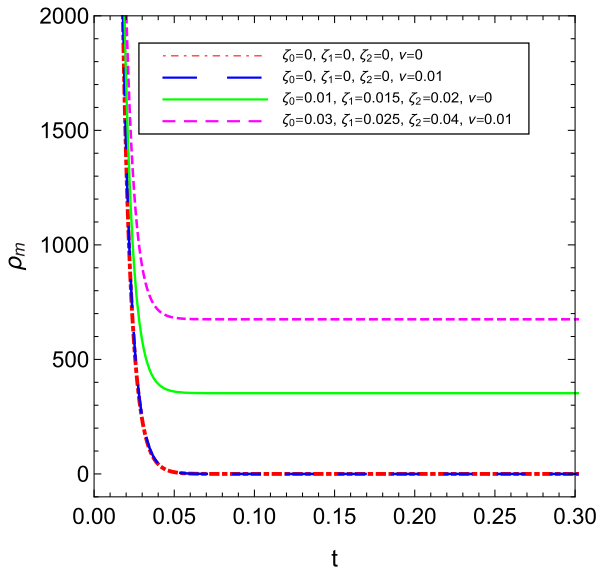

FIG. 1. The matter energy density as a function of cosmic time t for decaying vacuum with $\zeta = \zeta_0 + \zeta_1 \frac{\dot{a}}{a} + \zeta_2 \frac{\ddot{a}}{\dot{a}}$.

cosmological parameter, known as "deceleration parameter," q, which is defined as

$$q = -\frac{\ddot{a}}{a}\frac{1}{H^2} = -\left(1 + \frac{\dot{H}}{H^2}\right). \tag{19}$$

Using (16), the deceleration parameter is calculated as

$$q = -1 + \frac{3}{2}\frac{\frac{(1-\zeta_1-\zeta_2-\nu)}{(1-\frac{3}{2}\zeta_2)}\sigma^2 \csc^2 h\left(\frac{3}{2}\frac{(1-\zeta_1-\zeta_2-\nu)}{(1-\frac{3}{2}\zeta_2)}\sigma t\right)}{\left(\frac{\zeta_0}{2(1-\zeta_1-\zeta_2-\nu)} + \sigma \coth\left(\frac{3}{2}\frac{(1-\zeta_1-\zeta_2-\nu)}{(1-\frac{3}{2}\zeta_2)}\sigma t\right)\right)^2}. \tag{20}$$

From (20), we observe that the model transits from decelerated phase to accelerated phase. As t increases, the deceleration parameter decreases, and as $t \to \infty$, it approaches to $q = -1$. The rate of deceleration parameter attaining to -1 depends on the viscous terms.

For sake of completeness, we discuss another important cosmological parameter, known as effective equation of state (EOS) parameter, which is defined as

$$w_{\text{eff}} = -1 - \frac{2}{3}\frac{\dot{H}}{H^2}. \tag{21}$$

Using (16), Eq. (21) gives

$$w_{\text{eff}} = -1 + \frac{\frac{(1-\zeta_1-\zeta_2-\nu)}{(1-\frac{3}{2}\zeta_2)}\sigma^2 \csc^2 h\left(\frac{3}{2}\frac{(1-\zeta_1-\zeta_2-\nu)}{(1-\frac{3}{2}\zeta_2)}\sigma t\right)}{\left(\frac{\zeta_0}{2(1-\zeta_1-\zeta_2-\nu)} + \sigma \coth\left(\frac{3}{2}\frac{(1-\zeta_1-\zeta_2-\nu)}{(1-\frac{3}{2}\zeta_2)}\sigma t\right)\right)^2}. \tag{22}$$

It can be observed that the effective EOS parameter decreases to negative values and finally saturated to $w_{\text{eff}} = -1$ corresponding to a de Sitter epoch in future time of evolution.

IV. SOME PARTICULAR SOLUTIONS

In order to calculate specific expressions for cosmological parameters of the viscous model with decaying vacuum energy, let us analyze three particular popular proposals depending on the choice of ζ defined in Eq. (13).

A. Case I: $\zeta = \zeta_0 = \text{const}$

This is the simplest parametrization of Eckart's bulk viscosity model. Many authors [70,71,78,85,88,89,92,102–104] have studied the viscous cosmological models with a constant bulk viscous coefficient. In this case, the evolution equation (14) reduces to

$$\dot{H} + \frac{3}{2}(1-\nu)H^2 - \frac{3}{2}\zeta_0 H = \frac{1}{2}c_0. \tag{23}$$

Solving (23) or directly taking $\zeta_1 = \zeta_2 = 0$ in (16), for $\nu < 1$, we get

$$H = \frac{\zeta_0}{2(1-\nu)} + \sigma_1 \coth\left(\frac{3}{2}(1-\nu)\sigma_1 t\right), \tag{24}$$

where $\sigma_1 = \sqrt{\left(\frac{\zeta_0}{2(1-\nu)}\right)^2 + \frac{H_0^2(\Omega_{\Lambda 0}-\nu)}{(1-\nu)}}$. It can be observed that the solution reduces to the standard Λ for $\zeta_0 = 0$ and $\nu = 0$, whereas for $\zeta_0 = 0$ and $\nu \neq 0$ it gives the solution for the $\Lambda(t)$ model from quantum field theory [29]. The scale factor is given by

$$a(t) = e^{\frac{\zeta_0}{2(1-\nu)}t}\left(\sinh\left(\frac{3}{2}(1-\nu)\sigma_1 t\right)\right)^{\frac{2}{3(1-\nu)}}, \tag{25}$$

which shows that the scale factor increases exponentially as t increases. From (25), one can observe that, in general, it is not possible to express cosmic time t in terms of the scale factor a. It is possible only if $\zeta_0 = 0$. In the absence of bulk viscosity, we obtain the result of decaying vacuum model as discussed in Ref. [29]. Furthermore, for constant Λ, the solution reduced to the ΛCDM model with no viscosity.

The deceleration parameter and effective EOS parameter are, respectively, given by

$$q = -1 + \frac{3}{2}\frac{(1-\nu)\sigma_1^2 \csc^2 h\left(\frac{3}{2}(1-\nu)\sigma_1 t\right)}{\left(\frac{\zeta_0}{2(1-\nu)} + \sigma_1 \coth\left(\frac{3}{2}(1-\nu)\sigma_1 t\right)\right)^2} \tag{26}$$

and

$$w_{\text{eff}} = -1 + \frac{(1-\nu)\sigma_1^2 \csc^2 h\left(\frac{3}{2}(1-\nu)\sigma_1 t\right)}{\left(\frac{\zeta_0}{2(1-\nu)} + \sigma_1 \coth\left(\frac{3}{2}(1-\nu)\sigma_1 t\right)\right)^2}. \tag{27}$$

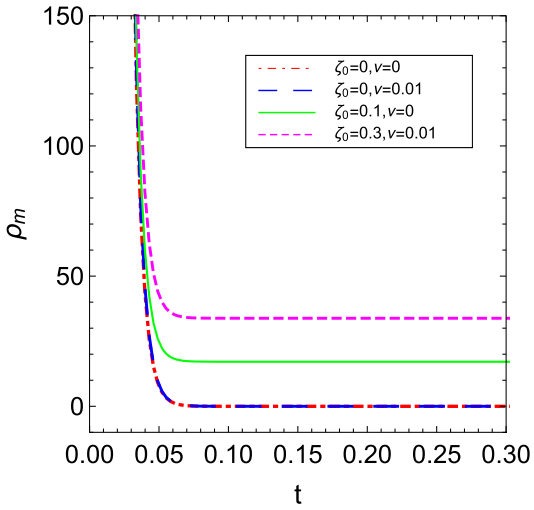

FIG. 2. The time evolution of matter energy density for the decaying vacuum model with viscosity $\zeta = \zeta_0$.

The time evolutions of q and w_{eff} are similar to the evolutions of these parameters as discussed for the general form of viscous term in Sec. III.

The continuity equation (18) in this case has the form

$$\dot{\rho_m} + 3(1-\nu)H\rho_m = 9(1-\nu)\zeta_0 H^2. \tag{28}$$

Solving (28), one may find the time evolution of the matter density. We will present only a numerical solution of this equation. In Fig. 2, we plot the time evolution of matter energy density $\rho_m(t)$ for different combinations of ζ_0 and ν. This figure shows that the matter density diverges at the beginning of cosmic evolution, decreases as t increases, and finally approaches to a finite value as $t \to \infty$ for $\zeta \neq 0$ and $\nu \neq 0$. In the absence of viscosity or decaying vacuum energy, the matter energy density tends to zero as $t \to \infty$.

B. Case II: $\zeta = \zeta_0 + \zeta_1 H$

We assume that the bulk viscous coefficient is a linear combination of two terms: ζ_0 and $\zeta_1 H$, i.e., $\zeta = \zeta_0 + \zeta_1 H$. In the literature, many authors [73,79,80] have assumed such a form of ζ to study the dynamics of Universe. In this case, Eq. (14) reduces to

$$\dot{H} + \frac{3}{2}(1-\zeta_1-\nu)H^2 - \frac{3}{2}\zeta_0 H = \frac{1}{2}c_0. \tag{29}$$

Solving Eq. (29) or directly putting $\zeta_2 = 0$ in Eq. (16), the solution for the Hubble parameter for $(\zeta_1+\nu) < 1$ is given by

$$H = \frac{\zeta_0}{2(1-\zeta_1-\nu)} + \sigma_2 \coth\left(\frac{3}{2}(1-\zeta_1-\nu)\sigma_2 t\right), \tag{30}$$

where $\sigma_2 = \sqrt{\left(\frac{\zeta_0}{2(1-\zeta_1-\nu)}\right)^2 + \frac{H_0^2(\Omega_{\Lambda 0}-\nu)}{(1-\zeta_1-\nu)}}$. The corresponding expression for the scale factor in normalized unit has the form

$$a = e^{\frac{\zeta_0}{2(1-\zeta_1-\nu)}t}\left[\sinh\left(\frac{3}{2}(1-\zeta_1-\nu)\sigma_2 t\right)\right]^{\frac{2}{3(1-\zeta_1-\nu)}}. \tag{31}$$

The respective deceleration parameter and effective EOS parameter are calculated as

$$q = -1 + \frac{3(1-\zeta_1-\nu)\sigma_2^2 \operatorname{csc}^2 h\left(\frac{3}{2}(1-\zeta_1-\nu)\sigma_2 t\right)}{2\left(\frac{\zeta_0}{2(1-\zeta_1-\nu)} + \sigma_2 \coth\left(\frac{3}{2}(1-\zeta_1-\nu)\sigma_2 t\right)\right)^2} \tag{32}$$

and

$$w_{\text{eff}} = -1 + \frac{(1-\zeta_1-\nu)\sigma_2^2 \operatorname{csc}^2 h\left(\frac{3}{2}(1-\zeta_1-\nu)\sigma_2 t\right)}{\left(\frac{\zeta_0}{2(1-\zeta_1-\nu)} + \sigma_2 \coth\left(\frac{3}{2}(1-\zeta_1-\nu)\sigma_2 t\right)\right)^2}. \tag{33}$$

The time evolutions of q and w_{eff} are similar to the evolutions of these parameters as discussed for the general form of the viscous term in Sec. III.

The continuity equation (18) in this case has the form

$$\dot{\rho_m} + 3(1-\nu)H\rho_m = 9(1-\nu)(\zeta_0 H^2 + \zeta_1 H^3). \tag{34}$$

We present only a numerical solution of Eq. (34). In Fig. 3, we plot the time-dependent matter energy density $\rho_m(t)$ for different combinations of ζ_0, ζ_1, and ν. It is observed from the figure that the matter density diverges at the beginning of cosmic evolution, decreases as time passes, and finally approaches to a finite value as $t \to \infty$ for $\zeta \neq 0, \zeta_1 \neq 0$, and

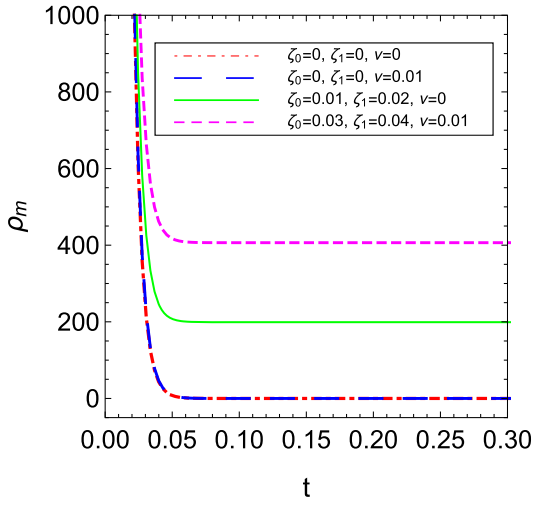

FIG. 3. The time evolution of matter energy density for the decaying vacuum model with viscosity $\zeta = \zeta_0 + \zeta_1 H$.

$\nu \neq 0$. In the absence of viscous terms or decaying vacuum energy, the matter energy density tends to zero as $t \to \infty$.

C. Case III: $\zeta = \zeta_1 H$

Finally, let us consider the case where the bulk viscous coefficient is proportional to the Hubble parameter, i.e., $\zeta = \zeta_1 H$. Such a form of ζ has been studied by many authors [54,60,73,81,105,106]. In this case, the evolution equation (14) for Hubble parameter reduces to

$$\dot{H} + \frac{3}{2}(1 - \zeta_1 - \nu)H^2 - \frac{1}{2}c_0 = 0. \tag{35}$$

The above equation with change of a variable from t to $x = \ln a$ can be written as

$$\frac{dh^2}{dx} + 3(1 - \zeta_1 - \nu)h^2 = 3(\Omega_{\Lambda 0} - \nu), \tag{36}$$

where $h = H/H_0$ is the dimensionless Hubble parameter and $\Omega_{\Lambda 0} = \rho_{\Lambda 0}/3H_0^2$. Assuming $(\zeta_1 + \nu) < 1$ and using the normalized scale factor–redshift relation $a = (1+z)^{-1}$, we can express the normalized Hubble function $E(z) \equiv H(z)/H_0$ as

$$E(z) = \frac{1}{(1-\zeta_1-\nu)^{1/2}} \times [(1-\zeta_1-\Omega_{\Lambda 0})(1+z)^{3(1-\zeta_1-\nu)} + \Omega_{\Lambda 0} - \nu]^{1/2}. \tag{37}$$

From the above equation, it is clear that, for $\nu = 0$ and $\zeta_1 = 0$, we recover exactly the ΛCDM expansion model, whereas only $\zeta_1 = 0$ gives the solution obtained in Ref. [41]. It is observed that at very late time we get a cosmological-constant-dominated era, $H \approx H_0\sqrt{\frac{\Omega_{\Lambda 0}-\nu}{(1-\zeta_1-\nu)}}$, which implies a de Sitter phase of the scale factor. Using $H = \dot{a}/a$, the solution for the scale factor in terms of cosmic time t is given by

$$a = \left(\frac{(1-\zeta_1-\Omega_{\Lambda 0})}{\Omega_{\Lambda 0}-\nu}\right)^{\frac{1}{3(1-\zeta_1-\nu)}} \times \left[\sinh\left(\frac{3}{2}\sqrt{(1-\zeta_1-\nu)(\Omega_{\Lambda 0}-\nu)}H_0 t\right)\right]^{\frac{2}{3(1-\zeta_1-\nu)}}. \tag{38}$$

It can be observed that the scale factor evolves as power-law expansion, i.e., $a \propto t^{2/3(1-\zeta_1-\nu)}$, for small values of t, whereas it expands exponentially, i.e., $a \propto \exp\sqrt{\frac{(\Omega_{\Lambda 0}-\nu)}{3(1-\zeta_1-\nu)}}H_0 t$, for large values of time t. In other words, the model expands with decelerated rate in early time of its evolution and expands with accelerated rate in late time of its evolution.

From Eq. (38), we can find the cosmic time in terms of the scale factor, which is given by

$$t(a) = \frac{2}{3H_0\sqrt{(1-\zeta_1-\nu)(\Omega_{\Lambda 0}-\nu)}}\sinh^{-1}\left[\left(\frac{a}{a_I}\right)^{\frac{3(1-\zeta_1-\nu)}{2}}\right], \tag{39}$$

where $a_I = \left(\frac{(1-\zeta_1-\Omega_{\Lambda 0})}{(\Omega_{\Lambda 0}-\nu)}\right)^{1/3(1-\zeta_1-\nu)}$.

Using (37), the value of q in terms of redshift is calculated as

$$q(z) = -1 + \frac{3}{2}\frac{(1-\zeta_1-\Omega_{\Lambda 0})(1+z)^{3(1-\zeta_1-\nu)}}{\left[\frac{(\Omega_{\Lambda 0}-\nu)}{(1-\zeta_1-\nu)} + (1-\frac{(\Omega_{\Lambda 0}-\nu)}{(1-\zeta_1-\nu)})(1+z)^{3(1-\zeta_1-\nu)}\right]}. \tag{40}$$

The above equation shows that the dynamics of q depends on the redshift which describes the transition of the Universe from decelerated to accelerated phase. We observe that, as $z \to -1$, $q(z)$ approaches to -1. However, the model decelerates or accelerates if $\Omega_{\Lambda 0} = \nu$, which gives $q = -1 + 1.5(1-\zeta_1-\nu)$. Thus, a cosmological constant is required for a transition phase. Also, for $z = 0$, we find the present value of q which is given by

$$q_0 = -1 + 1.5(1 - \zeta_1 - \Omega_{\Lambda 0}). \tag{41}$$

The transition redshift $z_{\rm tr}$ of the Universe, which is defined as a zero point of the deceleration parameter, $q = 0$, can be calculated as

$$z_{\rm tr} = -1 + \left(\frac{2(\Omega_{\Lambda 0}-\nu)}{(3(1-\zeta_1-\nu)-2)(1-\zeta_1-\Omega_{\Lambda 0})}\right)^{\frac{1}{3(1-\zeta_1-\nu)}}. \tag{42}$$

In this case, the effective EOS parameter is defined by $w_{\rm eff} = -1 - \frac{1}{3}\frac{d\ln h^2}{dx}$, where $x = \ln a$ and $h = H/H_0$. Using Eq. (37), we get

$$w_{\rm eff}(z) = -1 + \frac{(1-\zeta_1-\Omega_{\Lambda 0})(1+z)^{3(1-\zeta_1-\nu)}}{\left[\frac{(\Omega_{\Lambda 0}-\nu)}{(1-\zeta_1-\nu)} + (1-\frac{(\Omega_{\Lambda 0}-\nu)}{(1-\zeta_1-\nu)})(1+z)^{3(1-\zeta_1-\nu)}\right]}. \tag{43}$$

The present value of $w_{\rm eff}$ at $z = 0$ is given by

$$w_{\rm eff}(z=0) = -1 + (1 - \zeta_1 - \Omega_{\Lambda 0}). \tag{44}$$

We can observe that the model will accelerate provided $3w_{\rm eff}(z=0) + 1 = -2 + 3(1-\zeta_1-\Omega_{\Lambda 0}) < 0$.

Let us discuss the behavior of the matter energy density in this model as a function of scale factor (or redshift). Transforming the time derivative into derivative with

respect to the scale factor, the conservation equation (18) reduces to a differential equation for matter density:

$$\frac{d\rho_m}{da}+\frac{3(1-\nu)}{a}\rho_m=\frac{9(1-\nu)\zeta_1}{a}H^2. \tag{45}$$

Using (37) into (45) and integrating, we find

$$\rho_m=\left(\rho_{m0}-\frac{3\zeta_1H_0^2(\Omega_{\Lambda0}-\nu)}{(1-\zeta_1-\nu)}\right)a^{-3(1-\zeta_1-\nu)}+\frac{3\zeta_1H_0^2(\Omega_{\Lambda0}-\nu)}{(1-\zeta_1-\nu)}, \tag{46}$$

where $\rho_{m0}=\rho_m(a=1)$ is the present matter density. Substituting Eq. (38) in the above equation, one may obtain the explicit time evolution of the matter density if desired. It can be observed from Eq. (46) that the matter density no longer evolves as $\rho_m=\rho_{m0}\,a^{-3}$. There is a correction in the exponent of the scale factor and some additional constant terms. This is due to the fact that matter is exchanging energy from vacuum and viscous term. We also note that, as $t\to\infty$, $\rho_m=3\zeta_1H_0^2(\Omega_{\Lambda0}-\nu)/(1-\zeta_1-\nu)$; i.e., matter density does not approach zero in infinitely far future due to viscosity. In the absence of a viscous term, the matter density tends to zero as $t\to\infty$. The detailed discussion on the evolutions of matter energy density and other cosmological parameters of this particular model is presented in Sec. VII.

In the following section, we constrain the parameters of this model by using the latest observational datasets and analyze the evolutions of all above discussed various cosmological parameters using the best-fit values. We compare the proposed model with the existing model through the stability criteria.

V. GROWTH OF PERTURBATIONS

In cosmic structure formation, it is assumed that the present abundant structure of the Universe was developed through gravitational amplification of small density perturbations generated in its early evolution. In this section, we briefly discuss the linear perturbation within the framework of viscous fluid with varying $\Lambda(t)$. We refer the reader to Refs. [107,108] for the detailed perturbation equations, since here we have discussed some basic equations only. The differential equation for the matter density contrast $\delta_m\equiv\delta\rho_m/\rho_m$ for our model considered here can be approximated as follows [109]:

$$\delta_m''+\left(\frac{3}{a}+\frac{H'(a)}{H(a)}\right)\delta_m'-\frac{4\pi G\rho_m}{H^2(a)}\frac{\delta_m}{a^2}=0, \tag{47}$$

where prime represents derivative with respect to the scale factor a. The above second-order differential equation turns out to be accurate, since the main effects come from the different expression of the Hubble function. We consider the Hubble function as obtained in case III in Sec. IV. Equation (47) describes the smoothness of the matter perturbation in the extended viscous $\Lambda(t)$ model.

The linear growth rate of the density contrast, f, which is related to the peculiar velocity in the linear theory [110], is defined as

$$f(a)=\frac{d\ln D_m(a)}{d\ln a}, \tag{48}$$

where $D_m(a)=\delta_m(a)/\delta_m(a=1)$ is the linear growth function. The weighted linear growth rate, denoted by $f\sigma_8$, is the product of the growth rate $f(z)$, defined in (48), and $\sigma_8(z)$. Here, σ_8 is the root-mean-square fluctuation in spheres with radius $8h^{-1}$ Mpc scales [111,112], and it is given by [113]

$$\sigma_8(z)=\frac{\delta_m(z)}{\delta_m(z=0)}\sigma_8(z=0). \tag{49}$$

Using (48) and (49), the weighted linear growth rate is given by

$$f\sigma_8(z)=-(1+z)\frac{\sigma_8(z=0)}{\delta_m(z=0)}\frac{d\delta_m}{dz}. \tag{50}$$

In what follows, we perform the observational analysis of case III in Sec. IV to estimate the parameters of the model and analyse the evolution and dynamics of the model in detail.

VI. DATA AND METHODOLOGY

In this section, we present the data and methodology used in this work. We constrain the parameters of the GR-ΛCDM and $\zeta=\zeta_1H$ with varying Λ models using a large, robust, and latest set of observational data which involve observations from (i) distant type Ia supernovae (SNe Ia); (ii) a compilation of cosmic chronometer measurements of Hubble parameter $H(z)$ at different redshifts; (iii) baryonic acoustic oscillations (BAO); and (iv) $f(z)\sigma_8(z)$ data. A brief description of each dataset follows.

A. Pantheon SNe Ia sample

The most known and frequently used cosmological probe are distant type Ia supernovae (SNe Ia) which are used to understand the actual evolution of the Universe. A supernova explosion is an extremely luminous event, with its brightness being comparable with the brightness of its host galaxy [114]. We use the recent SNe Ia data points, the so-called Pantheon sample which includes 1048 data points of luminosity distance in the redshift range $0.01<z<2.26$. Specifically, one could use the observed distance

modulo $\mu_{\rm obs}$ to constrain cosmological models. The Chi-squared function for SNe Ia is given by

$$\chi^2_{\rm SNe\,Ia} = \sum_{i=1}^{1048} \Delta\mu^T C^{-1} \Delta\mu, \tag{51}$$

where $\Delta\mu = \mu_{\rm obs} - \mu_{th}$. Here, $\mu_{\rm obs}$ is the observational distance modulus of SNe Ia and is given as $\mu_{\rm obs} = m_B - \mathcal{M}$, where m_B is the observed peak magnitude in the rest frame of the B band and $\mathcal{M}$ is the absolute B-band magnitude of a fiducial SNe Ia, which is taken as -19.38. The theoretical distance modulus $\mu_{\rm th}$ is defined by

$$\mu_{\rm th}(z, \mathbf{p}) = 5\log_{10}\left(\frac{D_L(z_{\rm hel}, z_{\rm cmb})}{1\ {\rm M\,pc}}\right) + 25, \tag{52}$$

where $\mathbf{p}$ is the parameter space and D_L is the luminosity distance, which is given as $D_L(z_{\rm hel}, z_{\rm cmb}) = (1 + z_{\rm hel}) r(z_{\rm cmb})$. Here, $r(z_{\rm cmb})$ is given by

$$r(z) = cH_0^{-1} \int_0^z \frac{dz'}{E(z', \mathbf{p})}, \tag{53}$$

where c is the speed of light, $E(z) \equiv H(z)/H_0$ is the dimensionless Hubble parameter, and $z_{\rm hel}$ and $z_{\rm cmb}$ are heliocentric and CMB frame redshifts, respectively. Here, C is the total covariance matrix which takes the form $C = D_{\rm stat} + C_{\rm sys}$, where the diagonal matrix $D_{\rm stat}$ and covariant matrix $C_{\rm sys}$ denote the statistical uncertainties and the systematic uncertainties, respectively.

B. BAO measurements

In this work, we have used six points of BAO datasets from several surveys, which includes the Six Degree Field Galaxy Survey (6dFGS), the Sloan Digital Sky Survey (SDSS), and the LOWZ samples of the Baryon Oscillation Spectroscopic Survey (BOSS) [115–117].

The dilation scale $D_v(z)$ introduced in [118] is given by

$$D_v(z) = \left(\frac{d_A^2(z) z}{H(z)}\right)^{1/3}. \tag{54}$$

Here, $d_A(z)$ is the comoving angular diameter distance and is defined as

$$d_A(z) = \int_0^z \frac{dy}{H(y)'}. \tag{55}$$

Now, the corresponding Chi-squared function for the BAO analysis is given by

$$\chi^2_{\rm BAO} = A^T C^{-1}_{\rm BAO} A, \tag{56}$$

where A depends on the considered survey and $C^{-1}_{\rm BAO}$ is the inverse of the covariance matrix [117].

C. $H(z)$ data

The cosmic chronometer (CC) data, which are determined by using the most massive and passively evolving galaxies based on the "galaxy differential age" method, are model independent (see Ref. [119] for detail). In our analysis, we use 32 CC data points of the Hubble parameter measured by differential age technique [119] between the redshift range $0.07 \le z \le 1.965$. The Chi-squared function for $H(z)$ is given by

$$\chi^2_{H(z)} = \sum_{i=1}^{32} \frac{[H(z_i, \mathbf{p}) - H_{\rm obs}(z_i)]^2}{\sigma^2_{H(z_i)}}, \tag{57}$$

where $H(z_i, \mathbf{p})$ represents the theoretical values of Hubble parameter with model parameters, $H_{\rm obs}(z_i)$ is the observed values of Hubble parameter, and σ_i represents the standard deviation measurement uncertainty in $H_{\rm obs}(z_i)$.

D. $f(z)\sigma_8(z)$ data

In Sec. IV, we have mainly discussed the background evolution of the growth perturbations and defined the weighted linear growth rate by Eq. (50). To make a more complete discussion on the viscous $\Lambda(t)$ model in perturbation evolution, we focus on an observable quantity of $f(z)\sigma_8(z)$. We use 18 data points of "Gold-17" compilation of robust and independent measurements of weighted linear growth $f(z)\sigma_8(z)$ obtained by various galaxy surveys as compiled in Table III in Ref. [120]. In order to compare the observational dataset with that predicted by our model, we define the Chi-square function as

$$\chi^2_{(f\sigma_8)} = \sum_{i=1}^{18} \frac{[f\sigma_8^{\rm the}(z_i, \mathbf{p}) - f\sigma_8^{\rm obs}(z_i)]^2}{\sigma^2_{f\sigma_8(z_i)}}, \tag{58}$$

where $f\sigma_8^{\rm the}(z_i, \mathbf{p})$ is the theoretical value computed by Eq. (50) and $f\sigma_8^{\rm obs}(z_i)$ is the observed data [120].

Using the observational data as discussed above, we use the MCMC method by employing the EMCEE PYTHON package [121] to explore the parameter spaces of viscous model with decaying vacuum density as discussed in Sec. III by utilizing different combinations of datasets. The combinations are as follows:

(i) BASE: The combination of two datasets SNeIa + BAO is termed as "BASE," whose joint χ^2 function is defined as $\chi^2_{\rm tot} = \chi^2_{\rm SNe\,Ia} + \chi^2_{\rm BAO}$.
(ii) +CC: We combine CC data to the BASE, where $\chi^2_{\rm tot} = \chi^2_{\rm SNe\,Ia} + \chi^2_{\rm BAO} + \chi^2_{H(z)}$.
(iii) $+f\sigma_8(z)$: The BASE data are complemented with CC and $f\sigma_8$, where $\chi^2_{\rm tot} = \chi^2_{\rm SNe\,Ia} + \chi^2_{\rm BAO} + \chi^2_{H(z)} + \chi^2_{f\sigma_8}$.

We consider the ΛCDM model as a reference model, and its parameters are also constrained with the above sets of data.

TABLE I. Constraints on parameters of ΛCDM for different set of observation data. Here, BASE denotes "SNe Ia + BAO."

ΛCDM			
Parameter	BASE	+CC	$+f\sigma_8$
H_0	$68.987^{+0.263}_{-0.276}$	$69.001^{+0.238}_{-0.223}$	$68.793^{+0.193}_{-0.221}$
Ω_Λ	$0.701^{+0.013}_{-0.020}$	$0.699^{+0.016}_{-0.015}$	$0.684^{+0.015}_{-0.014}$
σ_8			$0.794^{+0.014}_{-0.015}$
S_8			$0.811^{+0.022}_{-0.022}$
z_{tr}	$0.670^{+0.038}_{-0.038}$	$0.674^{+0.035}_{-0.035}$	$0.625^{+0.041}_{-0.041}$
q_0	$-0.549^{+0.020}_{-0.023}$	$-0.551^{+0.020}_{-0.020}$	$-0.523^{+0.025}_{-0.025}$
w_0	$-0.699^{+0.013}_{-0.015}$	$-0.701^{+0.013}_{-0.013}$	$-0.682^{+0.017}_{-0.017}$
t_0 (Gyr)	$13.73^{+0.017}_{-0.017}$	$13.69^{+0.015}_{-0.015}$	$13.54^{+0.013}_{-0.013}$

TABLE II. Constraints on parameters of the viscous $\Lambda(t)$ model using different sets of observation data.

Viscous Λ(t)			
Parameter	BASE	+CC	$+f\sigma_8$
H_0	$68.843^{+0.274}_{-0.238}$	$68.913^{+0.262}_{-0.261}$	$68.684^{+0.259}_{-0.241}$
Ω_Λ	$0.680^{+0.018}_{-0.020}$	$0.684^{+0.013}_{-0.020}$	$0.674^{+0.012}_{-0.016}$
ζ_1	$0.006^{+0.007}_{-0.004}$	$0.006^{+0.008}_{-0.004}$	$0.003^{+0.005}_{-0.002}$
ν	$0.004^{+0.003}_{-0.003}$	$0.003^{+0.004}_{-0.002}$	$0.003^{+0.004}_{-0.002}$
σ_8			$0.790^{+0.008}_{-0.010}$
S_8			$0.822^{+0.019}_{-0.019}$
z_{tr}	$0.664^{+0.031}_{-0.042}$	$0.665^{+0.031}_{-0.037}$	$0.626^{+0.028}_{-0.038}$
q_0	$-0.533^{+0.025}_{-0.020}$	$-0.535^{+0.023}_{-0.020}$	$-0.516^{+0.022}_{-0.017}$
w_0	$-0.689^{+0.017}_{-0.013}$	$-0.690^{+0.015}_{-0.013}$	$-0.677^{+0.014}_{-0.011}$
t_0 (Gyr)	$13.52^{+0.019}_{-0.019}$	$13.48^{+0.017}_{-0.017}$	$13.47^{+0.013}_{-0.015}$

VII. RESULTS AND DISCUSSION

In this section, we present the main results obtained through the observational data on the viscous $\Lambda(t)$ model of the form $\zeta = \zeta_1 H$ with $\Lambda = c_0 + 3\nu H^2$ (refer to case III in Sec. IV). We also present the cosmological observation forthe ΛCDM model using the three combination of datasets. The viscous $\Lambda(t)$ model has four free parameter spaces $\{H_0, \Omega_\Lambda, \zeta_1, \nu\}$, whereas ΛCDM has two free parameters $\{H_0, \Omega_\Lambda\}$. We calculate the best-fit values by minimizing the combination of χ^2 function for the above defined datasets. We also provide the fitting values of the ΛCDM for comparison with the viscous $\Lambda(t)$ model. The constraints of the statistical study are presented in Tables I and II. Figures 4–6 show the $1\sigma(68.3\%)$ and $2\sigma(95.4\%)$ confidence level (CL) contours with marginalized likelihood distributions for the cosmological parameters of ΛCDM and viscous $\Lambda(t)$ models considering combination of different datasets, respectively. It is observed from Tables I and II that the constraints on the parameter spaces of ΛCDM and viscous with $\Lambda(t)$ are nearly the same.

Using best-fit values of parameters obtained from BASE, +CC, and $+f\sigma_8$ data into Eq. (40), the evolutions of the deceleration parameter with respect to the redshift are shown in Figs. 7–9 for the viscous $\Lambda(t)$ model along with the ΛCDM model. It is observed that with each dataset $q(z)$ varies from positive to negative and shows the similar trajectory that is comparable to the ΛCDM model. Thus, both the models depict a transition from the early decelerated phase to the late-time accelerated phase. Furthermore, $q(z)$ approaches to -1 in late time of evolution. Thus, the models successfully generate late-time cosmic acceleration along with a decelerated expansion in the past. Figures 7–9 show that the transition from decelerated to accelerated phase take place at redshift $z_{\rm tr} = 0.664^{+0.031}_{-0.042}$ with BASE data, $z_{\rm tr} = 0.665^{+0.031}_{-0.037}$ with +CC data, and $z_{\rm tr} = 0.626^{+0.028}_{-0.037}$ with $+f\sigma_8$ data. The datasets BASE, +CC, and $+f\sigma_8$ yield the present deceleration parameter q_0 as $-0.533^{+0.025}_{-0.020}$, $-0.535^{+0.023}_{-0.020}$, and $-0.516^{+0.022}_{-0.017}$, respectively (cf. Table II). The present values of z_{tr} and q_0 are very close and, thus, are in good agreement to ΛCDM as presented in Table I.

The evolutions of the Hubble parameter $H(z)$ of viscous $\Lambda(t)$ model with respect to the redshift are shown in Figs. 10–12. Throughout the expansion, viscous $\Lambda(t)$ is

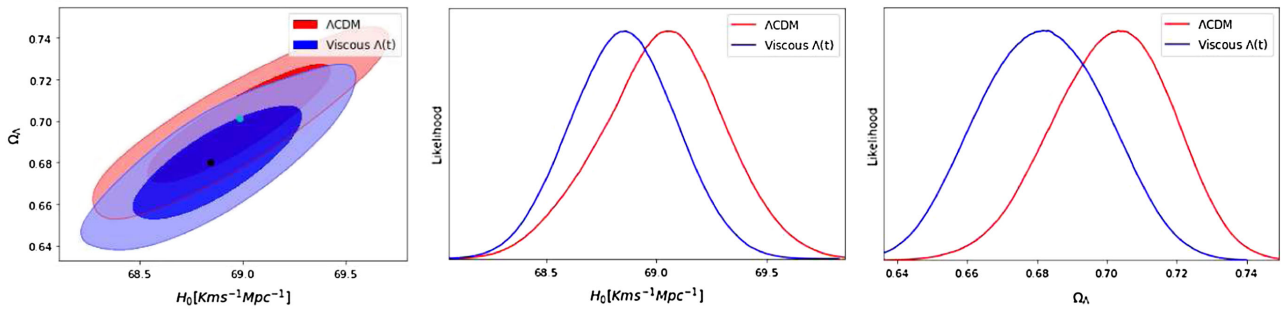

FIG. 4. Two-dimensional confidence contours of the $H_0 - \Omega_\Lambda$ and one-dimensional posterior distributions of H_0 and Ω_Λ for the ΛCDM and viscous $\Lambda(t)$ models using "BASE" data. The green and black dot on the contour represent the best-fit value of ΛCDM and viscous $\Lambda(t)$ models, respectively.

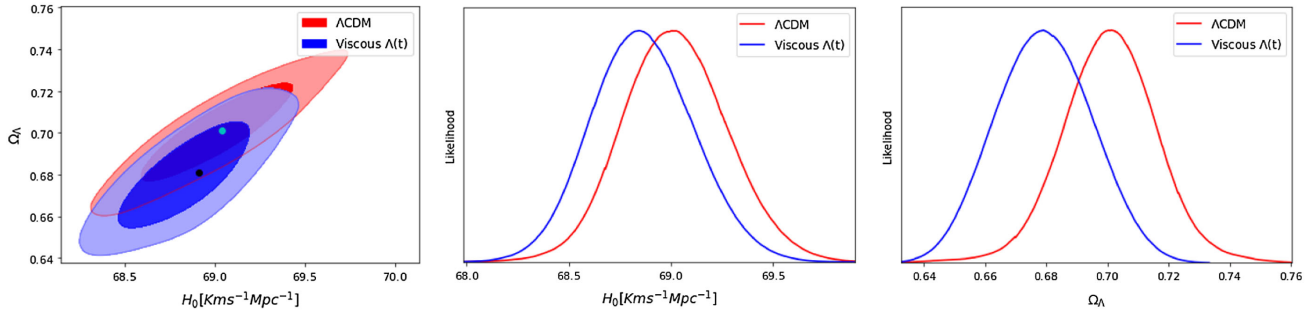

FIG. 5. Two-dimensional confidence contours of the $H_0 - \Omega_\Lambda$ and one-dimensional posterior distributions of H_0 and Ω_Λ for the ΛCDM and viscous $\Lambda(t)$ models using "+CC" data. The green and black dot on the contour represent the best-fit value of ΛCDM and viscous $\Lambda(t)$ models, respectively.

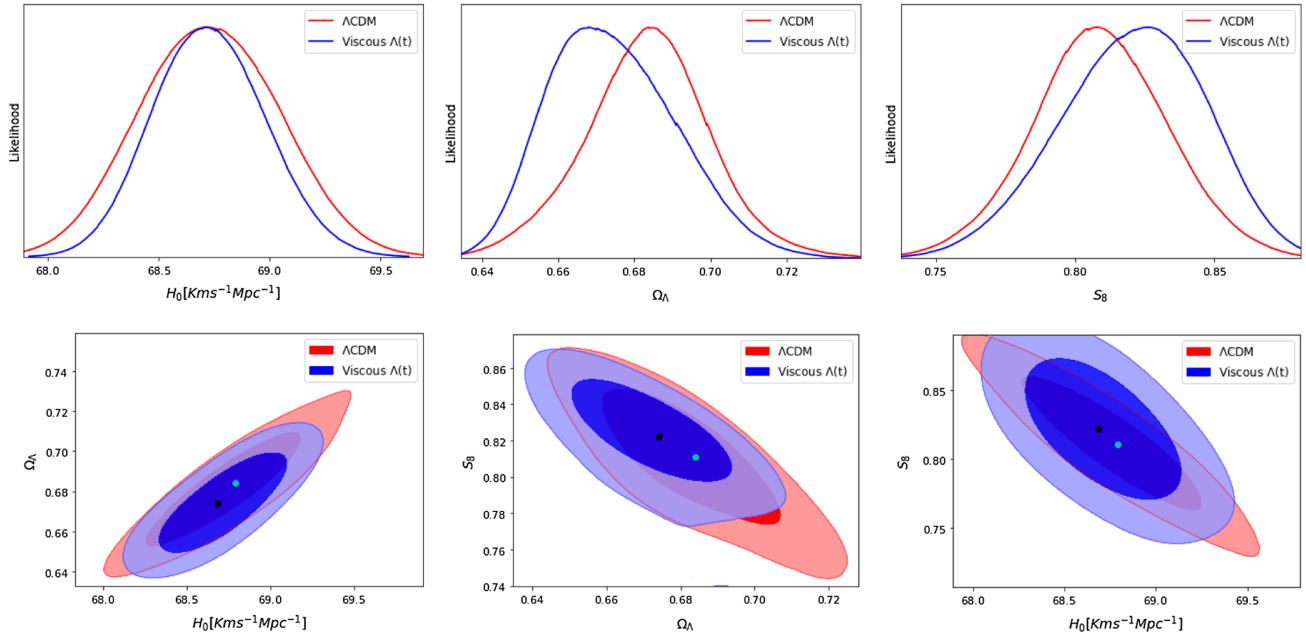

FIG. 6. Two-dimensional confidence contours of $H_0 - \Omega_\Lambda$, $\Omega_\Lambda - S_8$, and $H_0 - S_8$ and one-dimensional posterior distributions of H_0, Ω_Λ, and S_8 for the ΛCDM and viscous $\Lambda(t)$ models using "$+f\sigma_8$" data. The green and black dot on the contour represent the best-fit value of ΛCDM and viscous $\Lambda(t)$ models, respectively.

coinciding with the ΛCDM model and the model paths cover the majority of the dataset with the error bar of Hubble parameter, indicating that the viscous $\Lambda(t)$ agrees well with the ΛCDM model for all three combinations of datasets. In the considered cosmological scenario, the present age of the Universe is found to be $t_0 \approx 13.52$ Gyr, $t_0 \approx 13.48$ Gyr, and $t_0 \approx 13.47$ Gyr, respectively, as presented in Table II. The ages thus obtained are very much compatible with that obtained from the ΛCDM model with the same datasets (cf. Table I).

Using the best-fit values of parameters in Eq. (43), the evolutions of the effective EOS parameter $w_{\rm eff}$ are shown in Figs. 13–15. We conclude that, for large redshifts, $w_{\rm eff}$ has small negative value $w_{\rm eff} > -1/3$, and in the future the model asymptotically approaches to $w_{\rm eff} = -1$. The trajectory of $w_{\rm eff}$ for BASE and +CC datasets coincides with the evolution of the ΛCDM model. However, it slightly varies with the best-fit values obtained through $+f\sigma_8(z)$ data points. It can be observed that the viscous $\Lambda(t)$ model behaves like a quintessence in early time and cosmological constant in late time. The present values of $w_{\rm eff}$ are found to be $-0.689^{+0.017}_{-0.013}$, $-0.690^{+0.015}_{-0.013}$, and $-0.677^{+0.014}_{-0.011}$ with BASE, +CC, and $+f\sigma_8$ datasets, respectively, which are very close to the current value of the ΛCDM model as presented in Table I.

From Tables I and II, let us discuss the present value H_0 of Hubble parameter in the case of viscous $\Lambda(t)$ and ΛCDM models. The viscous $\Lambda(t)$ model gives $H_0 = 68.843^{+0.274}_{-0.238}$ km/s/Mpc with BASE data, the +CC data give $H_0 = 68.913^{+0.262}_{-0.261}$ km/s/Mpc, and, finally, the $+f\sigma_8$

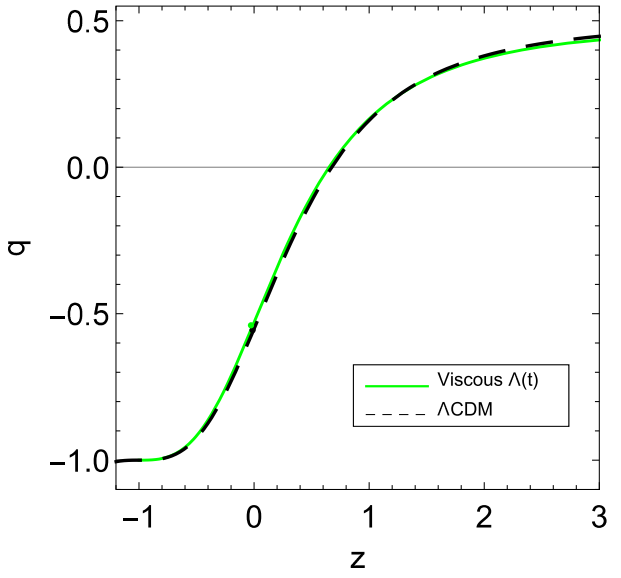

FIG. 7. The redshift evolution of the deceleration parameter for viscous $\Lambda(t)$ using BASE dataset. The evolution of deceleration parameter in the standard ΛCDM model is also shown as the dashed curve. A dot denotes the current value of q (hence q_0).

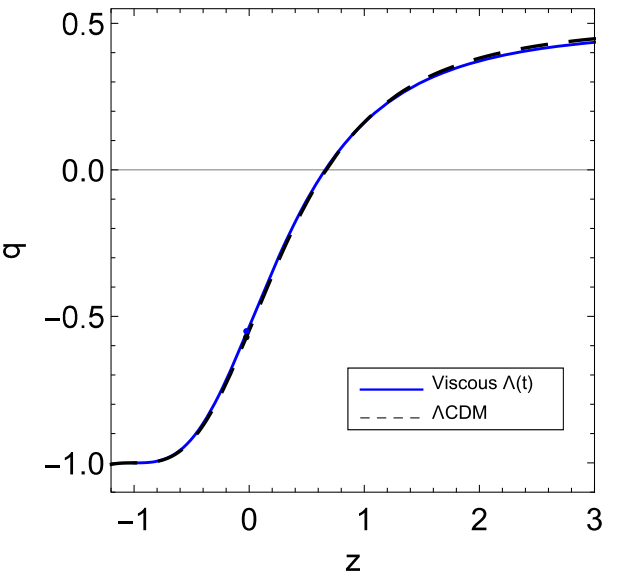

FIG. 8. The redshift evolution of the deceleration parameter for viscous $\Lambda(t)$ using +CC dataset. The evolution of deceleration parameter in the standard ΛCDM model is also shown as the dashed curve. A dot denotes the current value of q (hence q_0).

renders the present value: $H_0 = 68.684^{+0.259}_{-0.241}$ km/s/Mpc. Recently, the local measurement $H_0 = 73.04 \pm 1.04$ km/s/Mpc from Riess *et al.* [122] exhibits a strong tension with the Planck 2018 release $H_0 = 67.4 \pm 0.5$ km/s/Mpc [7] at the 4.89σ confidence level. The residual tensions of our fitting results with respect to the

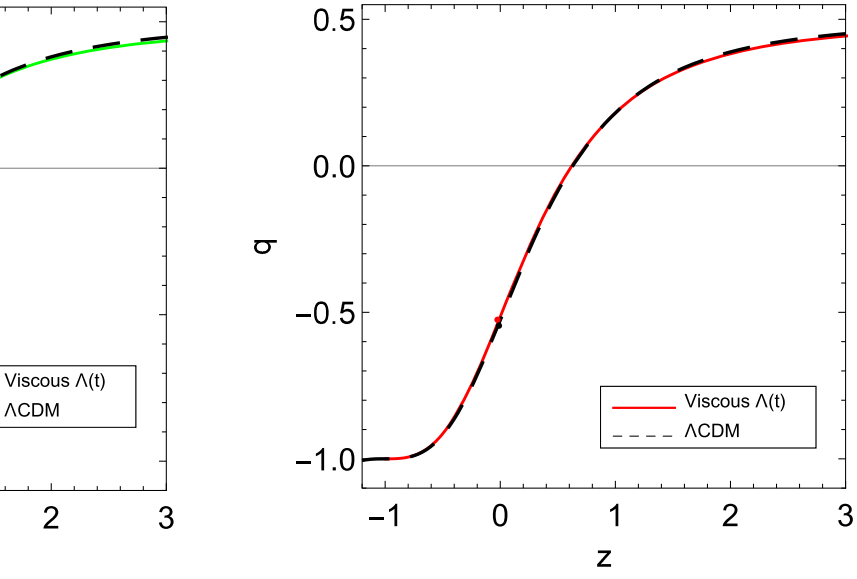

FIG. 9. The redshift evolution of the deceleration parameter for viscous $\Lambda(t)$ using $+f\sigma_8$ dataset. The evolution of deceleration parameter in the standard ΛCDM model is also shown as the dashed curve. A dot denotes the current value of q (hence q_0).

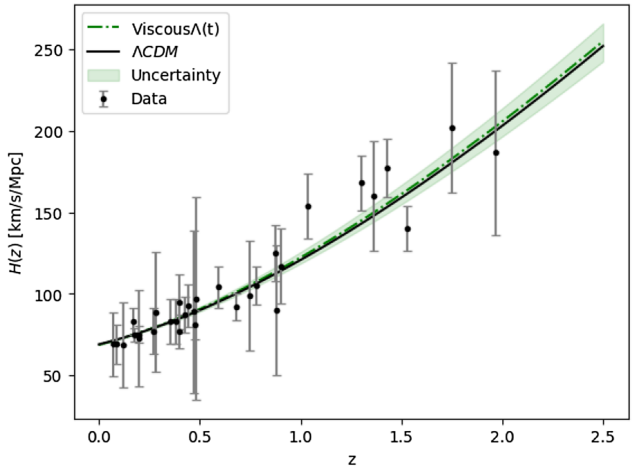

FIG. 10. Best fits using BASE dataset over $H(z)$ data for viscous $\Lambda(t)$ (green dot-dashed line) and ΛCDM (black solid line) are shown. The gray points with uncertainty bars correspond to the 32 CC sample.

latest local measurement $H_0 = 73.04 \pm 1.04$ km/s/Mpc [122] are 3.92σ, 3.85σ, and 4.07σ, respectively.

Let us focus on σ_8 and S_8, which play a very relevant role in structure formation. The best-fit values of these parameters for ΛCDM and viscous $\Lambda(t)$ models using BASE + CC + $f\sigma_8$ data are reported in Tables I and II, respectively. We can read off $\sigma_8 = 0.794^{+0.014}_{-0.015}$ for the ΛCDM model (cf. Table I), whereas the viscous $\Lambda(t)$ model prediction is $\sigma_8 = 0.790^{+0.008}_{-0.010}$ (cf. Table II). This is a very good result, which can be rephrased in terms of the fitting value of the

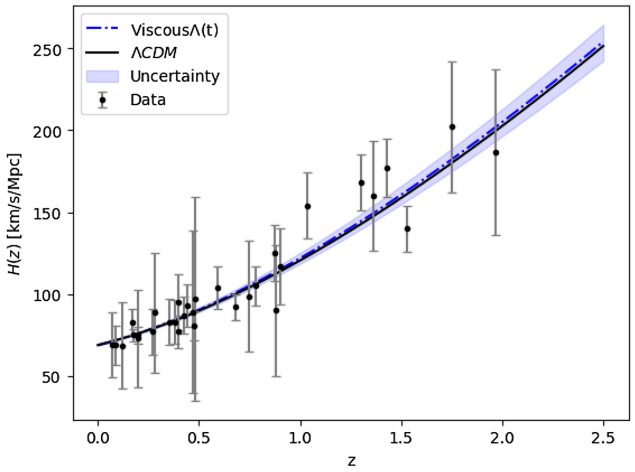

FIG. 11. Best fits using +CC dataset over $H(z)$ data for viscous $\Lambda(t)$ (blue dot-dashed line) and ΛCDM (black solid line) are shown. The gray points with uncertainty bars correspond to the 32 CC sample.

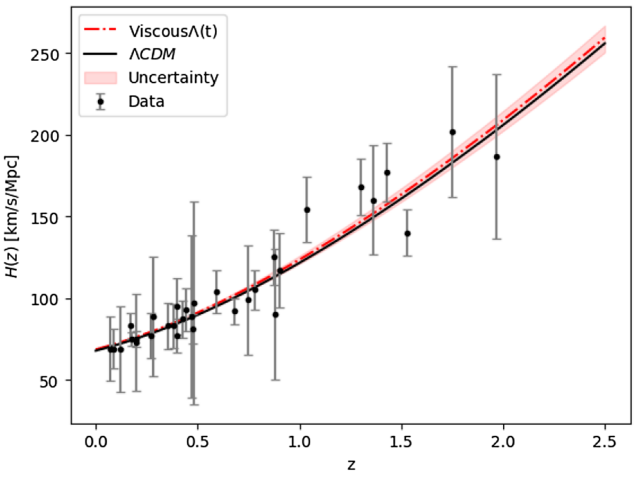

FIG. 12. Best fits using $+f\sigma_8$ dataset over $H(z)$ data for viscous $\Lambda(t)$ (red dot-dashed line) and ΛCDM (black solid line) are shown. The gray points with uncertainty bars correspond to the 32 CC sample.

related LSS observable $S_8 = \sigma_8\sqrt{(1-\Omega_\Lambda)/0.3}$ quoted in Tables I and II: $S_8 = 0.811 \pm 0.022$ for ΛCDM and $S_8 = 0.822 \pm 0.019$ for the viscous $\Lambda(t)$ model. The values of σ_8 and S_8 for the viscous $\Lambda(t)$ model are compatible for 1σ confidence level with ΛCDM. Our result predicts that the tensions in σ_8 and S_8 are reduced to 0.23σ and -0.38σ, respectively. The behavior of $f(z)\sigma_8(z)$ as a function of redshift is plotted in Fig. 17. We can see that the evolution of $f\sigma_8$ for both viscous $\Lambda(t)$ and ΛCDM models is consistent with the observational data points.

Table III presents the χ^2 and reduced χ^2 of ΛCDM and viscous $\Lambda(t)$ models, respectively, for the used datasets. To compute reduced χ^2, denoted as $\chi^2_{\rm red}$, we use

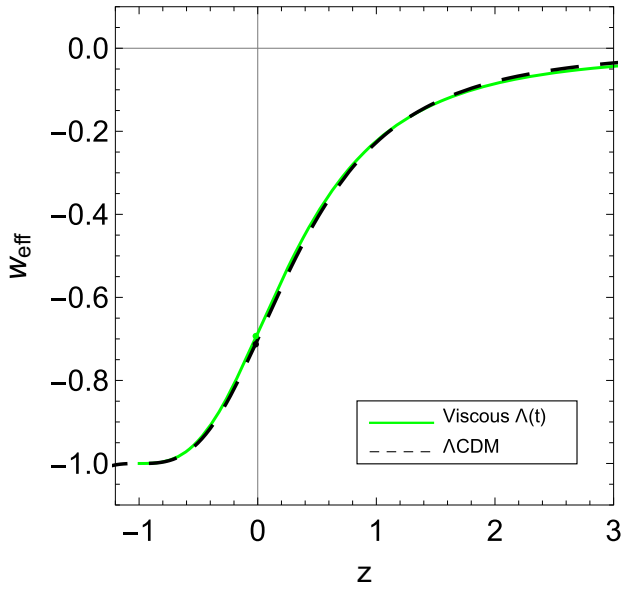

FIG. 13. Effective EOS parameter as a function of redshift z for viscous $\Lambda(t)$ using BASE dataset. The evolution of EOS parameter in the standard ΛCDM model is also represented as the dashed curve. A dot denotes the present value of the EOS parameter.

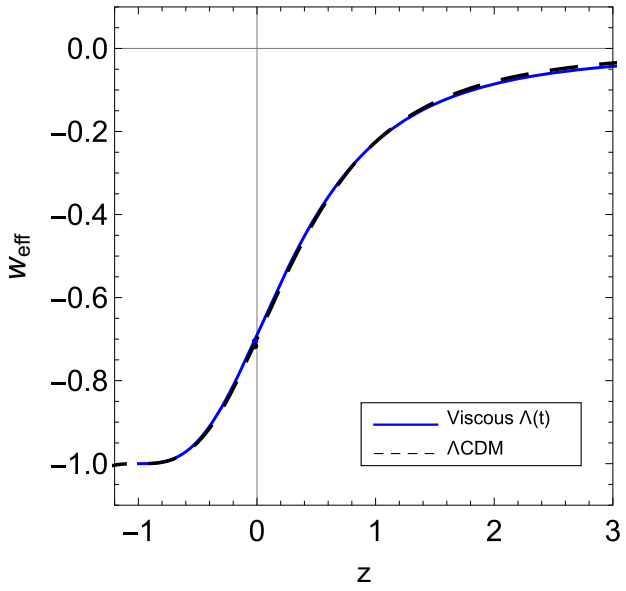

FIG. 14. Effective EOS parameter as a function of redshift z for viscous $\Lambda(t)$ using +CC dataset. The evolution of EOS parameter in the standard ΛCDM model is also represented as the dashed curve. A dot denotes the present value of the EOS parameter.

$\chi^2_{\rm red} = \chi^2_{\rm min}/(N-d)$, where N is the total number of data points and d is the total number of fitted parameters, which differs for the various models. It should be noted that, when a model is fitted to data, a value of $\chi^2_{\rm red} < 1$ is regarded as the best fit, whereas a value of $\chi^2_{\rm red} > 1$ is regarded as a poor

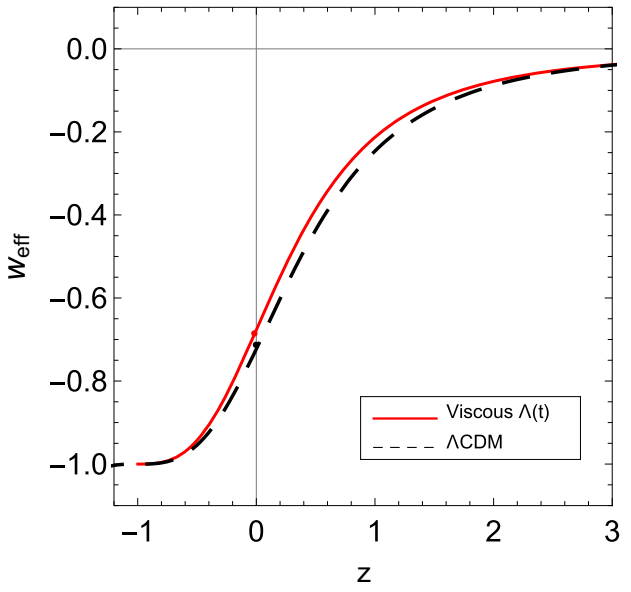

FIG. 15. Effective EOS parameter as a function of redshift z for viscous $\Lambda(t)$ using $+f\sigma_8$ dataset. The evolution of EOS parameter in the standard ΛCDM model is also represented as the dashed curve. A dot denotes the present value of the EOS parameter.

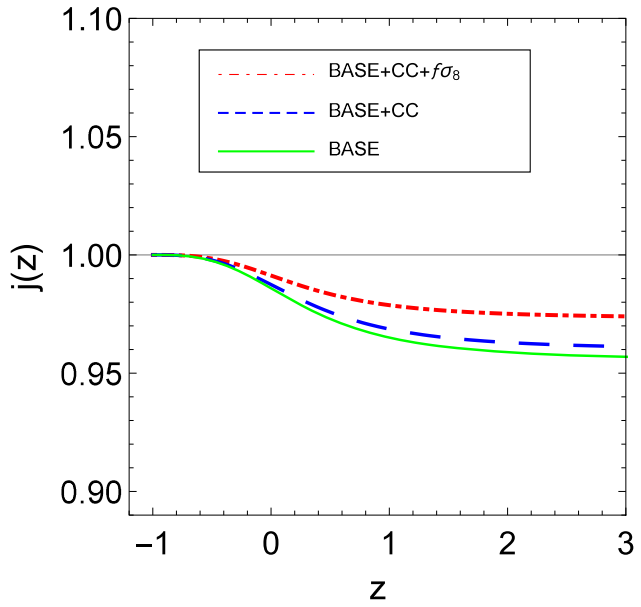

FIG. 16. Jerk parameter $j(z)$ with redshift z using best-fit values of parameters for the viscous $\Lambda(t)$ model. The horizontal line represents the ΛCDM model.

fit. In our observations, we have used $N = 1054$ data points for BASE (SNe Ia and BAO), $N = 1086$ data points for BASE + CC, and $N = 1104$ data points for BASE + CC + $f\sigma_8$. The number of free parameters of viscous $\Lambda(t)$ is $d = 4$, whereas for ΛCDM it is $d = 2$. Using this information, the $\chi^2_{\rm red}$ for both the models are given in Table III. It can be observed that the value of $\chi^2_{\rm red}$ is less than unity with every dataset for both the models, which shows that both models are in a very good fit with these observational datasets and the observed data are consistent with the considered models.

Using the three combination of datasets, we are also interested in investigating the cosmographical aspects of the models, such as the jerk parameter, which is defined as

$$j = \frac{\dddot{a}(t)}{aH^3} = q(2q+1) + (1+z)\frac{dq}{dz}. \tag{59}$$

The jerk parameter, which is a dimensionless third derivative of the scale factor, can provide us the simplest approach to search for departures from the ΛCDM model. It is noted that, for the ΛCDM model, $j = 1(\text{const})$ always. Thus, any deviation from $j = 1$ would favor a non-ΛCDM model. In contrast to a deceleration parameter which has negative values indicating an accelerating Universe, the positive values of the jerk parameter show an accelerating rate of expansion. In Fig. 16, the evolutions of jerk parameter are shown for ΛCDM and viscous $\Lambda(t)$ models using the best-fit values of parameters obtained from three

TABLE III. Values of Chi-squared, reduced Chi-squared, AIC and BIC of ΛCDM, and viscous $\Lambda(t)$ models. The ΛCDM model is considered as a reference model to calculate the ΔAIC and ΔBIC.

	BASE		+CC		$+f\sigma_8$	
Values	ΛCDM	Viscous $\Lambda(t)$	ΛCDM	Viscous $\Lambda(t)$	ΛCDM	Viscous $\Lambda(t)$
χ^2	518.017	515.074	525.457	522.390	842.630	831.112
d	2	4	2	4	2	4
N	1054	1054	1086	1086	1104	1104
$\chi^2_{\rm red}$	0.492	0.498	0.484	0.481	0.764	0.755
AIC	522.028	523.055	529.468	530.427	846.641	839.112
BIC	531.938	542.915	539.438	550.351	856.643	859.139
ΔAIC		1.026		0.959		−7.492
ΔBIC		10.977		10.913		2.496

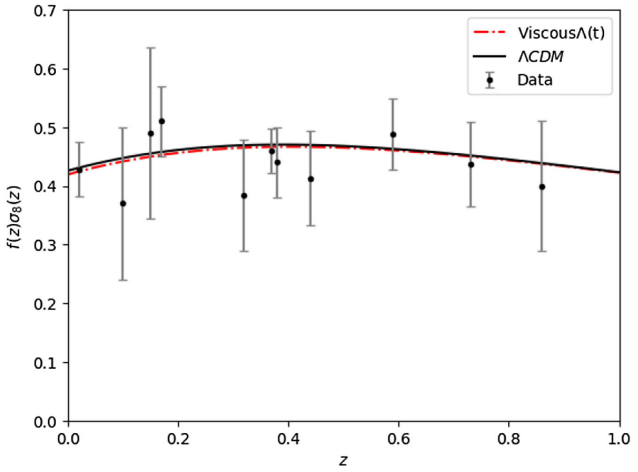

FIG. 17. Theoretical curves for the $f(z)\sigma_8(z)$ corresponding to ΛCDM and viscous $\Lambda(t)$ model along with some of the data points employed in our analysis. To generate this plot we have used the best-fit values of the cosmological parameters listed in Tables I and II for $+f\sigma_8$ data.

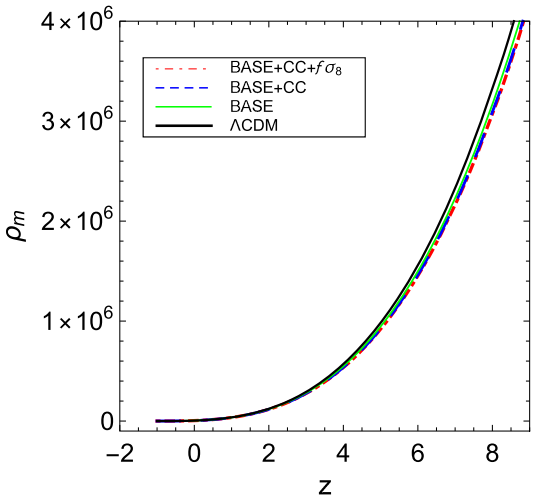

FIG. 18. The matter energy density as a function of redshift for decaying vacuum with viscous term $\zeta = \zeta_1 H$ using the best-fit values obtained from different combinations of datasets.

combination of datasets. It is obvious from the figure that this parameter remains positive and less than unity in the past and eventually tends to unity in late time. Thus, the jerk parameter deviates in early time, but it attains the same value as ΛCDM in late time.

Using the best-fit values of parameters from Table II in Eq. (46), we plot the matter energy density as a function of redshift for different combinations of datasets in Fig. 18. It is observed that the matter density was too large at the beginning of the cosmic evolution. As $z \to -1$, the matter energy density tends to a finite value for all combinations of datasets.

VIII. SELECTION CRITERION

There are two widely used selection criterion, namely, AIC and BIC, to measure the goodness of the fitted models compared to a base model. AIC is an essentially selection criteria based on the information theory, whereas the BIC is based on the Bayesian evidence valid for a large sample size. In cosmology, AIC and BIC are used to discriminate cosmological models based on the penalization associated with the number of free parameters of the considered models. The AIC parameter is defined through the relation [123]

$$\mathrm{AIC} = \chi^2_{\mathrm{min}} + \frac{2dN}{N-d-1}, \tag{60}$$

where d is the free parameters in a model, N the observational data points, and χ^2_{min} the minimum value of the χ^2 function. AIC penalizes according to the number of free parameters of that model. To discriminate the proposed model m_1 with the reference model m_2, we calculate $\Delta AIC_{m_1m_2} = AIC_{m_1} - AIC_{m_2}$, which can be explained as "evidence in favor" of model m_1 as compared to model m_2. In this paper, we consider ΛCDM model as a reference model (m_2).

The value $0 \le \Delta AIC_{m_1m_2} < 2$ refers to strong evidence in favor of the model m_1; for $2 \le \Delta AIC_{m_1m_2} \le 4$, there is average strong evidence in favor of the model m_1; for $4 < \Delta AIC_{m_1m_2} \le 7$, there is little evidence in favor of the model m_1; and for $\Delta AIC_{m_1m_2} > 8$, there is no evidence in favor of the model m_1.

On the other hand, the BIC can be defined as [124]

$$\mathrm{BIC} = \chi^2_{\mathrm{min}} + d \ln N. \tag{61}$$

Similar to ΔAIC, $\Delta BIC_{m_1m_2} = BIC_{m_1} - BIC_{m_2}$ gives evidence against the model m_1 with reference to model m_2. For $0 \le \Delta BIC_{m_1m_2} < 2$ gives not enough evidence of the model m_1; for $2 \le \Delta BIC_{m_1m_2} < 6$, we have evidence against the model m_1; and for $6 \le \Delta BIC_{m_1m_2} < 10$, there is strong evidence against the model m_1. Finally, if $\Delta\mathrm{BIC} > 10$, then there is strong evidence against the model, and it is probably not the best model.

The values of ΔAIC and ΔBIC with respect to ΛCDM as the referring model are shown in Table III. According to our results, $\Delta\mathrm{AIC}(\Delta\mathrm{BIC}) = 1.026(10.977)$ with respect to the BASE dataset, $\Delta\mathrm{AIC}(\Delta\mathrm{BIC}) = 0.959(10.913)$ with +CC dataset, and for $+f\sigma_8$ dataset, we have $\Delta\mathrm{AIC}(\Delta\mathrm{BIC}) = -7.492(2.416)$. Thus, under AIC there is strong evidence in favor of the viscous $\Lambda(t)$ model, whereas under BIC there is strong evidence against the viscous $\Lambda(t)$ model with BASE and +CC datasets and positive evidence against the model with the $+f\sigma_8$ dataset.

IX. CONCLUSION

In this work, we have studied the analytical and observational consequences of cosmology inspired by dissipative phenomena in fluids according to Eckart theory with varying VED scenarios for spatially flat homogeneous and isotropic FLRW geometry. We have assumed the interaction of two components: viscous dark matter and vacuum energy density satisfying the conservation equation (8). We have solved the field equations by assuming the most general form of bulk viscous coefficient, viz., $\zeta = \zeta_0 + \zeta_1 H + \zeta_2(\ddot{a}/aH)$. We have also explored three particular cases of bulk viscosity—namely, (i) $\zeta = \zeta_0$; (ii) $\zeta = \zeta_1 H$; and (iii) $\zeta = \zeta_0 + \zeta_1 H$—to observe the effect of viscosity with varying VED. These viscous models have different theoretical motivations, but not all of them are able to constrain observationally. We have constrained only the viscous model $\zeta = \zeta_1 H$ with varying VED. The motivation of the present work is to study the dynamics and evolutions of a wide class of viscous models with time-varying vacuum energy density in the light of the most recent observational data. Current observations do not rule out the possibility of varying DE. It has been observed that the dynamical Λ could be useful to solve the coincidence problem. Although the functional form of $\Lambda(t)$ is still unknown, a QFT approach has been proposed within the context of the RG. Thus, we have used the varying VED of the functional form $\rho_\Lambda = c_0 + 3\nu H^2$ in all of the viscous models presented in this paper. The motivation for this functional form stems from the general covariance of the effective action in QFT in curved geometry. It has been shown that the $\Lambda(t)$ provides either a particle production processes or increasing the mass of the viscous dark matter particles. In what follows, we summarize the main results of the four different viscous $\Lambda(t)$ models.

In case of the viscous $\Lambda(t)$ models with $\zeta = \zeta_0$, $\zeta = \zeta_0 + \zeta_1 H$, and $\zeta = \zeta_0 + \zeta_1 H + \zeta_2(\ddot{a}/aH)$, we have found the analytical solutions of the various cosmological parameters, like $H(t)$, $a(t)$, $\rho_m(t)$, $q(t)$, and $w_{\rm eff}(t)$. It has been observed that all these three viscous $\Lambda(t)$ models expand exponentially with cosmic time t. The models show the transition from decelerated phase to accelerated phase in late time. The matter energy density $\rho_m(t)$ approaches to a finite value in late time evolution of the Universe. This happens due to the presence of bulk viscosity. The deceleration parameter $q(t)$ tends to -1 as $t \to \infty$. It is important to note that it is $H(z)$ that is actually the observable quantity in cosmology which can be examined with current observations. However, assuming a suitable choice of model parameters, we have discussed numerically the evolutions and dynamics of these models. In the case of viscous $\Lambda(t)$ model with $\zeta = \zeta_1 H$, we have obtained the various cosmological parameters. We have performed a joint likelihood analysis in order to put the constrain on the main parameters by using the three different combinations of observational data: BASE, +CC, and $+f\sigma_8$. To discriminate our model with the concordance ΛCDM model, we have also performed the statistical analysis for ΛCDM by using the same observational datasets. Our finding shows that this viscous $\Lambda(t)$ model can accommodate a late time accelerated expansion. It has been observed that we can improve significantly the performance of the model by using BASE + CC + $f\sigma_8$.

From observational consistency points of view, we have examined the evolution of the viscous $\Lambda(t)$ model on Hubble parameter, deceleration parameter, and equation of state parameter by using the best-fit values of parameters. It has been observed that the model depicts transition from an early decelerated phase to late-time accelerated phase, and the transition takes place at $z_{tr} = 0.664^{+0.031}_{-0.042}$ with BASE data, $z_{\rm tr} = 0.665^{+0.031}_{-0.037}$ with +CC data, and $z_{\rm tr} = 0.626^{+0.028}_{-0.037}$ with $+f\sigma_8$ data. The present viscous $\Lambda(t)$ model has $q_0 = -0.533^{+0.025}_{-0.020}$, $q_0 = -0.535^{+0.023}_{-0.020}$, and $q_0 = -0.516^{+0.022}_{-0.017}$, respectively. Thus, both $z_{\rm tr}$ and q_0 values are in good agreement with that of the ΛCDM model. The ages of the Universe obtained for this model with each dataset are very much compatible with the ΛCDM model. The proposed model has a small negative value of EOS parameter for large redshifts and asymptotically approaches to cosmological constant for small redshifts. Thus, the viscous $\Lambda(t)$ model behaves like quintessence in early time and cosmological constant in late time. The residual tensions of our fitting results with respect to the latest local measurement $H_0 = 73.04 \pm 1.04$ km/s/Mpc [122] are 3.92σ, 3.85σ, and 4.07σ, respectively. In Ref. [125], the authors found $H_0 = 69.13 \pm 2.34$ km/s/Mpc assuming the ΛCDM. Such a result almost coincides with H_0 that we obtained in Tables I and II for ΛCDM and viscous $\Lambda(t)$ models. We have explored the σ_8 and S_8 parameters using the combined datasets of BASE + CC + $f\sigma_8$. The constraints on σ_8 and S_8 from this combined analysis are $\sigma_8 = 0.790^{+0.008}_{-0.010}$ and $S_8 = 0.822^{+0.019}_{-0.019}$, respectively, which are very close to the values of ΛCDM. The tension of our fitting results in σ_8 and S_8 for the viscous $\Lambda(t)$ model with respect to respective σ_8 and S_8 of ΛCDM is 0.23σ and -0.38σ, respectively. The evolution of $f\sigma_8$ as displayed in Fig. 17 shows that the behavior of $f\sigma_8$ is consistent with the observational data points. It has been noticed that the best-fit results are consistent in the vicinity of Planck data [7].

It has been observed that the value of $\chi^2_{\rm red}$ is less than unity with every dataset, which shows that the model is in a very good fit with these observational datasets and the observed data are consistent with the considered model. The jerk parameter remains positive and less than unity in past and eventually tends to unity in late time. Thus, the jerk parameter deviates in early time, but it attains the same value as ΛCDM in late time. To discriminate the viscous $\Lambda(t)$ with the ΛCDM, we have examined the selection

criterion, namely, AIC and BIC. According to the selection criteria ΔAIC, we have found that the viscous $\Lambda(t)$ model is positively favored over the ΛCDM model for BASE, +CC, and $+f\sigma_8$ datasets. Similarly, with respect to ΔBIC our model has a very strong evidence against the model for BASE and +CC datasets, whereas, when we add $+f\sigma_8$ dataset, there is no significant evidence against the model. As a concluding remark, we must point out that the viscous models with decaying VED may be preferred as potential models to examine the dark energy models beyond the concordance cosmological constant. The viscous effects with decaying VED can drive an accelerated expansion of the Universe. Thus, a viable cosmology can be constructed with viscous fluids and decaying VED. With new and more accurate observations and with more detailed analyses, it would be possible to conclusively answer the compatibility of viscous model with dynamical vacuum energy.

ACKNOWLEDGMENTS

V. K. thanks Delhi Technological University, India for providing a research fellowship to carry out this work.

[1] A. G. Riess *et al.*, Astron. J. **116**, 1009 (1998).
[2] S. Perlmutter *et al.*, Astrophys. J. **517**, 565 (1999).
[3] C. L. Bennet *et al.*, Astrophys. J. Suppl. Ser. **148**, 1 (2003).
[4] M. Tegmark *et al.*, Phys. Rev. D **69**, 103501 (2004).
[5] S. Alam *et al.*, Mon. Not. R. Astron. Soc. **470**, 2617 (2017).
[6] M. H. Amante, J. Magaña, V. Motta, M. A García-Aspeitia, and T. Verdugo, Mon. Not. R. Astron. Soc. **498**, 6013 (2020).
[7] N. Aghanim *et al.* (Planck Collaboration), Astrophys. Astron. **641**, A6 (2020).
[8] R. R. Caldwell, R. Dave, and P. J. Steinhardt, Astrophys. Space Sci. **261**, 303 (1998).
[9] L.-M. Wang, R. R. Cardwell, J. P. Ostriker, and P. J. Steinhardt, Astrophys. J. **530**, 17 (2000).
[10] P. J. Steinhardt, Phil. Trans. R. Soc. A **361**, 2497 (2003).
[11] P. J. E. Peebles and B. Ratra, Rev. Mod. Phys. **75**, 559 (2003).
[12] S. Weinberg, Rev. Mod. Phys. **61**, 1 (1989).
[13] S. M. Carrol, Living Rev. Relativity **4**, 1 (2001).
[14] T. Padmanabhan, Phys. Rep. **380**, 235 (2003).
[15] I. Zlatev, L.-M. Wang, and P. J. Steinhardt, Phys. Rev. Lett. **82**, 896 (1999).
[16] K. Freese, F. C. Adams, J. A. Frieman, and E. Mottola, Nucl. Phys. **A287**, 797 (1987).
[17] J. C. Carvalho, J. A. Lima, and I. Waga, Phys. Rev. D **46**, 2404 (1992).
[18] J. A. Lima and J. M. Maia, Phys. Rev. D **49**, 5597 (1994).
[19] J. A. Lima, Phys. Rev. D **54**, 2571 (1996).
[20] P. Wang and X. Meng, Classical Quantum Gravity **22**, 283 (2005).
[21] E. Elizalde, S. Nojiri, S. D. Odintsov, and P. Wang, Phys. Rev. D **71**, 103504 (2005).
[22] J. S. Alcaniz and J. A. S. Lima, Phys. Rev. D **72**, 063516 (2005).
[23] H. A. Borges and S. Carneiro, Gen. Relativ. Gravit. **37**, 1385 (2005).
[24] J. Solà and H. Stefancic, Mod. Phys. Lett. A **21**, 479 (2006).
[25] S. Carneiro, C. Pigozzo, H. A. Borges, and J. S. Alcaniz, Phys. Rev. D **74**, 023532 (2006).
[26] H. A. Borges, S. Carneiro, J. C. Fabris, and C. Pigozzo, Phys. Rev. D **77**, 043513 (2008).
[27] S. Carneiro, M. A. Dantas, C. Pigozzo, and J. S. Alcaniz, Phys. Rev. D **77**, 083504 (2008).
[28] S. Basilakos, Mon. Not. R. Astron. Soc. **395**, 2374 (2009).
[29] S. Basilakos, M. Plionis, and J. Solà, Phys. Rev. D **80**, 083511 (2009).
[30] F. E. M. Costa and J. S. Alcaniz, Phys. Rev. D **81**, 043506 (2010).
[31] C. Pigozzo, M. A. Dantas, S. Carneiro, and J. S. Alcaniz, J. Cosmol. Astropart. Phys. 08 (2011) 022.
[32] J. Solà, J. Phys. Conf. Ser. **283**, 012033 (2011).
[33] J. Grande, J. Solà, S. Basilakos, and M. Plionis, J. Cosmol. Astropart. Phys. 11 (2011) 007.
[34] D. Bessada and O. D. Miranda, Phys. Rev. D **88**, 083530 (2013).
[35] J. Solà, J. Phys. Conf. Ser. **453**, 012015 (2013).
[36] E. L. D. Perico, J. A. S. Lima, S. Basilakos, and J. Solà, Phys. Rev. D **88**, 063531 (2013).
[37] M. Szydlowski and A. Stachowski, J. Cosmol. Astropart. Phys. 10 (2015) 066.
[38] A. Gomez-Valent and J. Solà, Mon. Not. R. Astron. Soc. **448**, 2810 (2015).
[39] J. Solà and A. Gomez-Valent, Int. J. Mod. Phys. D **24**, 1541003 (2015).
[40] E. A. Novikov, Mod. Phys. Lett. A **31**, 1650092 (2016).
[41] A. P. Jayadevan, M. Mukesh, A. Shaima, and T. K. Mathew, Astrophys. Space Sci. **364**, 67 (2019).
[42] I. Shapiro and J. Solà, J. High Energy Phys. 02 (2002) 006.
[43] J. Solà, J. Phys. A **41**, 164066 (2008).
[44] J. Grande, J. Solà, and H. Stefancic, J. Cosmol. Astropart. Phys. 08 (2006) 011.
[45] C. P. Singh and J. Solà, Eur. Phys. J. C **81**, 960 (2021).
[46] M. Rezaei, J. Solà, and M. Malekjani, Mon. Not. R. Astron. Soc. **509**, 2593 (2022).
[47] W. Zimdahl, D. J. Schwarz, A. B. Balakin, and D. Pavón, Phys. Rev. D **64**, 063501 (2001).
[48] A. B. Balakin, D. Pavón, D. J. Schwarz, and W. Zimdahl, New J. Phys. **5**, 85 (2003).
[49] C. Eckart, Phys. Rev. **58**, 276 (1940).
[50] L. D. Landau and E. M. Lifshitz, *Fluid Mechanics* (Butterworth Heinermann, Oxford, 1987), Vol. 6.
[51] W. A. Hiscock and L. Lindblom, Phys. Rev. D **31**, 725 (1985).

[52] I. Müller, Z. Phys. **198**, 329 (1967).
[53] W. Israel and J. M. Stewart, Phys. Lett. A **58**, 213 (1976).
[54] Ø. Grøn, Astrophys. Space Sci. **173**, 191 (1990).
[55] R. Maartens, Classical Quantum Gravity **12**, 1455 (1995).
[56] A. A. Coley, R. J. Van den Hoogen, and R. Maartens, Phys. Rev. D **54**, 1393 (1996).
[57] W. Zimdahl, Phys. Rev. D **53**, 5483 (1996).
[58] I. Brevik and S. D. Odintsov, Phys. Rev. D **65**, 067302 (2002).
[59] I. Brevik and A. Hallanger, Phys. Rev. D **69**, 024009 (2004).
[60] C. P. Singh, S. Kumar, and A. Pradhan, Classical Quantum Gravity **24**, 455 (2007).
[61] C. P. Singh, Pramana J. Phys. **71**, 33 (2008).
[62] S. Nojiri and S. D. Odintsov, Phys. Lett. B **649**, 440 (2007).
[63] I. Brevik, O. Gorbunova, and D. Saez-Gomez, Gen. Relativ. Gravit. **42**, 1513 (2010).
[64] H. Velten, J. Wang, and X. Meng, Phys. Rev. D **88**, 123504 (2013).
[65] J. Wang and X. Meng, Mod. Phys. Lett. A **29**, 1450009 (2014).
[66] K. Bamba and S. D. Odintsov, Eur. Phys. J. C **76**, 18 (2016).
[67] I. Brevik, Ø. Grøn, J. de Haro, S. D. Odintsov, and E. N. Saridakis, Int. J. Mod. Phys. D **26**, 1730024 (2017).
[68] G. M. Kremer and F. P. Devecchi, Phys. Rev. D **67**, 047301 (2003).
[69] J. C. Fabris, S. V. B. Goncalves, and R. de Sá Ribeiro, Gen. Relativ. Gravit. **38**, 495 (2006).
[70] I. Brevik and O. Gorbunova, Gen. Relativ. Gravit. **37**, 2039 (2005).
[71] M.-G. Hu and X.-H. Meng, Phys. Lett. B **635**, 186 (2006).
[72] J. Ren and X.-H. Meng, Phys. Lett. B **633**, 1 (2006).
[73] X.-H. Meng, J. Ren, and M.-G. Hu, Commun. Theor. Phys. **47**, 379 (2007).
[74] J. R. Wilson, G. J. Mathews, and G. M. Muller, Phys. Rev. D **75**, 043521 (2007).
[75] G. J. Mathews, N. Q. Lan, and C. Kolda, Phys. Rev. D **78**, 043525 (2008).
[76] A. Avelino and U. Nucamendi, AIP Conf. Proc. **1083**, 1 (2008).
[77] A. Avelino, U. Nucamendi, and F. S. Guzman, AIP Conf. Proc. **1026**, 300 (2008).
[78] A. Avelino and U. Nucamendi, J. Cosmol. Astropart. Phys. 04 (2009) 006.
[79] X. H. Meng and X. Dou, Commun. Theor. Phys. **52**, 377 (2009).
[80] A. Avelino and U. Nucamendi, J. Cosmol. Astropart. Phys. 08 (2010) 009.
[81] C. P. Singh and P. Kumar, Eur. Phys. J. C **74**, 3070 (2014).
[82] A. Sasidharan and T. K. Mathew, Eur. Phys. J. C **75**, 348 (2015).
[83] B. D. Normann and I. Brevik, Mod. Phys. Lett. A **32**, 1750026 (2017).
[84] D. Wang, Y.-J. Yan, and X.-H. Meng, Eur. Phys. J. C **77**, 660 (2017).
[85] C. P. Singh and A. Kumar, Eur. Phys. J. Plus **133**, 312 (2018).
[86] C. P. Singh and A. Kumar, Mod. Phys. Lett. A **33**, 1850225 (2018).
[87] C. P. Singh and M. Srivastava, Eur. Phys. J. C **78**, 190 (2018).
[88] C. P. Singh and A. Kumar, Astrophys. Space Sci. **364**, 94 (2019).
[89] C. P. Singh and S. Kaur, Astrophys. Space Sci **365**, 2 (2020).
[90] C. P. Singh, Nouvo Cimento B **122**, 89 (2007).
[91] C. P. Singh and S. Kumar, Astrophys. Space Sci. **323**, 407 (2009).
[92] N. Mostafapoor and Ø. Grøn, Astrophys. Space Sci. **333**, 357 (2011).
[93] J. Hu and H. Hu, Eur. Phys. J. Plus **135**, 718 (2020).
[94] L. Herrera-Zamorano, A. Hernández-Almada, and Miguel A. García-Aspeitia, Eur. Phys. J. C **80**, 637 (2020).
[95] S. Weinberg, *Gravitation and Cosmology: Principles and Applications of the General Theory of Relativity* (Wiley, New York, 1972).
[96] S. L. Adler, Rev. Mod. Phys. **54**, 729 (1982).
[97] L. Parker and D. J. Toms, Phys. Rev. D **32**, 1409 (1985).
[98] I. L. Shapiro and J. Sola, Phys. Lett. B **682**, 105 (2009).
[99] F. A. Oliveira, F. E. M. Costa, and J. A. S. Lima, Classical Quantum Gravity **31**, 045004 (2014).
[100] A. Avelino, R. G. Salcedo, T. Gonzalez, U. Nucamendi, and I. Quiros, J. Cosmol. Astropart. Phys. 08 (2013) 012.
[101] A. Sasidharan and T. K. Mathew, J. High Energy Phys. 06 (2016) 138.
[102] C. P. Singh and Ajay Kumar, Gravitation Cosmol. **25**, 58 (2019).
[103] T. Padmanabhan and S. M. Chitre, Phys. Lett. A **120**, 433 (1987).
[104] A. Montiel and N. Breton, J. Cosmol. Astropart. Phys. 08 (2011) 023.
[105] I. Brevik, Phys. Rev. D **65**, 127302 (2002).
[106] J. Hu and H. Hu, Eur. Phys. J. Plus **135**, 718 (2020).
[107] J. Sola, J. de Cruz Pérez, and A. Gómez-Valent, Mon. Not. R. Astron. Soc. **478**, 4357 (2018).
[108] A. Gomez-Valent and J. Sola Peracaula, Mon. Not. R. Astron. Soc. **478**, 126 (2018).
[109] J. de Cruz, J. Sola, and C. P. Singh, arXiv:2302.04807.
[110] P. J. E. Pebbles, *Principles of Physical Cosmology* (Princeton University Press, Princeton, NJ, 1993).
[111] Y.-S. Song and W. J. Percival, J. Cosmol. Astropart. Phys. 10 (2009) 004.
[112] D. Huterer, D. Kirkby *et al.*, Astropart. Phys. **63**, 23 (2015).
[113] S. Nesseris and L. Perivolaropoulos, Phys. Rev. D **77**, 023504 (2008).
[114] D. M. Scolnic *et al.*, Astrophys. J. **859**, 101 (2018).
[115] C. Blake *et al.*, Month. Not. R. Astron. Soc. **418**, 1707 (2011).
[116] W. J. Percival *et al.*, Mon. Not. R. Astron. Soc. **401**, 2148 (2010).
[117] R. Giostri, M. Vargas dos Santos, I. Waga, R. R. R Reis, M. O. Calvão, and B. L. Lago, J. Cosmol. Astropart. Phys. 03 (2012) 027.
[118] D. Eisenstein, Astrophys. J. **633**, 560 (2005).
[119] M. Moresco *et al.*, Living Rev. Relativity **25**, 6 (2022).

[120] S. Nesseris, G. Pantazis, and L. Perivolaropoulos, Phys. Rev. D **96**, 023542 (2017).
[121] Daniel Foreman-Mackey, D. W. Hogg, D. Lang, and J. Goodman, Publ. Astron. Soc. Pac. **125**, 306 (2013).
[122] A. G. Riess *et al.*, Astrophys. J. Lett. **934**, L7 (2022).
[123] H. Akaike, IEEE Trans. Autom. Control **19**, 716 (1974).
[124] G. Schwarz, Ann. Stat. **6**, 461 (1978).
[125] Y. Wang, Lixin, Xu, and G. B. Zhao, Astrophys. J. **849**, 84 (2017).

Astronomy and Computing 53 (2025) 100992

Contents lists available at ScienceDirect

Astronomy and Computing

journal homepage: www.elsevier.com/locate/ascom

Full length paper

Exploring interacting bulk viscous model with decaying vacuum density

Vinita Khatri [a], C.P. Singh [a,*], Milan Srivastava [b]

[a] Department of Applied Mathematics, Delhi Technological University, Delhi 110042, India
[b] Department of Mathematics, Sharda School of Basic Sciences and Research, Sharda University, India

ARTICLE INFO

Keywords:
Dark energy
Viscous cosmology
Varying Λ
Cosmological parameters

ABSTRACT

In the present work, we study a cosmological model composed of a viscous dark matter interacting with decaying vacuum energy in a spatially flat Universe. In the first part, we find the analytical solution of different cosmological parameters by assuming the physically viable forms of bulk viscosity and decaying vacuum density with the interaction term. The second part is dedicated to constrain free parameters of the interacting viscous model with decaying vacuum energy by employing latest observational data of *Pantheon+*, Cosmic Chronometer and $f(z)\sigma_8(z)$. We find that the interacting model just deviate very slightly from well-known concordance ΛCDM model and can alleviate effectively the current H_0 tension between local measurement by R21 and global measurement by Planck 2018, and the excess in the mass fluctuation amplitude σ_8 essentially vanish in this context. We report the Hubble constants as $H_0 = 72.100^{+1.700}_{-1.700}$, and $72.200^{+1.000}_{-2.000}$ $\mathrm{kms^{-1}Mpc^{-1}}$, deceleration parameters as $q_0 = -0.532^{+0.022}_{-0.024}$, and $-0.531^{+0.022}_{-0.022}$, and equation of state parameters as $\omega_0 = -0.689^{+0.016}_{-0.016}$, and $-0.688^{+0.016}_{-0.016}$ for ΛCDM and interacting models, respectively. It is found that the interacting model is in good agreement with ΛCDM. Further, we discuss the amplitude of matter power spectrum σ_8 and its associated parameter S_8 using $f(z)\sigma_8(z)$ data. Finally, the information selection criterion and Bayesian inference are discussed to distinguish the interacting model with ΛCDM model.

1. Introduction

In modern cosmology, understanding of two dark components: dark energy (DE) and dark matter (DM) of the Universe is so far the most challenging research area in cosmology. The discovery of accelerated expansion (Riess et al., 1998; Perlmutter et al., 1999) has motivated to comprehend the composition of these dark entities. Dark matter, which interacts only gravitationally with ordinary matter, explains the measurement of rotation curves of spiral galaxies (Persic et al., 1996). The most important theories for DM are scalar fields and supersymmetry models (Magaña and Matos, 2012; Hernández-Almada and García-Aspeitia, 2018; Martin, 1998). On the other hand, dark energy, which has negative pressure, is considered for the accelerated expansion of the Universe. The most interesting candidates are the cosmological constant (CC), phantom energy, quintessence, Chaplygin gas, modified theories of gravity, etc. (Sahni and Starobinsky, 2000; Peebles and Ratra, 2003; Copeland et al., 2006). The cosmological constant as DE so-called Lambda-cold-dark matter, abbreviated as ΛCDM is still the best candidate to explain the cosmological observations. However, ΛCDM model suffers with some theoretical problems (Weinberg, 1989; Padmanabhan, 2003) when its origin is considered as quantum vacuum fluctuations.

Some works in literature have shown that some dynamical DE models are able to resolve the problems of ΛCDM. In this respect, the cosmological models with time-varying vacuum energy are the promising models to resolve the issues. Although there is no fundamental theory to describe a time-varying vacuum, a phenomenological technique has been proposed to parametrized CC. Shapiro and Solà (2002) and Solà (2008) proposed a running vacuum models (RVMs) on the basis of renormalization group (RG) formalism of Quantum Field Theory (QFT) in curved spacetime. In the context of RVMs, it is considered that the vacuum energy density evolves slowly with the cosmic expansion. It has been illustrated that both the background and linear perturbation levels of the cosmic evolutions can be described by the RVMs. The vacuum energy is typically determined in curved space–times using renormalization group procedures, which depend on the Hubble parameter H and its time derivative and is given by the form $\rho_\Lambda(H,\dot{H}) = M_{Pl}^2\Lambda(H,\dot{H})$ (Solà, 2013). In literature, many authors (Carvalho et al., 1992; Lima and Carvalho, 1994; Bertolami, 1986; Özer and Taha, 1987; Peebles and Ratra, 1988; Overduin and Cooperstock, 1998) have studied the time-varying vacuum energy models. In recent years, the RVMs have been carefully confronted against many cosmological data, which have received a significant success (Wang and Meng, 2005;

* Corresponding author.
E-mail addresses: vinitakhatri_2k20phdam501@dtu.ac.in (V. Khatri), cpsingh@dce.ac.in (C.P. Singh), milan.srivastava@sharda.ac.in (M. Srivastava).

https://doi.org/10.1016/j.ascom.2025.100992
Received 8 December 2024; Accepted 21 July 2025
Available online 6 August 2025

Elizalde et al., 2005; Borges and Carneiro, 2005; Carneiro et al., 2006; Borges et al., 2008; Carneiro et al., 2008; Basilakos, 2009; Basilakos et al., 2009; Costa and Alcaniz, 2010; Pigozzo et al., 2011; Bessada and Miranda, 2013; Solà and Gómez-Valent, 2015; Solà et al., 2017a,b, 2018, 2019, 2021; Jayadevan et al., 2019; Singh and Solà, 2021; Khatri and Singh, 2023).

On the other hand, viscous fluid cosmology is an interesting research area to understand the accelerated expansion of the Universe. It has been observed that irreversible processes in the evolution of the Universe may also be responsible for explaining the recent accelerated expansion. There are two types of viscosity: bulk and shear, however, bulk viscosity is the one that plays an important role in the evolution of the Universe as it satisfies the cosmological principle. Bulk viscous models have been studied using two approaches: the Eckart (1940), and Israel and Stewart (1976) theories. Eckart (1940) proposed a non-causal theory of viscous of first order which was later modified by Landau and Lifshitz (1987). In this theory, all equilibrium states are unstable (Hiscock and Lindblom, 1985) and the signals can propagate through the fluids faster than the speed of light (Müller, 1967). The Israel-Stewart formalism is a full causal theory of second order which avoids the casuality problem. When the relaxation time goes to zero, the causal theory reduces to the Eckart's first order theory. Despite of the causality problem, Eckart theory is widely used due to its simplicity. In both theories, the bulk viscous term is included in Einstein field equations through an effective pressure, written in the form $\bar{p} = p + \Pi$ where p is pressure of matter contents such as dust-matter, DE or relativistic species (photons and neutrinos) and Π refers the bulk viscous pressure. In Eckart theory, the bulk viscous pressure is assumed as $\Pi = -3\zeta H$, where ζ is the bulk viscous coefficient and H the Hubble parameter. Some works related to Eckart theory have studied the evolution of the Universe at late time by assuming bulk viscous coefficient with a constant (Murphy, 1973; Padmanabhan and Chitre, 1987; Grøn, 1990; Maartens, 1995; Brevik and Gorbunovae, 2005; Normann and Brevik, 2017) and polynomial as functions of redshift or in terms of energy density (Singh et al., 2007; Xin-He and Xu, 2009; Avelino and Nucamendi, 2010; Hernández-Almada, 2019). Brevik et al. (2017) have presented a basic review on viscous cosmology. Some more authors (Fabris et al., 2006; Hu and Meng, 2006; Ren and Meng, 2006; Meng et al., 2007; Wilson et al., 2007; Mathews et al., 2008; Avelino and Nucamendi, 2008; Avelino et al., 2008; Avelino and Nucamendi, 2009; Meng and Dou, 2009; Mostafapoor and Grøn, 2011; Singh and Kumar, 2014; Sasidharan and Mathew, 2015; Bamba and Odintsov, 2016; Wang et al., 2017; Singh and Kumar, 2018a,b; Singh and Srivastava, 2018; Singh and Kumar, 2019; Singh and Kaur, 2020; Hu and Hu, 2020) have explored the viability of a bulk viscous Universe to explain the present accelerated expansion of the Universe.

Decaying vacuum energy density (VED) models and viscous fluid models are two appealing theoretical models that have been separately studied by many authors to solve some of problems facing by standard ΛCDM model. Despite the success of decaying vacuum energy and viscous fluid models, it should be noted that they have, separately, limitations in describing the entire cosmological evolution. Recently, Herrera-Zamorano et al. (2020), Ashoorioon and Davari (2023), Cruz et al. (2023), Singh and Khatri (2024) have studied the cosmological model with combination of these two notions in a single cosmological setting and have investigated their cosmological implications using observational data.

The ΛCDM's problems also motivate research into new physics beyond this standard model. In standard cosmology, it is usually assumed that DM and DE do not interact with each other. However, there is no physical basis for this assumption. In this regard, a popular approach is to investigate the cosmological models where the interaction between the DM and DE takes place. In this interaction theory, DM and DE are not separately conserved but they exchange energy (and /or momentum). However, the total energy (and/or momentum) is conserved. It is worth constraining the interacting models against the available wealth of precision cosmological data. This has motivated a large number of studies based on models where DM and DE share interactions, usually referred to as interacting dark energy (IDE) models. Chen et al. (2009, 2014) have performed a detailed phase-space analysis and studied the possibility of transient acceleration by considering the interaction between DE and DM. Several studies in the literature have been devoted to explore whether DM-DE interactions may help to resolve the enduring H_0 tension (Wang and Wang, 2014; Nunes et al., 2016; Valentino et al., 2017, 2020; Yang et al., 2018; Wang et al., 2022; Gariazzo et al., 2022; Marcel and Abebe, 2024). Ju-Hua et al. (2011), Kremer and Sobreiro (2012), Avelino (2012), Avelino et al. (2013), Harko and Lobo (2013), Leyva and Sepúlveda (2017), Atreya et al. (2018), Hernández-Almada et al. (2020) have studied the interacting viscous dark fluids for explaining the early and late time evolution of the Universe. The above cited works on bulk viscosity show that interacting viscous fluid models can be one of the possible mechanism to explain the present acceleration of the Universe.

In recent years, Hubble tension and σ_8 tension are the major challenge in cosmology, which highlight the need of further research to understand the evolution of the Universe. These tensions have created due to the discrepancy between the measurement the expansion rate by two different methods: Cosmic Microwave Background(CMB) and distance ladder. Researchers are actively working to understand these tensions by exploring the alternative modified theories beyond the standard ΛCDM model. Abdalla et al. (2022) have presented a cosmological review of particle physics, astrophysics and cosmology associated with cosmological tensions and anomalies, and proposed some interesting models which could alleviate H_0 and σ_8 tensions.

In light of the aforementioned discussions, it has been observed that the interacting scenario that include dynamical dark energy have attracted the interest in literature as they are efficient to resolve the H_0 and σ_8 tensions (Pan et al., 2019). The main purpose of the present work is to investigate a cosmological model for a spatially flat Friedmann-Lemaître-Robertson-Walker Universe including two components: a non-perfect and interacting viscous dark matter, and decaying vacuum energy that interact with viscous dark matter in Eckart's approach. We analyse the dynamics of interacting model by constraining the free parameters by performing a Markov chain Monte Carlo (MCMC) using the latest observational data. Further, we investigate how our interacting viscous model with decaying VED affects the perturbation level. To investigate the role of this model in structure formation, we employ the perturbation equation to determine the growth of matter fluctuations. Finally, we study the evolutions of various cosmological parameters and compare the perfect fluid case that corresponds to the ΛCDM model through the model selection criteria and Bayesian evidence analysis.

The paper is organized as follows. In Section 2, we present the general features of the proposed cosmological model for a spatially flat Friedmann-Lemaître-Robertson-Walker Universe where dissipative effects are present with interacting decaying VED. Section 3 deals with the analysis on Structure formation and perturbation equations. We present in Section 4 the cosmological probes that are used to constrain the model. Section 5 gives the results and discussions on various cosmological parameters with the trajectories and compares the proposed model with the concordance ΛCDM using information criterion and the Bayesian inference. The main results of the work are summarized and discussed in Section 6. Two more solutions are also presented in Appendix.

2. Interacting bulk viscous model with decaying VED

We start with a homogeneous and isotropic Universe described by the Friedmann-Lemaître-Robertson-Walker (FLRW) metric

$$ds^2 = -dt^2 + a^2(t)\left[dr^2 + r^2(d\theta^2 + sin^2\theta d\phi^2)\right], \quad (1)$$

where $a(t)$ represents the cosmic scale factor of the Universe. The Einstein field equations in General Relativity are given by

$$R_{\mu\nu} - \frac{1}{2}g_{\mu\nu}R = 8\pi G\tilde{T}_{\mu\nu}, \tag{2}$$

where $R = g_{\mu\nu}R_{\mu\nu}$ is the Ricci scalar, G is the Newton gravitational constant and $\tilde{T}_{\mu\nu} = T_{\mu\nu} + g_{\mu\nu}\rho_\Lambda$ is the total energy–momentum tensor, which accounts for contribution of viscous dark matter and vacuum energy. Here, $\rho_\Lambda = \Lambda/8\pi G$ is the energy density associated to Λ-term, so-called the vacuum energy density (VED). It should be emphasized that we employ the geometric units $8\pi G = c = 1$.

In this paper, we propose to study the cosmological dynamics of the Universe which include the interaction between the dark matter component including dissipation through a bulk viscous coefficient and a VED described by running coupling depending on the Hubble parameter (hereafter we refer interacting viscous $\Lambda(t)$ model).

The energy–momentum tensor, $T_{\mu\nu}$ for viscous matter is given by (Eckart, 1940)

$$T_{\mu\nu} = (\rho_m + P)u_\mu u_\nu + g_{\mu\nu}P \tag{3}$$

where ρ_m is the energy density DM, u_μ is the associated four-velocity and $P = p_m + \Pi$ is the sum of pressure of fluid contributed from the equilibrium pressure, p_m and the non-equilibrium pressure, Π due to bulk viscosity. It is assumed that deviation of any system from the local thermodynamical equilibrium is the source of bulk viscosity. In accordance with the second law of thermodynamics, the restoration of thermal equilibrium is a dissipative process that produces entropy. As a result of this entropy generation, the bulk viscous term causes an expansion in the system. We also assume that the energy–momentum tensor for vacuum energy similar to a perfect fluid, with equation of state, $p_\Lambda = -\rho_\Lambda$.

The viscous fluid in homogeneous and isotropic cosmological models is determined by its bulk viscosity. The Eckart's formalism serves as the basis for this theory (Eckart, 1940). It is basically obtained from the second order theory of non-equilibrium thermodynamics in the limit of vanishing relaxation time which was proposed by Israel and Stewart (1976). Inspired by the viscosity behaviour in fluid mechanics, being proportional to the speed, we assume $\Pi = -3\zeta H$, where H is the Hubble parameter and ζ is the bulk viscous coefficient, which is assumed to be positive on thermodynamic grounds. Furthermore, we consider the non-relativistic matter with $p_m = 0$ to be the bulk viscous fluid. Therefore, the sum of the vacuum energy pressure, $p_\Lambda = -\rho_\Lambda$ and viscous pressure $\Pi = -3\zeta H$ are the components contributing to the total pressure. These two extra ingredients have been introduced to get a more realistic fluid description of DM and DE and also a suitable comparison with ΛCDM model.

In the presence of a non-gravitational interaction between viscous dark matter and decaying vacuum energy, which is characterized by a coupling function $Q(t)$, also known as the interacting rate, the Friedmann equation and conservation equations can be written as

$$3H^2 = \rho_m + \rho_\Lambda, \tag{4}$$

$$\dot{\rho}_m + 3H\rho_m = 9\zeta H^2 + Q(t), \tag{5}$$

$$\dot{\rho}_\Lambda + 3H(\rho_\Lambda + p_\Lambda) = -Q(t), \tag{6}$$

where dot denotes derivative with respect to the cosmic time t. In Eqs. (5) and (6), $Q(t)$ denotes the interaction function providing the rate of energy transfer between viscous dark matter and decaying VED. It is to be noted that $Q(t) < 0$ gives energy transfer from viscous DM to decaying vacuum energy where as $Q(t) > 0$ gives energy transfer from decaying vacuum energy to viscous DM. Once the interaction function $Q(t)$ is specified, the background dynamics of the model can be found using (4)–(6). We can define $Q(t)$ by two ways: either by deriving the interaction function from some fundamental physics at the Lagrangian level or by assuming at phenomenological level and testing using observational data. Due to the absence of a fundamental physical theory, we will consider the second approach by assuming the interaction function as (Nojiri and Odintsov, 2011; Brevik et al., 2015)

$$Q = 3\alpha\rho_m H, \tag{7}$$

where the term α denotes the dimensionless coupling parameter and included in the fitting vector of free parameters which is to be constrained by the observational dataset.

For decaying VED, we assume a phenomenological application of renormalization group analysis, which can be written as (Solà et al., 2017b; Khatri and Singh, 2023)

$$\rho_\Lambda = c_0 + 3\nu H^2, \tag{8}$$

where $c_0 = 3H_0^2(\Omega_\Lambda - \nu)$ is the additive constant and fixed by the boundary condition $\rho_\Lambda(H_0) = \rho_{\Lambda 0}$. In this scenario, ν is the dimensionless vacuum parameter and is naturally anticipated to have extremely small magnitude i.e. $|\nu| \ll 1$. Thus, the positive magnitude of ν enables the vacuum's cosmic evolution. In this instance, we will fit ν to the cosmological data set by taking it as a free parameter.

Substituting (7) into (5), we get

$$\dot{\rho}_m = 9\zeta H^2 - 3(1-\alpha)\rho_m H \tag{9}$$

From (4)–(9), we get the following Hubble evolution equation,

$$\dot{H} + \frac{3}{2}(1-\alpha)H^2 = \frac{3}{2}\frac{\zeta}{(1-\nu)}H + \frac{1}{2}\left(\frac{1-\alpha}{1-\nu}\right)c_0. \tag{10}$$

The above evolution Eq. (10) has H and ζ as unknown quantities. We can get the solution of H only if the functional form of ζ is specified. We consider the bulk viscous coefficient ζ as proportional to the expansion rate of the Universe, i.e., to the Hubble parameter H, which can be expressed as (Grøn, 1990; Singh et al., 2007; Singh and Kumar, 2014; Brevik, 2002; Hu and Hu, 2020)

$$\zeta = \zeta_1 H \tag{11}$$

where ζ_1 is a dimensionless constant to be estimated from the observations. Substituting this relation into (10), we get

$$\dot{H} + \frac{3}{2}\left(\frac{(1-\nu)(1-\alpha)-\zeta_1}{1-\nu}\right)H^2 - \frac{1}{2}\left(\frac{1-\alpha}{1-\nu}\right)c_0 = 0. \tag{12}$$

The preceding equation with a variable change from t to $x = \log a$ together with $c_0 = 3H_0^2(\Omega_\Lambda - \nu)$ can be written as

$$\frac{dh^2}{dx} + 3\left(\frac{(1-\nu)(1-\alpha)-\zeta_1}{1-\nu}\right)h^2 = 3\left(\frac{(\Omega_\Lambda-\nu)(1-\alpha)}{1-\nu}\right), \tag{13}$$

where $h = H/H_0$ represents the Hubble parameter which is dimensionless and $\Omega_\Lambda = \rho_\Lambda/3H_0^2$. Assuming $(1-\nu)(1-\alpha)-\zeta_1 > 0$ and employing the redshift relation to the normalized scale factor, $a = (1+z)^{-1}$, Eq. (13) gives

$$E^2(z) = \tilde{\Omega}_{m,0}(1+z)^{3\left(\frac{(1-\nu)(1-\alpha)-\zeta_1}{(1-\nu)}\right)} + \tilde{\Omega}_{\Lambda,0}, \tag{14}$$

where

$$\tilde{\Omega}_{\Lambda,0} = \frac{(\Omega_\Lambda-\nu)(1-\alpha)}{(1-\nu)(1-\alpha)-\zeta_1}, \tag{15}$$

and

$$\tilde{\Omega}_{m,0} = 1 - \frac{(\Omega_\Lambda-\nu)(1-\alpha)}{(1-\nu)(1-\alpha)-\zeta_1} = 1 - \tilde{\Omega}_{\Lambda,0}. \tag{16}$$

In Eq. (14), $E(z) = H/H_0$ is dimensionless Hubble parameter and $\Omega_{i,0}$ (i = DM,DE) represents the current value of density parameter of viscous DM and decaying vacuum energy. For $E(0) = 1$, we have $\tilde{\Omega}_{m,0}+\tilde{\Omega}_{\Lambda,0} = 1$. The scale factor of expansion can be calculated by using $H = \dot{a}/a$ and integrating Eq. (14), the solution for the scale factor $a(t)$ is given by

$$a(t) = \left(\frac{\tilde{\Omega}_{m,0}}{\tilde{\Omega}_{\Lambda,0}}\right)^{\frac{(1-\nu)}{3[(1-\alpha)(1-\nu)-\zeta_1]}} \left(\sinh^{2/3}\left(\frac{t}{\tilde{t}}\right)\right)^{\frac{(1-\nu)}{(1-\alpha)(1-\nu)-\zeta_1}}, \tag{17}$$

where $\tilde{t} \equiv 2/(3H_0\sqrt{\frac{[(1-\nu)(1-\alpha)-\zeta_1](1-\alpha)(\Omega_\Lambda-\nu)}{(1-\nu)^2}})$. It can be observed from (17) that the scale factor reduces to $a(t) = (\Omega_{m,0}/\Omega_{\Lambda,0})^{1/3}\ \sinh^{2/3}(t/\tilde{t})$ for $\alpha = 0$, $\zeta_1 = 0$ and $\nu = 0$, which is the analytical solution of the scale factor for ΛCDM model. It can be observed from above equation that the scale factor varies as $a \propto t^{\frac{2(1-\nu)}{3[(1-\nu)(1-\alpha)-\zeta_1]}}$ during early times which the power-law expansion of the Universe. For late-time evolution the scale factor varies as $a \propto \exp\sqrt{\frac{(\Omega_\Lambda-\nu)}{3(1-\zeta_1-\nu)}}H_0 t$, which implies the de Sitter Universe.

To investigate the decelerated and accelerated phases of the expansion of the Universe as well as its transition during the evolution, we explore a crucial cosmological parameter, called 'deceleration parameter'. The definition of deceleration parameter q is

$$q = -\frac{\ddot{a}}{a}\frac{1}{H^2} = -\left(1 + \frac{\dot{H}}{H^2}\right). \tag{18}$$

Using (14) into (18), the deceleration parameter q in terms of redshift z is given by

$$q(z) = -1 + \frac{3}{2(1-\nu)} \left(\frac{((1-\alpha)(1-\Omega_\Lambda) - \zeta_1)(1+z)^{3\left(\frac{(1-\nu)(1-\alpha)-\zeta_1}{(1-\nu)}\right)}}{\frac{(\Omega_\Lambda-\nu)(1-\alpha)}{(1-\nu)(1-\alpha)-\zeta_1} + \left(1 - \frac{(\Omega_\Lambda-\nu)(1-\alpha)}{(1-\nu)(1-\alpha)-\zeta_1}\right)(1+z)^{3\left(\frac{(1-\nu)(1-\alpha)-\zeta_1}{(1-\nu)}\right)}}\right) \tag{19}$$

The aforementioned equation demonstrates how the redshift affects the dynamics of q. We note that the value of $q(z)$ approaches -1 in the future (negative redshift). Furthermore, we determine the present value of q for $z = 0$, denoted as (q_0), which is given by

$$q_0 = -1 + \frac{3}{2(1-\nu)}\left[(1-\alpha)(1-\Omega_\Lambda) - \zeta_1\right]. \tag{20}$$

The accelerating and decelerating phase of the Universe can be inferred from the negative and positive signs of the deceleration parameter, respectively. For $q_0 > 0$, the Universe exhibits expanding behaviour and goes through a deceleration phase. For $-1 < q_0 < 0$, represents the current state of the Universe which is the expanding and accelerating Universe.

For the sake of completion, we further calculate effective equation of state parameter w_{eff} as a function of redshift z,

$$w_{eff}(z) = -1 + \frac{1}{(1-\nu)} \left(\frac{((1-\alpha)(1-\Omega_\Lambda) - \zeta_1)(1+z)^{3\left(\frac{(1-\nu)(1-\alpha)-\zeta_1}{(1-\nu)}\right)}}{\frac{(\Omega_\Lambda-\nu)(1-\alpha)}{(1-\nu)(1-\alpha)-\zeta_1} + \left(1 - \frac{(\Omega_\Lambda-\nu)(1-\alpha)}{(1-\nu)(1-\alpha)-\zeta_1}\right)(1+z)^{3\left(\frac{(1-\nu)(1-\alpha)-\zeta_1}{(1-\nu)}\right)}}\right) \tag{21}$$

At $z = 0$, the present value of w_{eff} is determined by

$$w_{eff}(z=0) = -1 + \frac{1}{(1-\nu)}\left[(1-\alpha)(1-\Omega_\Lambda) - \zeta_1\right]. \tag{22}$$

3. Growth of perturbations in interacting model

The presence of cosmological fluctuations influences the background cosmology in which the perturbations evolve. Hence for the complete analysis of our interacting viscous $\Lambda(t)$ model we must take into account the effects on the large scale structure (LSS) formation data, which we incorporate into our observational analysis, in order to fully confront the model. As a result, we must take the matter density perturbations into consideration. Details on this portion of the analysis has been provided in many references (Solà et al., 2018; Gomez-Valent and Solà, 2018). Here, we simply cite the resulting differential equation, which is entirely consistent with the analysis of Singh and Khatri (2024) and references therein. For the interacting viscous $\Lambda(t)$ model, we use the standard perturbations equation for the linear matter density contrast $\delta_m \equiv \delta\rho_m/\rho_m$ as given below:

$$\delta_m'' + \left(\frac{3}{a} + \frac{H'(a)}{H(a)}\right)\delta_m' - \frac{4\pi G\rho_m}{H^2(a)}\frac{\delta_m}{a^2} = 0. \tag{23}$$

Here $()' \equiv d/da$ represents the derivative with respect to the scale factor. The aforementioned approximation to structure formation is sufficient for considering the primary consequences originate from the distinct expression of the Hubble function as compared to the ΛCDM. Thus, the preceding second-order differential Eq. (23) seems to be accurate. We examine the Hubble function (14) as it was determined in Section 2. The smoothness of the matter perturbation in the interacting viscous $\Lambda(t)$ model is described by Eq. (23).

The weighted linear growth, $f(z)\sigma_8(z)$, is typically used to compare the theoretical calculations with the structure formation data in the linear regime. Here, $\sigma_8(z)$ represents the r.m.s. mass fluctuations on $R_8 = 8\ h^{-1}$ Mpc at redshift z and $f(z) = d\ln\delta_m(a)/d\ln(a)$ is the growth factor. The details of the calculation are provided in coming Section 4.3.

4. Data and methodology

In this section, we use a variety of observational data and methodology in order to constrain the model parameters of ΛCDM and interacting viscous Λ(t) models which comprise observations from: (i) Pantheon+ dataset; (ii) Hubble dataset (Cosmic Chronometers); and (iii) $f(z)\sigma_8(z)$ dataset. The following subsections provide an overview of each data set.

4.1. Pantheon+ dataset

We consider an updated Pantheon+ sample (Scolnic et al., 2022) which is the successor of the Pantheon sample. This compilation comprises of 1701 light curves gathered by 1550 type Ia supernovae (SNe), providing detailed information for cosmological analysis. In addition to the most recent SNe sightings, the Pantheon+ collection expands upon earlier SNe compilations and offers a broad range of redshifts ranging from $z = 0.00122$ to 2.2613. The Chi-squared related to the Pantheon+ dataset is given by

$$\chi^2_{Pan+} = \sum_{i=1}^{1701} \vec{D}^T C^{-1}_{Pan+} \vec{D} \tag{24}$$

where $\vec{D} = m_{Bi} - M - \mu_{model}$. Here, m_{Bi} and M are the observed peak magnitude in the rest frame of the B band and absolute B-band magnitude respectively. The theoretical distance modulus μ_{model} is defined by

$$\mu_{model}(z_i) = 5\log_{10}\left(\frac{D_L(z_i)}{1Mpc}\right) + 25, \tag{25}$$

where $D_L(z)$ represents the luminosity distance, that is described by $D_L(z) = (1+z)H_0\int_0^z \frac{dz'}{H(z')}$. In Eq. (24), C denotes the total covariance matrix which takes the form $C = D_{stat} + C_{sys}$, where the diagonal matrix D_{stat} and covariant matrix C_{sys} denote the statistical uncertainties and the systematic uncertainties.

In contrast to the Pantheon dataset, the degeneracy between the absolute magnitude M and H_0 is broken in *Pantheon+*. In order to accomplish this, the vector $\vec{D}$ in Eq. (24) is written in terms of the distance moduli of SNe in Cepheid hosts. As a result, M can have an independent constraint, which leads to the following expression:

$$\vec{D}' = \begin{cases} m_{Bi} - M - \mu_i^{Cepheid} & i \in Cepheid \\ m_{Bi} - M - \mu_{model}(z_i) & Otherwise \end{cases} \tag{26}$$

where $\mu_i^{Cepheid}$ denotes the distance modulus, determined independently using Cepheid calibrators, and corresponds to the Cepheid host of the ith SNe. Hence, we can rewrite Eq. (24) as follows:

$$\chi^2_{Pan+} = \sum_{i=1}^{1701} \vec{D}'^T C^{-1}_{Pan+} \vec{D}' \tag{27}$$

4.2. Cosmic chronometers

The cosmic chronometers (CC) is another observational data obtained through the differential-age method. We can find the Hubble parameter values from CC method at distinct redshifts based on the relative age of passively evolving galaxies. For our analysis, we employ a compilation of 32 data points of the Hubble parameter derived through the differential age technique (Moresco et al., 2022) in the redshift range $0.07 \leq z \leq 1.965$ with errors. The Chi-squared function for CC is given by

$$\chi^2_{CC} = \sum_{i=1}^{32} \frac{[H(z,\theta) - H^{obs}(z_i)]^2}{\sigma^2_{H(z)}} \tag{28}$$

where $H(z)$ represents the theoretical prediction of the Hubble parameter calculated in Eq. (14) and $H^{obs}(z)$ are the observational data with errors $\sigma_{H(z)}$.

4.3. $f(z)\sigma_8(z)$ data

Finally, in this work we use the recent "Gold -17" compilation consisting of 18 independent measurements of $f(z)\sigma_8(z)$. These data points are based on Redshift Space Distortion (RSD) measurements from various observations of the Large Scale Structure (LSS) and complied in Table III of Nesseris et al. (2017).

The linear growth rate of matter perturbations is defined as follows:

$$f(z) = \frac{d\ln\delta_m}{d\ln a} \equiv -(1+z)\frac{\delta'_m(z)}{\delta_m(z)} \tag{29}$$

Here, (') denotes the derivative with respect to redshift. Further, in the linear regime $\sigma_8(z)$ is the redshift-dependent parameter which measures the growth of root-mean-square mass fluctuations in spheres with radius 8 h^{-1} Mpc scales which is given as:

$$\sigma_8(z) = \sigma_8(z=0)\frac{\delta_m(z)}{\delta_m(z=0)} \tag{30}$$

Combining (29) and (30), the weighted linear growth is determined by:

$$f\sigma_8(z) = -(1+z)\frac{\sigma_8(z=0)}{\delta_m(z=0)}\frac{d\delta_m}{dz} \tag{31}$$

The Chi-squared function of $f(z)\sigma_8(z)$ can be calculated as (Quelle and Maroto, 2020):

$$\chi^2_{f(z)\sigma_8(z)} = \sum_{i=1}^{18} \frac{[f\sigma_8(z_i) - (f\sigma_{8,i})_{ob}]^2}{\sigma_i^2} \tag{32}$$

Based on the EMCEE (Foreman-Mackey et al., 2013) python module, we employ the Markov Chain Monte Carlo (MCMC) statistical technique to examine the parameter space of our cosmological models and minimize the χ^2 function for both ΛCDM and interacting viscous $\Lambda(t)$ models. We consider the joint analysis by assuming the sum of all χ^2 functions:

$$\chi^2_{tot} = \chi^2_{Pan+} + \chi^2_{CC} + \chi^2_{f\sigma_8(z)}. \tag{33}$$

To perform this analysis, we choose uniform priors for the parameters of models which is listed in Table 1.

5. Result and discussion

In this section, we present the results of our observational analysis on ΛCDM and interacting viscous $\Lambda(t)$ models, including both the constraints and cosmological parameters from the current data. In the first subsection, we will present the parameters constraints achieved by observational analysis using the data discussed in Section 4. In second subsection, we will implement the Bayesian inference, and in last subsection, we will examine the model comparison through information criterion.

Table 1
Flat prior used on various parameters during statistical analysis.

Parameters	Priors
H_0	[50, 100]
Ω_Λ	(0, 1]
ζ_1	(0, 1]
ν	(0, 1]
α	(−1, 1]
σ_8	[0.6, 1.2]

Table 2
The values of parameters for ΛCDM and interacting viscous $\Lambda(t)$ models for combination of Pantheon+ , Hubble(CC) and $f(z)\sigma_8(z)$ observational datasets.

Parameter	ΛCDM	Interacting viscous $\Lambda(t)$
H_0	$72.100^{+1.7}_{-1.7}$	$72.200^{+1.000}_{-2.000}$
Ω_Λ	$0.688^{+0.029}_{-0.028}$	$0.679^{+0.033}_{-0.034}$
M	$-19.293^{+0.048}_{-0.048}$	$-19.291^{+0.051}_{-0.054}$
ζ_1	–	$0.010^{+0.011}_{-0.010}$
ν	–	$0.005^{+0.005}_{-0.005}$
α	–	$-0.004^{+0.005}_{-0.005}$
σ_8	$0.748^{+0.055}_{-0.055}$	$0.738^{+0.062}_{-0.058}$
S_8	$0.762^{+0.053}_{-0.055}$	$0.762^{+0.055}_{-0.052}$
q_0	$-0.532^{+0.022}_{-0.024}$	$-0.531^{+0.022}_{-0.022}$
z_{tr}	$0.643^{+0.041}_{-0.041}$	$0.648^{+0.042}_{-0.042}$
w_0	$-0.689^{+0.016}_{-0.016}$	$-0.688^{+0.016}_{-0.016}$
$t_0(Gyr)$	$13.74^{+0.019}_{-0.021}$	$13.75^{+0.023}_{-0.021}$

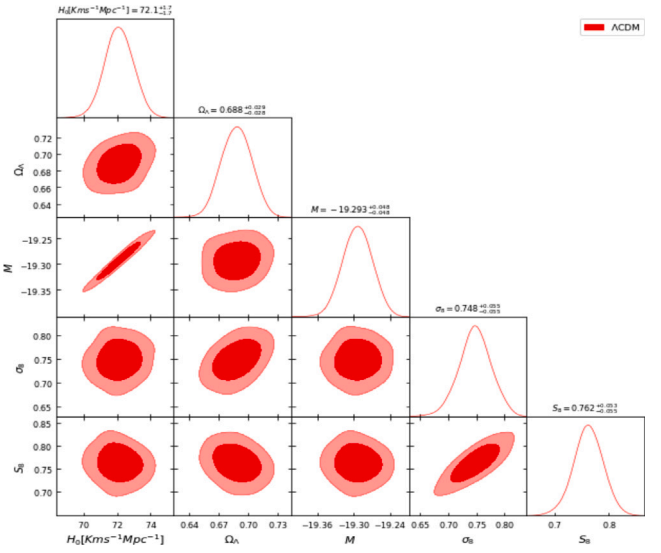

Fig. 1. The one-dimensional marginalized distributions and two-dimensional contour plots of ΛCDM model at 68.3% and 95.4% confidence levels using combined data of *Pantheon+, CC & $f(z)\sigma_8(z)$*.

5.1. Parameter constraints

The best-fit values of parameters of ΛCDM and interacting viscous $\Lambda(t)$ models using a combined $CC + f(z)\sigma_8(z) + Pan+$ data are summarized in Table 2. Figs. 1 and 2 show the 68.3% and 95.4% confidence regions and marginalized likelihood distributions for ΛCDM and interacting viscous $\Lambda(t)$ models, respectively. The GetDist code (Lewis, 2019) is utilized to retrieve their mean values and the aforementioned Figs. 1–2. In what follows we discuss the constraints on different cosmological as well as model parameters.

It is noted that the H_0 determined by Riess et al. (2022) is 73.04 ± 1.04 kms^{-1}Mpc^{-1}, so-called R21 where as Planck Collaboration

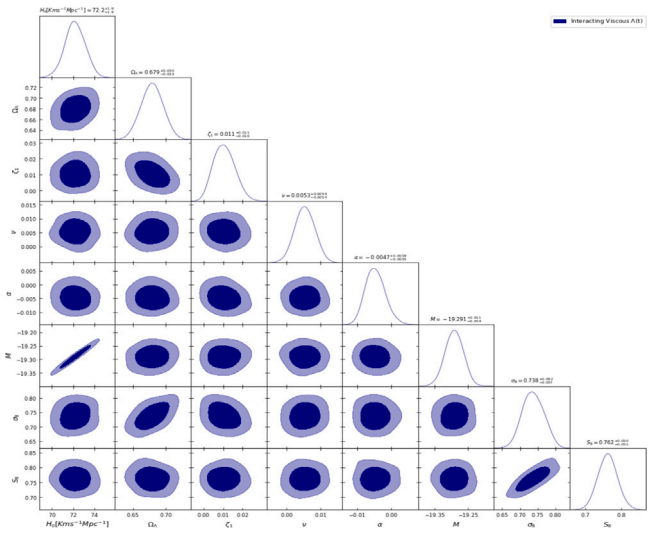

Fig. 2. The one-dimensional marginalized distributions and two-dimensional contour plots of interacting viscous $\Lambda(t)$ model at 68.3% and 95.4% confidence levels using combined data of *Pantheon+*, *CC* & $f(z)\sigma_8(z)$.

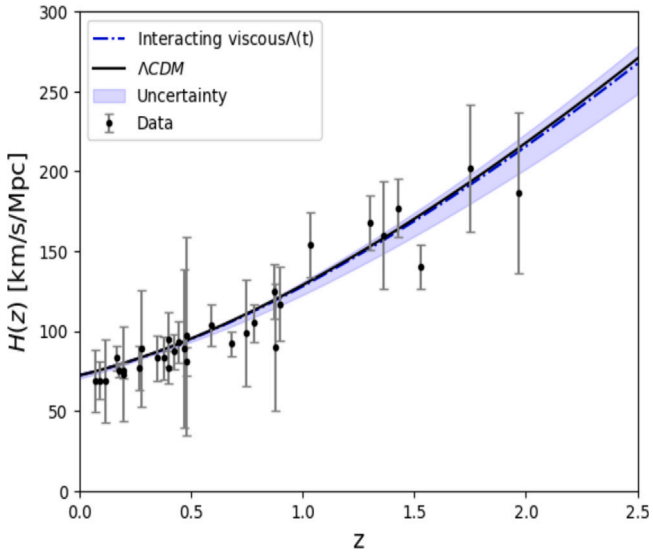

Fig. 3. The evolution of Hubble function $H(z)$ with redshift z. The solid black line corresponds to the ΛCDM model and the dashed blue line corresponds to the interacting viscous $\Lambda(t)$ model. The $H_{obs}(z)$ data are also plotted with their error bars.

(Aghanim et al., 2020) predicts $H_0 = 67.4 \pm 0.5$ kms^{-1}Mpc^{-1} at 5σ confidence level. This discrepancy is recognized as "Hubble tension". For ΛCDM model we obtain $H_0 = 72.100^{+1.7}_{-1.7}$ kms^{-1}Mpc^{-1}. This is in tension with both Planck (Aghanim et al., 2020) and R21 (Riess et al., 2022) results at 2.65σ and 0.47σ respectively. For interacting viscous $\Lambda(t)$ model, we obtain $H_0 = 72.200^{+1.000}_{-2.000}$ kms^{-1}Mpc^{-1} which is tension with both Planck and R21 results at 3.03σ and 0.46σ respectively. In other words, the H_0 measurement of interacting viscous $\Lambda(t)$ model is consistent with R21. The evolutions of $H(z)$ with redshift z are shown in Fig. 3 which predict that the trajectories cover majority of dataset with error bars of $H(z)$. This means that the interacting viscous $\Lambda(t)$ model agrees with the combination of dataset as well as ΛCDM model. In the interacting viscous $\Lambda(t)$ model, we obtain the viscosity coefficient, ζ_1 as $0.011^{+0.011}_{-0.010}$ and ν as $0.005^{+0.005}_{-0.005}$. The coupling parameter of the interaction term, α is calculated as $-0.004^{+0.005}_{-0.005}$. The negative value of α indicates that there is a possibility of the dark matter to decay into the dark energy.

Using the best-fit values, the evolutions of deceleration parameter with redshift for ΛCDM and interacting viscous $\Lambda(t)$ models with errors are plotted in Fig. 4. The trajectories show that the models have transition from decelerating phase to accelerating phase at transition redshift $z_{tr} = 0.643^{+0.041}_{-0.041}$ and $z_{tr} = 0.648^{+0.042}_{-0.042}$, respectively. The present value of deceleration parameter are found to be $q_0 = -0.532^{+0.022}_{-0.024}$ and $q_0 = -0.531^{+0.022}_{-0.022}$. These values of q_0 are within the range of the observational results, i.e., $q_0 = -0.64 \pm 0.12$ (Aghanim et al., 2020). In late time of evolution, $q(z)$ approaches to -1 in both models which is the future de Sitter phase.

In Fig. 5, we plot the effective EoS parameter as a function of redshift for best-fit values of ΛCDM and interacting viscous $\Lambda(t)$ models. It is observed that $w_{\rm eff} \to -1$ in the late-time in both the models, which implies that the models correspond to de Sitter phase in late-time. Using the best-fit, we get the present EoS parameters $w_{\rm eff}(z = 0) = -0.689 \pm 0.016$ and $w_{\rm eff}(z = 0) = -0.688 \pm 0.016$, respectively.

Next, we explore another tension between the theoretical prediction of the growth rate of matter perturbations with the observational growth rate data points for ΛCDM and interacting viscous $\Lambda(t)$ models. For both models the constraints on σ_8 and S_8 are given in Table 2. The amplitude of the matter power spectrum (σ_8) and its associated parameter $S_8 = \sigma_8\sqrt{(1-\Omega_\Lambda)/0.3}$ may be determined using the $f(z)\sigma_8(z)$ dataset and it is further possible to calculate the σ_8/S_8 tension. The combined dataset gives $\sigma_8 = 0.748^{+0.055}_{-0.055}$ and $S_8 = 0.762^{+0.053}_{-0.055}$ in the ΛCDM model and $\sigma_8 = 0.738^{+0.062}_{-0.057}$ and $S_8 = 0.762^{+0.055}_{-0.052}$ in interacting viscous $\Lambda(t)$ model. Our results are perfectly consistent with the combined use of the SDSS and KiDS/Viking data which gives $\sigma_8 = 0.760^{+0.025}_{-0.020}$ and $S_8 = 0.766^{+0.020}_{-0.014}$ (Heymans et al., 2021). It is to be noted that Planck collaboration gives $\sigma_8 = 0.806 \pm 0.005$ and $S_8 = 0.811 \pm 0.011$. Thus, the interacting viscous $\Lambda(t)$ model is in 1.14σ tension in σ_8 and 0.91σ tension in S_8 with the corresponding values of Planck (Aghanim et al., 2020). These tensions are not as large compared to H_0 tension as discussed above. This confirms that the measurement of σ_8 and S_8 using $CC + Pan+$ with $f(z)\sigma_8(z)$ data is fully consistent with ΛCDM. The trajectories of $f(z)\sigma_8(z)$ for ΛCDM and interacting viscous $\Lambda(t)$ models are plotted in Fig. 6. It can be observed that both the models are consistent with the observational data points.

Let us discuss the interacting viscous $\Lambda(t)$ model by defining a dimensionless parameter, known as jerk parameter, j. This parameter is purely kinematical and is associated with the third order derivative of the scale factor $a(t)$. It is defined as $j = \frac{\dddot{a}(t)}{aH^3}$ (Al Mamon and Bamba, 2018). In terms of the deceleration parameter, it can be expressed as follows (Al Mamon and Bamba, 2018):

$$j(z) = q(2q+1) + (1+z)\frac{dq}{dz}. \tag{34}$$

It can provide us the deviation of any model from the ΛCDM model. It is noted that jerk parameter always has constant value $j = 1$ for ΛCDM model. We report $j_0 = 0.992$ in interacting viscous $\Lambda(t)$ model which is quite comparable to the ΛCDM model. We plot the evolution of jerk parameter with respect to the redshift as shown in Fig. 7. We observe that the trajectory of $j(z)$ deviates from ΛCDM in early phase where as it approaches to $j = 1$ as $z \to -1$. Thus, jerk parameter points us the effects of interacting viscous $\Lambda(t)$ model over the ΛCDM model.

5.2. Model selection

In this section, we will discuss mainly reduced Chi-square and model selection criterion to observe the compatibility of the proposed model.

Let us first calculate the reduced Chi-square, χ^2_{red}, which is defined as $\chi^2_{red} = \chi^2_{min}/dof$. Here, dof denotes the degree of freedom which is equal to the number of observational data points (N) minus the number of parameters (K). It is to be noted that we have used $N = 1751$ and $K = 3$ in ΛCDM and $K = 6$ in interacting viscous $\Lambda(t)$ model with same number of data points. Table 4 presents the χ^2 and χ^2_{red} of ΛCDM and

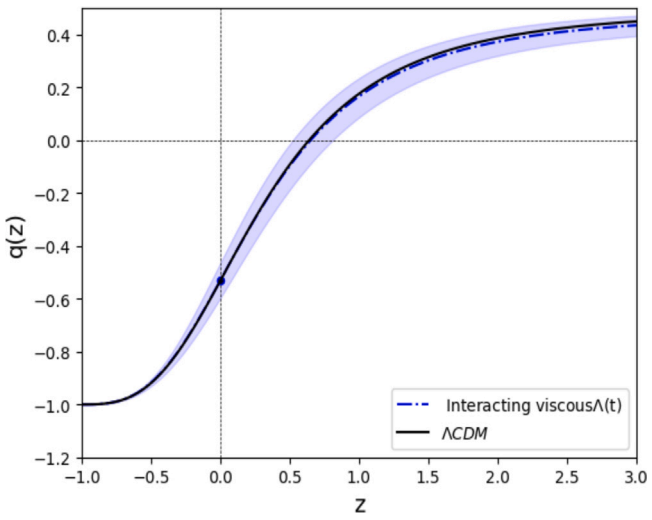

Fig. 4. The evolution of $q(z)$ with redshift z for interacting viscous $\Lambda(t)$ model and ΛCDM model using the best fit values. The present value q_0 is represented by a dot.

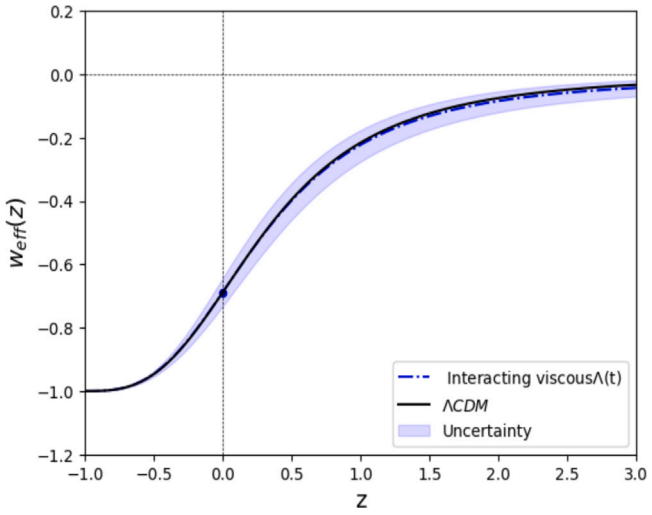

Fig. 5. The evolution of w_{eff} with redshift z for interacting viscous $\Lambda(t)$ model and ΛCDM model using the best fit values. The present value of $w_{eff}(z=0)$ is represented by a dot.

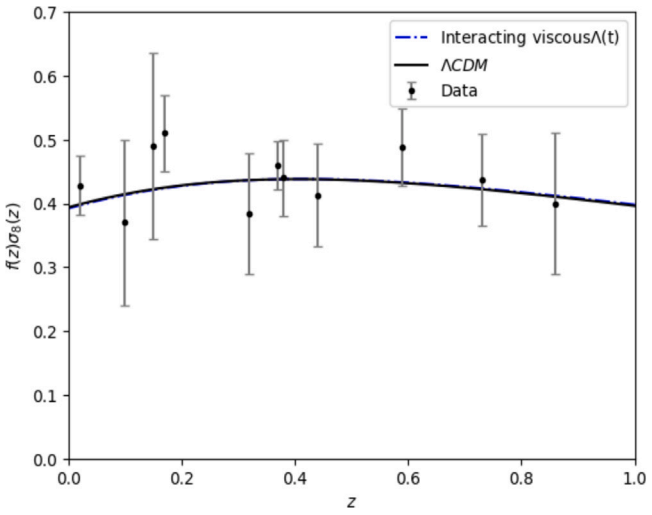

Fig. 6. The evolution of $f(z)\sigma_8(z)$ with redshift z for interacting viscous$\Lambda(t)$ model and ΛCDM model using the best fit values.

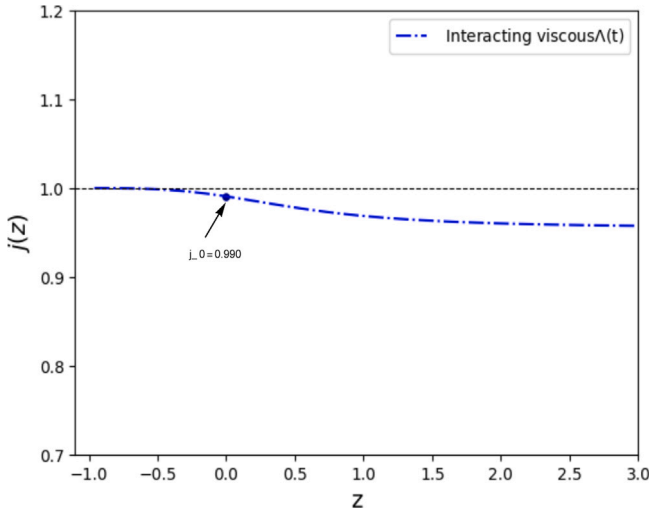

Fig. 7. The evolution of $j(z)$ with redshift z for interacting viscous $\Lambda(t)$ model the best fit values. The present value of $j_0(z=0)$ is represented by a dot and the horizontal line $j=1$ represents ΛCDM model.

interacting viscous $\Lambda(t)$ models, respectively. It is noted that a value $\chi^2_{red} < 1$ gives the best-fit with the data. We observed that both the models have the reduced χ^2 less than unity (for ΛCDM, $\chi^2_{red} = 0.447$ and for interacting viscous $\Lambda(t)$ model, it is $\chi^2_{red} = 0.448$). This shows that both the models are in very good fit with the observational data.

We discuss the another method which provides the statistical comparison of the proposed model with ΛCDM model. In this regard, there are two model selection criterion, namely, Akaike information criteria (AIC) and Bayesian information criteria (BIC). These selection criterion allow to compare models with different degree of freedom. They are defined as (Akaike, 1974; Schwarz, 1978)

$$AIC = \chi^2_{min} + \frac{2KN}{N-K-1}, \qquad BIC = \chi^2_{min} + K \ln N, \tag{35}$$

where N is the size of the data sample and K is the number of free parameters. In these approaches, the model with low values of AIC (BIC) is preferred by data. Considering the AIC (BIC) of ΛCDM model as reference model, denoted as $AIC_\Lambda(BIC_\Lambda)$, we compute $\Delta AIC = AIC_{model} - AIC_{\Lambda CDM}(\Delta BIC = BIC_{model} - BIC_{\Lambda CDM})$.

Following the rules described in Singh and Khatri (2024) and Hernández-Almada et al. (2020), the value $0 \leq \Delta AIC < 2$ indicates "strong evidence in favour" of the proposed model. For $2 \leq \Delta AIC \leq 4$, there is "averagely strong evidence in favour" of model. If $4 < \Delta AIC \leq 7$, then there is "little evidence in favour", whereas for $\Delta AIC > 7$, there is "no evidence in favour" of the proposed model.

Whereas, the value $0 \leq \Delta BIC < 2$ indicates "not enough evidence in favour" of the proposed model. For $2 \leq \Delta < 6$, there is "evidence against" the model, and for $6 \leq \Delta BIC < 10$, we have "strong evidence against" model. If $\Delta BIC \geq 10$ then there is "overwhelmingly strong evidence" against the proposed model, and it is not the best model (Liddle, 2007).

Table 4 displays the values of AIC (BIC) and corresponding ΔAIC (ΔBIC) for interacting viscous $\Lambda(t)$ model. According to our results, we have $\Delta AIC = 6.670$ and $\Delta BIC = 23.039$. This shows that there is "less support in favour" of the interacting viscous $\Lambda(t)$ model as far as AIC is concerned where as BIC gives "strong evidence against" the interacting viscous $\Lambda(t)$ model. This indicates that the evidence against our model is overwhelmingly strong and it is not the best-fit for the data according to BIC. This discrepancy arises because AIC tends to be more inclusive in model selection. Generally, AIC is more lenient with additional parameters, while BIC penalizes them. Thus, AIC limits the number of parameters, making it worthwhile.

Table 3
"Jeffreys' scale" for evaluating the strength of evidence between two comparing models, M_i versus M_j. The right column provides the convention for denoting the different levels of evidence above these thresholds.

$\ln \mathcal{B}_{ij}$	Strength of Evidence
< 1.0	Inconclusive
1.0	Weak evidence
2.5	Moderate evidence
5.0	Strong evidence

Table 4
Summary of $\ln \mathcal{E}$, $\ln \mathcal{B}$, χ^2, χ^2_{red}, AIC and BIC for the ΛCDM and interacting viscous $\Lambda(t)$ models for the following:

Values	ΛCDM	Interacting viscous $\Lambda(t)$
$\ln \mathcal{E}$	-793.120 ± 0.473	-795.697 ± 0.532
$\ln \mathcal{B}$	–	2.577
χ^2	781.708	782.344
K	3	6
N	1751	1751
χ^2_{red}	0.447	0.448
AIC	787.722	794.392
ΔAIC	–	6.670
BIC	804.112	827.152
ΔBIC	–	23.039

5.3. Bayesian inference

The Bayesian evidence serves as the foundation for assessing a model's performance in light of the data. In Bayesian data analysis, the correlation between the data, the model or hypotheses, and the prior knowledge is characterized by the joint probability distributions. Given the observed data, the conditional probability distribution of the unknowns can be used to uniquely infer the posterior distribution using Bayes theorem. The key statistic of Bayesian model selection is the Bayesian evidence $\mathcal{E}$ (Jeffreys, 1961; MacKay, 2003), which is employed in a model comparison problem by integrating the product of likelihood and posterior over the entire parametric space of the model. It is defined as (Liddle et al., 2006; Mukherjee et al., 2006; Liddle, 2007; Trotta, 2007)

$$\mathcal{E}(D|M) = \int_M \mathcal{L}(D|\Theta, M)\mathcal{P}(D|\Theta, M)d\Theta. \tag{36}$$

On the right-hand side, Θ is a set of free parameters for the given data D, M stands for the model, the vertical bar reads as 'given', and $\mathcal{L}$ and $\mathcal{P}$ stand for likelihood and prior probability distribution function of those parameters before the data, respectively.

In cosmology, this concept has been utilized extensively (Santos et al., 2017; Silva and Silva, 2021). When comparing two models, M_i versus M_j, one is interested in the ratio of the models' evidences known as *Bayes factor*, which is given by:

$$\mathcal{B}_{ij} \equiv \frac{\mathcal{E}_i}{\mathcal{E}_j} \tag{37}$$

Here, B_{ij} indicates the support for model i over model j.

Bayes factors are typically interpreted using the Jeffreys' scale (Jeffreys, 1961) which measures the strength of the evidence, given in Table 3. We accomplish this by estimating the values of the logarithm of Bayes factor ($\ln \mathcal{B}$) and the Bayesian evidence ($\ln \mathcal{E}$). Using the dataset and the priors mentioned in Table 1, the values of $\mathcal{E}$ and $\mathcal{B}$ are determined. We assume the ΛCDM as the reference model.

The results for the Bayesian evidence ($\ln \mathcal{E}$) and Bayes factor ($\ln \mathcal{B}$) for both ΛCDM and interacting viscous Λ(t) models examined in this work are summarized in Table 4. We find that the $\ln \mathcal{B}$ for interacting viscous Λ(t) model with respect to the ΛCDM model is obtained as 2.577 and thus the Bayesian evidence analysis shows that our model is "moderately supported" by the considered priors and dataset on Jeffreys' scale.

6. Conclusion

Inspired by dissipative phenomena and decaying vacuum energy, we have discussed some cosmological consequences of an alternative mechanism of accelerating Universe based on a class of interacting viscous model with decaying vacuum energy, referred as interacting viscous $\Lambda(t)$ model. The coupling between viscous fluid and vacuum energy density has been made through a coupling parameter, Q. Within the framework of Eckart thermodynamic theory the non-equilibrium pressure, Π is proportional to the Hubble parameter H with proportionality constant ζ, i.e., $\Pi = -3\zeta(t)H$. Thus, the effective pressure is assumed as sum of barotropic pressure, bulk viscous pressure and pressure due to vacuum energy, i.e., $\bar{p} = p_m + \Pi + p_\Lambda$. In the first part of work, we have obtained some main results for the scale factor, the Hubble parameter, the deceleration parameter, jerk parameter and EoS parameter by assuming the interaction term $Q = 3\alpha\rho_m H$. Although the nature of bulk viscosity and time-varying vacuum energy density are unknown, we have assumed $\zeta = \zeta_1 H$ for bulk viscous coefficient and $\rho_\Lambda = c_0 + 3\nu H^2$ for vacuum energy density. One can expect that the viscosity is affected by the expansion rate of the Universe and varying VED from the general covariance of the effective action in QFT. We have investigated the growth perturbation of interacting viscous $\Lambda(t)$ model. In the second part of this work, we have performed the Bayesian analysis using the latest background probes such as SNe Pantheon+, cosmic chronometer and $f(z)\sigma_8(z)$. We have compared the interacting viscous $\Lambda(t)$ model with ΛCDM using the Bayesian inference and model selection criterion such as AIC and BIC. The results show that the standard ΛCDM model is reproduced in the absence of parameters ζ, α and ν. In what follows, we summarize the main points of our analysis.

The constraints on model free parameters have been reported in Table 2. The best-fit value of H_0 according to a combination of Pantheon+, CC and $f(z)\sigma_8(z)$ is $H_0 = 72.200^{+1.000}_{-2.000}$ kms^{-1}Mpc^{-1}, which is tension with both Planck and R21 results at 3.03σ and 0.46σ, respectively. In other words, the tension in H_0 measurement is almost resolved in interacting viscous $\Lambda(t)$ model with respect to R21. The best fit values of present q and w_{eff} are $q_0 = -0.532^{+0.022}_{-0.024}$ and $w_{\rm eff}(z = 0) = -0.688 \pm 0.016$, respectively. From Fig. 4, it has been observed that the interacting viscous $\Lambda(t)$ model exhibits transition from an early decelerated phase to late-time accelerated phase and the transition takes place at $z_{tr} = 0.648^{+0.042}_{-0.042}$ which is close proximity $z_{tr} = 0.643^{+0.041}_{-0.041}$ to that of ΛCDM model. It has been found that the value of $\chi^2_{red} < 1$ which shows that the interacting viscous $\Lambda(t)$ model is in very good fit with the used data points. The jerk parameter remains positive and less than one in past, and tends to unity in late-time.

We have explored the σ_8 and S_8 parameters for ΛCDM and interacting viscous $\Lambda(t)$ models using the combined data set of Pantheon+, CC and $f(z)\sigma_8(z)$. The constraints on σ_8 and S_8 in interacting viscous $\Lambda(t)$ model are $\sigma_8 = 0.738^{+0.062}_{-0.057}$ and $S_8 = 0.762^{+0.055}_{-0.057}$ which are very close to ΛCDM model as reported in Table 2. The tensions of our fitting results in σ_8 and S_8 with respect to Plank results (Aghanim et al., 2020) are 1.14σ and 0.91σ, respectively. The evolution of $f(z)\sigma_8(z)$ has been plotted in Fig. 6 which shows that it is consistent with the observational data points.

It is noted that cosmological models are testable from the abundance of observational data as discussed above. However, an important distinction must be made between parameter fitting and model selection. As we know that the parameter fitting simply tells us how well a model fit the data. Model selection such as Bayesian inference and AIC and BIC are necessary to discriminate the proposed model with the existing model. The Bayesian inference analysis demonstrated the interacting viscous Λ(t) model is moderately supported by the considered dataset and priors. Further, there has been increasing interest in applying information criterion such as AIC and BIC for model selection. We have

examined the models using AIC and BIC for a fairer comparison. We have observed that the interacting viscous $\Lambda(t)$ model has "less support" according to the selection criteria ΔAIC. On contrary, with respect to ΔBIC, interacting viscous $\Lambda(t)$ model has "strong evidence against" the model with the considered datasets.

As a concluding remark we must point out that despite its intrinsic nature of bulk viscosity and decaying vacuum energy and its interaction are not well understood yet, the work presented in this paper suggests a possible description for resolving the H_0 and σ_8 tensions in cosmology. In principle, to give a robust approach for investigating the dark energy model beyond ΛCDM, background dynamics should be considered. Taking into account such interaction between the dark components may provide an opportunity to explain the present accelerating Universe. Indeed considering the interaction between the viscous fluid and decaying vacuum energy potentially enables us to resolve tensions in cosmological parameters.

CRediT authorship contribution statement

Vinita Khatri: Writing – original draft, Visualization, Software, Investigation, Data curation. **C.P. Singh:** Writing – review & editing, Visualization, Supervision, Methodology, Conceptualization. **Milan Srivastava:** Writing – review & editing, Visualization, Methodology.

Declaration of competing interest

The authors declare that they have no known competing financial interests or personal relationships that could have appeared to influence the work reported in this paper.

Acknowledgements

One of the author, VK would like to express gratitude to Delhi Technological University, India for providing Research Fellowship to carry out this work.

Appendix

The main aim in this appendix is to present some more analytical solutions of the cosmological parameters of the interacting viscous model with decaying vacuum energy density based on the different choices of ζ.

A.1. Solution with $\zeta = \zeta_0$

It is the most simple parametric form of the bulk viscous coefficient. Many authors (Brevik and Gorbunovae, 2005; Hu and Meng, 2006; Avelino and Nucamendi, 2009; Montiel and Breton, 2011) have studied the viscous cosmological models with constant bulk viscous coefficient. Using $\zeta = \zeta_0$ in Eq. (10), the Hubble evolution equation deduces the form

$$\dot{H} + \frac{3}{2}(1-\alpha)H^2 - \frac{3}{2}\frac{\zeta_0 H}{(1-\nu)}H = \frac{1}{2}\left(\frac{1-\alpha}{1-\nu}\right)c_0. \tag{A.1}$$

Solving (A.1) with the condition $H(t_0) = H_0$, we get

$$H = \frac{\zeta_0}{2(1-\nu)(1-\alpha)} + k\coth\left(\frac{3}{2}(1-\alpha)kt\right). \tag{A.2}$$

where $k = \frac{{\zeta_0}^2 + 4(\Omega_\Lambda - \nu)(1-\nu)(1-\alpha)^2 {H_0}^2}{4(1-\nu)^2(1-\alpha)^2}$. Integrating again with the condition $a(t_0) = 1$, we obtain the scale factor

$$a(t) = e^{\frac{\zeta_0}{2(1-\nu)(1-\alpha)}t}\left[\sinh\left(\frac{3}{2}(1-\alpha)kt\right)\right]^{\frac{2}{3(1-\alpha)}}, \tag{A.3}$$

Using (A.2), the deceleration parameter q and Effective EoS parameter w_{eff} are respectively given by

$$q = -1 + \frac{3}{2}\frac{(1-\alpha)k^2\csc^2 h(\frac{3}{2}(1-\alpha)kt)}{\left(\frac{\zeta_0}{2(1-\nu)(1-\alpha)} + k\coth(\frac{3}{2}(1-\alpha)kt)\right)^2}. \tag{A.4}$$

$$w_{eff} = -1 + \frac{(1-\alpha)k^2\csc^2 h(\frac{3}{2}(1-\alpha)kt)}{\left(\frac{\zeta_0}{2(1-\nu)(1-\alpha)} + k\coth(\frac{3}{2}(1-\alpha)kt)\right)^2}. \tag{A.5}$$

A.2. Solution with $\zeta = \zeta_0 + \zeta_1 H$

This form of bulk viscous coefficient has been discussed by several authors and the references therein (Avelino and Nucamendi, 2010). For $\zeta = \zeta_0 + \zeta_1 H$, where ζ_0 and ζ_1 are constants, the Eq. (10) simplifies into

$$\dot{H} + \frac{3}{2}(1-\alpha)H^2 - \frac{3}{2}\frac{\zeta_1 H^2}{(1-\nu)} - \frac{3}{2}\frac{\zeta_0 H}{(1-\nu)} = \frac{1}{2}\left(\frac{1-\alpha}{1-\nu}\right)c_0, \tag{A.6}$$

which can be integrated to calculate the Hubble function and the scale factor

$$H = \frac{\zeta_0}{2((1-\alpha)(1-\nu)-\zeta_1)} + k_1\ \coth\left(\frac{3}{2}\frac{((1-\alpha)(1-\nu)-\zeta_1)}{(1-\nu)}k_1 t\right), \tag{A.7}$$

$$a = e^{\frac{\zeta_0 t}{2((1-\alpha)(1-\nu)-\zeta_1)}} \times \left[\sinh\left(\frac{3}{2}\frac{((1-\alpha)(1-\nu)-\zeta_1)}{1-\nu}k_1 t\right)\right]^{\frac{2(1-\nu)}{3((1-\alpha)(1-\nu)-\zeta_1)}}, \tag{A.8}$$

where $k_1 = \frac{{\zeta_0}^2 + 4((1-\alpha)(1-\nu)-\zeta_1)((\Omega_\Lambda - \nu)(1-\alpha))H_0^2}{4((1-\nu)(1-\alpha)-\zeta_1)^2}$.

With this, we can calculate the deceleration parameter q and effective equation of state parameter w_{eff}, which are respectively given by

$$q = -1 + \frac{3(1-\zeta_1-\nu)\sigma_1^2\csc^2 h(\frac{3}{2}(1-\zeta_1-\nu)\sigma_1 t)}{2\left(\frac{\zeta_0}{2(1-\zeta_1-\nu)} + \sigma_1\coth(\frac{3}{2}(1-\zeta_1-\nu)\sigma_1 t)\right)^2} \tag{A.9}$$

and

$$w_{eff} = -1 + \frac{(1-\zeta_1-\nu)\sigma_1^2\csc^2 h(\frac{3}{2}(1-\zeta_1-\nu)\sigma_1 t)}{\left(\frac{\zeta_0}{2(1-\zeta_1-\nu)} + \sigma_1\coth(\frac{3}{2}(1-\zeta_1-\nu)\sigma_1 t)\right)^2} \tag{A.10}$$

Data availability

Data will be made available on request.

References

Abdalla, E., et al., 2022. J. High Energy Astrophys. 34, 49, arXiv:2203.06142.
Aghanim, N., et al., Planck Collaboration, 2020. Astrophys. Astron. 641, A6, arXiv:1807.06209 [astro-ph.CO].
Akaike, A., 1974. IEEE Trans. Autom. Control 19, 716.
Al Mamon, A., Bamba, K., 2018. Eur. Phys. J. C 78, 862.
Ashoorioon, A., Davari, Z., 2023. Astrophys. J. 959, 120.
Atreya, A., et al., 2018. J. Cosmol. Astropart. Phys. 02, 024.
Avelino, A., 2012. AIP Conf. Proc. 1473, 98.
Avelino, A., Nucamendi, U., 2008. AIP Conf. Proc. 1083, 1.
Avelino, A., Nucamendi, U., 2009. J. Cosmol. Astropart. Phys. 04, 006.
Avelino, A., Nucamendi, U., 2010. J. Cosmol. Astropart. Phys. 08, 009.
Avelino, A., et al., 2008. AIP Conf. Proc. 1026, 300.
Avelino, A., et al., 2013. Phys. Rev. D 88, 123004.
Bamba, K., Odintsov, S.D., 2016. Eur. Phys. J. C 76, 18.
Basilakos, S., 2009. Mon. Not. R. Astron. Soc. 395, 2347.
Basilakos, S., et al., 2009. Phys. Rev. D 80, 083511.
Bertolami, O., 1986. Nuovo Cim. B 93, 36.
Bessada, D., Miranda, O.D., 2013. Phys. Rev. D 88, 083530.
Borges, H.A., Carneiro, S., 2005. Gen. Relativity Gravitation 37, 1385.
Borges, H.A., et al., 2008. Phys. Rev. D 77, 043513.
Brevik, I., 2002. Phys. Rev. D 65, 127302, 2002.
Brevik, I., Gorbunovae, O., 2005. Gen. Relativity Gravitation 37, 2039.
Brevik, I., et al., 2015. Astrophys. Space Sci. 355, 399.
Brevik, I., et al., 2017. Internat. J. Modern Phys. D 26, 1730024, arXiv:1706.02543.
Carneiro, S., et al., 2006. Phys. Rev. D 74, 023532.
Carneiro, S., et al., 2008. Phys. Rev. D 77, 083504.
Carvalho, J.C., et al., 1992. Phys. Rev. D 46, 2404.
Chen, Xi-Ming, Gong, Y., Saridakis, E.N., 2009. J. Cosmol. Astropart. Phys. 04, 001, arXiv:0812.1117.

Chen, Xi-Ming, Gong, Y., Saridakis, E.N., 2014. Internat. J. Theoret. Phys. 53, 469, arXiv:1111.6743.
Copeland, E.J., et al., 2006. Internat. J. Modern Phys. D 15, 1753.
Costa, F.E.M., Alcaniz, J.S., 2010. Phys. Rev. D 81, 043506.
Cruz, N., et al., 2023. Phys. Dark Univ. 42, 101351.
Eckart, C., 1940. Phys. Rev. 58, 267.
Elizalde, E., et al., 2005. Phys. Rev. D 71, 103504.
Fabris, J.C., et al., 2006. Gen. Relativ. Grav. 38, 495.
Foreman-Mackey, D., et al., 2013. PASP 125, 306.
Gariazzo, S., et al., 2022. Phys. Rev. D 106, 023530.
Gomez-Valent, A., Solà, J., 2018. Mon. Not. R. Astron. Soc. 478, 126, arXiv:1801.08501.
Grøn, Ø., 1990. Astrophys. Space Sci. 173, 191.
Harko, T., Lobo, F.S.N., 2013. Phys. Rev. D 87, 044018.
Hernández-Almada, A., 2019. Eur. Phys. J. C 79, 751.
Hernández-Almada, A., García-Aspeitia, M.A., 2018. Internat. J. Modern Phys. D 27, 1850031.
Hernández-Almada, A., et al., 2020. Phys. Rev. D 101, 063516.
Herrera-Zamorano, L., et al., 2020. Eur. Phys. J. C 80, 637.
Heymans, C., et al., 2021. Astron. Astrophys. 646, A140, arXiv:2007.15632 [astro-ph.CO].
Hiscock, W.A., Lindblom, L., 1985. Phys. Rev. D 31, 725.
Hu, J., Hu, H., 2020. Eur. Phys. J. Plus 135, 718.
Hu, M.-G., Meng, X.-H., 2006. Phys. Lett. B 635, 186.
Israel, W., Stewart, J.M., 1976. Phys. Lett. A 58, 213.
Jayadevan, A.P., et al., 2019. Astrophys. Space Sci. 364, 67.
Jeffreys, H., 1961. Theory of Probability. Oxford University Press, Oxford.
Ju-Hua, Chen, et al., 2011. Chin. Phys. Lett. 28, 029801.
Khatri, V., Singh, C.P., 2023. Phys. Dark Univ. 42, 101300.
Kremer, G.M., Sobreiro, O.A.S., 2012. Braz. J. Phys. 42, 77.
Landau, L.D., Lifshitz, E.M., 1987. Fluid Mechanics, vol. 6, Butterworth Heinermann Ltd. Oxford.
Lewis, A., 2019. Getdist: a python package for analysing monte carlo samples. arXiv:1910.13970.
Leyva, Y., Sepúlveda, M., 2017. Eur. Phys. J. C 77, 426.
Liddle, A., 2007. Mon. Not. R. Astron. Soc. 377, L74.
Liddle, A., et al., 2006. Phys. Rev. D 74, 123506.
Lima, J.A.S., Carvalho, J.C., 1994. Gen. Relat. Gravit. 26, 909.
Maartens, R., 1995. Cl. Quantum Grav. 12, 1455.
MacKay, D.J.C., 2003. Information theory, Inference, and Learning Algorithm. Cambridge University Press, Cambridge.
Magaña, J., Matos, T., 2012. J. Phys. Conf. Ser. 378, 012012.
Marcel, A. van der Westhuizen, Abebe, Amare, 2024. J. Cosmol. Astropart. Phys. 01, 048.
Martin, S.P., 1998. Adv. Ser. Dir. High Energy Phys. 18, 1.
Mathews, G.J., et al., 2008. Phys. Rev. D 78, 043525.
Meng, X.H., Dou, X., 2009. Commun. Theor. Phys. (Beijing) 52, 377.
Meng, X.-H., et al., 2007. Commun. Theor. Phys. (Beijing) 47, 379.
Montiel, A., Breton, N., 2011. J. Cosmol. Astropart. Phys. 08, 023.
Moresco, M., et al., 2022. Living Rev. Relativ. 25, 6, arXiv:2201.07241 [astro-ph.CO].
Mostafapoor, N., Grøn, Ø., 2011. Astrophys. Space Sci. 333, 357.
Mukherjee, P., Parkinson, D., Liddle, A., 2006. Astrophys. J. 638, L51.
Müller, I., 1967. Z. Phys. 198, 329.
Murphy, G.L., 1973. Phys. Rev. D 8, 4231.
Nesseris, S., et al., 2017. Phys. Rev. D 96, 023542, arXiv:1703.10538.
Nojiri, S., Odintsov, S.D., 2011. Phys. Rep. 505, 59, arXiv:1011.0544.
Normann, B.D., Brevik, I., 2017. Modern Phys. Lett. A 32, 1750026.
Nunes, R.C., Pan, S., Saridakis, E.N., 2016. Phys. Rev. D 94, 023508.
Overduin, J.M., Cooperstock, F.I., 1998. Phys. Rev. D 58, 043506.
Özer, M., Taha, M.O., 1987. Nuclear Phys. B 287, 776.
Padmanabhan, T., 2003. Phys. Rep. 380, 235.
Padmanabhan, T., Chitre, S.M., 1987. Phys. Lett. A 120, 433.
Pan, S., et al., 2019. Phys. Rev. D 100, 103530, arXiv:1907.07540.
Peebles, P.J.E., Ratra, B., 1988. Astrophys. J. 325, L17.
Peebles, P.J.E., Ratra, B., 2003. Rev. Modern Phys. 75, 559.
Perlmutter, S., et al., 1999. Astrophys. J. 517, 565.
Persic, M., et al., 1996. Mon. Not. R. Astron. Soc. 281, 27.
Pigozzo, C., et al., 2011. J. Cosmol. Astropart. Phys. 08, 022, 2011.
Quelle, A., Maroto, A.L., 2020. Eur. Phys. J. C 80, 369.
Ren, J., Meng, X.-H., 2006. Phys. Lett. B 633, 1.
Riess, A.G., et al., 1998. Astron. J. 116, 1009.
Riess, A.G., et al., 2022. Astrophys. J. Lett. 934, L7, arXiv:2112.04510 [astro-ph.CO].
Sahni, V., Starobinsky, A., 2000. Internat. J. Modern Phys. A 9, 373.
Santos, B., et al., 2017. Phys. Rev. D 95, 123514.
Sasidharan, A., Mathew, T.K., 2015. Eur. Phys. J. C 75, 348.
Schwarz, G., 1978. Ann. Stat. 6, 461.
Scolnic, D., et al., 2022. Astrophys. J. 938 2, 113, arXiv:2112.03863.
Shapiro, I.L., Solà, J., 2002. J. High Energy Phys. 202, 006.
Silva, W.J.C. da, Silva, R., 2021. Eur. Phys. J. C 81, 403.
Singh, C.P., Kaur, S., 2020. Astrophys. Space Sci. 365, 2.
Singh, C.P., Khatri, V., 2024. Phys. Rev. D 109, 023508.
Singh, C.P., Kumar, P., 2014. Eur. Phys. J. C 74, 3070.
Singh, C.P., Kumar, A., 2018a. Eur. Phys. J. Plus 133, 312.
Singh, C.P., Kumar, A., 2018b. Modern Phys. Lett. A 33, 1850225.
Singh, C.P., Kumar, A., 2019. Grav. Cosmol. 25, 58.
Singh, C.P., Solà, J., 2021. Eur. Phys. J. C 81, 960.
Singh, C.P., Srivastava, M., 2018. Eur. Phys. J. C 78, 190.
Singh, C.P., et al., 2007. Cl. Quantum Grav. 24, 455.
Solà, J., 2008. Phys. A: Math. Theor. 41, 164066.
Solà, J., 2013. J. Phys. Conf. Ser. 453, 012015.
Solà, J., Gómez-Valent, A., 2015. Internat. J. Modern Phys. D 24, 1541003.
Solà, J., et al., 2017a. Phys. Lett. B 774, 317.
Solà, J., et al., 2017b. Astrophys. J. 836, 43.
Solà, J., et al., 2018. Mon. Not. R. Astron. Soc. 478, 4357.
Solà, J., et al., 2019. Phys. Dark Univ. 25, 100311.
Solà, J., et al., 2021. Eur. Phys. Lett. 134, 19001.
Trotta, R., 2007. Mon. Not. R. Astron. Soc. 378, 72.
Valentino, E. Di, et al., 2017. Phys. Rev. D 96, 043503.
Valentino, E. Di, et al., 2020. Phys. Dark Univ. 30, 100666.
Wang, P., Meng, X., 2005. Cl. Quantum Grav. 22, 283.
Wang, J.S., Wang, F.Y., 2014. Astron. Astrophys. 564, A137.
Wang, D., et al., 2017. Eur. Phys. J. C 77, 660.
Wang, et al., 2022. Mon. Not. R. Astron. Soc. 514, 1433.
Weinberg, S., 1989. Rev. Modern Phys. 61, 1.
Wilson, J.R., Mathews, G.J., Fuller, G.M., 2007. Phys. Rev. D 75, 043521.
Xin-He, M., Xu, D., 2009. Commun. Theor. Phys. (Beijing) 52, 377.
Yang, W., et al., 2018. J. Cosmol. Astropart. Phys. 09, 019.

Phys. Lett. B 871 (2025) 139994

Contents lists available at ScienceDirect

Physics Letters B

journal homepage: www.elsevier.com/locate/physletb

Letter

Interacting model of bulk viscous and decaying vacuum energy

Vinita Khatri, C. P. Singh *

Department of Applied Mathematics, Delhi Technological University Bawana Road, Delhi, 110042, India

ARTICLE INFO

Editor: P Brax

Keywords:
Cosmology
FLRW model
Bulk viscosity
Dark energy
Observational analysis

ABSTRACT

We discuss the dynamics of interacting viscous model with time-varying cosmological constant, $\Lambda(t)$, which is a natural generalization of the standard Lambda-Cold-Dark matter (ΛCDM) model in Friedmann-Lemaître-Robertson-Walker (FLRW) spacetime. The $\Lambda(t)$ is motivated by different cosmological approaches. Recent investigations involving the renormalization of quantum field theory (QFT) in curved spacetime yield a time-varying Λ, so-called running vacuum model (RVM) in which it acquires a dynamical component through quantum effects. We discuss both the background and perturbation equations for viscous RVM using a more generalized parametrization form of vacuum density. We employ the cosmic data, namely distant Type Ia Supernovae (Pantheon+), Baryonic Acoustic Oscillations DESI, Cosmic Chronometers and growth data. We anchor ΛCDM and viscous RVM on two Hubble constant priors of Planck2018 and SH0ES R22 that reflect the Hubble tension. Using these data samples we assess the viability and compare viscous RVM with the standard ΛCDM model. The Gelman-Rubin statistic (or R-hat statistic) is used to assess the convergence of Markov Chain Monte Carlo (MCMC) simulations. We also discuss the stability of viscous RVM using information criterion such as AIC, BIC and DIC. The constraints on parameters show that the viscous RVM is consistent with the standard ΛCDM model and alleviates the Hubble tension up to 0.569σ.

1. Introduction

Observational data from Type Ia Supernovae (SNeIa) [1,2], Weak Gravitational Lensing [3–5], Baryonic Acoustic Oscillations (BAO) [6–11], and Cosmic Microwave Background (CMB) [12–15] confirm that the Universe is dominated by two dark sectors: dark matter (DM) and dark energy (DE). Dark matter is essential for structure formation. It interacts with the standard model fields solely through gravity. Dark energy is responsible for the acceleration of expanding Universe.

Many cosmological observations indicate that General theory of Relativity (GTR) may not be the only ultimate theory which explains this accelerating phenomena. Therefore, it compels to modify either in matter part or gravitational part of Einstein field equations. The simplest modification is the introduction of cosmological constant(CC), Λ, into the Einstein field equations. A flat Friedmann-Lemaître-Robertson-Walker (FLRW) model with CC-term, known as ΛCDM (Λ plus Cold Dark matter) model of cosmology [16,17], is considered as the most effective model to explain the accelerating expansion of the Universe. However, this model suffers several theoretical and observational difficulties. Some remarkable examples are the cosmological constant problem and the coincidence problem(see, e.g., [18–21] for a review).

Nowadays, Hubble tension is one of the most intriguing problem with ΛCDM, which refers mismatching between the value of the Hubble constant H_0 inferred from early-Universe probes such as Planck CMB data [22] and direct local distance ladder measurements such as Type Ia supernovae and Cepheid variable stars [23–25]. In particular, the Planck collaboration gives $H_0 = 67.4 \pm 0.50\ km\ s^{-1}\ Mpc^{-1}$, while the $SH0ES$ collaboration finds $H_0 = 73.04 \pm 1.04\ km\ s^{-1}\ Mpc^{-1}$, a tension of 4.89σ. Another tension pertains to S_8 parameter, defined as $S_8 \equiv \sigma_8\sqrt{\Omega_m/0.3}$, where Ω_m is the fractional matter density and σ_8 is the variance of matter density field at $8\ Mpc$ scales. This tension refers mismatch in measurements of matter density fluctuations today as inferred from the CMB and galaxy surveys,(see, [26]). Due to these theoretical and observational shortcomings, it is necessary to look beyond the ΛCDM model.

In literature, many other cosmological models have been proposed to provide a conceptual framework for physical interpretation to DE. The most compelling representative for the DE is the CC, Λ which is traditionally connected to vacuum energy density (VED) through $\rho_\Lambda = \Lambda/8\pi G$, where G is the Newton's gravitational constant. In cosmology, the VED is a complex concept that has long challenged to the theoretical physicists and cosmologists, particularly since the introduction of Quantum Field Theory (QFT) and VED is a crucial notion in QFT. Recent developments in QFT suggest that the issues related to vacuum energy and its connection to the Λ-term can be largely resolved. The traditional vacuum energy can potentially align with the data in a more relaxed theoretical setting if the VED is properly renormalized in QFT within curved

* Corresponding author.
E-mail addresses: vinitakhatri_2k20phdam501@dtu.ac.in (V. Khatri), cpsingh@dce.ac.in (C.P. Singh).

https://doi.org/10.1016/j.physletb.2025.139994
Received 20 June 2025; Received in revised form 11 September 2025; Accepted 26 October 2025
Available online 30 October 2025

spacetime [27–29]. In literature, many works [30–49] have shown that a time-evolving Λ (or dynamical DE) could help in alleviating the problems faced by ΛCDM model. Motivated by the perturbation of QFT in a curved classical background, Solá and Gómez-Valent [28], and Moreno-Pulido and Solá [50] proposed a dynamical VED called in the literature 'running vacuum model'(RVM) in which the effective VED appears as an expansion in powers of the Hubble function and its time derivatives, i.e., $\rho_{vac} = \rho_{vac}(H, \dot{H}, \ddot{H}.)$. In RVMs, the dynamical dependency of the VED yields from proper renormalization of quantum effects in QFT in curve spacetime. Thus, the potential dynamics of VED is well motivated from different fundamental perspectives, and therefore, it creates the interest to study the dynamical VED in cosmology. One can find more literature review on RVMs in Refs. [51–59] and therein.

The other dark component is the cold dark matter(CDM) which is commonly described by pressureless fluid and is responsible for structure formation of the Universe. Some recent works [60–64] show that the Hubble tension and S_8 tension can be alleviated by inclusion of viscosity in the dark matter component due to late decoupling from the primordial plasma. The first attempt towards developing a general theory of dissipation in relativistic imperfect fluids was carried out by Eckart [65] and in a somewhat different formulation by Landau and Lifshitz [66]. These theories were further developed by Israel [67] and Israel and Stewart[68]. The possibility of explaining late-time accelerated expansion of the Universe, as an influence of the effective negative pressure due to bulk viscosity in the cosmic fluids, was first studied in [69,70] and since then several authors [71–92] have included bulk viscosity in cosmological models.

The works discussed above show that viscous DM models and a running VED models are capable in alleviating some of the tensions associated with the ΛCDM model. But these theories have separately some physical limitations to describe the entire evolution of the Universe. However, we can anticipate a more comprehensive physical scenario by combining these two theories to overcome the limitations of each individual approach. Such attempts have been carried out in Refs. [93–99]. In reference [100], the authors have shown that the viscous DM in addition to any dynamical DE alleviates H_0 and S_8 tensions.

In the light of aforementioned outlines, the main motivation of the present work is to address whether incorporating viscous DM with dynamical vacuum energy into a flat FLRW framework could provide a completely consistent cosmological evolution. In Ref. [99], the authors have explored the late-time evolution of the Universe through viscous DM and decaying vacuum with particular parametrization of decaying vacuum and bulk viscous coefficient $\zeta = \zeta_1 H$. This paper aims to examine the cosmological evolution by considering a more general parametrization for a running VED along with a simple parametrization of bulk viscous coefficient within Eckart's framework of relativistic non-perfect fluids. As a first step we shall determine the analytical solutions for Hubble function, deceleration parameter and effective equation of state parameter using certain phenomenological assumptions on bulk viscous coefficient and vacuum energy. It is learnt that viscous DM and RVM type of cosmological models can help to improve the best-fit to cosmological observations. Using latest observational data set, such as SNeIa (Pantheon+), BAO (DESI), Cosmic Chronometer (CC) and $f(z)\sigma_8(z)$, we find the best-fit values of parameters to check whether further improvement of the tensions can be attained as compared to ΛCDM model. The Gelman-Rubin statistic (or R-hat statistic) is used to assess the convergence of Markov Chain Monte Carlo (MCMC) simulations. To analyze the stability of our model, we additionally study information criterion such as AIC, BIC and DIC to discuss the stability of the model.

This paper is structured as follows: In Section 2 we introduce the mathematical formalism of bulk viscosity with RVM, evolution equations and motivation for assumptions on bulk viscous DM and running VED. In Section 3 we find the analytical solutions for the Hubble parameter, scale factor, equation of state parameter and deceleration parameter. In Section 4 we analyze the stability of our cosmological model using the scalar perturbation approach. In Section 5, we provide a brief overview of the various observational data used in this work as well as the method employed to constraint the free parameters of the models. We use two datasets: Baseline (SNeIa, CC and BAO(DESI)) and Baseline $+ f(z)\sigma_8(z)$ through out the paper. We also use the priors of Hubble constant of Planck2018 and SH0ES R22 with these datasets. The results are discussed in Section 6. In Section 7 we discuss the convergence diagnostic of Gelman-Rubin for our proposed model. The selection information criteria are presented in Section 8. Finally, the main findings are summarized in Section 9.

2. Viscous running vacuum model

Let us consider a cosmological framework described by the spatially homogeneous and isotropic flat Friedmann-Lemaître-Robertson-Walker (FLRW) metric

$$ds^2 = -dt^2 + a^2(t)\left[dr^2 + r^2(d\theta^2 + sin^2\theta d\phi^2)\right], \tag{1}$$

where $a(t)$ represents the scale factor as a function of cosmic time t and (r, θ, ϕ) are the co-moving coordinates.

As we know that the simplest explanation for the current observations is the unclumped form of energy density corresponds to positive Λ whose presence modifies the Einstein field equations to

$$G_{\mu\nu} = 8\pi G T_{\mu\nu} + \Lambda g_{\mu\nu}, \tag{2}$$

where $G_{\mu\nu} = R_{\mu\nu} - \frac{1}{2}g_{\mu\nu}R$ is the Einstein tensor, $T_{\mu\nu}$ is the energy-momentum tensor of viscous matter fields. Here and thereafter, we work in units where $8\pi G = c = 1$).

We consider the presence of two cosmic fluids: running VED and viscous DM. The first fluid represents a vacuum energy density described from the renormalization of QFT in curve spacetime which depends on the Hubble parameter and its time derivatives, $\rho_{vac} = \rho_{vac}(H, \dot{H})$. The energy-momentum tensor for the vacuum energy can be assumed to have the same form as $T_{\mu\nu}$, that is,

$$T^{vac}_{\mu\nu} = (\rho_{vac} + p_{vac})u_\mu u_\nu + g_{\mu\nu}p_{vac} \tag{3}$$

where ρ_{vac} and p_{vac} are the energy density and pressure, respectively for vacuum energy. For vacuum energy density we have $p_{vac} = -\rho_{vac}$.

As a second fluid, we assume the imperfect fluid characterized by bulk viscous coefficient as a part of pressureless cold dark matter. The energy-momentum tensor, $T_{\mu\nu}$, for such a viscous fluid modifies to [101]

$$T_{\mu\nu} = (\rho_m + P)u_\mu u_\nu + g_{\mu\nu}P, \tag{4}$$

where ρ_m denotes the matter density of the fluid and μ^μ is the associated fluid's four-velocity. It can be seen that the above Eq. (4), that the energy-momentum tensor resembles to that of a perfect however with an equivalent pressure $P = p_m + \Pi$, i.e, the sum of barotropic pressure of the matter fluid p_m and the viscous pressure Π. However, in this paper we assume pressureless viscous DM where $p_m = 0$ and the only pressure is bulk viscous, Π. In general, it is assumed that the bulk viscosity arises from deviation of the local thermodynamic equilibrium in any system. In thermodynamics as per the second law, the re-establishment of thermal equilibrium is a dissipative process resulting in entropy. As a consequence of this entropy generation, the bulk viscous term in the system expands.

The bulk viscosity is a characteristic of the viscous fluid in homogeneous and isotropic cosmological models. The majority of its foundation comes from Eckart's formalism [65] in the limit of vanishing relaxation time, which is derived from Israel and Stewart's [67] second order theory of non-equilibrium thermodynamics. The viscous pressure is characterized by $\Pi = -3\zeta H$, where H is the Hubble parameter and ζ is the bulk viscous coefficient that adheres the second law of the thermodynamics given that, $\zeta > 0$. As a result, it causes the effective pressure to be negative, which modifies the ideal fluid's energy-momentum tensor.

In our study, we combine these two components in a single cosmological scenario and explore their cosmological implications. Using the above framework, the Einstein's field Eq. (2) yield

$$3H^2 = \rho = \rho_m + \rho_{vac}, \tag{5}$$

$$2\dot{H} + 3H^2 = -p = 3\zeta H + \rho_{vac}, \tag{6}$$

where $H = \dot{a}/a$ is the Hubble parameter representing the rate at which the universe is expanding. As usual, the dot sign denotes derivative with respect to the cosmic time. In this work, we present a theory of the universe's evolution based on time varying vacuum energy density. From (2), the Bianchi identity imply that the coupling between vacuum energy and viscous CDM fluid must be of the type

$$u_\mu T^{\mu\nu}_{;\nu} = -u^\mu(\Lambda g^{\mu\nu})_{;\nu}, \tag{7}$$

or, equivalently,

$$\dot{\rho}_m + 3H(\rho_m - 3\zeta H) = -\dot{\rho}_{vac}, \tag{8}$$

This suggest that viscous CDM and varying Λ term are coupled. As a result, there is certain energy exchange amongst vacuum and the viscous CDM fluid. From Eqs. (5) and (8) together, the evolution equation for Hubble parameter is given by

$$\dot{H} + \frac{3}{2}H^2 = \frac{1}{2}\rho_{vac} + \frac{3}{2}\zeta H. \tag{9}$$

3. Solution of field equations

There are three independent unknown quantities, namely, H, ρ_{vac} and ζ in the evolution Eq. (9). One can obtain the solution only when both ρ_{vac} and ζ are defined. As previously mentioned, we shall consider the framework of FLRW spacetime in our study. Within the running vacuum model (RVM), the generic low-energy form of the vacuum energy density (VED) has been phenomenologically investigated on several prior times and with an impressive level of success. Moreover, it has consistently shown to be very competitive with the ΛCDM and even capable of outperforming the latter's fitting performance. In this work, we examine to what extent a viscous dark matter plus running vacuum framework is consistent with current cosmological data to describe the late-time expansion of the Universe. Motivated by the explicit QFT calculations on a FLRW background, the VED in the RVM takes following form [50,102]

$$\rho_{vac} = 3\left[c_0 + \frac{2}{3}\mu\dot{H}(z) + \nu H^2(z)\right], \tag{10}$$

where μ and ν are dimensionless parameters and expect that the values of these parameters should be less than one. The value of the additive constant c_0 is fixed by the boundary condition $\rho_{vac}(H_0) = \rho_{vac0}$ and the two evolving components, H^2 and $\dot{H}$ are independent and dimensionally homogeneous. Notice that in above Eq. (10), the parameter μ has an explicit factor $2/3$ for convenience. Additionally, for $\mu, \nu \to 0$, the model smoothly reduce to the concordance ΛCDM.

In literature various methods have been proposed for assuming the evolution of bulk viscosity and different viscous models are produced depending on the choice of ζ. In this work, we examine the bulk viscous term ζ is proportional to the Hubble parameter $H = \dot{a}/a$, i.e, to the expansion rate of the universe which can be expressed as [76,84,96,103–105]:

$$\zeta = \zeta_1 H. \tag{11}$$

Using (10) and (11), the evolution Eq. (9) has in the following form.

$$(1-\mu)\dot{H} + \frac{3}{2}(1-\nu-\zeta_1)H^2 = \frac{3}{2}c_0. \tag{12}$$

We can find the additive constant $c_0 = H_0^2[\Omega_{vac} - \nu + \mu(1-\Omega_{vac} - \zeta_1)]$, where $\Omega_{i,0} = \rho_{i,0}/\rho_{cr,0}$ with $\rho_{cr,0} = 3H_0^2/8\pi G$ is the current critical density at $a = 1$. Now, Eq. (12) immediately gives the Hubble function as

$$H^2(z) = H_0^2\left(\tilde{\Omega}_{vac,0} + \tilde{\Omega}_{m,0}(1+z)^{3\left(\frac{1-\nu-\zeta_1}{1-\mu}\right)}\right), \tag{13}$$

where

$$\tilde{\Omega}_{vac,0} = \frac{(\Omega_{vac} - \nu) + \mu(1-\Omega_{vac} - \zeta_1)}{(1-\nu-\zeta_1)}, \tag{14}$$

and

$$\tilde{\Omega}_{m,0} = 1 - \frac{(\Omega_{vac} - \nu) + \mu(1-\Omega_{vac} - \zeta_1)}{(1-\nu-\zeta_1)} = 1 - \tilde{\Omega}_{vac,0}. \tag{15}$$

Solving the above Eq. (13), we can find the evolution of various cosmological parameters of our model. Given the multiplicity of particles in Grand Unified Theory (GUT), the theoretical value of ν must be below 1. In the calculations carried out in [50], the coefficients μ, ν are expected to be of order $\approx M_X^2/m_{Pl}^2 << 1$, being M_X of order of a typical GUT scale. An estimate of ν in QFT indicates that it is of order 10^{-3} at most [106]. Here, we consider the fact that μ must be small and positive (i.e $0 < \mu << 1$) since the term $(1/1+z)^{3\left(\frac{1-\nu-\zeta_1}{1-\mu}\right)} \to 0$ for virtually any $(1/1+z) < 1$. Further ν can have any sign with $|\nu| << 1$.

By utilizing $H = \dot{a}/a$ and integrating the Eq. (13), one may determine the scale factor which is given by

$$a(t) = \left(\frac{\tilde{\Omega}_{m,0}}{\tilde{\Omega}_{vac,0}}\right)^{\frac{(1-\mu)}{3(1-\nu-\zeta_1)}} \left(\sinh^{2/3}\left(\frac{t}{\tilde{t}}\right)\right)^{\frac{(1-\mu)}{(1-\nu-\zeta_1)}}, \tag{16}$$

where $\tilde{t} \equiv 2/(3H_0\sqrt{\frac{(1-\nu-\zeta_1)[(\Omega_{vac}-\nu)+\mu(1-\Omega_{vac}-\zeta_1)]}{(1-\mu)^2}})$. It is evident from the above Eq. (16) that for $\nu = 0$, $\mu = 0$ and $\zeta_1 = 0$, the scale factor reduces to the ΛCDM model, i.e. $a(t) = (\Omega_{m0}/\Omega_{vac0})^{1/3}\ \sinh^{2/3}(t/\tilde{t})$. The above equation shows that the scale factor varies as $a \propto t^{\frac{2(1-\mu)}{3(1-\nu-\zeta_1)}}$ during early Universe expansion, which is power-law expansion. Further, the scale factor varies as $a \propto \exp\sqrt{\frac{(\Omega_{vac}-\nu)+\mu(1-\Omega_{vac}-\zeta_1)}{3(1-\zeta_1-\nu)}}H_0 t$ for late-time evolution, which implies the de Sitter universe. It follows that the model expands with deceleration in the early stages followed by acceleration in the later stages.

In order to investigate the decelerated and accelerated phases of the expansion of the Universe and the evolution during this time, we examine a crucial cosmological parameter, known as the 'deceleration parameter' q, which is defined as

$$q = -\left(1 + \frac{\dot{H}}{H^2}\right) = \frac{(1+z)}{E}\frac{dE}{dz} - 1 \tag{17}$$

where $E \equiv H(z)/H_0$ represents the dimensionless Hubble parameter. The positive value, $q > 0$ indicates a deceleration in the expansion of the Universe. At $q = 0$, the expansion of the Universe remains constant. When $-1 < q < 0$, it represents an accelerating Universe. It is to be noted that $q = -1$ signifies the exponential expansion, recognized as de Sitter expansion. Additionally, for $q < -1$, the Universe expands super-exponentially.

Using (13) into (17), the value of deceleration parameter q in terms of redshift is calculated as

$$q(z) = -1 + \frac{3}{2(1-\mu)} \times \left[\frac{(1-\nu-\zeta_1) - [(\Omega_{vac}-\nu)+\mu(1-\Omega_{vac}-\zeta_1)](1+z)^{3\left(\frac{1-\nu-\zeta_1}{1-\mu}\right)}}{\left[\frac{(\Omega_{vac}-\nu)+\mu(1-\Omega_{vac}-\zeta_1)}{(1-\nu-\zeta_1)} + \left(1 - \frac{(\Omega_{vac}-\nu)+\mu(1-\Omega_{vac}-\zeta_1)}{(1-\nu-\zeta_1)}\right)(1+z)^{3\left(\frac{1-\nu-\zeta_1}{1-\mu}\right)}\right]}\right].$$

Moreover, we compute q_0, the current value of q at $z = 0$, which is obtained as

$$q_0 = -1 + \frac{3}{2(1-\mu)}\left[(1-\zeta_1-\Omega_{vac}) + \mu(1-\Omega_{vac}-\zeta_1)\right]. \tag{18}$$

In order to help us better understand the accelerated phase, we consider another parameter, called as the equation of state (EoS) parameter w_{eff}, that is described as $w_{eff} = -1 - \frac{1}{3}\frac{d\ln h^2}{dx}$, where $x = \ln a$ and $h = H/H_0$ is the dimensionless parameter. Using (13), we obtain

$$w_{eff}(z) = -1 + \frac{1}{(1-\mu)} \times \left[\frac{(1-\nu-\zeta_1) - [(\Omega_{vac}-\nu)+\mu(1-\Omega_{vac}-\zeta_1)](1+z)^{3\left(\frac{1-\nu-\zeta_1}{1-\mu}\right)}}{\left[\frac{(\Omega_{vac}-\nu)+\mu(1-\Omega_{vac}-\zeta_1)}{(1-\nu-\zeta_1)} + \left(1 - \frac{(\Omega_{vac}-\nu)+\mu(1-\Omega_{vac}-\zeta_1)}{(1-\nu-\zeta_1)}\right)(1+z)^{3\left(\frac{1-\nu-\zeta_1}{1-\mu}\right)}\right]}\right].$$

Further, we compute the present value of $w_{eff}(z=0)$ which is determined as

$$w_{eff}(z=0) = -1 + \frac{1}{(1-\mu)}\left[(1-\zeta_1-\Omega_{vac}) + \mu(1-\Omega_{vac}-\zeta_1)\right]. \quad (19)$$

4. Growth of perturbations

The LSS observable $f(z)\sigma_8(z)$, which is primarily determined by Redshift Space Distortion measurements, plays a crucial role in understanding the formation of structures in the universe. In this section, we want to discuss a few points that will enable us to quickly review why improving the description of structure can also benefit our model in contrast to GR. In terms of the linear density contrast between the matter perturbations, $\delta_m = \delta\rho_m/\rho_m$, the precise differential equation is expressed as

$$\delta_m'' + \left(\frac{3}{a} + \frac{H'(a)}{H(a)}\right)\delta_m' - \frac{3}{2}\Omega_m(a)\frac{\delta_m}{a^2} = 0, \quad (20)$$

where the primes denote the derivative with respect to the scale factor. The $\Omega_m(a)$ can be derived from $\Omega_m(a) = 1 - \Omega_{vac}(a)$ where

$$\Omega_{vac}(a) = \nu + \frac{1}{H^2(a)}\left[H_0^2\left\{\left(\Omega_{vac}(a=1)-\nu\right)\right. \quad (21)$$

$$\left. + \mu\left(1-\Omega_{vac}(a=1)-\zeta_1\right)\right\} + \frac{2}{3}\mu a H(a)H'(a)\Big]. \quad (22)$$

The above equation utilizes the Hubble function that corresponds to the model under consideration. Due to the different Hubble function expression in each model, the above approximation for the structure formation equation is accurate.

In Ref. [99], Eq. (20) turns to be a very good approximation for the analysis of the matter perturbations and thus for present analysis, Eq. (20) is adequate. Details on this aspect of the analysis have been provided in numerous references [107,108]. Furthermore, in these references the impact is evaluated in considerable detail and the model's ability to reduce S_8 tension is predicated using the same fundamental process. Here, we shall utilize the Hubble function determined in Section-3, Eq. (13) to perform our analysis of the matter perturbation in Viscous RVM. The linear LSS regime's investigation is conveniently implemented using the weighted linear growth $f(z)\sigma_8(z)$, where $f(z)$ is the growth factor and is described by $f(z) = d\ln\delta_m/d\ln a$. Here, $\sigma_8(z)$ is the RMS mass fluctuation in spheres with radius $8h^{-1}$ Mpc scales. The calculation specifics are given in the upcoming Section 5.4.

5. Dataset and methodology

This section briefly describes the observational datasets and the statistical analysis methodology. We use following diverse array of observational datasets, which include latest Pantheon+ obtained from observations of Type Ia Supernovae (SNeIa), cosmic chronometer (CC), Baryonic Acoustic Oscillations (BAO) and $f(z)\sigma_8(z)$ to perform the statistical inference. We also consider two independent Hubble constant measurements that lead to the Hubble tensions [22,25].

5.1. SNeIa dataset:Pantheon+

The Pantheon+ analysis extends the Pantheon dataset by including Cepheid distance measurements to galaxies in the extended dataset of SNeIa. We use Pantheon+ SNeIa compilation [109–111] which includes the apparent magnitudes and redshifts corresponding to 1701 light curves in the redshift range $0.001 \le z \le 2.2613$ that were collected from 1550 SNeIa. Interestingly, the new Pantheon+ compilation incorporates redshifts lower than $z < 0.01$, in contrast to the Pantheon study.

More precisely, the distance modulus $u(z_i,\theta)$ of an object is defined as the difference between observed apparent magnitude, m and its absolute magnitude, M. At redshift z_i, the distance modulus is given as

$$u(z_i,\theta) = 5\log_{10}\left(\frac{D_L(z_i,\theta)}{1Mpc}\right) + 25, \quad (23)$$

where $D_L(z_i,\theta)$ represents the luminosity distance in Mpc, which is model-based and can be obtained by

$$D_L(z_i,\theta) = c(1+z_i)\int_0^z \frac{dz'}{H(z',\theta)}. \quad (24)$$

Furthermore, each SNeIa's apparent magnitude must be calibrated using an arbitrary fiducial absolute magnitude M. Consequently, we may consider M as a nuisance parameter in the MCMC analysis by marginalizing over it. The next step involves constraining the cosmological parameters by minimizing χ^2 probability given by [112]

$$\chi^2_{SNeIa} = \vec{D}^T C^{-1}_{Pantheon+}\vec{D}. \quad (25)$$

In this case, $\vec{D} = m - M - u(z_i,\theta)$, and C is the corresponding covariance matrix that takes into account the systematic and statistical uncertainty.

In contrast to the Pantheon dataset, the degeneracy between the H_0 and the absolute magnitude M is broken by redefining the $\vec{D}$ in Eq. (25) in terms of the distance moduli of SNeIa in Cepheid hosts. This permits M to be an independent constraint, resulting to the following expression:

$$\vec{D}' = \begin{cases} m - M - \mu_i^{Ceph} & i \in Cepheid \\ m - M - \mu_{model}(z_i) & Otherwise \end{cases} \quad (26)$$

where u_i^{Ceph} is the distance modulus which corresponds to the Cepheid host, and are independently determined through Cepheid calibrators. Eq. (25) can therefore be rewritten as follows:

$$\chi^2_{SNeIa} = \vec{D'}^T C^{-1}_{Pantheon+}\vec{D}'. \quad (27)$$

5.2. H(z) dataset: CC

Massive, slowly evolving galaxies with old stellar populations and minimal star formation rates can serve as cosmic chronometers (CC) by implementing the differential age technique. The CC approach is an excellent method for discovering the expansion history of the Universe. Depending on the basis of the relative age of passively evolving galaxies, we employ the most recent estimates of 32 CC data points, precise estimates, and model-independent data in the redshift region $0.07 < z < 1.965$. The whole set of data points together with the relevant references are compiled by [59] in Table 2, where the correlations between the data points are indicated by a *. We have taken into account the impact of the established correlations between the different data points as described in [113]. In the present work, the χ^2_{CC} function takes the following form

$$\chi^2_{CC} = \left(H_i - H_{model}(z_i)\right)^T C^{-1}_{ij}\left(H_j - H_{model}(z_j)\right), \quad (28)$$

where $(H - H_{model}(z))$ represents the difference vector between the measured values and the model predictions of the Hubble parameter, and C^{-1}_{ij} is the inverse covariance matrix of the data. The computation of full covariance matrix for cosmic chronometers has been described in Ref. [113].

5.3. BAO dataset

Another important piece of data is Baryonic Acoustic Oscillations (BAO). We use the most recent 13 BAO measurements from DESI DR2 including the BGS, LRG1, LRG2, LRG3+ELG1, ELG2, QSO and Lyα samples at effective redshifts $z_{eff} = 0.295, 0.51, 0.706, 0.934, 1.321, 1.484$ and 2.33, respectively. We use the Dark Energy Spectroscopic Instrument (DESI) BAO measurements from the Data Release 2 [114].

The BAO measurements depend on the sound horizon at the drag epoch r_d which is given by [115]

$$r_d = \int_{z_d}^{\infty} \frac{c_s(z)}{H(z)} dz, \tag{29}$$

where $z_d \simeq 1060$ is the redshift at baryon drag epoch and c_s is the speed of sound prior to recombination. The traverse comoving distance is defined as

$$D_M(z) = \int_0^z \frac{c}{H(z')} dz' \tag{30}$$

and the distance variable is represented by $D_H(z) = c/H(z)$. Further, the angle-average distance $D_V(z)$ which quantifies the average of the distances measured along, and perpendicular to the line of sight to the observer is given by the relation

$$D_V(z) = \left(z D_M(z)^2 D_H(z)\right)^{1/3}. \tag{31}$$

The BAO statistics can be implemented by using D_M/r_d, D_H/r_d and D_V/r_d and the covariance matrix. We can estimate the chi-squared function for BAO measurements as

$$\chi^2_{BAO} = \Delta Y C^{-1}_{BAO} \Delta Y \tag{32}$$

where C^{-1}_{BAO} is the inverse of the covariance matrix for BAO dataset [116, 117] and Y is taken as D_M/r_d, D_H/r_d, and D_V/r_d. Here Δ represents the difference between observed and model values.

5.4. $f(z)\sigma_8(z)$ dataset

The $f(z)\sigma_8(z)$ structure formation data are crucial in diagnosing dark energy. In this study, we utilize the recent compilation of "Gold-17" data which consists of 18 independent measurements of $f(z)\sigma_8(z)$. These data points are compiled in Table 3 of Ref. [118] and are essentially determined from RSD measurements from many observations of the Large Scale Structure (LSS). The current galaxy surveys grant observational data for the combination $f\sigma_8$ where f is the linear growth rate of the density contrast and σ_8 is the root mean square mass fluctuation in spheres. Within the linear framework, they are given by [119]

$$\sigma_8(z) = \frac{\delta_m(z)}{\delta_m(z=0)} \sigma_8(z=0) \tag{33}$$

and

$$f\sigma_8(z) = -(1+z)\frac{\sigma_8(z=0)}{\delta_m(z=0)} \frac{d\delta_m}{dz} \tag{34}$$

The corresponding chi-square function of $f(z)\sigma_8(z)$ can be computed as [120]:

$$\chi^2_{f(z)\sigma_8(z)} = \sum_{i=1}^{18} \frac{[f\sigma_8(z_i) - (f\sigma_{8,i})_{ob}]^2}{\sigma_i^2} \tag{35}$$

5.5. Hubble constant measurements

In the background of the Hubble tension, we use the Hubble constant estimated by the Planck ($H_0^{P18} = 67.4 \pm 0.5\ kms^{-1}Mpc^{-1}$ [22]) collaborations and the SH0ES ($H_0^{R22} = 73.04 \pm 1.04\ kms^{-1}Mpc^{-1}$ [25]). We take these values as priors in the parameter space of ΛCDM and viscous RVM models.

Statistical analysis is performed using MontePython code *emcee* [121] of Python library. In this code, Markov Chain Monte Carlo (MCMC) method [122] is used to perform the statistical analysis on the input data to constrain the parameters of the viscous RVM. As a comparison, we perform a similar MCMC for the ΛCDM model, also based on the same likelihood. The following combinations are employed for our study:

- **Baseline**: It consists of combination of 3 datasets, namely $SNe\ Ia + CC + BAO$ and the joint χ^2 function is $\chi^2_{Baseline} = \chi^2_{SNe\ Ia} + \chi^2_{CC} + \chi^2_{BAO}$.
- **Baseline $+ f(z)\sigma_8(z)$**: In this combination, Baseline dataset is complemented $f\sigma_8$, where $\chi^2_{Baseline+f\sigma_8} = \chi^2_{SNe\ Ia} + \chi^2_{CC} + \chi^2_{BAO} + \chi^2_{f\sigma_8}$.

In the next section, we use MCMC sampling technique and the *emcee* library together with the above two splices of full data to see how the results are affected by minimising their respective χ^2 values, that correspond to the likelihood by $\mathcal{L} \propto \exp\left(-\frac{\chi^2}{2}\right)$. We built two competing models with each datasets by taking into account the Planck and SH0ES measurements of the Hubble constant as independent priors, while the rest of the cosmological parameters take the initial flat priors. We refer to the models as $P18$ (with the prior H_0^{18}) and $R22$ (with the prior H_0^{22}) for simplicity.

6. Results

Let us explore the evolution of the primary cosmological parameters for the best-fit values of the parameters derived from Baseline and Baseline + $f(z)\sigma_8(z)$ datasets with $P18$ and $R22$ priors, rspectively. Tables 1 and 2 show the constraints on full and subsets of the data, respectively for ΛCDM and viscous RVM models. These results are obtained with a reasonable Gelman-Rubin convergence criterion of $R - 1 = 10^{-2}$, which has been discuss in Section 7. Figs. 1 and 2 depict the $1-\sigma$ and $2-\sigma$ contour plots of ΛCDM and viscous RVM from Baseline and Baseline + $f(z)\sigma_8(z)$ datasets with $P18$ and $R22$, respectively.

As we know that the one of the key cosmological parameter in cosmology is current value of the Hubble parameter. Recent observations have revealed differences in the Hubble constant H_0 between Planck CMB data [22] and SH0ES-calibrated SNe [25]. This discrepancy is described as "Hubble tension" which is one of the most lingering tensions in cosmology. Note that the Planck Collaboration [22] predicts $H_0^{P18} = 67.4 \pm 0.5\ kms^{-1}Mpc^{-1}$, while Riess et al. [25] estimates a higher value of $H_0^{R22} = 73.04 \pm 1.04\ kms^{-1}Mpc^{-1}$. This leads to a tension at the level of 4.89σ. Tables 1 and 2 demonstrate that the present value of H_0 for the viscous RVM are $H_0^{P18} = 67.403 \pm 0.49\ kms^{-1}Mpc^{-1}$ and $H_0^{R22} = 72.212 \pm 1.0\ kms^{-1}Mpc^{-1}$ from Baseline, respectively, which has 4.318σ level of tension. In contrast, H_0 obtained for ΛCDM model are $H_0^{P18} = 67.410 \pm 0.49\ kms^{-1}Mpc^{-1}$ and $H_0^{R22} = 72.776 \pm 0.99\ kms^{-1}Mpc^{-1}$, respectively with Baseline, respectively. This leads to a tension at the level of 4.857σ.

Similarly, we have reported the present H_0 for the proposed viscous RVM as $H_0^{P18} = 67.416 \pm 0.48\ kms^{-1}Mpc^{-1}$ and $H_0^{R22} = 72.212 \pm 1.0\ kms^{-1}Mpc^{-1}$, respectively obtained from Baseline + $f(z)\sigma_8(z)$, which leads to a tension of 4.323σ level. The ΛCDM model have $H_0^{P18} = 67.391 \pm 0.51\ kms^{-1}Mpc^{-1}$ and $H_0^{R22} = 72.678 \pm 1.00\ kms^{-1}Mpc^{-1}$ which has a tension of 4.709σ level. The analysis of present values of Hubble constant show that the viscous RVM minimizes the Hubble tension up to 0.569σ and 0.564σ, respectively with the datasets used for this observation. The Hubble constant values also remain consistent with the Planck measurement regardless of the prior used.

Fig. 3 show the evolutions of $H(z)$ with redshift z for ΛCDM and viscous RVM using the baseline + P18 and Baseline + R22, respectively. Fig. 4 is same as in Fig. 3 but considering the results obtained with the Baseline + $f(z)\sigma_8(z)$ dataset. It is observed that the trajectories cover the majority of the dataset with $H(z)$ error bars. This indicates that both the datasets used for analysis agree with the viscous RVM. Further, in the current scenario the present age of the Universe is $13.7Gyr$ which is compatible with ΛCDM model with same combination of datasets.

Focusing on the deceleration parameter q, which plays a crucial role in describing deceleration, acceleration or transition of the Universe, we find present values of $q(z)$ for viscous RVM $q_0 = -0.520 \pm 0.014$ and $q_0 = -0.523 \pm 0.013$ with transition redshift $z_{tr} = 0.646 \pm 0.009$ and $z_{tr} = 0.650 \pm 0.007$, respectively for the Baseline with P18 and R22, whereas Baseline + $f(z)\sigma_8(z)$ dataset with P18 and R22 give $q_0 = -0.523 \pm 0.015$ and $q_0 = -0.524 \pm 0.016$ with $z_{tr} = 0.650 \pm 0.009$ nd $z_{tr} = 0.653 \pm 0.009$, respectively (see, Table 3). These value of q_0 are quite comparable to

Table 1
Cosmological constraints on ΛCDM model by Baseline and Baseline+$f(z)\sigma_8(z)$ with Hubble constants priors by the Planck (P18) and the SH0ES (R22) values, respectively, obtained via MCMC analysis.

Model	Dataset	H_0	Ω_Λ	r_d	M	σ_8	S_8
ΛCDM	Baseline + P18	67.410 ± 0.49	0.690 ± 0.008	148.810 ± 1.5	-19.438 ± 0.016	–	–
	Baseline + R22	72.776 ± 0.99	0.691 ± 0.009	137.998 ± 2.1	-19.272 ± 0.030	–	–
ΛCDM	Baseline + f(z)σ_8(z) + P18	67.391 ± 0.51	0.692 ± 0.007	149.060 ± 1.4	-19.437 ± 0.017	0.753 ± 0.026	0.751 ± 0.022
	Baseline + f(z)σ_8(z) + R22	72.678 ± 1.00	0.693 ± 0.008	138.290 ± 2.1	-19.275 ± 0.030	0.752 ± 0.028	0.762 ± 0.024

Table 2
Cosmological constraints on viscous RVM by Baseline and Baseline+$f(z)\sigma_8(z)$ with Hubble constants priors by the Planck (P18) and the SH0ES (R22) values, respectively, obtained via MCMC analysis.

Model	Dataset	H_0	Ω_Λ	ζ_1	ν	μ	r_d	M	σ_8	S_8
viscous RVM	Baseline + P18	67.403 ± 0.49	0.667 ± 0.012	0.013 ± 0.004	0.005 ± 0.003	0.004 ± 0.003	148.49 ± 1.5	-19.435 ± 0.017	–	–
	Baseline + R22	72.212 ± 1.0	0.669 ± 0.013	0.012 ± 0.005	0.006 ± 0.003	0.003 ± 0.002	137.81 ± 2.2	-19.271 ± 0.031	–	–
viscous RVM	Baseline + f(z)σ_8(z) + P18	67.416 ± 0.48	0.670 ± 0.011	0.012 ± 0.005	0.006 ± 0.003	0.004 ± 0.003	148.62 ± 1.4	-19.435 ± 0.016	0.745 ± 0.028	0.782 ± 0.021
	Baseline + f(z)σ_8(z) + R22	72.212 ± 1.0	0.669 ± 0.013	0.012 ± 0.004	0.006 ± 0.002	0.004 ± 0.002	137.81 ± 2.1	-19.271 ± 0.030	0.749 ± 0.027	0.784 ± 0.024

Table 3
Present values of cosmological parameters for ΛCDM and viscous RVM with Hubble constant priors by the Planck (P18) and the SH0ES (R22) values.

Model	Dataset	q_0	$w_{eff}(z=0)$	z_{tr}	t_0(Gyr)	j_0
ΛCDM	Baseline + P18	-0.535 ± 0.012	-0.690 ± 0.009	0.645 ± 0.007	13.775 ± 0.256	1
	Baseline + R22	-0.537 ± 0.014	-0.691 ± 0.008	0.648 ± 0.005	13.790 ± 0.268	1
ΛCDM	Baseline + f(z)σ_8(z) + P18	-0.538 ± 0.012	-0.692 ± 0.008	0.649 ± 0.007	13.787 ± 0.245	1
	Baseline + f(z)σ_8(z) + R22	-0.539 ± 0.013	-0.693 ± 0.007	0.652 ± 0.008	13.811 ± 0.288	1
Viscous RVM	Baseline + P18	-0.520 ± 0.014	-0.680 ± 0.006	0.646 ± 0.009	13.805 ± 0.284	0.978 ± 0.004
	Baseline + R22	-0.523 ± 0.013	-0.681 ± 0.009	0.650 ± 0.007	13.834 ± 0.274	0.978 ± 0.006
Viscous RVM	Baseline + f(z)σ_8(z) + P18	-0.523 ± 0.015	-0.682 ± 0.008	0.650 ± 0.009	13.825 ± 0.240	0.979 ± 0.007
	Baseline + f(z)σ_8(z) + R22	-0.524 ± 0.016	-0.683 ± 0.007	0.653 ± 0.009	13.839 ± 0.249	0.980 ± 0.005

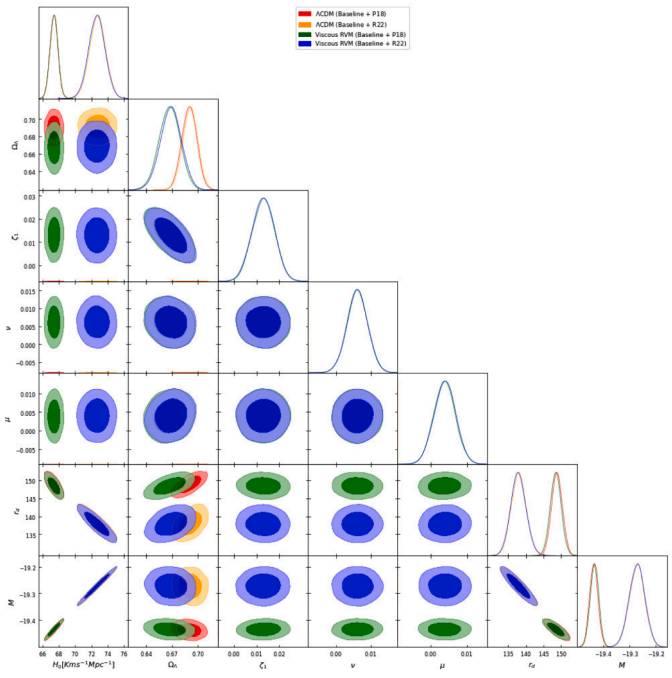

Fig. 1. Likelihood contours on the ΛCDM and viscous RVM cosmological parameters with the Baseline dataset + the Hubble constant priors from the Planck (P18) and the SH0ES (R22) values at $1-\sigma$ and $2-\sigma$ confidence levels.

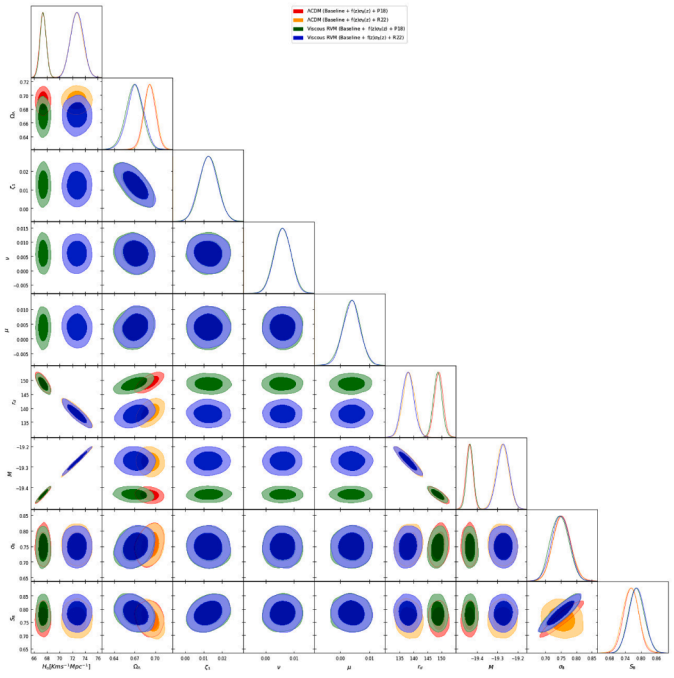

Fig. 2. The same as in Fig. 1 but for the Baseline+$f(z)\sigma_8(z)$ dataset + the Hubble constant priors from the Planck (P18) and the SH0ES (R22) values at $1-\sigma$ and $2-\sigma$ confidence levels.

those obtained by the ΛCDM model. The evolution of $q(z)$ with redshift z for viscous RVM models with errors are plotted in Figs. 5 and 6, respectively for these two combinations of datasets. As $q(z)$ evolves, it clearly shows that Universe has decelerated in the past ($q > 0$) and accelerated recently ($q < 0$). In both models, $q(z)$ approaches -1 in the late-time, corresponding to the future de Sitter phase. The plots also demonstrate that the evolution of $q(z)$ for viscous running vacuum model is consistently compatible with the ΛCDM model across these datasets. We

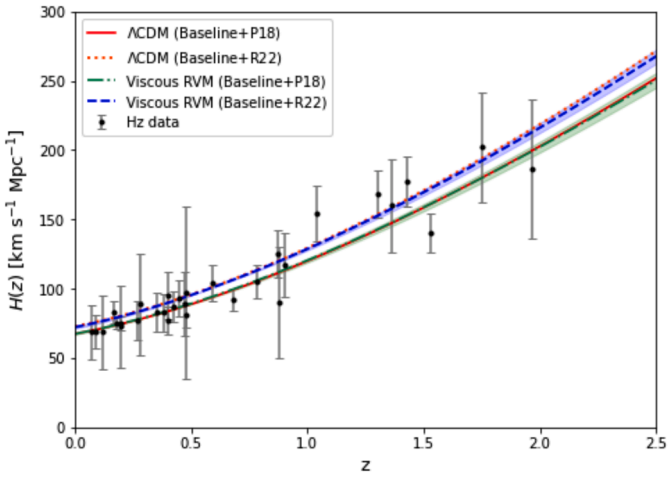

Fig. 3. The evolution of $H(z)$ with z for ΛCDM model and viscous RVM, using Baseline dataset. The 32 observational data points of $H(z_i)$ are displayed with their associated error bars.

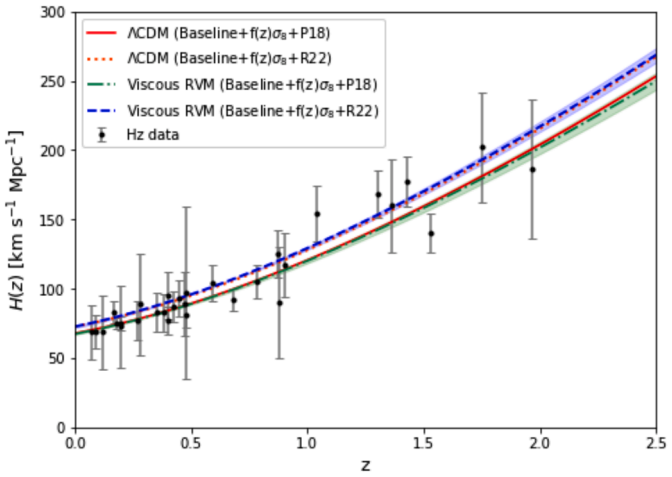

Fig. 4. The same as in Fig. 3 but considering the results obtained with the Baseline + $f(z)\sigma_8(z)$ dataset.

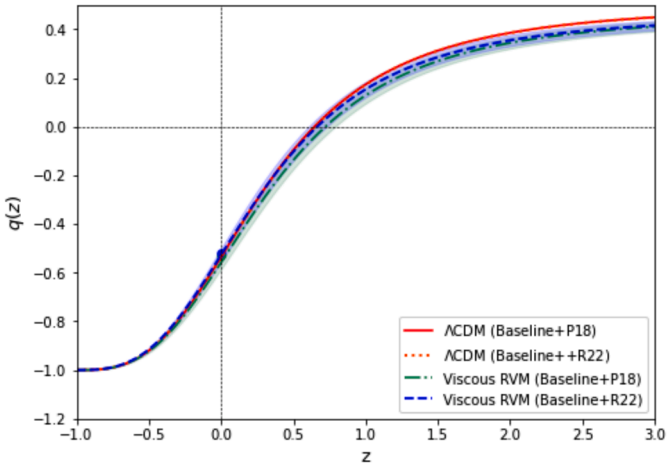

Fig. 5. Deceleration parameter with redshift z for the ΛCDM model and Viscous RVM, using the results obtained from the Baseline dataset.

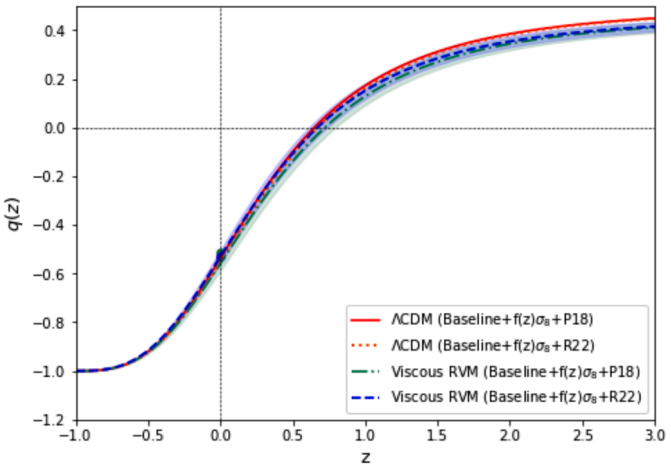

Fig. 6. The same as in Fig. 5 but considering the results obtained with the Baseline + $f(z)\sigma_8(z)$ dataset.

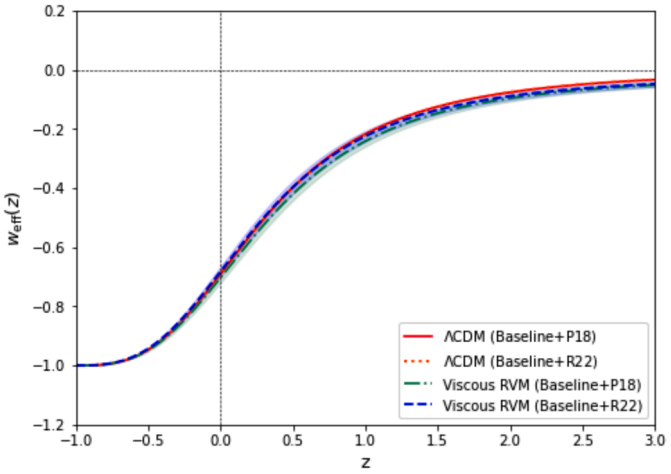

Fig. 7. Effective equation of state parameter with redshift z for the ΛCDM model and Viscous RVM, using the results obtained from the Baseline dataset.

find that the best-fit values of q_0 and z_{tr} align well with the predictions of ΛCDM model and other previous findings by many researchers using different approaches [99,123–126].

Further, based on the estimated model parameters, the evolutions of the effective equation of state parameter, $w_{eff}(z=0)$ are shown in Figs. 7 and 8 for all dataset combinations. In both models, it is found that the Universe transits from quintessence to de Sitter phase. The present effective EoS parameters for viscous RVM with respect to Baseline and Baseline + $f(z)\sigma_8(z)$ along with P18 and R22 are align with the theoretical predictions for the present value of ΛCDM model.

As we know that the second tension in cosmology is referred as the growth tension. This arises as the result of the discrepancy between the Planck value of the cosmological parameters Ω_m and σ_8 from weak gravitational lensing survey, cluster counts,and the redshift space distortion data. Given the degenerate impacts of these two parameters in lensing surveys, typically weighted amplitude of matter fluctuations $S_8 = \sigma_8\sqrt{(1-\Omega_\Lambda)/0.3}$ is employed as a parameter to compare the consistency with other observations. The weak gravitational lensing surveys provide constraints via cosmic shear, e.g. $S_8 = 0.759^{+0.024}_{-0.021}$ from the Kilo-Degree Survey (KiDS-1000)[127] which is in 3σ tension with the prediction of the Planck Legacy analysis of the cosmic microwave background. The values of σ_8 and S_8 for viscous RVM are $\sigma_8 = 0.745 \pm 0.028$ and $S_8 = 0.782 \pm 0.021$ using Baseline + $f(z)\sigma_8(z)$ with P18, and $\sigma_8 = 0.749 \pm 0.027$ and $S_8 = 0.784 \pm 0.024$ for Baseline + $f(z)\sigma_8(z)$ with R22. We find

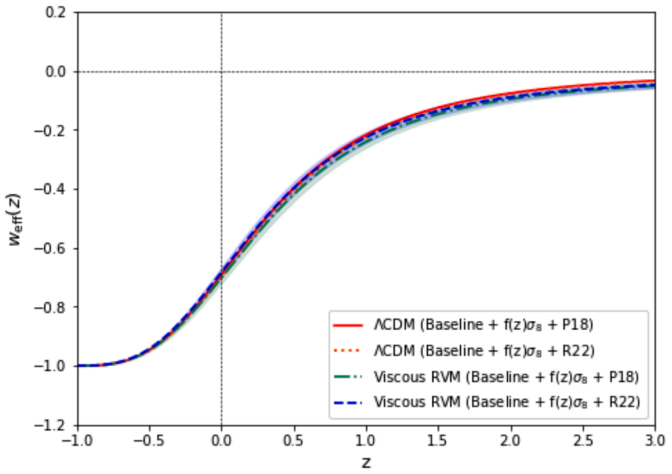

Fig. 8. The same as in Fig. 7 but considering the results obtained with the Baseline + $f(z)\sigma_8(z)$ dataset.

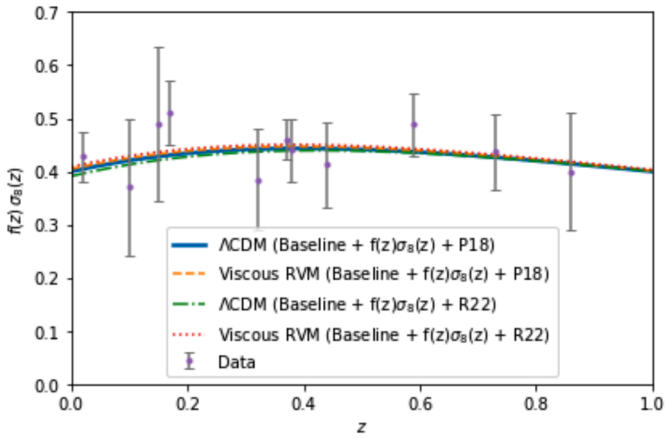

Fig. 9. $f(z)\sigma_8(z)$ with redshift z for the ΛCDM model and Viscous RVM, using the results obtained from the Baseline + $f(z)\sigma_8(z)$ dataset.

reasonable results for the matter sector including the perturbation. These values of $S_8(\sigma_8)$ are aligned with the KiDS-1000 [127]. However, viscous RVM shows a difference of 1.36σ with P22 and 1.27σ with R22 when compare with $S_8(\sigma_8) = 0.814^{+0.011}_{-0.012}(0.802^{+0.022}_{-0.018})$ of KiDS-Legacy [128]. We present the redshift evolution of the growth rate parameter $f\sigma_8(z)$ for ΛCDM and viscous RVM, compared against recent observational measurement of $f\sigma_8(z)$ (see Tables 1 and 2). These comparisons are shown in Fig. 9. We constraint viscous RVM by Baseline + $f(z)\sigma_8(z)$ with P18 and R22 which closely follow the ΛCDM curve.

The results of MCMC analysis for χ^2 and reduced Chi-squared $\chi^2_{red} = \chi^2_{min}/(N-d)$, where N and d are respectively the total number of data points used and number of free parameters, for ΛCDM and viscous RVM are reported in Table 5. It is noted that we have $N = 1747$ for Baseline and $N = 1765$ for Baseline + $f\sigma_8$ including P18 or R22. In viscous RVM, $d = 5$ and in ΛCDM, we have $d = 2$. Table 5 reveals that the χ^2_{red} is less than unity for both the models with both combinations of datasets. Note that a value of $\chi^2_{red} < 1$ is considered the best-fit with data while $\chi^2_{red} > 1$ is considered a bad fit. This indicates that both the models fit these observational data sets quite effectively and that the observed data are compatible with the concerned models.

As a supplementary information, we include an additional purely kinematical parameter, which is called the jerk parameter $j(z)$ and is described as

$$j(z) = q(2q+1) + (1+z)\frac{dq}{dz}. \tag{36}$$

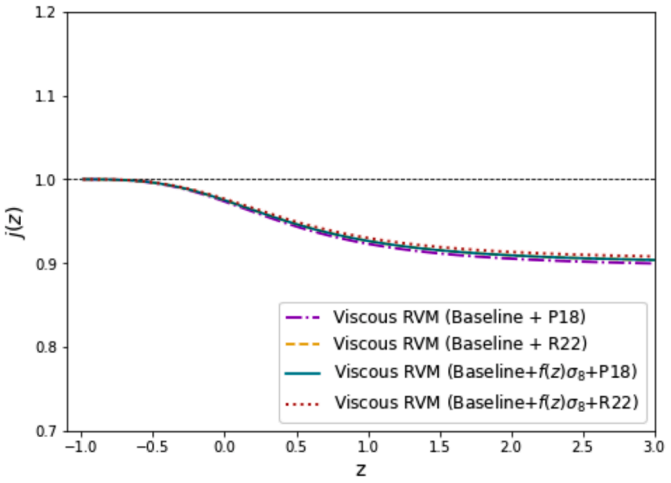

Fig. 10. Jerk parameter for Viscous RVM using the results obtained with the Baseline and Baseline + $f(z)\sigma_8(z)$ dataset.

It provide us with the departure of our model from the ΛCDM model. It is observed that for the ΛCDM model, jerk parameter always has a constant value of $j = 1$. The evolution of $j(z)$ for the viscous RVM and ΛCDM model are plotted in Fig. 10 using the best-fit parameter values derived from two different combinations of dataset. The positive value of $j(z)$ indicates an accelerating expansion of the Universe. The present values of jerk parameter for viscous RVM are $j_0 = 0.978 \pm 0.004$ for Baseline + P18 and $j_0 = 0.978 \pm 0.006$ for Baseline + R22 dataset, and $j_0 = 0.979 \pm 0.007$ for Baseline + $f\sigma_8(z)$ + P18 and $j_0 = 0.980 \pm 0.005$ for Baseline + $f\sigma_8(z)$ + R22 dataset, which slight deviation from the ΛCDM model. However, in late time, jerk parameter tends to 1 for all datasets.

7. Convergence diagnostics

Convergence diagnostics is a tool which is used to assess the stability state of the MCMC simulation. This diagnostics ensure the validity and reliability of the result obtained from MCMC analysis. The Gelman-Rubin (GR) diagnostic is one of the most commonly used techniques to evaluate the convergence of Markov Chain Monte Carlo (MCMC) simulations. This diagnostic works by running multiple Markov chains, denoted as $\{X_{i0}, X_{i1}, \ldots, X_{in-1}\}$ for $i = 1, \ldots, m$, with each chain initialized from an over-dispersed starting distribution compared to the target distribution π. Gelman and Rubin [129] presented approaches to construct such initial distributions, although in practice, these starting points are often selected arbitrarily. When running these m parallel chains, two variance estimators are computed for a variable $X \sim \pi$. The first is the within-chain variance:

$$W = \sum_{i=1}^{m}\sum_{j=0}^{n-1}(X_{ij} - \bar{X}_i)^2/(m(n-1)) \tag{37}$$

where $\bar{X}_i$ is the mean of the ith chain.

The second is the pooled (between-chain) variance estimate:

$$\hat{V} = \frac{n-1}{n}W + \frac{B}{n} \tag{38}$$

where

$$B = n\left(\sum_{i=1}^{m}\frac{(\bar{X}_i - \bar{X}_\cdot)^2}{m-1}\right) \tag{39}$$

with $\bar{X}_\cdot$ representing the overall mean across all chains.

Gelman and Rubin [129] suggested comparing the ratio of the pooled to the within-chain variance, known as the potential scale reduction factor (PSRF):

$$\hat{R} = \frac{\hat{V}}{W} \tag{40}$$

Table 4
The $\hat{R}$ values of parameters for ΛCDM and viscous RVM models with Hubble constant priors by the Planck (P18) and the SH0ES (R22) values.

Model	Dataset	H_0	Ω_Λ	ζ_1	ν	μ	r_d	M	σ_8
ΛCDM	Baseline + P18	1.0003	1.0002	–	–	–	1.0005	1.0004	–
	Baseline + R22	1.0003	1.0000	–	–	–	1.0002	1.0003	–
ΛCDM	Baseline + f(z)σ_8(z) + P18	1.0000	1.0000	–	–	–	1.0000	1.0000	1.0008
	Baseline + f(z)σ_8(z) + R22	1.0000	1.0000	–	–	–	1.0001	1.0000	1.0000
Viscous RVM	Baseline + P18	1.0000	1.0000	1.0004	1.0001	1.0006	1.0000	1.0000	–
	Baseline + R22	1.0008	1.0001	1.0002	1.0007	1.0001	1.0006	1.0006	–
Viscous RVM	Baseline + f(z)σ_8(z) + P18	1.0003	1.0000	1.0006	1.0000	1.0004	1.0002	1.0003	1.0000
	Baseline + f(z)σ_8(z) + R22	1.0008	1.0000	1.0002	1.0009	1.0000	1.0009	1.0007	1.0000

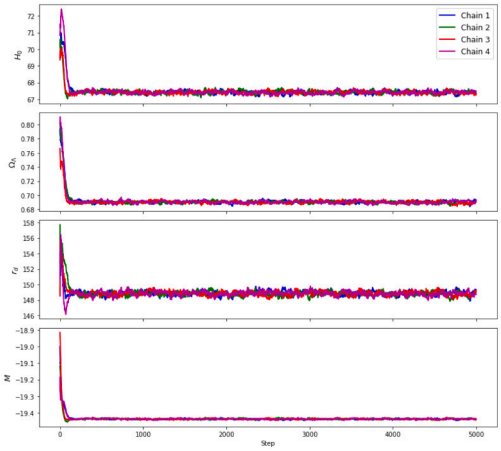

Fig. 11. Trace plot ΛCDM model using Baseline dataset with P18.

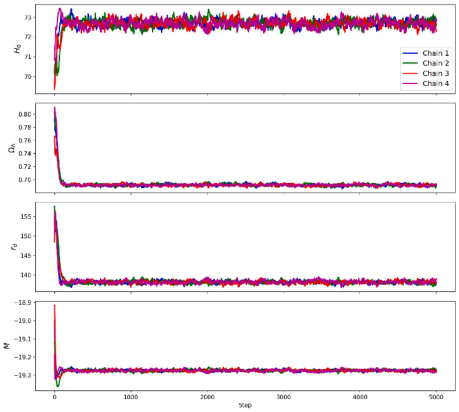

Fig. 12. Trace plot ΛCDM model using Baseline dataset with R22.

A value of $\hat{R}$ close to 1 indicates convergence. As more samples are drawn and the chains mix, $\hat{R}$ approaches 1.

In this work, to assess the convergence of our Markov Chain Monte Carlo sampling, we execute four independent chains using the emcee package. Each chain was initialized from a different starting position to ensure diverse exploration of the parameter space. We ran each chain for a total of 5000 iterations. To eliminate the influence of initial transients, we treat the first 2000 samples from each chain as burn-in and excluded them from all subsequent analyses. After discarding these burn-in samples, we evaluate convergence by calculating the Gelman-Rubin statistic $\hat{R}$ for each model parameter. The $\hat{R}$ values of parameters of ΛCDM and viscous RVM model are given in Table 4 which shows that both the models converge to 1 for both datasets, indicating that the chains had converged satisfactorily. In addition, we visualize the sampling behavior by plotting trace plots for each parameter of ΛCDM and viscous RVM models using baseline and baseline + $f(z)\sigma(z)$ datasets, respectively as shown in Figs. 11–18, which further confirm that the chains are well-mixed and stable after burn-in. Figs. 12–17

8. Model selection statistics

Finally, we assess the statistical relevance of the data fitting and the observational compatibility of the models by applying the well-known Akaike Information Criterion (AIC), the Bayesian Information Criterion (BIC), and the Deviance Information Criterion (DIC). These criteria evaluate fitted models against a reference model. AIC comes from information theory and is essentially a frequentist criterion, while the BIC is derived from an estimate of the Bayesian evidence that holds true for high sample sizes.

In cosmology, AIC and BIC have been utilized to distinguish cosmological models on the basis of penalization related to the number of parameters that the model requires to explain the data. Specifically, in Ref. [99], the author uses AIC and BIC to perform cosmological model selection in order to determine the parameter set that better fits the data. Subsequently, in this work we compare among models in light of AIC

Table 5
The reduced chi-squared $\chi^2_{red} = \chi^2/N - d$, AIC, BIC, DIC values for viscous RVM model with the Hubble constant Priors by the Planck (P18) and the SH0ES (R22) values.

Model	Dataset	$\chi^2_{\min}$	d	N	χ^2_{red}	AIC	BIC	DIC	ΔAIC	ΔBIC	ΔDIC
ΛCDM	Baseline + P18	1581.053	2	1747	0.906	1585.053	1595.984	1585.969	–	–	–
	Baseline + R22	1582.420	2	1747	0.907	1586.420	1597.351	1586.222	–	–	–
ΛCDM	Baseline + f(z)σ_8(z) + P18	1593.451	2	1765	0.903	1597.451	1608.403	1597.411	–	–	–
	Baseline + f(z)σ_8(z) + R22	1594.890	2	1765	0.905	1598.890	1609.841	1599.567	–	–	–
Viscous RVM	Baseline + P18	1573.334	5	1747	0.903	1583.334	1610.662	1585.404	−1.719	14.678	−0.565
	Baseline + R22	1573.531	5	1747	0.903	1583.531	1610.859	1586.044	−2.889	13.508	−0.178
Viscous RVM	Baseline + f(z)σ_8(z) + P18	1587.194	5	1765	0.902	1597.194	1624.573	1598.255	−0.257	16.170	0.844
	Baseline + f(z)σ_8(z) + R22	1589.721	5	1765	0.903	1599.721	1627.100	1600.326	0.831	17.259	0.759

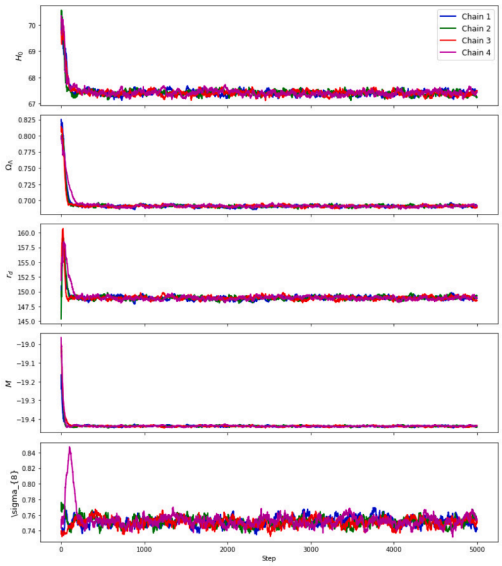

Fig. 13. Trace plot ΛCDM model using Baseline + f(z)$\sigma_8(z)$ dataset with P18.

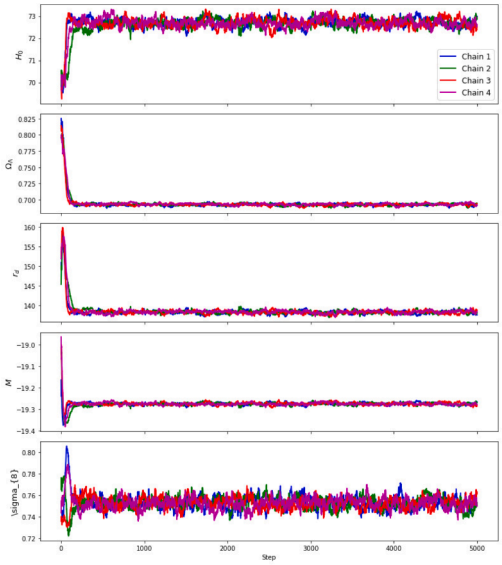

Fig. 14. Trace plot ΛCDM model using Baseline + f(z)$\sigma_8(z)$ dataset with R22.

and BIC, as well as the Deviance information criterion (DIC) utilizing the combinations of $Pantheon+, CC, BAO, f(z)\sigma_8(z)$ datasets. By using statistical analysis, we can identify which models are "more favorable" by considering the dataset and number of parameters.

The AIC is defined by [130]

$$AIC = \chi^2_{min} + \frac{2dN}{N-d-1}. \tag{41}$$

On the other hand, the BIC is defined as [131]

$$BIC = \chi^2_{min} + d \ln N. \tag{42}$$

Further, we assess the evidence of the model by analysing the Deviance information criterion (DIC)[132]. The effective number of parameters p_D, also known as Bayesian complexity of a model is expressed as

$$p_D = \overline{D(\theta)} - D(\bar{\theta}), \quad where \quad D(\theta) = -2 \ln \mathcal{L}(\theta) \tag{43}$$

Here, D is the deviance of the likelihood and the bars denotes the averages over the posterior distribution. In other words, p_D is the difference of the mean of the deviance and the deviance of the mean. We can define

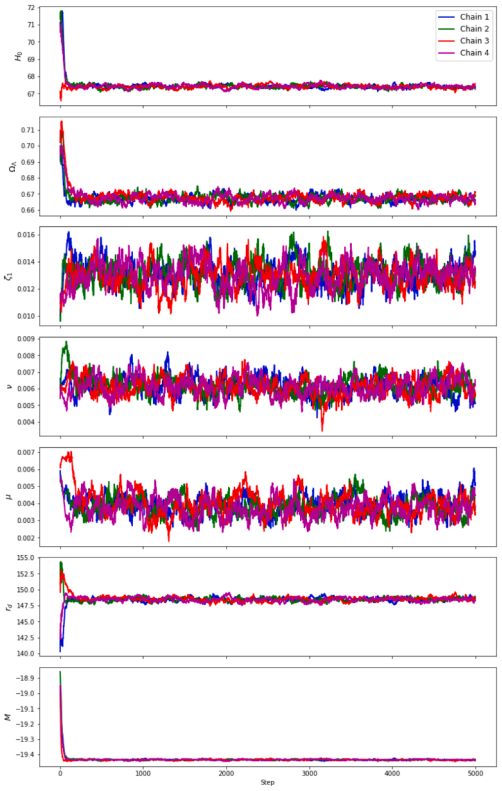

Fig. 15. Trace plot Viscous RVM using Baseline dataset with P18.

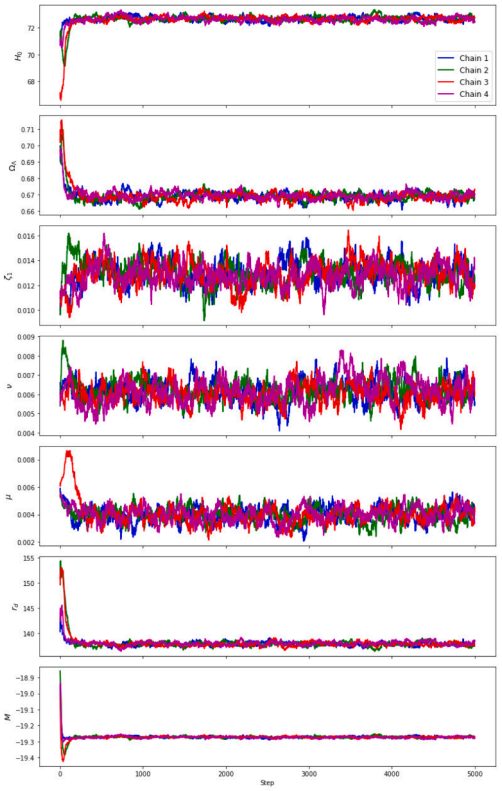

Fig. 16. Trace plot Viscous RVM using Baseline dataset with R22.

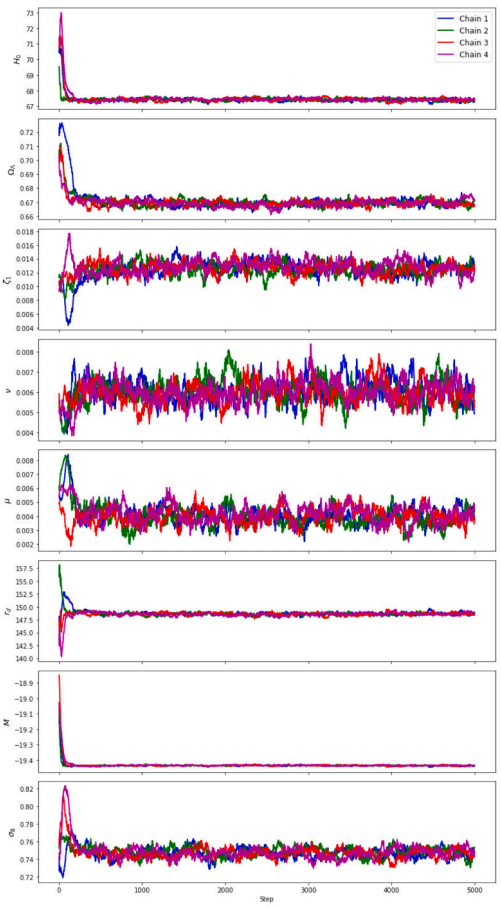

Fig. 17. Trace plot Viscous RVM using Baseline + f(z)$\sigma_8(z)$ dataset with P18.

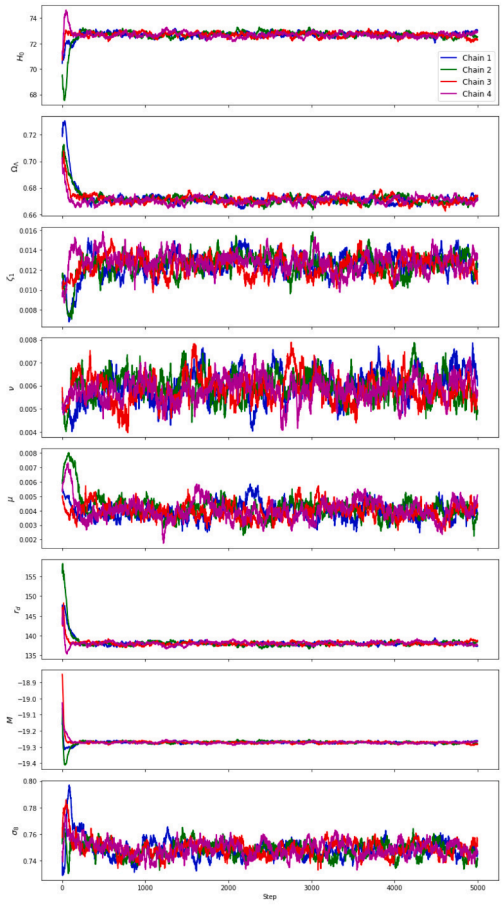

Fig. 18. Trace plot Viscous RVM using Baseline + f(z)$\sigma_8(z)$ dataset with R22.

p_D in terms of χ^2 as well. i.e.,

$$p_D = \overline{\chi^2(\theta)} - \chi^2(\bar{\theta}), \quad where \quad \chi^2 = -2\ln\mathcal{L} \tag{44}$$

The DIC is then defined by [133]

$$DIC \equiv D(\bar{\theta}) + 2p_D = \overline{D(\theta)} + p_D \tag{45}$$

Indeed, we can easily see from the definitions that when parameters are well-constrained, the DIC moves closer to the AIC rather than the BIC since $D(\bar{\theta}) \to -2\ln\mathcal{L}$ and $p_D \to n$.

Let us compute the comparison between our model l and the standard ΛCDM model k which is expressed as $\Delta AIC_{l,k} = AIC_l - AIC_k$, and it is interpreted as the model l is preferable over the model k. The support for the model is interpreted based on the thresholds in $\Delta AIC_{l,k}$, $\Delta AIC_{l,k}$ and $\Delta AIC_{l,k}$ with respect to the reference model, i.e., ΛCDM. For $\Delta AIC_{l,k} < 2$ indicates strong support for model over reference model, "average" support for $2 \leq \Delta AIC_{l,k} \leq 4$ and "considerably less support" if $4 < \Delta AIC_{k,l} \leq 7$ and $\Delta AIC > 10$ indicates essentially "no support for the model" [134]. Similarly, we can calculate $\Delta BIC_{l,k} = BIC_l - BIC_k$. A $\Delta BIC_{l,k} < 2$ indicates no distinguishable evidence; values between $2 \leq \Delta BIC_{l,k} < 6$ indicate mild to positive evidence against the model; a value between $6 \leq \Delta BIC_{l,k} < 10$ gives strong evidence against the model, and $\Delta BIC_{l,k} > 10$ represents very strong evidence against the model favoring the reference model [135]. The interpretation of ΔDIC generally aligns with that of ΔAIC [136].

Table 5 displays the values of ΔAIC, ΔBIC and ΔDIC assuming the ΛCDM as the referring model. We find the values of $(\Delta AIC, \Delta BIC, \Delta DIC) = (-1.719, 14.678, -0.565)$ for Baseline + P18 and $(\Delta AIC, \Delta BIC, \Delta DIC) = (-2.889, 13.508, -0.178)$ for Baseline + R22, and $(\Delta AIC, \Delta BIC, \Delta DIC) = (-0.257, 16.170, 0.844)$ for Baseline + $f(z)\sigma_8(z)$ + P18 and $(\Delta AIC, \Delta BIC, \Delta DIC) = (0.831, 17.259, 0.759)$ for Baseline + $f(z)\sigma_8(z)$ + R22. The values of $\Delta AIC(\Delta DIC)$ show that the datasets have strong support in favor of viscous RVM model. In contrast, the evaluation based on ΔBIC, we find that both the datasets exhibit a strong support for the ΛCDM model.

This discrepancy arises because AIC (DIC) tends to be more inclusive in model selection. The BIC imposes a stronger penalty on models with more number free parameters than AIC(DIC) and that the penalization function is proportional to the number of points in the dataset.

9. Conclusion

In this work, we have examined a bulk viscous cosmological model in the framework of time-varying vacuum energy density, where the bulk viscosity coefficient is proportional to the Hubble parameter H. Additionally, we have assumed a generic form of the VED which is proportional to $\dot{H}$ and H. This type of model has been the subject of discussions in the literature [20,28,29,137,138] and the references therein. These models have withstand numerous benchmark tests against all kinds of contemporary data with success and proved their robustness and viability as strong competitors to the standard ΛCDM model. This is true not only in terms of their ability to fit the recent cosmological data, but also important in terms of elevating the significance of the ΛCDM and its extensions in the context of theoretical physics. The primary distinctive characteristic of the RVM is predicting the existence of dynamical dark energy (DDE) related with the vacuum. In other words, the running vacuum manifests itself as a type of DDE, but it is actually (quantum) vacuum, and not merely an additional phenomenon taken out of the dark energy's blackbox to imitate or replace the core idea of vacuum energy in QFT. Since the VED in QFT must be renormalized, the rigid cosmological term Λ does not exist in the RVM paradigm. The renormalization

scale is dynamic; hence, the calculated quantum corrections result in a time-evolving VED with the expansion [29]. In the context of QFT in curved spacetime, precise calculations have recently reinforced the general structure of the RVM. As mentioned in the references [50,53,54], the smooth VED dynamics in the RVM was long anticipated based on semi-qualitative renormalization group arguments and it was only confirmed recently in an entire QFT context. In RVM framework, a true cosmological constant does not exist and it is reasonable to assert that a rigid parameter of this kind, is not predicted in renormalizable QFT [29].

Regarding the analysis presented in this work, we have focused on the implementation of viscous RVM, in order to facilitate a better comparison with earlier studies, especially the most recent one in Ref. [99]. In our approach, we have described a novel and comprehensive parametrization of bulk viscous coefficient and VED. The viscous RVM has one additional parameter μ. The dynamical component of the VED is proportional to the scalar of curvature, $\dot{H}$ and H^2, with its coefficient μ and ν respectively. Although such a coefficient can be analytically explained in QFT, in practical application it has to be fitted to the overall cosmological data because it depends on the masses of all the quantized matter fields. We have employed the chosen parameterizations in order to derive analytical solutions for different cosmological parameters, including $H(z)$, $a(t)$, $q(z)$, $w(z)$ and $j(z)$.

We have validated our findings using observational data from a wide range of sources, which comprises of, SNeIa pantheon+, CC, BAO and $f(z)\sigma_8(z)$ datasets. The priors of the present Hubble constant from Planck and SH0ES have been implied with these two datasets. Applying the MCMC methodology, the constraints of the model parameters of ΛCDM and viscous RVM have been estimated which are presented in Tables 1 and 2. When a global fit is made to the cosmological dataset using two different combinations, including the Baseline and Baseline + $f(z)\sigma_8(z)$, and the rigid option $\nu, \mu, \zeta = 0$ (i.e., Λ = constant corresponding to the ΛCDM model) is compared with the viscous RVM ($\nu, \mu, \zeta \neq 0$), we observed that a mild dynamics of the cosmic vacuum ($\nu, \mu \sim 10^{-3}$) and viscosity ($\zeta \sim 0.01$) is strongly preferred. We have evaluated convergence by calculating the Gelman-Rubin statistic $\hat{R}$ for each model parameter. The $\hat{R}$ values of parameters of ΛCDM and viscous RVM model are given in Table 4 which shows that both the models converge to 1 for both datasets, indicating that the chains had converged satisfactorily. The analysis of present values of Hubble constant show that the viscous RVM minimizes the Hubble tension up to 0.569σ and 0.564σ, respectively with the datasets used for this observation. The Hubble constant values also remain consistent with the Planck measurement regardless of the prior used. In other words, the MCMC analysis naturally favors the Planck value of H_0. This holds when both the Baseline and Baseline $+f(z)\sigma_8(z)$ have been considered. We have also found the reasonable results for the matter sector including the perturbation. These values of $S_8(\sigma_8)$ are aligned with the KiDS-1000 [127]. However, viscous RVM shows a difference of 1.36σ with P22 and 1.27σ with R22 when compare with $S_8(\sigma_8) = 0.814^{+0.011}_{-0.012}(0.802^{+0.022}_{-0.018})$ of KiDS-Legacy [128]. The analysis of other cosmological parameters such as deceleration parameter, EoS parameters and jerk parameter and their corresponding present values reveal that the viscous RVM describes the Universe transits from a decelerated phase to accelerated phase. The comparison with ΛCDM model demonstrates the efficacy of our parametrization of viscous RVM in determining the late-time cosmic acceleration.

We have reported the model selection criteria such as AIC, BIC and DIC of proposed viscous RVM with reference to the ΛCDM model. According to ΔAIC(ΔDIC), viscous RVM has "strong evidence in favour", and as far as ΔBIC is concerned, we have obtained the values > 10 and hence strong support of ΛCDM model.

To conclude, it is intriguing that the interacting viscous DM and vacuum energy density, i.e., viscous RVM provides the present values of Hubble constant which alleviates the Hubble tension. The viscous RVM which have been considered seems to be consistent with ΛCDM model in terms of evolution and present values of cosmological parameters such as the Hubble parameter, deceleration parameter, EoS parameter and jerk parameter. Our model is able to explain the accelerated expansion of the Universe with the consistency of observational datasets. Our findings imply that the dark energy is most likely dynamical and assumes the running vacuum form with viscosity. The potential for late-time new physics in the dark sector, which may be concealed behind these ongoing cosmological tensions, cannot yet be ruled out. The future data will play a crucial role in further validating the viscous RVM.

CRediT authorship contribution statement

Vinita Khatri: Writing - original draft, Supervision, Formal analysis; **C. P. Singh:** Methodology, Conceptualization, Writing - review & editing.

Data availability

No data was used for the research described in the article.

Declaration of competing interest

The authors declare that they have no known competing financial interests or personal relationships that could have appeared to influence the work reported in this paper.

Acknowledgement

The authors are thankful to the reviewers for the important comments that resulted in an improved version of the manuscript. Vinita Khatri acknowledges Delhi Technological University, New Delhi, for awarding Research Fellowship.

References

[1] A.G. Riess, et al, Astron. J. 116 (1998) 1009. https://doi.org/10.1086/300499
[2] S. Perlmutter, et al, Astrophys. J. 517 (1999) 565. https://doi.org/10.1086/307221
[3] J. Benjamin, et al Mon, Not, Roy, Astron. Soc. 381 (2007) 702. https://doi.org/10.1111/j.1365-2966.2007.12202.x
[4] L. Amendola, M. Kunz, D. Sapone, J. Cosmol. Astropart. Phys. 04 (2008) 13. https://doi.org/10.1088/1475-7516/2008/04/013
[5] L. Fu, et al, Astron. Astrophys. 479 (2008). https://doi.org/10.1051/0004-6361:20078522
[6] M. Tegmark, et al, Phys. Rev. D 69 (2004) 103501. https://doi.org/10.1103/PhysRevD.69.103501
[7] S. Cole, et al Mon, Not, Roy, Astron. Soc. 362 (2005) 505. https://doi.org/10.1111/j.1365-2966.2005.09318.x
[8] D.J. Eisenstein, et al, Astrophys. J. 633 (2005) 560. https://doi.org/10.1086/466512
[9] W.J. Percival, et al Mon, Not, Roy, Astron. Soc. 401 (2010) 2148. https://doi.org/10.1111/j.1365-2966.2009.15812.x
[10] C. Blake, et al Mon, Not, Roy, Astron. Soc. 415 (2011) 2876. https://doi.org/10.1111/j.1365-2966.2011.18903.x
[11] B.A. Reid, et al Mon, Not, Roy, Astron. Soc. 426 (2012) 2719. https://doi.org/10.1111/j.1365-2966.2012.21779.x
[12] E. Komatsu, et al, Astrophys. J. Suppl. 180 (2009) 330. https://doi.org/10.1088/0067-0049/180/2/330
[13] N. Jarosik, et al, Astrophys. J. Suppl. 192 (2011). https://doi.org/10.1088/0067-0049/192/2/14
[14] E. Komatsu, et al, Astrophys. J. Suppl. 192 (2011). https://doi.org/10.1088/0067-0049/192/2/18
[15] P.A. Ade, et al, Astron. Astrophys. 594 (2016). A, https://doi.org/10.1051/0004-6361/201525830
[16] P.J.E. Peebles, Astrophys. J. 284 (1984) 439. https://doi.org/10.1086/162425
[17] P.J.E. Peebles, Principles of Physical Cosmology, Princeton University Press, 1993. https://doi.org/10.1515/9780691206721
[18] S. Weinberg, Rev. Mod. Phys 61 (1989) 1. https://doi.org/10.1103/RevModPhys.61.1
[19] V. Sahni, A. Starobinsky, Int. J. Mod. Phys. D 9 (2000) 373. https://doi.org/10.1142/S0218271800000542
[20] J. Solá, J. Phys. Conf. Ser. 453 (2013) 12015. https://doi.org/10.1088/1742-6596/453/1/012015
[21] L. Perivolaropoulos, F. Skara, New Astron. Rev. 95 (2022) 101659. https://doi.org/10.1016/j.newar.2022.101659
[22] N. Aghanim, et al, Astron. Astrophys. 641 (2020). A, https://doi.org/10.1051/0004-6361/201833910

[23] W.L. Freedman, Nat. Astron. 1 (2017) 121. https://doi.org/10.1038/s41550-017-0121
[24] E.D. Valentino, Nat. Astron. 1 (2017) 569. https://doi.org/10.1038/s41550-017-0236-8
[25] A.G. Riess, et al, Astrophys. J. Lett. 934 (2022). L, https://doi.org/10.3847/2041-8213/ac5c5b
[26] R. Dalal, et al, Phys. Rev. D 108 (2023) 123519. https://doi.org/10.1103/PhysRevD.108.123519
[27] P.J. Steinhardt, Phil. Trans. Roy. Soc. Lond. A 361 (2003) 2497. https://doi.org/10.1098/rsta.2003.1290
[28] J. Solá, A. Gomez-Valent, Int. J. Mod. Phys. D 24 (2015) 1541003. https://doi.org/10.1142/S0218271815410035
[29] J.S. Peracaula, Phil. Trans. Roy. Soc. Lond. A 380 (2022) 20210182. https://doi.org/10.1098/rsta.2021.0182
[30] A.M. Abdel-Rahman, Nuovo Cim. B 102 (1988) 225. https://doi.org/10.1007/BF02726570
[31] A.M. Abdel-Rahman, Phys. Rev. D 45 (1992) 3497. https://doi.org/10.1103/PhysRevD.45.3497
[32] J.D. Barrow, Phys. Lett. B 180 (1986) 335. https://doi.org/10.1016/0370-2693(86)91198-6
[33] J.D. Barrow, P. Parsons, Phys. Rev. D 55 (1997) 1906. https://doi.org/10.1103/PhysRevD.55.1906
[34] A. Beesham, Gen. Rel. Grav. 26 (1994) 159. https://doi.org/10.1007/BF02105151
[35] M.S. Berman, Phys. Rev. D 43 (1991) 1075. https://doi.org/10.1103/PhysRevD.43.1075
[36] J.C. Carvalho, J.A. Lima, I. Waga, Phys. Rev. D 46 (1992) 2404. https://doi.org/10.1103/PhysRevD.46.2404
[37] W. Chen, Y.S. Wu, Phys. Rev. D 41 (1990) 695. https://doi.org/10.1103/PhysRevD.41.695
[38] T. Damour, G.W. Gibbons, J.H. Taylor, Phys. Rev. Lett. 61 (1988) 1151. https://doi.org/10.1103/PhysRevLett.61.1151
[39] T.B. Enginol, Phys. Lett. A 139 (1989) 127. https://doi.org/10.1016/0375-9601(89)90345-9
[40] D. Kalligas, P. Wesson, C.W. Everitt, Gen. Rel. Grav. 24 (1992) 351. https://doi.org/10.1007/BF0076041
[41] D. Kalligas, P.S. Wesson, C.W. Everitt, Gen. Rel. Grav. 27 (1995) 645. https://doi.org/10.1007/BF02108066
[42] Y.K. Lau, Aust. J. Phys. 38 (1985) 547. https://doi.org/10.1071/PH850547
[43] Y.K. Lau, S.J. Prokhovnik, Aust, J. Phys. 39 (1986) 339. https://doi.org/10.1071/PH860339
[44] J.A. Lima, M. Trodden, Phys. Rev. D 53 (1996) 4280. https://doi.org/10.1103/PhysRevD.53.4280
[45] P.J.E. Peebles, B. Ratra, Astrophys. J. 325 (1988). L, https://doi.org/10.1086/185100
[46] T. Singh, A. Beesham, W.S. Mbokazi, Gen. Rel. Grav. 30 (1998) 573. https://doi.org/10.1023/A:1018866107585
[47] R.F. Sistero, Gen. Rel. Grav. 23 (1991) 1265. https://doi.org/10.1007/BF00756848
[48] J.A. Lima, J.M. Maia, Phys. Rev. D 49 (1994) 5597. https://doi.org/10.1103/PhysRevD.49.5597
[49] I. Waga, Astrophys. J. 414 (1993) 436. https://doi.org/10.1086/173090
[50] C. Moreno-Pulido, J.S. Peracaula, Eur. Phys. J. C 80 (2020) 692. https://doi.org/10.1140/epjc/s10052-020-8238-6
[51] A. Gómez-Valent, J.S. Peracaula, Eur. Phys. Lett. 120 (2018) 39001. https://doi.org/10.1209/0295-5075/120/39001
[52] J.S. Peracaula, et al, Eur. Phys. Lett. 134 (2021) 19001. https://doi.org/10.1209/0295-5075/134/19001
[53] C. Moreno-Pulido, J.S. Peracaula, Eur. Phys. J. C 82 (2022) 551. https://doi.org/10.1140/epjc/s10052-022-10484-w
[54] C. Moreno-Pulido, J.S. Peracaula, Eur. Phys. J. C 82 (2022) 1137. https://doi.org/10.1140/epjc/s10052-022-11117-y
[55] C. Moreno-Pulido, J.S. Peracaula, S. Cheraghchi, Eur. Phys. J. C 83 (2023) 637. https://doi.org/10.1140/epjc/s10052-023-11772-9
[56] A. Gómez-Valent, J. Solá, S. Basilakos, JCAP 2015 (2015) 1. https://doi.org/10.1088/1475-7516/2015/01/004
[57] J. Solá, A. Gómez-Valent, J. De, C. Perez, Astrophys. J. 811 (2015). L, https://doi.org/10.1088/2041-8205/811/1/L14
[58] J. Solá, A. Gómez-Valent, J. De, C. Perez, Astrophys. J. 836 (2017). L, https://doi.org/10.3847/1538-4357/836/1/43
[59] J. Solá, et al, Universe, 262, https://doi.org/10.3390/universe9060262
[60] M. Raveri, Phys. Rev. D 93 (2016) 43522. https://doi.org/10.1103/PhysRevD.93.043522
[61] S. Anand, P. Chaubal, A. Mazumdar, S. Mohanty, J. Cosmol. Astropart. Phys. 11 (2017) 5. https://doi.org/10.1088/1475-7516/2017/11/005
[62] J.D. Bowman, Nature 555 (2018) 67. https://doi.org/10.1038/nature25792
[63] E. Elizalde, M. Khurshudyan, S.D. Odintsov, R. Myrzakulov, Phys. Rev. D 102 (2020) 123501. https://doi.org/10.1103/PhysRevD.102.123501
[64] B.D. Normann, I.H. Brevik, Mod. Phys. Lett. A 36 (2021) 2150198. https://doi.org/10.1142/S0217732321501984
[65] C. Eckart, Phys. Rev. 58 (1940) 919. https://doi.org/10.1103/PhysRev.58.919
[66] L.D. Landau, E.M. Lifshitz, Fluid Mechanics, 2nd Ed., Elsevier:Butterworth Heinemann, 1987.
[67] W. Israel, Ann. Phys. 100 (1976) 310. https://doi.org/10.1016/0003-4916(76)90064-6
[68] W. Israel, J.M. Stewart, Phys. Lett. A 58 (1976) 213. https://doi.org/10.1016/0375-9601(76)90075-X
[69] W. Zimdahl, D.J. Schwarz, A.B. Balakin, D. Pavon, Phys. Rev. D 64 (2001) 63501. https://doi.org/10.1103/PhysRevD.64.063501
[70] A.B. Balakin, D. Pavon, D.J. Schwarz, W. Zimdahl, New J. Phys. 5 (2003) 85. https://doi.org/10.1088/1367-2630/5/1/385
[71] G.M. Kremer, F.P. Devecchi, Phys. Rev. D 67 (2003) 47301. https://doi.org/10.1103/PhysRevD.67.047301
[72] J.C. Fabris, S.V.B. Goncalves, R.D. Ribeiro, Gen. Relativ. Gravit. 38 (2006) 495. https://doi.org/10.1007/s10714-006-0236-y
[73] I. Brevik, O. Gorbunova, Gen. Relativ. Gravit. 37 (2005) 2039. https://doi.org/10.1007/s10714-005-0178-9
[74] M.G. Hu, X.H. Meng, Phys. Lett. B 635 (2006) 186. https://doi.org/10.1016/j.physletb.2006.02.059
[75] J. Ren, X.H. Meng, Phys. Lett. B 633 (2006) 1. https://doi.org/10.1016/j.physletb.2005.11.055
[76] X.H. Meng, J. Ren, M.G. Hu, Commun. Theor. Phys. 47 (2007) 379. https://doi.org/10.1088/0253-6102/47/2/036
[77] J.R. Wilson, G.J. Mathews, G.M. Fuller, Phys. Rev. D 75 (2007) 43521. https://doi.org/10.1103/PhysRevD.75.043521
[78] G.J. Mathews, N.Q. Lan, C. Kolda, Phys. Rev. D 78 (2008) 43525. https://doi.org/10.1103/PhysRevD.78.043525
[79] A. Avelino, U. Nucamendi, AIP Conf. Proc, 1083, https://doi.org/10.1063/1.3058568
[80] A. Avelino, U. Nucamendi, F.S. Guzmán, AIP Conf. Proc, 1026, https://doi.org/10.1063/1.2965067
[81] A. Avelino, U. Nucamendi, J. Cosmol. Astropart. Phys. 04 (2009) 6. https://doi.org/10.1088/1475-7516/2009/04/006
[82] X.H. Meng, D. Xu, Commun. Theor. Phys. 52 (2009) 377. https://doi.org/10.1088/0253-6102/52/2/36
[83] A. Avelino, U. Nucamendi, J. Cosmol. Astropart. Phys. 08 (2010) 9. https://doi.org/10.1088/1475-7516/2010/08/009
[84] C.P. Singh, P. Kumar, Eur. Phys. J. C 74 (2014) 3070. https://doi.org/10.1140/epjc/s10052-014-3070-5
[85] A. Sasidharan, T.K. Mathew, Eur. Phys. J. C 75 (2015) 348. https://doi.org/10.1140/epjc/s10052-015-3567-6
[86] B.D. Normann, I. Brevik, Mod. Phys. Lett. A 32 (2017) 1750026. https://doi.org/10.1142/S0217732317500262
[87] D. Wang, Y.J. Yan, X.H. Meng, Eur. Phys. J. C 77 (2017) 660. https://doi.org/10.1140/epjc/s10052-017-5212-z
[88] C.P. Singh, A. Kumar, Eur. Phys. J. Plus. 133 (2018) 312. https://doi.org/10.1140/epjp/i2018-12122-y
[89] C.P. Singh, A. Kumar, Mod. Phys. Lett. A 33 (2018) 1850225. https://doi.org/10.1142/S0217732318502255
[90] C.P. Singh, M. Srivastava, Eur. Phys. J. C 78 (2018) 190. https://doi.org/10.1140/epjc/s10052-018-5683-6
[91] C.P. Singh, A. Kumar, Astrophys. Space Sci. 364 (2019) 94. https://doi.org/10.1007/s10509-019-3583-3
[92] C.P. Singh, S. Kaur, Astrophys. Space Sci. 365 (2020). https://doi.org/10.1007/s10509-019-3713-y
[93] C.P. Singh, Nuovo Cimento B 122 (2007) 89. https://doi.org/10.1393/ncb/i2007-10048-9
[94] C.P. Singh, S. Kumar, Astrophys. Space Sci. 323 (2009) 407. https://doi.org/10.1007/s10509-009-0137-0
[95] N. Mostafapoor, Ø.G. n, Astrophys. Space Sci. 333 (2011) 357. https://doi.org/10.1007/s10509-011-0690-1
[96] J. Hu, H. Hu, Eur. Phys. J. Plus. 135 (2020) 718. https://doi.org/10.1140/epjp/s13360-020-00623-1
[97] L. Herrera-Zamorano, A. Hernández-Almada, M.A. Garcia-Aspeitia, Eur. Phys. J. C 80 (2020) 637. https://doi.org/10.1140/epjc/s10052-020\protect\penalty-\@M-8225-y
[98] C. Norman, G. Gomez, E. Gonzalez, G. Palma, A. Rincon, Phys. Dark Univ 42 (2023) 101351. https://doi.org/10.1016/j.dark.2023.101351
[99] C.P. Singh, V. Khatri, Phys. Rev. D 109 (2024) 23508. https://doi.org/10.1103/PhysRevD.109.023508
[100] A. Ashoorioon, Z. Davari, Astrophys. J. 959 (2023) 120. https://doi.org/10.3847/1538-4357/ad0372
[101] S. Weinberg, Gravitation and Cosmology: Principles and Applications of the General Theory of Relativity, New York, U. S. A, John Wiley and Sons, Inc, 1972.
[102] C. Moreno-Pulido, J.S. Peracaula, Eur. Phys. J. C 82 (2022) 551. https://doi.org/10.1140/epjc/s10052-022-11117-y
[103] Ø.G. n, Astrophys. Space Sci. 173 (1990) 191. https://doi.org/10.1007/BF00643930
[104] C.P. Singh, S. Kumar, A. Pradhan, Class. Quantum Grav. 24 (2007) 455. https://doi.org/10.1088/0264-9381/24/2/011
[105] I. Brevik, Phys. Rev. D 65 (2002) 127302. https://doi.org/10.1103/PhysRevD.65.127302
[106] J. Solá, J. Phys. A 41 (2008) 164066. https://doi.org/10.1088/1751-8113/41/16/164066
[107] J.S. Peracaula, J. De, C. Pérez, A. Gómez-Valent, Mon. Not. R. Astron. Soc. 478 (2018) 4357. https://doi.org/10.1093/mnras/sty1253
[108] A. Gómez-Valent, J.S. Peracaula, Mon. Not. R. Astron. Soc. 478 (2018) 126. https://doi.org/10.1093/mnras/sty1028
[109] D.M. Scolnic, et al, Astrophys. J. 859 (2018) 101. https://doi.org/10.3847/1538-4357/aab9bb
[110] D.M. Scolnic, et al, Astrophys. J. 938 (2022) 113. https://doi.org/10.3847/1538-4357/ac8b7a

[111] D. Brout, et al, Astrophys. J. 938 (2022) 110. https://doi.org/10.3847/1538-4357/ac8e04
[112] A. Conley, et al, Astrophys. J. Suppl. Ser. 192 (2011) 1. https://doi.org/10.1088/0067-0049/192/1/1
[113] M. Moresco, et al, Astrophys. J. 898 (2020) 82. https://doi.org/10.3847/1538-4357/ab9eb0
[114] M.A. Karim, et al, [DESI] https://arxiv.org/abs/2503.14738.
[115] H. Wang, Z.Y. Peng, Y.S. Piao, 2024. https://arxiv.org/abs/2406.03395.
[116] CobayaSampler Collaboration, DESI BAO Data Repository.
[117] CobayaSampler Collaboration, DESI BAO Covariance Matrix File.
[118] S. Nesseris, G. Pantazis, L. Perivolaropoulos, Phys. Rev. D 96 (2017) 23542. https://doi.org/10.1103/PhysRevD.96.023542
[119] S. Nesseris, L. Perivolaropoulos, Phys. Rev. D 77 (2008) 23504. https://doi.org/10.1103/PhysRevD.77.023504
[120] A. Quelle, A.L. Maroto, Eur. Phys. J. C 80 (2020) 369. https://doi.org/10.1140/epjc/s10052-020-7941-7
[121] D. Foreman-Mackey, D.W. Hogg, D. Lang, J. Goodman, Publ. Astron. Soc. Pac. 125 (2013) 306. https://doi.org/10.1086/670067
[122] W.K. Hastings, Biometrika 57 (1970) 97. https://doi.org/10.1093/biomet/57.1.97
[123] A. Hernández-Almada, et al, Eur. Phys. J. C 79 (2019) 12. https://doi.org/10.1140/epjc/s10052-018-6521-6
[124] M. Koussour, Chin, J. Phys 83 (2023) 454. https://doi.org/10.1016/j.cjph.2023.04.003
[125] D. Wang, et al, Eur. Phys. J. C 83 (2023) 670. https://doi.org/10.1140/epjc/s10052-023-11744-z
[126] M. Koussour, N. Myrzakulov, S. Myrzakulova, M. Sofuoglu, Results Phys. 55 (2023) 107. https://doi.org/10.1016/j.rinp.2023.107166
[127] M. Asgari, et al, Astron. Astrophys. 645 (2021). A, https://doi.org/10.1051/0004-6361/202039070
[128] B. Stölzner, et al, https://doi.org/10.48550/arXiv2503.19442
[129] A. Gelman, D.B. Rubin, Statist. Sci. 7 (4) (1992) 457. https://doi.org/10.1214/ss/1177011136
[130] H. Akaike, IEEE Trans. Autom. Control 19 (1974) 716. https://doi.org/10.1109/TAC.1974.1100705
[131] G. Schwarz, Ann. Stat. 6 (1978) 461. https://doi.org/10.1214/aos/1176344136
[132] A.R. Liddle, Mon. Not. R. Astron. Soc. 377 (2007). L, https://doi.org/10.1111/j.1745-3933.2007.00306.x
[133] D.J. Spiegelhalter, N.G. Best, B.P. Carlin, A.V.D. Linde, J. Roy. Stat. Soc. Ser. B 64 (2002) 583. https://doi.org/10.1111/1467-9868.00353
[134] K. Burnham, D. Anderson, Model Selection and Multimodel Inference: A Practical Information- Theoretic Approach, Springer, New York, New York, 2003.
[135] R.E. Kass, A.E. Raftery, J. Am Statist. Assoc. 90 (1995) 773. https://doi.org/10.2307/2291091
[136] M. Rezaei, M. Malekjani, Eur. Phys. J. Plus. 136 (astro-ph.CO) (2021) 219. arXiv:2102.10671.
[137] J. Solá, J. Phys. Conf. Ser. 283 (2011) 12033. https://doi.org/10.1088/1742-6596/283/1/012033
[138] J. Solá, AIP Conf. Proc. 1606, 19, 2014. https://doi.org/10.1063/1.4891113

Astrophysics and Space Science (2023) 368:16
https://doi.org/10.1007/s10509-023-04173-7

RESEARCH

Constraining the time-varying vacuum energy models in Brans-Dicke theory

Vinita Khatri[1] · **C.P. Singh**[1]

Received: 29 July 2022 / Accepted: 8 March 2023 / Published online: 20 March 2023

Abstract

In this work, we constrain the time-varying vacuum energy models in Brans-Dicke theory within the framework of a flat Friedmann-Lamaître-Robertson-Walker space-time by using the latest observational data. In the first step, the analytical solution of field equations are found by considering the two functional forms of cosmological constant, viz. power-series form: $\Lambda = n_1 H + n_2 H^2$ and power-law form: $\Lambda \propto a^{-n}$, where n_1, n_2 and n are all constants, and H and a are the Hubble parameter and scale factor, respectively. Then, to test the viability of the models, the latest data sample such as Hubble $H(z)$ data, Type Ia supernovae and baryon acoustic oscillations are used to constrain the model parameters. We apply the Markov Chain Monte Carlo (MCMC) method to find the best-fit values of the space parameters of both the models. The cosmological implications of the models are discussed by using the best-fit values of parameters. It is found that both the models are in good agreement with the datasets and are consistent with the analytical solutions. We use jerk parameter and selection criteria (AIC and BIC) to find the consistency of the proposed models with the observation as compared to ΛCDM model. Both the models explain the late-time acceleration of the Universe.

Keywords Cosmology · Vacuum dark energy model · Brans-Dicke theory

1 Introduction

In the current view of modern cosmology, the nature and origin behind the current accelerating expansion of the Universe constitute a major problem. The analysis and interpretation of many observational data like Type Ia supernova (Perlmutter et al. 1999; Riess et al. 2004; Astier et al. 2006), galaxy clustering (Feldman et al. 2003), cosmic microwave background radiation (Spergel et al. 2007) and other cosmological observations (Komatsu et al. 2009, 2011; Sanchez et al. 2011; Ade et al. 2014, 2016) provide a cosmic expansion of the Universe that involves a recent accelerated expansion. This phenomena has been discussed either by adding an energy component in energy-momentum tensor usually called "dark energy" (DE) which has negative pressure, or modifying the general theory of relativity. The cosmological constant (CC), which was initially introduced by Einstein to make the static Universe, is a natural and simplest candidate of DE. This DE model, so-called standard Lambda-cold dark matter (ΛCDM) model, contains the cold dark matter for explaining cluster formation and a CC, Λ. Although the ΛCDM model fits accurately the current observational data and describes well the observed Universe, this model faces two serious problems, namely, the fine-tuning and the cosmological coincidence problems (Weinberg 1989; Copeland et al. 2006).

In the recent years, these longstanding problems have galvanized a variety of alternative theories for the cosmic acceleration beyond the ΛCDM model. One of such theories includes dynamical Λ instead of just assuming the Λ as a constant. A varying Λ has been proposed in literature to alleviate the CC problems. A number of works was proposed using varying Λ even before the discovering of the accelerating Universe (Ozer and Taha 1986; Peebles and Ratra 1988; Carvalho et al. 1992; Lima 1996; Overduin and Cooperstock 1998). This $\Lambda(t)$ model may act as an important alternative to the ΛCDM model. The $\Lambda(t)$ model is based on vacuum quantum fluctuations in the curved space-time. The resulting effective vacuum energy density depends on the

✉ C.P. Singh
cpsingh@dce.ac.in

V. Khatri
vinitakhatri_2k20phdam501@dtu.ac.in

[1] Department of Applied Mathematics, Delhi Technological University, Bawana Road, Delhi, 110 042, India

space-time curvature which decays from high initial values to smaller ones as the Universe expands (Carneiro 2003).

Due to lack of a concrete theory to model a time-varying Λ function, we generally parametrize the vacuum energy density by using phenomenological approach. In quantum field theory, the renormalization group (RG) (Shapiro and Solá 2000) describes a dynamical vacuum energy, in which the Λ-term varies as $\Lambda \sim H^2$, where H is the Hubble parameter. In a series of recent papers (Schützhold 2002; Borges and Carneiro 2005; Carneiro et al. 2006, 2008; Basilakos 2009; Basilakos et al. 2009; Perico et al. 2013; Bessada and Miranda 2013; Lima et al. 2013; Szydlowski and Stachowski 2015; Jayadevan et al. 2019), a number of flat Friedmann-Lemaître-Robertson-Walker (FLRW) type cosmologies have been studied by assuming the vacuum energy density as a truncated power-series in terms of Hubble parameter H. Carneiro et al. (2008) proposed a cosmological model by assuming the vacuum term as proportional to the Hubble parameter, $\Lambda \propto H$. Carvalho et al. (1992) and Grande et al. (2006) proposed a time-dependent vacuum, $\Lambda \sim c_1 H^2$ (here c_1 is a constant), which arises from the RG in quantum field theory. Bessada and Miranda (2013) have studied the evolution of the model with a phenomenological law $\Lambda = \Lambda_0 + 3\beta H^2$. Basilakos (2009) and Basilakos et al. (2009) investigated the properties of flat FLRW model by assuming the function form of $\Lambda(t)$ as a power series expansion in H up to the second order, $\Lambda \sim n_1 H + n_2 H^2$, where n_1 and n_2 are constants. Later on, Oliveira et al. (2014) have discussed the cosmological consequences of a model in which the vacuum varies as a truncated power series of the Hubble parameter.

On the other hand, the scalar tensor theories have been reconsidered extensively in literature, in particular, the Brans-Dicke (BD) scalar-tensor theory. Brans and Dicke (1961) introduced this scalar tensor theory to incorporate the Mach's principle in general relativity. In this theory, a scalar field ψ is included in the Einstein-Hilbert action that makes the Newtonian gravitational constant G as a function of coordinates. We replace the gravitational constant G by an inverse of time-varying scalar field ψ, which couples to gravity with a coupling parameter ω. However, in the limit $\omega \to \infty$, BD theory reduces to the corresponding general relativity. In recent years, this theory has received significant attention as it successfully describes the early inflationary era and late-time evolution of the Universe. Many authors (Pimental 1985; Johri and Kalyani 1994; Ram and Singh 1999; Sen et al. 2001; Banerjee and Pavon 2001a,b; Sen and Sen 2001; Mota and Barrow 2004; Das et al. 2006; Arik and Çalik 2006; Arik et al. 2008; Xu et al. 2010; Singh 2012; Karchi and Shojaie 2016; Kumar and Singh 2017; Singh and Kumar 2017; Srivastava and Singh 2018; Singh and Kaur 2019; Sharif and Syed Asit Ali Shah 2019; Karimkhani and Khoadam-Mohammadi 2019; Singh and Kaur 2020) have extensively studied FLRW model in the framework of BD theory. Since the vacuum energy models have the dynamical behavior, it is more suitable to consider the models in a dynamical framework such as BD theory.

In the present paper, we extend the successful approach recently presented on BD cosmology with decaying vacuum energy by Singh and Solà Peracaula (2021) with the some other suitable form of $\Lambda(t)$. However, the model could not gain the consistency with the analytical solutions. Here, we assume two different functional form of time-varying Λ: a power series up to the second order of H and a power-law form. We focus our attention on exact solutions and discuss the observational aspects of $\Lambda(t)$ models in the framework of BD theory. Additionally, we perform a Bayesian MCMC method to constrain the space parameters using the observational data of Type Ia supernova, Hubble data and baryon acoustic oscillations. Using the best-fit values of parameters we discuss the evolution of the Universe through Hubble parameter, deceleration and equation of state parameters, and check the consistency of the analytical solution sofar obtained for the both models. The model selection criteria and jerk parameters are also discussed and compared the models with the standard ΛCDM model.

The paper is organized as follows: In Sect. 2, we propose the model and basic field equations in BD theory with cosmological constant. The analytical solutions of the field equations are presented in Sects. 3 and 4 with two different functional forms of $\Lambda(t)$. In Sect. 5, we discuss the latest observational data and method to constrain the main parameters of our vacuum models. In Sect. 6, we analyze the models by using the best-fit values of model parameters. Section 7 discusses the statistical criteria of AIC and BIC in respect of the models along with ΛCDM. In Sect. 8, we draw our conclusions.

2 BD field equations with dynamical vacuum energy

We start with a spatially homogeneous and isotropic flat Friedmann-Lemaître-Robertson-Walker (FLRW) line element in standard spherical coordinates $x^i = (t, r, \theta, \phi)$

$$ds^2 = -dt^2 + a^2(t)\left[dr^2 + r^2(d\theta^2 + sin^2\theta d\phi^2)\right], \qquad (1)$$

where $a(t)$ is the scale factor of the Universe. The field equations of BD theory in the presence of cosmological constant (in the unit $c = 1$) is given by (Uhera and Kim 1982; Kim 2005)

$$G_{\mu\nu} = R_{\mu\nu} - \frac{1}{2}g_{\mu\nu}R = \frac{8\pi}{\psi}\tilde{T}_{\mu\nu} + \frac{8\pi}{\psi}T^{BD}_{\mu\nu}, \qquad (2)$$

where ψ is the scalar field known as BD scalar field, ω is a dimensionless BD coupling constant and $\tilde{T}_{\mu\nu} \equiv$

$T_{\mu\nu} - g_{\mu\nu}\rho_\Lambda$ is the total energy-momentum tensor, that is, the sum of the matter and vacuum contributions. Here $\rho_\Lambda = \Lambda/8\pi G = \Lambda\psi/8\pi$ is the vacuum energy density which has the equation of state (EoS) $p_\Lambda = -\rho_\Lambda$, and $T_{\mu\nu} = (\rho_m + p_m)\,u_\mu u_\nu + p_m\, g_{\mu\nu}$ is the ordinary energy-momentum tensor of perfect fluid, where ρ_m is the energy density of matter, p_m is the corresponding pressure and u_μ is the four-velocity vector. Thus, we consider $\tilde{T}_{\mu\nu}$ as a perfect fluid form of energy-momentum tensor which is given by

$$\tilde{T}_{\mu\nu} = (\rho + p)\,u_\mu u_\nu + p\, g_{\mu\nu}, \tag{3}$$

where $\rho = \rho_m + \rho_\Lambda$ and $p = p_m + p_\Lambda$.

In Eq. (2), $T^{BD}_{\mu\nu}$ is considered as the energy-momentum tensor for the BD scalar which is defined by

$$T^{BD}_{\mu\nu} = \frac{1}{8\pi}\Big[\frac{\omega}{\psi}\left(\nabla_\mu\psi\nabla_\nu\psi - \frac{1}{2}g_{\mu\nu}\nabla_\alpha\psi\nabla^\alpha\psi\right) + \nabla_\mu\nabla_\nu\psi - g_{\mu\nu}\nabla_\alpha\nabla^\alpha\psi\Big]. \tag{4}$$

The BD wave equation is given by

$$\Box\psi = \frac{8\pi}{(2\omega+3)}\left(T^{\mu}_{\mu} - 4\rho_\Lambda\right), \tag{5}$$

where T^{μ}_{μ} is the trace of $T_{\mu\nu}$.

For energy-momentum tensors (3) and (4), the BD field equations (2) and (5) for metric yield

$$3H^2 + 3H\frac{\dot{\psi}}{\psi} - \frac{\omega}{2}\frac{\dot{\psi}^2}{\psi^2} = \frac{8\pi}{\psi}\rho, \tag{6}$$

$$2\dot{H} + 3H^2 + \frac{\ddot{\psi}}{\psi} + 2H\frac{\dot{\psi}}{\psi} + \frac{\omega}{2}\frac{\dot{\psi}^2}{\psi^2} + = -\frac{8\pi}{\psi}p, \tag{7}$$

$$\ddot{\psi} + 3H\dot{\psi} = \frac{8\pi}{(2\omega+3)}(\rho - 3p), \tag{8}$$

where dots means time derivatives and $H = \dot{a}/a$ is the Hubble parameter. Let us assume the perfect fluid like form of BD energy-momentum tensor as $T^{BD}_{\mu\nu} = (\rho_{BD} + p_{BD})u_\mu u_\nu + p_{BD}g_{\mu\nu}$, where the energy density and pressure for BD are defined as

$$\rho_{BD} = \frac{1}{8\pi}\left[\frac{\omega}{2}\left(\frac{\dot{\psi}^2}{\psi}\right) - 3H\dot{\psi}\right], \tag{9}$$

$$p_{BD} = \frac{1}{8\pi}\left[\frac{\omega}{2}\left(\frac{\dot{\psi}^2}{\psi}\right) + 2H\dot{\psi} + \ddot{\psi}\right]. \tag{10}$$

The consistency of the BD field equations (2) yield

$$\nabla_\nu\left(R^{\mu\nu} - \frac{1}{2}g^{\mu\nu}R\right) = 0 = \nabla_\nu\left(\frac{8\pi}{\psi}\tilde{T}^{\mu\nu} + \frac{8\pi}{\psi}T^{\mu\nu}_{BD}\right). \tag{11}$$

Assuming that the matter with vacuum and scalar field conserve separately, i.e., $\tilde{T}^{\mu\nu}$ obeys the usual conservation law, $\nabla_\nu\tilde{T}^{\mu\nu} = 0$, which leads to

$$\dot{\rho_m} + 3H(\rho_m + p_m) = -\dot{\rho_\Lambda}. \tag{12}$$

One should note here that the EoS of the vacuum energy density follows the same usual form, i.e., $p_\Lambda(t) = -\rho_\Lambda(t) = -\psi\Lambda(t)/8\pi$ despite it evolves with time. From (11), we obtain

$$8\pi\tilde{T}^{\mu\nu}\,\nabla_\nu\left(\frac{1}{\psi}\right) + \nabla_\nu\left(\frac{8\pi}{\psi}T^{\mu\nu}_{BD}\right) = 0, \tag{13}$$

which simplifies to

$$\dot{\rho}_{BD} + 3H(\rho_{BD} + p_{BD}) = (\rho_m + \rho_\Lambda + \rho_{BD})\frac{\dot{\psi}}{\psi}. \tag{14}$$

In this paper, we assume that the scalar field ψ is related to scale-factor a by a power-law relation (Pimental 1985; Banerjee and Pavon 2007; Sheykhi 2010):

$$\psi = \psi_0\, a(t)^\epsilon, \tag{15}$$

where ψ_0 and ϵ are constants. Using (15) into (6), we get

$$H^2 = \frac{2}{(6 + 6\epsilon - \omega\epsilon^2)}\frac{8\pi}{\psi}(\rho_m + \rho_\Lambda), \tag{16}$$

where $\Lambda = 8\pi\rho_\Lambda/\psi$. One can find that the standard cosmology is recovered in the limit of $\epsilon \to 0$.

Finally, using (12) and (16), we find

$$\dot{H} + \frac{(3+\epsilon)}{2}H^2 = \frac{3\Lambda}{(6 + 6\epsilon - \omega\epsilon^2)}. \tag{17}$$

In the following sections, we find the exact solutions with two forms of $\Lambda(t)$: power-series and power-law forms.

3 A power series $\Lambda(t)$ model

In this paper, we assume the time-varying Λ as a truncated power series of the Hubble parameter up to the second order [hereafter, Λ_{PS}-model], that is, (Basilakos 2009; Basilakos et al. 2009; Oliveira et al. 2014)

$$\Lambda(t) = n_1 H + n_2 H^2, \tag{18}$$

where n_1 is a constant with dimension of H, while n_2 is a dimensionless constant. The first term, i.e., $\Lambda \propto H$ was discussed in Refs. (Schützhold 2002; Borges and Carneiro 2005; Carneiro et al. 2006, 2008) where as the second term, i.e., $\Lambda \propto H^2$ was proposed in Refs. (Carvalho et al. 1992;

Grande et al. 2006). Thus, Eq. (18) is a combination of linear and quadratic form of $\Lambda(t)$. Using (18) into (17), we get

$$\dot{H}+\left(\frac{3+\epsilon}{2}-\frac{3n_2}{(6+6\epsilon-\omega\epsilon^2)}\right)H^2=\frac{3n_1H}{(6+6\epsilon-\omega\epsilon^2)}. \tag{19}$$

Now, considering the current value of Λ as $\Lambda_0=3H_0^2\Omega_\Lambda$, where Ω_Λ is the density parameter for vacuum, Eq. (18) gives $n_1=H_0(\beta-3\Omega_m)$, where $\Omega_\Lambda=1-\Omega_m$. Here, Ω_m is the matter density parameter. Using this value of n_1, Eq. (19) can be rewritten as

$$\frac{dh}{dx}+\left(\frac{(3+\epsilon)(6+6\epsilon-\omega\epsilon^2)-6(3-\beta)}{2(6+6\epsilon-\omega\epsilon^2)}\right)h =\frac{3(\beta-3\Omega_m)}{(6+6\epsilon-\omega\epsilon^2)} \tag{20}$$

where $x=ln\,a$ and $h=H/H_0$ is the dimensionless Hubble parameter and $\beta=3-n_2$ (or $|n_2|\ll 1$). It is obvious from (20) that $\beta>3\Omega_m$, where $0<\beta<3$.

On solving (20), the dimensionless Hubble parameter as a function of the scalar factor can be written as

$$h(a)=\frac{6(\beta-3\Omega_m)}{(3+\epsilon)(6+6\epsilon-\omega\epsilon^2)-6(3-\beta)} +\left(1-\frac{6(\beta-3\Omega_m)}{(3+\epsilon)(6+6\epsilon-\omega\epsilon^2)-6(3-\beta)}\right)a^{-k}, \tag{21}$$

where $k=\frac{(3+\epsilon)(6+6\epsilon-\omega\epsilon^2)-6(3-\beta)}{2(6+6\epsilon-\omega\epsilon^2)}$. It is to be noted that for $\epsilon\to 0$, we recover the result obtained in Ref. (Oliveira et al. 2014) and further for $\beta\to 3$ i.e. $n_2\to 0$ and $\epsilon\to 0$, we recover the dynamical Λ solution derived in Ref. (Carneiro et al. 2006).

Considering $a=(1+z)^{-1}$, we can define the normalized Hubble expansion $E(z)$ as

$$E(z)=\frac{H}{H_0}=\tilde{\Omega}_{\Lambda 1}+\tilde{\Omega}_{m1}(1+z)^k, \tag{22}$$

where

$$\tilde{\Omega}_{\Lambda 1}=1-\tilde{\Omega}_{m1}=\frac{6(\beta-3\Omega_m)}{(3+\epsilon)(6+6\epsilon-\omega\epsilon^2)-6(3-\beta)}. \tag{23}$$

One can observe that for $\epsilon\to 0$ and $\beta\to 3$, Eq. (23) reduces to $\tilde{\Omega}_{\Lambda 1}=\Omega_\Lambda$. Assuming the scale factor to unity at present, i.e., $a_0=1$, the scale factor evolves with time as

$$a(t)=\left(\frac{e^{(k\tilde{\Omega}_{\Lambda 1}H_0\,t)}-1+\tilde{\Omega}_{\Lambda 1}}{\tilde{\Omega}_{\Lambda 1}}\right)^{1/k} \tag{24}$$

It is obvious from (24) that the scale factor varies as $a\sim t^{1/k}$, i.e., power-law expansion during the early times. Therefore, the model expands with decelerated rate. It is followed by a transition to an accelerating epoch where the scale factor varies $a\sim\exp(\tilde{\Omega}_{\Lambda 1}H_0\,t)$ in late time.

The observational data suggest that the accelerated expansion of the Universe is a recent phenomenon. It means that the Universe might be decelerated phase in the early epoch when there was no DE or when its effect was subdominant. Therefore, the Universe must have a transition from decelerating to accelerating phase. In this context, the deceleration parameter, which is defined as $q=-a\ddot{a}/\dot{a}^2$, plays an important role to describe the evolution history of the Universe. For this model, the deceleration parameter in terms of redshift is calculated as

$$q(z)=-1+\frac{k\,\tilde{\Omega}_{m1}\,(1+z)^k}{\tilde{\Omega}_{\Lambda 1}+\tilde{\Omega}_{m1}\,(1+z)^k}. \tag{25}$$

The present-day value q_0 can be found by putting $z=0$ in (25), which is given by

$$q_0=k\,\tilde{\Omega}_{m1}-1. \tag{26}$$

We now discuss the deceleration-acceleration transition redshift, z_{tr} which is defined as a redshift where $q(z)=0$ and it is given by

$$z_{tr}=-1+\left[\frac{2(6+6\epsilon-\omega\epsilon^2)\,\tilde{\Omega}_{\Lambda 1}}{\left((1+\epsilon)(6+6\epsilon-\omega\epsilon^2)-6(3-\beta)\right)\,\tilde{\Omega}_{m1}}\right]^{1/k}. \tag{27}$$

At this stage, we also discuss another important parameter, known as equation of state (EoS) parameter which describes the dynamics of the Universe. In this model, we discuss the effective EoS parameter, which is defined as $w_{eff}=-1-\frac{2a}{3}\frac{dh}{da}$. Using (21) in this expression, we get

$$w_{eff}(z)=-1+\frac{2k\tilde{\Omega}_{m1}}{3h}(1+z)^k. \tag{28}$$

The present value of EoS parameter is given by

$$w_{eff}(z=0)=-1+\frac{2k}{3}\tilde{\Omega}_{m1}. \tag{29}$$

The condition for acceleration of the present universe is given by

$$3w_{eff}(z=0)+1=2\left(-1+k\tilde{\Omega}_{m1}\right). \tag{30}$$

It should ne noted here that for an accelerated expansion of the Universe the effective EoS parameter must be $w_{eff}<(-1/3)$. This condition is satisfied if $\tilde{\Omega}_{m1}<1/k$, which is

also compatible with the analysis of deceleration parameter as given in Eq. (26). From Eq. (28), it is found that $w_{eff}(z) \to -1$ as $z \to -1$, i.e., as $a \to \infty$. Thus, the model exhibits to de Sitter Universe and coincides with the ΛCDM model in later stages of its evolution.

In what follows, we check the consistency of the model. Using (9), (10) and (16) into (14), we get

$$2(\omega\epsilon - 3)\dot{H} + (\omega\epsilon^2 + 6\omega\epsilon - 12)H^2 = 0. \tag{31}$$

We substitute the solution of Hubble function H from (22) into (31), we get

$$2k(\omega\epsilon - 3)\tilde{\Omega}_{m1}(1+z)^k + (12 - \omega\epsilon^2 - 6\omega\epsilon) \times (\tilde{\Omega}_{\Lambda 1} + \tilde{\Omega}_{m1}(1+z)^k) = 0. \tag{32}$$

It can be observed that, in general, the above equation is not satisfied. However, we can get a relation between the constants at present epoch, i.e., for $z = 0$, which is given by

$$2k(\omega\epsilon - 3)\tilde{\Omega}_{m1} + (12 - \omega\epsilon^2 - 6\omega\epsilon) = 0. \tag{33}$$

Once we get the best-fit values of model parameters by observations, we can check the consistency of the Eq. (33) for the present epoch.

4 A power-law $\Lambda(t)$ model

Bertolami (1986), Ozer and Taha (1987), and Chen and Wu (1990) have studied the model with vacuum energy density in general relativity which evolves as $\Lambda \propto a^{-2}$. In the following, we assume that the vacuum energy density evolves as the general power of the scale factor (hereafter Λ_{PL}-model):

$$\Lambda(a) = 3\gamma a^{-n}, \tag{34}$$

where γ is a constant. Using (34) in (17) and simplifying, we get

$$\frac{dH^2}{da} + \frac{(3+\epsilon)}{a}H^2 = \frac{18\gamma}{(6 + 6\epsilon - \omega\epsilon^2)}a^{-n-1}. \tag{35}$$

Using the present value of vacuum energy density, $\Lambda_0 = 3H_0^2\Omega_\Lambda$ into (34), we get $\gamma = \Omega_\Lambda H_0^2$. Using this value of γ, the solution of (35) with $H(a=1) = H_0$ in terms of redshift is given by

$$E(z) = \frac{H}{H_0} = \left[\tilde{\Omega}_{m2}(1+z)^{(3+\epsilon)} + \tilde{\Omega}_{\Lambda 2}(1+z)^n\right]^{1/2}, \tag{36}$$

where

$$\tilde{\Omega}_{\Lambda 2} = \frac{18\Omega_\Lambda}{(6 + 6\epsilon - \omega\epsilon^2)(3 + \epsilon - n)}, \tag{37}$$

and

$$\tilde{\Omega}_{m2} = 1 - \frac{18\Omega_\Lambda}{(6 + 6\epsilon - \omega\epsilon^2)(3 + \epsilon - n)}. \tag{38}$$

The deceleration parameter which is defined in the previous section is redefined as $q = -1 - \frac{a}{2H^2(a)}\frac{dH^2}{da}$ and it gives

$$q = -1 + \frac{1}{2}\frac{(3+\epsilon)\tilde{\Omega}_{m2}(1+z)^{(3+\epsilon)} + n\tilde{\Omega}_{\Lambda 2}(1+z)^n}{\tilde{\Omega}_{m2}(1+z)^{(3+\epsilon)} + \tilde{\Omega}_{\Lambda 2}(1+z)^n}. \tag{39}$$

It is clear from (39) that $q(z)$ tends to -1 in the future (negative redshifts). The present value q_0 is obtained as

$$q_0 = -1 + \frac{(3+\epsilon)\tilde{\Omega}_{m2} + n\tilde{\Omega}_{\Lambda 2}}{2}. \tag{40}$$

The transition redshift is given by

$$z_{tr} = \left(\frac{(2-n)\tilde{\Omega}_{\Lambda 2}}{(1+\epsilon)\tilde{\Omega}_{m2}}\right)^{1/(3+\epsilon-n)} - 1, \tag{41}$$

where as the effective EoS parameter is calculated as

$$w_{eff} = -1 + \frac{1}{3}\frac{(3+\epsilon)\tilde{\Omega}_{m2}(1+z)^{(3+\epsilon)} + n\tilde{\Omega}_{\Lambda 2}(1+z)^n}{\tilde{\Omega}_{m2}(1+z)^{(3+\epsilon)} + \tilde{\Omega}_{\Lambda 2}(1+z)^n}. \tag{42}$$

The w_{eff} at $z = 0$ is obtained as

$$w_{eff}(z=0) = -1 + \frac{1}{3}\left((3+\epsilon)\tilde{\Omega}_{m2} + n\tilde{\Omega}_{\Lambda 2}\right). \tag{43}$$

From above equation, we observe that the condition for acceleration of the present Universe $3w_{eff}(z=0) + 1 < 0$ is satisfied if $(3+\epsilon)\tilde{\Omega}_{m2} + n\tilde{\Omega}_{\Lambda 2} < 2$, which is also compatible with the analysis of deceleration parameter. From Eq. (43), it is found that $w \to -1$ as $z \to -1$, i.e., as $a \to \infty$. Thus, the model attains to de Sitter Universe and coincides with the ΛCDM model in late time evolution.

Let us check also the consistency of the model. Substituting the solution of Hubble function $H(z)$ obtained in Eq. (36) in Eq. (31), we get

$$(\omega\epsilon - 3)[(3+\epsilon)\tilde{\Omega}_{m2}a^{-(3+\epsilon)} + n\tilde{\Omega}_{\Lambda 2}a^{-n}] - (\omega\epsilon^2 + 6\omega\epsilon - 12)[\tilde{\Omega}_{m2}a^{-(3+\epsilon)} + \tilde{\Omega}_{\Lambda 2}a^{-n}] = 0. \tag{44}$$

We can get the relation between the constants at present epoch which is as follows.

$$(\omega\epsilon - 3)[(3+\epsilon)\tilde{\Omega}_{m2} + n\tilde{\Omega}_{\Lambda 2}] - (\omega\epsilon^2 + 6\omega\epsilon - 12) = 0. \tag{45}$$

We will check the above consistency equation for the model once the best-fit values of model parameters by observations are obtained.

5 Data sample and methodology

In this section we discuss the observational constraints on the free parameters of Λ_{PS} and Λ_{PL} models by using the latest observational data of $H(z)$, Type Ia supernovae and baryon acoustic oscillations.

5.1 Hubble data

The Hubble parameter measurements (abbreviated as $H(z)$) is an effective tools to constrain the free parameters of the model. In literature, there are two different techniques, differential-age method (Stern et al. 2010) and radial BAO method (Gaztañaga et al. 2009) to measure the Hubble parameter. We use 30 data points of Hubble parameter obtained by the so-called differential-age technique applied passively evolving galaxies in the redshift range $0.07 \leq z \leq 1.965$ as listed in Table 3 of Ref. (Solà et al. 2017). These Hubble data inputs are uncorrelated with the BAO data points.

The chi-square is defined as

$$\chi^2_{H(z)} = \sum_{i=1}^{30} \left[\frac{H_{obs}(z_i) - H_{th}(z_i, \mathbf{p})}{\sigma_{H,i}} \right]^2, \tag{46}$$

where $H_{th}(z_i)$ is the theoretical values and $H_{obs}(z_i)$ represents observed values as given in Table 3 of Ref. (Solà et al. 2017) and $\mathbf{p}$ is the set of space parameters.

5.2 Type Ia supernovae

We use the recent Type Ia supernovae (SNe) data points, the so-called Pantheon sample which includes 1048 data points of luminosity distance in the redshift range $0.01 < z < 2.3$ (Scolnic et al. 2018). This sample contains PanSTARRS1 Medium Deep Survey, SDSS, Low-z and HST samples (Scolnic et al. 2018). The chi-square function for Pantheon SNe data is

$$\chi^2_{SNe(Pan)} = \Delta\mu^T \cdot C^{-1} \cdot \Delta\mu, \tag{47}$$

where $\Delta\mu = \mu_i^{obs} - \mu^{th}(z_i, \mathbf{p})$. The observed distance modulus, μ_i^{obs} reads $\mu_{obs} = m_B - M_B$, where m_B is the observed peak magnitude in the rest frame of the B band and M_B is the absolute magnitude nuisance of SNe. The theoretical distance modulus, μ^{th}, which depends on redshift and the cosmological parameters, is defined by

$$\mu^{th}(z, \mathbf{p}) = 5\ \log_{10}[d_L(z, \mathbf{p})/10\ pc] + \mathcal{M}, \tag{48}$$

where $d_L(z)$ is the luminosity distance which is given by

$$d_L(z, \mathbf{p}) = (1+z)c \int_0^z \frac{dz'}{H(z', \mathbf{p})}, \tag{49}$$

where c is the speed of light. Also, $\mathcal{M}$ is the nuisance parameter in which H_0 and M_B can be absorbed. It is to be noted that M has been assumed to be 23.83. It is mentioned that C is the total covariance matrix which takes the form $C = D_{stat} + C_{sys}$, where the diagonal matrix D_{stat} and covariant matrix C_{sys} denote the statistical uncertainties and the systematic uncertainties, respectively.[1]

Simple analytical models of light curve predict that the SNe peak luminosity is proportional to the mass of nickel synthesized which in turn, to a good approximation, is a fixed fraction of the Chandrasekhar mass ($M_{Ni} \propto M_{Ch}$), which satisfies $M \propto G^{-3/2}$ (Khokhlov et al. 1993; Gomez-Gomar et al. 1998; Karimkhani and Khoadam-Mohammadi 2019). Based on the fact that luminosity $L \propto M_{Ch}$, a modification is required to the absolute magnitude of a SNe in the case of varying G. Thus, for the luminosity distance we have $L \propto G^{-3/2}$, i.e., for a slow decrease of G with time, the distant supernovae should be dimmer than predicted for a standard scenario. Using the definition of absolute magnitude

$$M = -2.5 \log \frac{L}{L_\odot}, \tag{50}$$

the modulus distance relation (48) must be corrected as (Li et al. 2015; Karimkhani and Khoadam-Mohammadi 2019)

$$\mu^{th}(z, \mathbf{p}) = 5\ \log_{10}[d_L(z, \mathbf{p})/10\ pc] + \frac{15}{4} \log \frac{G}{G_0} + \mathcal{M}. \tag{51}$$

Since, in BD theory, $G \propto \psi^{-1}$, where $\psi = \psi_0 a^\epsilon$, we rewrite (51) as

$$\mu^{th}(z, \mathbf{p}) = 5\ \log_{10}[d_L(z, \mathbf{p})/10\ pc] + \frac{15}{4}\epsilon \log(1+z) + \mathcal{M}. \tag{52}$$

5.3 Baryon acoustic oscillations (BAO_{dz})

In recent years, measurements of BAO have been proven as an important geometric probe that we can employ to constrain the dark energy models. In this paper, we have used BAO estimator $d_z(z)$ collected by Blake et al. (2011). It can computed as follows:

$$d_z(z_i, \mathbf{p}) = \frac{r_s(z_d)}{D_V(z_i)}, \tag{53}$$

where

$$r_s(z_d) = \int_{z_d}^{\infty} \frac{cdz}{H(z)\sqrt{3\left(1 + \frac{\delta\rho_b}{\delta\rho_\gamma}\right)}} \tag{54}$$

[1] https://archive.stsci.edu/prepds/ps1cosmo/index.html.

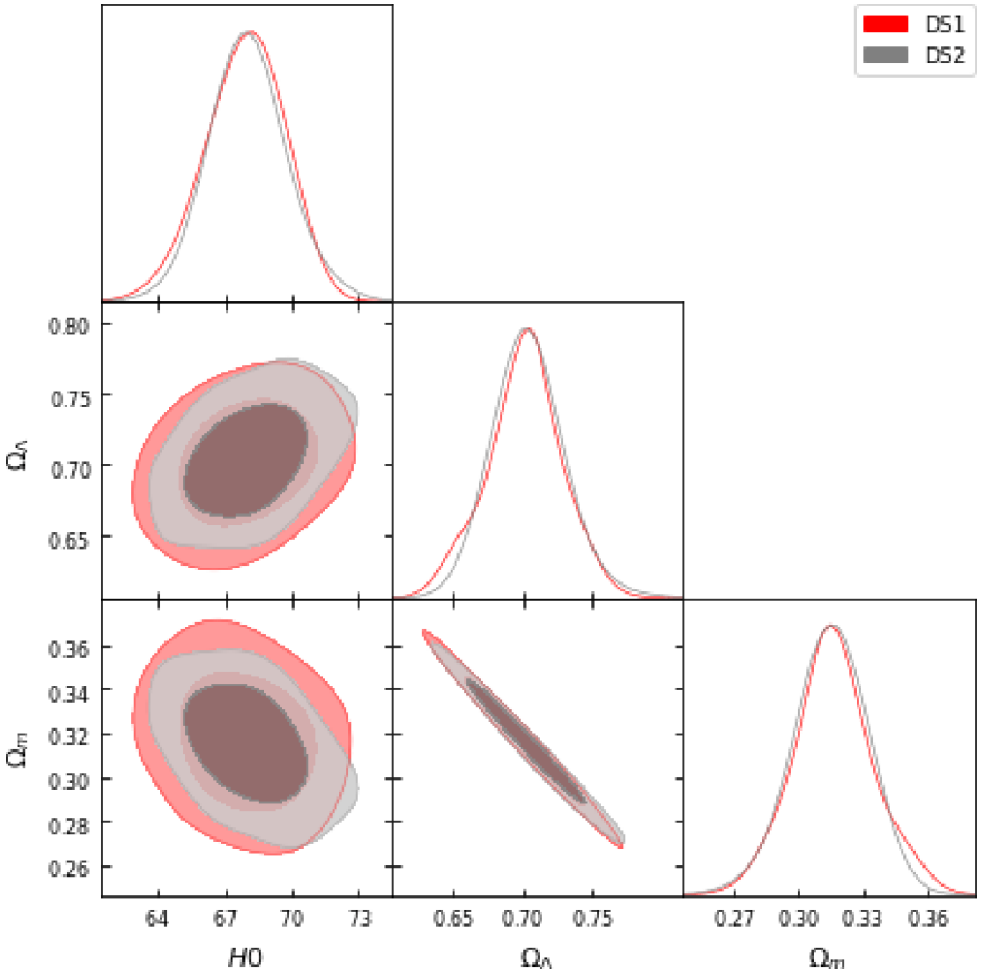

Fig. 1 Two-dimensional confidence contours and one-dimensional posterior distributions on free parameters in ΛCDM model obtained from the datasets $DS1 : SNe + H(z)$ (red contours) and $DS2 : SNe + H(z) + BAO_{dz}$ (grey contours)

is the comoving sound horizon prior to the drag redshift epoch, z_d, i.e., the epoch at which baryons are released from the Compton drag of photons, and ρ_b and ρ_γ are the baryon and photon densities, respectively.

The remaining term, $D_V(z)$ is the "dilation scale" introduced by Eisenstein et al. (2005) and can be calculated by

$$D_V(z) \equiv \left[(1+z)^2 D_A^2(z)\frac{c\,z}{H(z)}\right]^{\frac{1}{3}}. \tag{55}$$

Here, $D_A(z) = (1+z)^{-2} d_L(z, \mathbf{p})$ is the angular diameter distance.

The chi-square function for BAO_{dz} is defined as (Gomez-Valent et al. 2015a,b)

$$\chi^2_{BAO_{dz}}(\mathbf{p}) = \sum_{i=1}^{6}\left[\frac{d_{z,th}(z_i, \mathbf{p}) - d_{z,obs}(z_i)}{\sigma_{z,i}}\right]^2 \tag{56}$$

The values of $z_i, d_{z,obs}, \sigma_{z,i}$ can be found in Table 3 of Blake et al. (2011).

6 Results and discussion

In our analysis, we use the publicly available MCMC sampling algorithm in emcee python library (Foreman-Mackey et al. 2013) to generate the chain. In MCMC method, the best-fit of the parameters are maximized by using the probability function $\mathcal{L} \propto \exp(-\chi^2/2)$.

In order to find the best fit, we minimize the overall χ^2 function using two different combinations of datasets, namely, $DS1 : \chi^2_{min} = \chi^2_{Sne} + \chi^2_{H(z)}$ and $DS2 : \chi^2_{min} = \chi^2_{SNe} + \chi^2_{H(z)} + \chi^2_{BAO_{dz}}$. The main cosmological parameters are ϵ, ω and H_0 which are common for both models. In addition to this Λ_{PS}-model has two extra parameters Ω_m and β, and Λ_{PL}-model has two extra parameters n and Ω_Λ. We constrain the space parameters in three models: ΛCDM, Λ_{PS} and Λ_{PL}. The contours of our statistical analyses are shown in Figs. 1, 2, 3 and best-fit values of parameters are summarized in Table 1 that arise from the joint analysis described above. Using fitting values of parameters of ΛCDM, Λ_{PS} and Λ_{PL} models, a comparative study of Λ_{PS} and Λ_{PL} models with concordance ΛCDM are as follows:

17

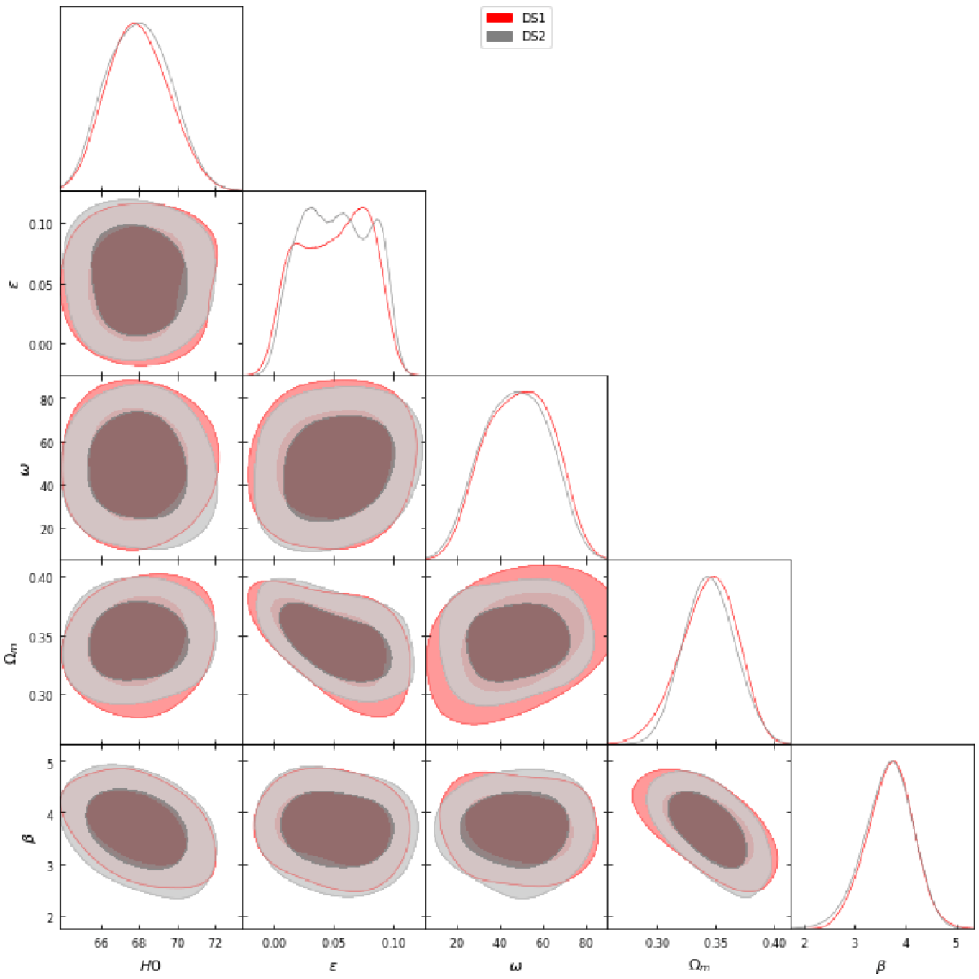

Fig. 2 Two-dimensional confidence contours and one-dimensional posterior distributions on free parameters in the Λ_{PS} model obtained from the datasets $DS1 : SNe + H(z)$ (red contours) and $DS2 : SNe + H(z) + BAO_{dz}$ (grey contours)

Table 1 The fit values of parameters of ΛCDM, Λ_{PS} and Λ_{PL}, respectively obtained from $DS1 : SNe + H(z)$ and $DS2 : SNe + H(z) + BAO_{dz}$ datasets. The H_0 parameter is expressed in Km s^{-1} Mpc^{-1}

$Models \rightarrow$	ΛCDM		Λ_{PS}		Λ_{PL}	
$Parameters \downarrow$	$DS1$	$DS2$	$DS1$	$DS2$	DS1	DS2
H_0	$68.179^{+2.008}_{-1.670}$	$68.126^{+1.311}_{-1.788}$	$67.801^{+1.688}_{-1.634}$	$67.706^{+1.617}_{-1.575}$	$67.266^{+1.440}_{-1.683}$	$67.182^{+1.615}_{-1.612}$
ϵ	–	–	$0.036^{+0.032}_{-0.037}$	$0.036^{+0.031}_{-0.037}$	$0.038^{+0.034}_{-0.030}$	$0.038^{+0.035}_{-0.029}$
ω	–	–	$48.234^{+18.385}_{-19.161}$	$48.384^{+18.593}_{-19.664}$	$46.489^{+20.241}_{-18.530}$	$46.151^{+19.415}_{-19.238}$
β	–	–	$3.710^{+0.414}_{-0.447}$	$3.709^{+0.419}_{-0.417}$	–	–
n	–	–	–	–	$0.219^{+0.101}_{-0.136}$	$0.222^{+0.116}_{-0.136}$
Ω_m	$0.313^{+0.018}_{-0.016}$	$0.314^{+0.015}_{-0.018}$	$0.344^{+0.023}_{-0.024}$	$0.341^{+0.026}_{-0.024}$	–	–
Ω_Λ	$0.708^{+0.023}_{-0.027}$	$0.706^{+0.027}_{-0.022}$	–	–	$0.672^{+0.021}_{-0.021}$	$0.669^{+0.021}_{-0.021}$
χ^2_{min}	569.617	10684.353	553.587	10659.909	544.063	10633.291
AIC	575.639	10690.355	563.642	10669.964	554.685	10643.346
ΔAIC	–	–	11.997	20.391	20.954	47.029
BIC	578.714	10693.458	568.750	10675.084	559.226	10684.474
ΔBIC	–	–	9.964	18.374	19.488	8.984

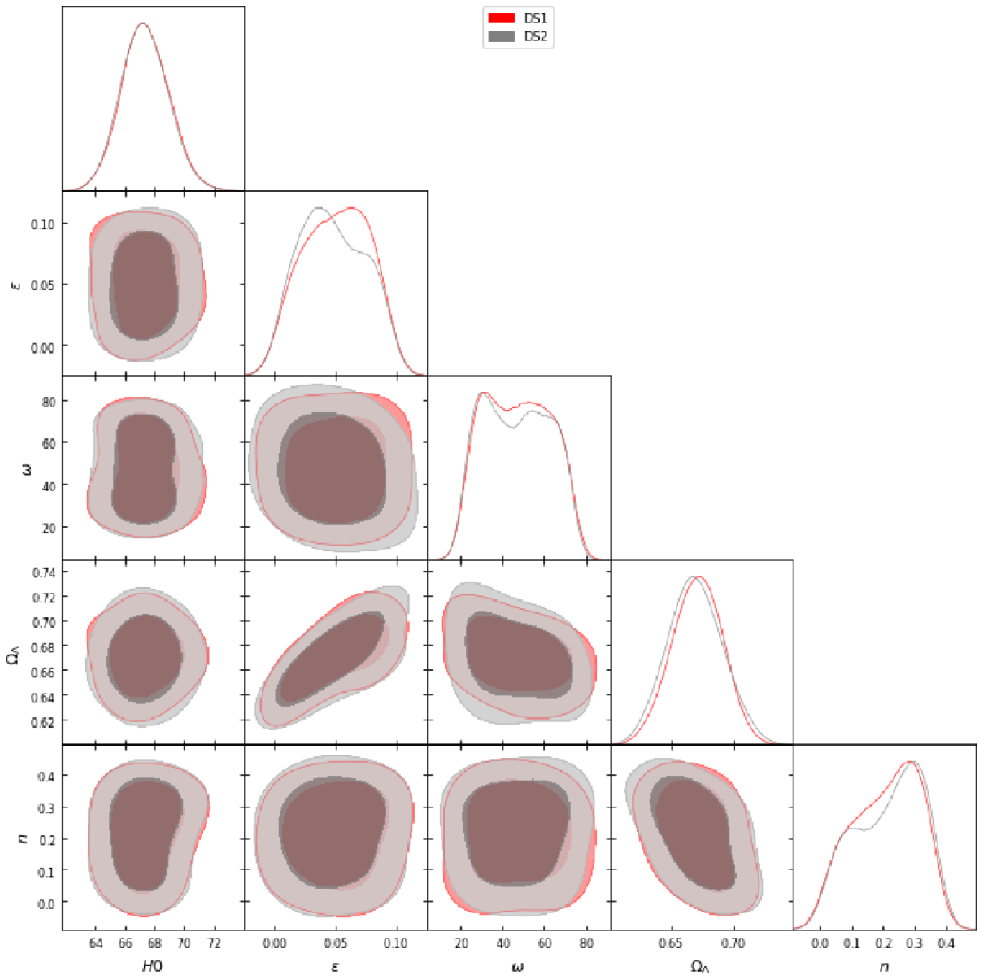

Fig. 3 Two-dimensional confidence contours and one-dimensional posterior distributions on free parameters in the Λ_{PL} model obtained from datasets $DS1 : SNe + H(z)$ (red contours) and $DS2 : SNe + H(z) + BAO_{dz}$ (grey contours)

Table 2 The transition value z_{tr} and the present values of q, w_{eff} of ΛCDM, Λ_{PS} and Λ_{PL}, respectively

$Model \rightarrow$	ΛCDM		Λ_{PS}		Λ_{PL}	
$Values \downarrow$	$DS1$	$DS2$	DS1	DS2	DS1	DS2
z_{tr}	$0.651^{+0.048}_{-0.048}$	$0.647^{+0.055}_{-0.055}$	$0.735^{+0.051}_{-0.180}$	$0.735^{+0.064}_{-0.180}$	$0.667^{+0.045}_{-0.052}$	$0.607^{+0.045}_{-0.052}$
q_0	$-0.541^{+0.032}_{-0.032}$	$-0.535^{+0.031}_{-0.031}$	$-0.770^{+0.23}_{-0.23}$	$-0.780^{+0.23}_{-0.23}$	$-0.459^{+0.018}_{-0.018}$	$-0.459^{+0.018}_{-0.018}$
$w_{eff}(z=0)$	$-0.694^{+0.021}_{-0.021}$	$-0.690^{+0.021}_{-0.021}$	$-0.850^{+0.15}_{-0.15}$	$-0.850^{+0.16}_{-0.16}$	$-0.639^{+0.012}_{-0.012}$	$-0.639^{+0.012}_{-0.012}$

In Λ_{PS} model, we find $\Omega_m = 0.344^{+0.023}_{-0.024}$ and $\Omega_m = 0.341^{+0.026}_{-0.024}$ from $DS1$ and $DS2$, respectively which are subsequently higher than the respective values $\Omega_m = 0.313^{0.018}_{-0.016}$ and $\Omega_m = 0.314^{+0.015}_{-0.018}$ of ΛCDM model. However, these results are close to $\Omega_m = 0.32^{+0.01}_{-0.02}$ obtained in Ref. (Basilakos et al. 2009) in general relativity.

The respective transition from deceleration to acceleration takes place at the redshift $z_{tr} = 0.735^{+0.051}_{-0.180}$ and $z_{tr} = 0.735^{+0.064}_{-0.180}$, which show that the transitions occur earlier than ΛCDM model as mentioned in Table 2, and also $z_{tr} = 0.660$ as obtained in Ref. Aghanim et al. (2020).

The present values of q and w_{eff} are listed in Table 2 which show that the q_0 and $w_{eff}(z=0)$ of Λ_{PS} are lower than the ΛCDM obtained from $DS1$ dataset. However, these values, which are obtained with dataset $DS2$, are little-bit higher than ΛCDM model. From Figs. 6 and 8, we observe that as $z \rightarrow -1$, both q and EoS parameter w_{eff} tend to -1. The present values of Hubble parameter are $H_0 = 67.801^{+1.688}_{-1.634}$ Km s^{-1} Mpc^{-1} and $H_0 = 67.706^{+1.617}_{-1.575}$ Km s^{-1} Mpc^{-1}, which are good agreement with Planck result (Aghanim et al. 2020), where $H_0 = 67.7 \pm 0.46$ Km s^{-1} Mpc^{-1}. However, these values are slightly lower than the values of ΛCDM obtained from the same datasets.

In this model we have two extra free parameters, namely ϵ and β with respect to the ΛCDM model. In dataset $DS1$ we find $\epsilon = 0.036^{+0.032}_{-0.037}$ and $\beta = 3.710^{+0.414}_{-0.447}$ whereas for $DS2$ dataset, we have $\epsilon = 0.036^{+0.031}_{-0.037}$ and $\beta = 3.709^{+0.419}_{-0.417}$.

The χ^2 is an important quantity which is used to data fitting process. In this analysis, we find $\chi^2 = 553.587$ and $\chi^2 = 10659.909$, respectively with respect to $DS1$ and $DS2$ datasets. The reduced chi-square is defined as $\chi^2_{red} = \chi^2_{min}/\nu$, where $\nu = (N - n)$ is the degree of freedom (dof). Here, N is total number of combined data, which are 1078 and 1084 and n is the number of estimated free parameters of model, which is 5 for each dataset $DS1$ and $DS2$, respectively. If $\chi^2_{red} \leq 1$, then the fit is good and the observed data is consistent with proposed model. For Λ_{PS} model, it is $\chi^2_{red} = 0.515$ and $\chi^2_{red} = 9.879$, respectively. Thus, the data $DS1$ is compatible with the considered model.

An another way to analyze the departure from the concordance ΛCDM model is through the *jerk parameter (j)*, which is a dimensionless third order derivative of the scale factor $a(t)$ with respect to cosmic time t. It is defined as (Blandford et al. 2004; Rapetti et al. 2007)

$$j = \frac{\dddot{a}(t)}{aH^3} = -q + (1+z)\frac{dq}{dz} + 2q(1+q), \tag{57}$$

where q is the deceleration parameter as given by (25) and (39). This parameter gives the information about the dynamics of DE corresponding to $j(z) = 1$ (constant) for ΛCDM model. Any deviation from $j = 1$ would favor a non-ΛCDM model. The plot of jerk parameter $j(z)$ is shown in Fig. 10 using the best-fit values of parameters obtained from DS1 and DS2 datasets in (57). It is found that $j(z) \to 1$ as $z \to -1$ which incorporates the flat ΛCDM model well in late times. The current value $j(z)$ at $z = 0$ is $j_0 = 0.6214$ and $j_0 = 0.6247$ with DS1 and DS2 datasets, respectively which differ from $j_0 = 1$ at present-day.

In Λ_{PL}, we find $\Omega_\Lambda = 0.672 \pm 0.021$ from $DS1$ and $\Omega_\Lambda = 0.669 \pm 0.021$ from $DS2$, which are comparatively lower than the value $\Omega_\Lambda = 0.708^{+0.023}_{-0.027}$ and $\Omega_\Lambda = 0.706^{+0.027}_{-0.022}$, respectively. The redshift transition values are $z_{tr} = 0.667^{+0.045}_{-0.052}$ and $z_{tr} = 0.607^{+0.045}_{-0.052}$, which are consistent with the values of ΛCDM model.

The present values of Hubble constant for this model are $H_0 = 67.266^{+1.440}_{-1.683}$ and $H_0 = 67.182^{+1.615}_{-1.612}$ obtained from DS1 and DS2 datasets which are slightly lower than the values of ΛCDM model. The evolution of $H(z)$ for this model with ΛCDM are shown in Fig. 4 and 5. The present values of q are higher than ΛCDM model whereas the $w_{eff}(z = 0)$ are very closed to standard model (refer to Table 2). From Fig. 6, 7, 8, 9, we observe that as $z \to \infty$, $q \to -0.779$ and -0.802, where as $w_{eff} \to -0.850$ and -0.864 for datasets $DS1$ and $DS2$, respectively. This model shows the quintessence-like behavior $(-1 < w \leq 0)$ in late-time evolution. This model has two extra parameters, namely ϵ and n with respect to the ΛCDM model. The best-fit values of these parameters are $\epsilon = 0.038^{+0.034}_{-0.030}$ and $n = 0.219^{+0.101}_{-0.136}$ from $DS1$ dataset, and $\epsilon = 0.038^{+0.035}_{-0.029}$ and $n = 0.222^{+0.116}_{-0.136}$

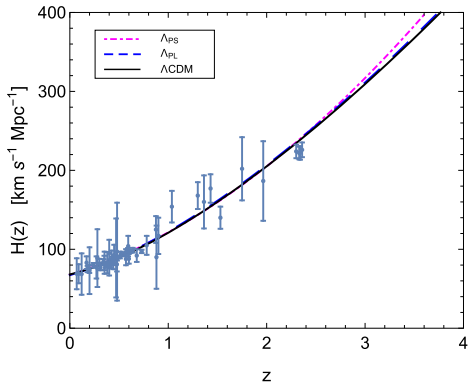

Fig. 4 Best fits over $H(z)$ obtained from $DS1$ dataset. The grey bars show the data points of $H(z)$

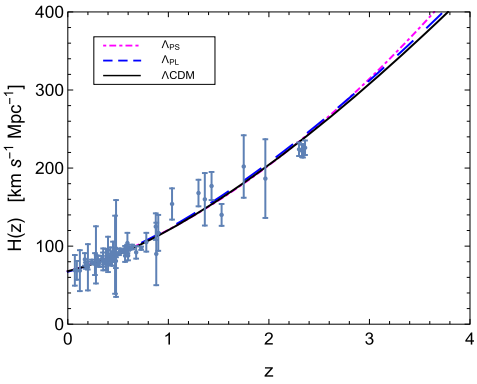

Fig. 5 Best fits over $H(z)$ obtained from $DS2$ dataset. The grey bars show the data points of $H(z)$

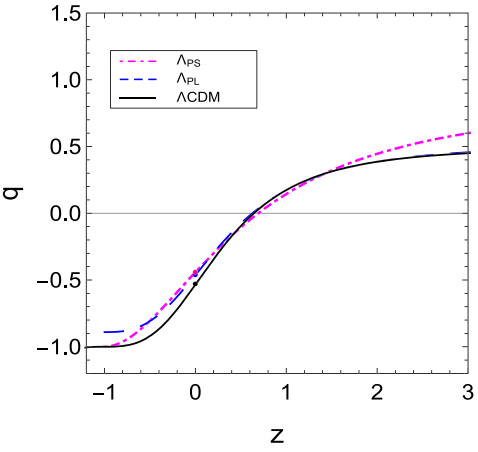

Fig. 6 Plot of evolution of deceleration parameter with redshift using fitting values of parameters obtained from $DS1$ dataset. The dot denotes the present value of deceleration parameter

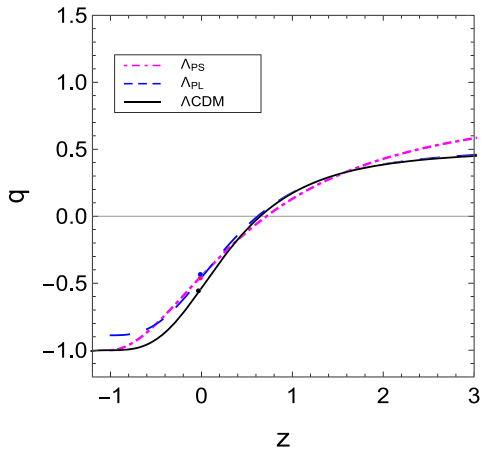

Fig. 7 Plot of evolution of deceleration parameter with redshift using fitting values of parameters obtained from $DS2$ dataset. The dot denotes the present value of deceleration parameter

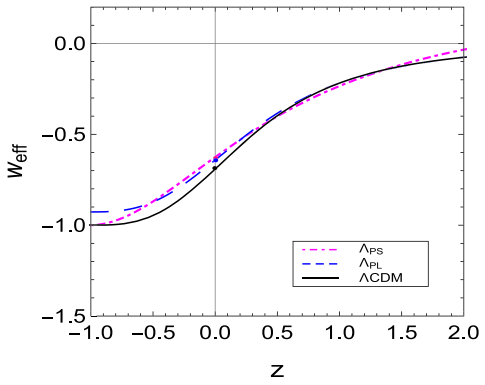

Fig. 8 Plot of evolution of EoS parameter with redshift using fitting values of parameters obtained by $DS1$ dataset. The dot denotes the present value of EoS parameter

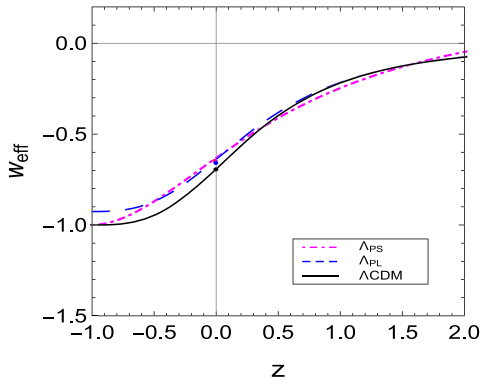

Fig. 9 Plot of evolution of EoS parameter with redshift using fitting values of parameters obtained by $DS2$ dataset. The dot denotes the present value of EoS parameter

from $DS2$. The values of n are much larger than the value $n = -0.06 \pm 0.04$ obtained in Ref. (Basilakos et al. 2009).

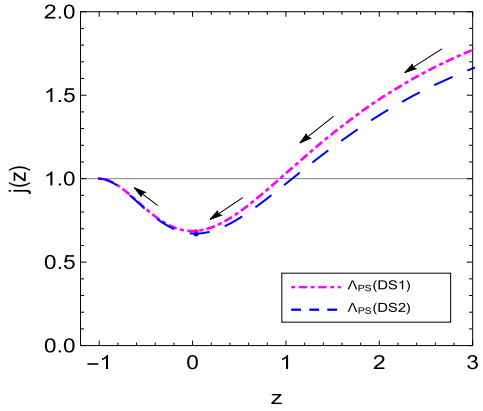

Fig. 10 Plot of evolution of jerk parameter $j(z)$ with redshift z using fitting values of parameters of Λ_{PS}. The horizontal line represents the ΛCDM model

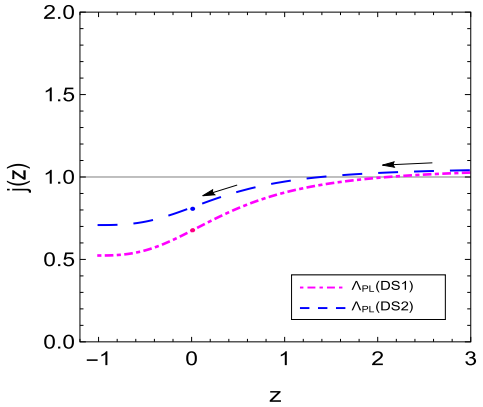

Fig. 11 Plot of evolution of jerk parameter $j(z)$ with redshift z using fitting values of parameters of Λ_{PL}. The horizontal line represents the ΛCDM model

The respective chi-square values from DS1 and DS2 datasets are $\chi^2 = 544.063$ and $\chi^2 = 10633.291$ for which $\chi^2_{red} = 0.507$ and $\chi^2_{red} = 9.854$. Thus, the χ^2_{red} is less than unity for $DS1$ dataset which show that the model provides a very good fit to this dataset.

The plot of jerk parameter $j(z)$ as a function of redshift z is shown in Fig. 11 using the best-fit values of parameters obtained from DS1 and DS2 datasets. It is observed that the Λ_{PL} deviates from the ΛCDM model at current epoch ($j_0 = 0.6004$ and $j_0 = 0.6574$, respectively) as well as $z \to -1$. These deviations from ΛCDM model need attention which would be found to know the real cause behind the cosmic acceleration.

In a paper (Singh and Solà Peracaula 2021), the authors explored two functional forms of Λ: $\Lambda = \text{const.}$ and $\Lambda = \sigma H$, so-called Λ_{H1} and Λ_{H2} models in BD theory. It was found that the BD version of the Λ-cosmology, i.e., Λ_{H1} is on an essentially equal footing position as compared to the concordance model in the light of observational fits. However, despite the quality fit of the Λ_{H2}, the model does

not adapt to the consistency equation and Ω_Λ comes to very poor with this equation which is not acceptable in the present scenario. It has been shown that model Λ_{H1}, in the context of the BD theory, is more favored than Λ_{H2} and is comparable to the concordance ΛCDM model within general relativity.

In the present Λ_{PS} and Λ_{PL} models, the observational values obtained from DS1 and DS2 datasets are much more favored and satisfy the consistency equations (33) and (45), respectively, which show that the Λ_{PS} and Λ_{PL} models are also analytically consistent. The analytical values of Ω_Λ are much favored with the observed values obtained from DS1 and DS2 datasets in both the models. The version of the BD framework with these dynamical forms of Λ improve the efficiency with respect to the two datasets used. This can also be observed by information criteria as discussed below.

7 Selection criteria

In order to compare the proposed models with ΛCDM, we implement the selection information criteria in terms of the strength of the evidence according to Akaike information criteria (AIC) (Akaike 1974) and Bayesian information criteria (BIC) (Schwarz 1978). These information criteria penalize the presence of extra degree of freedom (d.o.f.). For detail discussion about these criteria, we refer to Ref. (Liddle 2007). The AIC and BIC are respectively defined as

$$AIC = \chi^2_{min} + \frac{2nN}{N-n-1}, \tag{58}$$

and

$$BIC = \chi^2_{min} + n\log(N), \tag{59}$$

where n is the number of free parameters and N is the size of the data sample. It is to be noted that the dataset $DS1$ has a total of 1078 data points (1048 data points of SNe and 30 points of $H(z)$), where as the dataset $DS2$ has 1084 data points (1048 data points of SNe, 30 points of $H(z)$ and 6 points of BAO_{dz}).

Assuming AIC (or BIC) value of ΛCDM as the reference, the AIC (or BIC) differences are defined as $\Delta AIC_i = AIC_i - AIC_{\Lambda CDM}$ (or $\Delta BIC_i = BIC_i - BIC_{\Lambda CDM}$), where i denotes either the Λ_{H1} or the Λ_{H2} model. A model having $0 \leq \Delta AIC$ (or ΔBIC) ≤ 2 gives "weak evidence in favor". In contrast, for $2 < \Delta AIC < 4$ and $2 \leq \Delta BIC < 6$, the model has "positive evidence in favor", where as for $6 \leq \Delta AIC$ (or ΔBIC) < 10, the model is considered to have "strong evidence in favor" and finally, for ΔAIC (or ΔBIC) > 10, the model has "very strong evidence in favor" (Liddle 2007). The AIC and BIC and their difference values ΔAIC and ΔBIC for models *PS-model* and *PL-model* with reference to the corresponding values of AIC and BIC of ΛCDM model are given in Table 1.

According to AIC and BIC in $DS1$ dataset, we find $\Delta AIC(\Delta BIC) = 11.997(9.964)$ for Λ_{PS} whereas it is $\Delta AIC(\Delta BIC) = 20.954(19.488)$ for Λ_{PL}. Similarly, in $DS2$ dataset, we find $\Delta AIC(\Delta BIC) = 20.391(18.374)$ for Λ_{PS} and $\Delta AIC(\Delta BIC) = 47.029(8.984)$ for Λ_{PL}. These values suggest that according to AIC, there is a *very strong evidence in favor* whereas as per BIC there is a *strong evidence in favor* of these two models.

8 Conclusion

In this work, we have discussed the dynamics of a flat FLRW model in BD theory with varying vacuum energy density. We have assumed two different functional forms of vacuum energy density, namely power series expansion in H up to the second order excluding constant term (Λ_{PS}-model) and power-law form in terms of scale factor (Λ_{PL}-model), in order to parametrize the vacuum energy density. In the first step, we have solved the BD field equations analytically using these two forms of vacuum energy density. These two models have different theoretical solutions. We have discussed the cosmological consequences of cosmic acceleration based on these two forms of interacting Λ scenarios. Secondly, we have performed two different combinations of joint likelihood analysis $DS1 = SNe + H(z)$ and $DS2 = SNe + H(z) + BAO_{dz}$ for each model including ΛCDM model in order to put the constraints on the main free parameters by χ^2 minimizing technique. It is noted that there are extra parameters, namely ϵ and β in Λ_{PS}, and ϵ and n in Λ_{PL} with respect to the ΛCDM model. The fit values of these free parameters are provided in Table 1.

Figures 1-3 show the two-dimensional confidence contours and one-dimensional posterior distributions on the free parameters in ΛCDM, Λ_{PS} and Λ_{PL} models obtained from two different datasets. The best-fit values of the model's parameters, transition redshift z_{tr}, q_0 and $w_{eff}(z=0)$ are displayed in the Tables 1 and 2, respectively. Using the fitting values we have discussed the dynamical behavior of various cosmological parameters, like $H(z)$, $q(z)$, $w_{eff}(z)$ and $j(z)$ by plotting the trajectories of evolution with redshift as shown in Figs. 4-11. In view of the observational datasets, we find datasets $DS1$ and $DS2$ are very much compatible for the considered models. The present values H_0, q_0 and $w_{eff}(z=0)$ are very close to the ΛCDM model. However, the current value of jerk parameter j_0 deviates from concordance model. We have found that the Λ_{PS} model behaves as a de Sitter model in late-time evolution of the Universe where as the Λ_{PL} model behaves as a quintessence DE with an EoS lying in $(-1 < w \leq 0)$. The χ^2_{red} implies the same goodness of the models considered here. Also, using

the best-fit values of models parameters, we have found that the consistency equations (33) and (45) for the both models are satisfied. In what follows, we have summarized our main results in more detail.

Assuming ΛCDM as a reference model, we have discussed the performance of these two proposed models. We have found that both the Λ_{PS} and Λ_{PL} models show a smooth transition from deceleration ($q > 0$) epoch to acceleration ($q < 0$) epoch in recent past. The trajectories of $q(z)$ clearly show that the models generate decelerated expansion in past and late time cosmic acceleration in present. Figures 6 and 7 also show the transition from decelerated to accelerated expansion happen in the range $0.667 \leq z_{tr} \leq 0.735$ which are comparatively same as ΛCDM model. The parameters $q(z)$, w_{eff} and $j(z)$ tend to ΛCDM model in late-time evolution in Λ_{PS}. In Λ_{PL}, these parameters do not tend to respective values of ΛCDM in late-time evolution. It has been observed that both the model are well consistent with $H(z)$ data at low redshifts. Therefore, we conclude that both the models are well fitted with the present $H(z)$ data.

As for as the AIC and BIC statistical criteria is concerned, we have discussed these two criteria for the models against the ΛCDM to observe the performance of each model beyond the standard concordance ΛCDM model and have analyzed any deviation against or in favor of these models. According to ΔAIC and ΔBIC we have found large positive values which show that Λ_{PS} and Λ_{PL} models have *strong evidence in favor* over the ΛCDM model with reference to datasets $DS1$ and $DS2$. Finally, it should be mentioned that the results of our studied could be improved if more observational data is involved.

Acknowledgements The authors thank the anonymous reviewer for thoughtful remarks and suggestions. One of the authors, VK is thankful to Delhi Technological University, New Delhi for providing Research Fellowship to carry out this work.

Author contributions C.P. Singh has written the main manuscript text, conceptualization, investigation, methodology and observation part. Vinita Khatri has prepared the figures and observation part. Both the authors have reviewed the manuscript and agreed for submission.

Data Availability The manuscript has no associated data. The datasets used in this paper are openly available on https://doi.org/10.17909/T95Q4X.

Declarations

Competing interests The authors declare no competing interests.

References

Ade, P.A.R., et al.: Astron. Astrophys. **517**, A16 (2014)
Ade, P.A.R., et al.: Astron. Astrophys. **594**, 13 (2016)
Aghanim, N., et al. (Planck Collaboration): Astron. Astrophys. **641**, A6 (2020). arXiv:1807.06209
Akaike, H.: IEEE Trans. Autom. Control **19**, 716 (1974)
Arik, M., Çalik, M.: Mod. Phys. Lett. A **21**, 1241 (2006)
Arik, M., Çalik, M., Sheftel, M.B.: Int. J. Mod. Phys. D **17**, 225 (2008)
Astier, P., et al.: Astron. Astrophys. **447**, 31 (2006)
Banerjee, N., Pavon, D.: Phys. Rev. D **63**, 043504 (2001a)
Banerjee, N., Pavon, D.: Class. Quantum Gravity **18**, 593 (2001b)
Banerjee, N., Pavon, D.: Phys. Lett. B **647**, 447 (2007)
Basilakos, S.: Mon. Not. R. Astron. Soc. **395**, 2347 (2009)
Basilakos, S., Plionis, M., Solà, J.: Phys. Rev. D **80**, 083511 (2009)
Bertolami, O.: Nuovo Cimento B **93**, 36 (1986)
Bessada, D., Miranda, O.D.: Phys. Rev. D **88**, 083530 (2013)
Blake, C., et al.: Mon. Not. R. Astron. Soc. **418**, 1707 (2011)
Blandford, R.D., et al.: ASP Conf. Ser. **339**, 27 (2004). arXiv:astro-ph/0408279
Borges, H.A., Carneiro, S.: Gen. Relativ. Gravit. **37**, 1385 (2005)
Brans, C.H., Dicke, R.H.: Phys. Rev. **124**, 925 (1961)
Carneiro, S.: Int. J. Mod. Phys. D **12**, 1669 (2003)
Carneiro, S., Pigozzo, C., Borges, H.A.: Phys. Rev. D **74**, 023532 (2006)
Carneiro, S., Dantas, M.A., Pigozzo, C., Alcaniz, J.S.: Phys. Rev. D **77**, 083504 (2008)
Carvalho, J.C., Lima, J.A.S., Waga, I.: Phys. Rev. D **46**, 2404 (1992)
Chen, W., Wu, Y.S.: Phys. Rev. D **41**, 695 (1990)
Copeland, E.J., Sami, M., Tsujikawa, S.: Int. J. Mod. Phys. D **15**, 1753 (2006)
Das, S., Corasaniti, P.S., Khoury, J.: Phys. Rev. D **73**, 083509 (2006)
Eisenstein, D.J., et al. (SDSS Collab.): Astrophys. J. **633**, 560 (2005). arXiv:astro-ph/0501171
Feldman, H.A., et al.: Astrophys. J. **596**, L131 (2003)
Foreman-Mackey, D., Hogg, D., Lang, D., Goodman, J.: Publ. Astron. Soc. Pac. **125**, 306 (2013)
Gaztañaga, E., Cabré, A., Hui, L.: Mon. Not. R. Astron. Soc. **399**, 1663 (2009)
Gomez-Gomar, J., Isern, J., Jean, P.: Mon. Not. R. Astron. Soc. **295**, 1 (1998)
Gomez-Valent, A., et al.: J. Cosmol. Astropart. Phys. **01**, 004 (2015a). arXiv:1409.7048
Gomez-Valent, A., et al.: J. Cosmol. Astropart. Phys. **12**, 048 (2015b). arXiv:1509.03298
Grande, J., Sola, J., Stefancic, H.: J. Cosmol. Astropart. Phys. **8**, 11 (2006)
Jayadevan, A.P., et al.: Astrophys. Space Sci. **364**, 67 (2019)
Johri, V.P., Kalyani, D.: Gen. Relativ. Gravit. **26**, 1217 (1994)
Karchi, A.P.K., Shojaie, H.: Int. J. Mod. Phys. D **25**, 1650045 (2016)
Karimkhani, E., Khoadam-Mohammadi, A.: Astrophys. Space Sci. **364**, 177 (2019)
Khokhlov, A., Mueller, E., Hoeflich, P.: Astron. Astrophys. **270**, 223 (1993)
Kim, H.: Mon. Not. R. Astron. Soc. **364**, 813 (2005)
Komatsu, E., et al.: Astrophys. J. Suppl. Ser. **180**, 330 (2009)
Komatsu, E., et al.: Astrophys. J. Suppl. Ser. **192**, 11 (2011)
Kumar, P., Singh, C.P.: Astrophys. Space Sci. **362**, 52 (2017)
Li, J.-X., Wu, F.-Q., Li, Y.-C., Gong, Y., Chen, X.-L.: Res. Astron. Astrophys. **15**(12), 2151 (2015)
Liddle, A.R.: Mon. Not. R. Astron. Soc. **377**, L74 (2007)
Lima, J.A.S.: Phys. Rev. D **54**, 2571 (1996)
Lima, J.A.S., Basilakos, S., Solà, J.: Mon. Not. R. Astron. Soc. **431**, 923 (2013)
Mota, D.F., Barrow, J.D.: Mon. Not. R. Astron. Soc. **349**, 291 (2004)
Oliveira, F.A., Costa, F.E.M., Lima, J.A.S.: Class. Quantum Gravity **31**(04), 045004 (2014)
Overduin, J.M., Cooperstock, S.: Phys. Rev. D **58**, 043506 (1998)
Ozer, M., Taha, O.: Phys. Lett. B **171**, 363 (1986)
Ozer, M., Taha, O.: Nucl. Phys. B **287**, 776 (1987)
Peebles, P.L.E., Ratra, B.: Astrophys. J. **325**, L17 (1988)
Perico, E.L.D., et al.: Phys. Rev. D **88**, 063531 (2013)

Perlmutter, S., et al.: Astrophys. J. **517**, 565 (1999)
Pimental, L.O.: Astrophys. Space Sci. **112**, 175 (1985)
Ram, S., Singh, C.P.: Nuovo Cimento B **114**, 245 (1999)
Rapetti, D., Allen, S.W., Amin, M.A., Blandford, R.D.: Mon. Not. R. Astron. Soc. **375**, 1510 (2007)
Riess, A.G., et al.: Astrophys. J. **607**, 665 (2004)
Sanchez, A.G., et al.: Mon. Not. R. Astron. Soc. **425**, 415 (2011)
Schützhold, R.: Phys. Rev. Lett. **89**, 081302 (2002)
Schwarz, G.: Ann. Stat. **6**, 461 (1978)
Scolnic, D.M., et al.: Astrophys. J. **859**, 101 (2018)
Sen, S., Sen, A.A.: Phys. Rev. D **63**, 124006 (2001)
Sen, A.A., Sen, S., Sethi, S.: Phys. Rev. D **63**, 107501 (2001)
Shapiro, I.L., Solá, J.: Phys. Lett. B **475**, 236 (2000)
Sharif, M., Syed Asit Ali Shah: Mod. Phys. Lett. A **34**, 1950083 (2019)
Sheykhi, A.: Phys. Rev. D **81**, 023525 (2010)
Singh, C.P.: Astrophys. Space Sci. **338**, 411 (2012)
Singh, C.P., Kaur, S.: Phys. Rev. D **100**, 084057 (2019)
Singh, C.P., Kaur, S.: Astrophys. Space Sci. **365**, 2 (2020)
Singh, C.P., Kumar, P.: Int. J. Theor. Phys. **56**, 3297 (2017)
Singh, C.P., Solà Peracaula, J.: Eur. Phys. J. C **81**, 960 (2021)
Solà, J., Gomez-Valent, A., de Cruz Perez, J.: Astrophys. J. **836**, 43 (2017)
Spergel, D.N., et al.: Astrophys. J. Suppl. Ser. **170**, 377 (2007)
Srivastava, M., Singh, C.P.: Int. J. Geom. Methods Mod. Phys. **15**, 1850124 (2018)
Stern, D., Jimenez, R., Verde, L., Kaminokowski, M., Stanford, S.A.: J. Cosmol. Astropart. Phys. **02**, 08 (2010)
Szydlowski, M., Stachowski, A.: J. Cosmol. Astropart. Phys. **066**, 10 (2015)
Uhera, K., Kim, C.W.: Phys. Rev. D **26**, 2575 (1982)
Weinberg, S.: Rev. Mod. Phys. **61**, 1 (1989)
Xu, L., et al.: Mod. Phys. Lett. A **25**, 1441 (2010)

Physics of the Dark Universe 42 (2023) 101300

Contents lists available at ScienceDirect

Physics of the Dark Universe

journal homepage: www.elsevier.com/locate/dark

Brans–Dicke cosmology with cosmological term $\Lambda(H) = c_0 + 3\nu H^2$

Vinita Khatri, C.P. Singh *

Department of Applied Mathematics, Delhi Technological University, Bawana Road, New Delhi 110 042, India

ARTICLE INFO

Article history:
Received 5 June 2023
Received in revised form 19 July 2023
Accepted 22 July 2023

Keywords:
Cosmology
Dark energy
FLRW model
Brans–Dicke theory
Cosmological constant

ABSTRACT

In this paper, we study the dynamics of a flat Friedmann–Lemaître–Robertson–Walker (FLRW) cosmological model by considering varying vacuum energy density (VED) in Brans–Dicke (BD) cosmology. For this purpose, we consider the well-motivated VED of the form $\Lambda(H) = c_0 + 3\nu H^2$, where c_0 and ν are dimensionless constants. We first adopt a theoretical method to find the exact solutions for various cosmological parameters of two models, namely Λ_{RG1} and Λ_{RG2}. In Λ_{RG1} model, the scale factor evolves as a power-law expansion which gives the deceleration parameter a constant value. Hence, this type of model does not show the transition phase. The second model Λ_{RG2} describes the transition phase from deceleration to acceleration. In the second part, we perform two joint likelihood analysis in order to find the constrain on the main free parameters of the Λ_{RG2} model using the latest observational data sets including SNe Pantheon, $H(z)$ data, BAO/CMB data and local H_0 by SH0ES. Performing the two different combination of datasets, we find that the model shows prior decelerated epoch followed by late time accelerated epoch. We also compare the decaying VED with traditional Λ cosmology, which help us to define the evolution of the VED model. The results show that varying VED model in BD theory is consistent with data and the cosmic evolutions are in good agreement with the concordance ΛCDM and BD with constant Λ models. The AIC and BIC selection criteria are also discussed.

1. Introduction

The astrophysical observation datasets [1–6] for different redshift lead a strong evidence for a spatially flat and accelerating Universe in the present time. This accelerated expansion is characterized by an unknown energy component which is popularly called as "dark energy" (DE). The DE constitutes $\sim$ 68% of the total energy density and has negative pressure to cause the observed accelerating Universe. The nature of the DE still remains a complete mystery. The simplest type of DE is the cosmological constant [7]. A flat Friedmann–Lemaître–Robertson–Walker (FLRW) model with a cosmological term, known as Lambda-cold-dark matter (ΛCDM) is well consistent with the current observational data. However, this model has still some problems such as the fine-tuning problem and the cosmic coincidence problem. In literature, many other cosmological models have been proposed to describe this phenomena. In particular, cosmological models with time-dependent VED seem to be challenging because these models may explain unification of early and late-time evolution of the Universe.

Bertolami [8], and Ozer and Taha [9] proposed a cosmological model of time-varying cosmological constant, $\Lambda(t)$ and claimed that it could be a possible candidate of DE. Later on, many authors [10–14] have studied the cosmological model with time-varying cosmological constant. The renormalization of quantum field theory (QFT) provides a time-varying VED in which the Λ component evolves as $\Lambda \sim H^2$, where H is the Hubble parameter [15]. Wang and Meng [16] have given a more interesting and realistic decay law. Although, there exists no fundamental theory to model the time-varying VED, a phenomenological approach has been proposed to parametrize $\Lambda(t)$. In literature, many authors [17–33] have carried out analysis on decaying VED in which VED has been phenomenologically assumed in various possible ways, as a function of scale factor or Hubble parameter. Such attempts suggest that decaying VED model describe not only the acceleration of the Universe but also solve both cosmological constant and coincidence problems.

Although Einstein's general theory of relativity is a very successful theory, the research on its alternative theories are getting a lot of attention during the last two decades. There are many reasons behind the alternative theories. The motivation comes from the attempt to quantize gravity, which requires higher order modifications on the Einstein–Hilbert (EH) action. Some motivation comes from the dark components (DE and DM) which might be the effects caused by the modifications on large scales of GR. It may also possible due to the unification of gravity with other forces, which requires the modifications on EH action.

Brans and Dicke [34] proposed a scalar-tensor theory of gravitational field based on Mach's principal and Dirac's large number

* Corresponding author.
E-mail addresses: vinitakhatri2k20_phdam501@dtu.ac.in (V. Khatri), cpsingh@dce.ac.in (C.P. Singh).

https://doi.org/10.1016/j.dark.2023.101300
2212-6864/

hypothesis (LNH), known as Brans–Dicke (BD) theory of gravitation. Brans–Dicke scalar-tensor theory is one of the most simple and most studied theory of gravity. In this theory, the gravitational interaction is mediated by both the curvature of the space–time represented by a non flat metric tensor and also a scalar field. The scalar field in the original BD theory is a long range one which sets the coupling BD parameter ω_{BD} to very high values, $\omega_{BD} > 40000$ that makes the BD theory indistinguishable from General Relativity (GR). In order to overcome this, a potential term, is added to brings the effective mass to the scalar a short range. This arbitrary potential effectively plays the role of a cosmological constant in BD theory. However, addition of arbitrary potential to the action is not the only way to bring an effective cosmological constant to this theory. It is possible to extend BD theory by adding a cosmological constant term whose coupling with the scalar field is exactly same as its coupling to the Ricci curvature scalar in original BD action. The main difference between these extensions of BD theory is that, in latter case, the scalar field is still long range one. Hence, BD theory with cosmological constant keeps the spirit of original BD theory by having a long range scalar field even in the presence of cosmological constant. BD theory has important consequences in different areas which makes it worthwhile to study. The extra degree of freedom due to presence of cosmological constant term gives very interesting solutions and results which are not present in BD theory.

The action and field equations for BD theory are well-known. They involve the ordinary (tensor) gravitational field of GR, $g_{\mu\nu}$, but also the scalar BD field ϕ and the (dimensionless) BD parameter, ω_{BD}. We include the cosmological constant associated to vacuum energy density, ρ_Λ as a fundamental ingredient of the theory. In fact, we wish to consider the same matter and vacuum components as in the concordance ΛCDM except that we replace GR paradigm by the BD one. Vacuum dynamics, and in general dynamical DE can be phenomenologically favorable, even if not firmly established yet. The idea that the DE could be not just the cosmological constant of Einstein equations but a dynamical variable, or just some appropriate function of the cosmic time, i.e., there must be some decay-law of vacuum energy density, sometimes on purely phenomenological grounds. In particular, models with time-dependent VED seem to be promising. Many of these models, however, are of pure phenomenological nature since these models are parametrized in a totally ad hoc manner and having no obvious connection with any fundamental theory, therefore, these need testing.

This kind of theory was renewed, owing to its association with superstrings theories [35–50]. In recent years, many authors [51–59] have studied BD theory with cosmological constant in explaining the DE phenomena.

In this work, we combine BD gravity with the idea of dynamical DE. More especially, we show that if one tries to encapsulate the slow evolution of the BD field in terms of the current GR paradigm, the effective theory that emerges is a variant of the ΛCDM framework in which ρ_Λ acquires a time-evolving component and plays the role of an approximate dynamical VED. Although the correct form of this varying VED is not known, a quantum field theory (QFT) approach within the context of renormalization group (RG) have been proposed phenomenologically. Therefore, we assume the phenomenological form of the dependence of the cosmological constant on the square of the Hubble parameter with a constant term. In the absence of this square term of Hubble parameter, it reduces to the concordance ΛCDM model. Thus, due to this additional term, the model deviate from the ΛCDM. Our analysis includes both analytical and observational. We perform the joint statistical analysis using the latest observational data including Hubble data, Type Ia Supernova Pantheon data, baryon acoustic oscillation data and cosmic microwave background data, and local Hubble constant, H_0 by SH0ES. The evolution of various cosmological parameters such as Hubble parameter, deceleration parameter and equation of state parameter are discussed.

We organize our paper as follows. Section 2 presents the model and field equations of a flat Friedmann–Lemaître–Robertson–Walker cosmological model in BD theory with varying cosmological constant. In Section 3, we present the exact solution for two different models depending on the choice of VED. In Section 4, we describe the datasets used in this paper and the method to constraint the free parameters of the model. The results are discussed in detail for the various cosmological parameters such as deceleration parameter, Hubble parameter and equation of state parameter in Section 5. Section 6 discusses the model selection criteria of AIC and BIC of the models assuming ΛCDM as a reference model. In Section 7, we conclude the main findings of our work.

2. The field equations in BD theory

Assuming homogeneity and isotropy, the Friedmann–Lemaître–Robertson–Walker (FLRW) metric for a flat Universe is

$$ds^2 = -dt^2 + a^2(t)d\Omega^2_{k=0}, \tag{1}$$

with $d\Omega^2_{k=0} = dr^2 + r^2(d\theta^2 + \sin^2\theta d\phi^2)$ which represents the spatial line element associated to the hypersurfaces of homogeneity corresponding to a three sphere. Here, (r, θ, ϕ) are defined as the co-moving coordinates, t denotes the proper cosmic time and $a(t)$ represents the scale factor of the Universe. We use units in which $c = \hbar = 1$.

The scalar-tensor theories, especially the BD theory provides a very suitable alternative theory to GR. The BD theory includes both a scalar field ϕ and metric tensor $g_{\mu\nu}$ to describe the gravitational interaction. This interaction is due to the curvature of the space–time and the effect of scalar field. The BD theory in its original form does not contain the cosmological constant, however, in this paper, we consider BD theory with a cosmological constant. A very straightforward extension of GR theory with cosmological constant to BD theory with cosmological constant is just following the original BD prescription by replacing Newton coupling constant G with a scalar field ϕ and adding a dynamical term coupled by an arbitrary parameter ω_{BD}, known as BD parameter. Hence, the action of the BD theory can be described by the following action in Jordan frame, in which the matter Lagrangian $\mathcal{L}_m$ is not coupled to the scalar field, as [35,39,60]

$$S = \int d^4x\sqrt{-g}\left[\frac{1}{16\pi}\left(\phi R - \frac{\omega_{BD}}{\phi}\nabla_\alpha\phi\nabla^\alpha\phi\right) - \rho_\Lambda + \mathcal{L}_m\right], \tag{2}$$

where ϕ is new degree of freedom representing the BD scalar field, which is non-minimally coupled to curvature, R. The dynamics of ϕ is the inverse of the Newtonian constant G. The factor ω_{BD} is a dimensionless BD coupling constant and $\mathcal{L}_m$ is the Lagrangian density of the matter fields. Here, $\rho_\Lambda = \Lambda/8\pi G = \Lambda\phi/8\pi$ is VED associated with the cosmological constant Λ. Setting $\Lambda = 0$ one can obtain the original BD theory [34]. It is to be noted that this theory reduces to general relativity with Λ when ϕ becomes constant. The other symbols have their usual meaning.

Varying the action (2) with respect to both the metric $g_{\mu\nu}$ and the BD scalar field ϕ, we obtain the following field equations of motion.

$$G_{\mu\nu} = R_{\mu\nu} - \frac{1}{2}g_{\mu\nu}R = \frac{8\pi}{\phi}\tilde{T}_{\mu\nu} + \frac{8\pi}{\phi}T^{BD}_{\mu\nu}, \tag{3}$$

and

$$\nabla_\alpha\nabla^\alpha\phi = \frac{8\pi}{(2\omega_{BD}+3)}(T^{m\lambda}_{\lambda} - 4\rho_\Lambda), \tag{4}$$

where $\tilde{T}_{\mu\nu}$ is the total energy–momentum tensor (EMT) consisting of the sum of the matter and VED related through $\tilde{T_{\mu\nu}} = T^{m}_{\mu\nu} - g_{\mu\nu}\rho_\Lambda$ and assume it as a perfect fluid form:

$$\tilde{T}_{\mu\nu} = (\rho + p)\, u_\mu u_\nu + p\, g_{\mu\nu}, \tag{5}$$

with $\rho = \rho_m + \rho_\Lambda$ and $p = p_m + p_\Lambda$, where ρ_m and ρ_Λ are the matter energy density and VED, respectively, while p_m and p_Λ are the corresponding thermodynamical pressure and vacuum pressure, respectively. In this work, we consider the pressure of dust matter containing the dark matter, $p_m = 0$.

The EMT for BD scalar, $T^{BD}_{\mu\nu}$ in (3) is defined by

$$T^{BD}_{\mu\nu} = \frac{1}{8\pi}\Bigg[\frac{\omega_{BD}}{\phi}\left(\nabla_\mu\phi\nabla_\nu\phi - \frac{1}{2}g_{\mu\nu}\nabla_\alpha\phi\nabla^\alpha\phi\right) + \left(\nabla_\mu\nabla_\nu\phi - g_{\mu\nu}\nabla_\alpha\nabla^\alpha\phi\right)\Bigg], \tag{6}$$

In the framework of metric (1), we can write down the BD field Eqs. (3) as follows:

$$3H^2 + 3H\frac{\dot{\phi}}{\phi} - \frac{\omega_{BD}}{2}\frac{\dot{\phi}^2}{\phi^2} = \frac{8\pi}{\phi}\rho, \tag{7}$$

$$2\dot{H} + 3H^2 + \frac{\ddot{\phi}}{\phi} + 2H\frac{\dot{\phi}}{\phi} + \frac{\omega_{BD}}{2}\frac{\dot{\phi}^2}{\phi^2} = -\frac{8\pi}{\phi}p, \tag{8}$$

$$\ddot{\phi} + 3H\dot{\phi} = \frac{8\pi}{(2\omega_{BD}+3)}(\rho - 3p). \tag{9}$$

where an overdot means derivative with respect to cosmic time t and $H = \dot{a}/a$ is the Hubble parameter. The Bianchi identity of $\nabla_\nu G^{\mu\nu} = 0$ in Eq. (3) leads to the following consistency relation.

$$\nabla_\nu\left(R^{\mu\nu} - \frac{1}{2}g^{\mu\nu}R\right) = 0 = \nabla_\nu\left(\frac{8\pi}{\phi}\tilde{T}^{\mu\nu} + \frac{8\pi}{\phi}T^{\mu\nu}_{BD}\right). \tag{10}$$

Let us assume that the EMT, $\tilde{T}_{\mu\nu}$ obeys the usual energy conservation equation $\tilde{T}^{\mu\nu}_{;\nu} = 0$, which gives

$$\dot{\rho_m} + 3(\rho_m + p_m)\frac{\dot{a}}{a} = -\dot{\rho_\Lambda}. \tag{11}$$

We assume that EMT for BD scalar field, $T^{BD}_{\mu\nu}$ regards as a perfect fluid, i.e., $T^{BD}_{\mu\nu} = (\rho_{BD} + p_{BD})u_\mu u_\nu + p_{BD}g_{\mu\nu}$, where

$$\rho_{BD} = \frac{1}{8\pi}\left[\frac{\omega_{BD}}{2}\left(\frac{\dot{\phi}^2}{\phi}\right) - 3H\dot{\phi}\right], \tag{12}$$

$$p_{BD} = \frac{1}{8\pi}\left[\frac{\omega_{BD}}{2}\left(\frac{\dot{\phi}^2}{\phi}\right) + 2H\dot{\phi} + \ddot{\phi}\right]. \tag{13}$$

Now, using (11) the Bianchi identity Eq. (10) gives

$$8\pi\tilde{T}^{\mu\nu}\,\nabla_\nu\left(\frac{1}{\phi}\right) + \nabla_\nu\left(\frac{8\pi}{\phi}T^{\mu\nu}_{BD}\right) = 0, \tag{14}$$

which simplifies to

$$\dot{\rho}_{BD} + 3H(\rho_{BD} + p_{BD}) = (\rho_m + \rho_\Lambda + \rho_{BD})\frac{\dot{\phi}}{\phi}. \tag{15}$$

Following [36,43,45], let us assume that the BD scalar ϕ varies as a power-law of the scale factor, namely $\phi = \phi_0\, a(t)^\epsilon$, where ϕ_0 and ϵ are constants. The value of ϵ is assumed to be small in order to make the consistency with G. Therefore, large ω_{BD} results the product $\epsilon\omega_{BD}$ as an order unity [43]. It is noted that the Cassini experiment set a very high lower bound on ω_{BD}.

It is interesting to note that in Ref. [51] such power-law form of BD scalar has been assumed to study the dynamics of BD cosmology with a cosmological term. It has been observed that the power-law form of BD scalar can conveniently improve the fitting of the cosmological data [52]. Therefore, we expect that this assumption would also be helpful in a different form of time-varying VED model in BD theory.

Thus, using the power-law form of BD scalar, Eq. (7) reduces to

$$H^2 = \frac{2}{(6 + 6\epsilon - \omega_{BD}\epsilon^2)}\frac{8\pi}{\phi}(\rho_m + \rho_\Lambda). \tag{16}$$

Eq. (16) shows that the standard cosmology of general relativity can be recovered in the limit of $\epsilon \to 0$. Considering the dust matter $p_m = 0$, Eqs. (11) and (16) give a single evolution equation for Hubble parameter as

$$\dot{H} + \frac{(3+\epsilon)}{2}H^2 = \frac{3}{(6 + 6\epsilon - \omega_{BD}\epsilon^2)}\frac{8\pi}{\phi}\rho_\Lambda = \frac{3\Lambda}{(6 + 6\epsilon - \omega_{BD}\epsilon^2)}, \tag{17}$$

where $\rho_\Lambda = \Lambda/8\pi G = \Lambda\phi/8\pi$. The above equation is solvable once we know the functional form of Λ. In the next Section, we find the solution of Eq. (17) using time-dependent cosmological constant.

3. Solution with time-varying Λ

In this paper, we assume $\Lambda(t)$ as a combination of constant term and a quadratic term in H [28,51], that is,

$$\Lambda(H) = c_0 + 3\nu H^2, \tag{18}$$

where c_0 and ν are constants. The motivation for assuming variable Λ of the form (18) originates from quantum field theory (QFT) [61], for a detail review, see, Refs. [62–64]. This functional form of $\Lambda(t)$ has been used to study the evolution of the cosmic star formation rate and constrained the model parameter $\nu \leq 0.1$ [26,62].

It is to be noted that in Ref. [59], the authors have studied the Friedmann cosmology with decaying vacuum energy in BD theory with $\Lambda = c_0$ and $\Lambda = \sigma H$. It has been found that cosmological model with constant Λ gives the consistent results where as the model with $\Lambda = \sigma H$ does not show consistency with the observational data used. Therefore, we extend our work by assuming the functional form of $\Lambda(H)$ as defined in (18) with the possibility that it would describe the current accelerating Universe and fit well with the latest observational data. The following two subsections study two different cosmological models depending on the choice of Λ component defined in Eq. (18), namely $\Lambda = 3\nu H^2$ and $\Lambda = c_0 + 3\nu H^2$ and perform the qualitative and observational analysis (see, the model $\Lambda = c_0$ in Ref. [59]).

3.1. Model with $\Lambda \propto H^2$

We assume that the cosmological term is proportional to the quadratic Hubble parameter (hereafter, Λ_{RG1} model). This form of $\Lambda(t)$ can be obtained from Eq. (18) by setting $c_0 = 0$, which gives [11,65–68]

$$\Lambda(H) = 3\nu H^2, \tag{19}$$

where ν is a constant and is expected to be $|\nu| \ll 1$. Using (19) into (17), we get

$$H' + \left(\frac{3+\epsilon}{2} - \frac{9\nu}{(6 + 6\epsilon - \omega_{BD}\epsilon^2)}\right)\frac{H}{a} = 0, \tag{20}$$

where a prime represents dH/da. On solving (20), we get

$$H(z) = H_0\,(1+z)^{\left(\frac{3+\epsilon}{2} - \frac{9\nu}{6+6\epsilon-\omega_{BD}\epsilon^2}\right)}, \tag{21}$$

where H_0 denotes the current Hubble parameter at $t = 0$ and $z = (a_0/a) - 1$ is the redshift (thereafter, we take $a_0 = 1$). Using $H = \dot{a}/a$, the scale factor is given by

$$a = \left[\left(\frac{3+\epsilon}{2} - \frac{9\nu}{(6+6\epsilon-\omega_{BD}\epsilon^2)}\right) H_0 t\right]^{\frac{1}{\left(\frac{3+\epsilon}{2} - \frac{9\nu}{6+6\epsilon-\omega_{BD}\epsilon^2}\right)}}, \quad (22)$$

We find the power-law solution of the scale factor which shows that the model decelerates, marginally inflates or accelerates depending on $\left(\frac{3+\epsilon}{2} - \frac{9\nu}{(6+6\epsilon-\omega_{BD}\epsilon^2)}\right) > 1$, $\left(\frac{3+\epsilon}{2} - \frac{9\nu}{(6+6\epsilon-\omega_{BD}\epsilon^2)}\right) = 1$ or $\left(\frac{3+\epsilon}{2} - \frac{9\nu}{(6+6\epsilon-\omega_{BD}\epsilon^2)}\right) < 1$, respectively.

In cosmology, the deceleration parameter, q plays an vital role to study the deceleration–acceleration phase and its transition. This dimensionless parameter is defined as

$$q = -a\ddot{a}/\dot{a}^2. \quad (23)$$

Using (22) in to (23), we get $q = \left(\frac{3+\epsilon}{2} - \frac{9\nu}{(6+6\epsilon-\omega_{BD}\epsilon^2)}\right) - 1$, which is a constant. This shows that the model either decelerates ($q > 0$), marginally inflates ($q = 0$) or accelerates ($q < 0$) depending on the bracket term is greater, equal or less than one. Thus, the model does not describe transition from decelerating phase to accelerating phase. We can say that, this model does not fit the present observational data as desired. In general, a time varying q describes the phase transition.

Let us test the consistency of the solution obtained for this model. Using (7), (12) and (13), Eq. (15) gives

$$2\epsilon(\omega_{BD}\epsilon - 3)\dot{H} = \epsilon(12 - \omega_{BD}\epsilon^2 - 6\omega_{BD}\epsilon)H^2. \quad (24)$$

Using the solution (21) into (24), one can get

$$2(\omega_{BD}\epsilon - 3)\left(\frac{3+\epsilon}{2} - \frac{9\nu}{(6+6\omega_{BD}-\omega_{BD}\epsilon^2)}\right) - \left(\omega_{BD}\epsilon^2 + 6\omega_{BD}\epsilon - 12\right) = 0, \quad (25)$$

which gives a relation between the constants.

3.2. Model with $\Lambda = c_0 + 3\nu H^2$

In the previous subsection, we observe that the form $\Lambda = 3\nu H^2$ gives power-law solution and constant value of deceleration parameter, which shows that the Λ_{RG1} model cannot describe the current transition phase of the Universe. Therefore, to observe the phase transition we now consider the form of Λ with the addition of a constant c_0, i.e., $\Lambda = c_0 + 3\nu H^2$ as defined in Eq. (18). This type of model (hereafter Λ_{RG2} model) was first proposed in Ref. [69] using renormalization group (RG) in quantum field theory, which have been further extensively studied in the literature, cf. Refs. [26,62,63,70].

Using (18), Eq. (17) reduces to

$$\frac{dH^2}{dx} + \left(\frac{3+\epsilon}{2} - \frac{9\nu}{(6+6\epsilon-\omega_{BD}\epsilon^2)}\right) H^2 = \frac{6c_0}{(6+6\epsilon-\omega_{BD}\epsilon^2)}, \quad (26)$$

where $x = \ln a$. By defining $\Lambda_0 = 3H_0^2\Omega_\Lambda$, Eq. (18) gives $c_0 = 3H_0^2(\Omega_\Lambda - \nu)$, where "0" represents the present cosmic time. Therefore, Eq. (26) can be rewritten as

$$\frac{dH^2}{dx} + \left(\frac{3+\epsilon}{2} - \frac{9\nu}{(6+6\epsilon-\omega_{BD}\epsilon^2)}\right) H^2 = \frac{18H_0^2(\Omega_\Lambda - \nu)}{(6+6\epsilon-\omega_{BD}\epsilon^2)}, \quad (27)$$

The solution of (27) in terms of redshift is given by

$$H^2(z) = H_0^2\left[\frac{18(\Omega_\Lambda - \nu)}{(3+\epsilon)(6+6\epsilon-\omega_{BD}\epsilon^2) - 18\nu} + \left(1 - \frac{18(\Omega_\Lambda - \nu)}{(3+\epsilon)(6+6\epsilon-\omega_{BD}\epsilon^2) - 18\nu}\right)(1+z)^k\right], \quad (28)$$

where $k = \left(\frac{(3+\epsilon)(6+6\epsilon-\omega_{BD}\epsilon^2)-18\nu}{(6+6\epsilon-\omega_{BD}\epsilon^2)}\right)$.

Using the dimensionless Hubble parameter $E(z) = H/H_0$, Eq. (28) can be represented as

$$E^2(z) = \tilde{\Omega}_\Lambda + \tilde{\Omega}_m(1+z)^k, \quad (29)$$

where

$$\tilde{\Omega}_\Lambda = 1 - \tilde{\Omega}_m = \frac{18(\Omega_\Lambda - \nu)}{(6+6\epsilon-\omega_{BD}\epsilon^2)(3+\epsilon) - 18\nu} \quad (30)$$

From above equations it is to be noted that the solution (22) of the Ref. [59] in case of standard BD model with constant cosmological constant can be recovered by taking $\nu = 0$ and further $\epsilon = 0$ gives the standard ΛCDM regime, the standard scaling law of non-relativistic matter and a strictly constant VED [62]. Again, in the absence of BD theory $\epsilon = 0$, i.e. $\phi = \phi_0 = 1/G$ and $\nu \neq 0$, the model Λ_{RG2} reduces to the ΛCDM regime, the standard scaling law of non-relativistic matter and varying VED [62,63].

We observe from (29) that in the limit $a \to 0$, the Hubble parameter, $H \approx H_0\tilde{\Omega}_m a^{-k/2}$, which implies that the model decelerates. However, in the limit $a \to \infty$, we have $H \approx H_0\sqrt{\tilde{\Omega}_\Lambda}$, which corresponds to a pure de Sitter phase. Thus, the model transits from a decelerated phase to a late time accelerated phase.

Integrating and simplifying (28), the scale factor has the solution

$$a(t) = \left(\frac{\tilde{\Omega}_m}{\tilde{\Omega}_\Lambda}\right)^{1/k} \sinh^{2/k}\left(\frac{k\sqrt{\tilde{\Omega}_\Lambda}}{2} H_0\, t\right). \quad (31)$$

It is observed that at early times the scale factor varies as $a \propto t^{2/k}$, i.e, power-law expansion and during late-time, it varies as $a \propto \exp\left(\sqrt{\tilde{\Omega}_\Lambda}\, H_0 t\right)$, which shows the de Sitter phase of the Universe.

The Hubble parameter in terms of cosmic time t is given by

$$H(t) = H_0\sqrt{\tilde{\Omega}_\Lambda}\, \coth\left(\frac{k\sqrt{\tilde{\Omega}_\Lambda}}{2} H_0 t\right), \quad (32)$$

whereas the cosmic time t in terms of the scale factor a is expressed by

$$t(a) = \frac{2}{k\sqrt{\tilde{\Omega}_\Lambda}\, H_0} \sinh^{-1}\left(\sqrt{\frac{\tilde{\Omega}_\Lambda}{\tilde{\Omega}_m}}\, a^{k/2}\right). \quad (33)$$

Thus, the current age t_0 of the Universe is given by

$$t_0 = \frac{2(6+6\epsilon-\omega_{BD}\epsilon^2)}{(3+\epsilon)(6+6\epsilon-\omega_{BD}\epsilon^2)\sqrt{\tilde{\Omega}_\Lambda} H_0} \sinh^{-1}\left(\sqrt{\frac{\tilde{\Omega}_\Lambda}{\tilde{\Omega}_m}}\right). \quad (34)$$

It is straight forward to calculate the deceleration parameter q as defined in Eq. (23), which can be obtained as

$$q(z) = -1 + \frac{k\tilde{\Omega}_m(1+z)^k}{2\left[\tilde{\Omega}_{\Lambda 1} + \tilde{\Omega}_m(1+z)^k\right]}. \quad (35)$$

Now, the present value of q corresponds to $z = 0$ is calculated as

$$q_0 = -1 + \frac{1}{2}\frac{(3+\epsilon)(6+6\epsilon-\omega_{BD}\epsilon^2) - 18\Omega_\Lambda}{(6+6\epsilon-\omega_{BD}\epsilon^2)}. \quad (36)$$

We observe that the present transition from decelerated to accelerated phase, q(at $z=0$) $=0$ occurs at $18\Omega_\Lambda=(1+\epsilon)(6+6\epsilon-\omega_{BD}\epsilon^2)$. The transition redshift, z_{tr} at $q(z)=0$ is given by

$$z_{tr}=\left[\frac{2(6+6\epsilon-\omega_{BD}\epsilon^2)\tilde{\Omega}_\Lambda}{[(1+\epsilon)(6+6\epsilon-\omega_{BD}\epsilon^2)-18\nu]\tilde{\Omega}_m}\right]^{1/k}-1 \tag{37}$$

For sake of completeness, we discuss another parameter known as equation of state (EoS) parameter w, which also describes the different phases of the evolution of the Universe. It is observed that $3w+1<0$ describes the accelerated expansion of the Universe. The EoS parameter (hereafter, effective EoS parameter, w_{eff}) is defined by

$$w_{eff}=-1-\frac{2}{3}\frac{aH'}{H}. \tag{38}$$

For this model, we have

$$w_{eff}=-1+\frac{1}{3}\frac{k\tilde{\Omega}_m(1+z)^k}{[\tilde{\Omega}_\Lambda+\tilde{\Omega}_m(1+z)^k]}. \tag{39}$$

The above equation gives w_{eff} at $z=0$ as

$$w_{eff}(z=0)=-1+\frac{1}{3}\frac{(3+\epsilon)(6+6\epsilon-\omega_{BD}\epsilon^2)-18\Omega_\Lambda}{(6+6\epsilon-\omega_{BD}\epsilon^2)}. \tag{40}$$

The condition $3w_{eff}(z=0)+1<0$ is satisfied if $18\Omega_\Lambda>(1+\epsilon)(6+6\epsilon-\omega_{BD}\epsilon^2)$. From Eq. (39), it is observed that $w_{eff}\to-1$ as $z\to-1$. Thus, the model corresponds to the ΛCDM model.

Substituting the solution (28) into the consistency Eq. (24), we obtain

$$k(\omega_{BD}\epsilon-3)\tilde{\Omega}_m a^{-k}+(12-\omega_{BD}\epsilon^2-6\omega_{BD}\epsilon)[\tilde{\Omega}_\Lambda+\tilde{\Omega}_m a^{-k}]=0. \tag{41}$$

One can observe that the above equation are not always consistent. Therefore, we assume that this equation satisfies at present, i.e. $a=a_0=1$. Thus, Eq. (41) at present reduces to

$$k(\omega_{BD}\epsilon-3)\tilde{\Omega}_m-(\omega_{BD}\epsilon^2+6\omega_{BD}\epsilon-12)=0, \tag{42}$$

where $\tilde{\Omega}_\Lambda+\tilde{\Omega}_m=1$.

4. Data and statistical method

In this section we will discuss the observational data and the statistical method to constraint the parameters of model.

4.1. Data

In our analysis, we use the most recent and relevant observational data as follows:

1. *Type Ia supernova (SNe):* SNe is the most powerful tool to study DE because of their role as standardizable candles. The Pantheon sample [71] consists of 40 binned data points of the bolometric apparent magnitude covering the redshift range $0.014\le z\le 1.62$ with. The compute the theoretical one as

$$m_{th}(z)=\mathcal{M}+5\ \log_{10}[d_L(z)/10pc], \tag{43}$$

where $\mathcal{M}$ is a nuisance parameter. The dimensionless luminosity distance, $d_L(z)$ is defined as

$$d_L(z)=\frac{(1+z)c}{H_0}\int_0^z\frac{dz'}{E(z',\theta)}, \tag{44}$$

where c is the speed of light which has been taken as unity in this model. The chi-squared function, χ^2 for SNe data is given by

$$\chi^2_{Pan}=(m_{th}-m_{obs})Cov^{-1}(m_{th}-m_{obs})^T, \tag{45}$$

where Cov^{-1} is the inverse of the covariance matrix which consists of systematic covariance Cov_{sys} and statistical matrix D_{stat} having diagonal component [71,72], and m_{obs} is the observed quantity of m [73].

2. *Baryon acoustic oscillations (BAOs) and cosmic microwave background (CMB):* BAOs provide another independent test for constraining the property of DE. We use BAO measurements from the Sloan Digital Sky Survey ($SDSS(R)$) [74], the 6dF Galaxy survey [75], *BOSS CMASS* [76] and three parallel measurements from *WiggleZ* survey [77]. The combined dataset gives tight constraints on DE models. In this work, we follow them to constrain different vacuum models using their combined BAO dataset. This data can be used to measure the angular diameter, $d_A(z,\theta)$, which is given by

$$d_A(z_*,\theta)=c\int_0^{z_*}\frac{dz'}{H(z',\theta)} \tag{46}$$

where z_* represents the photons decoupling redshift which is taken as $z_*\approx 1090$ [78]. Also, the volume–distance, $D_v(z,\theta)$ is defined by $D_v(z,\theta)=\left(\frac{d_A^2(z,\theta)cz}{H(z,\theta)}\right)^{\frac{1}{3}}$. Using the measurements obtained from the ratio of the BAO dilation scale to the sound horizon scale and CMB acoustic scale at the drag epoch, the χ^2 function for BAO/CMB can be defined as [79]

$$\chi^2_{BAO/CMB}=A^TC^{-1}A \tag{47}$$

where

$$A=\begin{bmatrix}\frac{d_A(z_*,\theta)}{D_v(0.106,\theta)}-30.84\\ \frac{d_A(z_*,\theta)}{D_v(0.35,\theta)}-10.33\\ \frac{d_A(z_*,\theta)}{D_v(0.57,\theta)}-6.72\\ \frac{d_A(z_*,\theta)}{D_v(0.44,\theta)}-8.41\\ \frac{d_A(z_*,\theta)}{D_v(0.6,\theta)}-6.66\\ \frac{d_A(z_*,\theta)}{D_v(0.73,\theta)}-5.43\end{bmatrix}$$

and C^{-1} represents the inverse of the covariance matrix [79]. The correlation coefficient has been taken from Ref. [80].

3. *Hubble data:* The Hubble data $H(z)$ is applied to constrain the model parameters independently. We use 36 measurements of $H(z)$ in which first 31 measurements are determined from the cosmic chronometric (CC) technique [81], two measurements determined from the BAO signal in Lyman-α forest distribution alone or cross-correlated with quasistellar objects (QSOs) [82,83] and last three correlated measurements from the radial BAO signal in the galaxy distribution [84].
The χ^2 function of $H(z)$ for 33 Hubble measurement including CC and Lyman-α, is given by

$$\chi^2_{CC+Ly\alpha}=\sum_{i=1}^{33}\frac{[H^{obs}(z_i)-H^{th}(z_i)]^2}{\sigma_i^2}, \tag{48}$$

where $H^{th}(z_i)$ is the theoretical and $H^{obs}(z_i)$, the observed values at redshift z_i, and σ_i^2 is the standard deviation of each $H^{obs}(z_i)$.
The χ^2 for the last 3 correlated measurements from BAO signals in galaxy distribution is given by

$$\chi^2_{gal}=A^T\mathbf{C}^{-1}A, \tag{49}$$

where $\mathbf{C}$ is the covariance matrix given by [84]

$$\mathbf{C}=\begin{bmatrix}3.65 & 1.78 & 0.93\\ 1.78 & 3.65 & 2.20\\ 0.93 & 2.20 & 4.45\end{bmatrix}$$

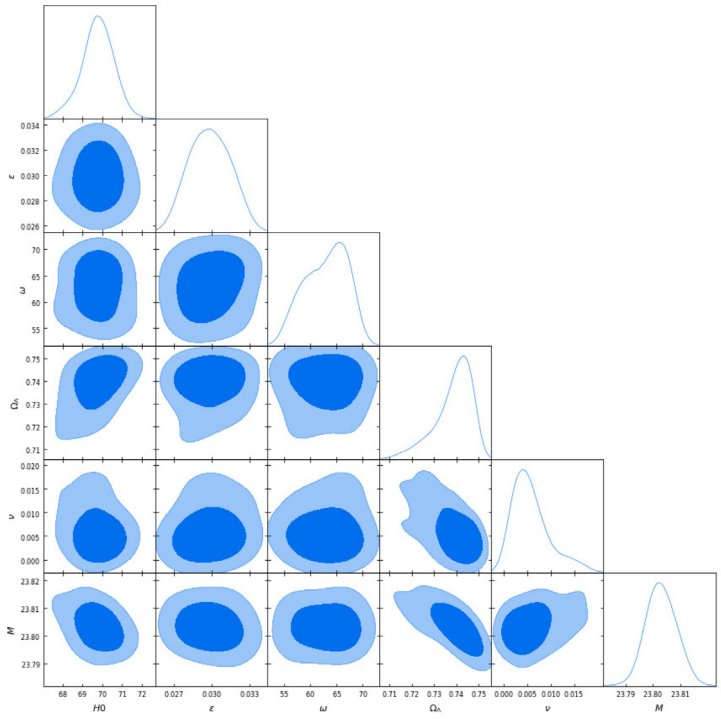

Fig. 1. The 2− dimensional contours and 1− dimensional posterior distribution of the free parameters of Λ_{RG2} model using the combined dataset $DS1 = SNe + H(z) + BAO/CMB + H_0$.

and

$$A = \begin{bmatrix} H_{obs}(0.38) - H_{th}(0.38) \\ H_{obs}(0.51) - H_{th}(0.51) \\ H_{obs}(0.61) - H_{th}(0.61) \end{bmatrix}$$

Thus, the final χ^2 function of $H(z)$ is defined by

$$\chi^2_{H(z)36} = \chi^2_{CC+Ly\alpha} + \chi^2_{gal}. \quad (50)$$

4. Local Hubble constant: Finally, we use $H_0 = 73.5 \pm 1.4$ Km s^{-1} Mpc^{-1}, which is locally measured by SH0ES as reported in Ref. [85].

4.2. Statistical method

We study two combinations of data set, labeled as $DS1 : SNe + BAO/CMB + H(z) + H_0$ and $DS2 : SNe + BAO/CMB + H(z)$ to minimize the total χ^2 -function of the model. The corresponding chi-squared are defined as

$$\chi^2_{DS1} = \chi^2_{Pan} + \chi^2_{BAO/CMB} + \chi^2_{H(z)36} + H_0, \quad (51)$$

and

$$\chi^2_{DS2} = \chi^2_{Pan} + \chi^2_{BAO/CMB} + \chi^2_{H(z)36}. \quad (52)$$

We perform a Bayesian Markov Chain Monte Carlo (MCMC) analysis based on *EMCEE* module [86]. In our study, we assume prior values for model parameters, viz., $60 \leq H_0 \leq 80$, $0 < \epsilon < 1$, $0 < \omega_{BD} \leq 500$, $0 < \nu < 1$ and $0.6 \leq \Omega_\Lambda \leq 0.8$.

5. Results and discussion

In this section, we present the main results obtained by observational data sets: DS1 and DS2, and describe the physical properties of the vacuum model accordingly. We summarize the best-fit of free parameters of Λ_{RG2} model in Table 2. To make a comparison with the Λ_{RG2} model, we also present the fitting values of ΛCDM (cf. Table 1). The contour maps of parameters Ω_Λ, ϵ, ω_{BD} and ν of Λ_{RG2} model with 1σ (68.3%) and 2σ (95.4%) confidence level are shown in Figs. 1 and 2, respectively.

Figs. 3 and 4 present the evolution of the deceleration parameter for the best fit values of parameters obtained from DS1 and DS2 data sets for Λ_{RG2} model. It is observed that $q(z)$ with each data set varies with redshift z from positive to negative and show the same trajectory as ΛCDM model. Thus, the model shows transition from early deceleration to the late time acceleration. It can be observed that $q(z) \to -1$ in late-time of evolution. Figs. 3 and 4 also show that the transition from decelerated to accelerated phase occurs at the redshift $z_{tr} = 0.707^{+0.094}_{-0.707}$ with DS1 data and $z_{tr} = 0.678^{+0.013}_{-0.011}$ with DS2 data (cf. Table 4.). The joint

Table 1
Constraints of the parameters, and AIC and BIC for ΛCDM model obtained from joint analysis of data sets DS1 and DS2 [59].

Sample	Ω_Λ	H_0	χ^2_{min}	AIC	BIC
$DS1$	$0.680^{+0.015}_{-0.010}$	$71.545^{+1.175}_{-0.820}$	34.78	40.78	48.04
$DS2$	$0.690^{+0.032}_{-0.028}$	$68.545^{+2.102}_{-1.742}$	34.69	40.69	47.91

Table 2
Constraints on the parameters, and AIC and BIC for Λ_{RG2} model obtained from joint analysis of data sets DS1 and DS2.

Parameters ↓	$DS1$	$DS2$
ϵ	$0.029^{+0.002}_{-0.002}$	$0.029^{+0.002}_{-0.002}$
ν	$0.005^{+0.004}_{-0.003}$	$0.007^{+0.007}_{-0.005}$
ω	$68.870^{+3.968}_{-5.192}$	$62.673^{+4.736}_{-5.527}$
Ω_Λ	$0.741^{+0.006}_{-0.010}$	$0.730^{+0.011}_{-0.017}$
H_0	$69.780^{+0.801}_{-0.717}$	$67.951^{+1.076}_{-1.145}$
χ^2_{min}	41.03	38.82
AIC	51.03	48.82
BIC	63.13	60.85
ΔAIC	10.25	8.13
ΔBIC	15.09	12.94

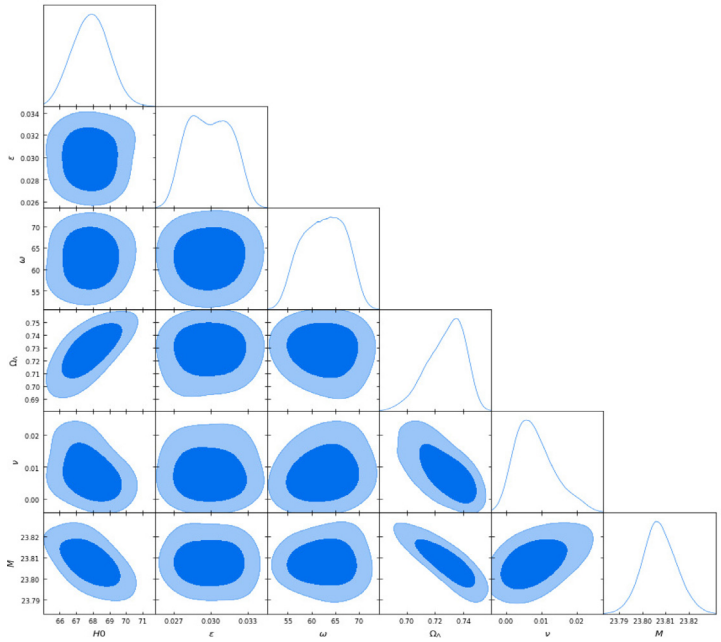

Fig. 2. The 2− dimensional contours and 1− dimensional posterior distribution of the free parameters of Λ_{RG2} model using the combined dataset $DS2 = SNe + H(z) + BAO/CMB$.

Table 3
Values of z_{tr}, q_0, $w_{eff}(z=0)$ and t_0 for ΛCDM model [59].

Sample	z_{tr}	q_0	$w_{eff}(z=0)$	t_0
$DS1$	$0.701^{+0.024}_{-0.020}$	$-0.594^{+0.014}_{-0.018}$	$-0.729^{+0.009}_{-0.012}$	$13.48^{+0.450}_{-0.230}$ Gyr
$DS2$	$0.672^{+0.028}_{-0.025}$	$-0.554^{+0.024}_{-0.030}$	$-0.703^{+0.016}_{-0.020}$	$13.69^{+0.09}_{-0.09}$ Gyr

datasets DS1 and DS2 yield the present deceleration parameter q_0 as $-0.572^{+0.067}_{-0.015}$ and $-0.555^{+0.016}_{-0.023}$, respectively. These results show that the parameters z_{tr} and q_0 are in good agreement with that of ΛCDM model (cf. Table 3).

Using the parameter constraints in analytical solution of Hubble parameter (28), the evolutions of the Hubble parameter $H(z)$ with the error bar of Hubble data set are shown in Figs. 5 and 6. For sake of comparison the ΛCDM model is also plotted. The cosmic evolution of Λ_{RG2} is coinciding each other through out the expansion history with ΛCDM model. The trajectories of the model for both data sets DS1 and DS2 cover most of the data set of error bar of Hubble parameter, which shows that the Λ_{RG2} model is in good agreement with ΛCDM model.

In this cosmological scenario, the current age of the Universe with each dataset are found to be $t_0 = 14.07^{+0.018}_{-0.022}$ Gyr and $t_0 = 13.95^{0.020}_{-0.020}$ Gyr, respectively. The age of the Universe obtained are very much compatible with that obtained from the ΛCDM (cf. Table 3), and $t_0 \approx 14.37$ Gyr and $t_0 \approx 13.7$ obtained through the combined data set of WMAP, BAO and SNe [5]. Using data set DS1, the present value of Hubble parameter is extracted as $H_0 = 69.780^{+0.801}_{-0.717}$ $\text{Kms}^{-1}\text{Mpc}^{-1}$, which is slightly lower than $H_0 = 71.545^{+1.175}_{-0.820}$ $\text{Kms}^{-1}\text{Mpc}^{-1}$ based on the observation from ΛCDM model applied to DS1 dataset. With DS2 dataset, it is $H_0 = 67.951^{+1.076}_{-1.145}$ $\text{Kms}^{-1}\text{Mpc}^{-1}$ which is consistent with the observational value of ΛCDM model $H_0 = 68.545^{+2.102}_{-1.742}$ $\text{Kms}^{-1}\text{Mpc}^{-1}$. These values show a variation from $H_0 = 71.9^{+2.6}_{-2.7}$ $\text{Kms}^{-1}\text{Mpc}^{-1}$ of WMAP sky survey [5].

The evolution of effective EoS parameters w_{eff} are shown in Figs. 7 and 8 for Λ_{RG2} and ΛCDM models obtained through the combined data sets DS1 and DS2. We may conclude that for large redshifts, w_{eff} has small negative value $w_{eff} > -1/3$ and in future

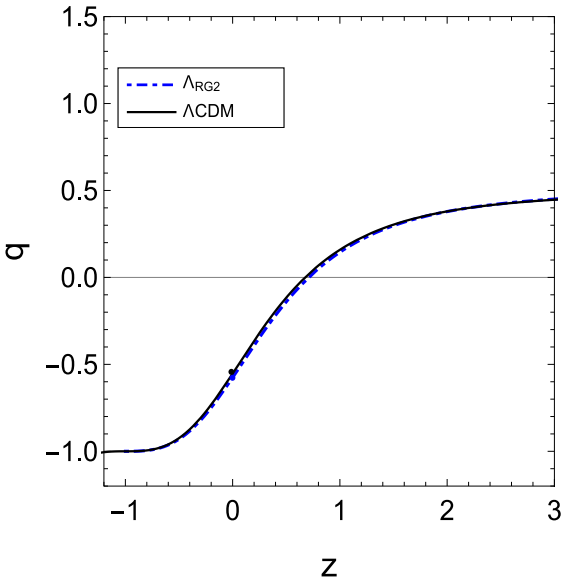

Fig. 3. Figure shows the evolution of the deceleration parameter for Λ_{RG2} and ΛCDM using data combination DS1. A dot on a curve represents the current value q_0.

Table 4
Values of z_{tr}, q_0, $w_{eff}(z=0)$ and t_0 for Λ_{RG2} model.

Sample	z_{tr}	q_0	$w_{eff}(z=0)$	t_0
$DS1$	$0.707^{+0.094}_{-0.077}$	$-0.571^{+0.067}_{-0.015}$	$-0.714^{+0.004}_{-0.009}$	$14.07^{+0.018}_{-0.022}$ Gyr
$DS2$	$0.678^{+0.013}_{-0.011}$	$-0.555^{+0.016}_{-0.023}$	$-0.703^{+0.011}_{-0.015}$	$13.95^{+0.020}_{-0.020}$ Gyr

the model asymptotically approaches to $w_{eff} = -1$. The each trajectory of w_{eff} coincides with the evolution of ΛCDM model. The Λ_{RG2} model behaves like a quintessence. The present value of w_{eff} is found to be $-0.714^{+0.004}_{-0.009}$ and $-0.703^{+0.011}_{-0.015}$ with DS1 and DS2 datasets, respectively, which are very close to the current value of w_{eff} of ΛCDM model (cf. Table 3).

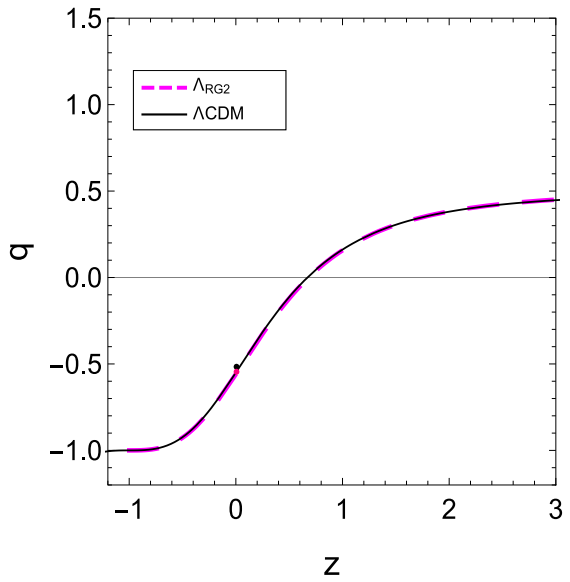

Fig. 4. Figure shows the evolution of the deceleration parameter for Λ_{RG2} and ΛCDM using data combination DS2. A dot on a curve represents the current value q_0.

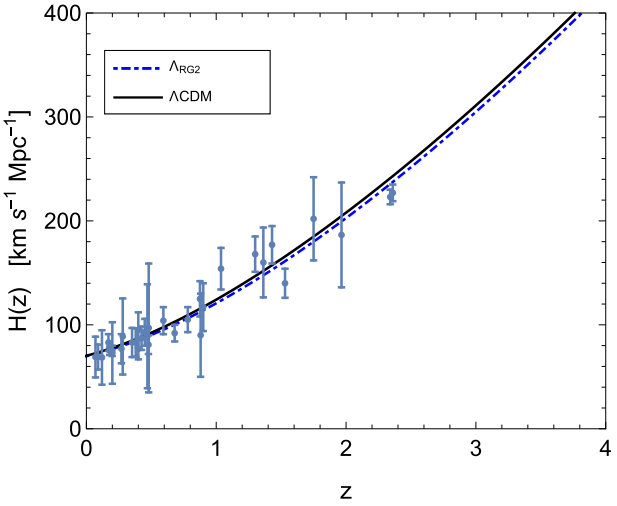

Fig. 5. Best fits using DS1 data set over $H(z)$ data for Λ_{RG2} (blue dash–dot line) and ΛCDM (black solid line) are shown. The grey points with uncertainty bars correspond to the 36 $H(z)$ sample.

The combined data sets DS1 and DS2 give the minimal chi-squared viz. χ^2 as 41.038 and 38.820, respectively. Let us calculate the reduced χ^2_{red}, which can be obtained as $\chi^2_{red} = \chi^2_{min}/(N - d)$, where N is the total number of data and d is the number of fitted parameters, which vary for the different models. In our observation, we have used $N = 83$ data points for DS1: 40 data points of SNe Pantheon, 36 Hubble data, 6 data set of BAO/CMB and 1 of local Hubble constant H_0, $N = 82$ data points for DS2 consists of 40 data points of SNe Pantheon, 36 Hubble data, 6 data set of BAO/CMB, and $d = 5$ for Λ_{RG2} model. Using these information, we get $\chi^2_{red} = 0.526$ and 0.504, respectively with DS1 and DS2 data sets which provide a very good fit with these observation data sets. A model with $\chi^2_{red} < 1$ or closer to 1 is considered as a best-fit where as $\chi^2_{red} > 1$ is considered a bad fit.

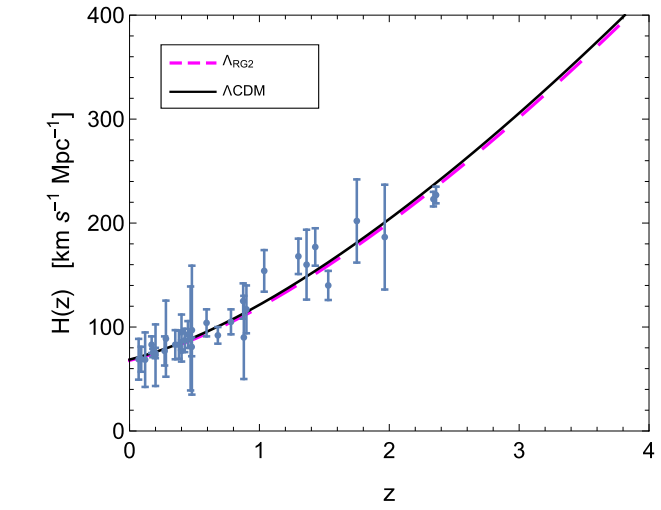

Fig. 6. Best fits using DS2 data set over $H(z)$ data for Λ_{RG2} (magenta dashed line) and ΛCDM (black solid line) are shown. The grey points with uncertainty bars correspond to the 36 $H(z)$ sample.

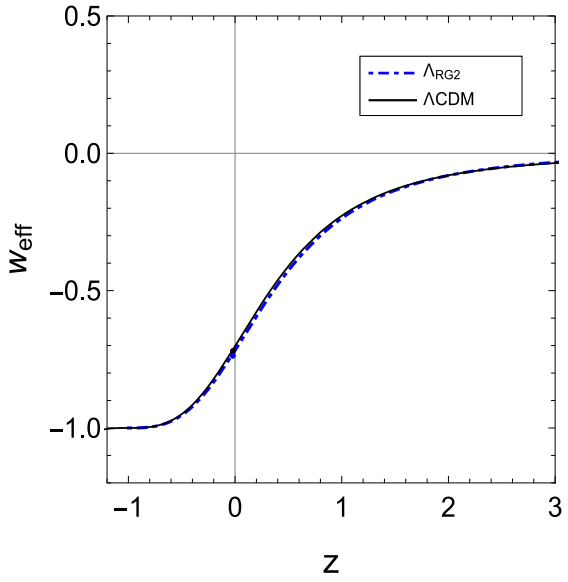

Fig. 7. Figure shows the evolution of effective EoS parameter as a function of redshift z for Λ_{RG2} and ΛCDM using data combination DS1. A dot on a curve represents the current value $w_{eff}(z = 0)$.

6. Selection criterion

We now study model selection information criteria like, Akaike Information Criterion (AIC) [87] and Bayesian Information Criterion (BIC) [88] for Λ_{RG2} and ΛCDM models. The AIC (or BIC) model selection criteria has been developed to summarize the data evidence in favor or against of a model. The AIC and BIC are respectively defined as

$$AIC = \chi^2_{min} + 2d; \qquad BIC = \chi^2_{min} + d \ln N; \tag{53}$$

where d and N are the number of free parameters and data points used in the analysis, respectively. In this approach, the model with lower values of AIC (or BIC) is preferred by data.

Considering ΛCDM as the reference model, we can calculate $\Delta AIC = AIC_{\Lambda_{RG2}} - AIC_{\Lambda CDM}$ and $\Delta BIC = BIC_{\Lambda_{RG2}} - BIC_{\Lambda CDM}$. In case of AIC, if $\Delta AIC < 2$, the data strongly support the given model. If $2 < \Delta AIC < 4$, there is average support and the range $4 <$

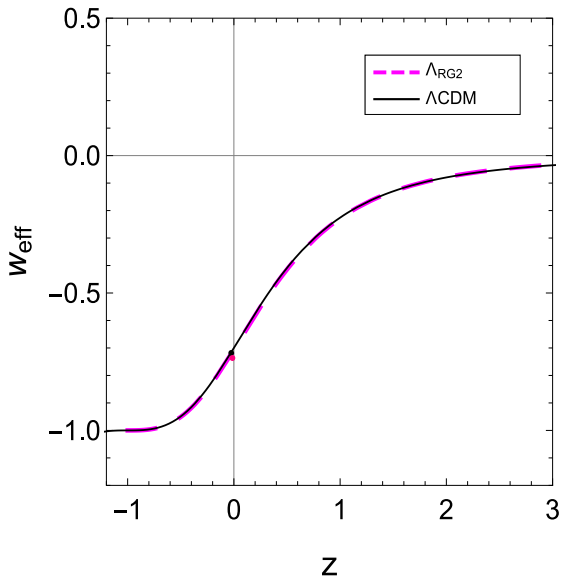

Fig. 8. Figure shows the evolution of effective EoS parameter as a function of redshift z for Λ_{RG2} and ΛCDM using data combination DS2. A dot on a curve represents the current value $w_{eff}(z=0)$.

$\Delta AIC < 10$ still supports the model but less than the preferred one. For the value of $\Delta AIC > 10$, the data does not support the given model. Similarly, in case of BIC, $\Delta BIC < 2$ indicates no evidence against the model. If $2 < \Delta BIC < 6$, there is positive evidence against the model. A value in the range $6 < \Delta BIC < 10$ suggests a strong evidence against the model and a very strong evidence against the model for $\Delta BIC > 10$. Thus, based on our $\Delta AIC(\Delta BIC)$ results given in Table 2 for Λ_{RG2} model with reference to ΛCDM, we find $\Delta AIC(\Delta BIC) = 10.25(15.09)$ for $DS1$ dataset whereas in $DS2$ dataset, it is $\Delta AIC(\Delta BIC) = 8.13(12.94)$. These values suggest that Λ_{RG2} model is not supported from a model selection point of view. These results show that BIC penalizes the free parameters more strongly than AIC.

7. Conclusion

In this paper, we have discussed the dynamics of a flat FLRW model with decaying VED in BD theory. Many authors, as mentioned in introductory part, have studied the FLRW model with varying Λ in GR assuming the phenomenological form of $\Lambda(t)$. We have considered the cosmological model in dynamical BD theory of gravity to explore the role played by the scalar field and varying $\Lambda(t)$ in describing the late-time evolution of the Universe.

Kim [39] presented BD theory with cosmological constant as a unified model for DM and DE. It was found that the BD theory predicts the emergence of a yet-unknown zero acceleration epoch, which is an intermediate stage acting as a crossing bridge between the decelerating matter-dominated era and the accelerating phase. Pérez and J. Solà [52] reconsidered BD theory in which the model can be formulated in ΛCDM form, but at the expense of replacing constant cosmological constant with a dynamical form.

In Ref. [59], the authors have studied the Friedmann cosmology with decaying vacuum energy in BD theory with $\Lambda = c_0$ and $\Lambda = \sigma H$. It has been found that cosmological model with constant Λ gives the consistent results where as the model with $\Lambda = \sigma H$ does not show the consistency with the observational data used. Therefore, if one tries to encapsulate the slow evolution of the BD-field in terms of the current GR framework (in which G and Λ remain both constant), the effective theory that emerges is a variant of the ΛCDM framework in which ρ_Λ acquires a time-evolving component of a very specific nature. This plays the role of an approximate dynamical VED. The resulting ΛCDM-like model appears as if $\rho_\Lambda = \Lambda/(8\pi G)$ were a dynamical VED composed of a constant term plus a small dynamical term, i.e., $\rho_\Lambda = c_0 + 3\nu H^2$, so-called Λ_{RG2} model. Therefore, this model is not exactly the traditional ΛCDM, but has additional features.

The Λ_{RG2} model deserves a particular consideration since it has extra parameters ϵ and ν. We have found that Λ_{RG2} model is favored by the overall observational data, $DS1$ and $DS2$ when it is compared with the standard ΛCDM model of cosmology. The output of Λ_{RG2} model for the datasets brings the model to the forefront position with respect to the standard ΛCDM and BD with constant Λ models as discussed in a paper [59]. Thus, when fitted to the cosmological data, we have found that the BD cosmology with variable Λ, transcribed in such a GR paradigm, appears to be competitive with the ΛCDM and emulates the dynamical VED model. Current values of various parameters show that the BD model mimics quintessence at present and de Sitter in late-time. In what follows, we summarize the result of both the Λ_{RG1} and Λ_{RG2} models:

We have studied a flat FLRW model in BD theory by assuming two different functional forms of VED, viz. $\Lambda_{RG1}: \Lambda = 3\nu H^2$ and $\Lambda_{RG2}: \Lambda = c_0 + 3\nu H^2$. We have found that Λ_{RG1}-model does not able to fit with the observational data. This model gives power-law expansion of the Universe which does not show the phase transition. The Universe decelerates or accelerates depending on the values of model parameters. A similar discussion has been carried out by many authors [11,70]. On the other hand, the Λ_{RG2} model is well compared with standard ΛCDM model. Firstly, we have obtained the analytical solution of the basic cosmological functions of flat FLRW model in BD theory for these two models. The second part of the work consists of performing a Bayesian MCMC analysis using two different joint combinations of observational data of SNe Pantheon, $H(z)$ data, BAO/CMB and local Hubble constant to obtain the best fit parameters for Λ_{RG2} model. We have constrained the parameter ν using these observational data and found to be $0.005^{+0.004}_{-0.003}$ with DS1 data and $0.007^{+0.007}_{-0.005}$ with DS2 data.

The observational data sets DS1 and DS2 yield the density parameter Ω_Λ as $0.741^{+0.006}_{-0.010}$ and $0.730^{+0.011}_{-0.017}$, respectively. If we look the consistency of the Λ_{RG2} model, Eq. (42) must be satisfied by using best fit values of the free parameters of the model obtained numerically as listed in Table 2 or it gives the same value of one of the free parameters of the model. Hence, using the best fit values of parameters of DS1 and DS2 listed in Table 2 into the consistency relation (42), we found the free parameter Ω_Λ as 0.723 and 0.730, respectively. These results of Ω_Λ are perfectly consistent with the values of Ω_Λ as mentioned above obtained from the observations using DS1 and DS2 datasets (cf. Table 2). In what follows, we summarize the main results of our analysis.

Based on the best-fit values of model parameters obtained from two different combined datasets, the evolution of the cosmological quantities have been plotted as a function of redshift. In case of Λ_{RG2} model, we have observed that the scale factor expands with decelerated rate in early times and accelerated at late-time of the evolution. We have estimated the deceleration–acceleration transition redshift that takes place at $z_{tr} = 0.707^{+0.094}_{-0.707}$ and $z_{tr} = 0.678^{+0.678}_{-0.011}$, which are consistent with the ΛCDM model. The deceleration parameter exhibits a transition from decelerated phase to an accelerated phase. The effective EoS parameter is small negative values at high redshift but tend to -1 as $z \to -1$, showing the ΛCDM behavior.

The evolutions of various cosmological parameters, like $H(z)$, $q(z)$ and $w_{eff}(z)$ have been shown in Figs. 3–8 by using the fitting values of model parameters obtained from $DS1$ and $DS2$

for ΛCDM and BD Λ_{RG2} models, respectively. Using these datasets we have analyzed whether the BD Λ_{RG2} is capable to fit the observations in a comparable way to the concordance GR-ΛCDM model. The best-fit values and evolution of various parameters of these two models, namely Λ_{RG2} and GR-ΛCDM show that the evolutions of the both models are coincide to each other. It means that the BD model with variable Λ may be the considered as a competitive model to GR-ΛCDM model. We have also compared the models with reduced chi-squared value with DS1 and DS2 datasets. We have found that $\chi^2_{red} = 0.526$ and $\chi^2_{red} = 0.504$, respectively which are very close to the values of GR-ΛCDM ($\chi^2_{red} = 0.429$ and $\chi^2_{red} = 0.433$). It means that both the models provide a very good fit with these observational datasets. It is well-known that the discrepancy is much smaller than the expected if the reduced chi-squared value is less than one. Using the best fit values, the current age of the Universe are found to be $t_0 \sim 14.07$ Gyr and $t_0 \sim 13.95$ Gyr from DS1 and DS2 datasets, respectively.

In the final remark, we have discussed the possibility, in contrast to ΛCDM case, that Λ is not a constant but a function of the cosmic time, i.e., $\rho_\Lambda = \rho_\Lambda(t)$. This varying VED is perfectly allowed within the FLRW metric in a dynamical frame of BD theory. It has been observed that the choice of functional form of Λ is very important in describing the dynamics of the Universe, especially the late time acceleration. In the absence of BD theory, we recover exactly the varying vacuum models as discussed in Ref. [62,63]. Our results show that both the models, GR-ΛCDM amd BD-Λ_{RG2}, fit the observational datasets used here in very well. In late-time evolution, both the models show a similar evolution and approach to the de Sitter Universe. Thus, the Λ_{RG2} model successfully reproduces the expected epochs and shows a good agreement with the ΛCDM model.

Declaration of competing interest

The authors declare that they have no known competing financial interests or personal relationships that could have appeared to influence the work reported in this paper.

Data availability

No data was used for the research described in the article.

Acknowledgments

The authors are thankful to the anonymous reviewers for the comments and suggestions to improve the quality of the manuscript. VK expresses her sincere thank to Delhi Technological University, New Delhi for providing Research Fellowship to carry out this work.

References

[1] A.G. Riess, et al., Astrophys. J. 116 (1998) 1009.
[2] S. Perlmutter, et al., Astrophys. J. 517 (1999) 565.
[3] P. de Bernardis, et al., Nature 404 (2000) 955.
[4] M. Tegmark, et al., Phys. Rev. D 74 (2006) 123507.
[5] E. Komatsu, et al., Astrphys. J. Suppl. Ser. 180 (2009) 330.
[6] A.G. Riess, et al., Astrophys. J. 730 (2011) 119.
[7] P.J.E. Peebles, B. Ratra, Rev. Modern Phys. 75 (2003) 559.
[8] O. Bertolami, Nuovo Cimento B 93 (1986) 36.
[9] M. Ozer, O. Taha, Nuclear Phys. B 287 (1987) 776.
[10] P.J.E. Peebles, B. Ratra, Astrophys. J. 325 (1988) L17.
[11] J.C. Carvalho, J.A.S. Lima, I. Waga, J. Phys. Rev.D. 46 (1992) 2404.
[12] O. Bertolami, P.J. Martins, Phys. Rev. D 61 (2000) 064007.
[13] J.S. Alcaniz, J.M.F. Maia, Phys. Rev. D 67 (2003) 043502.
[14] J.D. Barrow, T. Clifton, Phys. Rev. D 73 (2006) 103520.
[15] I.L. Shapiro, J. Sola, Phys. Lett. B 475 (2000) 236.
[16] P. Wang, X. Meng, Class. Quantum Gravityity 22 (2005) 283.
[17] E. Elizalde, S. Nojiri, S.D. Odintsov, P. Wang, Phys. Rev. D 71 (2005) 103504.
[18] J.S. Alcaniz, J.A.S. Lima, Phys. Rev. D 72 (2005) 063516.
[19] H.A. Borges, S. Carneiro, Gen. Relativ. Gravit. 37 (2005) 1385.
[20] J. Solà, H. Stefancic, Modern Phys. Lett. A 21 (2006) 479.
[21] S. Carneiro, C. Pigozzo, H.A. Borges, J.S. Alcaniz, Phys. Rev. D 74 (2006) 23532.
[22] H.A. Borges, S. Carneiro, J.C. Fabris, C. Pigozzo, Phys. Rev. D 77 (2008) 043513.
[23] S. Carneiro, M.A. Dantas, C. Pigozzo, J.S. Alcaniz, Phys. Rev. D 77 (2008) 083504.
[24] F.E.M. Costa, J.S. Alcaniz, Phys. Rev. D 81 (2010) 043506.
[25] C. Pigozzo, M.A. Dantas, S. Carneiro, J.S. Alcaniz, J. Cosmol. Astropart. Phys. 08 (2011) 022.
[26] D. Bessada, O.D. Miranda, Phys. Rev. D 88 (2013) 083530.
[27] M. Szydlowski, A. Stachowski, J. Cosmol. Astropart. Phys. 066 (2015) 1510.
[28] A.P. Jayadevan, M. Mukesh, A. Shaima, T.K. Mathew, Astrophys. Space Sci.. 364 (2019) 67.
[29] S. Basilakos, Mon. Not. R. Astron. Soc. 395 (2009) 2374.
[30] J. Solà, J. Phys. Conf. Ser. 283 (2011) 012033.
[31] J. Grande, J. Solà, S. Basilakos, M. Plionis, J. Cosmol. Astropart. Phys. 11 (2011) 007.
[32] J. Solà, J. Phys. Conf. Ser. 453 (2013) 012015.
[33] A. Gomez-Valent, J. Solà, Mon. Not. R. Astron. Soc. 448 (2015) 2810.
[34] C. Brans, R.H. Dicke, Phys. Rev. 124 (1961) 925.
[35] K. Uhera, C.W. Kim, Phys. Rev. D 26 (1982) 2575.
[36] L.O. Pimentel, Astrophys. Space Sci. 112 (1985) 175.
[37] N. Banerjee, D. Pavon, Classical Quantum Gravity 18 (2001) 593.
[38] L. Amendola, C. Quercellini, D. Tocchini-Valentini, A. Pasqui, Astrophys. J. 583 (2003) L53.
[39] H. Kim, Mon. Not. R. Astron. Soc. 364 (2005) 813.
[40] J.C. Fabris, S.V.B. Goncalves, R. de Sa Ribeiro, Gravit. Cosmol. 12 (2006) 49.
[41] T. Clifton, J.D. Barrow, Phys. Rev. D 73 (2006) 104022.
[42] A.E. Montenegro Jr., S. Carneiro, Class. Quantum Gravity 24 (2007) 313.
[43] N. Banerjee, D. Pavon, Phys. Lett. B 647 (2007) 447.
[44] G. Olivares, F. Atrio-Barandela, D. Pavon, Phys. Rev. D 77 (2008) 063513.
[45] A. Sheykhi, Phys. Rev. D 81 (2010) 023525.
[46] C.P. Singh, Astrophys. Space Sci. 338 (2012) 411.
[47] P. Kumar, C.P. Singh, Astrophys. Space Sci. 362 (2017) 52.
[48] C.P. Singh, P. Kumar, Int. J. Theor. Phys. 56 (2017) 3297.
[49] S. Ghaffari, M. Moradpour, I.P. Lobo, J.P.M. Graca, Valdir B. Bezerra, Eur. Phys. J. C 78 (2018) 706.
[50] P. Mukherjee ans S. Chakrabarti, Eur. Phys. J. C 79 (2019) 681.
[51] J. Solà, Internat. J. Modern Phys. D 27 (2018) 1847029, arXiv:1805.09810.
[52] J. de Cruz Pérez, J. Solà, Modern Phys. Lett. A 33 (2018) 1850228, arXiv:1809.03329.
[53] J. Solà, A. Gomez-Valent, J. de Cruz Pérez, C. Moreno-Pulido, Astrophys. J. Lett. 886 (2019) L6, arXiv:1909.02554.
[54] E. Karimkhani, A. Khodam-Mohammadi, Astrophys. Space Sci. 364 (2019) 117.
[55] C.P. Singh, Simran Kaur, Phys. Rev. D 100 (2019) 084057.
[56] C.P. Singh, Simran Kaur, Astrophys. Space Sci. 365 (2020) 2.
[57] J. Solà, A. Gomez-Valent, J. de Cruz Pérez, C. Moreno-Pulido, Class. Quantum Gravity 37 (2020) 245003.
[58] S. Kaur, C.P. Singh, Phys. Dark Universe 33 (2021) 100869.
[59] C.P. Singh, J. Solà Peracaula, Eur. Phys. J. C 81 (2021) 960.
[60] H. Özer, O. Delice, Eur. Phys. J. C 81 (2021) 326.
[61] I.L. Shapiro, Class. Quantum Gravity 25 (2008) 103005.
[62] S. Basilakos, M. Plionis, J. Sola, Phys. Rev. D 80 (2009) 083511.
[63] E.L.D. Perico, J.A.S. Lima, S. Basilakos, J. Solà, Phys. Rev. D 88 (2013) 063531.
[64] J. Solà Peracaula, J. de Cruz Pérez, A. Gomez-Valent, Mon. Not. R. Astron. Soc. 478 (2018) 4357, arXiv:1703.08218.
[65] I. Waga, Astrophys. J. 414 (1993) 436.
[66] J. Salim, I. Waga, Class. Quantum Gravity 10 (1993) 1767.
[67] R.C. Arcuri, I. Waga, Phys. Rev. D 50 (1994) 2928.
[68] A.I. Arbab, Gen. Relativ. Gravit. 29 (1997) 61.
[69] I.L. Shapiro, J. Sola, J. High Energy Phys. 02 (2002) 006.
[70] S. Basilakos, D. Polarski, J. Sola, Phys. Rev. D 86 (2012) 043010.
[71] D.M. Scolnic, et al., Astrophys. J. 859 (2018) 101.
[72] A. Conley, et al., Astrophys. J. Suppl. Ser. 192 (2011) 1.
[73] M. Betoule, et al., Astron. Astrophys. 568 (2014) A22.
[74] N. Padmanabhan, et al., Mon. Not. R. Astron. Soc. 427 (2012) 2132.
[75] F. Beutler, et al., Mon. Not. R. Astron. Soc. 416 (2011) 3017.
[76] L. Anderson, et al., Mon. Not. R. Astron. Soc. 441 (2014) 24.
[77] C. Blake, et al., Mon. Not. R. Astron. Soc. 425 (2012) 405.
[78] P.A.R. Ade, et al., Astron. Astrophys. 594 (2016) A13.
[79] M.V. de Santos, R.R.R. Reis, I. Waga, J. Cosmol. Astropart. Phys. 02 (2016) 66.
[80] G. Hinshaw, et al., Astrophys. J. Suppl. 208 (2013) 19.
[81] M. Moresco, et al., J. Cosmol. Astropart. Phys. 08 (2012) 006.
[82] T. Delubac, et al., Astron. Astrophys. 574 (2015) A59.
[83] A. Font-Ribera, et al., J. Cosmol. Astropart. Phys. 05 (2014) 027.
[84] S. Alam, et al., Mon. Not. R. Astron. Soc. 470 (2017) 2617.
[85] M.J. Reid, D.W. Pesce, A.G. Riess, Astrophys. J. 886 (2) (2019) L27.
[86] D. Foreman-Mackey, D. Hogg, D. Lang, J. Goodman, Publ. Astron. Soc. Pac. 125 (2013) 306, arXiv:1202.3665[astro-ph].
[87] H. Akaike, IEEE Trans. Automat. Control 19 (1974) 716.
[88] G. Schwarz, Ann. Statist. 6 (1978) 461.